UNIVERSITAT DE BARCELONA

CD98hc orchestrates amino acid and glucose availability, redox homeostasis and energetic and nucleotide metabolism

CD98hc sostiene la disponibilidad de aminoácidos y glucosa, la homeóstasis óxido-reducción y el metabolismo energético y de nucleótidos

Sara Cano Crespo

Universitat de Barcelona
Facultat de Biologia
Departament de Bioquímica i Biomedicina Molecular

CD98hc orchestrates amino acid and glucose availability, redox homeostasis and energetic and nucleotide metabolism.

CD98hc sostiene la disponibilidad de aminoácidos y glucosa, la homeostasis óxido-reducción y el metabolismo energético y de nucleótidos.

Sara Cano Crespo

Barcelona, 2019

Universitat de Barcelona
Facultat de Biologia
Departament de Bioquímica i Biomedicina Molecular
Institute for Research in Biomedicine (IRB Barcelona)
Programa de Doctorat en Biomedicina

CD98hc orchestrates amino acid and glucose availability, redox homeostasis and energetic and nucleotide metabolism.

CD98hc sostiene la disponibilidad de aminoácidos y glucosa, la homeostasis óxido-reducción y el metabolismo energético y de nucleótidos.

Memòria presentada per **Sara Cano Crespo** per optar al grau de doctora per la Universitat de Barcelona.

Sara Cano Crespo
Doctoranda

Manuel Palacín
Director i tutor

Barcelona, 2019

Contents

1. Most frequently used abbreviations 21

2. Introduction 29

2.1 Heteromeric AA Transporters in health and disease 31

2.1.1 The heavy subunits 32

2.1.2 The light subunits 33

2.2 CD98hc-associated transporters: AA availability and redox homeostasis 35

2.2.1 y^+LAT2: the mysterious transporter 35

2.2.2 xCT: the oxidative stress supervisor 35

2.2.3 LAT1: the essential AA importer 37

2.3 CD98hc in the spotlight of cancer 44

2.3.1 CD98hc-associated AA transport function 44

2.3.2 CD98hc-associated integrin signalling 48

2.4 CD98hc's metabolic connexions 49

2.4.1 CD98hc and GLUT1 49

2.4.2 The metabolic super-complex CD98hc-LAT1-MCT-CD147 54

2.5 Cell cycle progression and replication stress 56

2.5.1 A quick overview 56

2.5.2 Replication stress and the DNA damage response 59

2.6 Dissection of integrin signalling- and AA transport function- associated to CD98hc in cell proliferation 62

2.6.1 CD98hc-associated AA transport function *in vivo* 62

2.6.2 CD98hc-associated AA transport function *in vitro* 63

3. Objectives 67

4. Results 71

4.1 CD98hc is at the crossroad of oxidative stress and AA availability. 73

4.1.1 CD98hc protects cells against oxidative stress leading to cell survival 74

4.1.2 CD98hc supports the balance of intracellular AA content 76

4.1.3. CD98hc-deficient cell proliferation is restored after BCAA and AAA supplementation 79

4.1.4 Low 6AA cells: A cellular model to study the effects of BCAA and AAA scarcity 83

4.1.5 BCAA and AAA shortage inactivates mTORC1 signalling pathway in CD98hc KO cells 87

4.1.6 CD98hc ablation leads to eIF2α phosphorylation non mediated by AA scarcity 89

4.1.7 Lack of CD98hc triggers the reduction of global protein synthesis 94

4.2 CD98hc sustains appropriate nucleotide availability for proper cell cycle progression 96

4.2.1 Gene Set Enrichment Analysis reveals putative cell cycle alterations in CD98hc KO cells 97

4.2.2 Cells lacking CD98hc fail to progress adequately through the S-phase of the cell cycle 99

4.2.3 Lack of CD98hc and BCAA and AAA shortage lead to replicative stress 101

4.2.4 CD98hc and BCAA/AAA availability are required for appropriate cell division cycle accomplishment 106

4.2.5 CD98hc KO cells present defective pentose phosphate pathway and a general reduction in the nucleotide pool levels 108

4.2.6 Shortage of dNTPs underlies the replicative stress existing in CD98hc KO cells 114

4.3 CD98hc sustains the cellular energy metabolism 119

4.3.1 Ablation of CD98hc leads to downregulated GLUT1 transporter decreasing glucose uptake 119

4.3.2 CD98hc deficiency represses glycolysis 121

4.3.3 CD98hc ablation triggers the downregulation of the expression of both CD147 and MCT1 proteins 130

4.3.4 CD98hc ablation leads cells to re-route to OXPHOS 135

4.3.5 CD98hc ablation induces an increase in mitochondrial mass 137

4.3.6 Glutamine may account for OXPHOS activation in CD98hc KO cells 140

4.3.7. The shortage of BCAAs and AAAs has an impact in OXPHOS 143

5. Discussion 147

5.1 CD98hc is essential for *in vitro* cell survival and redox homeostasis 150

5.2 CD98hc sustains cellular the AA availability required for proper cell proliferation 154

5.3 CD98hc is required for nucleotides biosynthesis, ensuring the correct completion of the cell cycle 157

5.4 CD98hc regulates glucose utilization and sustains the energy metabolic program of the cell 162

6. Conclusions 171

7. Materials and Methods 175

7.1 Cell culture protocols 177

7.1.1 Cell lines and growing conditions 177

7.1.2 CRISPR/Cas9-mediated CD98hc knockout in HEK 293T cells 178

7.1.3 Cell freezing and thawing 182

7.1.4 Dipeptide and nucleoside supplementation 182

7.1.5 Transitory cell transfection 183
7.1.6 Cell proliferation assay 183
7.2 General molecular biology protocols 183
7.2.1 Protein extraction 183
7.2.1.1 Total cellular protein extraction 183
7.2.1.2 Total membranes extraction 184
7.2.2 Co-immunoprecipitation assays 184
7.2.3 Protein quantification 185
7.2.4 Immunoblotting 186
7.2.5 RNA extraction 186
7.2.6 RNA quantification 186
7.2.7 RNA reverse transcription to cDNA 188
7.2.8 Quantitative real-time PCR (RT-PCR) ..... 188_Toc9095954
7.2.9 DNA purification 190
7.2.10 Polymerase Chain Reaction (PCR) 191
7.3 Global protein synthesis measurement 191
7.3.1 Measurement of 35S-methionine incorporation 191
7.3.2 Protein synthesis measurement by SUnSET 192
7.4 Apoptosis assay: annexin V-propidium iodide staining 193
7.5 Cell cycle analysis 194
7.6 Quantification of ROS production: intracellular ROS and mitochondrial superoxide levels 196
7.7 Transcriptome analysis 197
7.7.1 RNA expression profiling 197
7.7.2 Bioinformatic analyses 198

7.8 Immunofluorescence 198
7.8.1 Mitosis analysis 198
7.8.2 Mitochondrial morphology analysis 199
7.9 AA uptake measurement 200
7.10 Targeted metabolomics assay 201
7.10.1 Metabolite extraction 201
7.10.2 Gas Chromatography (GC) - Mass spectrometry (MS) analysis 202
7.10.3 Liquid Chromatography (LC) - Mass spectrometry (MS) analysis 203
7.11 tRNA aminoacylation array 204
7.12 Intracellular AA quantification 207
7.13 Mitochondrial DNA copy number analysis 207
7.14 Glucose uptake measurement with 2-NBDG 208
7.15 Mitochondrial mass determination with Mitotracker-green 208
7.16 Oxygen consumption measurements 209
7.17 Statistical analysis 209
8. Resumen en castellano 211
8. 1 Introducción 213
8.1.1 Transportadores heteroméricos de aminoácidos 213
8.1.2 Transportadores asociados con CD98hc: asequibilidad de AAs y homeostasis óxido-reducción 214
8.1.3 La importancia de CD98hc en cáncer 218
8.1.3.1 La función de CD98hc asociada a transporte 218
8.1.3.2 CD98hc y señalización de integrinas 220

8.1.4 CD98hc: conexiones metabólicas 220

8.1.4.1 CD98hc y el transportador de glucosa GLUT1 220

8.1.4.2 El supercomplejo metabólico CD98hc-LAT1-MCT-CD147 221

8.1.5 Estrés replicativo y su impacto en la progresión del ciclo celular 223

8.2 Objetivos 224

8.3 Resultados y discusión 225

8.3.1 CD98hc protege a las células frente al estrés oxidativo manteniendo su viabilidad 226

8.3.2 CD98hc sostiene la adecuada asequibilidad de AA requerida para la proliferación celular 227

8.3.3 CD98hc es fundamental para la síntesis de nucleótidos, necesarios para la progresión del ciclo celular 229

8.3.4 CD98hc regula el metabolismo energético celular 231

8.4 Conclusiones 234

9. References 236

10. Appendix I 263

I.I A human cellular model to study the roles of CD98hc 263

I.II Publication: Prazosin induced lysosomal tubulation interferes with cytokinesis and theendocytic sorting of the tumour antigen CD98hc 269

11. Appendix II: 292

Publication: Amino Acid Transport Associated to Cluster of Differentiation 98 Heavy Chain (CD98hc) is at the Cross-road of Oxidative Stress and Amino Acid Availability 292

12. Appendix III 306

Publication: CD98hc (SLC3A2) sustains amino acid and nucleotide availability for cell cycle progression 306

Figure Contents

Figure 1. HATs structure. 32
Figure 2. HATcrystal structures. 34
Figure 3. xCT detoxifying activity. 36
Figure 4. Outline of AA-mediated mTORC1 signalling pathway. 39
Figure 5. eIF2α phosphorylation in stress responses.. 41
Figure 6. Outline: LAT1 in cancer. 46
Figure 7. Outline: xCT in cancer. 47
Figure 8. Glucose metabolism: an overview. 51
Figure 9. Deoxynucleotides biosynthesis. 53
Figure 10. Cell cycle progression diagram. 58
Figure 11. DNA damage response signalling pathway. 60
Figure 12. Both CD98hc-integrin signalling and -AA transport capacity promote cell proliferation *in vivo*. 63
Figure 13. β-Mercaptoethanol inhibits cell death and restores CD98hc KO cell survival. 64
Figure 14. CD98hc AA transport function is sufficient for efficient cell proliferation *in vitro*. 65
Figure 15. Expression of CD98hc-asscociated transporters in different human cell lines. 73
Figure 16. CD98hc protects cells from ferroptosis. 75
Figure 17. CD98hc ablation leads to increased oxidative stress. 76
Figure 18. CD98hc depletion leads to imbalanced intracellular AA content and to adaptations of CD98hc-independent transporters. 77
Figure 19. CD98hc ablation triggers the upregulation of the expression and activity of CAT3.. 78
Figure 20. PEPT1 expression is upregulated in CD98hc KO cells. 80
Figure 21. Supplementation with BCAA- and AAA-containing dipeptides restores proliferation of CD98hc KO cells. 81

Figure 22. PEPT1 expression matched the recovery of cell proliferation in CD98hc KO cells. 81
Figure 23. NRF2 expression matched the recovery of cell proliferation in CD98hc KO cells. 82
Figure 24. Supplementation with BCAA- and AAA-containing dipeptides does not recover the intracellular AA content. 82
Figure 25. Low 6AA media optimization. 83
Figure 26. Low 6AA cells present compromised proliferation. 84
Figure 27. BCAA and AAA shortage leads to imbalanced intracellular AA content.. 85
Figure 28. Comparison of the intracellular AA content in CD98hc KO and low 6AA cells.. 85
Figure 29. BCAA and AAA shortage triggers the upregulation of the expression of CAT3 and increased L-Arg uptake.. 86
Figure 30. Low 6AA do not present oxidative stress. 87
Figure 31. CD98hc ablation leads to downregulated mTORC1 signalling pathway due to the BCAA and AAA shortage. t. 88
Figure 32. BCAA and AAA shortage leads to downregulated mTORC1 signalling pathway. 88
Figure 33. CD98hc ablation leads to eIF2-mediated integrated stress response activation. 89
Figure 34. tRNA charging levels were marginally affected in CD98hc KO cells.. 90
Figure 35. BCAA and AAA shortage does not trigger eIF2-mediated integrated stress response activation. 91
Figure 36. CD98hc KO cells do not present unfolded protein response. 91
Figure 37. CD98hc KO cells present upregulate HRI expression. 92
Figure 38. ATF4 expression is repressed in CD98hc KO cells. 93
Figure 39. GADD34 expression is repressed in CD98hc KO cells. 94
Figure 40. SUnSET analysis of protein synthesis in WT and CD98hc KO cells... 95
Figure 41. Global protein synthesis is downregulated in CD98hc KO cells. 96
Figure 42. GSEA of transcriptional data from WT and CD98hc KO cells. 97

Figure 43. GSEA shows an enrichment in cell cycle related gene sets in CD98hc KO cells. 98
Figure 44. CD98hc depletion leads to increased S- and G2/M- phases. 99
Figure 45. CD98hc depletion leads to delayed S-phase. 100
Figure 46. CD98hc KO cells show an enrichment in the DNA damage response gene set. 103
Figure 47. CD98hc ablation leads to activated DNA damage response. 104
Figure 48. The loss of CD98hc induces apoptosis. 104
Figure 49. BCAA and AAA shortage leads to activated DNA damage response. 105
Figure 50. BCAA- and AAA- containing dipeptides partially reverse S-phase delay in CD98hc KO cells. 106
Figure 51. GSEA reveals enrichment in G2/M checkpoint gene set 107
Figure 52. CD98hc ablation leads to impaired mitotic rate. 107
Figure 53. BCAA and AAA shortage leads to impaired mitotic rate. 108
Figure 54. Lack of CD98hc triggers a general reduction in the nucleotide pool. 109
Figure 55. The pentose phosphate pathway flux is abrogated in CD98hc KO cells. 110
Figure 56. BCAA and AAA shortage triggers a reduction in the deoxynucleotide pool. 110
Figure 57. BCAA and AAA shortage leads to downregulated RRM2 expression. 111
Figure 58. Pentose phosphate pathway flux is not affected in low 6AA cells.. 112
Figure 59. BCAA and AAA shortage leads to downregulated c-myc expression. C 112
Figure 60. mTORC1 pathway inhibition leads to replicative stress and downregulated c-myc expression in WT cells. 113
Figure 61. CD98hc ablation leads to downregulated c-myc expression with no alterations in RRM2 expression. 114
Figure 62. Nucleosides partially reverse S-phase delay in CD98hc KO cells. 115
Figure 63. Nucleosides reduce the DNA damage response in CD98hc KO cells. 116

Figure 64. Nucleosides reverse mitotic rate in CD98hc KO cells. 117
Figure 65. Nucleosides reverse the replicative stress caused by BCAA and AAA deprivation in low 6AA cells. 118
Figure 66. CD98hc ablation leads to repressed GLUT1- and upregulated GLUT3-expression levels. 120
Figure 67. Ablation of CD98hc leads to reduced glucose uptake. 121
Figure 68. BCAA and AAA are less incorporated by CD98hc KO cells. 122
Figure 69. CD98hc KO cells are consuming less glucose than WT cells. 122
Figure 70. CD98hc KO cells present repressed glycolysis. 124
Figure 71. CD98hc KO cells show a reduction in TCA intermediaries. 125
Figure 72. Low 6AA cells enhanced glycolysis. 127
Figure 73. BCAA and AAA shortage increases conversion of pyruvate into citrate. 128
Figure 74. BCAA and AAA shortage trigger a decrease in the expression of lipogenic genes. 129
Figure 75. CD98hc-LAT1-CD147-MCT1 co-immunoprecipitate together. 131
Figure 76. CD98hc ablation leads to downregulated CD147 and MCT1 expression. 132
Figure 77. The lactate content in the extracellular media of CD98hc KO cells is lower than in the WT media. 133
Figure 78. LDH isoforms are expressed differentially in cell lacking CD98hc. 134
Figure 79. CD98hc KO cells show a decrease in ATP levels. 135
Figure 80. CD98hc KO cells present enhanced OXPHOS. 136
Figure 81. TCA cycle enzymes present altered expression in CD98hc KO cells. A,. 137
Figure 82. CD98hc KO cells present increased mitochondrial mass. 138
Figure 83. CD98hc ablation induces changes in the mitochondrial morphology. 139
Figure 84. CD98hc KO cells produce higher levels of mitochondrial ROS. 140
Figure 85. The glutaminolytic enzymes are upregulated in CD98hc KO cells. 141
Figure 86. ASNS is upregulated in CD98hc KO cells. 142

Figure 87. The conversion of pyruvate into alanine is increased in CD98hc KO cells.. 142
Figure 88 Supplementation with BCAA- and AAA-containing dipeptides reduces OXPHOS in CD98hc KO cells..... 143
Figure 89. Low 6AA cells present enhanced OXPHOS. 144
Figure 90. Low 6AA cells do not present increased mitochondrial mass. 145
Figure 91. CD98hc functions as a regulatory hub, orchestrating not only AA availability and redox homeostasis but also glucose and nucleotide synthesis, required for proper cell cycle progression. 150
Figure 92. CD98hc protects cells against oxidative stress leading to cell survival.. 154
Figure 93. CD98hc supports the balance of intracellular AA content..... 156
Figure 94. CD98hc is required for the correct completion of the cell cycle. 161
Figure 95. CD98hc regulates glucose utilization, controlling the energy metabolism of the cell. 166
Figure 96. Overview of the most relevant results reported in the present thesis.169
Figure 97. CRISPR/Cas9-mediated CD98hc knockout in HEK 293T cells..... 179
Figure 98. Generation of CRISPR/Cas9-mediated CD98hc knockout HEK 293T cells. 180
Figure 99. Confirmation of the deletion of CD98hc in CD98hc KO HEK 293T cells. 181
Figure 100. Co-immunoprecipitation of CD98hc and associated light chains, CD147 and MCT1..... 184
Figure 101. SUnSET, a nonradioactive method to monitor protein synthesis..... 193
Figure 102. Annexin V staining assay for apoptosis measurement. 194
Figure 103. The cell cycle profile of a sample can be determined by staining the DNA with propidium iodide..... 195
Figure 104. Mitotic phases and their corresponding P-H3 staining pattern.. 200
Figure 105. tRNA aminoacylation array. 206
Figure 106. Characterization of CD98hc KO HEK 293T cells. 266

Figure 107. The intracellular AA content is not affected in CD98hc KO HEK 293T cells.. 267

Table Contents

Table 1. HATs, transport system, substrate spectrum and associated disorders....33
Table 2. Antibodies used and details of usage..... 187
Table 3. Real time PCR SYBR Green primers..... 189
Table 4. Characterization of analysed metabolites..... 203
Table 5. Characterization of analysed nucleotides..... 204

Most frequently used abbreviations

AA: amino acid
AA+: cationic amino acid
AA^0: neutral amino acid
AAA: aromatic amino acid
Ab: antibody
ADP: adenosine diphosphate
AMP: adenosine monophosphate
AMPK: adenosine monophosphate-activated protein Kinase
asc1: alanine-serine-cysteine-1
ASNS: asparagine synthetase
ATF4: activating transcription factor 4
ATM: ataxia Telangiectasia Mutated protein
ATP: adenosine triphosphate
ATR: ataxia telangiectasia and rad3 related protein
a.u.: arbitrary units

BCAA: branched-chain amino acid
BCH: 2-aminoBiCyclo[2. 2. 1]Heptane-2-carboxylic acid
BHQ: tert-butylhydroquinone
BSA: bovine Serum Albumin

CAT: cationic amino acid transporter
CD147: cluster of differentiation 147
CD98hc: cluster of differentiation 98 heavy chain
CDK: cyclin-dependent kinase
cDNA: complementary DNA
CDP: cytidine diphosphate
CHK: checkpoint kinase
CMP: cytidine monophosphate
CSH: cysteine
CSSC: cysteine

dADP: deoxy-adenosine diphosphate
dAMP: deoxy-adenosine monophosphate
dCDP: deoxy- cytidine diphosphate
DCF: fluorescent 2′: 7′-dichlorofluorescein
dCMP: deoxy-cytidine monophosphate
DDR: DNA damage response
dGMP: deoxy- guanosine monophosphate
DMSO: dimethyl sulfoxide
DNA: deoxyribonucleic acid
DPM: disintegrations per minute

DSBs: DNA double strand breaks
dsDNA: double stranded DNA
dTDP: deoxythymidine diphosphate
DTT: dithiothreitol

EAA: essential amino acid
ECM: extracellular matrix
EDTA: ethylenediaminetetraacetic acid
eIF2: eukaryotic initiation factor 2
ER: endoplasmic reticulum
ES: enrichment score

FACS: fluorescence activated cell sorting
FBS: fetal bovine serum
FCCP: carbonyl cyanide-4-(trifluoromethoxy)phenylhydrazone
FDR: false discovery rate
FES: fibroblasts derived from embryonic stem cells

G6P: glucose-6-phosphatase
GADD34: DNA damage-inducible protein
GC: Gas chromatography
GC-MS: gas chromatography-coupled to mass spectrometry
GCN2: general control non-derepressible-2
GDP: guanosine diphosphate
GFP: green fluorescent protein
GLUT: glucose transporter
GMP: guanosine monophosphate
GPX: GSH peroxidase
GSEA: gene set enrichment analysis
GSH: glutathione (reduced form)
GSSG: glutathione (oxidized form)

H2DCFDA: 2':7'-dichlorodihydrofluorescein diacetate
H3: histone 3
HAT: heteromeric amino acid transporter
HEPES: hydroxyethyl piperazineethanesulfonic acid
HRI: heme-regulated inhibitor

IMP: inosine monophosphate.
IP: propidium iodide

ISR: integrated stress response

KD: knock down
KO: knock out

LAT1: L-type amino acid transporter 1
LAT2: L-type amino acid transporter 2
LC: liquid chromatography
LDH: lactate deshydrogenase

MCT: monocarboxylate transporter
MS: mass spectrometry techniques
mTORC1: mammalian target of rapamycin complex 1

NAD: nicotinamide adenine dinucleotide
nDNA: nuclear DNA
NEM: N-EthylMaleimide
NES: normalised enrichment score
NRF2: nuclear factor erythroid 2-related factor 2

OCR: oxygen consumption rate
OXPHOS: oxidative phosphorylation

P-: phosphorylated
PAGE: polyacrylamide gel electrophoresis
PBS: phosphate buffered saline
PCR: polymerase chain reaction
PDH: pyruvate dehydrogenase
PEI: polyethylenimine
PEPT1: peptide transporter 1
PERK: PKR-like ER kinase
PGC-1a: peroxisome proliferator-activated receptor γ coactivator
PKR: protein kinase double-stranded RNA-dependent
PPP: pentose phosphate pathway
Puro: puromycin

RIPA: radio-immunoprecipitation assay
RNA: ribonucleic acid

RNR: ribonucleotide reductase
ROS: reactive oxygen species
RPA: replication protein A
RPLP0: ribosomal phosphoprotein: large: P0
RRM2: ribonucleotide reductase regulatory subunit M2
RS: replicative stress
RT-PCR: real time-polymerase chain reaction

S6: ribosomal protein S6
SAS: sulfasalazine
SDHA: succinate dehydrogenase [ubiquinone] flavoprotein subunit
SDS: sodium dodecyl sulphate
SLC: solute carrier

TCA: tricarboxylic acid cycle
TFAM: transcription factor A, mitochondrial
tRNA: transference RNA

UDP: uridine diphosphate
UMP: uridine monophosphate

WT: wild type

y+LAT1: y^+L amino acid transporter 1
y+LAT2: y^+L amino acid transporter 2

β-ME: β mercaptoethanol

Amino acid abbreviations

A	Ala	alanine	**M**	Met	methionine
C	Cys	cysteine	**N**	Asn	asparagine
D	Asp	aspartic acid	**P**	Pro	proline
E	Glu	glutamic acid	**Q**	Gln	glutamine
F	Phe	phenylalanine	**R**	Arg	arginine
G	Gly	glycine	**S**	Ser	serine
H	His	histidine	**T**	Thr	threonine
I	Ile	isoleucine	**V**	Val	valine
K	Lys	lysine	**W**	Trp	tryptophan
L	Leu	leucine	**Y**	Tyr	tyrosine

Introduction

All cells take up nutrients from the surrounding environment and directed them into metabolic pathways in order to fuel the wide variety of functions that they exert (Vander Heiden et al. 2011). Among these nutrients, amino acids (AAs) are necessary for all living cells and organisms, not only as building blocks of proteins, but also as energy sources, precursors of metabolites and signalling molecules (Christensen, 1990).

Despite differences in structure and function, all living cells in multicellular organisms have a surrounding plasma membrane that serves as a barrier and a gatekeeper (Cooper, 2000). The selective permeability of biological membranes allows the cells to control and maintain their internal composition. In this regard, cell membranes restrict diffusion of AAs, and therefore, the action of specific transmembrane proteins that act as transporters is needed to allow AAs to pass across membranes (Cooper, 2000). Due to the compartmentalization of biochemical pathways in eukaryotes, they are present on the plasma membrane and on the membranes of intracellular organelles. In this frame, different families of transporters belonging to SLC (solute carrier) classification guarantee the absorption, distribution and excretion of AAs. At least SLC1, 3, 6, 7, 32, 36, 38, and 43 family members are known to play this role, characterized by different specificities, transport mechanisms, cellular localization and regulations (Hediger et al. 2013). Importantly, the absence, overexpression and malfunction of AA transporters is associated with a wide variety of disorders, reflecting the relevant roles they fulfil in human physiology (Bröer and Palacín 2011).

2.1 Heteromeric AA Transporters in health and disease

Forming part of the Amino acids, Polyamines and organic Cations (APC) transporter superfamily (Chang et al. 2004), Heteromeric AA Transporters (HATs) are one of the eleven families of the AA transporters in mammals that mediate the transport of AAs across the plasma membrane. These transporters have a

heteromeric structure, being composed by a heavy and the corresponding light subunit, linked by a disulfide bridge (**Figure1**) (Fotiadis, Kanai, and Palacín 2013).

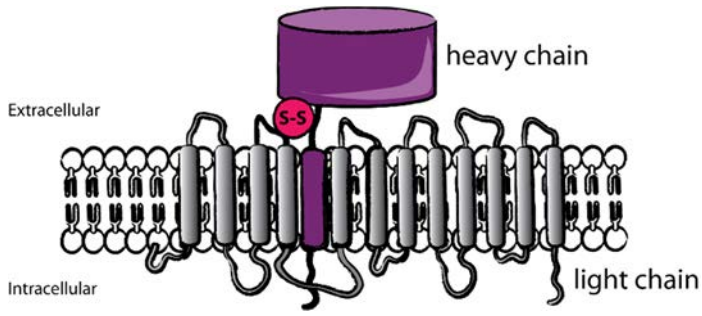

Figure 1. HATs structure. Heavy (depicted in purple) and light chains (depicted in grey) are linked by a disulfide bridge with conserved cysteine residues. The heavy and light subunits have one and twelve transmembrane segments, respectively, as indicated.

2.1.1 The heavy subunits

The heavy subunits are type II N-glycoproteins with an intracellular N-terminal, a single transmembrane domain and an extracellular C-terminal ectodomain. They act as ancillary proteins, taking the holotransporter to the plasma membrane (Estévez et al. 1998; Pfeiffer et al. 1998).

There are two heavy subunits from the SLC3 family, rBAT (SLC3A1) and CD98hc (SLC3A2; 4F2hc). The first one to be identified was rBAT, which was cloned and expressed in *Xenopus laevis* oocytes independently by three groups (Wells and Hediger 1992; Tate, Yan, and Udenfriend 1992; Bertran et al. 1992).

Then, on the basis of its homology, the 4F2 heavy chain (4F2hc), later renamed as cluster of differentiation 98 heavy chain (CD98hc), was recognised as the second heavy subunit (Joan Bertran et al. 1992; Wells et al. 1992), although this protein was originally identified with unknown function in 1982 as a lymphocyte activation antigen by the monoclonal antibody 4F2 (Hemler and Strominger 1982).

rBAT is mainly expressed in the epithelial cells of the kidney proximal tubule and the small intestine, with an apical localization. In contrast, CD98hc is ubiquitous, with a basolateral location in epithelial cells (Bertran et al. 1992).

2.1.2 The light subunits

Light chains are hydrophobic and not glycosylated proteins, formed by a 12-transmembrane domain with NH_2 and COOH termini located intracellularly (Gasol et al. 2004). Light subunits are the real catalytic part of the transporter, thereby mediating the AA transport across the plasma membrane (Reig et al. 2002).

Table 1. HATs, transport system, substrate spectrum and associated disorders. AA^0, neutral AAs; AA^+, basic AAs; BCAA, branched-chain AAs; AAA, aromatic AAs; CssC, cysteine

Heavy chain	Light chain	Transport system	Substrates	Associated disorders
rBAT	$b^{0,+}AT$	$b^{0,+}$	AA^0/AA^+ exchange; Arg, Lys and Orn reabsorption	Cystinuria (1, 2)
	AGT1		Reabsorption of CssC in exchange of Asp and Glu	
CD98hc	LAT1	L	Large AA^0 BCAA and AAA, Gln, Met, His	Cancer (3) Autism spectrum disorders (4)
	LAT2	L	Small AA^0 BCAA and AAA	Age-related hearing loss (5)
	y^+LAT1	y^+L	Na^+-LargeAA^0/AA^+ exchange	Lysinuric protein intolerance (LPI) (6)
	y^+LAT2	y^+L	Na^+-LargeAA^0/AA^+ exchange; Gln/Arg exchange	
	asc1	Asc	Small AA^0 exchange; D-serine; D-glycine	
	xCT	x_c^-	Glu/CssC exchange	Cancer (3) Ferroptosis (7) KSHV entry (8)

1, (Calonge et al. 1994); **2**, (Feliubadaló et al. 1999); **3**, (McCracken and Edinger 2013a); **4**, (Tărlungeanu et al. 2016); **5**, (Espino Guarch et al. 2018); **6**, (David Torrents et al. 1999); **7**, (Dixon, Lemberg, Lamprecht, Skouta, Zaitsev, Gleason, Patel, Bauer, Cantley, Yang, Morrison, and Stockwell 2012b); **8**, (Kaleeba and Berger 2006).

There are eight human light subunits, all members of the SLC7 family (LAT transporter branch). Two of them form dimers with rBAT: $b^{0,+}$AT (SLC7A9) and AGT1 (SLC7A13), and CD98hc dimerizes with six different light subunits: LAT1, y^+LAT2, y^+LAT1, LAT2, asc1 and xCT (SLC7A5, 6, 7, 8, 10 and 11 respectively) (**Table 1**). (Fotiadis, Kanai, and Palacín 2013; Nagamori et al. 2016). Light subunits confer substrate specificity to the heterodimer (**Table 1**).and, with the exception of asc1, they are obligatory exchangers with 1:1 stoichiometry.

A growing body of evidence shows that malfunction of the aforementioned transporters is associated with a broad range of disorders (**Table 1**), highlighting the relevance of their study.

Only recently the first structures of these transporters have been solved: i) bacterial asc transporter (BasC) in conformation outward-facing with and without substrate bound (**Figure 2A**) (Errasti-Murugarren et al. 2019) and ii) the human LAT1-CD98hc heterodimer (**Figure 2B**) (Yan et al. 2019).

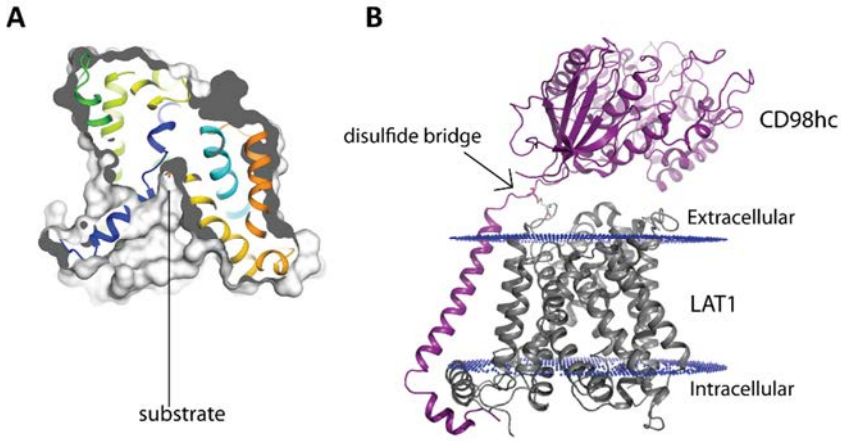

Figure 2. HATcrystal structures. **A**, crystal structure of BasC (3.4 Å). Helices are coloured in rainbow while protein surface is depicted in light grey. The sagittal plane shows the substrate (2-amino isobutyrate, orange) at the end of the vestibule open to the cytoplasm. **B**, structure of human LAT1–CD98hc (3.3 Å). CD98hc is depicted in purple; LAT1, depicted in grey, exhibits an inward open conformation. The disulfide bridge is indicated. *Images of the structures were made by Joana Fort.*

These structures open the path to dissect the molecular mechanisms of substrate binding and translocation, determine the molecular bases for interaction with other proteins and the structure-based design of ligands with therapeutic value.

2.2 CD98hc-associated transporters: AA availability and redox homeostasis

This thesis has wanted to get deeper into the understanding the cellular functions that rely on CD98hc-associated transporters, in particular, our cellular model, as well as all the cell lines tested in this study, present the following light chains associated to CD98hc:

2.2.1 y⁺LAT2: the mysterious transporter

y^+LAT2-CD98hc mediates sodium-independent transport of AA^+s and the sodium-dependent uptake of AA^0s (Torrents et al. 1998). It has a wide tissue distribution, including small intestine, brain, testis, kidney, heart and parotid gland (Bröer et al. 2000). The physiological role of this transporter is not clear at present, but it is believed to control the balance between the AA^0 and AA^+ levels in cells.

2.2.2 xCT: the oxidative stress supervisor

Cloning and characterization of mouse xCT light subunit was carried out by Bannai's group (Sato et al. 1999), and later in 2001, this human light subunit was cloned by our group (Bassi et al. 2001).

CD98hc-xCT is the responsible of the transport of anionic cystine in exchange of glutamate (Sato et al. 1999). Since cystine is very rare in the cytosol due to its rapid reduction to cysteine, whereas the concentration of glutamate is much higher in cells than in extracellular fluid, the physiological flows via this transporter comprise the entry of cystine and the exit of glutamate (Bannai 1986). Although cysteine is not an essential AA (EAA) and can be synthesized from homocysteine

and serine, most cells rely on system x_c^- to take up cystine from the extracellular environment.

Cystine taken up by the cell via system x_c^- is reduced by the enzyme glutathione-cystine transhydrogenase to its corresponding disulfide, cysteine, which is then incorporated into proteins and glutathione (GSH) (**Figure 3**) (Conrad & Sato, 2012). GSH is a tripeptide form by cysteine, glutamate, and glycine, among which cysteine is the rate-limiting precursor. Moreover, the first and rate-limiting step of its synthesis is catalysed by the enzyme glutamate-cysteine ligase, which indeed, is regulated at transcriptional and translational levels by cysteine availability (Lu 2009). Then, GSH in its reduced form functions as a co-substrate in ROS-detoxifying reactions catalysed by different enzymes, such as GSH peroxidase (GPX), thereby protecting cells from ROS-induced damage (**Figure 3**). Through the GPX-mediated reaction, GSH is oxidized to its oxidized form (G-S-S-G), which is then recycled back to GSH by GSH reductase (GR) at the expense of NADPH (**Figure 3**).

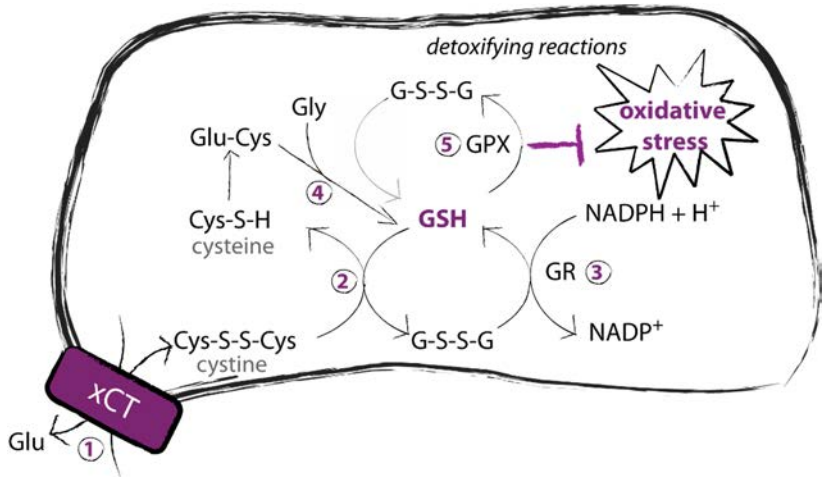

Figure 3. xCT detoxifying activity. 1. Cystine (Cys-S-S-Cys) is transported in exchange of glutamate by CD98hc-xCT inside the cell, where it is reduced to cysteine (Cys-S-H) by GSH-cystine transhydrogenase (**2**). This reaction has as substrates Cys-S-S-Cys and reduced glutathione (GSH) and produces Cys-S-H and oxidized glutathione (G-S-S-G). **3**. Glutathione reductase (GR) reduces again G-S-S-G to GSH. **4**. Free Cys-S-H is essential for the formation of GSH along with glutamate (Glu) and glycine (Gly). **5**. GSH peroxidase (GPX) uses GSH in detoxifying reactions that protect cells from oxidative stress.

In addition to the regulation of the intracellular levels of GSH, and in consequence, the cellular redox homeostasis, in recent years, xCT light chain has been associated with a new form of cell death termed ferroptosis.

Ferroptosis is a non-apoptotic cell death resulting from over-accumulation of lipid hydroperoxides in an iron-dependent manner. This increased lipid peroxidation is normally detoxified by a GPX, which uses GSH to convert lipid hydroperoxides into lipid alcohols, thereby repressing ferroptosis (Yang et al. 2014). Dixon and co-workers demonstrated that the blockage of CD98hc-xCT with specific inhibitors, such as erastin, sulsfosalazin (SAS) and sorafenib, induced depletion of GSH, loss of GPX activity and ferroptotic cell death in cells (Dixon et al. 2014; Dixon et al. 2012).

Furthermore, CD98hc-xCT is a well-known transporter overexpressed in cancer as part of the redox adaptations to survive under conditions of persistent oxidative stress (**chapter 2.3**).

2.2.3 LAT1: the essential AA importer

The identification of LAT1 as an AA transporter (Mastroberardino et al. 1998) allowed the study of the regulation of system L activity and its role in cell proliferation and tumorigenesis. LAT1 is expressed in most tested tumours and tumour cell lines, suggesting that CD98hc-LAT1 plays an important role in many growing cells (**chapter 2.3**).

CD98hc-LAT1 accounts for the sodium-independent exchange of large AA^0s: branched-chain AAs (BCAA) (leucine, isoleucine and valine), aromatic AAs (AAA) (tyrosine, tryptophan and phenylalanine), methionine, glutamine, and histidine (Uchino et al. 2002; Verrey et al. 1998), most of them EAAs.

EAAs have been found to regulate mRNA translation through at least two nutritional-sensing pathways, which are the mammalian mechanistic target of rapamycin (mTORC) and the eukaryotic initiation factor 2 (eIF2)-mediated

integrated stress response (ISR) (Kimball and Jefferson 2005). Thus, not surprisingly, the transporter CD98hc-LAT1 has been identified as a key player in both signalling pathways.

2.2.3.1 mTORC1 signalling pathway

The nutrient-sensing pathway mTORC1 responds to AA deprivation by downregulating general protein synthesis while reprograming cells for their special necessities (Efeyan, Comb, and Sabatini 2015). mTOR forms two distinct complexes named mTORC1 and mTORC2, of which mTORC1 plays a central role in cell growth and proliferation by responding to AA availability, being particularly sensitive to decreases in leucine, arginine and glutamine (Blommaart et al. 1995; Hara et al. 1998; Nicklin et al. 2009a). The presence of AAs is sensed at the lysosome by the protein complex Ragulator that causes the Rag proteins, a family of four related small guanosine triphosphatases (GTPases), to switch to their active conformation. These active proteins bind to Raptor and promote the relocalization of mTORC1 to the lysosome compartment, which also contains Rheb (**Figure 4**) (Sancak et al. 2008). Once the mTORC1 kinase domain is activated by direct binding with Rheb, it phosphorylates the two key effectors of the pathway, p70S6 kinase (S6K) and eIF4E binding protein 1 (4EBP1) (**Figure 4**) (Cargnello, Tcherkezian, and Roux 2015).

On one hand, S6K phosphorylates and regulates several protein substrates that are involved in mRNA metabolism and translation. Among those, there are the initiation factor eIF4B, a positive regulator of the 5′cap binding eIF4F complex, the tumour suppressor programmed cell death 4 (PDCD4), which is an inhibitor of eIF4B and it is degraded after phosphorylation, and the ribosomal protein S6, component of the 40S ribosomal subunit (**Figure 4**) (Magnuson, Ekim, and Fingar 2011). On the other hand, the mTORC1 substrate 4EBP1 is a translation inhibitor that binds and sequesters eIF4E, preventing the assembly of the eIF4F complex. In this sense, mTORC1 phosphorylates 4EBP1 at multiple sites to trigger its dissociation from the initiation complex and thereby allowing the 5′cap-dependent mRNA translation to occur (Gingras et al. 1999).

How AA scarcity is sensed by mTORC1 machinery needs to be further elucidated, although it is believed to involve the v-ATPase, a large protein complex that acidifies the lysosome acting as a proton pump (Zoncu et al. 2011), and intracellular sensors that interact directly with the AAs or their derivatives (Goberdhan, Wilson, and Harris 2016). For instance, Sestrin2 and the CASTOR proteins have been proposed as sensors of cytosolic leucine (H. Wang et al. 2015) and arginine (Chantranupong et al. 2016), respectively. In the same frame, transporters have emerged as important AA sensors controlling mTORC1 recruitment and activation at the surface of multiple intracellular compartments. Some examples are the proton-assisted amino acid transporters 1 (PAT1, SLC36A1) and 4 (PAT4, SLC36A4), required for AA-dependent mTORC1 activation in the lysosome and Golgi apparatus, respectively, or the lysosomal membrane protein SNAT9 (SLC38A9), which acts as a sensor of luminal arginine in lysosomes (Wang et al. 2015).

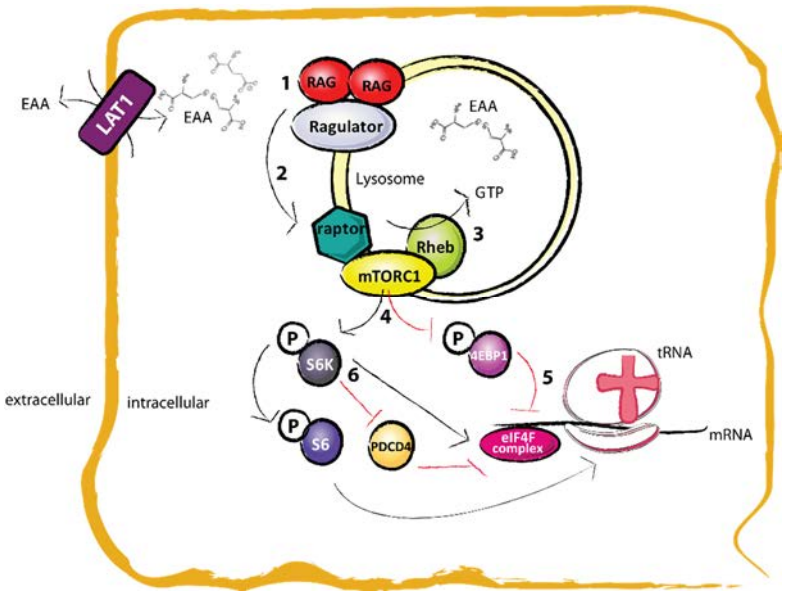

Figure 4. Outline of AA-mediated mTORC1 signalling pathway. AA availability leads to the activation of the RAG GTPases proteins (**1**) that trigger the recruitment of mTORC1 by raptor in the lysosome (**2**). There, Rheb activates mTORC1 (**3**), which phosphorylates the two key effectors, S6K and 4EBP1 (**4**). On one hand, the phosphorylation of the inhibitor 4EBP1 leads to its release from the eIF4F complex (**5**), allowing protein translation. On the other hand, S6K targeted different proteins enabling the initiation of protein synthesis (**6**).

Particularly, an interesting study performed by Milkereit and co-workers revealed that the lysosomal protein LAPTM4b recruits CD98hc-LAT1 to the lysosomal membrane in order to stimulate mTORC1 via V-ATPase (Milkereit et al. 2015). Those results evidenced, against what was believed until then, the presence of CD98hc-LAT1 and associated AA transport activity out of the plasma membrane.

The role for CD98hc-LAT1 in the regulation of mTORC1 pathway is widely accepted by the accumulating evidence. Indeed, it has been reported that genetic- (Cormerais et al. 2016; Elorza et al. 2012) or chemical LAT1 ablation with specific inhibitors, such as 2-aminobicyclo-(2,2,1)-heptane-2-carboxylic acid (BCH) (Nicklin et al., 2009), JPH203 (Cormerais et al. 2016; Oda et al. 2009) or D-phenylalanine (Nicklin et al., 2009), results in mTORC1 inhibition and impaired cell growth.

Besides AA availability, growth factors, through the activation of the canonical insulin and Ras signalling pathways (Inoki, Zhu, and Guan 2003), the cellular energy status, through the AMP-activated protein kinase (AMPK) (Hardie 2007), and oxygen levels, through multiple pathways (Wouters and Koritzinsky 2008), are known to affect mTORC1 activity.

2.2.3.2 eIF2-mediated Integrated Stress Response

AA deprivation, among other stress stimuli, leads to the activation of the eIF2-mediated Integrated Stress Response (ISR), a pro-survival gene expression programme (Taniuchi et al. 2016). Translation initiation involves the binding of methionine-tRNA (met-tRNA) to the 40S ribosomal subunit (Kimball and Jefferson 2005). This step is controlled by a complex consisting of eIF2-GTP-met-tRNA in which the exchange of GDP for GTP is mediated by the guanine nucleotide exchange factor eIF2B. The activity of eIF2B is regulated through phosphorylation of the α-subunit of eIF2 (eIF2α), whereby phosphorylation converts eIF2 in a competitive inhibitor of eIF2B protein (Krishnamoorthy et al. 2002). Thus, eIF2α phosphorylation, triggered by different stress signals, reduces the overall rate of

translation, allowing cells to overcome the stress or promoting their elimination if the damage cannot be repaired (**Figure 5**) (Taniuchi et al., 2016).

Four kinases (PERK (PKR-like ER kinase), PKR (protein kinase double-stranded RNA-dependent), GCN2 (general control non-derepressible-2), and HRI (heme-regulated inhibitor)) mediate the phosphorylation of the α subunit of eIF2 responding to different stress signals (**Figure 5**) (Donnelly et al. 2013).

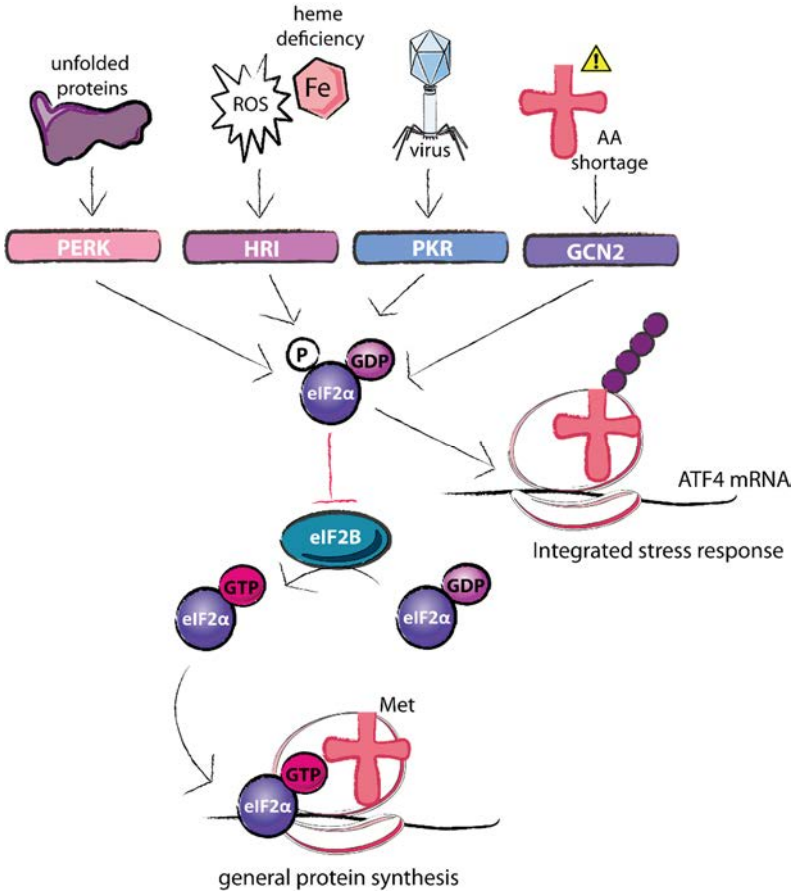

Figure 5. eIF2α phosphorylation in stress responses. To initiate the general gene translation it is necessary the formation of an eIF2·GTP·met·tRNA in the ribosome. eIF2B catalyzes the exchange of GDP for GTP on eIF2, however phosphorylated eIF2α (P-eIF2α) inhibits eIF2B activity and therefore the general protein translation of the cell. Moreover, P-eIF2α specifically promotes the translation of genes (e.g. **ATF4**) that activate the integrated stress response.

PERK

PERK is mainly activated by the accumulation of misfolded proteins in the endoplasmic reticulum (ER), a phenomenon termed ER stress. Accumulation of misfolded proteins causes the immunoglobulin binding protein (BiP) to dissociate from PERK, allowing its dimerization, autophosphorylation and consequent activation (Bertolotti et al. 2000).

PERK blocks the protein synthesis by activating the unfolded protein response (UPR), allowing the ER to refold misfolded proteins and dispose of those that are irreparably damaged (Bi et al. 2013).

Interestingly, a recent study conducted by Liu and colleagues, indicated that UPR was largely disrupted when CD98hc was depleted, highlighting a novel role for CD98hc in the regulation of ER stress (Liu et al. 2018)

PKR

PKR is mostly activated by viral infections through its regulatory N-terminal region that contains a double-stranded RNA binding domain (dsRBD). Once activated, it blocks the translation of viral mRNAs and promotes apoptosis (Galluzzi et al. 2008).

GCN2

As no AA compensates the absence of another in protein synthesis, cells are able to efficiently detect the lack of any AA. It is well established that in response to starvation for different AAs, GCN2 is activated through direct interaction of its histidyl-tRNA synthetase (HisRS)-related domain with uncharged tRNAs (Wek, Zhu, and Wek 1995). After the binding, a conformational change is induced, causing the dimerization and activation of the protein (Dey et al. 2007) and the subsequent eIF2α phosphorylation (Harding et al. 2000).

Particularly, in a study conducted by Anthony and co-workers, it was shown that rats fed with a diet lacking BCAAs or AAAs, all transported by CD98hc-LAT1,

caused enhanced eIF2α phosphorylation through GCN2 activation and protein synthesis decay (Anthony et al. 2001).

Consistently, two different studies have reported that disruption of LAT1, either genetically (Cormerais et al. 2016) or pharmacologically (Cormerais et al. 2019), induces GCN2 activation.

HRI

HRI kinase was firstly believed to have a role in reticulocytes under stress status related to iron and heme deficiencies, in a manner that when heme dissociates from the HRI protein, it was autophosphorylated at key residues and subsequently phosphorylated eIF2α (Kramer, Cimadevilla, and Hardesty 1976; Levin et al. 1976). However, it was later demonstrated that its expression was ubiquitous, suggesting a possible function in the translational regulation of non-erythroid tissues (Berlanga, Herrero, and de Haro 1998). In this regard, increasing research provides strong evidence of the activation of HRI under oxidative stress conditions in different cell types (Lu, Han, and Chen 2001; Suragani et al. 2012; Tidke et al. 2016)

Once the pathway is activated by any of the aforementioned kinases, global mRNA translation was attenuated by the phosphorylatyon of eIF2α while the ISR is induce, entailing the translation of specific mRNAs to remediate the stress and restore homeostasis. Among them, the transcription factor 4 (ATF4) (**Figure 5**) serves to enhance transcriptional expression of genes involved in AA metabolism and resistance to oxidative stress (Harding et al. 2000). Remarkably, ATF4 binds to AA response elements (AAREs) in CD98hc, LAT1 and xCT genes (Harding et al. 2003; Hideyo Sato et al. 2004; Q. Wang et al. 2011), pointing out the central role of HATs on the resolution of the stress upon the phosphorylation of eIF2α.

2.3 CD98hc in the spotlight of cancer

Metabolic flexibility is a term originally applied to the ability of helminths to generate their energetic requirements via aerobic or anaerobic pathways depending on the environmental conditions (Köhler 1985). Nowadays, the notion is widely used to describe the capability of a biological system to respond or adapt to conditional changes in metabolic demand (Pavlova and Thompson 2016). At the cellular level, it comprises extensive re-routing of anabolic and catabolic pathways in order to maintain the cellular homeostasis. In this regard, rapidly proliferating cells, among them, cancer cells, upregulate AA transporters as part of their metabolic reprogramming in order to fulfil their increased biosynthetic and bioenergetic needs and to maintain redox homeostasis (Pavlova and Thompson 2016).

2.3.1 CD98hc-associated AA transport function

The link of CD98hc associated transporters with cancer is nowadays well assessed. Since AAs are used, not only as building blocks for protein synthesis, but also as nitrogen and carbon sources for the synthesis of nucleotides, amino sugars and GSH (Ganapathy, Thangaraju, and Prasad 2009a; Vučetić et al. 2017), cancer cells upregulate their nutritional and antioxidant capacity by inducing the expression of the AA transporters CD98hc-LAT1 and CD98hc-xCT (McCracken & Edinger, 2013).

2.3.1.1. CD98hc-LAT1

LAT1 was found to be highly expressed in tumours of most human tissues according to the Gene expression database of normal and tumour tissues (GENT) (Shin et al. 2011), which evidences the relevant roles it plays in cancer. Moreover, the grade of the expression of LAT1 has been associated with chemotherapy resistance, poor prognosis and metastasis in several cancers (Namikawa et al. 2015; Sakata et al. 2009; Sommer et al. 2018; Yanagisawa et al. 2014).

Cancer cells gain considerable advantage from LAT1 overexpression due to different reasons: i) the increased demand of nutrients, such as EAA, uptaken by this transporter, for protein synthesis and energy supply, is a well-known hallmark of cancer cells (Ganapathy, Thangaraju and Prasad, 2009); ii) the persistent activation of mTORC1, in which, as described above (**section 2.2.3.1**), LAT1 plays a key role, is a peculiarity of all cancer cells (Pavlova and Thompson 2016) and iii) it has been reported that leucine is an allosteric regulator of glutamate dehydrogenase (GDH) (Yielding and Tomkins 1961). GDH catalyses the conversion of glutamate to a-ketoglutarate, playing a pivotal role in glutamine metabolism, which is particularly important in hypoxic or glucose limiting conditions and therefore, in cancer environment (Scalise et al. 2017).

Although the molecular mechanism of the induction of LAT1 in cancer cells remains poorly understood, extensive studies have identified at least three pathways implicated in the overexpression of this transporter in this context. Interestingly, LAT1 promoter has been identified to have a canonical binding site for the proto-oncogene c-myc (Hayashi and Anzai 2017a), thereby considered as a critical regulator for LAT1 expression. In the same line, the Hypoxia inducible factor 2α (HIF2α) is known to also bind this promoter so as to increase the expression of this transporter in specific cancers (Elorza et al. 2012). Finally, the transcription factors YAP/TAZ are able to induce LAT1 expression for conferring cellular growth advantages via activation of mTORC1 activity (Hansen et al. 2015).

These observations support the view that LAT1 functions as a key transporter for highly effective delivery of EAAs into cancer cells. In this regard, its inhibition is expected to have clinical benefits for cancer therapy. The design of inhibitors is the current main strategy followed in the search for the inactivation of this transporter. Among the competitive ones, the LAT1 inhibitor BCH has been reported to suppress cell proliferation in cancer cells (Kim et al. 2008; Oda et al. 2009) and significantly delayed tumour growth in tumour-bearing mice (Ohshima et al. 2016). Furthermore, JPH203 inhibits LAT1 activity, thereby decreasing cell viability and proliferation in different type of cancers (Rosilio et al. 2015; Yothaisong et al. 2017).

However, due to the strict dependency of the inhibition efficiency on the concentration of natural AAs, limited results have been obtained so far with these approaches (Augustyn et al. 2016). Considering this drawback, designing non-competitive inhibitors, or even those that could bind covalently to the substrate binding site of the transporter, is now being explored as a promising alternative strategy (Napolitano et al. 2017).

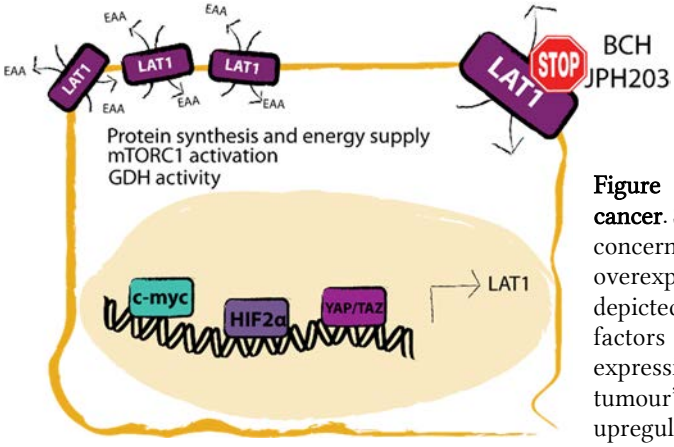

Figure 6. Outline: LAT1 in cancer. Some of the main aspects concerning LAT1 overexpression in cancer are depicted. The transcription factors that regulate its expression, major inhibitors and tumour's advantages from LAT1 upregulation are indicated.

2.3.1.2 CD98hc-xCT

The transporter xCT is overexpressed in several human cancers (Koppula et al. 2017). Remarkably, by analysing multiple microarray datasets from the NCI-60 cell line panel (a panel of 60 diverse human cancer cell lines used by the National Cancer Institute for therapeutic development), it was found that xCT is present in all of the cell lines (Reinhold et al. 2015). Furthermore, like LAT1, xCT is expressed on poor prognosis subsets of most solid tumours and it has been proposed as a reliable biomarker for high-grade malignancy (Cobler et al. 2018; Kinhosita et al. 2013; Toyoda et al. 2014).

The metabolic reprogramming carried out by cancer cells results in increased oxidative stress, thus, in order to induce their antioxidant capabilities, these cells need to increase the biosynthesis of antioxidants, including GSH (Chio and Tuveson 2017). In this context, xCT, which enables the entry of the main source of cystine in cells for GSH production (**section 2.2.2**), plays a vital role in the re-

establishment of the redox balance in cancer cells, fostering their metabolic flexibility.

Extensive studies have identified two transcription factors that regulate the induction of xCT expression, the already described ATF4, which would enhance the expression of the transporter in situations of nutritional or oxidative stresses (**section 2.2.3.2**), and the nuclear factor (erythroid-derived 2)-like 2 (NRF2).

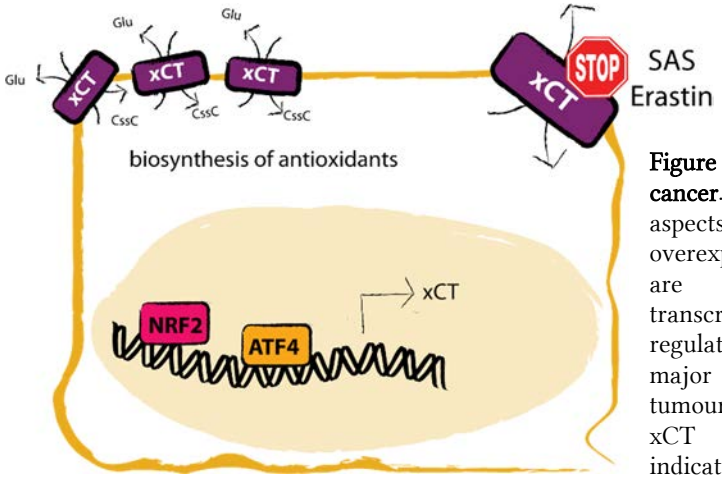

Figure 7. Outline: xCT in cancer. Some of the main aspects concerning xCT overexpression in cancer are depicted. The transcription factors that regulate its expression, major inhibitors and tumour's advantages from xCT upregulation are indicated.

NRF2 is considered a master regulator of oxidative stress in cells. Under basal conditions, NRF2 remains in the cytoplasm interacting with kelch-like-ECH-associated protein-1 (KEAP1), an adaptor protein for the Cullin3-dependent ubiquitin ligase complex. Thus, both proteins are constantly polyubiquitinated and degraded in the proteasome (Motohashi and Yamamoto 2004). Oxidative stress inducers trigger the oxidation of the reactive cysteine residues on KEAP1, resulting in the destabilization of the KEAP1-NRF2 complex. In this situation, NRF2 protein is stabilised and translocated into the nucleus to regulate the transcription of target genes involved in the antioxidant response, xCT among others (Motohashi and Yamamoto 2004; Sasaki et al. 2002).

Since xCT has been proposed as a potential target for cancer therapy, different pharmacological and genetic approaches have been applied to block its function, among which the most relevant compounds are SAS (Gout et al. 2001) and erastin

(Dixon et al. 2012). It has been demonstrated that both drugs markedly reduce tumour development (Timmerman et al. 2013;Yang et al. 2014), however, they have off-target effects, thereby restricting their use in clinical approaches.

2.3.2 CD98hc-associated integrin signalling

Integrins are heterodimeric cell adhesion receptors consisting of a β and an α-subunits, each of them being a type 1 transmembrane protein with a C-terminal cytoplasmic tail and a single transmembrane domain connected to the N-terminus outside the cell (Barczyk, Carracedo, and Gullberg 2010).

The extracellular matrix (ECM) acts as a scaffold for many proteins that play a pivotal role in tumour progression. As major adhesion molecules that support cell attachment to ECM, integrins are overexpressed in tumour cells in order to contribute to tumour progression and metastasis by increasing cell migration, invasion, proliferation and survival (Desgrosellier and Cheresh 2010).

Besides its function as an AA transporter, CD98hc interacts with β1 and β3 integrins, amplifying their downstream signalling (Feral et al. 2005). These two functions associated to CD98hc depend on different domains within the heavy subunit of the transporter. Whereas AA transport function requires the ectodomain for the association with the catalytic light subunit, the intracellular domain is necessary and sufficient for interacting with β1 integrins (de la Ballina et al., 2016; Fenczik et al., 2001).

In this regard, it has been shown that cells lacking CD98hc are, not only significantly defective in integrin-dependent cell spreading and migration, but they are also less protected from anchorage deprivation-induced apoptosis (anoikis) (Feral et al. 2005). Furthermore, CD98hc deletion in mouse embryonic stem (ES) cells effectively delays teratocarcinoma formation in mice. Interestingly, the tumorigenicity of the ES cells can be reconstituted by expressing a chimeric form of CD98hc which is able to interact with β1 integrins while is incapable of

transporting AAs (Feral et al. 2005). Together, these findings indicate that CD98hc contributes to integrin-dependent tumour progression.

In the same line, it was recently described a novel role for CD98hc as an indirect regulator, via the regulation of sphingolipid synthesis, of integrin mechanosensing (Boulter et al., 2018). In that study they found that ablation of CD98hc resulted in aberrant skin mechanical homeostasis as a consequence of defective mechanical sensing of β1 integrins through different signalling pathways. Loss of CD98hc decreased the expression of the enzyme dihydroceramide desaturase 2 (DES2), which triggered the block of *de novo* sphingolipid biosynthesis pathway (Boulter et al., 2018). This finding highlights the cross-talk between cell metabolism and integrin mechanosensing coordinated by CD98hc.

2.4 CD98hc's metabolic connexions

In addition to the classical dual role of CD98hc, being an ancillary subunit of HATs and simultaneously an integrin co-receptor, CD98hc has been reported to interact with other transmembrane proteins with relevant roles in cell metabolism, thereby suggesting potential novel functions of these transporters in this field of study.

2.4.1 CD98hc and GLUT1

Glucose metabolism governs several cellular functions, since glucose oxidation generates the major source of metabolic energy in eukaryotic cells (Thorens and Mueckler 2010). These functions are secondary to glucose uptake, which in most mammalian cells is controlled mainly by glucose transporters (GLUTs; SLC2A) family members.

Interestingly, Ohno and colleagues evidenced that CD98hc directly interacted with GLUT1, which is widely distributed throughout several tissues regulating the basal glucose uptake of the cells (Carvalho et al. 2011; Ohno et al. 2011a). CD98hc

contributed to its stabilization by preventing its degradation in the lysosome, leading to increased cellular glucose uptake (Ohno et al., 2011).

Increase in glucose consumption is a hallmark of cancer metabolism, since it helps to supply the energy needed for tumour cell proliferation. Consistent with this notion, GLUT1 is aberrantly expressed in many tumours (Carvalho et al. 2011) and its expression has been correlated with tumour grade and poor prognosis in different kind of cancers (Cantuaria et al. 2001; Hao et al. 2009; Rudlowski et al. 2003; B. Zhang, Xie, and Li 2019).

Hence, this unexpected observation not only unveils a novel connexion between CD98hc and the progression of cancer malignancy, but it also indicates that CD98hc is likely to be involved in the regulation of glucose metabolism.

Adenosine triphosphate (ATP), which provides the energy for supporting the key functions of cells, is formed mainly by two metabolic pathways, glycolysis and oxidative phosphorylation (OXPHOS), both mostly fuelled by glucose (**Figure 8**). However, glucose metabolism involves not only these two pathways but also others, including: the pentose phosphate pathway, which generates pentose phosphates for ribonucleotide synthesis and NADPH; the hexosamine pathway, responsible for the glycosylation reactions; glycogenesis, which produces glycogen for glucose storage and the serine biosynthesis pathway, which generates different AAs (**Figure 8**) (Hay 2016).

The pentose phosphate pathway: nucleotide metabolism

The pentose phosphate pathway (PPP), which branches from glycolysis at the first committed step of glucose metabolism (**Figure 8**), has a crucial role in the synthesis of ribonucleotides and is also a major source of NADPH (Cho et al. 2018). It is composed of two phases: the oxidative branch, and the non-oxidative branch. The oxidative one yields NADPH and ribulose-5P which is then converted into ribose-5P (**Figure 8**). The nonoxidative branch consists of a series of reactions that recruit additional glycolytic intermediates, such as fructose-6P and glyceraldehyde-3P (**Figure 8**) (Patra & Hay, 2014).

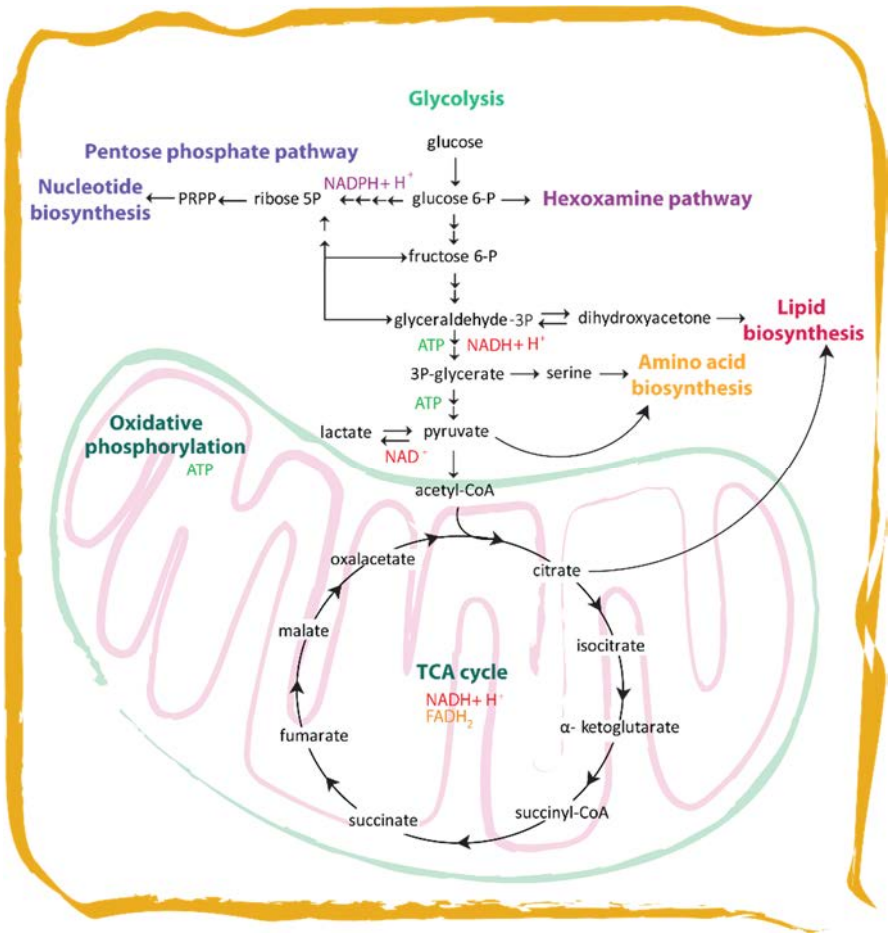

Figure 8. Glucose metabolism: an overview. Glucose is converted into pyruvate through glycolysis, generating ATP and NADH. Then, pyruvate can be converted either into lactate, regenerating NAD^+ (anaerobic glycolysis) or into acetyl-CoA, which enters in the TCA cycle in the form of citrate. Citrate is consumed and then regenerated by a sequence of reactions to complete the cycle, producing NADH and $FADH_2$, which are fed into the oxidative phosphorylation (electron transport) pathway to generate ATP. Alternatively, citrate can be exported back to the cytosol to be used for lipid synthesis. Glucose can be also used as a source of carbon to produce ribose-5P through the pentose phosphate pathway to make RNA and DNA, also yielding NADPH. In addition, glucose fuels the hexoxamine pathway, whose end-product is uridine diphosphate N-acetylglucosamine (UDP-GlcNAc), used for making glycosaminoglycans, proteoglycans, and glycolipids. The serine biosynthesis pathway, as long as other intermediates of glycolysis and the TCA cycle, generate AAs. PRPP, Phosphoribosyl pyrophosphate.

To maintain homeostasis, proliferating cells need to replenish nucleotides at the same rate as cell division. Thus, the progression of the cell cycle must be tightly

connected to the ability of the cell to acquire nutrients, generate metabolic energy and synthesize nucleotides. Moreover, dividing cells double their biomass as they complete a cell cycle, and thereby they have to increase protein biosynthetic rate. In this sense, to make protein faster, cells make more ribosomes, which in turn, requires more rRNA and therefore an increase in the rate of production of ribonucleotides (Lane & Fan, 2015).

Although there are salvage pathways through which the cells uses free bases, and cells can also take up nucleosides from the extracellular media (Young et al. 2013), most proliferating cells synthesize nucleotides *de novo* (**Figure 9**).

De novo synthesis of purine and pyrimidine nucleotides relies on metabolic pathways that provide carbon and nitrogen precursors, including the AAs aspartate, glutamine, serine and glycine, as well as glucose and CO_2. These major feeder pathways are glycolysis, the PPP, the serine-glycine pathway, the TCA cycle, and glutamine amidotransferase reactions (Lane & Fan, 2015).

The ribose-5P yielded by the PPP, functions as the scaffold for the purine ring biosynthesis, and also conforms the five-carbon sugar molecule of both purine and pyrimidine ribonucleotides (Berg et al. 2002). The five carbon atoms of the purine ring derive from CO_2, glycine and N^{10}-formyl-TetraHydroFolate (THF), is built directly on the activated Phosphoribosyl pyrophosphate (PRPP) generated from ribose-5P (**Figure 9**). On the contrary, the pyrimidine rings are synthesized first as uracil from aspartate, CO_2 (or bicarbonate) and glutamine and then attached to the ribose (**Figure 9**).

DNA synthesis requires a source of the four dNTPs, which derives from the ribonucleotides at the level of ribonucleotide diphosphates (rNDPs) by reduction at the 2′ position of the ribose subunit. This reaction is carried out by the ribonucleotide reductase (RNR), the only enzyme able to catalyse this rate-limiting step (Guarino, Salguero, and Kearsey 2014).

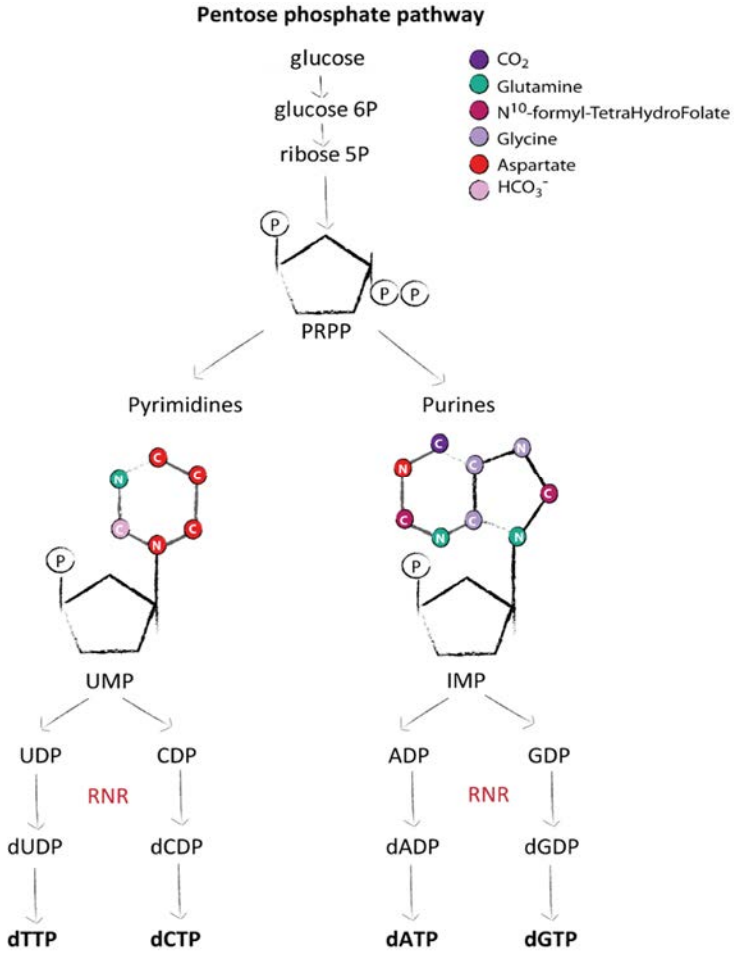

Figure 9. Deoxynucleotides biosynthesis. The pentose phosphate pathway generates phosphoribosyl pyrophosphate (PRPP), required for both purine and pyrimidine synthesis. The synthesis of any **pyrimidine** nucleotide begins with the formation of uridine monophosphate (UMP) in a reaction that requires aspartate, glutamine, bicarbonate and ATP. Then, the sugar-phosphate group from PRPP is added to the nitrogenous base. In **purine** synthesis, PRPP is turned into inosine monophosphate (IMP) by using glutamine, glycine, aspartate and ATP. IMP and UDP can be converted into different nucleotides by means of different reactions summarized in the diagram. DNA synthesis requires deoxynucleotides-triphosphate (dNTPs); nucleoside-diphosphates (NDPs) are converted into deoxynucleoside-diphosphates (dNDPs) by the ribonucleotide reductase (RNR). UDP, uridine diphosphate; CDP, cytidine diphosphate; ADP, adenosine diphosphate; GDP, guanosine diphosphate; dUDP, deoxyuridine diphosphate; dCDP, deoxycytidine diphosphate; dADP, deoxyadenosine diphosphate; dGDP, deoxyguanosine diphosphate; dTTP, deoxythymidine triphosphate; dCTP, deoxycytidine triphosphate; dATP, deoxyadenosine triphosphate; dGTP, deoxyguanosine triphosphate.

Since CD98hc likely regulates glucose metabolism, we envisioned that it may be also involved in nucleotide metabolism regulation. In addition, BCAAs, which are transported by CD98hc-LAT1 have been shown to constitute a potential alternative source of nitrogen for the synthesis of nucleotides in specific conditions (Mayers et al. 2016). Furthermore, BCAAs are able to control glucose metabolism by regulating pyruvate dehydrogenase (PDH) activity (Li et al. 2017), and like AAAs, can be shunted via anaplerosis to replenish the TCA cycle (Lerin et al. 2016; Stančíková and Rovenský 2015). However, little attention has been devoted to the involvement of BCAA and AAA availability in nucleotide metabolism.

2.4.2 The metabolic super-complex CD98hc-LAT1-MCT-CD147

CD147 (also named basigin, EMMPRIN, TCSF and HT7) is a multifunctional transmembrane glycoprotein expressed in a variety of human tissues and cells belonging to the immunoglobulin super family (Xin et al. 2016). Remarkably, it is overexpressed in a broad range of human malignant tumours (Muramatsu 2016), in which acts through multiple molecular mechanisms enhancing the tumour progression.

On one hand, CD147 stimulates the production of matrix metalloproteinases (MMPs) by adjacent stromal cells (Huang et al. 2015). For a tumour cell to metastasize from the primary tumour to other organs, it is necessary to breakdown the ECM components that are the physical barriers for the migration of the cells. In this regard, CD147, through the MMPs, plays a central role in tissue remodelling, promoting invasion and metastasis of cancer cells (Huang et al. 2015). On the other hand, it drives tumour angiogenesis by enhancing vascular endothelia growth factor (VEGF) levels in cancer cells (Pinheiro et al. 2015). Furthermore, CD147 is the ancillary protein of monocarboxylate transporters-1 (MCT-1) and MCT-4, ensuring their correct expression in the plasma membrane and regulating their activity as transporters of the lactic acid produced by anaerobic glycolysis (Kirk et al. 2000).

Interestingly, by using crosslinking agents coupled to liquid chromatography and mass spectrometry techniques (LC-MS), Xu and Hemler found that CD98hc formed part of the metabolic super-complex MCT-CD147-CD98hc-LAT1 (Xu and Hemler 2005). Results obtained in that study demonstrated that the expression of CD147 and CD98hc was correlated, in such a way that depletion of either them resulted in parallel reduction of both components, leading to defective cell proliferation (Xu and Hemler 2005).

Collectively, these findings suggest that CD98hc expression may regulate the expression of CD147, and by consequence MCT expression and activity, which is considered to be of vital importance for the metabolic plasticity in cancer (Ždralević et al. 2017).

The MCTs and the Warburg effect

The observation that tumour cells take up and catabolise glucose at a notably higher rate than their tissue of origin was firstly reported by Warburg in the middle 50's, which is known as the Warburg effect (Warburg 1956). This discovery led him to assume that cancer cells presented an impairment of the respiration through OXPHOS. After an intense debate in the subsequent years, it became clear that instead, high rates of glucose metabolism and glycolysis are maintained in tumours despite OXPHOS activity. On the contrary, most normal cells obey the Crabtree effect, a phenomenon firstly described in yeasts, which postulates that if a high rate of glycolysis is maintained, the need of oxidative phosphorylation done by the TCA cycle is reduced and therefore OXPHOS resulted repressed (Crabtree 1928). However, even though cancer cells are able to maintain the activation of both pathways, during tumour growth, the microenvironment becomes hypoxic, and under these conditions, rates of OXPHOS decreased while glycolysis is increased (Wheaton and Chandel 2011), thus, it is now well documented that that most rapidly developing tumours depend primarily on anaerobic glycolysis (Hay 2016).

Lactic acid is the end product of the Warburg effect and it is released abundantly by cancer cells through the MCTs, especially through MCT1, the most widely

expressed member of this family. Not surprisingly, MCT1 has been shown to be induced in a variety of cancers (Pérez-Escuredo et al. 2016). Lactate is necessary for all the major steps in cancer progression, not only stimulating angiogenesis, motility and migration, but also being directly involved in the "immune escape", as a consequence of the increased extracellular acidosis of tumour microenvironment (San-Millán and Brooks 2017). Furthermore, lactate is vital for the self-sufficiency of cancer cells by replenishing levels of nicotinamide adenine dinucleotide (NAD^+), thereby maintaining the equilibrium of the cytoplasmic redox pair ($NADH/NAD^+$) for continuation of glycolysis.

Considering this, the blockage of lactate export has emerged as a possible anti-cancer strategy since it would disrupt the Warburg effect in those cells. In this regard, several studies have shown that inhibition of either MCT1 or CD147 in cancer cells suppressed lactate export, glycolysis and tumour growth, paralleled with a reroute of the metabolism towards OXPHOS (Cormerais et al. 2016; Le Floch et al. 2011; Marchiq et al. 2015).

2.5 Cell cycle progression and replication stress

As it is reflected in previous sections, proliferation imposes biosynthetic requirements to support cell growth and division. In this respect, progression of the cell cycle is a highly demanding process tightly dependent on the ability of the cell to acquire nutrients, on the cellular redox status, and also on the production of energy to drive the constant *de novo* biosynthesis of nucleotides (Cooper, 2000). As previously described in the introduction of this thesis, CD98hc is able to regulate all the three key processes, suggesting a possible novel role of the multifunctional protein in cell cycle progression.

2.5.1 A quick overview

As illustrated in **Figure 10**, the cell cycle has two major phases: interphase and the mitotic (M) phase. Interphase comprises Gap (G1)-, DNA synthesis (S)-, and Gap2

(G2)- phases, during which cells undergo normal growth processes while also preparing for cell division. In somatic cells, chromosomes are replicated during the S-phase. After DNA replication, cells progress through the G2-phase, in which they are prepared for the subsequent mitosis, divided into several stages: prophase, prometaphase, metaphase, anaphase, and telophase.

The transition from one phase to another is tightly regulated by checkpoints, a mechanisms by which the cell actively halts progression through the cell cycle until conditions are favourable (Barnum and O'Connell 2014). Checkpoints are controlled by heterodimers composed by two key classes of regulatory molecules, cyclins and cyclin-dependent kinases (CDKs). The heteromeric complexes are activated at specific points of the cell cycle and in turn, activate or inactivate target proteins to orchestrate the coordinated entry into the next phase of the cycle (**Figure 10**). In most eukaryotes, cell cycle-regulated transcription can be grouped into three main waves coinciding with the main checkpoints: the G1/S, the G2/M and the mitotic checkpoint (Cooper, 2000).

The primary G1/S cell cycle checkpoint controls the commitment of cells to complete the G1-phase to enter into the S-phase. Upon pro-mitotic extracellular signalling, G1-phase cyclin-CDK complexes CDK4/6-Cyclin D and CDK2-Cyclin E, work in concert to promote the expression of transcription factors, mostly from the E2F family, which, along with their dimerization partner proteins and the pocket proteins, including retinoblastoma protein (RB), retinoblastoma-like protein 1 (p107) and retinoblastoma-like protein 2 (p130), promote the expression of S-phase cyclins and enzymes required for DNA replication (**Figure 10**).

In parallel, these complexes also promote the degradation of molecules that function as S-phase inhibitors by targeting them for ubiquitination (Lim and Kaldis 2013). Then, active S-phase cyclins-CDKs phosphorylate proteins that make possible the replication of the DNA.

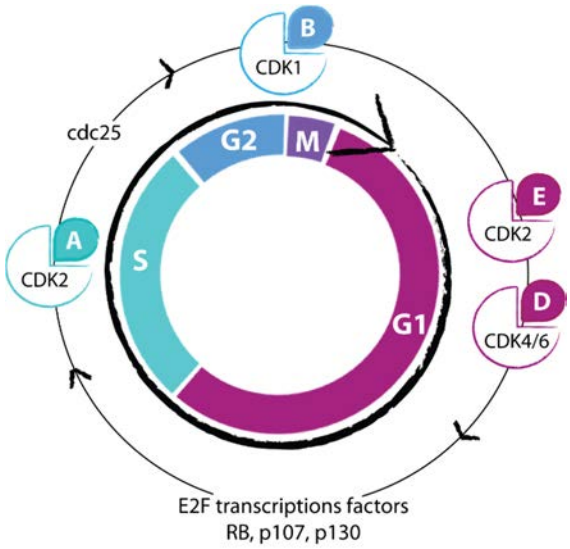

Figure 10. Cell cycle progression diagram. Cell cycle includes accurate duplication of the genome during the S-phase (S) and segregation of complete sets of chromosomes to each of the daughter cells in M-phase (M). It also contains G1-phase (G1), which connects the completion of M-phase to initiation of S-phase in the next cycle, and G2-phase (G2), which separates the S- and M- phases. The progression is driven by activation and inactivation of cyclin-dependent kinases (CDKs), which trigger the transition to subsequent phases of the cycle. Only the main players are depicted in the diagram. The CDKs and their corresponding cyclins are coloured according to the phase in which they exert their main function.

The G2/M DNA damage checkpoint prevents cells from entering mitosis if genomic DNA is damaged. Specifically, the activity of the CDK1-Cyclin B complex is pivotal in regulating the G2-phase transition, wherein CDK1 is maintained in an inactive state until cells approach the M-phase, then, the phosphatase cdc25 is activated and in turn induces CDK1 activity, which drives the cell into mitosis. Importantly, DNA damage leads to the activation of the DNA damage response pathway (DDR), which rely on two parallel cascades that ultimately serve to inactivate the CDK1-Cyclin B complex (Lim and Kaldis 2013) (**section 2.5.2**).

Mitotic cyclin-CDK complexes, which are synthesized but inactivated during S- and G2- phases, promote the initiation of mitosis by stimulating downstream proteins involved in chromosome condensation and mitotic spindle assembly. The segregation of sister chromatids at anaphase is under the mechanical control of the

mitotic spindle, comprised of microtubules and several motor proteins at both ends of the centrosome and kinetochores. Once all kinetochores are attached and aligned at the metaphase plate, anaphase is promoted by the activity of a large E3 ubiquitin ligase known as the anaphase-promoting complex (APC). The spindle checkpoint functions to prevent activation of APC whenever the chromosomes are not properly attached to the spindle in order to avoid aberrant segregation. It includes a large number of proteins, but most essential are the mitotic cyclins, Polo-like kinases (Plks), Aurora kinases and NIMA-related (Nek) kinases (Salaun, Rannou, and Prigent 2008).

2.5.2 Replication stress and the DNA damage response

Every time a cell divides, billions of nucleotides must be accurately copied in coordination with the succession of the cell cycle. A number of conditions, such as, oxidative stress (Barzilai and Yamamoto 2004; Maser et al. 1997), limitation of essential replication factors, including nucleotides (Poli et al. 2012) and replication machinery (Aguilera and García-Muse 2013), overexpression or constitutive activation of oncogenes (Halazonetis, Gorgoulis, and Bartek 2008) and altered protein synthesis (Rosner et al. 2009), are known to interfere with DNA replication and hamper its progression. This phenomenon, termed replication stress (RS) is characterized by the activation of the DDR and the subsequent DNA synthesis slows down (Mazouzi, Velimezi, & Loizou, 2014).

The DDR is a sophisticated network, which attempts to preserve genome stability, triggers the activation of cell-cycle checkpoints and the appropriate DNA repair pathways, or, in certain contexts, the initiation of apoptotic programs. This pathway is executed through a series of steps arranged in a hierarchical manner. The DNA lesions are detected by *sensor* proteins that recognize either the lesions themselves or the chromatin alterations caused by the DNA damage. Then, *transducers* are brought into action to transfer the damage signal to downstream *effectors* (**Figure 11**) (Maréchal and Zou 2013).

.

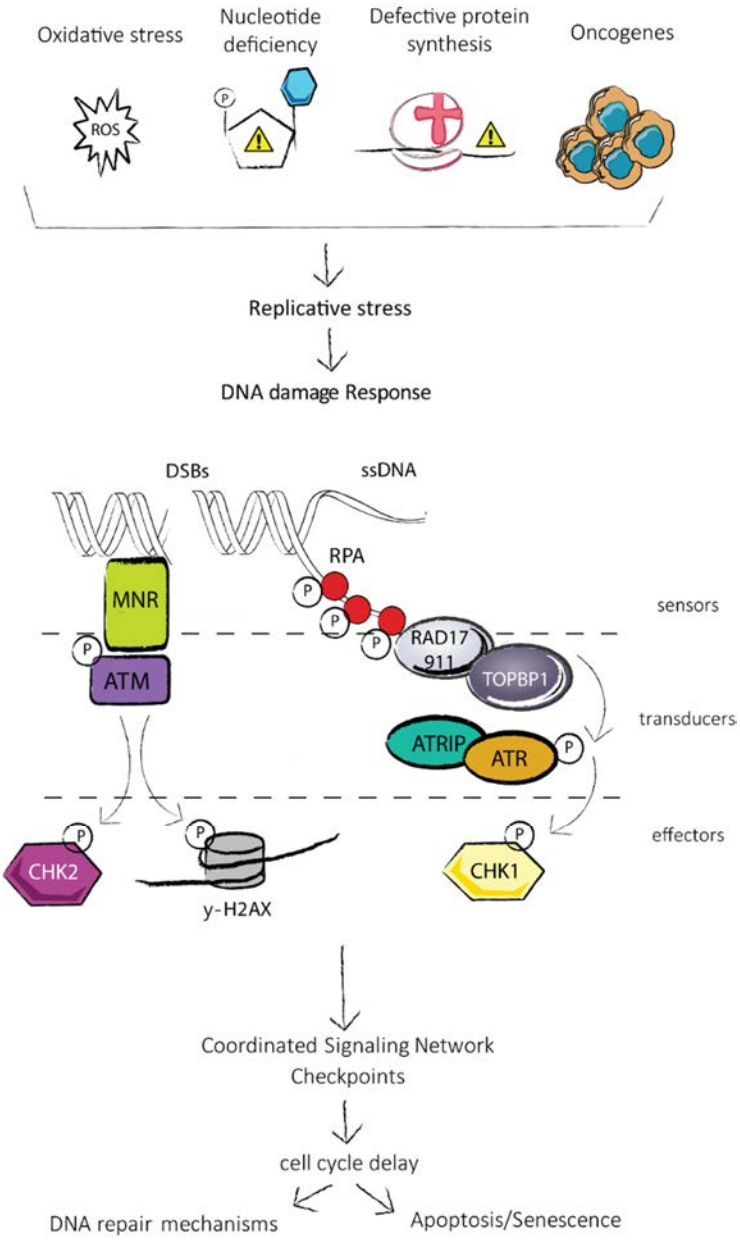

Figure 11. DNA damage response signalling pathway. DNA double strand breaks (DSBs) lead to activated ATM, which in turn phosphorylates and activates CHK2 and the histone variant H2AX. In addition, single strand DNA (ssDNA) activates the ATR pathway, which triggers the phosphorylation and activation of CHK1. Both checkpoints diffuse globally through the nucleus, where they inhibit new replication and, along with P-H2AX, activate the expression of different DNA repair proteins. As a consequence, cells undergo cell cycle delay that enables damage elimination. Sensors, transducers and effectors are indicated.

One of the central components of the DDR is the ataxia telangiectasia and rad3 related protein (ATR) (**Figure11**).DNA insults usually result in the development of stretches of single-stranded DNA (ssDNA) that are rapidly coated by the replication protein A (RPA). RPA acts as a signalling platform recruiting a wide variety of proteins, including ATRIP, which forms a complex with ATR, localizing the kinase at the DNA lesion (**Figure 11**). In addition, RPA recruits Rad17, which interacts with complex 911 (Rad9, Rad1, Hus1), responsible of the recruitment of TopBP1, the activator of ATR (**Figure 11**) Despite the many targets downstream of ATR, the key event that translates ATR activity into a checkpoint signal may mostly depend on one single substrate, which is the phosphorylation and subsequent activation of the checkpoint kinase 1 (CHK1) (**Figure 11**) (Mazouzi, Velimezi, & Loizou, 2014). CHK1 diffuses globally through the nucleus, where it inhibits new replication and activate a numerous other effectors for the damage repair achievement (Cabello et al. 2010). At the same time, ATR phosphorylates RPA, which is known to have different roles within the repair response (**Figure 11**) (Vassin et al. 2009).

Other key transducer is the serine threonine kinase ataxia telangiectasia mutated protein (ATM), which is mainly activated by DNA double strand breaks (DSBs). DSBs are recognized and directly bound by the complex MNR, required for the rapid localization and activation of ATM at the DNA breaks (**Figure 11**) (Manic et al. 2015). The spreading activity is primarily played by the checkpoint kinase 2 (CHK2), involved in different repair processes (Zannini, Delia, and Buscemi 2014). Furthermore, the phosphorylation of the histone variant H2AX by ATM is considered a key event in the DDR, acting as a platform for the recruitment of a variety of DNA repair proteins (**Figure 11**) (Zannini, Delia, and Buscemi 2014).

Although ATM and ATR have distinct DNA-damage specificities, they are known to crosstalk at multiple levels and interestingly, ATR is also activated by DSBs, presenting a broader spectrum of action (Maréchal and Zou 2013).

2.6 Dissection of integrin signalling- and AA transport function- associated to CD98hc in cell proliferation

Previous studies performed by Laura Rodriguez de la Ballina in our group assessed the role of CD98hc-associated AA transport function in cell proliferation and teratoma formation, both *in vitro* and *in vivo*.

2.6.1 CD98hc-associated AA transport function *in vivo*

As it is previously described in **section 2.3.2**, CD98hc-deficient ES cells failed to proliferate and form teratomas *in vivo* after injecting them in nude mice (Feral et al. 2005). In order to elucidate whether the tumorigenicity capacity of these cells depended on the integrin signalling- or the AA transport function- associated to CD98hc, different chimeric forms of CD98hc were generated (**Figure 12A**).

The capacity of forming teratomas was reconstituted by expressing a chimeric form of CD98hc (only containing cytoplasmic and transmembrane domains) which was able to interact with β1 integrins while the transport activity remain abolished (**Figure 12A**) (Feral et al. 2005). However, teratomas were significantly smaller than when CD98hc-deficient ES cells were reconstituted with wild-type (WT) CD98hc. This finding suggested that the partial teratoma growth could be ascribed to the lack of CD98hc-mediated AA transport function.

Rescue experiments using a chimeric form of CD98hc (containing ectodomain and transmembrane domains) capable of restoring AA transport (**Figure 12A**), showed that AA transport function was also able to promote cell proliferation *in vivo*, and indeed, maximal cell growth rates are only achieved when both CD98hc activities (AA transport and enhanced integrin signalling) function synergically (**Figure 12**) (de la Ballina et al., 2016).

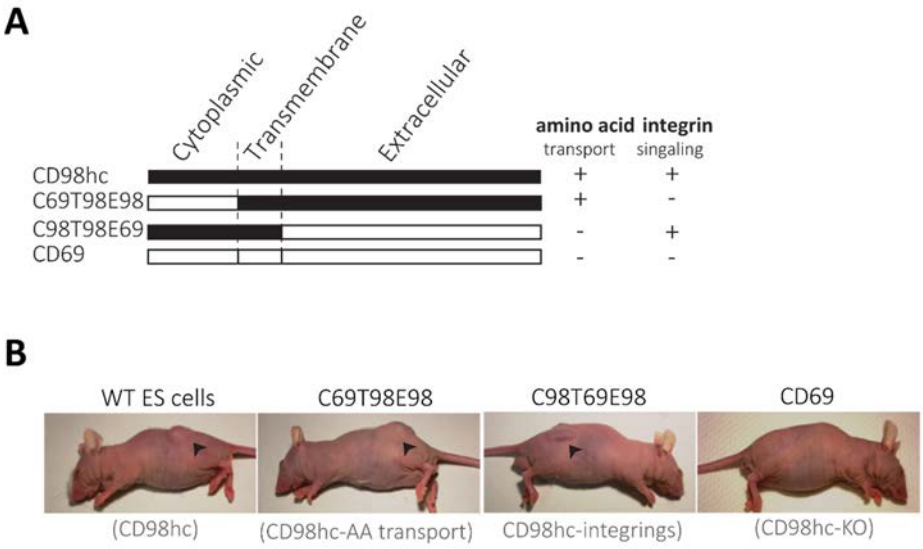

Figure 12. Both CD98hc-integrin signalling and -AA transport capacity promote cell proliferation *in vivo*. A, depiction of the chimeric proteins of CD98hc. B, mice were injected with corresponding ES cells and analysed after 26 days. Addapted from (de la Ballina et al., 2016).

2.6.2 CD98hc-associated AA transport function *in vitro*

In order to study CD98hc associated AA transport function *in vitro,* our group established a collaboration with Chloé C. Féral (Université de Nice-Sophia Antipolis, Nice, France) who had generated fibroblasts derived from CD98hc-/- ES cells, in which exon 1, encoding the transmembrane domain of CD98hc, was replaced by a neomycin cassette (Feral et al. 2005).

Laura Rodriguez de la Ballina characterised these cells and found that WT fibroblasts expressed CD98hc, but not rBAT heavy subunits. Concerning CD98hc-associated light subunits, such cells expressed LAT1, xCT and y^+LAT2. In contrast, CD98hc knock-out (KO) fibroblasts actually lacked CD98hc and the associated lights chains in the plasma membrane (de la Ballina 2011). To check the functional impact of these changes, transport activities were analysed in CD98hc KO and WT cells. As expected, transport activities corresponding to LAT1, xCT and y^+LAT2

were completely abolished in CD98hc KO cells (de la Ballina, 2011; de la Ballina et al., 2016). Next, *in vitro* cell proliferation was assessed, and strikingly, CD98hc KO cells did not survive under standard culture conditions unless medium was supplemented with β-mercaptoethanol (β-ME) (**Figure 13**).

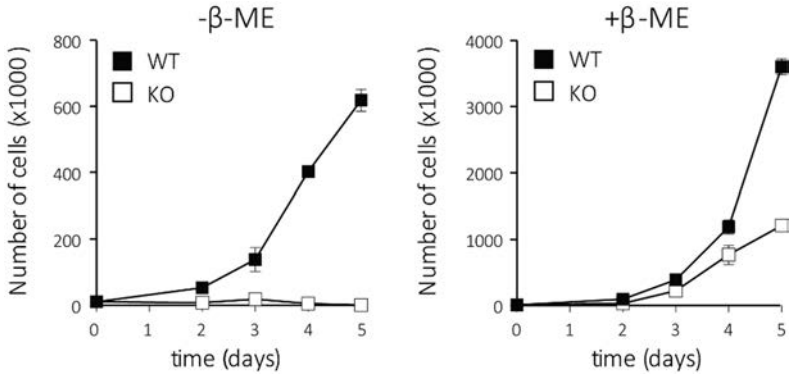

Figure 13. β-Mercaptoethanol inhibits cell death and restores CD98hc KO cell survival. WT and CD98hc KO cell proliferation is compared in the absence (left panel) and presence (right panel) of β-ME for 5 days (de la Ballina et al., 2016).

This phenomenon is attributed to the loss of xCT, since this transporter sustains cellular redox homeostasis by taking up cystine, which is necessary for GSH biosynthesis (**section 2.2.2**) (Forman, Zhang, and Rinna 2009; Okuno et al. 2003; Sato et al. 2005). β-ME supplementation allowed reduction of extracellular cystine into free cysteine, which can be subsequently imported by CD98hc-independent transporters.

Next, to specifically study the effect of CD98hc-mediated AA transport on intrinsic cell proliferation capacity, *in vitro* cell proliferation rate was compared in CD98hc KO cells when rescued with the different described chimeras of CD98hc (**Figure 12A**). CD98hc KO cells presented a major delay in proliferation *in vitro* compared to WT cells (**Figure 14A**) This deficiency was rescued by reconstitution with full-length CD98hc or with AA transport chimeras (i.e., chimeras that include the ectodomain of CD98hc, which stabilizes the light subunits (Rosell et al. 2014)).

However, when only the capacity of integrin signalling was reconstituted in CD98hc KO cells, *in vitro* cell proliferation was still impaired (**Figure 14B**).

Thus, these results indicate that CD98hc AA transport capacity is enough to drive proliferation *in vitro*, whereas integrin signalling is dispensable in these conditions. This finding highlights the essentiality of CD98hc-dependent AA transport for cell proliferation regardless of the surrounding environment.

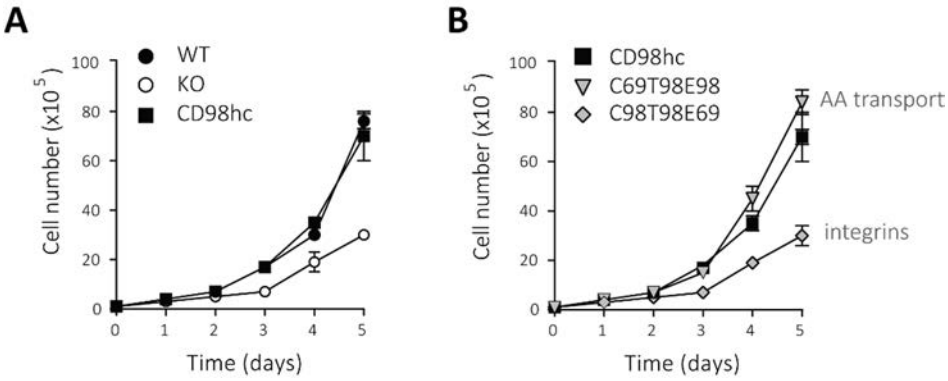

Figure 14. CD98hc AA transport function is sufficient for efficient cell proliferation *in vitro*. **A**, WT or CD98hc KO cells recovered with full-length CD98hc (labelled as CD98hc) or **B**, CD98hc KO cells recovered with chimeras restoring AA transport (C69T98E98) or integrin signalling (C98T98E69) functions were seeded on day 0 and grown for 5 days. Cells were counted every day. Results are expressed as the mean ± SEM of duplicates (de la Ballina et al., 2016).

Objectives

CD98hc is a multifunctional protein involved in a broad number of functions, including proliferation, spreading, migration and survival. It is the ancillary protein for six different HAT transporters (LAT1, LAT2, xCT, y^+LAT1, y^+LAT2 and asc1), among which CD98hc-LAT1 and CD98hc-xCT are overexpressed in cancer and associated with an aggressive tumour phenotype and poor prognosis.

Previous data gathered by Laura Rodriguez de la Ballina in the group determined that CD98hc -AA transport function and -integrin signalling are required for cell survival and proper cell proliferation *in vivo*. However, the integrin function associated to CD98hc is dispensable *in vitro,* which provide an advantage when studying the cellular functions that rely on CD98hc independently of integrin signalling in these conditions.

Although the role of LAT1 and xCT has been evaluated to address specific questions, the impact of eliminate CD98h, and therefore all the related transporters, is poorly studied.

Moreover, data provided by the studies described above, along with the results obtained throughout this thesis, suggest a potential role of CD98hc in energy metabolism and cell cycle progression, which has not been studied yet.

Collectively, this background motivated the present study with the following specific aims:

I. To investigate the role of CD98hc AA transport function in cell proliferation and redox homeostasis and to evaluate the possible stress signalling pathways involved.

II. To study the involvement of CD98hc in nucleotide biosynthesis and cell cycle progression.

III. To explore which is the impact of CD98hc in the energy metabolism of the cell.

Results

4.1 CD98hc is at the crossroad of oxidative stress and AA availability.

As reported in **section 2.6,** previous results determined that CD98hc AA transport function is required for cell survival and proper cell proliferation both *in vitro* and *in vivo* (de la Ballina et al., 2016). Reconstitution of CD98hc AA transport capacity in mouse CD98hc KO fibroblasts was enough to recover cell proliferation *in vitro*, in contrast to the restoration of CD98hc-mediated integrin signalling (de la Ballina et al., 2016). Thus, we aimed at further studying the cellular functions that rely on CD98hc independently of integrin signalling *in vitro* using WT and CD98hc KO mouse fibroblasts derived from ES cells as a cellular model.

These WT fibroblasts expressed the CD98hc-associated transporters xCT, LAT1 and y^+LAT2, as revealed by their mRNA expression and transport activities (de la Ballina 2011). Remarkably, expression of transporters associated with CD98hc was analysed in several human cell lines at mRNA levels and xCT, LAT1 and y^+LAT2 were expressed in all of them (**Figure 15**). Thus, the ES-derived fibroblasts provide a suitable *in vitro* model to establish the role of CD98hc.

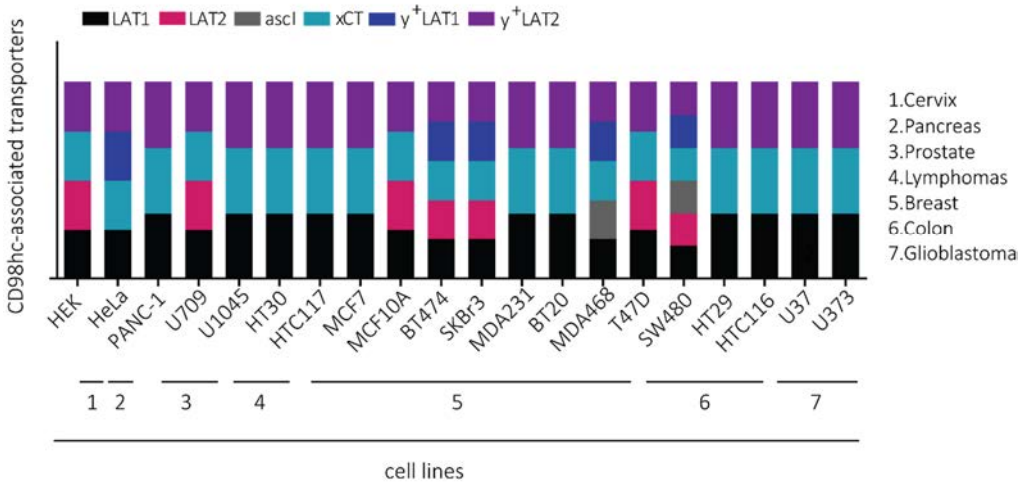

Figure 15. Expression of CD98hc-asscociated transporters in different human cell lines. mRNA expression of the light chains associated with CD98hc is depicted for the selected cell lines. Tissue of origin of the tumour-derived cell lines is indicated.

4.1.1 CD98hc protects cells against oxidative stress leading to cell survival

CD98hc KO fibroblasts failed to survive in standard culture conditions unless medium was supplemented with β-ME (**Introduction, Figure 13**) (de la Ballina et al., 2016). This phenomenon is attributed to the loss of xCT, since this transporter provides cellular redox homeostasis by taking up cystine, which is necessary for GSH biosynthesis (Forman, Zhang, and Rinna 2009; Okuno et al. 2003; Hideyo Sato, Shiiya, et al. 2005).

In this regard, it was previously described that invalidation of xCT activity results in an iron-dependent oxidative (non-apoptotic) cell death called ferroptosis (**Figure 16A**) (Bassi et al. 2012, 2014). In order to determine whether ferroptosis underlay the death of CD98hc KO cells, mRNA levels of ChaC glutathione-specific gamma-glutamylcyclotransferase 1 (CHAC1), which serves as a ferroptosis marker (Bassi et al. 2014), were determined. CD98hc KO cells showed a marked increase in CHAC1 mRNA levels compared to WT cells. In addition, WT cells treated the xCT inhibitor SAS (Gout et al. 2001) presented a similar increase in CHAC1 mRNA levels compared to non-treated cells to that observed in CD98hc KO cells (**Figure 16B**). β-ME supplementation allowed reduction of extracellular cystine into free cysteine, which could be subsequently transported by other non-CD98hc-associated transporters (**Figure 16A**) (Conrad & Sato, 2012). Consequently, β-ME supplementation protected cells from ferroptosis, as evidenced by restoration of CHAC1 mRNA levels in both CD98hc KO cells and WT cells treated with SAS (**Figure 16B**). Thus, culture media was supplemented with β-ME henceforward in order to guarantee cell survival.

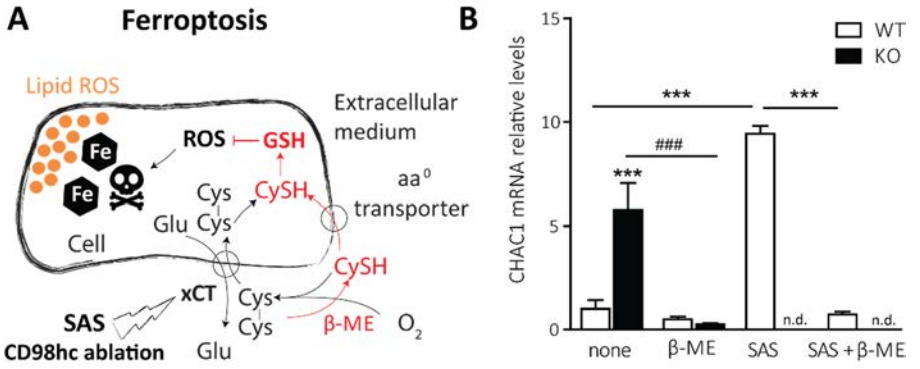

Figure 16. CD98hc protects cells from ferroptosis. **A**, ferroptosis cell death was depicted. Cystine (Cys-Cys) is transported by xCT inside the cell where it is reduced to cysteine (CysSH, essential for reduced GSH formation). GSH counterbalances ROS levels and therefore inhibits cell death by ferroptosis. Inhibition of xCT by SAS or CD98hc-xCT ablation lead to ferroptosis. By supplementing the culture medium with β-ME, free CysSH is able to be imported inside the cell by CD98hc-independent AA^0 transporters avoiding this kind of cell death. **B**, CHAC1 mRNA expression levels in WT and CD98hc KO cells grown with no additives (none), in the presence of 100 μM β-ME, 1 mM SAS, or the combination of both (β-ME + SAS). n.d., not determined. Quantification data correspond to the mean ± SEM of eight independent experiments. Statistical significance ***, $p \leq 0.001$ vs. WT cells, or ###, $p \leq 0.001$ vs. KO cells, was analysed using a Student's t-test.

However, even when supplemented with β-ME, CD98hc-KO cells presented increased redox-sensitive H_2DCFDA labelling compared to WT cells (**Figure 17A**). In addition, protein levels of NRF2, considered as a master regulator of the intracellular antioxidant response (Q. Ma 2013), were increased in cells lacking CD98hc when compared to WT cells (**Figure 17B**). In contrast, inhibition of xCT by SAS in WT cells did not increase NRF2 expression (**Figure 17B**). These findings suggest that CD98hc is required for *in vitro* cell survival due to its key role in cystine uptake via CD98hc-xCT, thereby protecting cells from ferroptosis. Moreover, CD98hc ablation induces oxidative stress independently of xCT activity and it is non-reverted by β-ME supplementation.

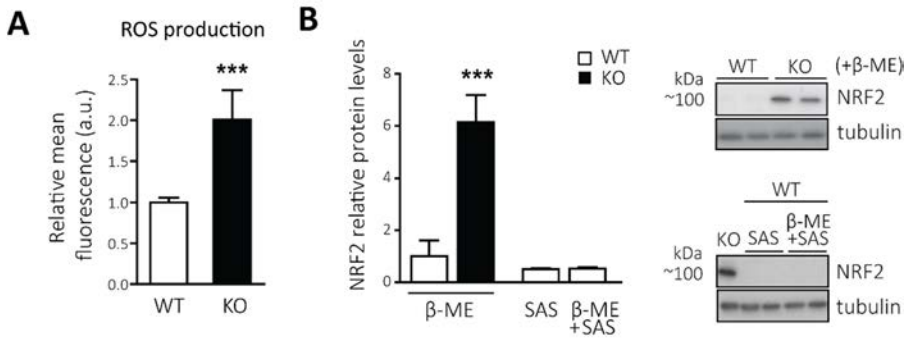

Figure 17. CD98hc ablation leads to increased oxidative stress. **A**, quantification of ROS levels using the free radical sensor H_2DCFDA (DCF) measured by flow cytometry. Bars represent the mean DCF fluorescence in WT and CD98hc KO cells. a.u., arbitrary units. n=6. **B**, comparison of NRF2 protein expression between WT and CD98hc KO cells grown in the presence of 100 μM β-ME, 1 mM SAS, or the combination of both (β-ME + SAS). n=6. Data are normalized by tubulin expression. Quantification data correspond to the mean ± SEM of the independent experiments (n) indicated for each graph normalized to WT cells. Statistical significance ***, $p \leq 0.001$ vs. WT cells was analysed using a Student's t-test.

4.1.2 CD98hc supports the balance of intracellular AA content

WT fibroblasts, as mentioned above (**section 2.6**), presented transport activities corresponding to system xc^-, system L, and system y^+L (de la Ballina et al., 2016). CD98hc is the ancillary protein that drives the trafficking of associated light chains to the plasma membrane (Verrey et al. 2004). Thus, CD98hc-KO cells should lack all CD98hc-associated transport subunits in the plasma membrane. Consistently, xc^-, L, and y^+L transport activities were absent in CD98hc KO cells (de la Ballina et al., 2016). In this regard, we hypothesized that deficiency of those transport activities might impact on the intracellular AA content of CD98hc KO cells. As shown in **Figure 18A**, cells lacking CD98hc presented an imbalanced AA content compared to WT cells. The cell content of both AA^+ (arginine, lysine, and histidine) and AA^0 (alanine, serine, asparagine, glutamine, and methionine) was increased in CD98hc-deficient compared to WT fibroblasts. In contrast, BCAA (valine, leucine, and isoleucine) and AAA (phenylalanine and tyrosine) showed a decreased intracellular content in CD98hc KO cells (**Figure 18A**).

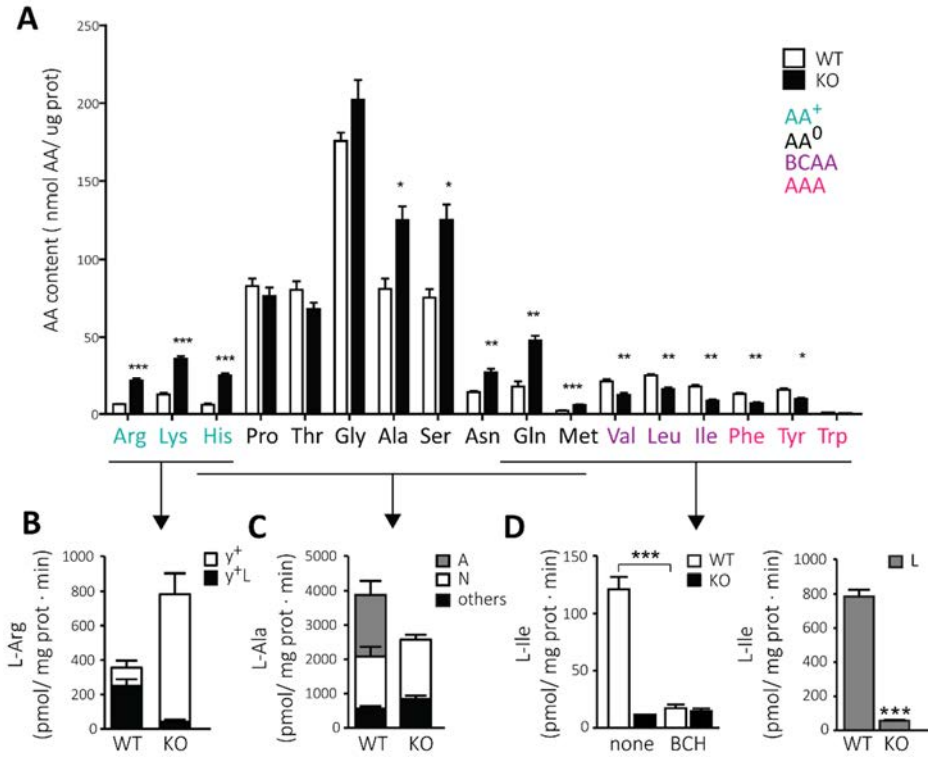

Figure 18. CD98hc depletion leads to imbalanced intracellular AA content and to adaptations of CD98hc-independent transporters. **A**, samples from WT and CD98hc KO cells were processed as described in *Materials and Methods* and quantitative analysis of AAs (nmol AA/μg protein) was performed. AAs are grouped by side chain properties as indicated. n=5. **B**, Na^+-dependent L-Arg (10 μM) uptake at 2 min (linear conditions of uptake) inhibitable by NEM (1mM) alone (system y^+) or in combination with L-Leu (1 mM) (system y^+L) was measured in WT and CD98hc KO cells. n=12. **C**, Na^+-dependent L-Ala (100 μM) uptake at 2 min (linear conditions of uptake) inhibitable by N-(methylamino)-isobutyric acid (10 mM) alone (system A), or in combination with L-Asn (10 mM) (system N), was measured in WT and CD98hc KO cells. Residual transport is depicted as *others*. n=8. **D**, Na^+-independent L-Ile (10 μM) uptake at 2 min (linear conditions of uptake) in the absence (none) and presence of BCH (1 mM) (left panel; n=8) and L-Ile (10 μM) uptake levels at 2 min in the presence of Na^+ (right panel; n=12) was measured in WT and CD98hc KO cells. Quantification data correspond to the mean ± SEM of the independent experiments (n) indicated for each graph. Statistical significance *, $p \leq 0.05$; **, $p \leq 0.01$; ***, $p \leq 0.001$ vs. WT was analysed using a Student's t-test. The abbreviated AAs correspond from left to right: arginine, lysine, histidine, proline, threonine, glycine, alanine, serine, asparagine, glutamine, methionine, valine, leucine, isoleucine, phenylalanine, tyrosine and tryptophan. *Transport activity analysis (B to D) was performed by Laura Rodriguez de la Ballina.*

Analysis of the transport activities revealed that in the absence of CD98hc, the activity of CD98hc-independent transporters was modulated (**Figure 18**) (de la Ballina et al., 2016). In agreement with the increased intracellular AA^+ content, L-

arginine uptake was much higher in CD98hc-deficient than in WT cells (**Figure 18B**) (de la Ballina et al., 2016). This transport activity was identified as exclusively system y^+, as N-ethylmaleimide (NEM) specifically inactivates system y^+ without affecting system y^+L (data not shown) (Deves, Angelo, and Chavez 1993). Next, we tested whether the expression levels of cationic amino acid transporters (CATs; system y^+) could account for such dramatically increased transport activity. In this regard, we detected a notably increase in CAT3 (**Figure 19A**) but not CAT1 and CAT2 (data not shown) mRNA levels in CD98hc KO compared to WT fibroblasts. Accordingly, CAT3 activity, inhibitable by CAT3-specific inhibitor D-arginine (data not shown) (Nicholson et al. 1998) was increased in CD98hc KO compared to WT cells (**Figure 19B**). These data indicate that CAT3 upregulation could account for increased content of AAs^+ in CD98hc KO cells.

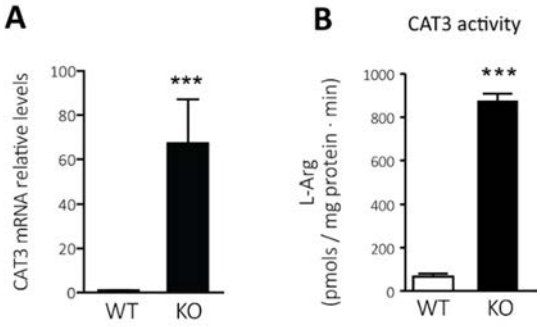

Figure 19. CD98hc ablation triggers the upregulation of the expression and activity of CAT3. **A**, comparison of CAT3 mRNA expression levels between WT and CD98hc KO cells. n=3. **B**, CAT3 transport activity measured as Na^+-independent uptake of L-arginine (Arg) (10 μM) at 2 min (linear conditions of uptake) inhibitable by D-Arg (5 mM) in the presence of L-Leu (1 mM) was measured in WT and CD98hc KO cells. n=3. Quantification data correspond to the mean ± SEM of the independent experiments (n) indicated for each graph normalized to WT cells. Statistical significance ***, $p \leq 0.001$ vs. WT cells was analysed using a Student's t-test. *CAT3 transport activity analysis (B) was performed by Laura Rodriguez de la Ballina.*

Regarding the transport of AA^0s, L-alanine uptake was analysed in WT and CD98hc KO cells. In WT cells it was identify the presence of system N (AA^0 Na^+-

dependent transporter) (Bröer 2014), system A (co-transporter of Na^+ and AA^0 mainly excluding BCAAs and AAAs (Bröer 2014)), and others (not ascribed to any specific transporter). Ablation of CD98hc resulted in the disappearance of system A transport activity whereas no differences were detected in system N. Considering that despite the depletion of system A, the intracellular content of AA^0s was increased in CD98hc KO cells (**Figure 18C**), AA^0s would be accumulated by unidentified causes (e.g., metabolism).

L-isoleucine uptake was measured in WT and CD98hc KO cells so as to study the BCAA transport, and it was found that depletion of CD98hc resulted in the abrogation of system L transport activity (responsible of the transport of BCAAs and AAAs; Na^+-independent and inhibitable by the leucine analogue BCH (**Figure 18D, left panel**) (Im et al. 2008). System L consists of four isoforms, LAT1 and LAT2, associated with CD98hc, and two independent of CD98hc, LAT3 and LAT4 (Bodoy et al. 2013; Fotiadis, Kanai, and Palacín 2013). These results suggested that no CD98hc-independent isoform of system L was compensated for LAT1 ablation in cells lacking CD98hc. Moreover, CD98hc KO cells presented only 10% of WT L-isoleucine uptake in the presence of sodium in the cell medium, suggesting that sodium-dependent leucine transporters did not compensate the lack of CD98hc-associated transporters (**Figure 18D, right panel**) (de la Ballina et al., 2016).

In all, the results of this section suggest that, at least in part, modulation of expression of other transporters non-related with CD98hc likely accounts for imbalanced intracellular AA content in CD98hc KO cells.

4.1.3. CD98hc-deficient cell proliferation is restored after BCAA and AAA supplementation

Considering the reduced intracellular content of the LAT1 substrates (valine, leucine, isoleucine, phenylalanine, and tyrosine) in CD98hc KO cells, we hypothesized that BCAA and AAA shortage could underlie the proliferation defect observed in these cells. In this regard, we found that the peptide transporter 1

(PEPT1) was overexpressed at mRNA (**Figure 20A**) and protein levels (**Figure 20B**) in CD98hc KO cells when compared to WT cells.

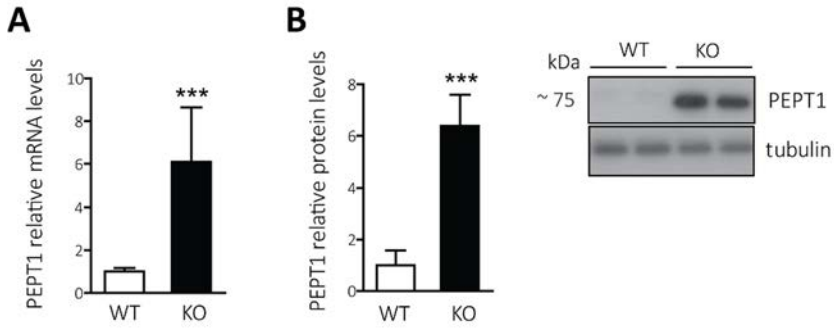

Figure 20. PEPT1 expression is upregulated in CD98hc KO cells. A, comparison of PEPT1 mRNA expression levels between WT and CD98hc KO cells. n=3. **B**, comparison of PEPT1 protein expression between WT and CD98hc KO cells. Data are normalized by tubulin expression. n=3. Quantification data correspond to the mean ± SEM of the independent experiments (n) indicated for each graph normalized to WT cells. Statistical significance ***, $p \leq 0.001$ vs. WT cells was analysed using a Student's t-test.

PEPT1 is a proton-dependent transporter responsible for cellular uptake of di- and tripeptides (Daniel and Kottra 2004). PEPT1 upregulation in CD98hc KO cells is likely related to the oxidative stress occurring in these cells, since regulation of PEPT1 expression is controlled by the cellular defence program activated by NRF2 (Geillinger et al. 2014). Taking advantage of the overexpression of PEPT1, alanyl-dipeptides containing BCAAs and AAAs were synthesized as described in *Materials and Methods* to supplement culture media. Remarkably, the proliferation capacity of CD98hc-deficient fibroblasts was restored to WT levels after dipeptide-supplementation for 5 days (**Figure 21**, **left panel**), whereas control-supplementation (L-alanine) showed no effect (**Figure 21**, **right panel**). These results point out the strong requirement of these AAs for proper cell proliferation.

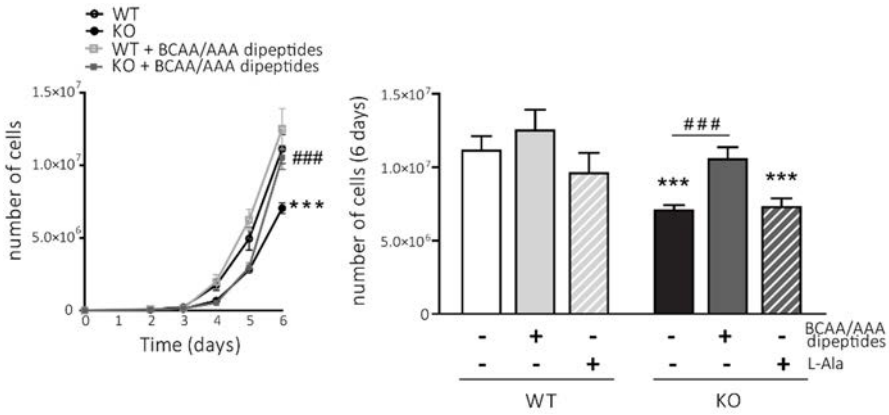

Figure 21. Supplementation with BCAA- and AAA-containing dipeptides restores proliferation of CD98hc KO cells. WT and CD98hc KO cells grown with no additives or in the presence of BCAA- and AAA- containing dipeptides was measured over 6 days. Cell counts at several time points are shown as the mean ± SEM of three independent experiments (left panel). Cell count at day 6 including KO + L-alanine (L-Ala) as control (right panel). Statistical significance ***, $p \leq 0.001$ vs. WT cells or ###, $p \leq 0.001$ vs. KO cells, was analysed using a Student's t-test.

Intriguingly, the rescue of cell proliferation was accomplished between days 5 and 6 after dipeptide addition (**Figure 21**). In order to further analyse this lapse, we performed a time-course analysis and found that upregulation of PEPT1 expression matched the recovery of cell proliferation, with the highest mRNA (**Figure 22A**) and protein (**Figure 22B**) expression being reached at days 5–6 after cell seeding.

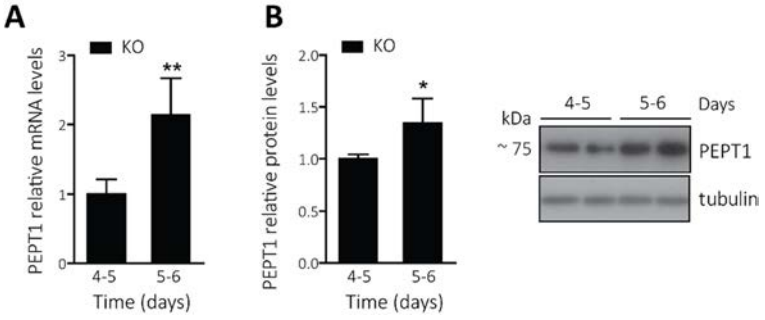

Figure 22. PEPT1 expression matched the recovery of cell proliferation in CD98hc KO cells. **A**, comparison of PEPT1 mRNA expression levels at indicated time points in CD98hc KO cells. n=3. **B**, comparison of PEPT1 protein expression at indicated time points in CD98hc KO cells. Data are normalized by tubulin expression. n=3. Quantification data correspond to the mean ± SEM of the independent experiments (n) indicated for each graph normalized to time point 4-5 days. Statistical significance *, $p \leq 0.05$; **, $p \leq 0.01$ vs. time point 4-5 days was analysed using a Student's t-test.

Accordingly, same upregulation pattern was observed regarding NRF2 protein levels (**Figure 23**). This outcome evidences a plausible explanation for the timing of the cell proliferation rescue in CD98hc KO cells.

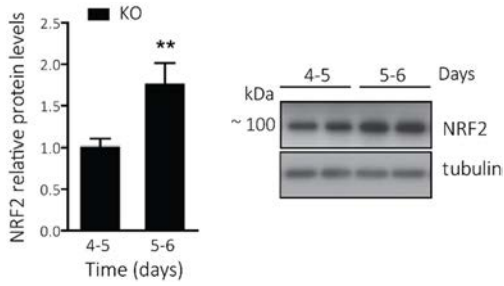

Figure 23. NRF2 expression matched the recovery of cell proliferation in CD98hc KO cells. Comparison of NRF2 protein expression at indicated time points in CD98hc KO cells. Data are normalized by tubulin expression. Quantification data correspond to the mean ± SEM of three independent experiments normalized to time point 4-5 days. Statistical significance **, $p \leq 0.01$ vs. time point 4-5 days was analysed using a Student's t-test.

Strikingly, the intracellular AA content of dipeptide-supplemented fibroblasts showed no recovery of either BCAA or AAA intracellular levels (**Figure 24**), pointing to the relevance of AA flux rather than AA content.

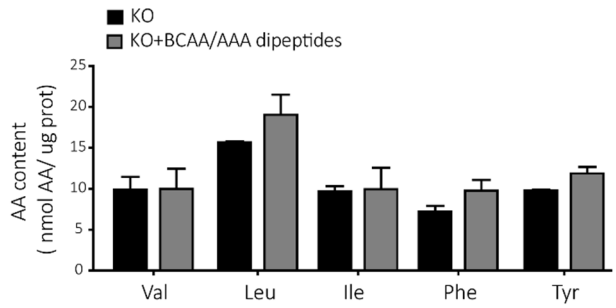

Figure 24. Supplementation with BCAA- and AAA-containing dipeptides does not recover the intracellular AA content. Samples from CD98hc KO cells alone or in the presence of dipeptides were processed as described in *Materials and Methods* and quantitative analysis of AAs (nmol AA/μg protein) was performed. Quantification data correspond to the mean ± SEM of three independent experiments. No statistical differences were found using a Student's t-test.

4.1.4 Low 6AA cells: A cellular model to study the effects of BCAA and AAA scarcity

In all, these results allowed us to establish that CD98hc, putatively due to the AA transport function of CD98hc, lies at the cross-road of oxidative and nutritional stress (de la Ballina et al., 2016). However, the relative contribution of each stressor to the phenotype of CD98hc KO cells was unknown. In an attempt to dissociate oxidative from nutritional stress, we generated a cellular model with only one of the stressors. To this end, we cultured WT cells in media with reduced concentrations of BCAAs and AAAs (**Figure 25**), under standard cell culture concentrations of cystine and β-ME.

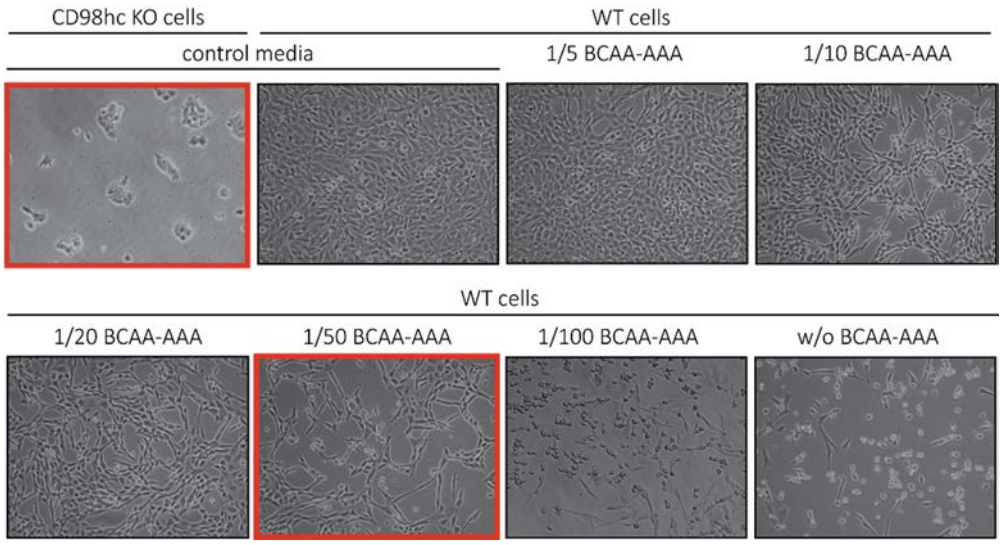

Figure 25. Low 6AA media optimization. WT cells were cultured for three days in different media with reduced BCAA-AAA concentrations. Ratios are referred to control media concentrations. A representative image of each condition is represented.

Cell culture medium was optimized to phenocopy the proliferation defect (**Figure 26A**) reported in the CD98hc KO model (**Introduction, Figure 13**) (de la Ballina et al., 2016). Thus, 1/50 of the BCAA and AAA concentration in regular DMEM media was selected and WT cells were cultured in media with these AA

concentrations, which are considered within the lower physiological levels in plasma (**Figure 26B**). Henceforward, these cells were referred to as low 6AA cells, and were compared to cells cultured in complete home-made DMEM media (control cells). Low 6AA and control cells were cultured in the presence β-ME to compare with CD98hc KO and WT cells.

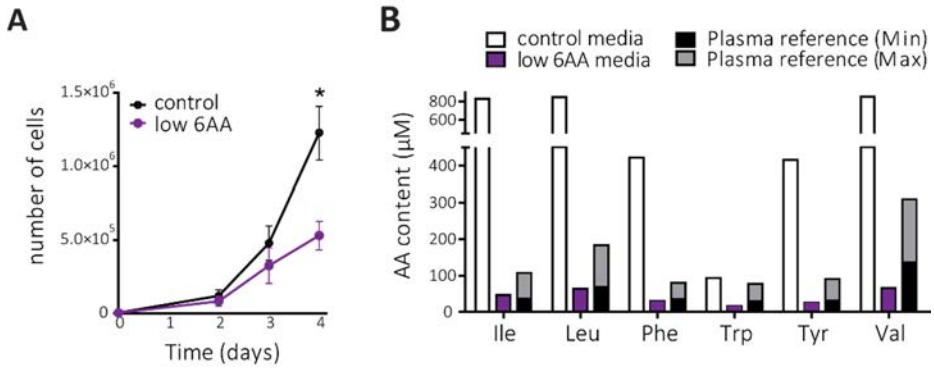

Figure 26. Low 6AA cells present compromised proliferation. A, proliferation of control and low 6AA cells was measured over 4 days. Quantification data correspond to the mean ± SEM of three independent experiments normalized to control cells. Statistical significance *, $p \leq 0.05$ vs. control cells was analysed using a Student's t-test. **B**, Final BCAA and AAA concentrations (μM) in control and low 6AA media are indicated and compared with minimum and maximum plasma physiological reference values.

Low 6AA cells showed a dramatic decrease in the content of BCAAs and AAAs in comparison to control cells (**Figure 27**). Strikingly, intracellular levels of AA^+ and neutral AA^0 were increased in low 6AA cells (**Figure 27**). This imbalance in the intracellular AA content (**Figure 27**) resembled the one observed in CD98hc-deficient cells (**Figure 18A**) (de la Ballina et al., 2016).

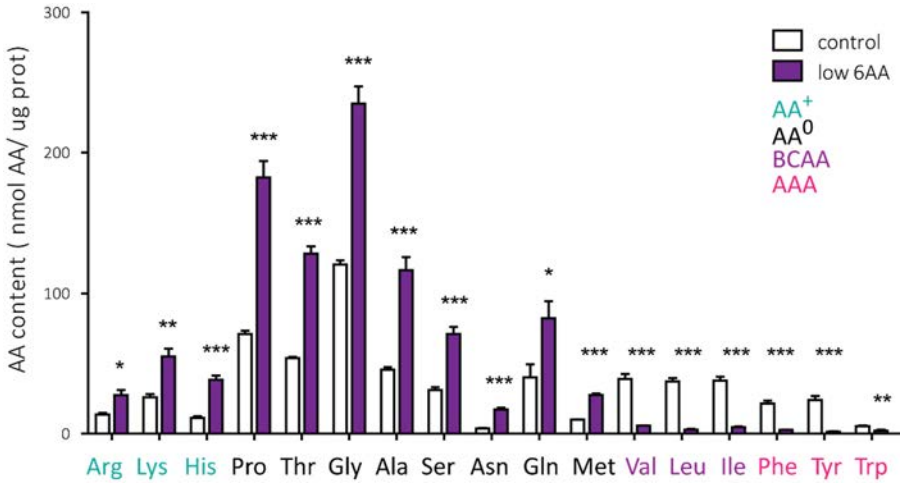

Figure 27. BCAA and AAA shortage leads to imbalanced intracellular AA content. Samples from control and low 6AA cells were processed as described in *Materials and Methods* and quantitative analysis of AAs (nmol AA/µg protein) was performed. AAs are grouped by side chain properties as indicated. Quantification data correspond to the mean ± SEM of five independent experiments. Statistical significance *, $p \leq 0.05$; **, $p \leq 0.01$; ***, $p \leq 0.001$ vs. control cells was analysed using a Student's t-test.

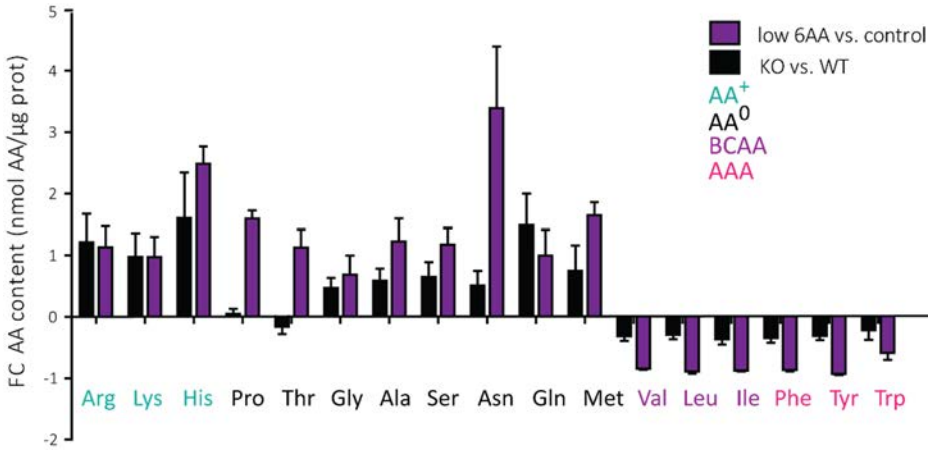

Figure 28. Comparison of the intracellular AA content in CD98hc KO and low 6AA cells. Comparative quantitative analysis of the intracellular AA content (nmol AA/µg protein) in CD98hc KO (n=7) and low 6AA cells (n=5). The fold change (FC, (KO/WT)-1 or (low 6AA /control)-1)) of the AA concentration of KO compared to WT cells and low 6AA compared to control cells is represented. AAs are grouped by side chain properties as indicated.

In order to check whether modulation of expression of other transporters could account for the increase in the AA^+ concentration, like it was observed in CD98hc KO cells, expression levels of AA^+ transporters was analysed in these cells. Low 6AA cells presented a higher mRNA expression levels of the CAT1 and CAT3 (not CAT2; data not shown) (y^+ transport system) and y^+LAT1 (not y^+LAT2; data not shown) (y^+L transport system) transporters (**Figure 29A**). This finding is in accordance with upregulated L-arginine uptake by both y^+L (inhibitable by 1 mM L-Leu and Na^+ (Devés, Chavez, and Boyd 1992)) and y^+ (the remained transport after inhibition with 1 mM L-Leu and Na^+) transport systems in low 6AA cells (**Figure 29B**). In the light of these results, extracellular BCAA and AAA restriction seems to be sufficient to trigger the intracellular AA imbalance observed in cells lacking CD98hc.

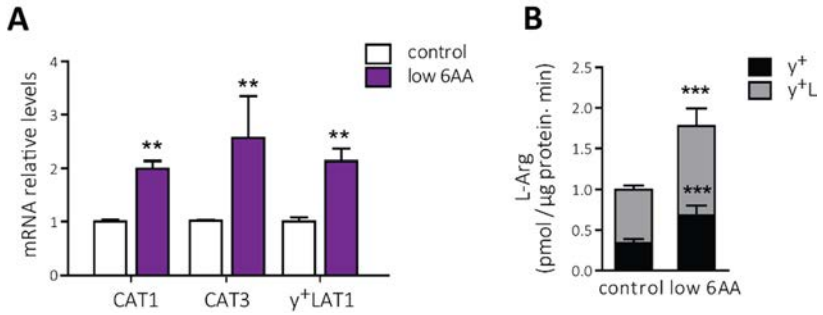

Figure 29. BCAA and AAA shortage triggers the upregulation of the expression of CAT3 and increased L-Arg uptake. A, comparison of CAT1, CAT3 and y^+LAT1 mRNA expression levels between control and low 6AA cells. n=3. B, L-Arg (10 µM) uptake at 2 min (linear conditions of uptake) in control and low 6AA cells was measured. L-Arg uptake inhibited by 1 mM L-Leu and Na^+ was identified as system y^+L, the remained transport was attributed to system y^+. n=4. Quantification data correspond to the mean ± SEM of the independent experiments (n) indicated for each graph normalized to control cells. Statistical significance **, $p \leq 0.01$; ***, $p \leq 0.001$ vs. control cells was analysed using a Student's t-test. *L-Arg uptake analysis (B) was performed by Josep Chillarón.*

Moreover, we assessed the presence of oxidative stress in low 6AA cells by using a redox-sensitive probe H_2DCFDA labelling and found no differences compared to control cells (**Figure 30A**). In addition, protein levels of NRF2 were comparable between low 6AA and control cells (**Figure 30B**). This indicated that low 6AA cells

did not present oxidative stress, in contrast to that observed in CD98hc KO cells (**Figure 30B** and **Figure 17**).

Hence, low 6AA cells are a suitable cellular model in which to study the effects of cellular BCAA and AAA deficiency, independently of ROS and other possible metabolic alterations that might be associated with CD98hc ablation.

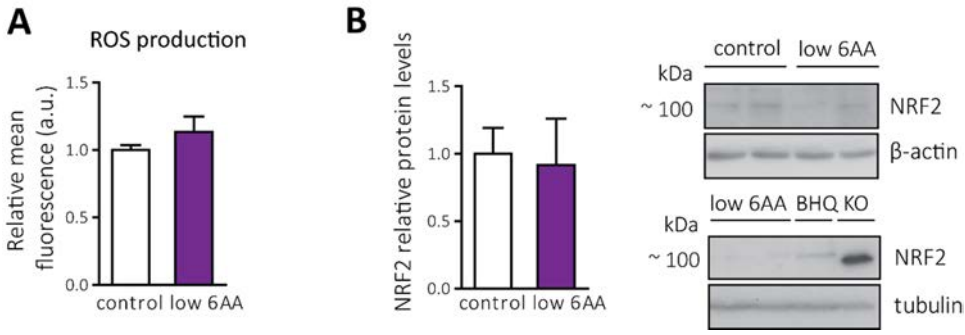

Figure 30. Low 6AA do not present oxidative stress. A, quantification of ROS levels using the free radical sensor H2DCFDA (DCF) was measured by flow cytometry. Bars represent the mean DCF fluorescence in control and low 6AA cells. a.u., arbitrary units. n>6. **B**, comparison of NRF2 protein expression between control and low 6AA cells (upper panel). 50 µg of protein extracts were loaded. Data are normalized by β-actin expression. Comparison of NRF2 protein expression between low 6AA and CD98hc KO cells (lower panel). 50 µg of protein extracts were loaded. Tert-butylhydroquinone (BHQ) treatment (50 µM, 1h) was used as a control. Data are normalized by tubulin expression. Quantification data correspond to the mean ± SEM of the independent experiments (n) indicated for each graph normalized to control cells. No statistical differences were found using a Student's t-test.

4.1.5 BCAA and AAA shortage inactivates mTORC1 signalling pathway in CD98hc KO cells

The nutrient-sensing pathway mTORC1 responds to amino acid deprivation downregulating global protein synthesis while reprograming cells for their particular needs (Efeyan, Comb, and Sabatini 2015). mTORC1 activation stimulates the subsequent phosphorylation of components of the translational machinery, including the ribosomal protein S6, one of the most widely studied downstream effectors targets of this pathway (**Introduction, Figure 4**) (Cargnello, Tcherkezian, and Roux 2015). Thus, we thought that the intracellular BCAA and

AAA shortage of CD98hc deficient cells may induce protein synthesis repression via mTORC1 inactivation. Accordingly, CD98hc KO cells showed lower levels of phosphorylated S6 (P-S6) in comparison to WT cells (**Figure 31**).

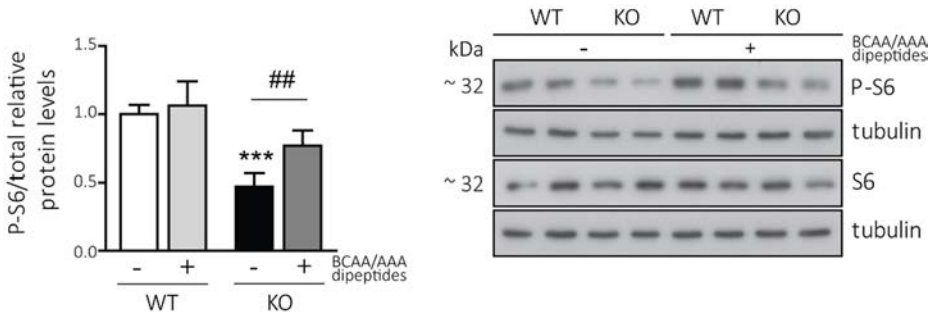

Figure 31. CD98hc ablation leads to downregulated mTORC1 signalling pathway due to the BCAA and AAA shortage. Comparison of S6 phosphorylation (P-S6) between WT and CD98hc KO cells with no additives or in the presence of BCAA- and AAA- containing dipeptides. Data are normalized by tubulin expression. Quantification data correspond to the mean ± SEM of four independent experiments normalized to WT cells. Statistical significance *** vs. WT cells or ##, $p \leq 0.01$ vs. KO cells, was analysed using a Student's t-test.

To confirm that BCAA and AAA limitation inhibited the mTORC1 signalling pathway in CD98hc KO cells, we added BCAA- and AAA-containing dipeptides to the culture media. This supplementation partially restored S6 phosphorylation (**Figure 31**). In addition, low 6AA cells presented repressed mTORC1 activation, as revealed by decreased P-S6 protein levels (**Figure 32**).

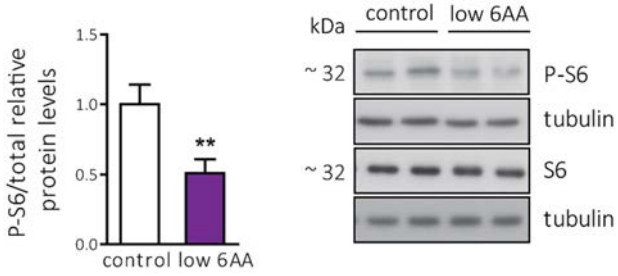

Figure 32. BCAA and AAA shortage leads to downregulated mTORC1 signalling pathway. Comparison of S6 phosphorylation (P-S6) between control and low 6AA cells. Data are normalized by tubulin expression. Quantification data correspond to the mean ± SEM of four independent experiments normalized to control cells. Statistical significance **, $p \leq 0.01$ vs. control cells was analysed using a Student's t-test.

These results suggest that the shortage of BCAAs and AAAs in CD98hc KO cells repress protein synthesis via the downregulation of mTORC1.

4.1.6 CD98hc ablation leads to eIF2α phosphorylation non mediated by AA scarcity

AA deprivation and oxidative stress lead to eIF2-mediated ISR activation (Castilho et al. 2014; Taniuchi et al. 2016b). eIF2α phosphorylation reduces the overall rate of the translation, allowing cells to either overcome the stress or be eliminated if the damage cannot be repaired (Introduction, **Figure 11**) (Dever 2002). CD98hc KO cells presented a marked increase in the phosphorylated levels of eIF2α (P-eIF2α) compared to WT cells (**Figure 33**). However, eIF2α remained phosphorylated after addition of BCAA- and AAA- containing dipeptides (**Figure 33**), thereby suggesting that nutritional status did not trigger the eIF2α-mediated ISR pathway in CD98hc KO cells.

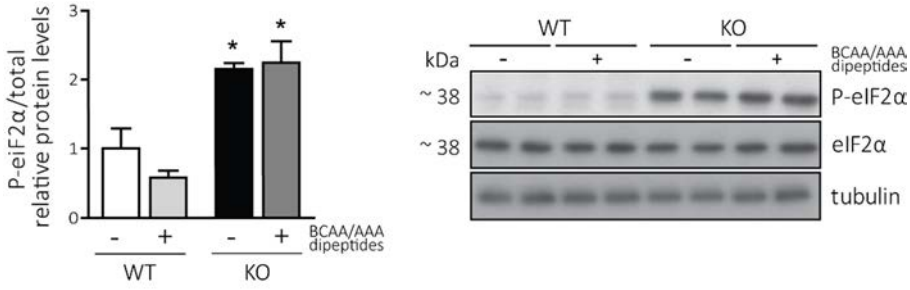

Figure 33. CD98hc ablation leads to eIF2-mediated integrated stress response activation. Comparison of eIF2α phosphorylation (P- eIF2α) between WT and CD98hc-KO cells with no additives or in the presence of BCAA- and AAA- containing dipeptides. Data are normalized by tubulin expression. Quantification data correspond to the mean ± SEM of three independent experiments normalized to WT cells. Statistical significance *, $p \leq 0.05$ vs. WT cells was analysed using a Student's t-test.

The phosphorylation of the α subunit of eIF2 mediated by AA deprivation is mediated by GCN2 activation (Donnelly, Gorman, Gupta, & Samali, 2013). GCN2 is activated through the binding of uncharged transfer RNAs (tRNAs) (Joshi, Kulkarni, and Pal 2013). Considering the absence of good antibodies for mouse

GCN2 detection, tRNA charging levels were measured by the tRNA-tailored microarrays as an indirect indication of GCN2 activation (**Materials and Methods, Figure 105**). The differentially charged tRNAs are represented as a heatmap. Importantly, tRNA charging levels were only marginally affected in CD98hc KO cells in comparison to WT. This observation suggests that GCN2 is not upstream of eIF2α phosphorylation in our CD98hc KO model.

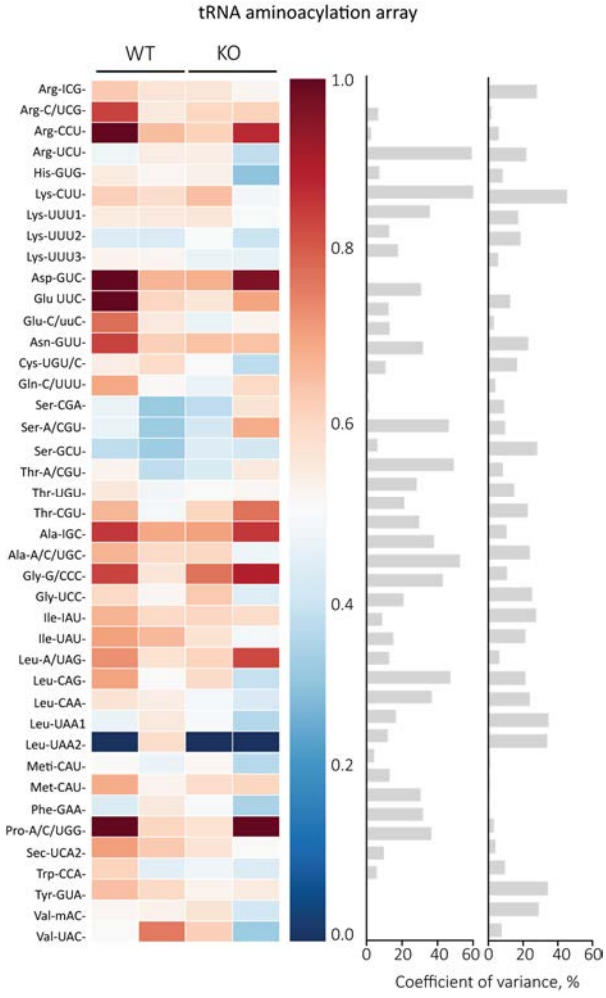

Figure 34. tRNA charging levels were marginally affected in CD98hc KO cells. tRNA microarrays of aminoacyl-tRNAs in CD98hc KO and WT cells. Representative array of two independent biological replicates is shown. Covariance analysis (plots on the right) for each isoacceptor is indicated. tRNAs are depicted by their anticodon and cognate AA. Meti and Mete, initiator and elongator $tRNA^{Met}$,respectively. Note that Leu-UAA1 and Leu-UAA2 are two $tRNA^{Leu}$(UAA) isodecoders that pair to the same codon UUA/G Leu codon but differ in their sequence outside the anticodon. *tRNA microarrays were performed by Christine Polte in Zoya Ignatova´s laboratory at The Institute of Biochemistry and Molecular Biology of the University of Hamburg, Germany.*

Moreover, phosphorylated levels of eIF2α remained unaffected in low 6AA cells when compared to control ones (**Figure 35**), reinforcing previous assumption.

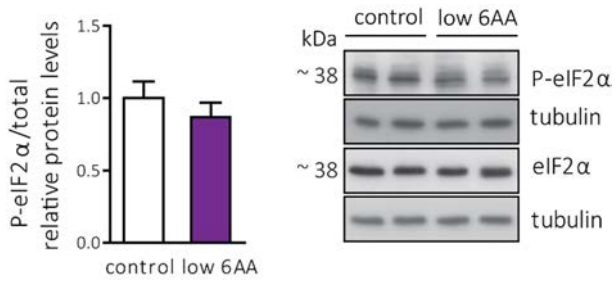

Figure 35. BCAA and AAA shortage does not trigger eIF2-mediated integrated stress response activation. Comparison of eIF2α phosphorylation between control and low 6AA cells. Data are normalized by tubulin expression. Quantification data correspond to the mean ± SEM of three independent experiments normalized to control cells. No statistical differences were found using a Student's t-test.

Four kinases (PERK, PKR, GCN2 and HRI) mediate the phosphorylation of the α subunit of eIF2 responding to different stress signals (Donnelly et al., 2013). We excluded the presence of unfolded protein response (UPR) in CD98hc KO cells, as evidenced by the lack of activating phosphorylation of PERK (Takayanagi et al. 2013) in these cells (**Figure 36**). Thapsigargin (Tg) treatment in WT cells was used as a positive control, since is the most widely used inhibitor of the sarco-endoplasmic reticulum (ER) Ca^{2+}-ATPase (SERCA), depleting the Ca^{2+} store in the ER and consequently, leading to ER stress and UPR (Sehgal et al. 2017).

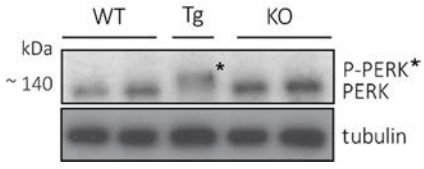

Figure 36. CD98hc KO cells do not present unfolded protein response. Comparison of PERK phosphorylation (P-PERK) between WT and CD98h KO cells. Thapsigargin (Tg) treatment (1 μM 3h) in WT cells was used as a positive control. Phosphorylation of PERK caused a mobility shift of the corresponding protein band (*). Data are normalized by tubulin expression. A representative Western blot is shown, similar results were obtained four times.

Considering the unlikely involvement of PKR, mainly activated by viral infections (García, Meurs, and Esteban 2007), we measured total protein levels of HRI kinase, which is known to be activated by oxidative stress (Lu, Han, & Chen, 2001). Consistent with the elevated intracellular levels of ROS (**Figure 17**), HRI expression was upregulated in CD98hc KO compared to WT cells (**Figure 37**). Arsenite (As^{3+}) treatment, which is known to activate HRI and therefore eIF2α phosphorylation (Lu, Han, & Chen, 2001), was used as a positive control (**Figure 37**).

Altogether these results point to HRI kinase as the best candidate to be the responsible of the activation of the ISR regulated by eIF2 in CD98hc KO cells, probably due to oxidative stress.

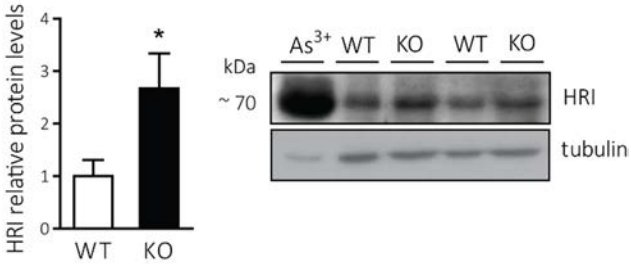

Figure 37. CD98hc KO cells present upregulate HRI expression. Comparison of HRI protein expression between WT and CD98hc KO cells. 50 µg of protein extracts were loaded. Arsenite (As^{3+}) treatment in WT cells (200 µm 1h) was used as a positive control. Data are normalized by tubulin expression. Quantification data correspond to the mean ± SEM of three independent experiments normalized to WT cells. Statistical significance *, $p \leq 0.05$ vs. WT cells was analysed using a Student's t-test.

Phosphorylated eIF2α causes a reduction in global protein synthesis while specifically promoting the translation of genes including the transcription factor ATF4, aiding cell survival and recovery (Lu, Harding, and Ron 2004). However, despite the robust phosphorylation of eIF2α, ATF4 mRNA (**Figure 38A**) and protein levels (**Figure 38B**) were substantially repressed in CD98hc KO cells.

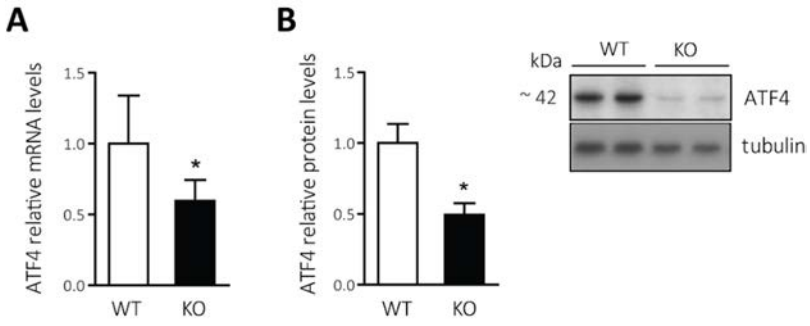

Figure 38. **ATF4 expression is repressed in CD98hc KO cells. A**, comparison of ATF4 mRNA expression levels between WT and CD98hc KO cells. n=3. **B**, comparison of ATF4 protein expression between WT and CD98hc KO cells. Data are normalized by tubulin expression. n=3. Quantification data correspond to the mean ± SEM of the independent experiments (n) indicated for each graph normalized to WT cells. Statistical significance *, $p \leq 0.05$ vs. WT cells was analysed using a Student's t-test.

Although the ISR serves essential adaptive functions, unabated induction of this stress response can contribute to morbidity. In this sense, dysfunctional ISR has already been reported in cells affected by chronic stresses (Cheung et al. 2007; Dey et al. 2010; Evstafieva et al. 2014; Kumar et al. 2003a; Woehlbier and Hetz 2011). This could be the case for CD98hc KO fibroblasts, which present chronic oxidative and nutritional stresses.

In the same line, induction of ATF4 in response to eIF-2α phosphorylation is immediately upstream of growth arrest and DNA damage-inducible protein (GADD34) activation (Ma and Hendershot 2003). GADD34 specifically promoted the dephosphorylation of eIF2α in a negative feedback loop that inhibits prolonged translational blockage and stress-induced gene expression (Brush, Weiser, and Shenolikar 2003; Harding et al. 2009; Novoa et al. 2001). In accordance with ATF4 repression, GADD34 protein levels were reduced in cells lacking CD98hc compared to WT cells (

Figure 39), reinforcing the idea that CD98hc KO cells present a dysfunctional eIF2-mediated ISR activation.

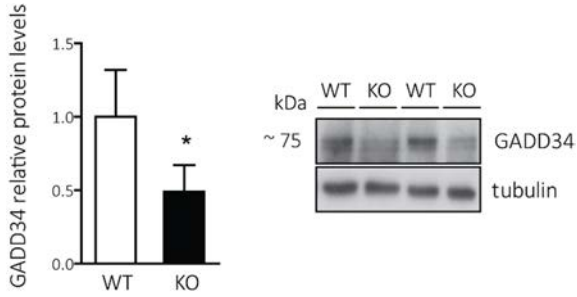

Figure 39. GADD34 expression is repressed in CD98hc KO cells. Comparison of GADD34 protein expression between WT and CD98hc KO cells. Data are normalized by tubulin expression. Quantification data correspond to the mean ± SEM of three independent experiments normalized to WT cells. Statistical significance *, $p \leq 0.05$ vs. WT cells was analysed using a Student's t-test.

4.1.7 Lack of CD98hc triggers the reduction of global protein synthesis

Previous reported data strongly suggested that in CD98hc KO cells, mTORC1 repression is mediated by the BCAA and AAA impoverishment, whereas eIF2-mediated ISR activation is likely related to oxidative stress. Next, we tested whether either of these stress-sensing pathways affected general protein synthesis. To this aim, we attempted to measure protein synthesis with the alternative non-radioactive methodology SUrface SEnsing of Translation (SUnSET). In SUnSET, a cell culture is pulsed with puromycin, an aminoacyl-tRNA analogue that is incorporated into the elongating peptides and leads to the termination of mRNA translation (**Material and Methods, Figure 101**). The amount of puromycin-labelled peptides determined by using anti-puromycin antibodies reflects the rate of protein synthesis (Schmidt et al. 2009). Strikingly, we found a huge increase in puromycin incorporation in CD98hc KO cells in comparison to WT cells (**Figure 40**), suggesting that protein synthesis was dramatically increased in these cells. To validate the method, cells were pre-incubated with the protein synthesis inhibitor cycloheximide (CHX) (Obrig et al. 1971), which fully blocked puromycin incorporation (**Figure 40**).

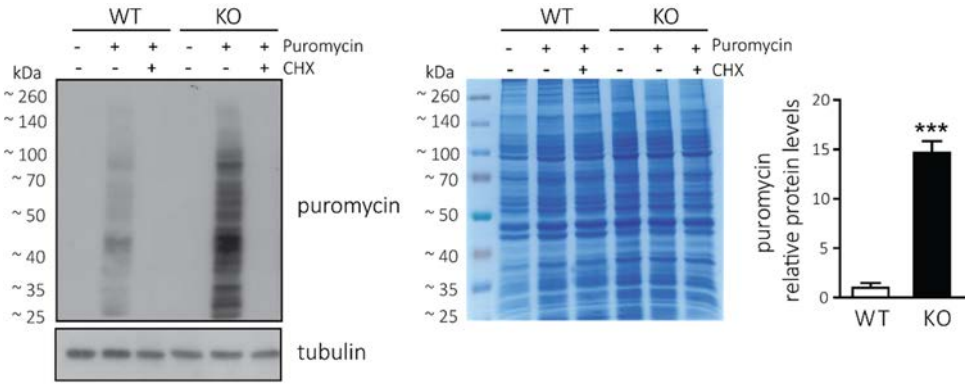

Figure 40. SUnSET analysis of protein synthesis in WT and CD98hc KO cells. Puromycin incorporation into elongating peptides (1 µM 30 min) was assessed by immunoblotting (left and right panels). Data are normalized by tubulin. Puromycin incorporation was blocked when cells were pre-incubated with cycloheximide (CHX) (25 nM 5 min). Coomassie staining was performed as loading control in Western blot analysis (middle panel). Quantification data correspond to the mean ± SEM of four independent experiments normalized to WT cells. Statistical significance ***, $p \leq 0.001$ vs. WT cells was analysed using a Student's t-test.

Previous result was unexpected since it did not correlate with the cell proliferation defect observed in cells lacking CD98hc (**Figure 21**). Moreover, the detected alterations in the stress-sensing pathways mTORC1 (**Figure 31**) and eIF2-mediated ISR (**Figure 33**), suggested that protein synthesis was likely downregulated in CD98hc KO cells (Efeyan, Comb, and Sabatini 2015), in disagreement with SUnSET results.

While trying to elucidate a possible explanation for these paradoxical results, an interesting paper came out highlighting the limitations of SUnSET technique for particular conditions (Marciano, Leprivier, and Rotblat 2018). Specifically, Marciano and co-workers demonstrated that puromycin labelling is not suitable for measuring global protein synthesis under conditions of nutritional starvation (Marciano, Leprivier, and Rotblat 2018). Since CD98hc KO cells undergo major alterations, not only in AA availability (**Figure 18**), but also in glucose metabolism (see below), we decided to measure protein synthesis with a classical methodology.

Thus, general protein synthesis was assessed by using [^{35}S] methionine labelling. This technique is a well-established method entails pulsing cells with radiolabelled

AAs, in this case [^{35}S]methionine, for a certain amount of time, and then measuring their incorporation into newly synthesized proteins by quantifying radioactivity (Tarver and Schmidt 1942). Considering the restricted AA uptake in CD98hc KO cells, due to the lack of CD98hc-associated AA transporters, the incorporated [^{35}S]methionine into protein was corrected by the total radioactivity entered in cells. A lower incorporation of [^{35}S]methionine was detected in CD98hc KO cells compared to WT cells, suggesting that, in accordance with the observed alterations in mTORC1 and eIF2α signalling pathways, protein synthesis was reduced in cells lacking CD98hc when compared to WT cells (**Figure 41**).

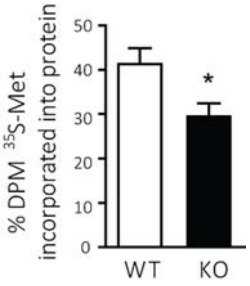

Figure 41. Global protein synthesis is downregulated in CD98hc KO cells. Comparison of ^{35}S-methionine (Met) incorporation into protein between WT and CD98hc KO cells. DPM, disintegrations per minute. Quantification data correspond to the mean ± SEM of four independent experiments. Statistical significance *, $p \leq 0.05$ vs. WT cells was analysed using a Student's t-test. *Protein synthesis was analysed by Josep Chillarón.*

Collectively, the results shown in this chapter suggest that CD98hc-associated transporters (xCT, LAT1, and y^+LAT2 in WT cells) are crucial to control reactive oxygen species and intracellular AA levels, thus sustaining cell survival and proliferation.

4.2 CD98hc sustains appropriate nucleotide availability for proper cell cycle progression.

Nutritional status regulates cell cycle progression, in part by controlling protein synthesis via the mTORC1 pathway (Cuyàs et al. 2014; Fingar et al. 2004; Rosner et al. 2009). Moreover, it is well established that nucleotide synthesis relies on feeder pathways involving glucose and AAs (Lane & Fan, 2015). Since CD98hc not only supports the balance of the intracellular AA content but may also regulate

glucose metabolism (Marchiq et al., 2015; Ohno et al., 2011), we hypothesized that CD98hc may have a role in the cell cycle.

4.2.1 Gene Set Enrichment Analysis reveals putative cell cycle alterations in CD98hc KO cells

Aiming at studying additional alterations that could take place in cells facing the loss of CD98hc and by consequence AA restriction, a comparative transcriptome analysis was performed in WT and CD98hc KO cells. Strikingly, we found that 20 % of the genes were differentially expressed in both groups (biological fold change > 2 and adjusted p-value < 0.05). Supporting this, Gene Set Enrichment Analysis (GSEA) using the KEGG database identified several gene categories altered between WT and CD98hc KO cells (**Figure 42; GEO accession code: GSE126781**).

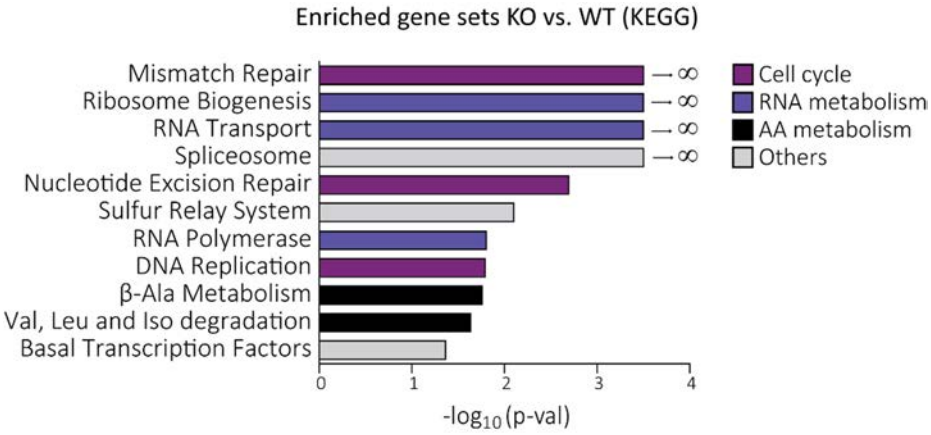

Figure 42. GSEA of transcriptional data from WT and CD98hc KO cells. Bars represent statistically significant enriched gene sets (nominal p-value < 5%, FDR < 25%) in CD98hc KO cells compared to WT cells according to KEGG data base. Bars are coloured according to the functional characterization indicated in the legend. X-axis: $-\log_{10}$ (p-val).

Remarkably, GSEA using the KEGG database showed a noticeable enrichment in gene sets closely related to cell cycle (**Figure 42**), including mismatch repair, DNA replication and nucleotide excision repair **(Figure 43A; GEO accession code:**

GSE126781). This outcome supported our hypothesis about the possible role of CD98hc in cell cycle dynamics.

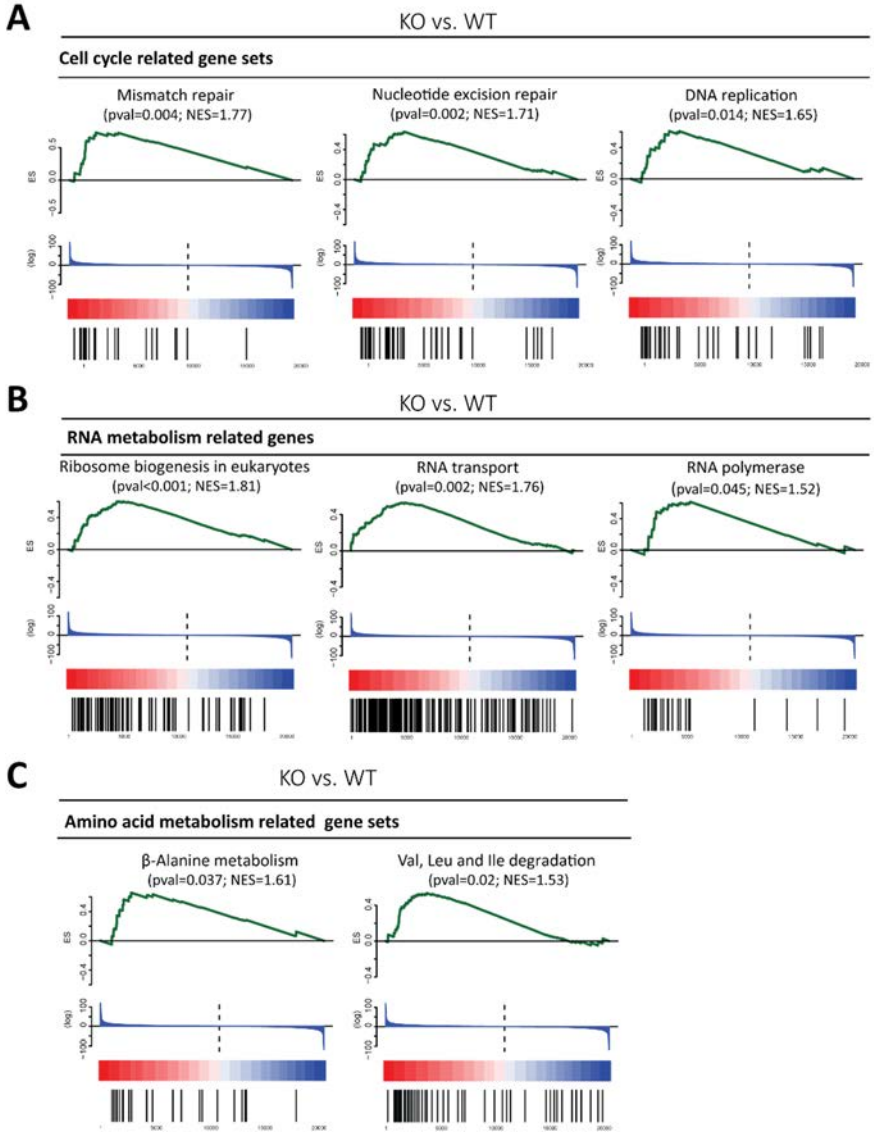

Figure 43. GSEA shows an enrichment in cell cycle related gene sets in CD98hc KO cells. Enrichment plots for the indicated gene sets related to cell cycle (**A**), RNA metabolism (**B**) and AA metabolism (**C**), obtained from GSEA using KEGG data base of transcriptional data from WT and CD98hc KO cells. Y-axis: value of the ranking metric; X-axis: the rank for all genes. Bottom: plot of the ranked list of all genes. The score at the peaks of the plots is the enrichment score (ES) for each gene set and those genes appear before or at the peak are defined as core enrichment genes for this gene set. P-value (p-val) and Normalized Enrichment Score (NES) are indicated for the included enrichment plots.

Furthermore, an enrichment was detected in gene sets associated with RNA (**Figure 42; Figue 43B; GEO accession code: GSE126781**) and AA metabolism (**Figure 42; Figure 43C; GEO accession code: GSE126781**) in CD98hc KO cells, probably caused by BCAA and AAA deficiency and defective protein synthesis.

4.2.2 Cells lacking CD98hc fail to progress adequately through the S-phase of the cell cycle

On the basis of previous data, we analysed cell cycle phase distributions by measuring DNA content using the DNA intercalating agent propidium iodide (PI) and flow cytometry in CD98hc-deficient and WT cells (**Figure 44**). Compared to WT, CD98hc KO cells showed increased S- (65 ± 0.7% vs. 53.3 ± 2.2%) and G2/M-phases (16 ± 0.5% vs. 14 ± 0.6%) at the expense of a reduction in G1-phase (18.8 ± 0.9% vs. 32.7 ± 2.5%) (**Figure 44**).

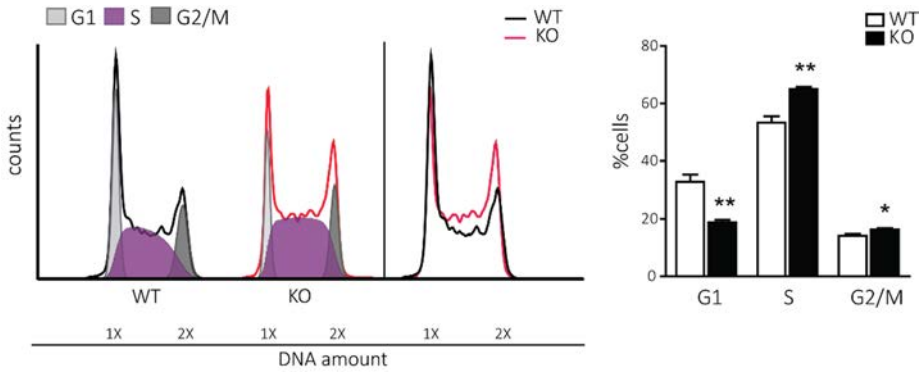

Figure 44. CD98hc depletion leads to increased S- and G2/M- phases. Cell cycle distribution was measured by flow cytometry using PI staining. 10.000 cells/condition were analysed. A representative cell cycle profile of WT and CD98hc KO cells is illustrated along with the overlap of their profiles (left panel). The graphical representation of cell cycle distribution (right panel) shows the percentage of cells in G1-, S- and G2/M- phases in WT and CD98hc KO cells. Quantification data correspond to the mean ± SEM of four independent experiments. Statistical significance *, $p \leq 0.05$; **, $p \leq 0.01$ vs. WT cells was analysed using a Student's t-test.

The increase in S-phase population cannot be attributed to an enhanced proliferative rate, since cells lacking CD98hc presented a major delay in proliferation in comparison to WT cells (**Figure 21**). Alternatively, the lack of CD98hc may slow down the progression of cells that are in the S-phase. To test whether CD98hc KO cells presented delayed DNA replication, cells were synchronised in S-phase with a double block of thymidine (Bjursell and Reichard 1973). The treatment achieved the retention of around 75% of cells in the DNA-synthesis phase (**Figure 45**).

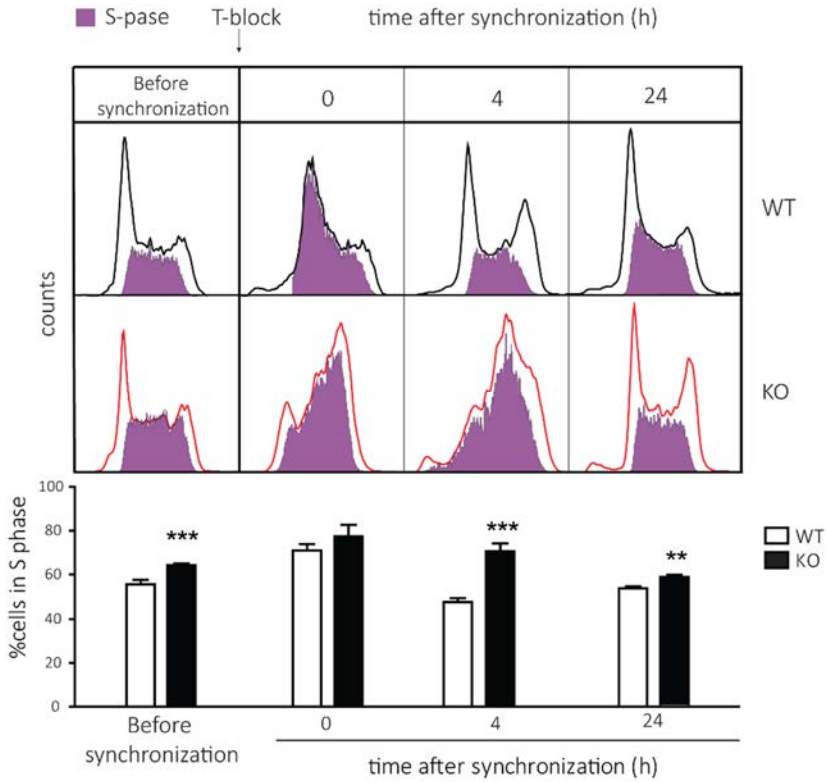

Figure 45. CD98hc depletion leads to delayed S-phase. WT and CD98hc KO cells were synchronized in S-phase with a double thymidine block (T-block). The DNA content was analysed by flow cytometry using PI staining. 10.000 cells/condition were analysed. The percentage of cells in each cell cycle stage was measured at indicated times after the release of the thymidine block. A representative cell cycle profile with highlighted S-phase (depicted in purple) is represented for each time point (upper panel). The percentage of cells in S-phase out of total was quantified at indicated time points for WT and CD98hc KO cells (lower panel). Quantification data correspond to the mean ± SEM of four independent experiments. Statistical significance **, $p \leq 0.01$; ***, $p \leq 0.001$ vs. WT cells was analysed using a Student's t-test.

S-phase progression was then monitored. Remarkably, 4 h after release, 70.7 ± 3.4% of CD98hc KO cells remained in S-phase compared to a 47.7± 1.8% in the case of WT cells (**Figure 45**). This observation confirms that cells lacking CD98hc fail to progress adequately through DNA synthesis.

4.2.3 Lack of CD98hc and BCAA and AAA shortage lead to replicative stress

During S-phase, cells must faithfully duplicate their genomes. In response to DNA damage, cells suffer replicative stress (RS), which is characterized by the activation of the DNA damage response (DDR) pathway and often accompanied by cell cycle arrest (Giglia-Mari, Zotter, and Vermeulen 2011; Zhou and Elledge 2000). We used the transcriptome analysis performed in WT and CD98hc KO cells to further interrogate whether the observed cell cycle arrest was accompanied by DNA damage and RS in CD98hc KO cells. In this regard, we created the *DNA damage response gene set*, which comprised 97 genes related to the regulation of DNA replication and repair and involved in DNA damage signalling pathways. The selection was carried out following the bibliography and available gene lists from commercial arrays (RT² Profiler™ PCR Array Human DNA Repair (PAHS-042Z), QUIAGEN;) (Shiotani and Zou 2009; Wu et al. 2013). The gene set was significantly enriched in CD98hc KO cells (p-val<0.001, NES = 1.83, FDR<0.001) (**Figure 46**).

In cases of RS, RPA senses the DNA damage and propagates the DDR (**Introduction, Figure 11**) (Zou and Elledge 2003). Phosphorylation of RPA (P-RPA) and CHK1 (P-CHK1), the final transducer of this signalling pathway, is widely accepted as the most specific indicators of DDR activation (Dai and Grant 2010; Marechal and Zou 2013; Nam and Cortez 2011). Cells lacking CD98hc presented a clearly enhanced DDR activation, as demonstrated by the increased in phosphorylated and total levels of CHK1 and RPA (**Figure 47**), in line with the transcriptomic analysis (**Figure 46**).

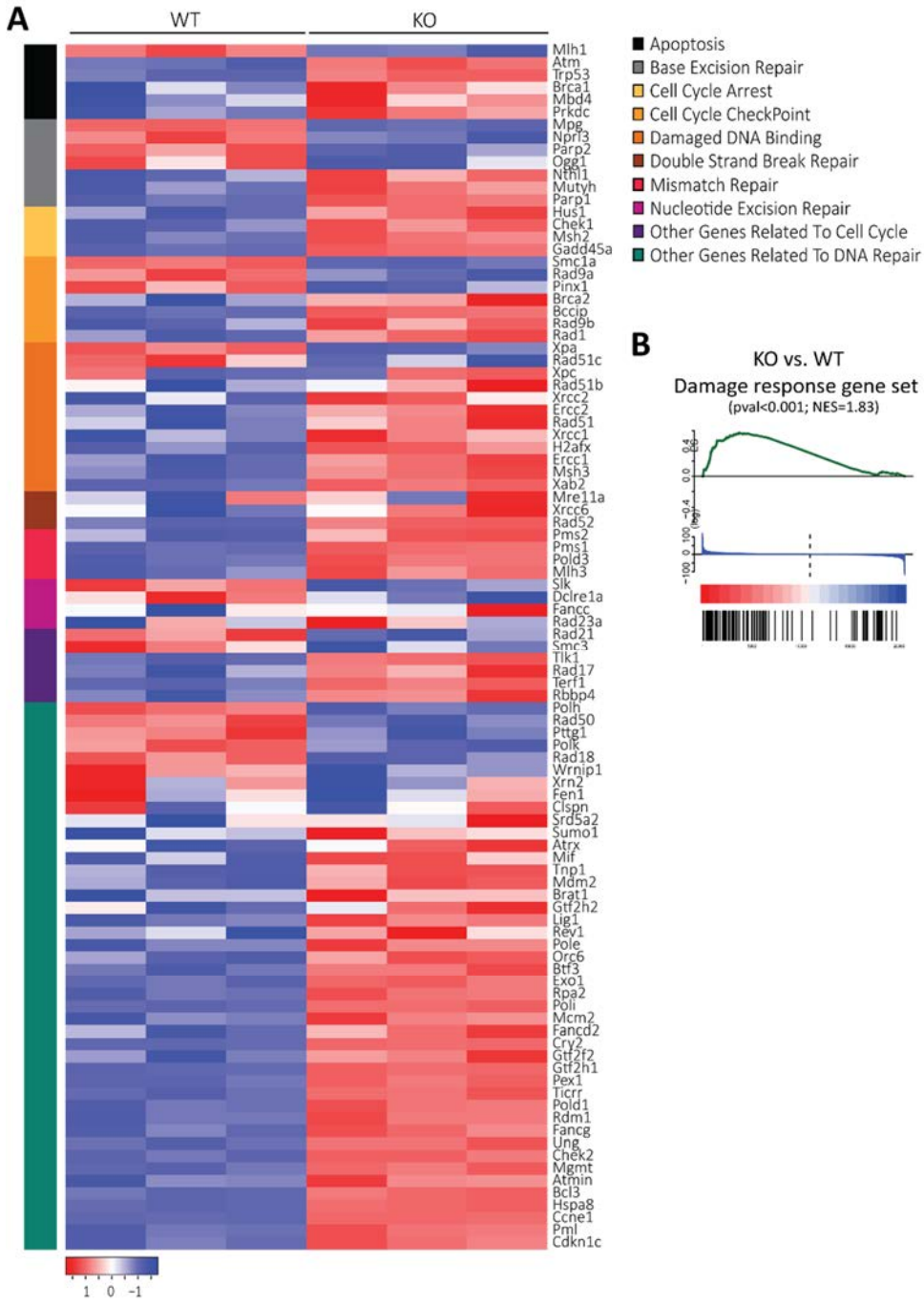
A
WT
KO
Mlh1
Atm
Trp53
Brca1
Mbd4
Prkdc
Mpg
Nprl3
Parp2
Ogg1
Nthl1
Mutyh
Parp1
Hus1
Chek1
Msh2
Gadd45a
Smc1a
Rad9a
Pinx1
Brca2
Bccip
Rad9b
Rad1
Xpa
Rad51c
Xpc
Rad51b
Xrcc2
Ercc2
Rad51
Xrcc1
H2afx
Ercc1
Msh3
Xab2
Mre11a
Xrcc6
Rad52
Pms2
Pms1
Pold3
Mlh3
Slk
Dclre1a
Fancc
Rad23a
Rad21
Smc3
Tlk1
Rad17
Terf1
Rbbp4
Polh
Rad50
Pttg1
Polk
Rad18
Wrnip1
Xrn2
Fen1
Clspn
Srd5a2
Sumo1
Atrx
Mif
Tnp1
Mdm2
Brat1
Gtf2h2
Lig1
Rev1
Pole
Orc6
Btf3
Exo1
Rpa2
Poli
Mcm2
Fancd2
Cry2
Gtf2f2
Gtf2h1
Pex1
Ticrr
Pold1
Rdm1
Fancg
Ung
Chek2
Mgmt
Atmin
Bcl3
Hspa8
Ccne1
Pml
Cdkn1c
1 0 −1
Apoptosis
Base Excision Repair
Cell Cycle Arrest
Cell Cycle CheckPoint
Damaged DNA Binding
Double Strand Break Repair
Mismatch Repair
Nucleotide Excision Repair
Other Genes Related To Cell Cycle
Other Genes Related To DNA Repair
B
KO vs. WT
Damage response gene set
(pval<0.001; NES=1.83)

Figure 46. CD98hc KO cells show an enrichment in the DNA damage response gene set. **A**, heat map for RNA expression level in WT and CD98hc KO cells of 97 genes involved in DNA damage signalling pathways. The genes featured were selected as indicated in *Materials and Methods* and grouped in the specified categories. Rows: genes; columns: samples. Range of colours (red to blue) shows the range of expression values (high to low comparing to the mean expression within all the samples). **B**, enrichment plot for DNA damage response gene set obtained from GSEA of transcriptional data from WT and CD98hc KO cells. Y-axis: value of the ranking metric; X-axis: the rank for all genes. Bottom: plot of the ranked list of all genes. The score at the peaks of the plots is the enrichment score (ES) for each gene set and those genes appear before or at the peak are defined as core enrichment genes for this gene set. P-value (p-val) and Normalized Enrichment Score (NES) are indicated.

The overexpression of these two DDR markers is probably the outcome of adaptation, which ensures that CD98hc KO cells survive in a context of chronic RS.

Furthermore, apoptosis is associated with inappropriate DNA damage resolution (Mazouzi, Velimezi, and Loizou 2014b). In this regard, we assessed the presence of apoptotic cell death in WT and CD98hc KO cells by using an annexin V binding assay. This methodology is based on the annexin V-affinity to phosphatidyl-serine (PS) (**Materials and Methods, Figure 102**) (Andre et al. 1990). Under normal physiological conditions, cells maintain a strictly asymmetric distribution of phospholipids in the cellular membranes with PS facing the cytosolic side. However, during apoptosis, this membrane asymmetry is rapidly lost, which results in the exposure of PS at the outer leaflet of the plasma membrane (Bevers et al. 1999). This phenomenon can be detected by annexin V labelling in combination with PI staining (Van Engeland et al. 1997). As shown in **Figure 48**, CD98hc KO cells presented increased apoptotic cell death compared to WT cells, which was already suggested by the transcriptome analysis data (**Figure 46**).

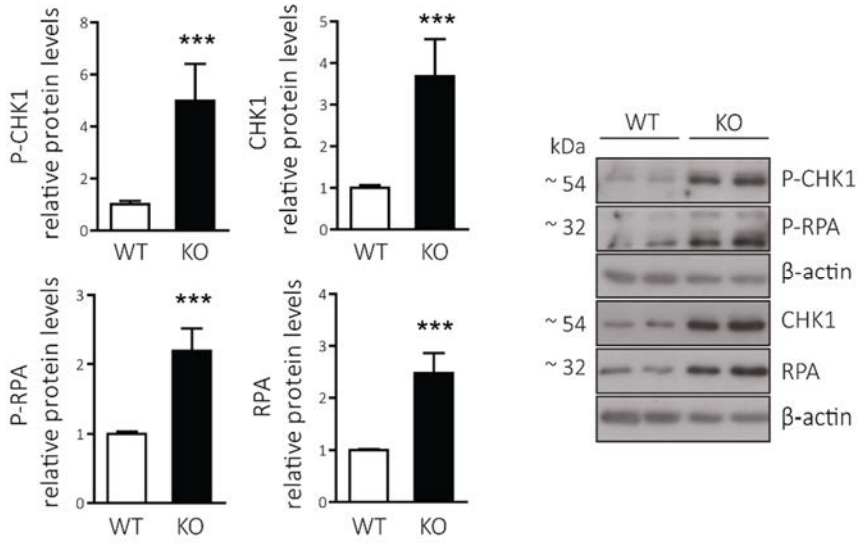

Figure 47. CD98hc ablation leads to activated DNA damage response. Comparison of phosphorylated and total protein levels of CHK1 and RPA between WT and CD98hc KO cells. Data are normalized by β-actin expression. Quantification data correspond to the mean ± SEM of four independent experiments normalized to WT cells. Statistical significance ***, $p \leq 0.001$ vs. WT was analysed using a Student's t-test.

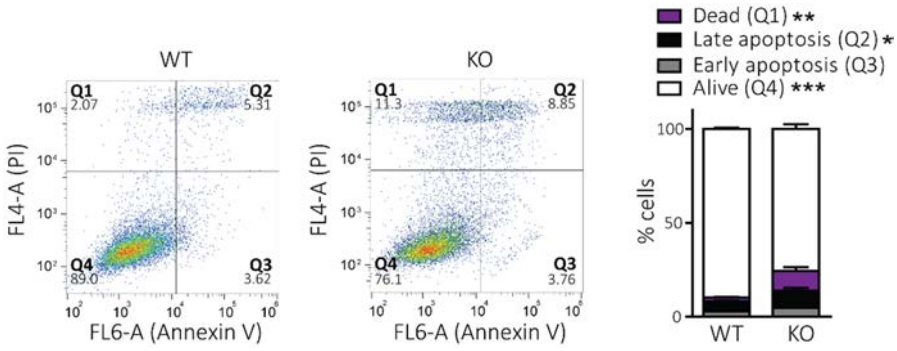

Figure 48. The loss of CD98hc induces apoptosis. Apoptosis in WT and CD98hc KO cells was measured by annexin V and PI staining followed by flow cytometry analysis. Representative diagrams are shown (left panel). Y-axis: PI fluorescence; X-axis: Annexin V fluorescence. The analysis allows to distinguish in between living cells (lower left quadrant, Q4), early apoptotic cells (lower right quadrant, Q3), late apoptotic cells (upper right quadrant, Q2), and dead cells (upper left quadrant, Q1). The percentage of cells in each state was quantified and is represented in a histogram (right panel). Quantification data correspond to the mean ± SEM of seven independent experiments. Statistical significance *, $p \leq 0.05$; **, $p \leq 0.01$; ***, $p \leq 0.001$ vs. WT cells was analysed using a Student's t-test.

To address whether BCAA and AAA limitation poses a challenge for the integrity of DNA replication in CD98hc KO cells, we evaluated the same DDR indicators in low 6AA cells. CHK1 and RPA phosphorylation was strongly upregulated in low 6AA cells compared to control cells (**Figure 49**). In this case, the total protein levels of both markers were decreased in low 6AA cells (**Figure 49**).

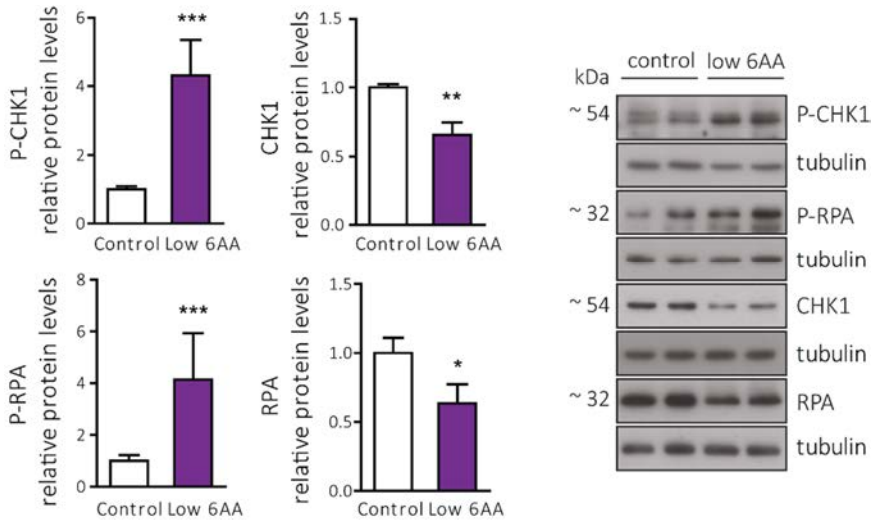

Figure 49. BCAA and AAA shortage leads to activated DNA damage response. Comparison of phosphorylated and total protein levels of CHK1 and RPA between control and low 6AA cells. Data are normalized by tubulin expression. Quantification data correspond to the mean ± SEM of three independent experiments normalized to control cells. Statistical significance *, $p \leq 0.05$; **, $p \leq 0.01$; ***, $p \leq 0.001$ vs. control cells was analysed using a Student's t-test.

Furthermore, to ascertain the implication of these AAs in cell cycle progression, the distribution of the different phases of the cell cycle was assessed by using PI staining and flow cytometry in WT and CD98hc KO cells cultured in the presence of BCAA- and AAA-containing dipeptides. Consistently, the S-phase delay was partially reduced in the treated-CD98hc KO cells compared to non-treated ones (**Figure 50**).

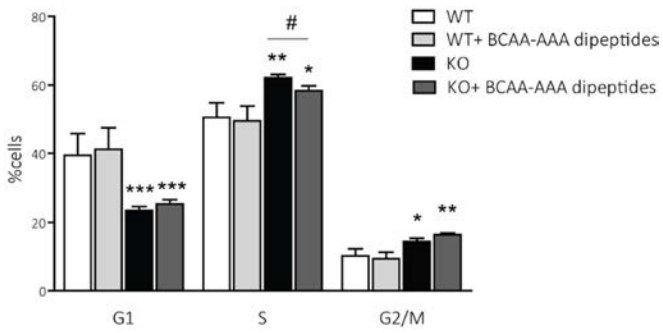

Figure 50. BCAA- and AAA- containing dipeptides partially reverse S-phase delay in CD98hc KO cells. Cell cycle distribution was measured by flow cytometry using PI staining. The graphical representation of cell cycle distribution shows the percentage of cells in G1-, S- and G2/M- phases in WT and CD98hc KO cells with no additives or in the presence of BCAA- and AAA- containing dipeptides. Quantification data correspond to the mean ± SEM of the four independent experiments. Statistical significance **, $p \leq 0.01$; ***, $p \leq 0.001$ vs. WT cells or #, $p \leq 0.05$; vs. KO cells was analysed using a Student's t-test.

Taken together, these results indicate that both loss of CD98hc and shortage of BCAAs and AAAs compromise the cell cycle, triggering RS.

4.2.4 CD98hc and BCAA/AAA availability are required for appropriate cell division cycle accomplishment

A key role of CHK1 within the DNA surveillance program is to stop cells from entering mitosis, thereby preventing the propagation of error-containing copies of the genome to daughter cells (Zhang and Hunter 2014). In this regard, we found an increase in the expression of genes implicated in the transition from G2-phase to mitosis in CD98hc KO cells according to the Hallmark database (**Figure 51**). This observation thus suggests that the entry into mitosis is compromised by the activation of the CHK1-mediated G2/M checkpoint.

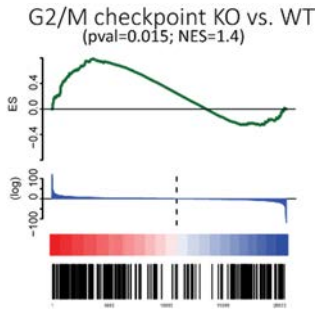

Figure 51. GSEA reveals enrichment in G2/M checkpoint gene set. Enrichment plot for the gene set G2/M checkpoint obtained from transcriptional data from WT and CD98hc KO cells using KEGG data base of. Y-axis: value of the ranking metric; X-axis: the rank for all genes. Bottom: plot of the ranked list of all genes. The score at the peak of the plot is the enrichment score (ES) for this gene set and those genes appear before or at the peak are defined as core enrichment genes for this gene set. P-value=0.015, Normalized Enrichment Score (NES) =1.4 and False Discovery Rate (FDR) <0.001).

Mitosis was analysed by immunofluorescence using the marker phospho-histone H3 (P-H3). Specific phosphorylation at serine 10 (Ser10) of histone H3 starts during late G2-phase and peaks in mitosis, when it undergoes different localization patterns during the mitotic phases, depending on chromatin condensation (**Materials and Methods, Figure 104**)) (Hendzel et al. 1997; Van Hooser et al. 1998). Thus, only patterns corresponding to cells undergoing mitosis were selected for quantification. CD98hc KO cells showed impaired mitotic rate comparing to WT cells (2.64% ± 0.3 vs. 3.8% ± 0.4%) (**Figure 52**).

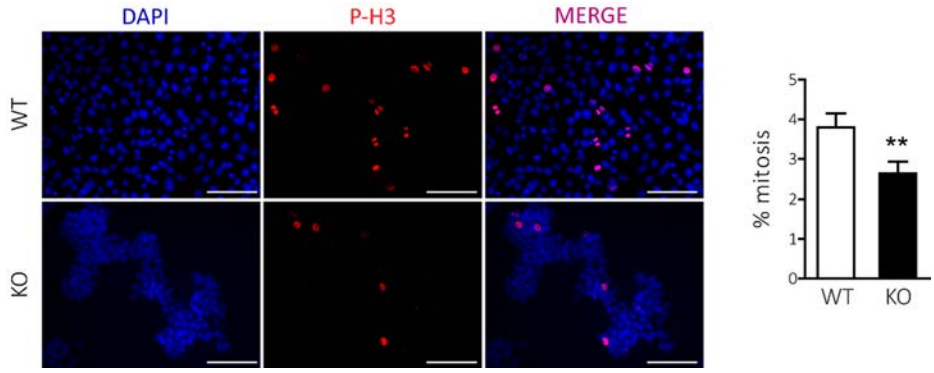

Figure 52. CD98hc ablation leads to impaired mitotic rate. Comparison of the mitotic rate between WT and CD98hc KO by immunofluorescence. The phosphorylation of Histone H3 (P-H3, red) was used as a marker for cells undergoing mitosis. DNA was stained with DAPI (blue). Representative images with around 200 nuclei are included (left panel). Scale bar is 50 microns. More than 30.000 nucleus were analysed per condition. The percentage of mitotic cells was quantified (right panel). Quantification data correspond to the mean ± SEM of seven independent experiments. Statistical significance **, $p \leq 0.01$ vs. WT was analysed using a Student's t-test.

Mitotic activity was also strongly diminished in cells sustained with BCAA and AAA partial deprivation (0.80 ± 0.1% vs. 3.67 ± 0.3 %) (**Figure 53**), thereby implying that these AAs participate in the orchestration of cell division.

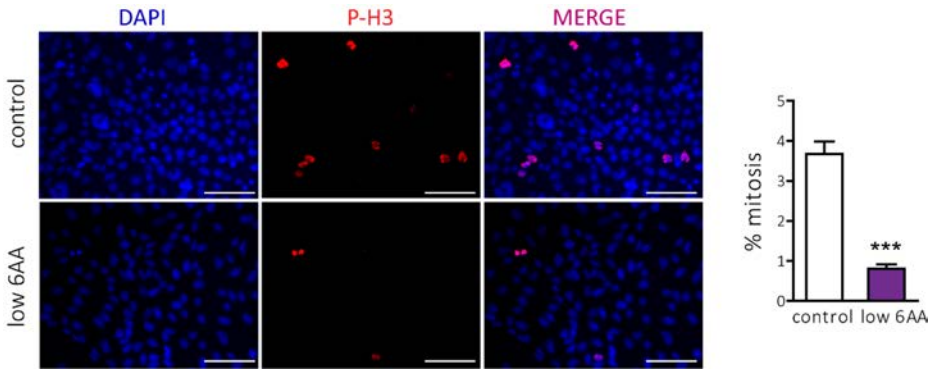

Figure 53. BCAA and AAA shortage leads to impaired mitotic rate. Comparison of the mitotic rate between control and low 6AA cells by immunofluorescence. The phosphorylation of Histone H3 (P-H3, red) was used as a marker for cells undergoing mitosis. DNA was stained with DAPI (blue). Representative images with around 200 nuclei are included (left panel). Scale bar is 50 microns. More than 30.000 nucleus were analysed per condition. The percentage of mitotic cells was quantified (right panel). Quantification data correspond to the mean ± SEM of seven independent experiments. Statistical significance ***, $p \leq 0.001$ vs. control cells was analysed using a Student's t-test.

4.2.5 CD98hc KO cells present defective pentose phosphate pathway and a general reduction in the nucleotide pool levels

To gain further insights into the connexion between the lack of CD98hc and the reported DNA damage, we examined whether there was any alteration in the nucleotide pool of CD98hc KO cells. To this end, we performed a targeted metabolomics assay to quantify the nucleotide content of these cells. Notably, CD98hc KO cells showed a remarkable general decrease in nucleotide levels when compared to WT cells (**Figure 54**).

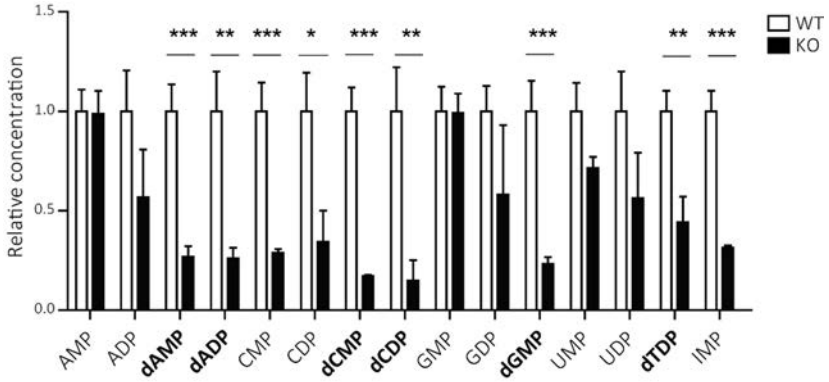

Figure 54. Lack of CD98hc triggers a general reduction in the nucleotide pool. Content of nucleotides in WT and CD98hc KO cells measured by a targeted metabolomics assay. Deoxynucleotides are depicted in bold letters. Quantification data correspond to the mean ± SEM of five independent experiments normalized to WT cells. Statistical significance *, $p \leq 0.05$; **, $p \leq 0.01$; ***, $p \leq 0.001$ vs. WT cells was analysed using a Student's t-test.

This finding suggested that the alteration underlying this massive reduction compromised the biosynthesis of both purine and pyrimidine nucleotides before the formation of their precursors. Ribose-5P, which is both a product and an intermediate of the PPP, plays a critical role in *de novo* nucleic acid synthesis and it is needed for the synthesis of both purine and pyrimidine ribonucleotides (Stincone et al. 2015). Cells metabolize glucose to generate glucose-6P, which can fuel either the PPP or glycolytic pathways. In order to analyse the activity of the PPP, we used uniformly labelled [U-^{13}C6]-glucose in combination with gas chromatography-coupled to mass spectrometry (GC-MS). The PPP flux was almost totally abrogated in CD98hc KO cells in comparison to WT cells, as indicated by the absence of ^{13}C-ribose-5P (M+5, five ^{13}C-labelled carbons) (**Figure 55A**). In addition, total content of ribose-5P was measured, and accordingly, it was prominently decreased in the KO cells (**Figure 55B**).

Taken together, our data suggest that CD98hc KO cells fail to synthesise the proper nucleotide pool as a result of reduced ribose-5P content, which is possibly attributable to the decrease in the PPP flux.

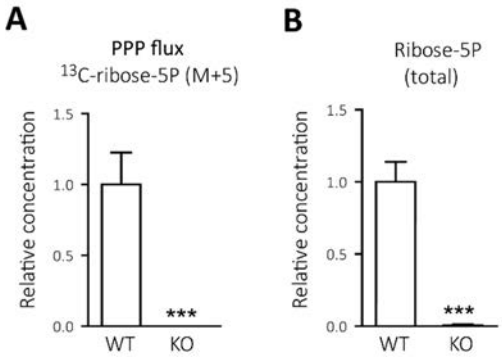

Figure 55. The pentose phosphate pathway flux is abrogated in CD98hc KO cells. A, the PPP flux was analysed by stable isotope tracer-based metabolomics in WT and CD98 KO cells. Cells were cultured with 5 mM uniformly labelled [U-^{13}C6]-glucose for 16 h. Ribose-5P with five ^{13}C carbons (M+5) was compared between WT and CD98hc KO cells. n=5. **B**, total content of ribose-5P was compared between WT and CD98hc KO cells. n=5. Quantification data correspond to the mean ± SEM of the independent experiments (n) indicated for each graph normalized to WT cells. Statistical significance ***, $p \leq 0.001$ vs. WT cells was analysed using a Student's t-test.

We next examined whether low 6AA cells also undergo alterations in nucleotide metabolism. Interestingly, in this case we found that shortage of BCAA and AAA triggered a reduction only in the deoxynucleotides, which are the final building blocks for DNA synthesis (**Figure 56**).

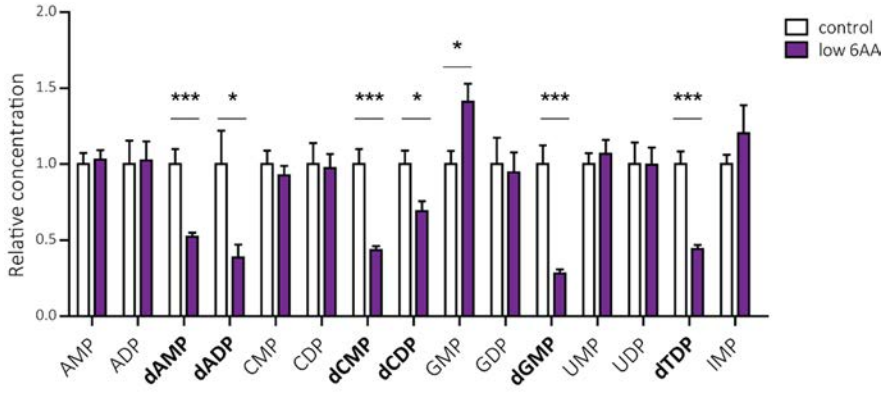

Figure 56. BCAA and AAA shortage triggers a reduction in the deoxynucleotide pool. Concentrations of nucleotides in control and low 6AA cells measured by a targeted metabolomics assay. Deoxynucleotides are depicted in bold letters. Quantification data correspond to the mean ± SEM of five independent experiments normalized to control cells. Statistical significance *, $p \leq 0.05$; ***, $p \leq 0.001$ vs. control cells was analysed using a Student's t-test.

This result suggested that low 6AA cells presented an impaired conversion of nucleotides to deoxynucleotides. The ribonucleotide reductase (RNR) is the only enzyme able to catalyse this rate-limiting step (Guarino, Salguero, and Kearsey 2014). Its activity is determined by levels of its ribonucleotide reductase regulatory subunit M2 (RRM2) (Nordlund and Reichard 2006). Protein levels of RRM2 were analysed and found to be strongly diminished in low 6AA compared to control cells (Figure 57)

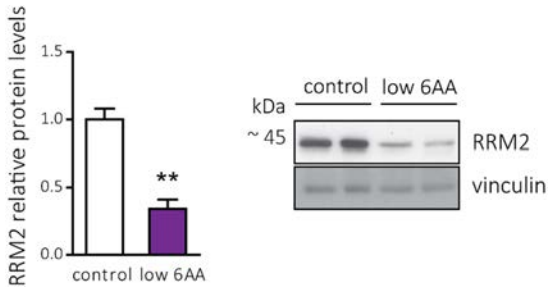

Figure 57. BCAA and AAA shortage leads to downregulated RRM2 expression. Comparison of RRM2 protein expression between control and low 6AA cells. Data are normalized by vinculin expression. Quantification data correspond to the mean ± SEM of four independent experiments normalized to control cells. Statistical significance **, $p \leq 0.01$ vs. control cells was analysed using a Student's t-test.

These results strongly indicate that the decrease in deoxynucleotide levels is caused by suppression of RRM2 expression in low 6AA cells. As expected, PPP activity was not affected in these cells as indicated by levels of ^{13}C-ribose-5P (M+5) (**Figure 58A**). Indeed, we found an increase in total levels this metabolite in low 6AA cells compared to control cells (**Figure 58B**).

The ability of the oncogenic protein c-myc to control DNA replication is well established (Aird et al. 2015; Dejure et al. 2017; Gao et al. 2009). Interestingly, c-myc enhances the biosynthesis of nucleotides by promoting the upregulation of the synthesis of deoxynucleotides through the upregulation of RRM2 (Mannava et al. 2008; Neretti et al. 2008). Thus, we hypothesized that low 6AA cells might suffer a reduction in c-myc expression levels. Protein levels of c-myc were analysed, and accordingly, low 6AA cells showed decreased c-myc protein levels compared to control cells (**Figure 59**).

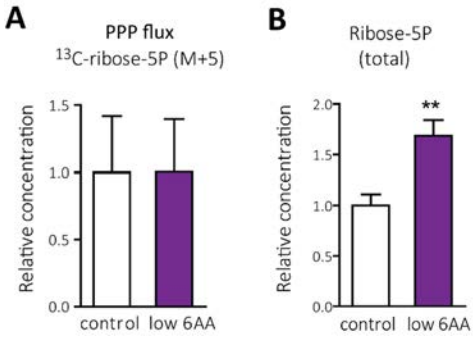

Figure 58. Pentose phosphate pathway flux is not affected in low 6AA cells. **A**, the PPP flux was analysed by stable isotope tracer-based metabolomics in control and low 6AA cells. Cells were cultured with 5 mM fully labelled [U-^{13}C6]-glucose for 16 h. Ribose-5P with five ^{13}C carbons (M+5) was compared between control and low 6AA cells. n=5. **B**, total content of ribose-5P was compared between control and low 6AA cells. n=5. Quantification data correspond to the mean ± SEM of the independent experiments (n) indicated for each graph normalized to WT cells. Statistical significance **, $p \leq 0.01$ vs. control cells was analysed using a Student's t-test.

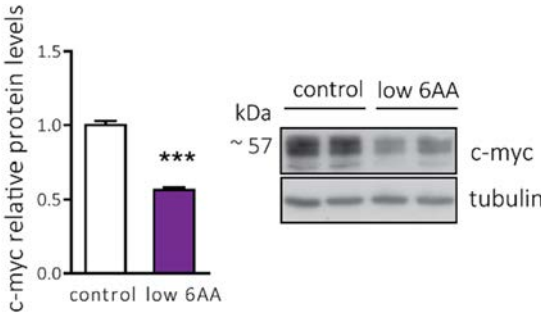

Figure 59. BCAA and AAA shortage leads to downregulated c-myc expression. Comparison of c-myc protein expression between control and low 6AA cells. Data are normalized by tubulin expression. Quantification data correspond to the mean ± SEM of three independent experiments normalized to control cells. Statistical significance ***, $p \leq 0.001$ vs. control cells was analysed using a Student's t-test.

Provided data suggested that c-myc downregulation may be a possible link between the shortage of BCAAs and AAAs and the altered expression of RRM2. In support of this idea, Csibi and co-workers demonstrated that mTORC1- S6K pathway, which is inhibited in low 6AA cells (**Figure 32**), is able to regulate c-myc translation (Csibi et al. 2014). In order to get a further insight into the role of mTORC1 pathway in c-myc regulation in this cellular model, c-myc expression was analysed after suppression of mTORC1 pathway in WT cells (**Figure 60**).

To this end, WT cells were treated with the widely used mTORC1 inhibitor rapamycin (Thoreen and Sabatini 2009). The marked decrease in the phosphorylated protein levels of S6 after rapamycin treatment served us as a control of the inhibition of the pathway in WT cells (**Figure 60**). We found that c-myc expression was also decreased in cells treated with rapamycin compared to non-treated cells (**Figure 60**). Interestingly, mTORC1 inhibition led to increased phosphorylation levels of the DDR marker CHK1 (**Figure 60**), indicating the presence of RS in these conditions.

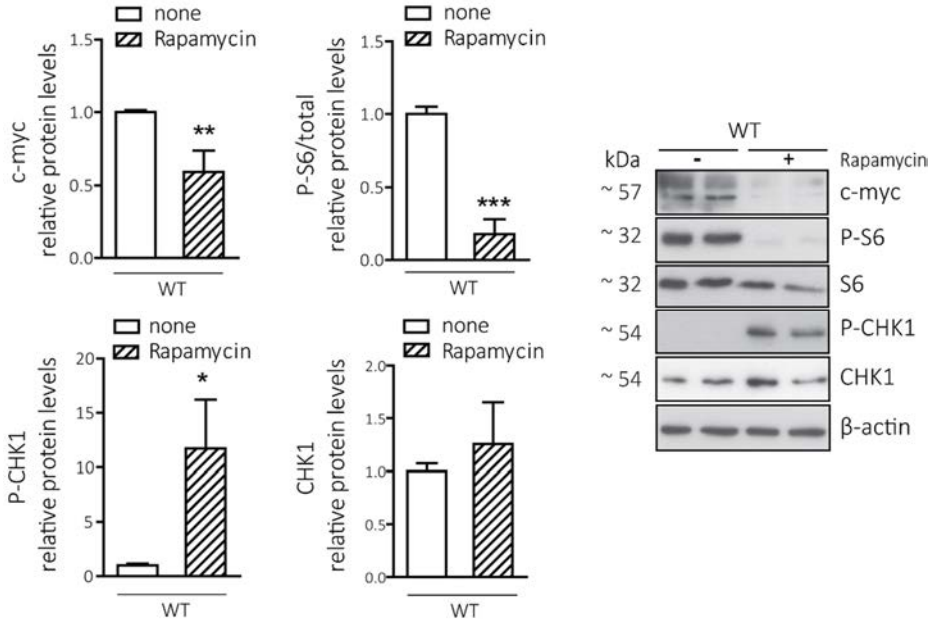

Figure 60. mTORC1 pathway inhibition leads to replicative stress and downregulated c-myc expression in WT cells. Comparison of c-myc, phosphorylated and total protein levels of CHK1 between treated and non-treated WT cells with rapamycin (2 μM 3h). Phosphorylated levels of S6 (P-S6) served as a control for mTORC1 pathway inhibition. Data are normalized by β-actin expression. Quantification data correspond to the mean ± SEM of three independent experiments normalized to non-treated WT cells. Statistical significance *, $p \leq 0.05$; **, $p \leq 0.01$; ***, $p \leq 0.001$ vs. non-treated WT cells was analysed a Student's t-test.

These results suggest that c-myc downregulation could be a possible connection between the shortage of BCAAs and AAAs, the downregulated RRM2 protein expression and the resulting RS.

In spite of the fact that CD98hc KO cells also presented c-myc downregulation (**Figure 61A**), we found no differences in RRM2 expression compared to WT cells (**Figure 61B**), reinforcing our assumption about the different mechanisms underlying the RS observed in CD98hc KO- and low 6AA- cellular models.

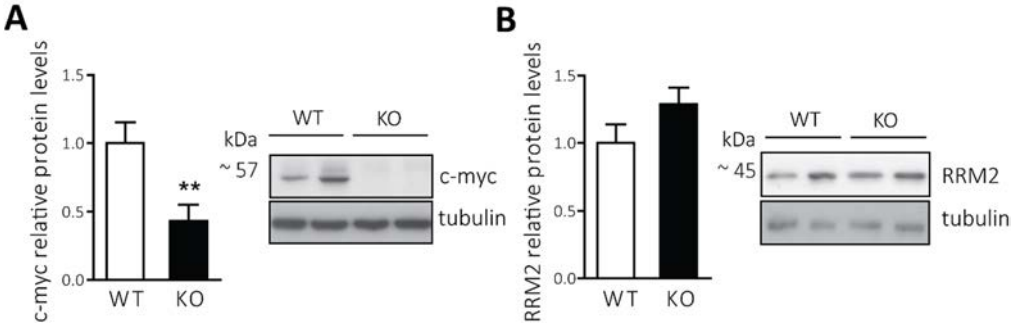

Figure 61. CD98hc ablation leads to downregulated c-myc expression with no alterations in RRM2 expression. **A**, comparison of c-myc protein expression between WT and CD98hc KO cells. Data are normalized by tubulin expression. (n=3). **B**, comparison of RRM2 protein expression between WT and CD98hc KO cells. Data are normalized by tubulin expression. n=3. Quantification data correspond to the mean ± SEM of the independent experiments (n) normalized to WT cells. Statistical significance **, $p \leq 0.01$ vs. WT cells was analysed using a Student's t-test.

4.2.6 Shortage of dNTPs underlies the replicative stress existing in CD98hc KO cells

We next sought to assess whether the decrease in nucleotides was responsible for the RS in CD98hc KO cells. To test this hypothesis, we examined whether exogenous supplementation of nucleosides could rescue S-phase delay in these cells. Hence, cell culture media was supplemented with the five (A, U, C, G and T) nucleosides, and cell cycle distribution was evaluated after 48 h of treatment. The percentage of cells that remained in the S fraction after nucleoside addition decreased from 66.6 ± 3.8 % to 57.8 ± 5.4 % in CD98hc KO cells (

Figure 62), whereas no differences were found in WT cells after the supplementation. This observation thus indicates that a shortage of nucleosides can pose a replication barrier that triggers the DDR in CD98hc KO cells

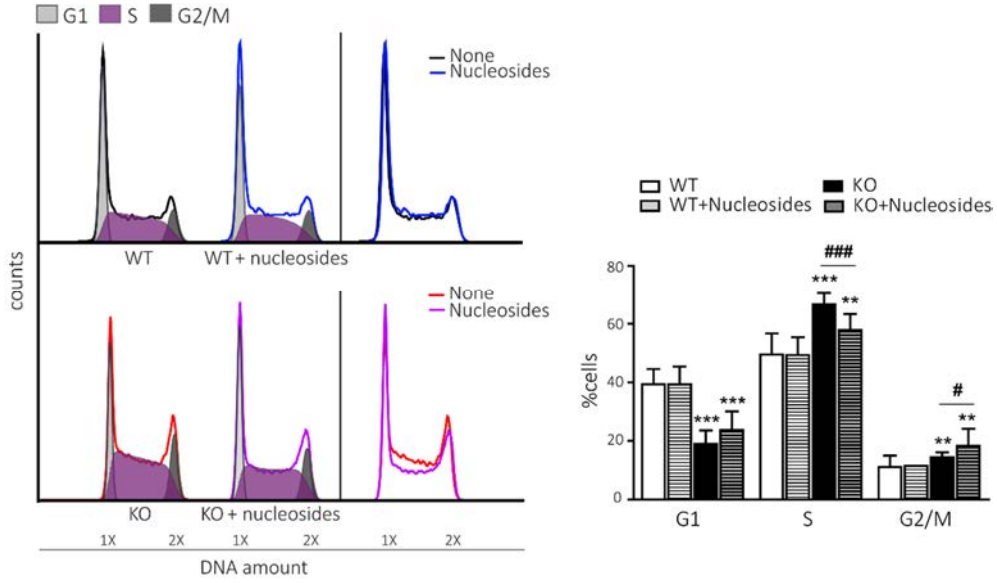

Figure 62. Nucleosides partially reverse S-phase delay in CD98hc KO cells. Cell cycle distribution was measured by flow cytometry using PI staining. A representative cell cycle profile of WT and CD98hc KO cells with no additives or in the presence of nucleosides (48 h) is shown, along with the overlap of their profiles (left panel). The graphical representation of cell cycle distribution shows the percentage of cells in G1-, S- and G2/M-phases (right panel). Quantification data correspond to the mean ± SEM of the four independent experiments. Statistical significance **, $p \leq 0.01$; ***, $p \leq 0.001$ vs. WT cells or #, $p \leq 0.05$; ###, $p \leq 0.001$ vs. KO cells was analysed using a Student's t-test.

To further corroborate our hypothesis, we next studied the effects of exogenous nucleosides on the activation of the DDR signalling pathway in CD98hc KO cells. The phosphorylation of CHK1 and RPA strongly decayed in CD98hc KO cells supplemented with exogenous nucleosides, compared to non-treated cells. In contrast, the total levels of the two proteins remained unchanged after supplementation (**Figure 63**).

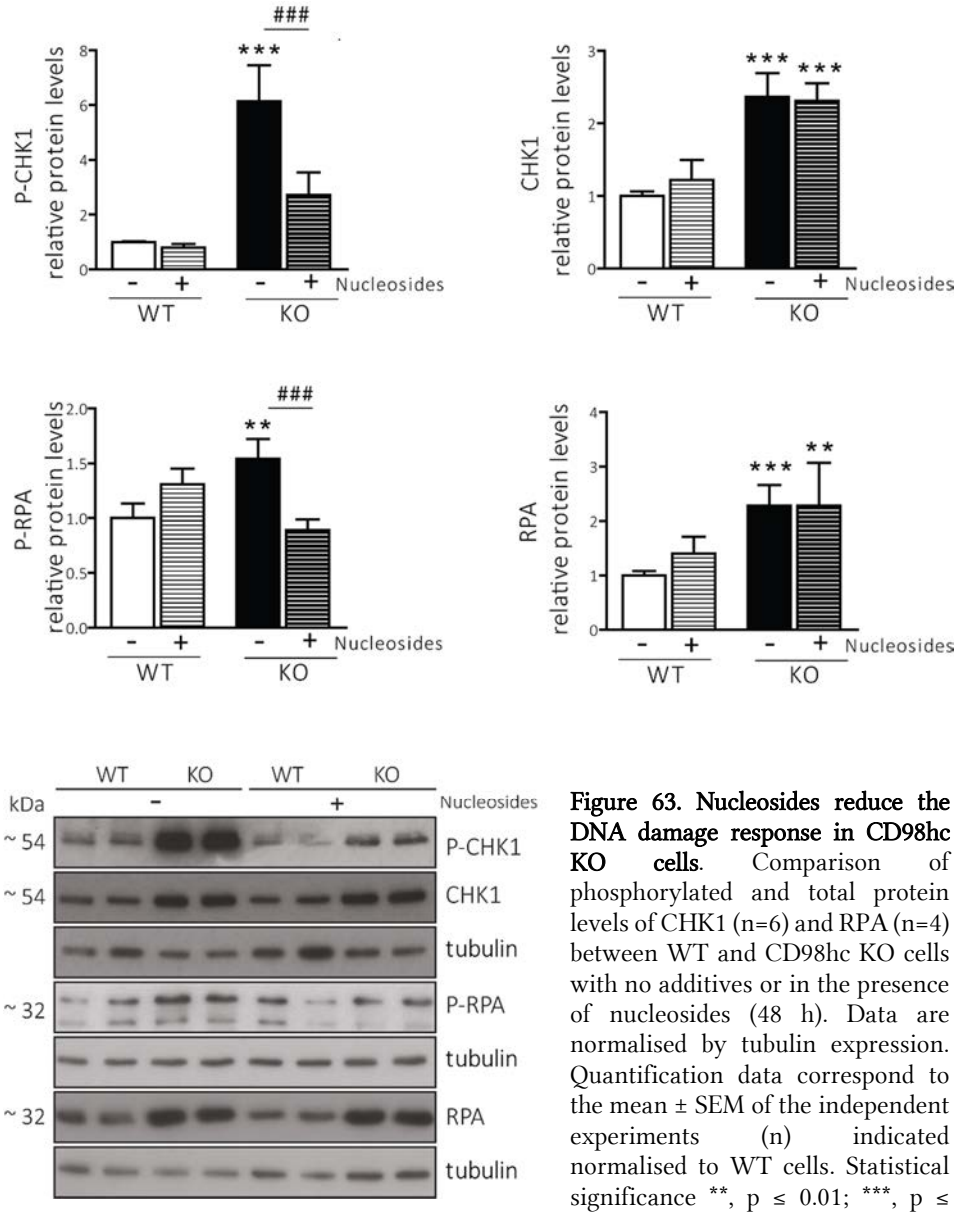

Figure 63. Nucleosides reduce the DNA damage response in CD98hc KO cells. Comparison of phosphorylated and total protein levels of CHK1 (n=6) and RPA (n=4) between WT and CD98hc KO cells with no additives or in the presence of nucleosides (48 h). Data are normalised by tubulin expression. Quantification data correspond to the mean ± SEM of the independent experiments (n) indicated normalised to WT cells. Statistical significance **, $p \leq 0.01$; ***, $p \leq 0.001$ vs. WT cells or ###, $p \leq 0.001$ vs. KO cells was analysed using a Student's t-test.

Finally, we examined the effects of nucleoside addition on progression through the cell division cycle. To this end, we used P-H3-labelling by immunofluorescence in order to select and quantify cells undergoing mitosis. Consistently with the whole

picture, the mitotic rate was significantly recovered in nucleoside supplemented-CD98hc KO cells (**Figure 64**).

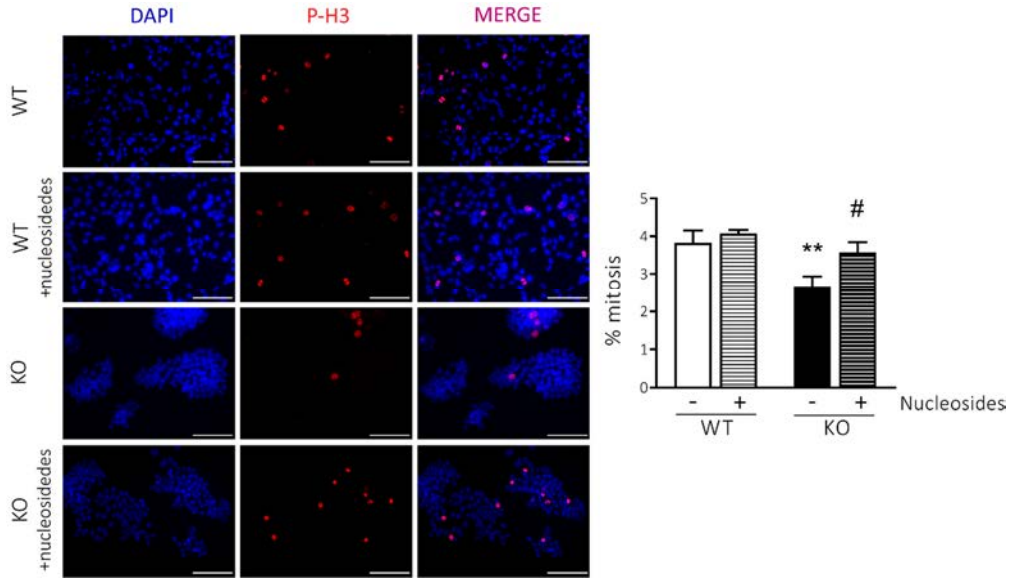

Figure 64. Nucleosides reverse mitotic rate in CD98hc KO cells. Comparison of mitotic rate between WT and CD98hc KO cells with no additives or in the presence of nucleosides (48 h) by immunofluorescence. The phosphorylation of Histone H3 (P-H3, red) was used as a marker for cells undergoing mitosis. DNA was stained with DAPI (blue). Representative images with around 200 nuclei are included (upper panel). Scale bar is 50 microns. Quantification of the percentage of mitotic cells is represented. More than 30,000 nuclei per condition from six independent experiments were analysed (lower panel). Statistical significance **, $p \leq 0.01$ vs. WT cells or #, $p \leq 0.05$ vs. KO cells was analysed using a Student's t-test.

The RS triggered by BCAA and AAA shortage in low 6AA cells was also related to a reduction in the nucleoside pool, since addition of exogenous nucleosides reversed the DDR response in these cells (**Figure 65**).

On the basis of our observations, we conclude that the shortage of nucleotides jeopardises faithful DNA replication in CD98hc KO cells, resulting in RS and cell cycle arrest. Moreover, BCAA and AAA deprivation causes a shortage of deoxynucleosides that also triggers RS in low 6AA cells.

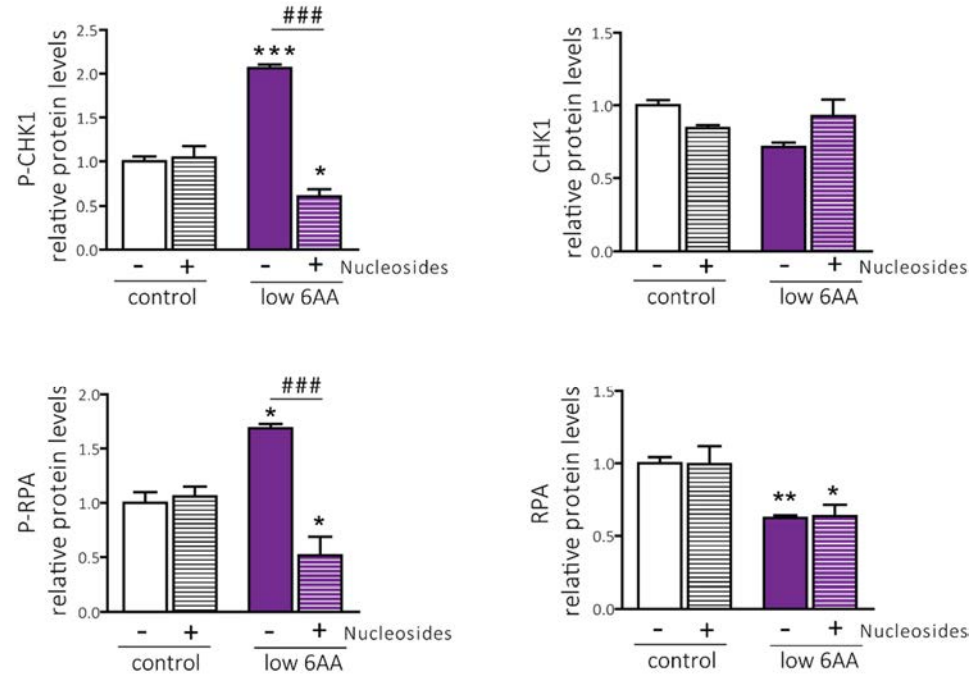

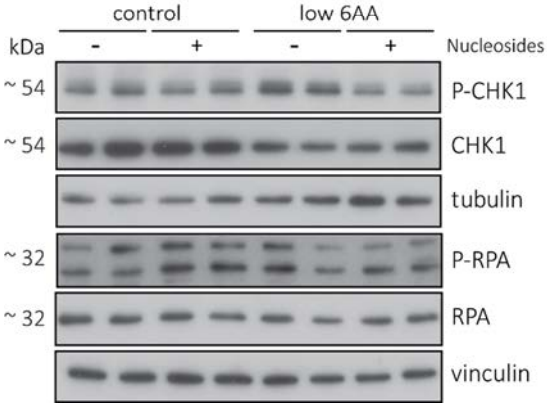

Figure 65. Nucleosides reverse the replicative stress caused by BCAA and AAA deprivation in low 6AA cells. Comparison of phosphorylated and total protein levels of CHK1 and RPA between control and low 6AA cells with no additives (n≥6) or in the presence of nucleosides (48 h) (n=4). Data are normalised by tubulin or vinculin expression. Quantification data correspond to the mean ± SEM of the independent experiments (n) indicated normalised to control cells. Statistical significance *, $p \leq 0.05$; **, $p \leq 0.01$; ***, $p \leq 0.001$ vs. control cells or ###, $p \leq 0.001$ vs. low 6AA cells was analysed using a Student's t-test.

4.3 CD98hc sustains the cellular energy metabolism

Based on the data shown in previous sections, we conclude that the mechanism by which the lack of CD98hc promotes the decrease in the nucleotide levels is unlikely to be determined exclusively by the shortage of BCAAs and AAAs, since low 6AA cells did not present altered PPP activity and showed a reduction only in the deoxynucleotide pool. Given these observations, we hypothesised that alterations in glucose metabolism may also underlie the abrogated PPP flux in CD98hc KO cells.

4.3.1 Ablation of CD98hc leads to downregulated GLUT1 transporter decreasing glucose uptake

Most mammalian cells depend on a continuous supply of glucose and therefore, the activity of the glucose metabolic pathways is tightly regulated. After uptake, glucose is broken down to extract energy through the glycolysis pathway and also shunts to fuel the PPP supplying the 5-carbon sugars and NADPH production (Alberts et al. 2002). Glucose uptake in mammalian cells is mainly mediated by GLUT transporter family members (Mueckler and Thorens 2013) and as described in the introduction, CD98hc is able to stabilise GLUT1 transporter, thereby increasing glucose transport activity in cells (Ohno et al., 2011).

In order to corroborate this statement in our CD98hc KO model, GLUT1 protein levels were analysed in WT and CD98hc KO cell membranes. Supporting the previous reported results, the expression of GLUT1 was strongly diminished in CD98hc KO compared to WT cells (**Figure 66A**)

Next, we used the transcriptome analysis performed in WT and CD98hc KO cells in order to know whether any other GLUT isoform was overcoming the downregulation of GLUT1. We found that the expression of the GLUT isoforms 1, 3 and 4 was increased in CD98hc KO cells when compared to WT cells (FCs= 1.8, 233 and 2.9, respectively; p-val<0.001; **GEO accession code: GSE126781**). Strikingly, we discovered that GLUT3 was the most differentially expressed gene

in the transcriptome. Accordingly, protein (**Figure 66A**) and mRNA (**Figure 66B**) levels were highly upregulated in CD98hc KO cells in comparison to WT cells.

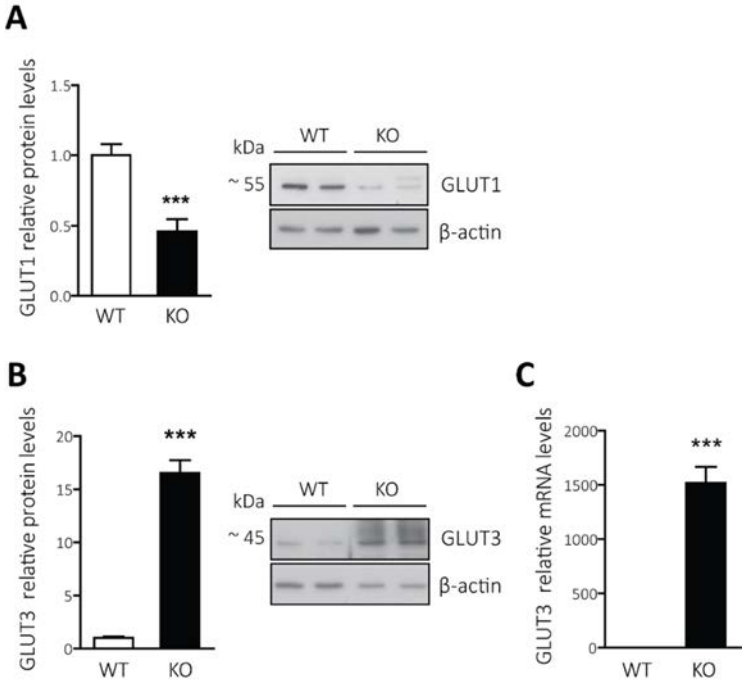

Figure 66. CD98hc ablation leads to repressed GLUT1- and upregulated GLUT3-expression levels. **A**, comparison of GLUT1 protein expression in total membranes between WT and CD98hc KO cells. n=4. Data are normalized by β-actin expression. **B**, comparison of GLUT3 protein expression in total membranes between WT and CD98hc KO cells. Data are normalized by β-actin expression. n=4. **C**, comparison of GLUT3 mRNA expression between WT and CD98hc KO cells. n=3. Quantification data correspond to the mean ± SEM of the indicated (n) independent experiments normalized to WT cells. Statistical significance ***, $p \leq 0.001$ vs. WT cells was analysed using a Student's t-test.

Then, we investigated whether the observed alterations in the expression of GLUTs had an impact in the glucose uptake by using the fluorescent substrate 2-(N-(7-nitrobenz-2-oxa-1,3-diazol-4-yl)amino)-2-deoxyglucose (2-NBDG). 2-NBDG is a deoxyglucose analogue that can be taken up by cells through GLUTs, but nevertheless, it cannot be metabolise and thus, it accumulates inside the cells (Yoshioka et al. 1996). Interestingly, we found that glucose uptake was reduced in CD98hc KO cells when compared to WT cells (**Figure 67**), suggesting that GLUT3

overexpression was not enough to supplement GLUT1 downregulation in CD98hc KO cells.

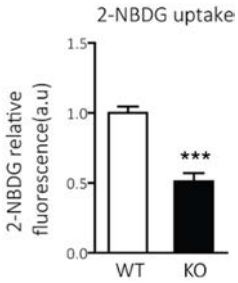

Figure 67. Ablation of CD98hc leads to reduced glucose uptake. Quantification of glucose uptake measured by flow cytometry by using the fluorescent glucose analogue 2-NBDG. Bars represent the mean 2-NBDG fluorescence in WT and CD98hc KO cells. a.u., arbitrary units. Quantification data correspond to the mean ± SEM of four independent experiments normalized to WT cells. Statistical significance ***, $p \leq 0.001$ vs. WT cells was analysed using a Student's t-test.

4.3.2 CD98hc deficiency represses glycolysis

To further examine the metabolic impact of CD98hc depletion in glucose metabolism, uniformly-labelled [U^{13}C6]-glucose metabolic tracer analysis was conducted in order to determine the contribution of glucose to intermediary metabolism in CD98hc KO and WT cells. Thus, cells were cultured in the presence of [U-^{13}C6]-glucose for 16 h and next, the incorporation of ^{13}C-glucose into different intermediates of the glycolytic pathway was monitored using gas chromatography-coupled to mass spectrometry (GC-MS).

First, the content of the three BCAA (valine, isoleucine and leucine) and the AAA tryptophan was checked. As expected, CD98hc KO cells culture media presented an increased BCAA and AAA content (**Figure 68, upper panel**) while the intracellular levels of these AA were reduced (**Figure 68, lower panel**). These results are reflective of the limited transport and eventually metabolization of these AA by CD98hc KO cells (**Figure 18**).

Moreover, CD98hc KO cells culture media presented more ^{13}C-glucose and non-labelled-glucose than the WT cells culture media after the 16 h of incubation (**Figure 69**), thereby implying a lower glucose uptake by cells lacking CD98hc, corroborating our previous result (**Figure 67**).

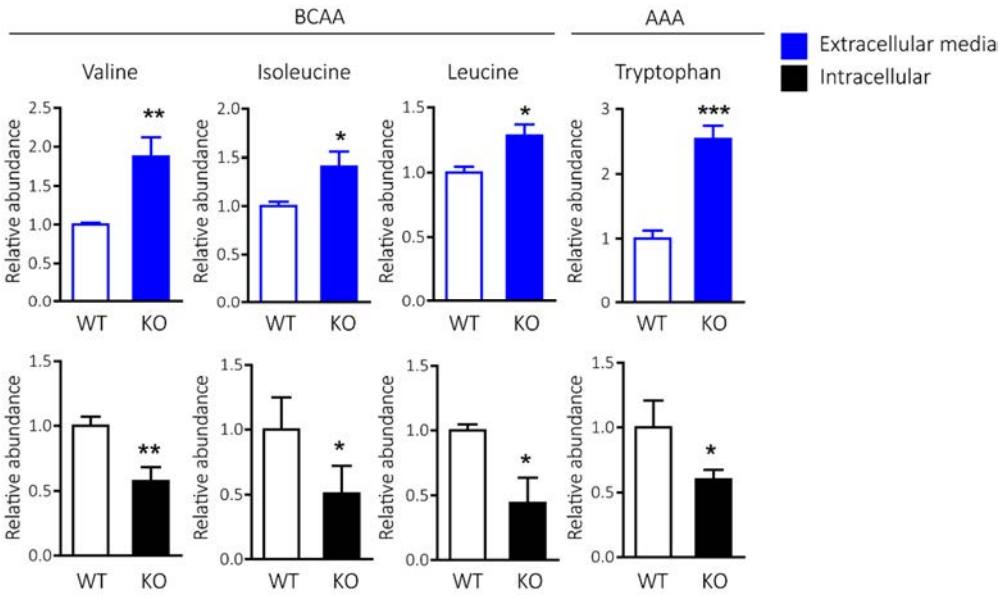

Figure 68. BCAA and AAA are less incorporated by CD98hc KO cells. Comparison of the content of the indicated AAs in WT and CD98hc KO cells and in their extracellular media. Quantification data correspond to the mean ± SEM of five independent experiments normalized to WT cells. Statistical significance *, $p \leq 0.05$; **, $p \leq 0.01$; ***, $p \leq 0.001$ vs. WT cells was analysed using a Student's t-test.

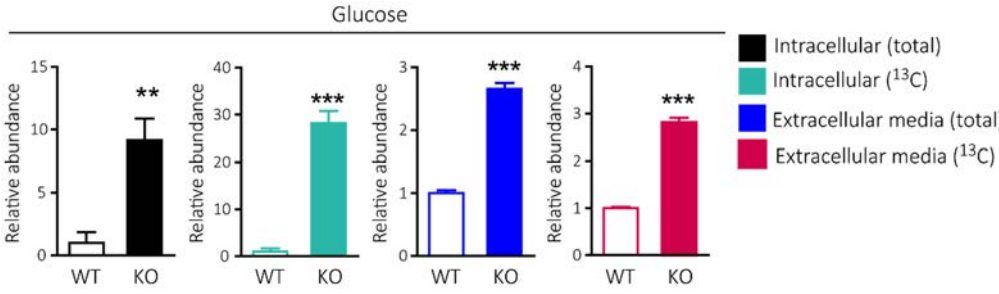

Figure 69. CD98hc KO cells are consuming less glucose than WT cells. Comparison of the abundance of the ^{13}C-glucose and non-labelled-glucose (total) between CD98hc KO and WT cells and in their respective culture media. Quantification data correspond to the mean ± SEM of five independent experiments normalized to WT cells. Statistical significance **, $p \leq 0.01$; ***, $p \leq 0.001$ vs. WT cells was analysed using a Student's t-test.

However, despite the lower transport of ^{13}C-glucose by CD98hc KO cells, the intracellular content of both non-labelled- and ^{13}C-glucose (M+6, six ^{13}C-labelled carbons) were highly increased in these cells compared to WT cells (**Figure 69**).

This outcome indicates that, beside decreased glucose uptake, glucose is being accumulated in CD98hc KO cells.

Once inside the cell, ^{13}C-glucose is phosphorylated to ^{13}C-glucose-6P, which can continue through the glycolytic pathway, producing other intermediates that are all uniformly labelled as shown in **Figure 70**.

When analyzing glycolysis metabolites, no statistically significant differences were found in the abundance of M+6 isotopologues of ^{13}C-glucose-6P and ^{13}C-fructose-6P and neither in the M+3 (three ^{13}C-labelled carbons) ^{13}C-dihydroxyacetone between WT and CD98hc KO cells, in parallel with a similar total content of them (**Figure 70**). However, the abundance of M+3 isotopologues of ^{13}C-3P-glycerate, ^{13}C-pyruvate and ^{13}C-lactate were notably decreased in cells lacking CD98hc compared to WT cells (**Figure 70**). In keeping with these observations, the content of unlabelled glyceraldehyde-3P and lactate were also diminished in the former cells (**Figure 70**). Although less incorporation of ^{13}C-glucose into ^{13}C-pyruvate was detected in CD98hc KO cells, no changes were found regarding total levels of this metabolite, suggesting another alternative source for its production (e.g., from extracellular 1 mM pyruvate) (**Figure 70**).

In all, our previous observations indicated that the glycolytic flux was notably impaired in CD98hc KO cells when compared to WT cells. The defective glycolytic capacity of these cells was unlikely to be as a consequence of the downregulation of the implicated enzymes, since the expression of hexokinase (HK), phosphofructokinase (PFK) and pyruvate kinase (PK), which catalyse the three key rate-limiting steps in glycolysis (X. Li, Gu, and Zhou 2015), were found to be increased in the data collected from the transcriptome analysis performed in CD98hc KO and WT cells (FCs= 3.5, 2.1 and 2.8, respectively, p-val<0.001; **GEO accession code: GSE126781**).

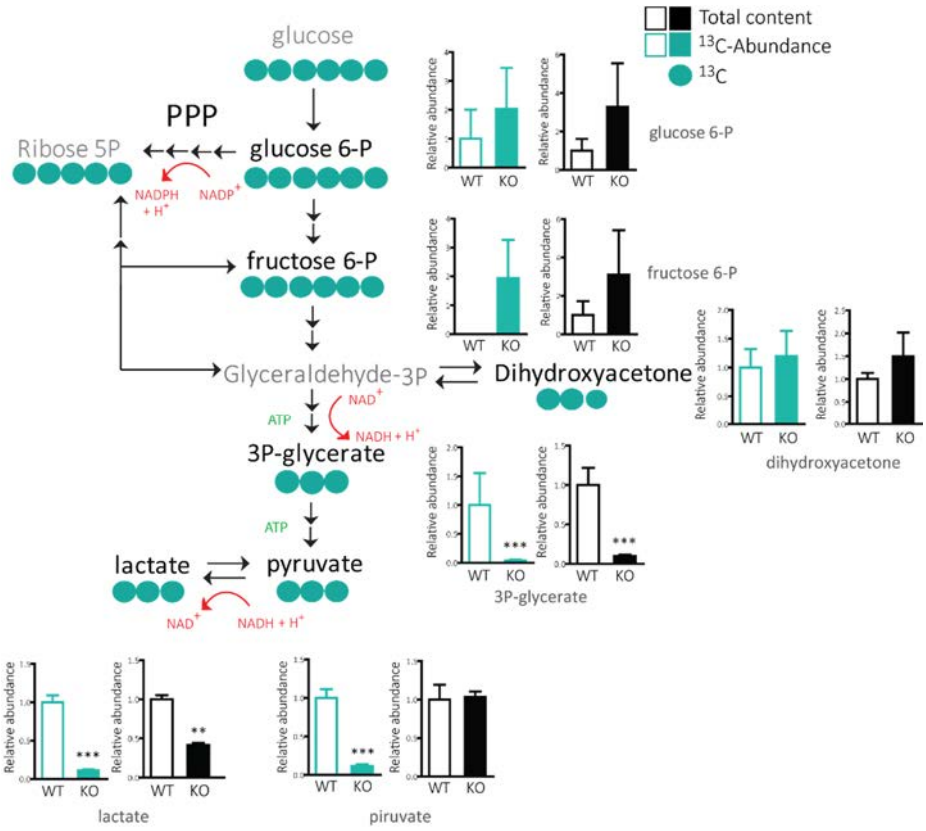

Figure 70. CD98hc KO cells present repressed glycolysis. Schematic diagram of ^{13}C glucose tracer labelling. Comparison of the abundance of the ^{13}C-isotopologues of all carbon atoms in the indicated compounds and total content of the indicated intermediates in CD98hc KO and WT cells. Intermediates depicted in grey are not analysed in this figure. Each reaction is represented by a single arrow. Quantification data correspond to the mean ± SEM of five independent experiments normalized to WT cells. Statistical significance **, $p \leq 0.01$; ***, $p \leq 0.001$ vs. WT cells was analysed using a Student's t-test.

^{13}C-pyruvate resulting from glycolysis can produce ^{13}C-lactate or alternatively enter into the TCA cycle via acetyl-CoA. This entry of ^{13}C-labelled acetyl-CoA results in two ^{13}C carbons (M+2; two ^{13}C-labelled carbons) in all metabolites in the first TCA cycle (**Figure 71**).

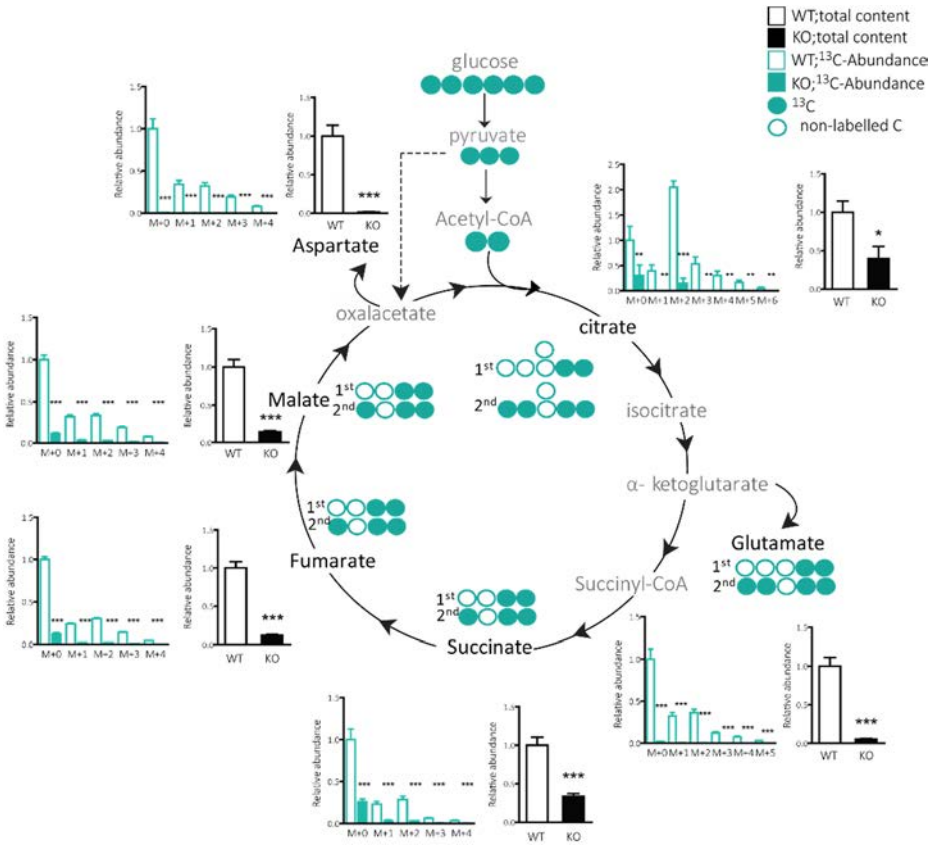

Figure 71. CD98hc KO cells show a reduction in TCA intermediaries. Schematic diagram of ^{13}C glucose tracer labelling in the TCA cycle. 1st and 2nd represent the ^{13}C-labelling after one and two TCA cycles via acetyl-CoA. Comparison of mass isotopomer distribution in CD98hc KO and WT cells. Intermediates depicted in grey are not analysed in this figure. Quantification data correspond to the mean ± SEM of five independent experiments normalized to WT cells. Statistical significance *, $p \leq 0.05$; **, $p \leq 0.01$; ***, $p \leq 0.001$ vs. WT cells was analysed using a Student's t-test.

After the first turn, the resultant ^{13}C-oxalacetate (M+2) can again condensate with ^{13}C-acetyl-CoA resulting in ^{13}C-citrate (M+4; four ^{13}C-labelled carbons), which continues with the cycle. In addition, ^{13}C-pyruvate can yield ^{13}C-oxalacetate via pyruvate carboxylase route, generating additional possibilities of ^{13}C-labelled carbons (M+X; in any number of the carbons of the considered metabolites) in the different TCA metabolites (**Figure 71**).

The incorporation of ^{13}C-glucose into the different isotopologues (M+X) of the TCA intermediates ^{13}C-citrate, ^{13}C-succinate, ^{13}C-fumarate, and ^{13}C-malate were

markedly reduced in CD98hc KO cells. Same results were obtained regarding the content of the same non-labelled metabolites (**Figure 71**). Notably, a five-fold decrease in ^{13}C-citrate (M+2) was observed in CD98hc KO cells compared to WT cells, indicating that there was less citrate generated from pyruvate in the former cells.

These data suggest that the abundance of the TCA cycle intermediaries is reduced in CD98hc KO cells. In addition, glucose is less incorporated in the TCA cycle compared to WT cells.

In order to evaluate the involvement of the BCAA and AAA shortage in CD98hc KO cells (**Figure 18**) in the observed alterations regarding glucose metabolism, low 6AA cells were cultured in the presence of [U-^{13}C6]-glucose for 16 h and the incorporation of ^{13}C-glucose into the different isotopologues (M+X) was examined (**Figure 72**).

No differences were found in total- and ^{13}C-glucose levels in low 6AA cells compared to control cells, suggesting that, in contrast to CD98hc KO cells, glucose is not being accumulated in low 6AA cells (**Figure 72**).

Remarkably, in sharp contrast to CD98hc KO cells, there was an increase in the incorporation of ^{13}C-glucose into ^{13}C-dihydroxyacetone (M+3) and ^{13}C-3P-glycerate and moreover, the content of the glycolytic intermediaries glucose-6P, fructose-6P, dihydroxyacetone and 3P-glycerate was also increased. However, no differences were found neither in the ^{13}C-glucose incorporation into pyruvate and lactate, nor in their total content of these metabolites (**Figure 72**). These data suggest that low 6AA cells present enhanced glycolytic flux.

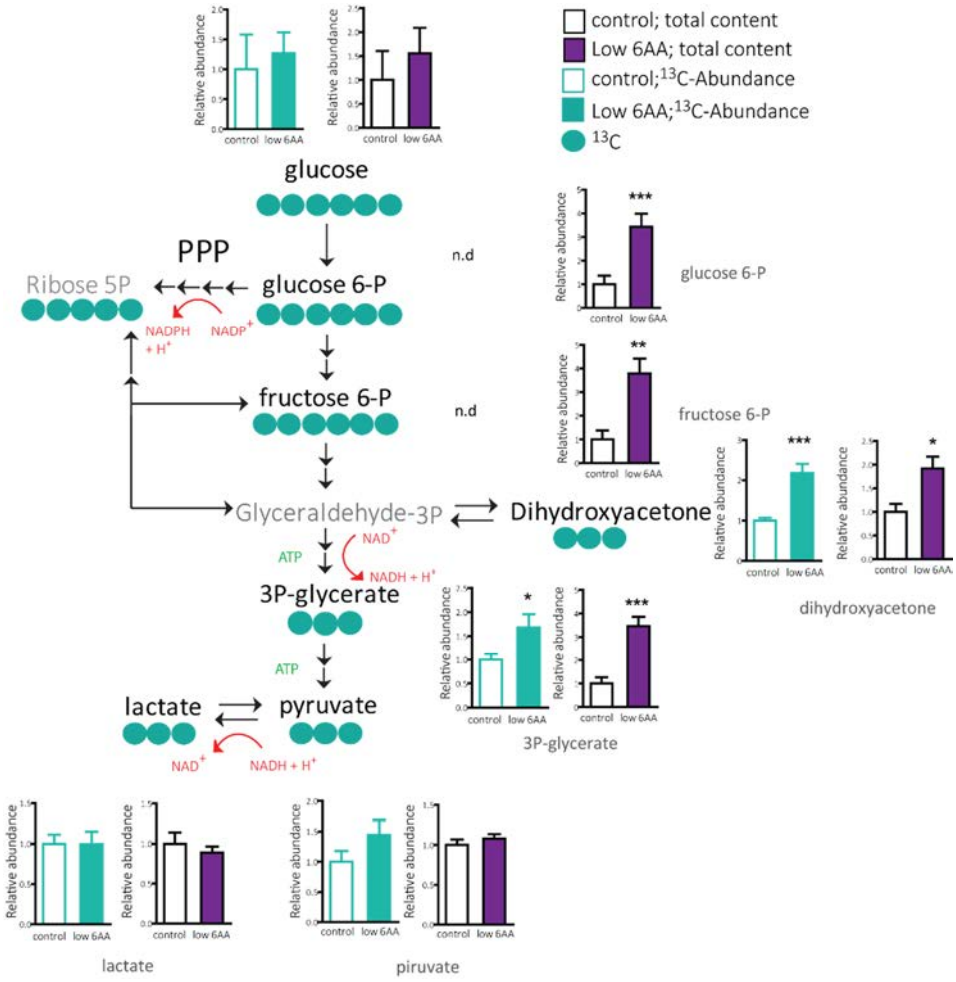

Figure 72. Low 6AA cells enhanced glycolysis. Schematic diagram of ^{13}C glucose tracer labelling. Comparison of the abundance of the ^{13}C-isotopologues and total content of the indicated intermediates in low 6AA and control cells. Intermediates depicted in grey are not analysed in this figure. Each reaction is represented by a single arrow. n.d., not detected. Quantification data correspond to the mean ± SEM of five independent experiments normalized to control cells. Statistical significance *, $p \leq 0.05$; **, $p \leq 0.01$; ***, $p \leq 0.001$ vs. control cells was analysed using a Student's t-test.

The isotopic labelling of the TCA intermediates was similar to that observed in control cells with the exception of citrate, whose abundance and the content of its different ^{13}C-isotopologues (M+X) were higher in low 6AA cells compared to control cells (**Figure 73**).

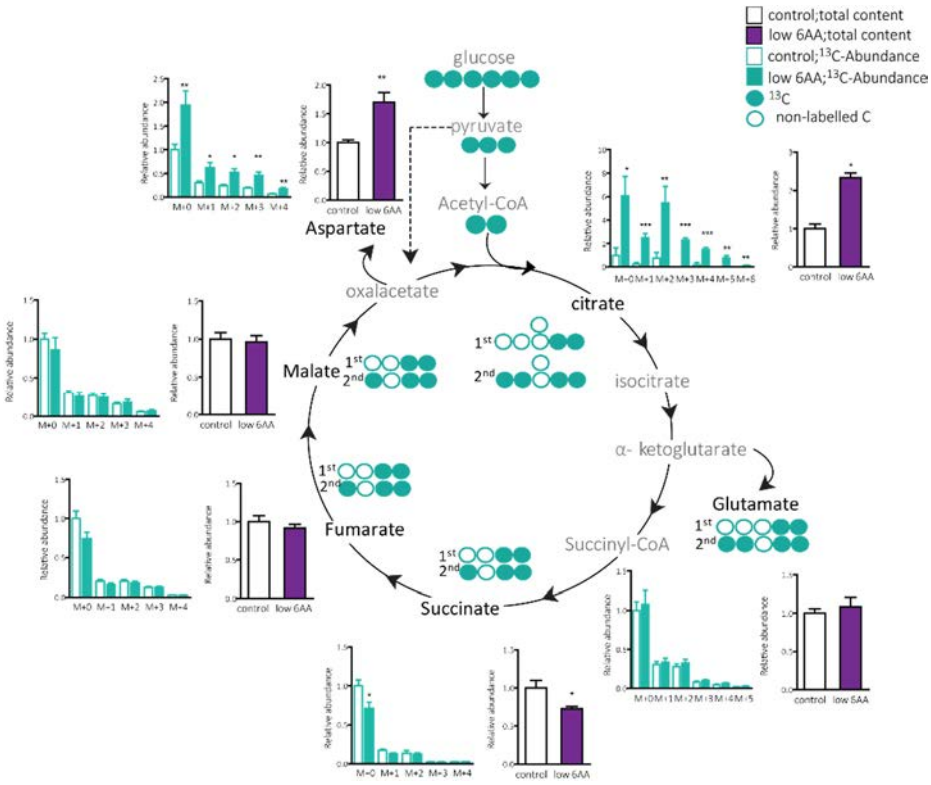

Figure 73. BCAA and AAA shortage increases conversion of pyruvate into citrate. Schematic diagram of ^{13}C glucose tracer labelling in the TCA cycle. 1st and 2nd represent the ^{13}C-labelling after one and two TCA cycles via acetyl-CoA. Comparison of mass isotopomer distribution in low 6AA and control cells. Intermediates depicted in grey are not analysed in this figure. Quantification data correspond to the mean ± SEM of five independent experiments normalized to WT cells. Statistical significance *, $p \leq 0.05$; **, $p \leq 0.01$; ***, $p \leq 0.001$ vs. control cells was analysed using a Student's t-test.

This result suggested that shortage of BCAA and AAA led to increased conversion of pyruvate into citrate, which was being accumulated in low 6AA cells. Probably this was a consequence of the deprivation of BCAAs and AAAs, which are known to regulate lipid metabolism (Du et al. 2012; Feller 2010; Zhang et al. 2017), and when limiting, lipogenesis results impaired (Du et al. 2012; Guo and Cavener 2007). The synthesis of *de novo* fatty acids and cholesterol starts with citrate in the cytosol which is converted to acetyl-coA. Then, fatty acid synthetase (FAS), the main biosynthetic enzyme in this pathway, catalyses the formation of fatty acids (Berg et al. 2002). The mRNA abundance of this lipogenic enzyme was downregulated in

low 6AA cells (**Figure 74A**). Since the transcription of this gene, and others related to fatty acid synthesis and cholesterol, is under the control of the transcription factors sterol regulatory element binding proteins (SREBPs) (Berg et al. 2002), we next determined the expression of SREBP1c and SREBP2. Consistently, the mRNA expression of these transcription factors was significantly downregulated (**Figure 74B**), pointing to a possible inhibition of lipid synthesis in low 6AA cells. In agreement with these findings, other studies have demonstrated the role of BCAA availability in the control of the expression of these lipogenic genes through the mTORC1 pathway (Bai et al. 2015; Guo and Cavener 2007; Kasuga et al. 2011).

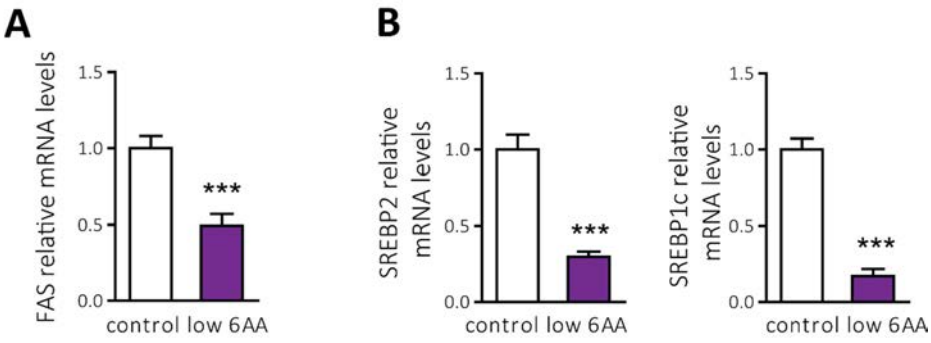

Figure 74. BCAA and AAA shortage trigger a decrease in the expression of lipogenic genes. **A**, comparison of FAS mRNA expression between control and low 6AA cells. n=3. **B**, comparison of SREBP2 and SREBP1c mRNA expression between control and low 6AA cells. n=3. Quantification data correspond to the mean ± SEM of the independent experiments (n) indicated for each graph normalized to control cells. Statistical significance ***, $p \leq 0.001$ vs. control cells was analysed using a Student's t-test.

Moreover, the decrease found in the total succinate levels in low 6AA cells (**Figure 73**) is likely reflective of the lower incorporation of BCAAs and AAAs via anaplerosis into the TCA cycle (Lieberman, Marks, and Peet 2013; Stančíková and Rovenský 2015).

The increased abundance of aspartate in low 6AA cells, paralleled with an augment in its different ^{13}C-isotopologues (M+X), may be reflective of its accumulation due to the defective cell proliferation of these cells and their likely reduced *de novo* nucleotide biosynthesis (Ahn and Metallo 2015).

Collectively, these data suggest that low 6AA were adapted to limited BCAA and AAA availability at the expense of higher glycolysis rate. However, this is not a plausible alternative for cells lacking CD98hc, since they not only present AA availability impairment, but also defective glucose metabolism. In this regard, besides the CD98hc-GLUT1 interplay, CD98hc may also regulate glucose metabolism via direct interaction with CD147 (Marchiq et al. 2015; Xu and Hemler 2005)

4.3.3 CD98hc ablation triggers the downregulation of the expression of both CD147 and MCT1 proteins

Xu and Hemler identified the metabolic super-complex MCT-CD147-CD98hc-LAT1 (Xu and Hemler 2005). Even more interesting is their finding about the correlated expression of CD98hc and CD147 proteins (Xu and Hemler 2005), since it has been reported that ablation of CD147, the ancillary protein of the lactate transporters MCTs, results in repressed glycolysis (Marchiq et al. 2015).

However, the specificity of the light subunits associated to CD98hc in this protein cluster had not been established. To gain further insight into this aspect, the c-myc-tagged human light subunits LAT1, LAT2, asc1, y^+LAT1 and xCT were transfected using the cellular model HEK293T. Next, co-immunoprecipitation assays were performed pulling down the light chains (**Materials and Methods, Figure 100**). Assuming that both CD98hc and the corresponding light chain are always together in the plasma membrane, data were corrected by the co-immunoprecipitated CD98hc protein. As shown in Figure 75, LAT1 was the light subunit that strongly immunoprecipitated CD147 and MCT1 proteins, corroborating that CD98hc-LAT1 is the transporter that mainly interacts with the complex.

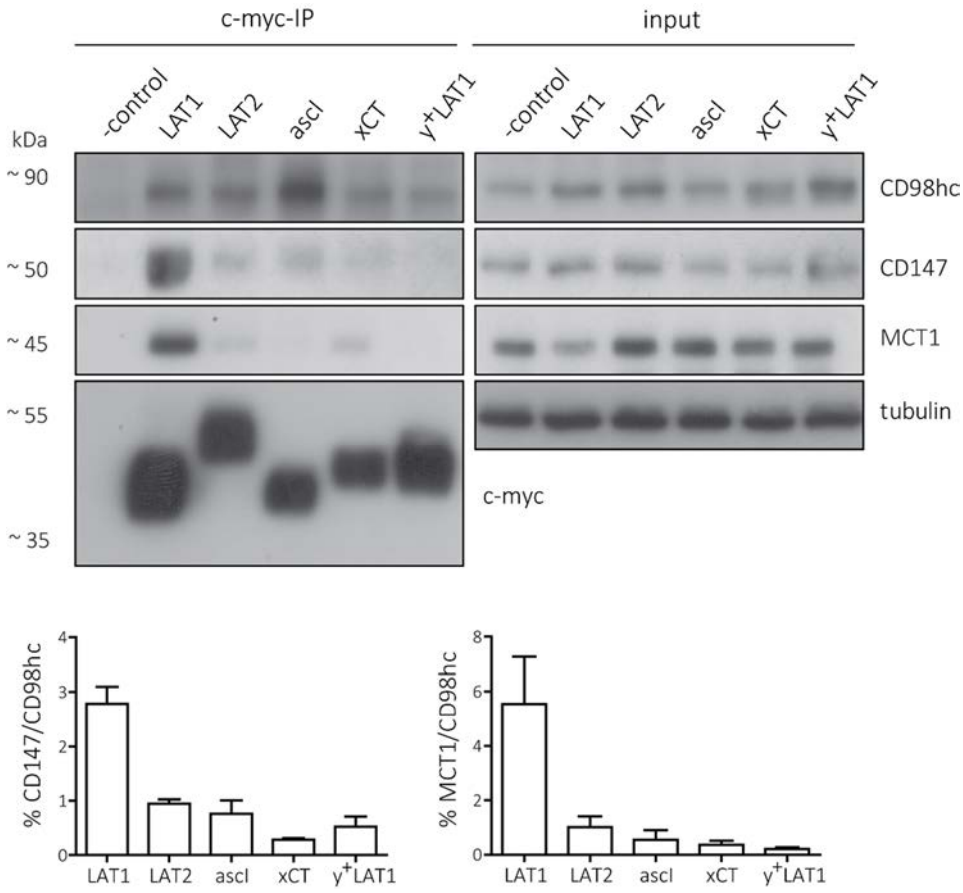

Figure 75. CD98hc-LAT1-CD147-MCT1 co-immunoprecipitate together. Co-immunoprecipitation (Co-IP) assay showing interaction between LAT1 and CD98hc, CD147 and MCT1. HEK293T cells were transfected with the indicated c-myc-tagged light chains and the co-IP was performed using anti-c-myc agarose. Note that light chains (~50 kDa) are highly hydrophobic and not glycosylated proteins, which results in anomalously high mobility in SDS-PAGE (35–40 kDa). Data are corrected by the co-immunoprecipitated CD98hc. Quantification data correspond to the mean ± SEM of the three independent experiments.

In order to analyse whether the downregulation of CD147, which in turn regulates de expression of MCT1 (Walters, Arendt, and Jelinek 2013), plays a role in the evidenced impaired glucose metabolism in CD98hc KO cells, expression of both proteins was analysed. Consistent with previous reported results, the expression of both CD147 and MCT1 proteins was markedly reduced in CD98hc KO cells compared to WT cells (**Figure 76**).

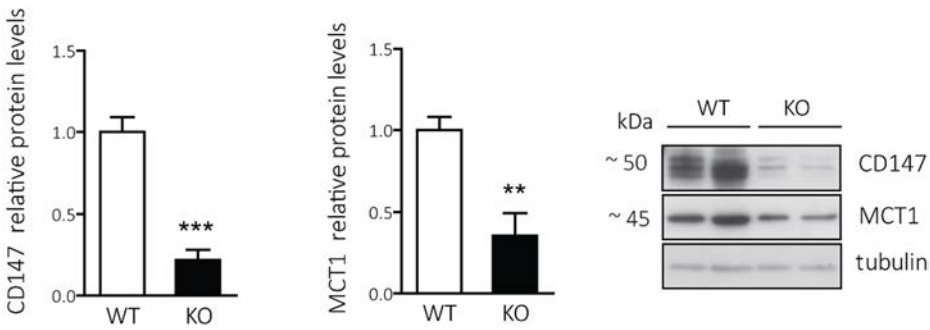

Figure 76. CD98hc ablation leads to downregulated CD147 and MCT1 expression. Comparison of CD147 and MCT1 protein expression between WT and CD98hc KO cells. Data are normalized by tubulin expression. Note that MCT1 is a 55 kDa protein that runs at ~45 kDa on SDS–PAGE. Quantification data correspond to the mean ± SEM of the three independent experiments normalized to WT cells. Statistical significance **, $p \leq 0.01$; ***, $p \leq 0.001$ vs. WT cells was analysed using a Student's t-test.

Both CD147 and MCT1 are overexpressed in cancer to support the Warburg effect (Huang et al. 2015; Walters, Arendt, and Jelinek 2013). Disrupting lactate production and export represents a promising approach for antineoplastic therapeutic targeting, since it is one of the main cellular sources for regenerating the NAD^+ required for glycolysis (Doherty et al. 2013). It was already shown above (**Figure 70**) that the abundance of lactate is lower in cells lacking CD98hc compared to WT cells. In order to determine whether cells lacking CD98hc indeed transport less lactate to the extracellular media, the content of lactate was quantified in the media of CD98hc KO and WT cells. Accordingly to the lower expression of MCT1, the abundance of the M+3 isotopologue of ^{13}C-lactate and its total content were reduced in the extracellular media of CD98hc KO cells (**Figure 77**). However, despite the downregulation of MCT1, lactate is not being accumulated in CD98hc KO cells, which suggests that it is less produced.

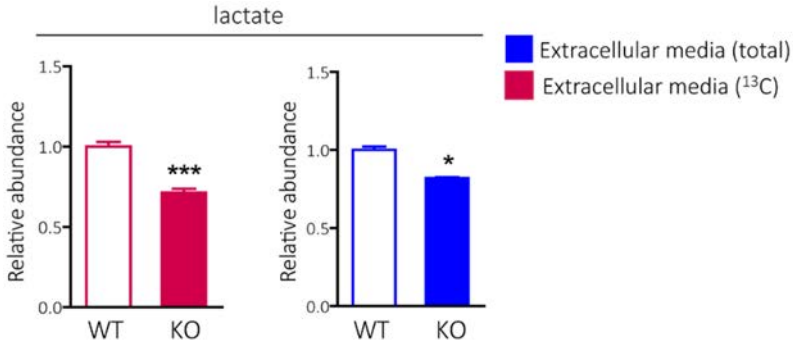

Figure 77. The lactate content in the extracellular media of CD98hc KO cells is lower than in the WT media. Comparison of the abundance of the ^{13}C-lactate (M+3) (left panel) and total content (right panel) in the extracellular media of CD98hc KO and WT cells. Quantification data correspond to the mean ± SEM of five independent experiments normalized to WT cells. Statistical significance*, p≤ 0.05; ***, p ≤ 0.001 vs. WT cells was analysed using a Student's t-test.

The enzyme lactate dehydrogenase (LDH) catalyses the bidirectional conversion of pyruvate and lactate with concomitant oxidation-reduction of the cofactor NAD^+/NADH (**Figure 78A**). LDH is a tetramer composed of two different subunits, LDHA and LDHB, which can assemble into different combinations (Doherty and Cleveland 2013). It is interesting to note that LDHA has a higher affinity for pyruvate and a higher V_{max} for pyruvate reduction than LDHB. By contrast, LDHB is thought to convert lactate to pyruvate, thereby performing the "reverse Warburg effect", allowing cells to use lactate as a nutrient source for oxidative metabolism (Doherty & Cleveland, 2013; Ždralević et al., 2018). Remarkably, mRNA levels of LDHA were decreased in CD98hc KO cells compared to WT cells (**Figure 78B**), whereas in sharp contrast, LDHB expression resulted highly increased in cells lacking CD98hc (**Figure 78C**).

Altogether, these results point to a reduction in the conversion of pyruvate into lactate, which may impact in the regeneration of NAD^+ molecules, a key step required for glycolysis to proceed (Ždralević et al. 2018).

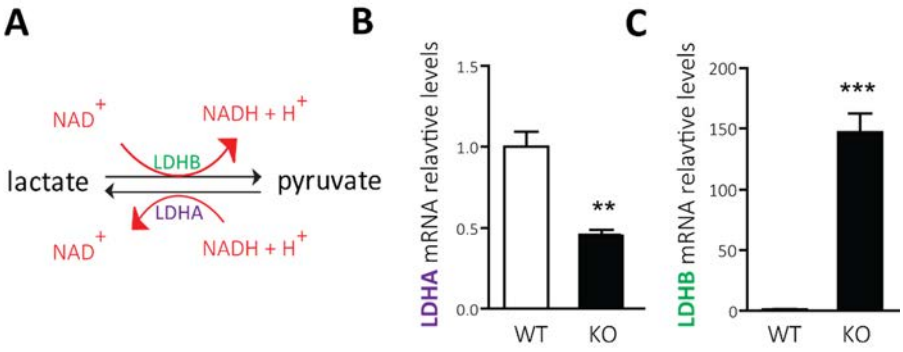

Figure 78. LDH isoforms are expressed differentially in cell lacking CD98hc. A, LDH catalyses the interconversion of pyruvate and lactate with concomitant interconversion of NADH and NAD^+. **B** and **C**, comparison of LDHA (**B**) and LDHB (**C**) mRNA expression between WT and CD98hc KO cells. Quantification data correspond to the mean ± SEM of three independent experiments normalized to WT cells. Statistical significance **, $p \leq 0.01$; ***, $p \leq 0.001$ vs. WT cells was analysed using a Student's t-test.

Several studies have shown that disruption of the anaerobic glycolysis, as a consequence of the inhibition of either the lactate transporters or the enzyme LDHA, results in a metabolic re-route to OXPHOS paralleled with a decrease in ATP levels and increased oxidative stress (Doherty et al. 2014; Fantin, St-Pierre, and Leder 2006; Gerlinger et al. 2012; Le et al. 2010).

In this regard, ATP levels were measured by a targeted metabolomics assay using LC-MS. In agreement with those studies, ATP levels were notably reduced in CD98hc KO cells when compared to WT cells (**Figure 79, left panel**). In addition, the AMP: ATP ratio, which is known to activate the AMP-activated protein kinase (AMPK), is increased in the former cells (**Figure 79, right panel**).

The previous reported "metabolic reprogramming" to OXPHOS in conditions of glycolysis disruption prompted us to investigate whether cells lacking CD98hc are able to survive at expense of a higher OXPHOS rate.

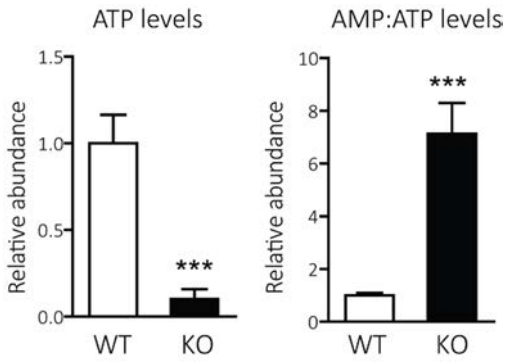

Figure 79. CD98hc KO cells show a decrease in ATP levels. Comparison of the content of ATP (left panel) and AMP:ATP ratio (right panel) in WT and CD98hc KO cells measured by a targeted metabolomics assay using LC-MS. Quantification data correspond to the mean ± SEM of five independent experiments normalized to WT cells. Statistical significance ***, $p \leq 0.001$ vs. WT cells was analysed using a Student's t-test.

4.3.4 CD98hc ablation leads cells to re-route to OXPHOS

In order to assess OXPHOS capacity, CD98hc KO and WT cells were analysed for mitochondrial respiration using the Seahorse technology (**Figure 80A**). Real-time oxygen consumption rate (OCR) measurement showed that basal respiration, representing the sum of all physiological mitochondrial oxygen consumption, was increased in cells lacking CD98hc (**Figure 80B**), indicating an enhanced respiratory function in these cells compared to WT cells. The non-mitochondrial respiration was quantified by injecting rotenone and antimycin A, inhibitors of complex I and III, respectively, and it was subtracted from the total OCR (**Figure 80**). The injection of oligomycin, an ATP synthase inhibitor, leads to a decrease in basal respiration that is reflective of the OCR used to generate ATP (**Figure 80**). Interestingly, OCR coupled to drive ATP production was also increased in CD98hc KO cells. Next, carbonyl cyanide-p-trifluoromethoxyphenyl-hydrazon (FCCP), a protonophore, was added to collapse the inner membrane gradient, driving the electron transport chain (ETC) to function to its maximal rate. The maximal respiration was found to be increased in CD98hc KO cells, while no differences were found in the proton leak when compared to WT cells (**Figure 80**), which is conducted by the protons that can return to the mitochondrial matrix independently of ATP synthase.

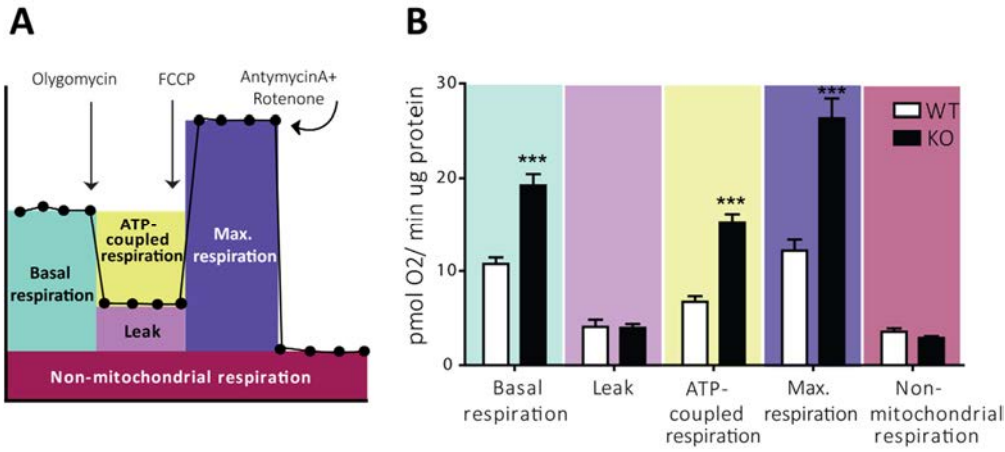

Figure 80. CD98hc KO cells present enhanced OXPHOS. **A**, schematic representation of the performed experiment. OCR is measured before and after the addition of indicated inhibitors to derive several parameters of mitochondrial respiration. **B**, comparison of the OCR between CD98hc KO and WT cells. Quantification data correspond to the mean ± SEM of six independent experiments. Statistical significance ***, $p \leq 0.001$ vs. WT cells was analysed using a Student's t-test.

These results suggest that CD98hc KO cells are forced to heavily rely on the OXPHOS system for energy production. Increased mitochondrial respiration can be achieved by increasing either the mitochondrial mass or the mitochondrial functionality.

Since mitochondrial functionality can be modulated by the regulation of the expression of the TCA cycle enzymes (**Figure 81A**) (Anderson et al. 2018), we took advantage of the transcriptome analysis performed in WT and CD98hc KO cells to analyse their expression. Several of the enzymes involved in the TCA cycle presented a slightly increase in the abundance of their transcripts in CD98hc KO cells when compared to WT cells (**Figure 81**). This outcome suggests a possible explanation for the increased OXPHOS capacity in CD98hc KO cells despite having a reduction in the intermediates of the TCA cycle (**Figure 71**).

A

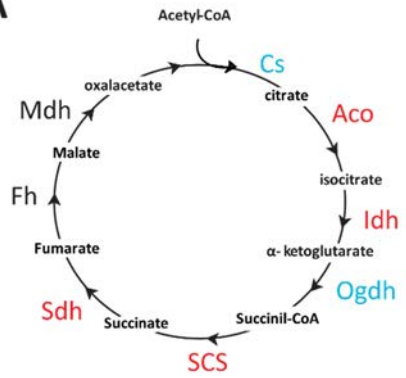

B

	Enzymes	FC	p-val
Cs	Citrate synthase	-1.20	0.01
Aco	Aconitase	1.29	0.05
Idh	Isocitrate dehydrogenase	1.15	0.03
Ogdh	Oxoglutarate dehydrogenase	-1.28	0.01
SCS	Succinate-CoA synthase	1.22	0.03
Sdh	Succinate dehydrogenase	1.31	0.00
Fh	Fumarase	-1.10	0.11
Mdh	Malate deshydrogenase	1.04	0.55

Figure 81. TCA cycle enzymes present altered expression in CD98hc KO cells. **A**, schematic diagram of the TCA cycle. Upregulated enzymes are depicted in red, downregulated enzymes are depicted in blue and enzymes are depicted in black when no differences were found between both cell groups. **B**, Fold change (FC) of the expression of the indicated enzymes in CD98hc KO vs. WT cells is indicated. p-val, p-value.

4.3.5 CD98hc ablation induces an increase in mitochondrial mass

Changes in mitochondrial mass may be another possible adaptation underlying the increased mitochondrial respiration in CD98hc KO cells.

In this regard, mitochondrial mass was assessed by different approaches. CD98hc KO cells presented upregulation in the protein expression levels of the voltage-dependent anion-selective channel protein 1 (VDAC1), a porin located in the outer membrane of mitochondria, widely used as a mitochondrial mass indicator (**Figure 82A**).

Moreover, staining with Mitotracker-green, a fluorescent mitochondrial stain which localizes to mitochondria regardless of mitochondrial membrane potential (Muñoz and Zorzano 2015), also suggested an increase in the mitochondrial abundance in CD98hc KO cells (**Figure 82B**).

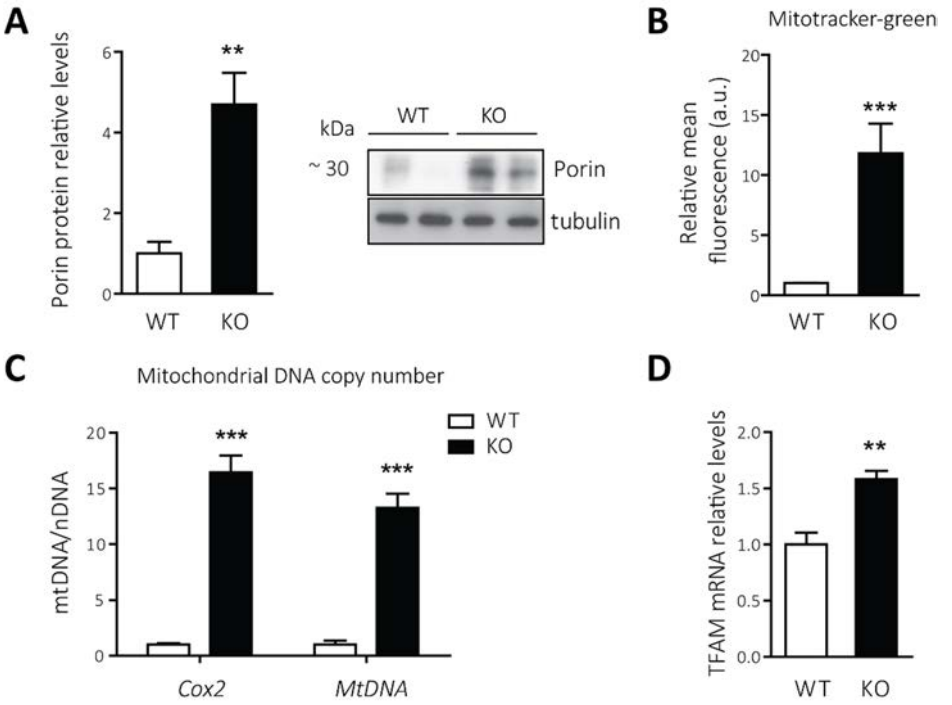

Figure 82. CD98hc KO cells present increased mitochondrial mass. **A**, comparison of porin protein levels between CD98hc KO and WT cells. Data are normalized by tubulin expression. n=4. **B**, analysis of mitochondrial mass using the specific mitochondrial molecular probe Mitotracker-green measured by flow cytometry. Bars represent the mean fluorescence in WT and CD98hc KO cells. a.u., arbitrary units. n=6. **C**, comparison of the mitochondrial DNA copy number in CD98hc KO and WT cells. The expression of the mitochondrial Cox2 and MtDNA regions was normalised by the expression of the nuclear gene Sdha. n=4. D, comparison of TFAM mRNA expression levels between CD98hc KO and WT cells. Quantification data correspond to the mean ± SEM of the indicated (n) independent experiments normalized to WT cells. Statistical significance **, $p \leq 0.01$;***, $p \leq 0.001$ vs. WT cells was analysed using a Student's t-test.

We then determined the mitochondrial DNA copy number by analysing the genomic expression of the mitochondrial gene cyclooxygenase-2 (*Cox2*) and a genomic mitochondrial region, hereafter referred to as *MtDNA*. The quantification of *Cox2* and *MtDNA* were then normalised by the genomic DNA copy number using the succinate dehydrogenase complex subunit A (*Sdha*) as a housekeeping nuclear gene. Consistent with our idea, we found an increase in the mitochondrial DNA copy number in CD98hc KO cells in comparison to WT cells (**Figure 82C**).

In keeping with this, mitochondrial transcription factor A (TFAM) mRNA levels, which controls the transcription of mitochondrial DNA encoded genes, as well as DNA replication during biogenesis (Lezza 2012), were also upregulated in cells lacking CD98hc (**Figure 82D**).

Collectively, these results point to a significant increase in the mitochondrial mass induced by the lack of CD98hc, which may be an adaptation of CD98hc KO cells to support their increased respiration by OXPHOS (**Figure 80**).

After assessing mitochondrial mass, we also analysed mitochondrial morphology in CD98hc KO cells by using the mitochondrial-targeted red fluorescent protein mitoDsRed. Cells lacking CD98hc clearly showed a markedly mitochondrial fragmentation compared to the well elongated mitochondrial network of WT cells (**Figure 83**).

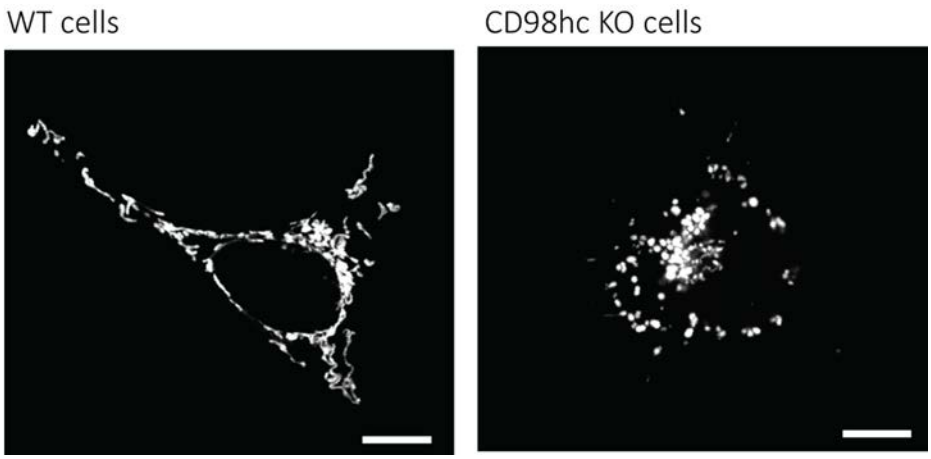

Figure 83. CD98hc ablation induces changes in the mitochondrial morphology. Mitochondrial morphology of CD98hc KO and WT cells using mitoDsRed labelling. Representative images experiment are shown. Similar results were obtained with a five independent experiments. Scale bars is 10 μm.

Since mitochondria harbour the major oxidative pathways in the cells, they generate superoxide ($O_2^{\bullet-}$) and hydrogen peroxide (H_2O_2) at the ETC, which are thought to augment the intracellular oxidative stress in cells (Cadenas, Davies, and

Adenas 2000). Because CD98hc KO cells presented enhanced mitochondrial respiration through OXPHOS and increased mitochondrial mass, we hypothesized that mitochondrial ROS may account too for the increased oxidative stress shown in these cells (**Figure 17**). In this regard, we measured levels of $O_2^{\bullet-}$ production by making use of the mitochondrial dye MitoSOX, which becomes fluorescent after oxidation specifically by $O_2^{\bullet-}$ (Muñoz and Zorzano 2015). Consistently, we found a huge increase in the production of this radical in CD98hc KO cells, as evidenced by enhanced MitoSOX fluorescence (**Figure 84**).

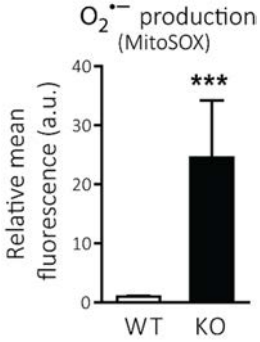

Figure 84. CD98hc KO cells produce higher levels of mitochondrial ROS. Analysis of mitochondrial ROS production using MitoSOX measured by flow cytometry. Bars represent the mean fluorescence in WT and CD98hc KO cells. a.u., arbitrary units. Quantification data correspond to the mean ± SEM of six independent experiments normalized to WT cells. Statistical significance ***, $p \leq 0.001$ vs. WT cells was analysed using a Student's t-test.

The reported data suggest that CD98hc KO cells have increased mitochondrial mass, probably as an adaptation to survive under nutritional stress conditions. This increase may underlie to some extent the enhanced mitochondrial respiration and the augmented ROS levels in CD98hc KO cells.

4.3.6 Glutamine may account for OXPHOS activation in CD98hc KO cells

While cytosolic ATP production relies mainly on glucose, mitochondrial OXPHOS can be fuelled by alternative substrates, such as fatty acids and AAs (Boroughs and Deberardinis 2016). In this regard, the induction of OXPHOS as a consequence of glycolysis abrogation, has been reported to be boosted by glutaminolysis (Fantin et al., 2006; Le et al., 2010; Marchiq et al., 2015; Ždralević, Vučetić, et al., 2018).

In an attempt to elucidate whether glutamine was used to maintain cell survival by supporting the anaplerosis of the TCA cycle via α-ketoglutarate (DeBerardinis et

al. 2007a) in CD98hc KO cells, we took advantage of the transcriptome analysis performed in WT and CD98hc KO cells to analyse the expression of the main enzymes involving in glutamine catabolism (**Figure 85, upper panel**). Interestingly, we found that most of the involved enzymes presented increased abundance of transcripts in cells lacking CD98hc compared to WT cells (**Figure 85, lower panel**).

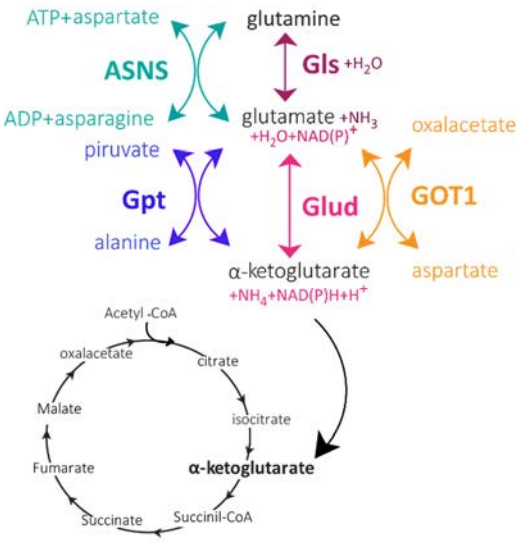

Figure 85. The glutaminolytic enzymes are upregulated in CD98hc KO cells. Schematic diagram of the conversion of glutamine to α-ketoglutarate (upper panel). Enzymes and substrates of the reactions are indicated. Fold change (FC) of the expression of the indicated enzymes in CD98hc KO vs. WT cells is indicated (lower panel) p-val; p-value.

	Enzymes	FC	p-val
Glud	glutamate dehydrogenase 1	2.10	0.00
Gpt2	glutamic pyruvate transaminase 2	1.40	0.00
Gpt	glutamic pyruvic transaminase	2.09	0.00
Got2	glutamic- oxaloacetic transaminase	1.20	0.02
Got1	glutamic-oxaloacetic transaminase	1.75	0.00
Gls2	glutaminase 2	1.29	0.02
Asns	asparagine synthetase	-1.08	0.68

Moreover, asparagine synthetase (ASNS), which converts aspartate and glutamine to asparagine and glutamate (**Figure 85**), has been proposed as a marker of glutamine-dependent OXPHOS (Balasubramanian, Butterworth, and Kilberg 2013), and it was found increased in CD98hc KO cells in comparison to WT cells (**Figure 86**).

Finally, it is interesting to note that, despite the lower content of ^{13}C-pyruvate in CD98hc KO cells, no changes were detected in the abundance of pyruvate-derived-alanine (^{13}C-alanine) and neither in the total content of this AA between CD98hc KO and WT cells (**Figure 87**).

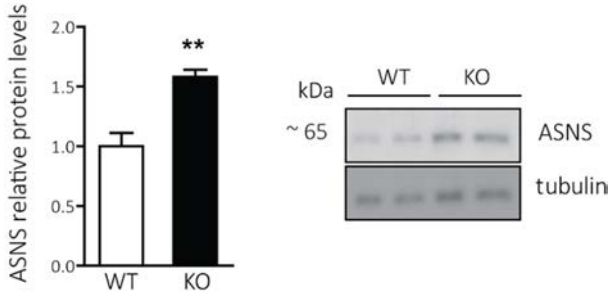

Figure 86. ASNS is upregulated in CD98hc KO cells. Comparison of ASNS protein expression levels between CD98hc KO and WT cells. Data are normalised by tubulin. Quantification data correspond to the mean ± SEM of three independent experiments normalised to WT cells. Statistical significance **, $p \leq 0.01$ vs. WT cells was analysed using a Student's t-test.

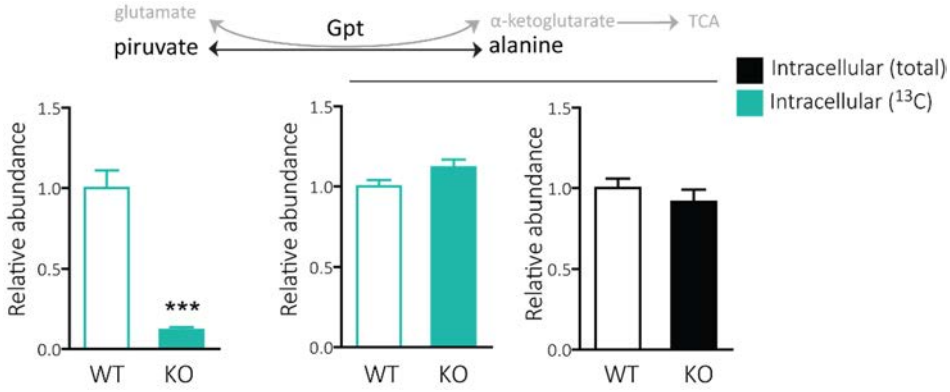

Figure 87. The conversion of pyruvate into alanine is increased in CD98hc KO cells. Comparison of the abundance of ^{13}C-pyruvate (M+3) and ^{13}C-alanine (M+3) in CD98hc KO and WT cells. Intermediates depicted in grey are not analysed in this figure. Quantification data correspond to the mean ± SEM of five independent experiments normalized to WT cells. Statistical ***, $p \leq 0.001$ vs. WT cells was analysed using a Student's t-test.

This result, along with the increased expression of the GPT, which catalyses the synthesis of α-ketoglutarate and alanine from pyruvate and glutamate (**Figure 85**), indicates that this reaction is displaced towards the production of α-ketoglutarate.

In all, our data support the view that CD98hc KO cells may depend on glutamine to fuel the TCA cycle, suggesting that CD98hc sustains a metabolic program based on glucose in detriment of glutaminolysis.

4.3.7. The shortage of BCAAs and AAAs has an impact in OXPHOS

In order to elucidate whether the BCAA and AAA limitation also posed a threat to the energy metabolism of the cell, mitochondrial respiration, using the Seahorse technology as described in **Figure 80A**, was assessed under the addition of BCAA- and AAA- containing dipeptides in the culture media.

Interestingly, the increase in both basal respiration and OCR coupled to ATP synthesis was partially restored in the dipeptide-supplemented CD98hc KO cells (**Figure 88**), suggesting the implication of these AAs in the mitochondria bioenergetics.

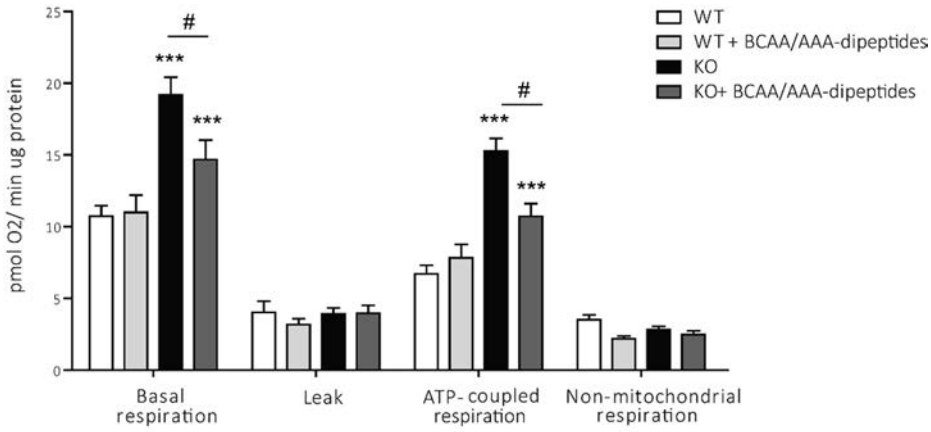

Figure 88 Supplementation with BCAA- and AAA-containing dipeptides reduces OXPHOS in CD98hc KO cells. Comparison of the OCR between CD98hc KO and WT cells alone or in the presence of BCAA- and AAA- containing dipeptides. Quantification data correspond to the mean ± SEM of six independent experiments. Statistical significance ***, $p \leq 0.001$ vs. WT cells or #, $p \leq 0.05$ vs. KO cells was analysed using a Student's t-test.

Supporting this idea, BCAA and AAA shortage led to increased mitochondrial respiration in low 6AA cells, as evidenced by the increase in the OCR, both in basal conditions and coupled to ATP production (**Figure 89**).

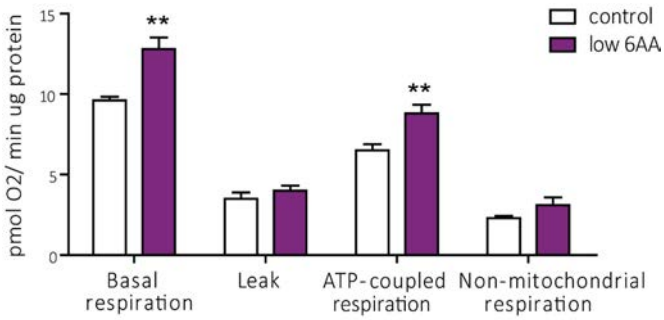

Figure 89. Low 6AA cells present enhanced OXPHOS. Comparison of the OCR between low 6AA and control cells. Quantification data correspond to the mean ± SEM of four independent experiments. Statistical significance **, $p \leq 0.01$ vs. control cells was analysed using a Student's t-test.

Interestingly, no differences were found in the mitochondrial mass in low 6AA cells in comparison to control cells, assessed by using the markers porin (**Figure 90A**) and mitotracker-green (**Figure 90B**).

All together, these data suggest that BCAA and AAA availability also plays a role in the bioenergetic metabolism of the cell, thus, when limiting, cells adapt by means of a metabolic reprogramming independently of the mitochondrial abundance in order to survive in these conditions.

Taken together, these results reported in this chapter indicate that CD98hc plays an important role in the regulation of the cellular energy metabolism of the cell. Remarkably, it controls the expression of the glucose transporter GLUT1 and the lactate transporter MCT1, along with its ancillary protein CD147, all three key for glucose metabolism. Additionally, CD98hc loss of function leads to the disruption of glycolysis paralleled with a re-routing to OXPHOS. In consequence, the PPP resulted impaired in CD98hc KO cells, which probably underlies the general reduction in the nucleotide pool observed in these cells.

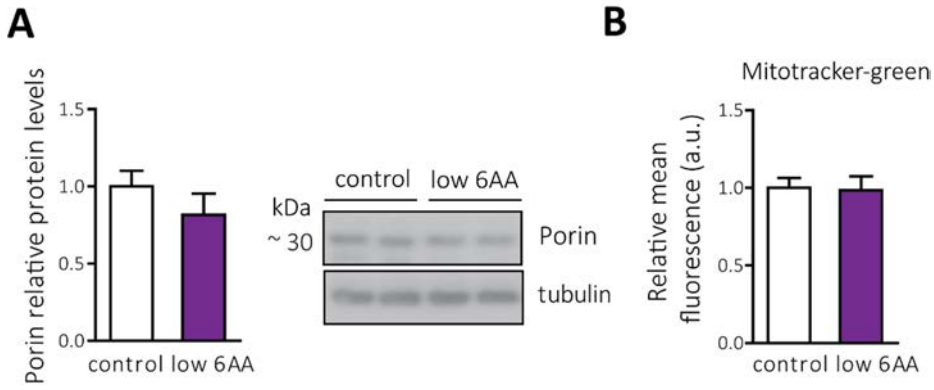

Figure 90. Low 6AA cells do not present increased mitochondrial mass. A, comparison of porin protein levels between low 6AA and control cells. Data are normalized by tubulin expression. n=3. **B**, analysis of mitochondrial mass using the specific mitochondrial molecular probe Mitotracker-green measured by flow cytometry. Bars represent the mean fluorescence in low 6AA and control cells. a.u., arbitrary units. n=3. Quantification data correspond to the mean ± SEM the indicated (n) independent experiments normalized to control cells. No statistical differences were found using a Student's t-test.

Discussion

All mammalian cells, whether they are cancerous or not, have to take up EAAs from external sources, whereas non-EAAs can be synthesized endogenously. However, in cells with high proliferation rates, as is the case with tumour cells, even these AAs need to be obtained from the surrounding environment, since their capacity of endogenous synthesis does not meet their increased nutritional demand (Bhutia et al. 2015). For this reason, tumour cells express AA transporters, such as CD98hc-LAT1 and CD98hc-xCT, at a higher level than normal cells (Bhutia et al. 2014, 2015; Fuchs and Bode 2005). Although the primary function of AA transporters is to provide AAs to serve as building blocks for protein synthesis, our results highlight that CD98hc functions as a regulatory hub, orchestrating not only cellular nutrient and redox homeostasis, but also glucose and nucleotide metabolism. Therefore, blocking the function of CD98hc and associated transporters should have detrimental effects specifically on tumour cells.

In this regard, this thesis has attempted to gain into the understanding of the role that CD98hc plays in different cellular functions in order to achieve a holistic comprehension of its relevance in both physiological and pathological conditions. To this end, we used WT and CD98hc KO mouse fibroblasts derived from ES cells as a cellular model. Concerning CD98hc associated transporters, WT cells express xCT, LAT1 and y^+LAT2 light subunits, all found in all the cell lines tested in this study, whereas CD98hc KO cells lack both expression and function of these transporters. Thus, these cells provide a suitable model for the proposed *in vitro* study. Furthermore, we generated low 6AA cells as a novel model through which to study the impact of BCAA and AAA shortage independently of oxidative stress and other metabolic alterations present in CD98hc KO cells.

The results of the present work can be grouped in four different categories (**Figure 91**).

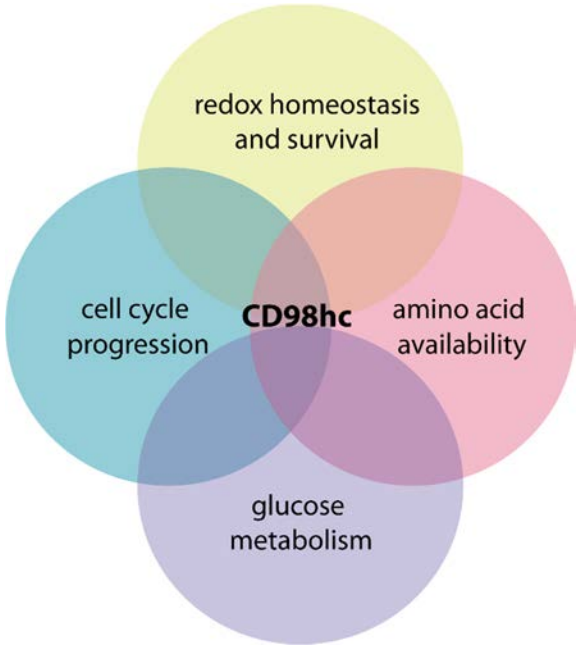

Figure 91. CD98hc functions as a regulatory hub, orchestrating not only AA availability and redox homeostasis but also glucose and nucleotide synthesis, required for proper cell cycle progression. The most important roles played by CD98hc, discussed below, are grouped in the four indicated categories.

5.1 CD98hc is essential for *in vitro* cell survival and redox homeostasis

ROS are produced by living organisms as a consequence of normal cellular metabolism. However, the shift in balance between the productions of ROS and the availability and action of antioxidants results in oxidative stress, associated with macromolecular damage and cell death (Birbe et al. 2012). Among the intracellular antioxidant molecules, GSH plays a central role in alleviating oxidative stress and in this regard, in cultured cells, xCT activity is considered essential for maintaining its intracellular levels (**Figure 92**)(Shiro Bannai and Tateishi 1986).

Consistently, we show that CD98hc KO cells do not survive under routine culture conditions unless media is supplemented with the reducing agent β-ME. Our results are in good agreement with the work performed by Sato and co-workers on

fibroblasts isolated from xCT deficient embryos (Sato et al. 2005). In that study, the cell death observed in xCT KO fibroblasts was ascribed to the increased oxidative stress cells suffer due to the loss of the transporter, but the mechanism underlying the cell death remained unknown. Our results, along with the data provided by the work of Dixon and colleagues, in which xCT transporter was specifically inhibited by SAS (Dixon et al. 2012), evidence that ablation of either xCT or CD98hc triggers the iron-dependent cell death ferroptosis due to the drop of GSH levels (**Figure 92**). These results are supported by a recent study in which it is demonstrated that ferroptosis also occurs upon cysteine starvation conditions (Chen et al. 2017).

Although xCT KO mice present a redox imbalance in plasma, these mice do not required the expression of the transporter to survive (Arensman et al. 2019; Sato et al. 2005), as it is the case in *in vitro* conditions. This is probably due to the different oxygen (O_2) levels range in both situations. Cell culture experiments are performed at atmospheric O_2 levels (21 %) whereas *in vivo,* O_2 levels range from 2 to 9 %, which does not contribute to increase oxidative stress and therefore anti-oxidant capabilities are less required (Jagannathan, Cuddapah, and Costa 2016). However, due to the sustained exacerbated metabolism and reprogramming carried out by cancer cells, tumours often become heavily reliant on antioxidant machinery. In those cases in which ROS counterbalance is highly required, modulation of redox status via the inhibition or ablation of xCT may offer a vulnerability point on the tumour outcome.

Even when ferroptosis is blocked by β-ME supplementation, consistently with aforementioned studies (Conrad & Sato, 2012; Dixon et al., 2014), CD98hc KO cells present accumulation of DCF fluorescence signal and increased NRF2 expression. These results, together with the fact that pharmacological inhibition of xCT with SAS does not promote NRF2 activation in WT cells, indicate that another source, independently of xCT loss, is likely underlying the oxidative stress existing in CD98hc KO cells.

One possible explanation, may be the increased mitochondrial mass and enhanced respiration by OXPHOS existing in cells lacking CD98hc. Mitochondria have long

been thought of as simply cellular power source, whose main function is to provide ATP. However, in 1961, Jensen demonstrated for the first time that these organelles also produce ROS (Jensen 1966). Nowadays, mitochondria is considered as a major source of ROS, especially through electron leakage from Complexes I and III of the ETC (Murphy 2009). This hypothesis is also supported by the increased MitoSOX fluorescence signal in CD98hc KO cells, which is a reliable readout for the mitochondrial $O_2^{\bullet-}$ production.

Another plausible cause that may account for the enhanced oxidative stress is the abrogated PPP flux occurring in CD98hc KO cells. The PPP gained significant attention in the late 50's due to the revelation that hemolytic anaemia, characterized by the abnormal breakdown of red blood cells induced by oxidant agents and correlated with the lack of GSH, could be triggered by genetically inherited deficiency of glucose-6P dehydrogenase (G6PDH), which catalyses the first committed step in the oxidative branch of the PPP (Carson et al. 1956). Today, it is widely accepted by the accumulating evidence that the PPP is a major source of NADPH, which protects against oxidative stress, directly in ROS detoxification reactions and also indirectly, via the regeneration of GSH (Patra & Hay, 2014). Supporting this statement, disruption of the pathway has been associated with depleted NADPH and GSH levels, resulting in a distortion of redox control, which can be prevented by administration of the potent antioxidant N-acetylcysteine (NAC) (Hanczko et al. 2009). Likewise, induction of the PPP forms part of the antioxidant response mediated by NRF2, since this transcription factor promotes the expression of the enzymes of the PPP (Zhang and Wang 2007).

Moreover, our data suggest that the increased oxidative stress may induce the phosphorylation of eIF2α in CD98hc KO cells (**Figure 92**). Although it is well established that in conditions of AA starvation, uncharged tRNAs activate GCN2 (Dong et al. 2000; Wek, Zhu, and Wek 1995), which in turn phosphorylates eIF2α (Anthony et al. 2001; Harding et al. 2000; P. Zhang et al. 2002), we show that BCAA and AAA limitation does not induce the phosphorylation of eIF2α in our model. However, to the best of our knowledge, neither tRNA charging, nor direct

activation of GCN2, has been evaluated after partial AA restriction rather than full deprivation. Our results indicate that BCAA and AAA restriction is not enough to cause a substantial increase in the level of deacylated tRNAs. Thus, our data suggest that GCN2 does not govern the activated eIF2-mediated ISR pathway in the CD98hc KO model, although its participation in the response cannot be ruled out. Supporting this, low 6AA cells, which in contrast to CD98hc KO cells do not present increased ROS, do not present any detectable change in the activity of eIF2α, despite the impaired proliferation rate present in these cells.

An alternative explanation for the observed activation of eIF2α pathway could be, as mentioned above, that increased levels of oxidative stress in CD98hc KO cells mediate eIF2α phosphorylation through activation of the kinase HRI, which is known to be activated in response to toxic ROS levels (**Figure 92**) (Lu, Han, and Chen 2001; McEwen et al. 2005; Suragani et al. 2012; Tidke et al. 2016). This hypothesis is also supported by the increased protein levels of HRI in CD98hc KO cells. However, in order to clarify this process, further research is needed to demonstrate that the counterbalance of the oxidative stress is able to restore normal expression levels of HRI and P-eIF2α.

Another aspect that remains to be defined is the reason why ATF4 is not upregulated despite the increased phosphorylated levels of eIF-2α in CD98hc KO cells. Dysfunctional ISR (suppressed ATF4 expression in the presence of phosphorylated eIF2α) has been previously reported in cases of chronic stresses, which could be the case of cells lacking CD98hc. This is the case for the hepatocytes from subjects with the metabolic syndromes Non-alcoholic fatty liver (NAFL) and non-alcoholic steatohepatitis (NASH) (Cheung et al. 2007), cells facing sustained mitochondrial dysfunction (Evstafieva et al. 2014) or exposed to UV irradiation (Dey et al., 2010) and this phenomena was also observed in brain ischemia and reperfusion contexts (Kumar et al. 2003).

Collectively, all these works evidence that apparently, cells have the capacity to selectively repress or activate key regulatory genes of the ISR pathway to direct the transcriptome and cell survival depending on the precise stress.

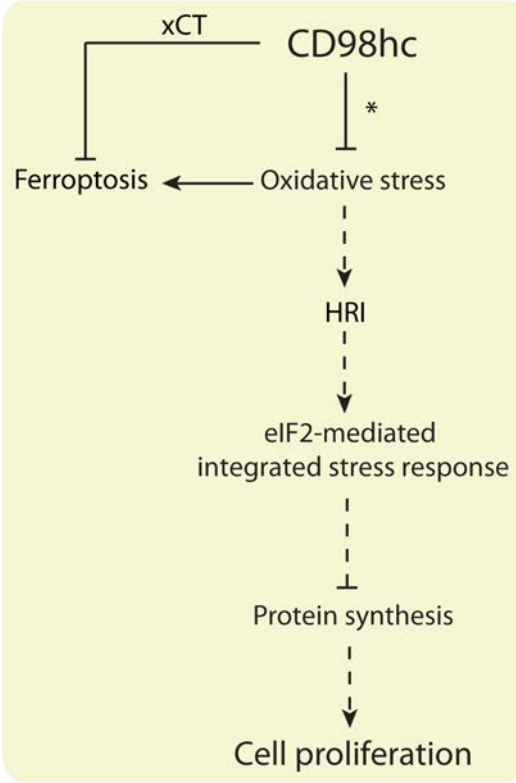

Figure 92. CD98hc protects cells against oxidative stress leading to cell survival. CD98hc-xCT is required for the counterbalance of the oxidative stress, thereby avoiding ferroptosis. In addition, independently of the loss of xCT, and likely related to metabolic alterations (*), CD98hc KO cells present increased oxidative stress, which probably underlies the HRI activation and the resulted phosphorylated-eIF2α. Activation of eIF2α-mediated ISR pathway is known to downregulate global protein synthesis and therefore the cell proliferation rate. Solid lines represent established connexions proposed in this work. Dashed lines represent connexions suggested by the data provided herein and literature.

5.2 CD98hc sustains cellular the AA availability required for proper cell proliferation

The substrate specificity of different AA transporters is often overlapping in order to ensure the system remain unaffected if one transporter fails (Vilches et al., 2018). Here, we report alterations in the intracellular content of several AAs after invalidation of a transporter component, highlighting that redundancy is not a characteristic feature of CD98hc-associated transporters (**Figure 93**).

Our data show that CD98hc KO cells present a shortage in several EAA, such as BCAAs and AAAs, all transported by CD98hc-LAT1 (**Figure 93**). This is consistent with the fact that around 90% of the L-isoleucine uptake is lost when CD98hc is absent. In addition, the metabolomic analysis performed in CD98hc KO and WT cells allows us to unequivocally determine that the entry of the analysed BCAAs

(leucine, isoleucine and valine) and the AAA tryptophan, is diminished in the former cells.

The global intracellular AA imbalance shown in CD98hc KO cells resemble that observed in low 6AA cells. In this work we propose that modulation of other transporters non-related to CD98hc may account, at least in part, for such AA imbalance. For instance, upregulation of CAT3 in CD98hc KO cells, and CAT1 and CAT3, in the case of low 6AA cells, could underlie the increased concentration of AA^+s (arginine, lysine and histidine), which are carried by those transporters (Fotiadis, Kanai, and Palacín 2013), in both cellular models. This assumption is supported by the research performed by Tărlungeanu and co-workers, who generated a blood brain barrier (BBB) conditional LAT1 KO mice (Tărlungeanu et al. 2016). As expected, deletion of LAT1 in the BBB triggers a decrease in the content of BCAAs in the brain, however, levels of other AAs, such as the AA^+ histidine, resulted highly increased. Like in our cellular models, the mouse brain shows a significant upregulation of CAT1 and CAT3 transporters (Tărlungeanu et al. 2016). All together, these findings suggest that the reduction in BCAAs and AAAs is enough to trigger a response within which other AA transporters are upregulated, resulting in an intracellular AA imbalance.

The shortage of BCAAs and AAAs, in agreement with the results obtained in other studies (Y. Cormerais et al. 2016; Elorza et al. 2012; Moberg et al. 2016; Neishabouri, Hutson, and Davoodi 2015; Nicklin et al. 2009a; Persaud et al. 2018), drives the downregulation of the nutrient-sensing pathway mTORC1 (**Figure 93**). In support of this notion, low 6AA cells present similar mTORC1 pathway inhibition to that observed on CD98hc KO cells, and accordingly, both cellular models present a major defect in cell proliferation (**Figure 93**). Addition of BCAA- and AAA-containing dipeptides in the CD98hc null model recovered cell proliferation together with a partial re-activation of mTORC1.

Controversially, due to a technical misconception, we previously reported increased phosphorylation state of S6, and in consequence, induction of mTORC1 pathway in CD98hc KO cells when compared to WT cells (de la Ballina et al., 2016).

Since WT and CD98hc KO cells proliferate at different rates, dissimilar confluences are reached at the day of the cell harvest if same number of cells are seeded for the experimental analysis of mTORC1 pathway. When cells reach a critical number and density, cell confluence leads to contact inhibition of proliferation (CIP) due to, among other regulatory mechanisms, the inhibition of mTORC1 pathway (Leontieva, Demidenko, and Blagosklonny 2014), which was possibly the case for WT cells. When ensuring similar confluence between WT and CD98hc KO cells, we show an unequivocally downregulation of the pathway in the KO cells. This setback awarded us to be extremely cautious with regard to confluence in the culture of both cells groups thereafter.

Moreover, our results show that ablation of CD98hc leads to a reduced protein synthesis rate, probably governed by mTORC1 downregulation, although we cannot discard the involvement of the phosphorylated eIF2α response (**Figure 93**).

Altogether, these data evidence the strong requirement of BCAAs and AAAs for protein synthesis and proper cell proliferation. Indeed, it is interesting to note that a reduction of the concentration of BCAAs and AAAs in the cell culture media to levels which are considered within the lower physiological levels in plasma, is enough to trigger detrimental consequences in the homeostasis of the cells.

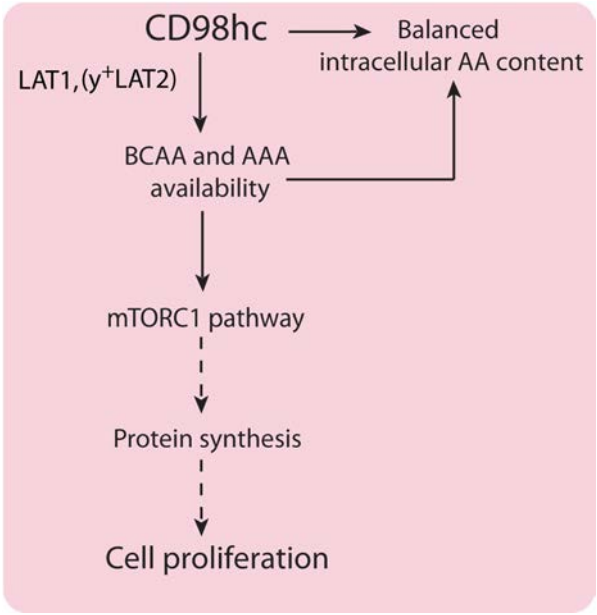

Figure 93. CD98hc supports the balance of intracellular AA content. CD98hc sustains BCAA and AAA availability, mostly mediated via LAT1, although contribution of y^+LAT2 cannot be discarded, for protein synthesis and cell proliferation. Solid lines represent established connexions proposed in this work. Dashed lines represent connexions suggested by the data provided herein and literature.

5.3 CD98hc is required for nucleotides biosynthesis, ensuring the correct completion of the cell cycle

The progression of the cell cycle is tightly dependent on the ability of the cell to acquire nutrients and produce energy to drive the constant *de novo* biosynthesis of nucleotides (DeBerardinis et al., 2007; Moffatt and Ashihara, 2002), which, when limiting, may affect genome integrity in diverse ways (Bester et al. 2011; Giannattasio and Branzei 2017; Zeman and Cimprich 2014). Our results indicate that CD98hc is essential for the biosynthesis of the nucleotides (**Figure 94**). Consistent with this, lack of CD98hc promotes a dramatic reduction in the nucleotide pool, which leads to ATR-CHK1-dependent DDR activation and the subsequent protective arrest in S-phase.

The induction of the DDR in CD98hc KO cells subjected to chronic RS is likely to be governed by the overexpression of the components of the pathway (CHK1 and RPA), probably as a result of an adaptation. In support of this notion, other studies have proposed that this behaviour is an adaptation to the chronic RS, for instance in cancer (Albiges et al. 2014; Cho et al. 2005; David et al. 2016; Hwang et al. 2018; Mak et al. 2015; Verlinden et al. 2007). In this regard, attending to the rational that the more CHK1 protein cells have, the better able they are to handle the DNA damage stress caused by the harsh tumour microenvironment, López-Contreras and colleages unveiled the advantages from having an extra allele of CHK1 for protecting from RS in cancer cells (López-Contreras et al. 2012).

Expression of mammalian CHK1 and RPA (both mRNA and protein) peaks at S- and G2- phases of the cell cycle (Kaneko et al. 1999). Thus, we cannot discard the possibility that the observed increase in the total protein levels of CHK1 and RPA in CD98hc KO cells, was related to some extent to the fact that the cell population retained in S-phase in these cells is higher than in WT, due to RS. However, since low 6AA cells, which also present RS, do not induce CHK1 and RPA expression, this possibility is unlikely. At the same time, this result also reveals differences between the chronic and acute stresses that cause the RS in these two cellular

models. In this regard, low 6AA cells present phosphorylated levels of CHK1 and RPA markedly increased, while total levels of both proteins resulted repressed. This coupling between activating phosphorylation and subsequent downregulation of total levels of CHK1 has been described as a mechanism through which detrimental accumulation of this protein upon acute induction of genotoxic stresses is prevented (Zhang et al. 2005).

CHK1 responds to RS by phosphorylating its key target cdc25A, which subsequently undergoes proteasomal degradation. As a result, the activity of CDK1/B complex is reduced, leading to G2/M arrest and reduced mitosis (Krämer et al. 2004; Thanasoula et al. 2012). Data provided by the transcriptome analysis suggest that the reduced mitotic rate in CD98hc null cells is due to the activation of the G2/M checkpoint. Moreover, this outcome is consistent with the increase in the percentage of cells lacking CD98hc in the G2/M fraction, which may reflect a delay in the G2-phase caused by mitotic blockage (Patil, Pabla, and Dong, 2013). However, despite these correlations, further experiments should be performed in order to confirm the degradation of cdc25A in CD98hc KO cells.

Following the same strategy as Fernandez-Capetillo's group (Ruiz et al. 2015), we rescued the replication-induced DNA damage in CD98hc KO cells by the addition of nucleosides in the culture media, as reflected in the marked decrease of the phosphorylation of RPA and CHK1 proteins. Consistently, nucleoside-supplemented CD98hc KO cells resumed cycle progression, thus reversing the observed S-phase arrest. Furthermore, the provision of nucleosides also rescued the slowed entry into mitosis. Thus, collectively, these findings highlight that CD98hc is critical for the prevention of derangements in nucleotide levels, to our knowledge, a novel role non-described until now. The link between the lack of CD98hc and the limiting nucleotide levels should be confirmed in additional cell lines in order to test whether this connexion is universal. Nevertheless, we took advantage of a recent study performed by Boulter and colleagues in CD98hc KO dermal model generated to asses the cross-regulation of CD98hc and integrins in the mechanical homeostasis of the dermis (Boulter et al., 2018). A metabolomics

screen was carried out and they found alterations in metabolites belonged to a wide variety of metabolic pathways, including, as expected, AA metabolism and for instance lipid metabolism, in which they focused their study. However, paying attention into the metabolic profile of the CD98hc KO cells, we found the following nucleotides: UDP, UMP, ADP, AMP, IMP, dCMP, GMP and CMP, all significantly decreased in these cells compared to WT cells, with the exception of IMP (Boulter et al., 2018), in good agreement with our data.

The PPP is a major pathway for glucose catabolism and the main source of ribose-5P, which forms the sugar backbone of all nucleotides (Jiang, Du, and Wu 2014). In this study, we propose that the abrogation of the PPP flux and, consequently, the drastic reduction of ribose-5P, explains the decreased levels of nucleotides in CD98hc KO cells (**Figure 94**). In support of this notion, other studies have demonstrated that both ribose-5P availability (Boer and Sperling 1995; Pilz, Willis, and Boss 1984) and impaired PPP activity (Cosentino, Grieco, and Costanzo 2011; Fornalewicz et al. 2017; Qu et al. 2017; Yu et al. 2015) trigger alterations in nucleotide biosynthesis and DNA replication. However, the mechanism by which the PPP is downregulated in CD98hc KO cells remains to be clarified.

It is well established that the oncogenic protein c-myc, often constitutively overexpressed in cancer, controls DNA replication by multiple metabolic networks (Aird et al. 2015; Dejure et al. 2017; Gao et al. 2009). Regarding its relation with the PPP, c-myc was found to enhance the expression of the two rate-limiting enzymes glucose-6P dehydronenase (G6PDH) (Yang et al. 2018), which catalyses the first reaction of the oxidative branch of the PPP, and the phosphoribosyl-pyrophosphate synthetase 2 (PRPS2) (Cunningham et al. 2014), responsible for the synthesis of PRPP from ribose-5P, precursor of both pyrimidine and purine nucleotides. Taking this consideration, one could postulate that the downregulated levels of this oncogene in CD98hc KO cells may have an impact on activity of the PPP.

Furthermore, mTORC1 signalling, inhibited in cells lacking CD98hc, also sustains the metabolic flux of the oxidative branch of the PPP by promoting the expression of genes involved in this pathway (Düvel et al. 2010).

Alternatively, the mechanism underlying the downregulation of the PPP may be related to alterations in glucose utilization and energy metabolism, discussed above (**chapter 5.4**).

On the basis of our data, we determine that the mechanism underlying the decreased nucleotide pool in cells lacking CD98hc is unlikely to be caused exclusively by the shortage of BCAAs and AAAs. This hypothesis is supported by the fact that low 6AA cells do not present alterations in the PPP activity and show a reduction only in the deoxynucleotide pool. The intracellular concentration of deoxynucleotides is tightly regulated by the expression of RRM2, the only enzyme that catalyses the rate-limiting step for the *de novo* conversion of ribonucleosides to deoxyribonucleosides(**Figure 94**) (Aird et al. 2013; Lopez-Contreras et al. 2015). Consistently, low 6AA cells present a severe downregulation of RRM2 protein levels, which probably dictates the RS reported in this model, which indeed, is also recovered by the addition of nucleosides.

However, the link between BCAA and AAA restriction and RRM2 downregulation in low 6AA cells remains to be further addressed. In this regard, it has been reported that c-myc enhances the biosynthesis of nucleotides by promoting deoxynucleotide synthesis through the upregulation of RRM2 (Mannava et al. 2008; Neretti et al. 2008). Thus, it is feasible that the decreased expression of c-myc observed in low 6AA cells underlies the reduced RRM2 expression (**Figure 94**).

In this regard, the impact of AA limitation, concretely glutamine scarcity, on c-myc expression levels has been already reported (Dejure et al., 2017). However, although glutamine deprivation inhibits mTORC1 activity, they demonstrated that this downregulation had no effects on c-myc levels. However, in agreement with other studies (Csibi et al. 2014), mTORC1 pathway downregulation is enough to trigger a decrease in the protein expression levels of c-myc in our cell model,

suggesting a possible link between the shortage of BCAAs and AAAs and the downregulation of c-myc and RRM2 expression in low 6AA cells. Nevertheless, further experimental research is required in order to address the detailed mechanism underlying this process. For instance, the analysis of the expression RRM2 upon rapamycin treatment or the recovery of c-myc expression attempting to restore RRM2 protein abundance and therefore the deoxynucleotide pool, are some of the experimental approaches that would clarify our assumption.

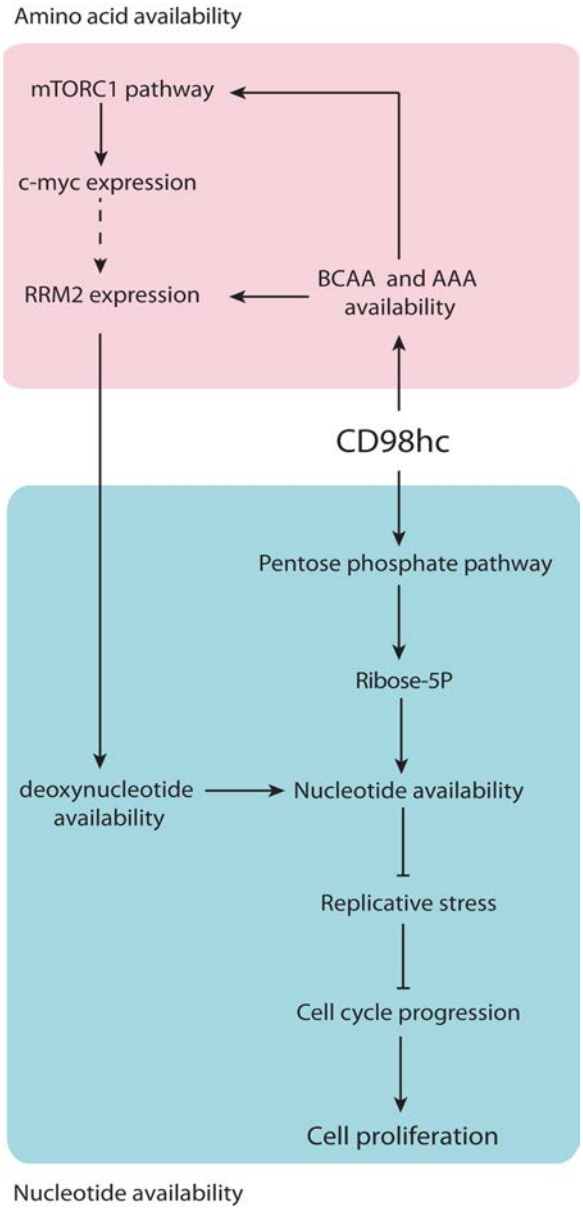

Figure 94. CD98hc is required for the correct completion of the cell cycle. CD98hc regulates the cellular nucleotide content likely through the regulation of the PPP flux, which enables cells to progress adequately throughout the cell cycle. In addition, BCAA and AAA availability has an impact in the reduction of ribonucleotides to the corresponding deoxynucleotides, thereby balancing the cellular nucleotide content. Solid lines represent established connexions proposed in this work. Dashed lines represent connexions suggested by the data provided herein and literature.

5.4 CD98hc regulates glucose utilization and sustains the energy metabolic program of the cell

The data reported herein suggest that the nutrient stress conditions of living without CD98hc force cells to use mitochondrial oxidative metabolism to cope with the energetic demands and maintain proliferation and survival.

CD98hc KO cells, in good agreement with the results obtained by Ohno *et al.*, present downregulated levels of GLUT1, presumably as a consequence of its degradation due to the absence of CD98hc (**Figure 95**) (Ohno et al., 2011). GLUT1 mRNA levels and GLUT3 at both mRNA and protein levels resulted upregulated in CD98hc KO cells, probably attempting to compensate the degradation of GLUT1. Supporting these results, the overexpression of GLUT transporters as an adaptation to survive in challenging conditions in terms of glucose availability has already been reported (Adekola, Rosen, and Shanmugam 2012; Boado and Pardridge 2002).

However, despite GLUT3 overexpression, glucose uptake rate remains decreased in CD98hc KO cells, suggesting that such overexpression is insufficient to overcome the loss of GLUT1. In addition, even though a lower amount of glucose is transported intracellularly, glucose is accumulated inside the cells, evidencing a serious impediment to use this metabolite as an energy supply. In the same line, and consistent with this assumption, glycolysis is dramatically reduced in cells lacking CD98hc (**Figure 95**).

Our results support the view that CD98hc KO cells activate mitochondrial respiration via OXPHOS to face the energetic demand imposed by their inability to synthesize glycolytic ATP (**Figure95**).In fact, this is reflected in the dramatically reduction of ATP levels existing in these cells (**Figure 95**). This energetic shift in respiration is probably achieved, among other possibilities, by the observed increase in the mitochondrial mass.

The link between a decay in ATP levels and the induction of mitochondrial biogenesis via the activation AMPK is well established (Long and Zierath 2006). Upon changes in energy availability, and thus, changes in the ATP-to-ADP or ATP-to-AMP ratios, AMPK is activated and stimulates glucose utilization in order to replenish ATP stores. AMPK increases the glucose uptake via the upregulation of GLUT transporters (J. H. Kim et al. 2010), and it also promotes mitochondrial biogenesis aiming at increasing the oxidative capacity of the cell (Herzig and Shaw 2018). Additional studies should be adressed to define whether the downstream effectors of AMPK that contribute to the regulation of mitochondrial biogenesis, such as the peroxisome proliferator-activated receptor-ɣ co-activator 1 (PGC1), the oestrogen-related receptors (ERRs) or the peroxisome proliferator-activated receptor (PPAR) family of transcription factors, are involved in the enhanced mitochondrial mass observed our CD98hc KO model. In the line of this discussion, in a recent study performed by Balsa and colleagues, it was demonstrated that glucose deprivation causes a metabolic switch towards OXPHOS at the expense of increased expression of mitochondrial proteins that form part of the ETC super-complexes. Like in CD98hc KO cells, despite such metabolic reprogramming, glucose-deprived cells present a reduced ATP content and increased AMP:ATP ratio (Balsa et al. 2019).

Furthermore, supporting our results, disruption of glycolysis via different mechanisms, e.g. deletion or inhibition of glucose-6P isomerase (GPI), which catalyse the interconversion between glucose-6P and fructose-6P (de Padua et al. 2017), the lactate transporters MCT1 and MCT4 (Benjamin et al. 2018; Cormerais et al. 2016; Granja et al. 2014), their ancillary protein CD147 (Y. Cormerais et al. 2016; Granja et al. 2014) or the enzyme LDH (Brand et al. 2016; Fantin, St-Pierre, and Leder 2006), also triggers a metabolic reprogramming towards mitochondrial respiration due to different mechanistic routes.

Regarding the inhibition of MCT1 and CD147, both downregulated in CD98hc KO cells, it was reported that it results in an intracellular accumulation of lactate (Benjamin et al. 2018; Y. Cormerais et al. 2016; Granja et al. 2014). MCTs couple

the transport of lactate and H^+ with an obligatory 1:1 stoichiometry across the plasma membrane, thus, the blockage of the lactate export and therefore its intracellular accumulation would lead to, on one hand, a decrease in the intracellular pH (pHi) levels, and on the other hand, a halt in the conversion of pyruvate into lactate. Consequently, cytosolic acidification would reduce the glycolytic rate via inhibition of the rate-limiting enzyme phosphofructokinase (PFK) (Calderon-Montano et al. 2011). In addition, high intracellular lactate concentrations can result in end-product inhibition of LDH (Stambaugh and Post 1966) and, as a consequence, loss of NAD^+ regenerating capacity. Since NAD^+ is reduced to NADH during glycolysis, a constant supply of this metabolite is required to maintain a continuous rate of this pathway (Benjamin et al. 2018).

However, despite the decreased expression of CD147 and MCT1 in cells lacking CD98hc (**Figure 95**), we did not observe an accumulation of intracellular lactate. Indeed, the content of this metabolite is reduced in these cells and also in their extracellular media, suggesting that it is being produced to a lesser extent than in the WT cells. This assumption is also supported by the fact that ^{13}C-glucose is much less incorporated into lactate in the null cells. This lower conversion could be due to the reduced glycolysis rate per se, but it also may be potentiated by the suppression of LDHA in parallel with the increased expression of LDHB, which favours the catalysis of the lactate oxidation to pyruvate, coupled with NADH regeneration (**Figure 95**). Interestingly, this coupling between levels of both LDH isoforms has previously been described as a result of the activation of the AMPK-mTORC1 axis (Nam, Oh, and Shin 2016).

Considering that lactate is not being accumulated in cells lacking CD98hc, it is unlikely that a decrease in the pHi levels is affecting the activity of the PFK in these cells. Indeed, the incorporation of glucose into 3P-glycerate is the first step in which glycolysis is compromised. Interestingly, this is the first glycolotic reaction in which NAD^+ is needed, suggesting that levels of this cofactor may underlay the alterations in this pathway. In this regard, NAD^+ and NADH levels should be determined to clarify this hypothesis. If any alteration was detected

regarding NAD^+ concentration, manipulation of the NAD^+/NADH ratio, for instance, by using the novel genetically encoded tool *Lb*NOX generated to recycle NAD^+ in Mootha's laboratory (Titov et al. 2016) or by supplementing the culture media with its precursor NMN (Yoshino, Baur, and Imai 2018), would potentially promotes the restoration of the glycolytic rate.

Besides the aforementioned putative connexions between glucose metabolism and the loss of CD98hc, it is worth bearing in mind that the concomitant BCAA and AAA shortage may also be involved in the metabolic rewiring described in the CD98hc KO model. Indeed, our data demonstrated that shortage of these AAs increased the mitochondrial OXPHOS in low 6AA cells. Moreover, addition of BCAA- and AAA- containing dipeptides into CD98hc KO media reduces the mitochondrial OCR coupled to ATP production in the KO cells. These results suggest that cell adaptation to limited EAA availability can occur at the expense of higher OCR coupled to an increased ATP production in the mitochondria (**Figure 95**), although the mechanism by which they reprogram the metabolism remains elusive.

Previous results highlight the ability of BCAAs and AAAs to regulate the energy metabolism of the cell. Although the role of these AAs in metabolism has rarely been study, two recent works have brought light into this issue. On one hand, it has been described that branched chain ketoacid dehydrogenase kinase (BCKDK) deficiency, which is a negative regulator of branched-chain α-ketoacid dehydrogenase complex (BCKDHc), the key enzyme of the BCAA catabolism, results in the permanent activation of BCKDHc, promoting BCAA hypercatabolism. "Metabolically speaking" this would be the antagonist of our model, and accordingly, BCKDK KO fibroblasts present decreased OXPHOS (Oyarzabal et al. 2016). Likewise, ablation of the mitochondrial targeted 2C-type serine/threonine protein phosphatase (PP2Cm), which disrupts BCAA catabolism has been shown to repress glucose utilization in heart (Li et al. 2017).

Although glucose is the major energy source, cells can also use a diversity of carbon substrates able to be oxidised in the TCA cycle. Oxidation of glutamine in

the mitochondria is a major metabolic fate of this AA and a primary source of energy for proliferating cells. In this way, glutamine can be routed through the TCA cycle to maintain OXPHOS in a process called glutaminolysis (Ahn and Metallo, 2015). This substrate plasticity enables cells to rewire their metabolic pathways, which is considered one of the major hallmarks in cancer (Yang, Venneti, and Nagrath 2017). Indeed, a bulk of studies demonstrate that glutaminolysis guarantees cell survival in cases of inefficient glucose metabolism (Fan et al., 2014; Fantin et al., 2006; Le et al., 2010; Marchiq et al., 2015; Ždralević et al., 2018). In the light of our results, it seems feasible that cells lacking CD98hc have adapted to use glutamine to boost mitochondrial respiration in order to survive. However, further experiments are necessary to confirm this suggestion, for instance by using the same ^{13}C isotope-assisted method we used to quantify glucose metabolism.

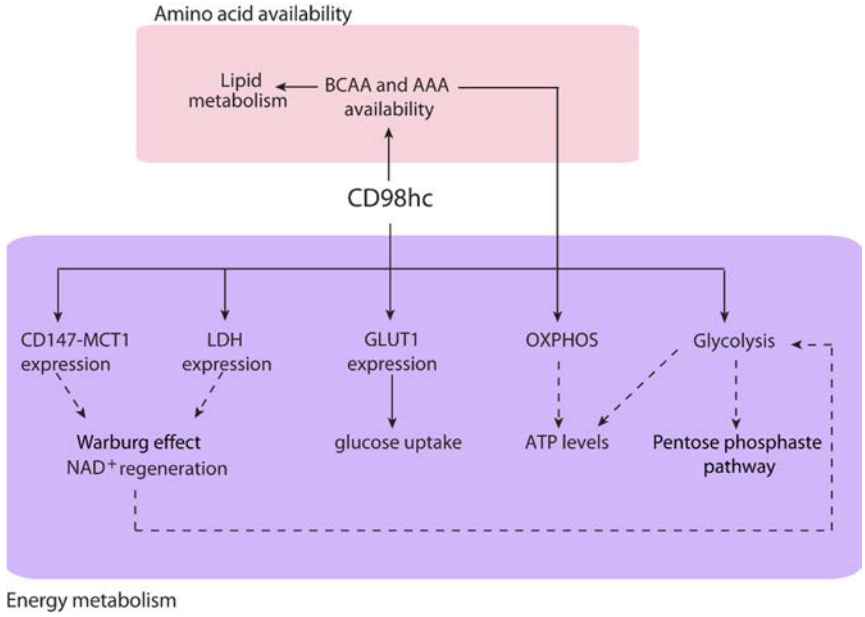

Figure 95. CD98hc regulates glucose utilization, controlling the energy metabolism of the cell. CD98hc controls the expression of CD147, MCT1, LDH and GLUT1, all key for glucose metabolism. Moreover, CD98hc expression influences OXPHOS, glycolysis and PPP rates, which in turn has an impact in the ATP levels of the cell. In addition, BCAA and AAA availability is also able to regulate the cellular metabolism of the cell. Solid lines represent established connexions proposed in this work. Dashed lines represent connexions suggested by the data provided herein and literature.

In summary, in this study we have evaluated the extensive cellular functions related to redox homeostasis, protein synthesis, cell cycle regulation and energy metabolism that rely on CD98hc. Our data further support the belief that CD98hc is a putative target in pathophysiological scenarios, especially in the context of cancer treatment. On the one hand, targeting CD98hc downregulates tumour growth by decreasing the redox counterbalance capacity of the cells, mediated by CD98hc-xCT. On the other hand, CD98hc ablation limits the required balance in the AA content for proper protein synthesis and cell proliferation, mostly harmonised by CD98hc-LAT1. Moreover, it leads to disrupted glucose utilization, disturbing the Warburg effect, triggering decay in ATP levels and blocking nucleotide biosynthesis, which ultimately results in cell cycle arrest (**Figure 96**). Finally, although not studied in the present thesis, CD98hc loss of function compromises integrin-regulated signalling pathways needed for tumour growth and invasion (Fenczik et al. 1997; Feral et al. 2005; de la Ballina et al. 2016).

To date, many studies have focused on the search for either inhibitors of xCT (Balza et al. 2013) or LAT1 (Häfliger et al., 2018; Hayashi and Anzai, 2017; Im et al., 2008; Oda et al., 2009) transporters as anti-cancer strategies. Even though these strategies are appealing approaches, yet limited results have been obtained so far. Generating drugs against CD98hc could represent a novel option, widening the therapeutic window of cancer therapy by inducing an immediate impairment in the diverse cellular functions described above (**Figure 96**).

Moreover, the arrest in S-phase may enhance the sensitivity of cancer cells to chemotherapeutic (Mills, Kolb, and Sampson 2018; X. Wang et al. 2018) and radiotherapeutics (Bull et al. 2004; M. Y. Li et al. 2017; Otani et al. 2016) agents. In the same line, the reported results suggest that CD98hc ablation leads to increased reliance on oxidative mitochondrial respiration, which would make cells lacking CD98hc extremely sensitive to inhibitors of the ETC. Thus, combinatorial therapy involving the ablation of CD98hc emerges as a promising strategy for anti-cancer therapeutic purposes. CD98hc-targeting drugs could be delivered locally to tumours where this protein is strongly overexpressed.

Finally, the results obtained in this thesis add light into the different cellular functions that rely on BCAA and AAA availability. Beyond cancer disease, many other disorders, such as the severe protein malnutrition syndrome Kwashiorkor (Giovanni et al. 2016; Hsu et al. 2014), cardiovascular diseases (Ferguson and Wang 2016; Li et al. 2017), insulin resistance (Würtz et al. 2013), diabetes (Hernández-Alvarez et al. 2017), Parkinson's disease (Ohtsuki et al. 2010), Autism Spectrum Disorder (Tărlungeanu et al. 2016) or Maple syrup urine disease (Burrage et al. 2014; Schadewaldt and Wendel 1997), have been related to alterations in BCAA or AAA availability and catabolism, stressing the importance of their further study and characterization.

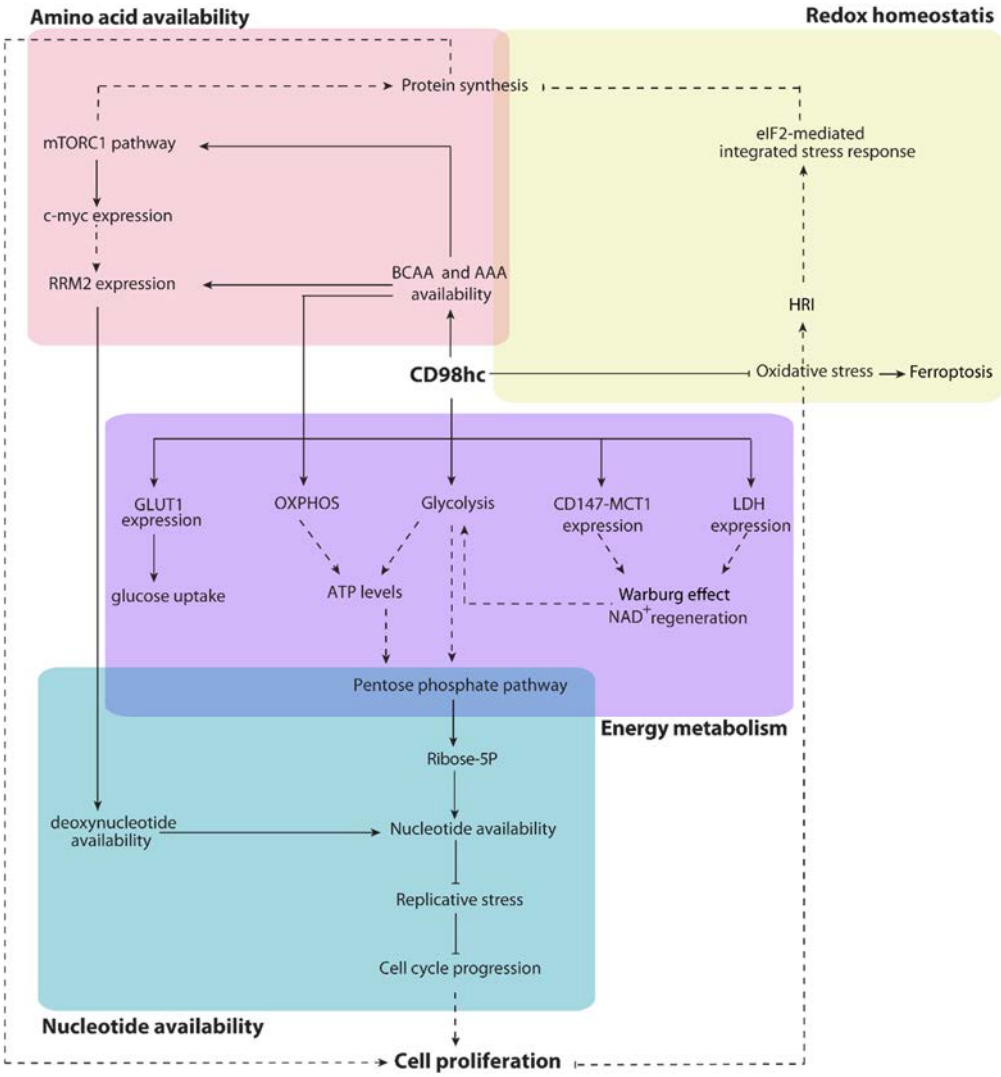

Figure 96. Overview of the most relevant results reported in the present thesis.

Conclusions

I. CD98hc protects cells against oxidative stress, preventing ferroptosis and leading to cell survival.

II. CD98hc promotes proper cell proliferation by sustaining the balance of intracellular amino acid content needed to regulate the nutrient-sensing signalling pathway mTORC1. Moreover, ablation of CD98hc leads to the activation of the integrated stress response mediated by eI2Fα, probably due to the increased oxidative stress. Both pathways would contribute to the defective global protein synthesis observed in cells lacking CD98hc.

III. CD98hc sustains the BCAA and AAA availability required to maintain the expression of RRM2 and thereby the deoxynucleotide synthesis, necessary for cell cycle progression and proliferation.

IV. The lack of CD98hc triggers a reduction in the glucose uptake and glucose-related metabolic pathways, such as glycolysis and the pentose phosphate pathway, forcing cells to use mitochondrial oxidative metabolism in order to maintain the cellular ATP levels, which suggests a metabolic rewiring.

V. CD98hc supports the production of ribose-5P and therefore is required for nucleotide biosynthesis. Loss of CD98hc leads to a dramatic reduction in the nucleotide pool, causing replicative stress, enhanced DNA damage response, S-phase delay and diminished rate of mitosis.

Materials and Methods

7.1 Cell culture protocols

7.1.1 Cell lines and growing conditions

WT and CD98hc KO fibroblasts derived from mouse embryonic stem cells were generated by Chloé C. Féral (Université de Nice - Sophia Antipolis, Nice, France) (Feral et al. 2005).

WT and CD98hc KO fibroblasts were cultured in DMEM high glucose (21969035, Thermo Fisher Scientific) medium supplemented with 10% v/v FBS (SH30066.03, HyClone), 20 mM Hepes, pH 7.3, 100 μM non-essential amino acids (EAAs) (11140035, Thermo Fisher Scientific), 2 mM L-glutamine (25030-024, Thermo Fisher Scientific), 100 μM β-mercaptoethanol (β-ME) (31350010, Thermo Fisher Scientific) and 100 U/mL Penicillin-Streptomycin (15140122, Thermo Fisher Scientific).

WT fibroblasts referred to as control and low 6AA cells were cultured for 3 days in DMEM medium (D9800-13, Stratech) supplemented with 10% v/v FBS (SH30066.03, HyClone), 20 mM Hepes, pH 7.3, 100 μM non-EAAs (11140035, Thermo Fisher Scientific), 2 mM L-glutamine (25030-024, Thermo Fisher Scientific), 100 μM β-ME (31350010, Thermo Fisher Scientific), 100 U/mL Penicillin-Streptomycin (15140122, Thermo Fisher Scientific), 25 mM glucose, 1 mM sodium pyruvate, 44 mM sodium bicarbonate and the same concentration of AAs as complete DMEM media, with the exception of BCAAs and AAAs in low 6AA media (16 μM L-isoleucine, 16 μM L-leucine, 8 μM L- phenylalanine, 1.5 μM L-tryptophan, 7.8 μM L-tyrosine and 16 μM L-valine). Total amino acid concentrations are indicated in **Figure 26**.

Where indicated, cells were treated with 1 mM sulfasalazine (SAS) (S0883-10G, Sigma-Aldrich), and 3 μM rapamycin (sc-3504, Santa Cruz) 3 h.

CD98hc KO HEK 293T cells were generated by CRISPR/Cas9 technology as describe below (**7.1.2**). WT and CD98hc KO HEK 293T cells were cultured in same growing conditions as WT and CD98hc KO fibroblasts.

Cells were maintained at 37°C and 5% v/v CO_2 in a humidified incubator and were periodically tested with a PCR detection kit to ensure that they were mycoplasma-free (MP0035, Sigma-Aldrich).

7.1.2 CRISPR/Cas9-mediated CD98hc knockout in HEK 293T cells

To generate CD98hc knockout cells, CRISPR/Cas9 system was used according to the manufacturer's instructions (Santa Cruz).

Phase 1: CRISPR/Cas9 KO and HDR plasmid transfection

HEK 293T cells were seeded onto 6-well plates and were grown until 50% confluence. Then, they were co-transfected with the CD98hc CRISPR/Cas9 KO plasmid (**Figure 97A**) (sc-400501, Santa Cruz) and the CD98hc homology-directed repair (HDR) plasmid (**Figure 97B**) (sc-400501-HDR, Santa Cruz). Transfection was performed as indicated above (**7.1.5**) with 1 ug of each plasmid per well. CD98hc CRISPR/Cas9 KO plasmid consists of a pool of 3 plasmids designed to disrupt gene expression by causing a double-strand break in 5'-GATTCTCTATGTCCCGAACC- 3', 5'-TCGGGACATAGAGAATCTGA- 3' and 5'-TCATCCCCGTAGCTGAAAAC- 3' and CD98hc HDR plasmid contains a puromycin resistance gene in order to allow the selection of stably transfected cells with successful integration (**Figure 97**). Successful co-transfection of the CRISPR/Cas9 CD98hcKO- and HDR- plasmids was visually confirmed via fluorescent microscopy by detection of GFP and RFP, respectively (**Figure 98A**).

Phase 2: Puromycin selection

DMEM medium was changed with fresh medium containing 1 ug/ml puromycin (sc-108071B, Santa Cruz). Expanded pools of cells resistant to puromycin were maintained for three passages in the corresponding selective medium.

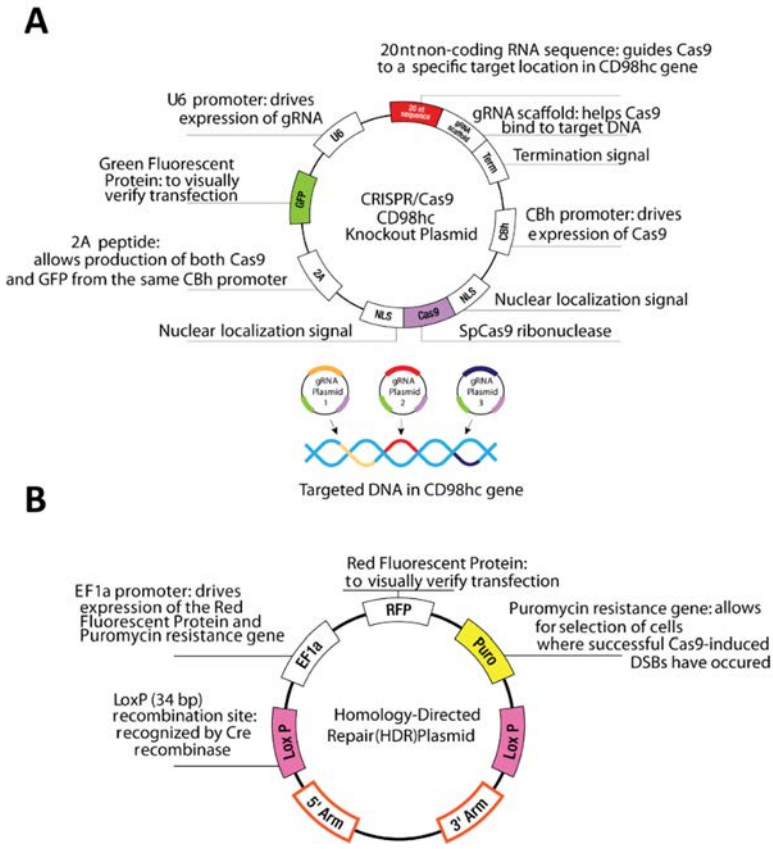

Figure 97. CRISPR/Cas9-mediated CD98hc knockout in HEK 293T cells. HEK293T cells were co-transfected with CD98hc CRISPR/Cas9 KO plasmid (A) and CD98hc homology-directed repair (HDR) plasmid (B).

Phase 3: Single clone generation

Cultures were further enriched for cells expressing high levels of RFP by sorting on a FACS (BD FACSAria™Fusion; BD Biosciences) (**Figure 98B** and **Figure 98C**). Sorter was used to deposit single cells into a 96-well plate for clonal selection in *The Flow Cytometry Facility of the Parc Científic de Barcelona.* Several clones were obtained, expanded and assayed for CD98hc expression. The knockout of CD98hc was confirmed by Western blot (**Figure 99A**), RT-PCR (**Figure 99B**) and PCR (**Figure 99C**) analyses.

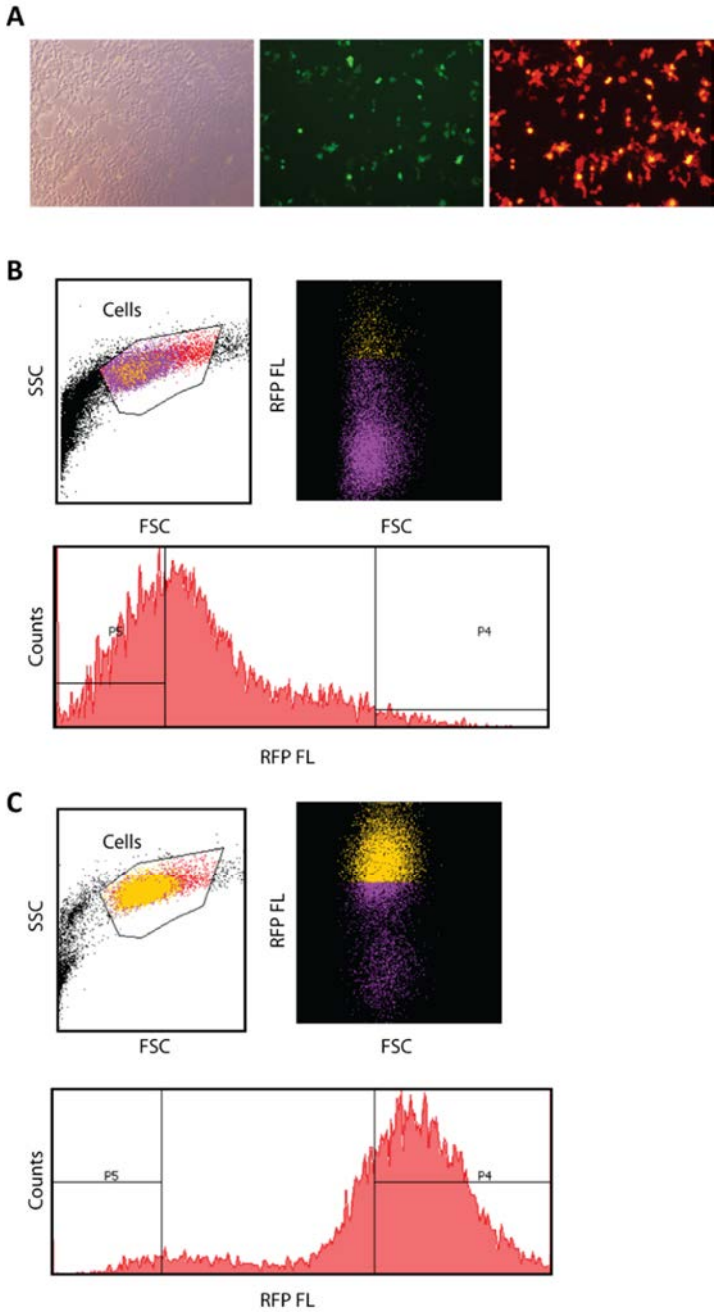

Figure 98. Generation of CRISPR/Cas9-mediated CD98hc knockout HEK 293T cells. **A**, co-transfection of the CRISPR/Cas9 CD98hcKO- and HDR- plasmids was monitored via fluorescent microscopy by detection of GFP and RFP, respectively. **B** and **C**, cell cultures were further enriched for cells expressing high levels of RFP (yellow) by sorting on a FACS. First and second selections correspond to **B** and **C**, respectively. Note that in the second round most of the cells presented high levels of RFP (yellow). Cells that express RFP are depicted in purple.

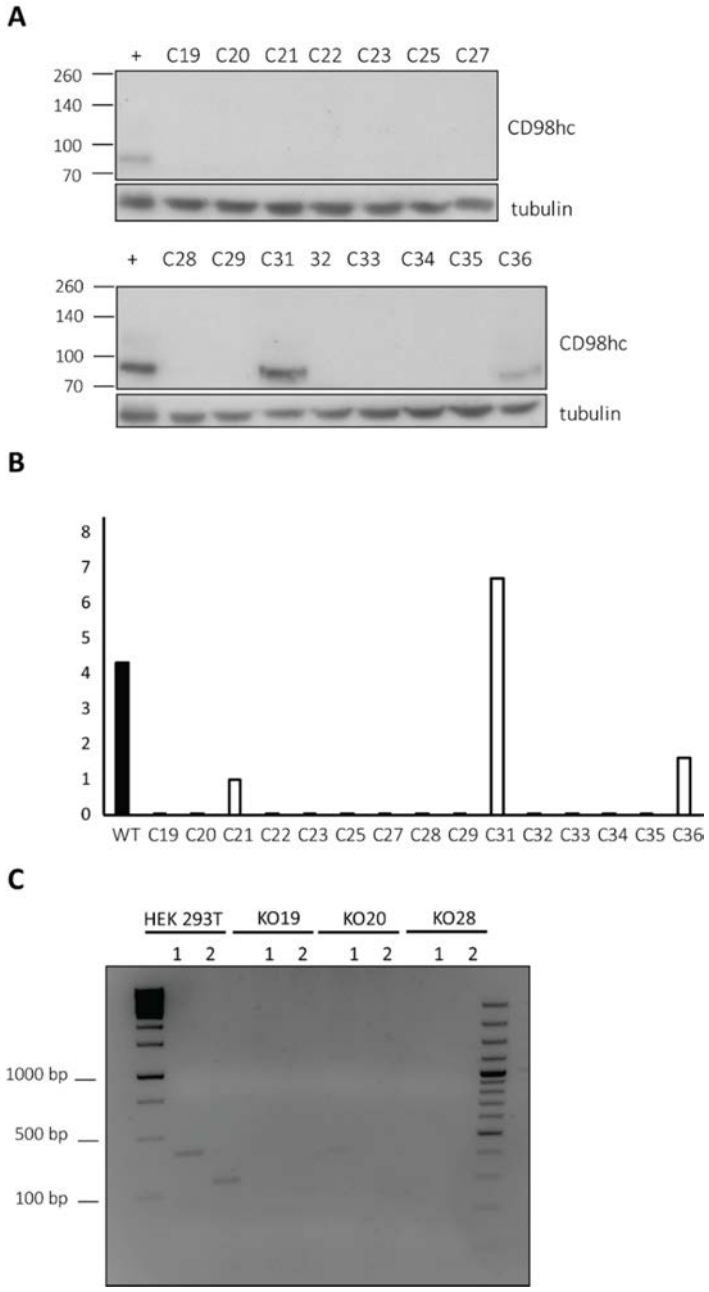

Figure 99. Confirmation of the deletion of CD98hc in CD98hc KO HEK 293T cells. **A,** several clones (C) were tested for CD98hc protein expression by Western blot. **B**, several clones were tested for CD98hc mRNA expression by RT-PCR. **C**, *CD98HC* deletion was checked in the genomic DNA of clones 19, 20 and 28 by PCR amplification. 1 and 2 correspond to different pair of amplification primers. The expected size of the amplicons is 394 and 185 base pairs, respectively.

7.1.3 Cell freezing and thawing

Cellular stocks were kept at liquid nitrogen or storaged at -80ºC. Cells were detached from the culture dish by trypsinization and pelleted. Freezing solution (90 % serum, 10 % DMSO (#D2650, Sigma-Aldrich) was added to the cell pellet, not exceeding $10x10^6$ cells/ml, and suspension was transferred to cold cryotubes which are immediately transferred to the -80ºC freezer before ultimately transferring cells to the liquid nitrogen container.

For frozen cell recovery, the cryotubes were placed in warm water, agitating gently until completely thawed. Rapid thawing (60 to 90 sec at 37ºC) provides the best recovery for most cell cultures. The contents of the vials were poured to T75 flasks which were incubated normally.

7.1.4 Dipeptide and nucleoside supplementation

BCAA- and AAA-containing dipeptides were synthesised by *The Synthesis of Peptides Unit (U3) of the CIBER in Bioengineering, Biomaterials and Nanomedicine (CIBER-BBN)* at the Barcelona Science Parc. Briefly, dipeptides were synthesized in solution by coupling of the corresponding protected N- and C-terminal AAs using 2-(1H-benzotriazol-1-yl)-1,1,3-tetramethylmethyl-uroniumhexafluoro phosphate (HBTU) in dimethylformamide as the coupling reagent. Once the reaction was finalized, protected dipeptides were precipitated with cold water, centrifuged, and washed again with cold water. Protecting groups were eliminated by the addition of trifluoroacetic acid, and after 1 h final dipeptides were precipitated by the addition on cold diethyl ether. Dipeptides were redissolved in H_2O and lyophilized. Purity was estimated by HPLC and HPLC-MS.

Where indicated, each dipeptide was supplemented at a concentration of 0.25x of the corresponding BCAA or AAA concentration in complete DMEM medium: BCAAs: isoleucine (200 μM), leucine (200 μM), and valine (25 μM), or AAAs: phenylalanine (25 μM), tyrosine (200 μM), and tryptophan (100 μM).

Where indicated, nucleosides (ES-008-D, EmbryoMax) were supplemented for 48 h (150 µM cytidine, 150 µM guanosine, 150 µM uridine, 150 µM adenosine and 50 µM thymidine).

7.1.5 Transitory cell transfection

Cells were seeded onto 6-well plates over-night. A reaction mix containing 6 ng of the plasmid of interest was prepared in 2 mL tubes (Eppendorf). 1,560 mL of NaCl and 78 mL of pollyethylenimine (PEI) (#23966, Polyscience) were added into the 2 mL tube and after vortex the mix is incubated for 15 min at room temperature, then it is again mixed and added on top of the cells attached to the culture dishes with fresh medium. 24 h after transfection the next step of the protocol was performed depending on the experiment.

7.1.6 Cell proliferation assay

WT and CD98hc KO cells were seeded in duplicate at 1×10^4 cells per well onto 6-well plates. Cell medium were daily changed. Where indicated, BCAA- and AAA-containing dipeptides were added as described above (**7.1.4**).

Control and low 6AA cells were seeded in duplicate in corresponding media at 1×10^4 cells per well onto 6-well plates.

Cells were collected and counted at indicated time points using the Neubauer chamber method.

7.2 General molecular biology protocols

7.2.1 Protein extraction

7.2.1.1 Total cellular protein extraction

Total cellular protein extracts for immunoblotting analysis were performed as follows: cells were rinsed in ice-cold PBS and scraped from culture plates in lysis

buffer: 150 mM NaCl, 10 mM Tris, pH 7.2, 0.1% w/v SDS, 1% w/v Triton X-100, 1% w/v deoxycholate, 5 mM EDTA, phosphatase inhibitor cocktail (524628-1SET, Merck Chemicals & Life Science S.A.) and protease inhibitor mixture (11836153001, Sigma-Aldrich). Homogenates were further homogenized by passing them through a 25G syringe, rotated for 1 h at 4 °C and centrifuged at 13,000 rpm for 15 min at 4 °C.

7.2.1.2 Total membranes extraction

If total membrane extraction was required, cells were rinsed in homogenization buffer: 25 mM Hepes, 4 mM EDTA, 250 mM sucrose, phosphatase inhibitor cocktail (524628-1SET, Merck Chemicals & Life Science S.A.) and protease inhibitor mixture (11836153001, Sigma-Aldrich). After passing the homogenates through a 25G syringe, cell extracts were disrupted by three rounds of 30 sec sonication. Then, centrifugation at 10,000 g for 10 min at 4°C was performed and supernatants were transferred to microcentrifuge tubes and centrifuged at 200,000 g for 1 h at 4°C in a TLA-55 rotor (Beckman Coulter).

7.2.2 Co-immunoprecipitation assays

The interaction between CD98hc and associated light chains, CD147 and MCT1 was assessed by co-immunoprecipitation assays by pulling down each c-myc-tagged-light chain previously transfected in HEK 293T cells (**Figure 100**).

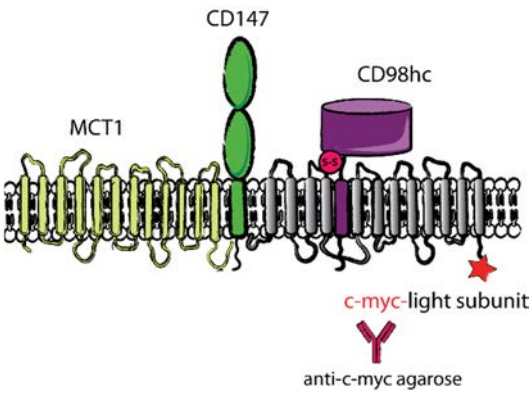

Figure 100. Co-immunoprecipitation of CD98hc and associated light chains, CD147 and MCT1. c-myc-tagged light chains were transfected in HEK 293T cells and they were pulled down with anti-c-myc agarose. Endogenous co-immunoprecipitated CD98hc, MCT1 and CD147 was analysed.

Cells were transfected as indicated above (**7.1.5**) with the following plasmids: pCDN3 (negative control), c-myc-LAT1, c-myc-LAT2, c-myc-y$^+$LAT1, c-myc-xCT and c-myc-asc1.

24 h after transfection, cells were harvested in lysis buffer: 25 mM HEPES pH 7.5, 150 mM NaCl, 5 mM MgCl, 1% Brij 99 with protease inhibitors (11697498001, Sigma-Aldrich). Cells were then disrupted using a 25G-syringe and solubilise at 4 °C for 1 h with rotation. After centrifugation at 10,000 g for 5 min, supernatant was kept and protein quantification was performed using the Pierce BCA Protein assay kit (23225, Thermo Fisher Scientific) as described in **7.2.3**.

Before performing the co-immunoprecipitation assay, anti-c-myc agarose conjugated (A 7470, Sigma-Aldrich) was prepared. The desired amount of the 1:1 suspension of the anti-c-myc agarose conjugate (50 µl per sample) was washed 5 times with 1ml PBS.

1 mg of protein sample was added to the settled resin and if necessary, volume was brought to 400 µL with PBS. Samples were rotated over-night at 4°C. Then, the resin was washed 6 times with 2CMC (critical micelle concentration) of Brij 99. After the final wash, supernatant was aspirated leaving ~10 µL above the resin. 20 µL 2X of SDS sample buffer was added and samples were incubated 5 min at 95°C before being analysed by immunoblotting (**7.2.4**).

7.2.3 Protein quantification

Protein quantification was performed using the Pierce BCA Protein assay kit (23225, Cultek). A standard curve is generated between 0.5 mg/mL to 20 mg/mL using 2 mg/mL BSA from the kit. Samples were distributed in a 96-well-plate and 200 µL of reaction mixture (A+B solutions at 50:1 ration from the kit) was added to each well. The plate is incubated 20 min at 37 °C and absorbance was measured at 562nm. Protein concentration was calculated by interpolation from the standard curve.

7.2.4 Immunoblotting

Cells were lysed in radioimmunoprecipitation assay (RIPA) buffer (**7.2.1.1**) and after centrifugation at 10,000 g for 15 min at 4°C, protein concentrations were determined using the Pierce BCA protein assay (**7.2.3**). Protein extracts (20 µg, unless specified otherwise) were separated by electrophoresis on 10% or 15% SDS polyacrylamide gel and transferred onto Immobilon membranes (IPVH00010, Millipore). Membranes were blocked in 5% non-fat milk or 3% BSA according to datasheet specifications and incubated with the primary antibodies indicated in **Table 2.** Immunoreactive bands were detected with the horseradish peroxidase antibodies indicated in **Table 2** using the ECL system (RPN2106, Sigma-Aldrich). Analysis and quantification of immunoreactive bands were performed using ImageJ software.

7.2.5 RNA extraction

Total RNA from the cell culture was extracted using an RNA extraction kit (12183018A, PURELINK RNA MINI KIT, Invitrogen) following the manufacturer's instructions. Briefly, cells cultured in 6-well plates were scraped in 300 uL of PureLink RNA Mini Kit's lysis buffer with DTT. Samples were then homogenized by passing them through a 25G syringe 10 times and 300 uL 70% ethanol were added in order to keep 1:1 volumes. After vortex, samples were placed into purification columns from PureLink RNA Mini Kit and RNA was purified following the instructions according to protocol. A DNAse treatment step was included.

7.2.6 RNA quantification

RNA samples were quantified using the Nanodrop spectrometer (Thermo Fisher Scientific). RNA purity was determined by the A260/A280 and A260/A230 absorbance ratios. A A260/A280 ratio of 1.8 is accepted as pure DNA, whereas pure RNA is at 2.0. If this ratio is lower than expected could entail sample contamination with DNA, phenol, proteins or other contaminants that absorb

preferentially at or near 280 nm. Moreover, pure nucleic acid result in a higher 260/230 ratio than 260/280 ratio. Lower ratios can be ascribed to contaminants, such as EDTA, carbohydrates or phenol from the RNA extraction.

Table 2. Antibodies used and details of usage.

Target	Raised in	Working conditions	Cat.number	Source
Primary antibodies				
P-S6	rabbit	1:2000	#2211S	Cell Signaling
S6	mouse	1:8000	sc-74459	Santa Cruz
P-eIF2α	rabbit	1:1000	#9721	Cell Signaling
eIF2α	rabbit	1:1000	#9722	Cell Signaling
HRI	goat	1:500	sc-21949	Santa Cruz
P-CHK1	rabbit	1:2000	#2348	Cell Signaling
CHK1	mouse	1:2000	#2360	Cell Signaling
P-RPA	rabbit	1:2000	A300-245A-T	Bionova Cientifica
RPA	Rat	1:2000	#2208	Cell Signaling
NRF2	rabbit	1:1000	ab62352	Abcam
RRM2	rabbit	1:1000	GTX103193	GeneTex
tubulin	mouse	1:5000	#T5168	Sigma-Aldrich
vinculin	mouse	1:5000	ab18058	Abcam
β-actin	mouse	1:5000	A1978	Sigma-Aldrich
PEPT1	rabbit	1:5000		custom made by Dr. H. Daniel
PERK	rabbit	1:1000	sc-13073	Santa Cruz
ATF4	rabbit	1:1000	#11815	Cell Signaling
GADD34	rabbit	1:1000	sc-8327	Santa Cruz
c-myc	rabbit	1:1000	#5605	Cell Signaling
GLUT1	rabbit	1:1000	GT-11-A	Alpha Diagnostic
GLUT3	rabbit	1:500		custom made by Gwyn Gould
CD147	mouse	1:1000	sc-21746	Santa Cruz
MCT1	mouse	1:1000	sc-365501	Santa Cruz
CD98hc	rabbit	1:1000	sc-9160	Santa Cruz
porin	mouse	1:1000	ab14734	Abcam
ASNS	rabbit	1:500	GTX103569	GeneTex
Secondary antibodies				
anti-mouse	donkey	1:10,000	715-035-150	Jackson Immuno Research Europe
anti-rabbit	donkey	1:10,000	711-035-152	Jackson Immuno Research Europe
anti-rat	chicken	1:15,000	sc-2956	Santa Cruz
anti-goat	donkey	1:10,000	705-035-003	Jackson Immuno Research Europe

7.2.7 RNA reverse transcription to cDNA

RNA was reverse-transcribed with the reverse transcriptase SuperScript RTII (18064014, Invitrogen). Briefly, 1 µg of RNA diluted in RNase-free water was added to PCR tubes to a final volume of 10 µL. A mix containing: 1 µL deoxynucleotides (10 mM stock 1:1:1:1 of dATP, dCTP, dGTP, dTTP) and 1 µL oligodT (500 µg/mL stock) was added per sample. Samples were heated at 65°C for 5min to ensure linearization of RNA molecules. Then, a mix containing: 4 µL of 5X First-Strand Buffer, 2 µL 0.1M DTT, 1 µL of RNAseOUT (40 U/ µL stock) were added in each sample and samples were heated at 42°C for 2 min before the addition of 1 µL of SuperScrip II reverse transcriptase (200 U/ µL stock). Reverse-Transcription Polymerase Chain Reaction (RT-PCR) was set for 53 min at 42°C to allow DNA polymerization. Then, samples were heated for 15 min at 70°C to stop the reaction and cooled down to 4°C to ensure preservation. Generated cDNA was diluted to 1/2 (50 ng/ µL) with Milli-Q H_2O and stored at -20°C.

7.2.8 Quantitative real-time PCR (RT-PCR)

Sets of specific primers indicated in **Table 3** were used for amplification using the ABI Prism 7900 HT real-time PCR machine (Applied Biosystems) and SYBR Green PCR Master Mix (4368702, Thermo Fisher Scientific) for quantitative RT-PCR. Assay Master Mix for SYBR Green analysis (7 µL per sample) was prepared by combining 5 µL of SYBR Green PCR Master Mix and 2 uL (1.25 µM stock) of primer mix (forward and reverse). The reaction volume was set to 10 µL per well with 3 µL of cDNA (25 ng). Plates of 384 wells were loaded with 3 µL of cDNA and then, master mix (7 µL) was loaded. RT-PCR negative controls were loaded to identify crosscontamination and 3 technical replicates were analysed per sample. All measurements were normalized to RPLP0. Alternatively, in the case of mtDNA copy number assessment (**7.14**), genomic DNA was diluted to achieve a concentration of 100 pg/ µL.

Table 3. Real time PCR SYBR Green primers.

gene	F/R	5'-3' sequence
mouse		
CD98hc	F	GAAGATCAAGGTGGCGGAGGAC
	R	CAAGTACTCCAGATGGCTCTTCAGACC
LAT1	F	GTGTGCGGCGTCTTCTCCATC
	R	GAAGCCGAGCAAAATGATGAGG
LAT2	F	CTCCGGAATCTTTGTCTCACCGAAAG
	R	CTTCCCAGCTGTGAAGATATCTTGAACC
xCT	F	GGTGTAATCCGTCTCCACAGA
	R	GACTTGTGTCTCTTCCTGAAAATGCATC
y+LAT1	F	CTAAAGGGCAATGCGAGCAAGCTG
	R	GGTGGTACCCAGTTCAGCGTAACAAAG
y+LAT2	F	CCTTTATCCGTCTGTGGGTCTCACTTC
	R	CAGAGTACAGGGCAAGAGAGAGGTCTCC
asc1	F	GTGGGTGAACAGCTCCAGCGTAC
	R	CCACGAAAAGTAGCCCAGCAGC
CAT1	F	GGACACGGAGCGGAAAATACACC
	R	GCTCCCTGCTGTACTGGTTCATGGTC
CAT2	F	GAAGATCAAGGTGGCGGAGGAC
	R	CAAGTACTCCAGATGGCTCTTCAGACC
CAT3	F	GGCTCCCTCTGTGCACTTTCTA
	R	TAGCAAGGACACGGAACAGGA
CHAC1	F	CTTGAAGACCGTGAGGGCTG
	R	GTGGGGTGGCCACATAGG
GLUT1	F	AGCCCTGCTACAGTGTAT
	R	AGGTCTCGGGTCACATC
GLUT3	F	CTCTTCAGGTCACCCAACTACGT
	R	CCGCGTCCTTGAAGATTCC
c-myc	F	CGGACACACAACGTCTTGGAA
	R	AGGATGTAGGCGGTGGCTTTT
ATF4	F	CCTGAACAGCGAAGTGTTGG
	R	TGGAGAACCCATGAGGTTTCAA
PEPT1	F	GCCGGACCAGATGCAGACGG
	R	GCGGGTACACCACAGCGTCC
SREBP2	F	TGTAATCAATGGCCTTCCTCAGA
	R	CAAAATCATAGAGTTGAAGGACTTAGTCA
SREBP1c	F	CCTGTCTCACCCCCAGCATA
	R	GGAGCCATGGATTGCACATT
FAS	F	CCATGCCCAGAGGGTGGTTG
	R	AGCGGCCATTTCCATTGCCC
LDHA	F	TGTCTCCAGCAAAGACTACTGT
	R	GACTGTACTTGACAATGTTGGGA
LDHB	F	AGTCTCCCGTGCATCCTCAA
	R	AGGGTGTCCGCACTCTTCCT
RPLP0	F	CACTGGTCTAGGACCCGAGAAG
	R	GGTGCCTCTGGAGATTTTCG
TFAM	F	AACACCCAGATGCAAAACTTTCA
	R	GACTTGGAGTTAGCTGCTCTTT

gene	F/R	5'-3' sequence
human		
CD98hc	F	GACCCCTGTTTTCAGCTACG
	R	TCAGGGAAGCTGGACTCATC
LAT1	F	GGAAGGGTGATGTGTCCAATC
	R	TAATGCCAGCACAATGTTCCC
LAT2	F	GCCCTCACCTTCTCCAACTAC
	R	CGCACACTGGAACAGTTGAC
xCT	F	GCTGGCTGGTTTTACCTCAA
	R	AGCACATAGCCAATGGTGAC
y⁺LAT1	F	CCTTTGGAGGATTCCTTGCTT
	R	GTTCCCCATTTGACATAGGCA
y⁺LAT2	F	ACTACATCATCCAGCCGTCC
	R	GCGTAAGTGAACGTGTCCTG
asc1	F	TCAAGAAGGAGATCGGGCT
	R	CAGACGAACAGGGCCAGA
CAT1	F	CTTCATCACCGGCTGGAACT
	R	GGGTCTGCCTATCAGCTCGT
CAT2	F	GTTGACTGCAGGGGTCATTT
	R	ACATTTGGGCTGGTCGTAAG
CAT3	F	TCCAAGACTCTGTGCTCCCT
	R	GACCAAATCTGCGAAATGCT
RPLP0	F	CACTGGTCTAGGACCCGAGAAG
	R	GGTGCCTCTGGAGATTTTCG

7.2.9 DNA purification

Genomic DNA (gDNA) was purified using the DNeasyR Blood & Tissue Kit columns (69504, Qiagen) according to manufacter's instructions. Briefly, cells were tripsinized and centrifuged for 5 min at 300 g and cell pellets were resuspended in PBS to a final volume of 200 µL. 20 µL of QIAGEN Proteinase K were added into each sample. 200 µL of Lysis buffer (A) was added into the samples and they were mixed by pulse-vortexing for 15 sec. Then, samples were incubated at 56°C for 10 min. 200 µL of Ethanol (96–100%) were added to the samples and they were mixed again by pulse-vortexing for 15 sec. After mixing, mixtures were placed into the QIAamp Spin Columns and centrifuged at 6,000 g for 1 min. The QIAamp Spin Columns were placed in clean 2 mL collection tubes and after adding 500 µL of QIAGEN Buffer AW1, samples were centrifuged at 6,000 g for 1 min. Again, the QIAamp Spin Columns were placed in clean 2 mL collection tubes and 500 µL of QIAGEN Buffer AW2 were added into the samples. Next, samples were centrifuged at full speed (20,000 g) for 3 min. The columns were placed in clean

1.5 mL microcentrifuge tubes and 50 µL of distilled water were added. Samples were incubated at room temperature for 5 min, and then centrifuged at 6,000 x g for 1 min.

The purified DNA was quantified using the Nanodrop spectrometer (Thermo Fisher Scientific) as described for RNA quantification (**7.2.6**).

7.2.10 Polymerase Chain Reaction (PCR)

In order to check *CD98HC* gene disruption in CD98hc KO HEK293T cells, a pair of primers that amplified the targeted DNA was designed: CD98hc1 (sense, 5′-GCAAGGCTCCTGACTTCCTT-3′; antisense 5′-ATTTGCCCAAAGCCACATAG-3′); CD98hc2 (sense, 5′-GTAGTGCAGGTGGGGAAG-3′; antisense, 5′-AGTCAGCAGAATGGCTCCT-3′). The mix reaction was brought to a final volume of 50 µL: 10 µM of each primer, 100 ng/µL DNA, 5 µL Pfu DNA Polymerase buffer (M7741, Promega), 2 µL Mg^{2+}, 10 mM dNTPs, 1 µL Pfu DNA Polymerase (M7741, Promega) and H_2O.

The PCR program used was: 95°C (5 min), 25 cycles of 95°C (30 s)-55°C (30 s)-72°C (3 min), 72°C (10 min), 15°C (∞).

DNA fragment size was checked by electrophoresis in 1% agarose gels with SYBR Safe DNA Gel Stain (S33102, Thermo Fisher Scientific).

7.3 Global protein synthesis measurement

7.3.1 Measurement of 35S-methionine incorporation by TCA precipitation

Cells were washed twice with PBS and incubated for 1 min at 37°C with labelling media (Met/Cys-free DMEM with the usual supplements, dialysed FBS and 120 µCi/mL of ^{35}S-Methionine/Cysteine (Perkin Elmer)). Next, cycloheximide (C4859, Sigma-Aldrich) was added for 1 min at 37°C at a final concentration of 100 µg/mL.

Cells were then washed three times with cold PBS (plus 5 mM Met and Cys). They were then harvested in 0.5 mL of cold PBS and pelleted by centrifugation for 3 min at 3000 g at 4°C. Cells were lysed for 30 min at 4°C with NET buffer: 50 mM Tris HCl pH 7.4, 150 mM NaCl, 5 mM EDTA, 0.5 % IGEPAL, with protease inhibitors, and, after centrifugation for 10 min at 10,000 g, the supernatant was precipitated with cold 10 % trichloroacetic acid in order to measure the amount of intracellular radioactivity incorporated into proteins. The percentage of intracellular radioactivity incorporated was calculated. *Protein synthesis measurement was performed by Josep Chillarón.*

7.3.2 Protein synthesis measurement by SUnSET

SUnSET is a non-radioactive method which allows the monitoring and quantification of global protein synthesis (Schmidt et al. 2009). Importantly, puromycin is a structural analogue of tyrosyl-transfer RNA (**Figure 101A**), and, as such, can be incorporated into elongating peptide chains via the formation of a peptide bond (**Figure 101B**). The binding of puromycin to a growing peptide results in the termination of peptide elongation, and leads to the release of the truncated puromycin bound peptide from the ribosome (**Figure 101C**). Puromycin-labelled peptides can be monitored by immunoblotting with an antibody against puromycin (**Figure 101C**). The rate at which puromycin-labelled peptides are formed reflects the overall rate of protein synthesis.

Cells were cultured onto 6-well plates until sub-confluence conditions. 1 μM puromycin was added into cell culture media for 30 min. Then cells were harvested and subjected to immunoblotting analysis (**7.2.4**).

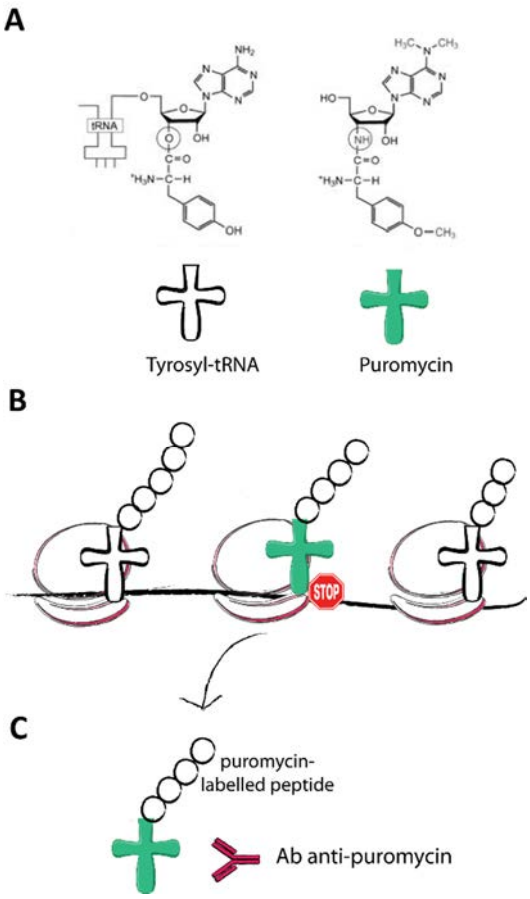

Figure 101. SUnSET, a nonradioactive method to monitor protein synthesis. **A**, comparison of the molecular structure of tyrosyl-tRNA and puromycin. **B**, puromycin is incorporated in the growing peptide chains via the formation of a peptide bound. **C**, once bound, the puromycin-labelled peptide is unable to undergo further elongation and it is released from the ribosome. The rate at which puromycin-labelled peptides are formed can be monitored by immunoblotting.

7.4 Apoptosis assay: annexin V-propidium iodide staining

The annexin V–FITC (A23204, Invitrogen) and propidium (IP) (P4864, Sigma-Aldrich) double staining technique was used to evaluate apoptosis. The annexin V binding assay is based on the ability of annexin V to bind in a calcium-dependent manner to phosphatidylserine (PS) (**Figure 102**) (van Genderen et al. 2006). In normal healthy cells PS is located in the inner leaflet of the plasma membrane. However, during apoptosis plasma membrane is disestablished and PS is externalized, thus annexin V is able to attach these residues (**Figure 102**). By using annexin V conjugated with a fluorophore apoptosis can be monitored. Addition of PI was performed to detect cell viability.

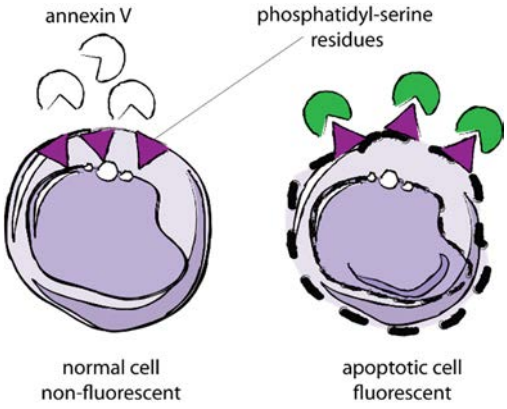

Figure 102. Annexin V staining assay for apoptosis measurement. Exposure of PS on the extracellular surface in apoptotic cells leads to binding of annexin V reagent and fluorescence signal is detected.

Cells were seeded onto 6-well plates at a density of 1×10^5 cell/mL. A positive control was performed by treating cells with 1 μM of staurosporine (S5921, Sigma-Aldrich) for 3 h. Cells were then harvested, washed in PBS and centrifuged. They were resuspended in 100 μL of annexin V binding buffer. Samples were incubated with 5 μL of annexin V conjugate and 1 μL of IP for 15 min at room temperature. Then, 300 μL of binding buffer was added to each sample, which were then subjected to flow cytometry (Gallios Flow Cytometer, Beckman Coulter). FSC-Area (forward scatter) and SSC-Area (side scatter) gating was applied to discriminate single cell population from debris. FITC and PI fluorescence were detected at 515 nm and 620 nm, respectively. 10,000 events were recorded for each sample. Fluorescence was displayed on a scatter plot with PI and FITC quadrant gates. Data acquisition was performed using FlowJO software.

7.5 Cell cycle analysis

Analysis of the cell's replication station state was achieved by using propidium iodide (PI) (P4864, Sigma-Aldrich), which binds to double stranded DNA by intercalating between base pairs. Cell in G1-phase will have one copy of DNA and will therefore have 1X fluorescence intensity. Cells in G2/M-phase of the cell cycle will have two copies of DNA and accordingly will have 2X intensity (**Figure 103**). Cells in S-phase are synthesizing DNA and therefore they will have fluorescence values between the 1X and 2X populations (**Figure 103**). The analysis with PI

staining by flow cytometry results in a histogram consisting of three populations: two Gaussian curves (1X and 2X peaks) and the S-phase population.

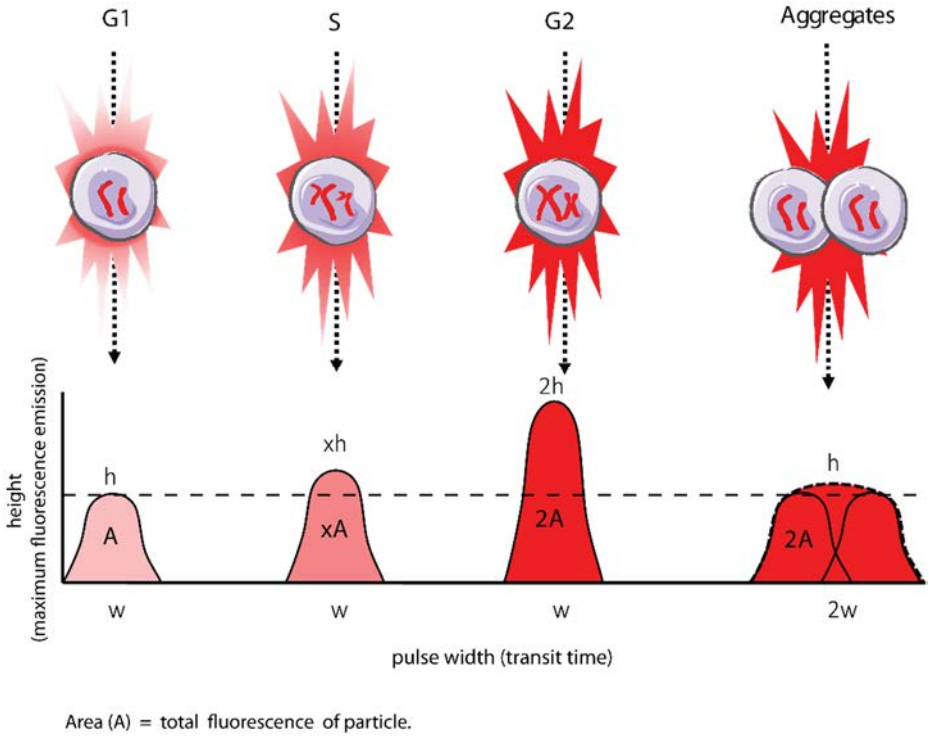

Figure 103. The cell cycle profile of a sample can be determined by staining the DNA with propidium iodide. PI stains DNA stoichiometrically, allowing differentiation of cells in G1-, S- and G2/M- phases, as well as identification of aggregates, which can be discarded form the analysis by analysing all the parameters indicated.

Cells can stick to one another and while passing through the laser at the same time, two cells in G0/1-phase that are stuck together will have as much nuclear fluorescence as one in G2/M-phase. This will result in analyzed G2/M percentages that are erroneously high. However, aggregates can be discarded by controlling the pulse width parameter: single cells will have similar pulse width (transit time) values and on the contrary, aggregates will have double total fluorescent area but also double transit time (**Figure 103**). Maximum fluorescence emission, pulse width and total fluorescence of the particles were analyzed to identify singlets.

Cells were seeded onto 6-well plates at a density of 1×10^5 cell/mL with no additives or in the presence of nucleosides or BCAA- and AAA- containing dipeptides.

When indicated, cells were synchronised by double thymidine block (Bjursell and Reichard 1973; H. T. Ma and Poon 2011). In that case, cells were incubated with 2 mM of thymidine (T1895, Sigma-Aldrich) for 16 h. Next, they were incubated for 8 h in complete medium without thymidine, and another block (2 mM thymidine) was performed for 16 h. After the double block, cells were released in complete medium for the indicated times.

For cell cycle analysis, the unattached cells were collected from the growth media and pooled before washing the culture with PBS. Next, PBS was pooled and cells were trypsinised. Cells were then fixed in 70% ethanol and stored at -20°C for at least 2 h. Before the analysis, cells were centrifuged and resuspended in PI-Triton X-100 staining solution: 2 mg RNase A (740505, Cultek), (0.1% (v/v) Triton X-100 (9036-19-5, Merck), 500 µM PI, for 30 min at RT. Samples were then subjected to flow cytometry (Coulter EPICS (R) XL Flow Cytometry System).

Forward and side scatter area gating were used to identify singlets. Interval gates were placed on the detected peaks corresponding to the phases of the cell cycle. Percentage of cells in G1-, S-, and G2/M-phases was determined using MCycle software. Cell cycle profiles were generated using FlowJO software.

7.6 Quantification of ROS production: intracellular ROS and mitochondrial superoxide levels

The levels of intracellular free radicals were assayed by measuring intracellular oxidation of H_2DCFDA (C6827, Thermo Fisher Scientific). H_2DCFDA is a non-fluorescent compound that is converted to highly fluorescent 2′, 7′-dichlorofluorescein (DCF) upon cleavage of the acetate groups by intracellular esterases and oxidation.

The levels of mitochondrial superoxide were assayed by measuring intracellular oxidation of MitoSOX (M36008, Thermo Fisher Scientific), which is a live-cell permeant that rapidly and selectively target the mitochondria. Once in the mitochondria, MitoSOX is oxidized by superoxide (not by other ROS species, oxidation of the probe is prevented by superoxide dismutase) and exhibits red fluorescence.

Cells were seeded onto 6-well plates in corresponding media. Cultures were incubated with 1 μM H_2DCFDA or 2 μM MitoSOX for 30 min. Wells without probe were used as autofluorescence controls. Cells were pre-treated with 100 μM H_2O_2 for 1 h or 50 nM antimycin for 30 min as positive controls for DCF and MitoSOX oxidation, respectively.

Cells were then harvested and washed in PBS, intracellular fluorescence was measured using the Gallios Flow Cytometer system (Beckman Coulter).

7.7 Transcriptome analysis

7.7.1 RNA expression profiling

Total RNA from the cell culture was extracted using an RNA extraction kit (12183018A, PURELINK RNA MINI KIT, Invitrogen) following the manufacturer's instructions (**7.2.5**). RNA integrity was assessed using RNA Nano Assay (Agilent Bioanalyzer 2100) and RNA quantification were executed using Nanodrop ND 1000 Spectrophotometer (**7.2.6**). cDNA library preparation and amplification were performed from 25 ng total RNA using WTA2 (Sigma-Aldrich) with 17 cycles of amplification. 8 μg of cDNA was subsequently fragmented by DNAseI and biotinylated by terminal transferase obtained from GeneChip Mapping 250k Nsp Assay Kit (Affymetrix). The hybridisation mixture was prepared following the Gene Atlas protocol (Affymetrix). Each sample target was hybridised to a Mouse Genome 430 PM array. After hybridisation for 16 h at 45°C, washing and staining was performed in the GeneAtlas Fluidics Station (Affymetrix). The arrays were scanned in a GeneAtlas Imaging Station (Affymetrix). All processing was

performed following the manufacturer's recommendations. CEL files were generated from DAT files using Affymetrix Command Console software. To generate the log2 expression estimates, overall array intensity was normalised between arrays and the probe intensity of all probes in a probe set was summarised to a single value using the RMA (Robust Multichip Average) algorithm (Irizarry, Bolstad, et al. 2003). *Microarray processing was performed at Functional Genomics Facility at IRB Barcelona.*

7.7.2 Bioinformatic analyses

Affymetrix arrays were normalized using RNA. Background correction and summarization (Irizarry, Hobbs, et al. 2003) as implemented in the "affyPLM" package (Bolstad 2005) from the R statistical framework (R Core Development Team 2008). Annotations for the HT-430 array version na34 were downloaded from Affymetrix: Affymetrix Analysis Centre. Netaffx https://www.affymetrix.com/analysis/index.affx. A linear model was fitted in order to identify differentially expressed genes between conditions of interest with batch scan as covariate. The "lmFit" function from the "limma" package (D. Wu et al. 2015) was used for fitting the model. Gene set enrichment analysis (GSEA), as implemented in (Subramanian et al. 2005), was performed on all the genes in the array ranked by the t-statistic obtained from the model. For each gene, the t-statistic of the most variable probe was used as a representative. We also ran GSEA on custom gene sets. *Bioinformatics analysis was performed by Camille Stephan-Otto Attolin in the Bioinformatics-Biostatistics Unit of IRB Barcelona.*

7.8 Immunofluorescence

7.8.1 Mitosis analysis

Cells were cultured in 24-wells plates with coverslips until subconfluence conditions. Then, cells were fixed in 4% paraformaldehyde (PFA) (sc-281692, Santa Cruz) in PBS for 20 min and washed with 50 mM NH_4Cl. They were then permeabilised and blocked in 0.1% triton X-100 (9036-19-5, Merck), 2% FBS (F7524,

Sigma-Aldrich) in PBS for 10 min. The coverslips were incubated with anti-phospho-Histone (P-H3) antibody (06-570, Merck) diluted 1:100 in 2% FBS PBS for 30 min. They were then washed with PBS, incubated in secondary antibody diluted 1:400 in 2% FBS PBS for 30 min and washed again with 0.5% triton X-100 PBS. They were then washed with PBS, stained with Hoechst 33342 (H3570, Invitrogen) diluted 1:20,000 in PBS and then washed again with PBS. Coverslips were mounted on microscope slides with Flouromount (17984-25, Thermo Fisher Scientific). WideField images were obtained using Olympus IX 81 microscope with objective lenses of 20x/ 0.45 LUCPlanFL N and 40x/ 0.75 UPlan FL N and ScanR Acquisition Software v2.3. *Microscopy acquisitions were performed in The Advanced Digital Microscopy Facilities of IRB Barcelona*.

Image processing and quantification were performed using ImageJ software. Nuclei segmentation was performed using a tailor-made ImageJ macro. Mitosis was measured manually attending the different patterns displayed by P-H3. Specific phosphorylation at serine 10 (Ser10) of H3 starts during late G2-phase and peaks during mitosis. Depending on chromatin condensation, P-H3 undergoes different localization patterns during the mitotic phases (**Figure 104**) (Hendzel et al. 1997; Van Hooser et al. 1998). Thus, only patterns corresponding to cells undergoing mitosis were selected for quantification, discarding cells with patterns matching to G2-phase.

7.8.2 Mitochondrial morphology analysis

Cells were seeded onto 6-well plates with coverslips and transitory transfected as described above (**7.1.5**) with the pDsRed2-Mito Vector (632421, CloneTech). Then, cells were fixed in 4% paraformaldehyde (PFA) (sc-281692, Santa Cruz) in PBS for 20 min and washed with 50 mM NH_4Cl. They were then washed with PBS, stained with Hoechst 33342 (H3570, Invitrogen) diluted 1:20,000 in PBS and then washed again with PBS. Coverslips were mounted on microscope slides with Flouromount (17984-25, Fisher Scientific). WideField images were obtained using Olympus IX

81 microscope with objective lenses of 20x/ 0.45 LUCPlanFL N and 40x/ 0.75 UPlan FL N and ScanR Acquisition Software v2.3.

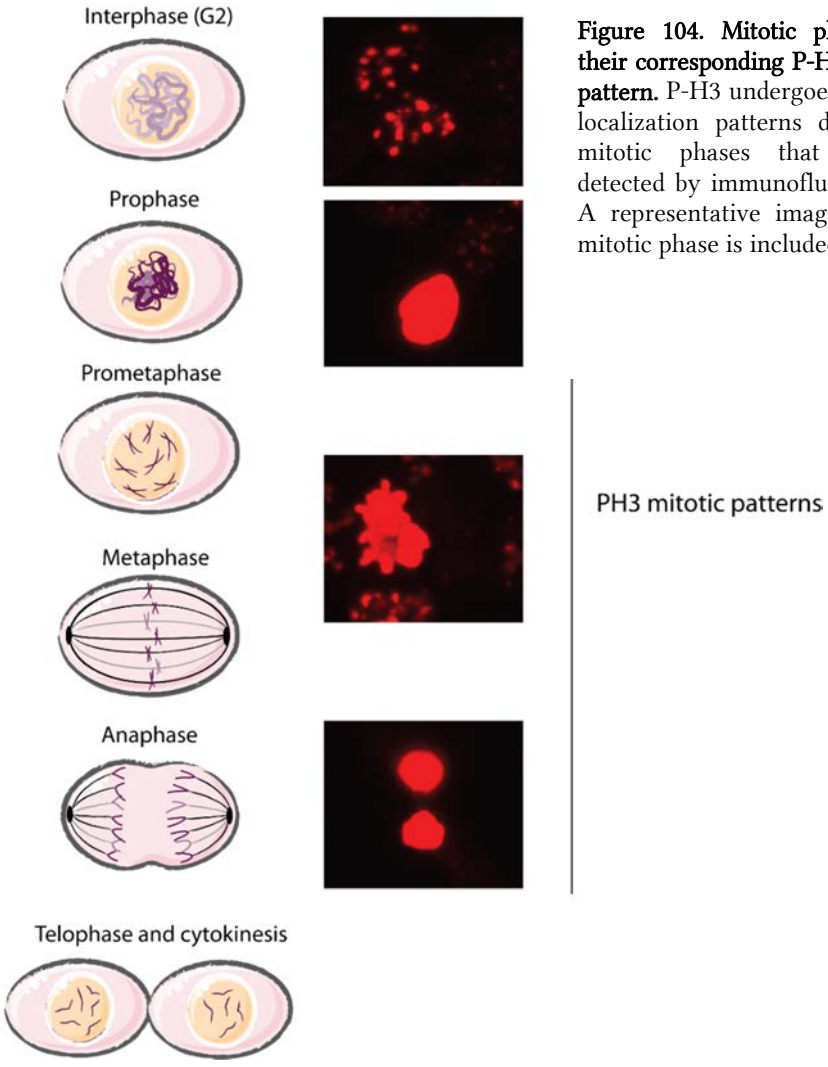

Figure 104. Mitotic phases and their corresponding P-H3 staining pattern. P-H3 undergoes different localization patterns during the mitotic phases that can be detected by immunofluorescence. A representative image of each mitotic phase is included.

7.9 AA uptake measurement

Transport activities were studied on whole WT, CD98hc KO, control and low 6AA cells as previously described (Reig et al., 2002) by measuring the transport of 10 μM of the corresponding radiolabelled AA (American Radiolabelled Chemicals).

Transport activities were confirmed using 1 mM specific inhibitors or pretreating cells with 1 mM N-ethylmaleimide for 3 min when needed.

Transports assays corresponding to ***Figure 18*** *were performed by Laura Rodriguez de la Ballina. Transports assays corresponding to* ***Figure 29B*** *were performed by Josep Chillarón.*

7.10 Targeted metabolomics assay

Metabolomics methodologies are divided in two distinct groups; untargeted metabolomics, a comprehensive analysis of all the measurable analytes in a sample, and targeted metabolomics, the measurement of defined metabolites which have been chemically characterized and biochemically annotated. Targeted approaches are usually focused on a few pathways of interest where candidate genes are already defined. The advantages of this kind of approach include a higher degree of sensitivity and easier identification of compounds than untargeted approaches (Roberts et al. 2012). In the present study, nucleotides and metabolites involved in glycolysis, TCA cycle and pentose phosphate pathway were analysed in WT, CD98hc KO, control and low 6AA cells.

7.10.1 Metabolite extraction

Cells were cultured in 150 mm dishes for 16 h in the presence of fully labelled glucose (^{13}C6-glucose, Sigma-Aldrich) before the harvest. Then, media were collected and cell pellets were scrapped, collected and frozen. Control and ^{13}C6-glucose medium (DMEM, control and low 6AA) were also analysed as controls. For better detection of differences in glucose metabolism between different conditions, cells should be grown the time enough to consume around 40% of the glucose added into the extracellular media. A previous glucose-consume time course was performed before the experiment and 16 h was determined as the best time point to performe the experiment.

Briefly, pellets were resuspended in 300 µL of cold acetonitrile:methanol:water (5:4:1, v:v:v) containing ^{13}C-glycerol (5 µL/mL) as internal standard. 10 µL of ^{13}C3-

glycerol (150 µl/ml) was also added to 200 µL of medium. Metabolites from cells were extracted with three rounds of liquid N_2 immersion and sonication, followed by 1 h in ice before centrifugation at 14,500 rpm (10 min at 4°C). Samples of media were lyophilised and resuspended in 500 µl of cold acetonitrile:methanol:water (5:4:1, v:v:v). After vortexing, they were placed in ice for 1 h and centrifuged at 14,500 rpm (10 min at 4°C). Metabolite extractions of cells and media were split in aliquots of 200 and 400 µL for GC-MS, respectively, and 50 µL for LC-MS analysis. *Metabolite extractions were performed by Alejandra Junza in the Metabolomics Platform leading by Oscar Yanes in the Department of Electronic Engineering (DEEEA) from Universitat Rovira i Virgili (Tarragona).*

7.10.2 Gas Chromatography (GC) - Mass spectrometry (MS) analysis

Samples were dried under a stream of N_2 gas and lyophilised before chemical derivatisation with 40 µL methoxyamine in pyridine (30 µg/mL) for 45 min at 60°C. Samples were also silylated using 25 µL N-methyl-N-trimethylsilyltrifluoroacetamide with 1% trimethylchlorosilane (Thermo Fisher Scientific) for 30 min at 60°C to increase the volatility of metabolites. A 7890A GC system coupled to a 7000 QqQ mass spectrometer (Agilent Technologies) was used for isotopologue determination. Derivatised samples were injected (1 µL) into the gas chromatograph system with a split inlet (5:1) equipped with a J&W Scientific HP-5ms stationary phase column (30 m × 0.25 mm i.d., 0.1 µm film, Agilent Technologies). Helium at a flow of 1.5 mL/min was used as carrier gas. The temperature gradient was from 70 to 190°C at a heating rate of 11°C /min and from 190 to 325°C at 21°C /min. Metabolites were ionized using positive chemical ionization (CI) with isobutene as reagent gas. Mass spectral data on the 7000 QqQ were acquired in scan mode selected ion clusters of the different metabolites (**Table 4**) *GC-MS analysis was performed by Alejandra Junza in the Metabolomics Platform leading by Oscar Yanes in the Department of Electronic Engineering (DEEEA) from Universitat Rovira i Virgili (Tarragona).*

Table 4. Characterization of analysed metabolites.

Metabolite	RT (min)	m/z	Metabolite	RT (min)	m/z
Proline	3.06	188	Malate	8.71	351
Pyruvate	3.57	190	Tryptophan	14.26	355
Alanine	7.18	306	Glutamate	10.12	364
Lactate	3.72	235	Glyceraldehyde 3P	11.22	416
Fumarate	6.98	261	Dihydroxyacetone P	11.46	416
Valine	5.47	262	Lysine	12.21	435
Succinate	6.60	263	2P- Glycerate	11.79	475
Isoleucine	6.14	276	3P-Glycerate	11.99	475
Leucine	6.41	276	Citrate	12.06	481
Glycine	6.56	292	Glucose	12.68	570
Glycerol ($^{13}C_3$) IS	6.20	312	Ribose 6P	13.92	620
Ketoglutarate	9.66	320	Fructose 6P	14.89	722
Serine	7.23	322	Glucose 6P	14.94	722
Aspartate	9.06	350			

RT, retention time; m/z, mass-to-charge ratio.

7.10.3 Liquid Chromatography (LC) - Mass spectrometry (MS) analysis

To determine nucleotides, cell extracts were analysed using an UHPLC system coupled to a 6490 QqQ mass spectrometer (Agilent Technologies). Cell extracts were injected (5 µL) and metabolites were separated using an InfinityLab Poroshell 120 HILIC-Z column (2.7 µm, 2.1×100 mm, Agilent). The mobile phases used for the metabolite separation were A: 50 mM ammonium acetate with 5 µM medrionic acid; and B: acetonitrile. The chromatographic gradient was isocratic for 0.5 min at 80% B, from 0.5 to 7.5 min decreased to 70% B and from 7.5 to 8.5 min decreased to 50%, and maintained for 30 sec. From 9.0 min to 9.2 min the percentage of B rose quickly to 80 % and finally the column was equilibrated at 80 % B until min 11. Flow rate was 0.7 mL/min. The QqQ mass spectrometer worked in MRM mode using the transitions in **Table 5** to determine nucleotides. The electrospray ionization source (ESI) worked in positive and negative mode. *LC-MS analysis was performed by Alejandra Junza in the Metabolomics Platform leading by Oscar*

Yanes in the Department of Electronic Engineering (DEEEA) from Universitat Rovira i Virgili (Tarragona).

Table 5. Characterization of analysed nucleotides

Metabolite	RT (min)	1st Transition (CE (V))	2nd Transition (CE (V))	Polarity
AMP	3.13	348 → 136 (16)	348 → 119 (56)	Positive
ADP	4.64	428 → 136 (32)	428 → 348 (16)	Positive
ATP	5.67	508 → 136 (32)	508 → 410 (12)	Positive
dAMP	2.79	332 → 136 (8)	332 → 81 (12)	Positive
dADP	4.34	412 → 136 (20)	412 → 81 (36)	Positive
dATP	5.39	492 → 136 (20)	492 → 81 (28)	Positive
CMP	4.40	324 → 112 (8)	324 → 95 (48)	Positive
CDP	5.89	404 → 112 (12)	404 → 95 (56)	Positive
CTP	6.91	484 → 112 (24)	484 → 97 (28)	Positive
dCMP	3.92	308 → 112 (12)	308 → 95 (56)	Positive
dCDP	5.51	388 → 112 (12)	388 → 81 (20)	Positive
dCTP	6.53	468 → 112 (12)	468 → 81 (36)	Positive
GMP	4.46	364 → 152 (8)	364 → 135 (52)	Positive
GDP	5.88	444 → 152 (32)	444 → 135 (60)	Positive
GTP	6.82	524 → 152 (32)	524 → 135 (56)	Positive
dGMP	4.01	348 → 152 (8)	348 → 135 (56)	Positive
dGDP	5.51	428 → 152 (28)	428 → 135 (56)	Positive
dGTP	6.50	508 → 152 (20)	508 → 81 (40)	Positive
UMP	3.19	325 → 97 (8)	325 → 41 (48)	Positive
UDP	4.67	403 → 159 (24)	403 → 79 (52)	Negative
UTP	5.70	483 → 159 (40)	483 → 385 (20)	Negative
dTDP	3.89	401 → 79 (60)	401 → 159 (24)	Negative
dTTP	4.98	483 → 81 (32)	483 → 63 (60)	Positive
IMP	3.76	349 → 137 (16)	349 → 110 (60)	Positive

RT, retention time; CE, collision energy; V, volts.

7.11 tRNA aminoacylation array

To determine the fraction of aminoacyl-tRNAs from the total tRNAs, we used tRNA-tailored microarrays following the protocol described previously (Avcilar-Kucukgoze et al. 2016). Note that isoacceptors and isodecoders can be distinguished, as long as their sequence differs in 8 or more nucleotides.

Since RNA molecules are highly unstable, all buffers and procedures were performed under RNase-free conditions.

Cells were grown until sub-confluence in T75 flasks. Then, cells were trypsinised, collected and centrifuged at 400 g for 5 min. Cell pellets were resuspended in 500 µL of buffer 0.3 M NaAcetate (pH 4.5), 10 mM EDTA. Total RNA was isolated using acidic phenol to preserve the aminoacyl moiety. Thus, 500 µL of acidic phenol pH 4.5 (A980.2, Carl Roth) was added in each sample. 3 cycles of vortex and snap-freezing samples in dry ice were performed. Phases were separated by centrifugation at 20,000 g 4°C for 15 min. Aqueous phase (upper phase, ~500 µL) was selected and mixed with 1 volume of acidic phenol. After vortex phases were separated again by centrifugation at 20,000 g 4°C for 15 min. Aqueous phase was carefully separated and 1 volume of isopropanol was added. 1 µL of glycogen was added to make the RNA pellet more visible. Samples were placed at -80°C for at least 30 min. Then, they were centrifuged for 25 min at 20,000 g at 4°C. Supernatants were removed and the pellets were resuspended in buffer 0.3 M NaAcetate (NaOAc) (pH 4.5), 10 mM EDTA and a 2.7 x volume of ethanol was added. Samples were again placed at -80°C for at least 30 min and then centrifuged for 25 min at 20,000 g at 4°C. The resulted pellet was resuspended in buffer 0.01 M NaOAc pH = 4.5, 1mM EDTA (~50-100 µL).

RNA integrity and concentration was checked and measured. 17 µg of RNA were resuspenended in 170 µL of buffer 10 mM NaOAc 1mM EDTA and samples were split in two for total- and aminoacylated- tRNA microarray detection (**Figure 105**). Once the tRNA was isolated, the method is based on the protection against periodate oxidation of the 3' end of the aminoacyl-tRNA if there is an AA attached. Total tRNA was isolated and split in two halves. One half was treated with periodate, which oxidizes the 3´ ends of uncharged tRNA, this step destroys their ability to be ligated with the oligonucleotide required for fluorescence labelling. The other half served as a control for total amount of tRNA measurement. Both samples were ligated with a fluorescent-oligonucleotide and they were subsequently hybridized to an array containing probes for all individual tRNAs to determine the ratio between the two fluorophores (**Figure 105**).

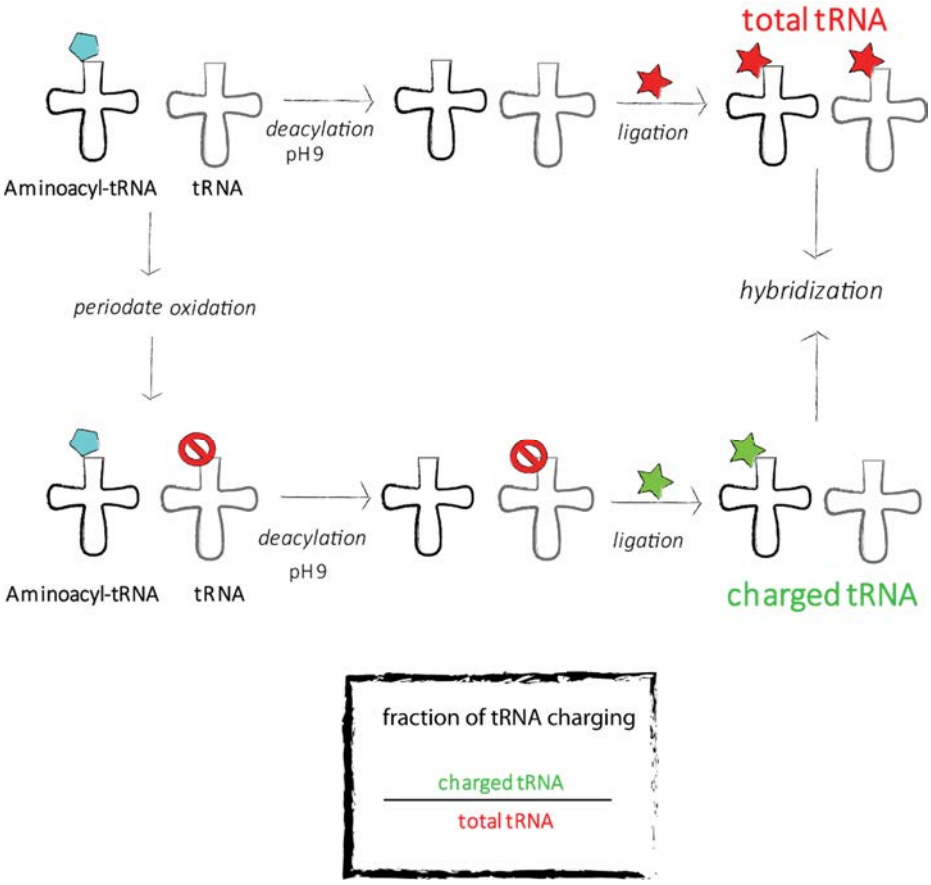

Figure 105. tRNA aminoacylation array. This method is based on the protection against periodate oxidation of the 3' end of the aminoacyl-tRNA if there is an AA attached. Total tRNA is isolated and split in two halves. To measure the amount of charged tRNA, one half is treated with periodate, which oxidizes the 3´ ends of uncharged tRNA, destroying their ability to be ligated with the fluorescent-oligonucleotide. The other non-treated half serves as a control for the amount of total tRNA. Both samples are labelled with a fluorescent-oligonucleotide and they are hybridized to an array containing probes for all individual tRNAs to determine the ratio between the two fluorophores.

The arrays were normalised to spike-standards, and quantification and normalisation was performed using in-house Phyton and R scripts. *Microarrays were performed by Christine Polte in Zoya's laboratory group in the Institute of Biochemistry and Molecular Biology of Hamburg (Germany).*

7.12 Intracellular AA quantification

Intracellular AA content was analysed using the Mass Trak Amino Acid Derivatization kit (186003836, Waters) and following the manufacturer's instructions. Briefly, WT and CD98hc KO cells, alone or in the presence of BCAA- and AAA- containing dipeptides and control and low 6AA cells were collected and homogenised in water. 100 µL of 50 µM norvaline was added to 100 µL of each sample as an internal standard. Samples were vortex for 10 sec and centrifuged at 16,000 g for 5 min. Next, 20 µL of supernatant from each sample was mixed with 60 µL of NaOH 0.5M/Borate buffer in a chromatography injection vial. After vortexing for 10 sec, 20 µL of 6-aminoquinolyl-N-hydroxysuccinimidyl carbamate (AQC) solution was added to the vials for AA derivatisation. Samples were then vortexed for 20 sec and incubated for 1 min at room temperature followed by 10 min at 55°C. Sample preparations were injected into an Ultra High Performance Liquid Chromatograph (Shimadzu) (injection volume: 1 µL). Chromatography was performed using MassTrak AAA columns (2.1 x 150 mm, 1.7 µm) (Waters). Solutions A and B were used as mobile phases (A: MassTrak AAA Eluent A Concentrate, diluted 1:10; B: MassTrak AAA Eluent B) and MassTrak standard gradient was used as provided in the kit. Detection was performed at 260 nm. AAs were quantified with Labsolutions software (Shimadzu). *AA concentrations were evaluated in the Servei de Bioquímica i Genètica Molecular of Hospital Clínic of Barcelona by Judit García.*

7.13 Mitochondrial DNA copy number analysis

In order to quantify the mitochondrial DNA as a readout of the mitochondrial mass, the number of copies of the mitochondrial gene cyclooxygenase-2 (*Cox2*) and the mitochondrial region referred as *MtDNA* were quantified and normalized to the nuclear DNA content. For this propose, the number of copies of the nuclear gene succinate dehydrogenase A (*Sdha*) were also quantified. The genomic DNA (gDNA) was extracted from cells from using DNeasyR Blood & Tissue Kit columns (69504, Qiagen) (**7.2.9**) and gDNA was quantified and diluted to achieve a concentration between of 100 pg/µL. Quantitative RT-PCR was performed using

the ABI Prism 7900 HT real-time PCR machine (Applied Biosystems) and the SYBR Green PCR Master Mix (4368702, Thermo Fisher Scientific). The following sets of specific primers were used: *Cox2* (sense, 5′-CTACAAGACGCCACAT-3′; antisense 5′-GAGAGGGGAGAGCAAT-3′); *mtDNA* (sense, 5′-ACCGCAAGGGAAAGATGAAA-3′; antisense 5′-AGGTAGCTCGTTTGGTTTCGG -3′); *Sdha* (sense, 5′-TACTACAGCCCCAAGTCT-3′; antisense 5′-TGGACCCATCTTCTATGC-3′).

7.14 Glucose uptake measurement with 2-NBDG

This assay is based on direct incubation of cells with a fluorescent non-metabolizable D-glucose analogue 2-[N-(7-nitrobenz-2-oxa-1,3-diazol-4-yl) amino]-2-deoxy-D-glucose (2-NBDG) (186689-07-6, Abcam) followed by flow cytometric detection of fluorescence produced by the cells.

Cells were seeded in a 6-well plates over-night. The next day, 2-NBDG was added to a final concentration of 200 µg/mL in glucose-free medium for 30 min. After the incubation, cells were washed twice with PBS and collected by centrifugation for 5 min at 400 g at room temperature. Pellets were resuspended in 200 µL of Cell-Based Assay Buffer and propidium iodide (PI) was added to exclude dead cells. Samples were then subjected to flow cytometry (Coulter EPICS (R) XL Flow Cytometry System) and fluorescence was detected at excitation/emission = 485/535 nm.

7.15 Mitochondrial mass determination with Mitotracker-green

Cells were seeded onto 6-well plates in corresponding media. Cultures were incubated with 100 nM MitoTracker-green (M7514, Thermo Fisher Scientific) for 20 min. Wells without probe were used as autofluorescence controls. Cells were then harvested and washed in PBS, and intracellular fluorescence was measured using the Gallios Flow Cytometer system (Beckman Coulter).

7.16 Oxygen consumption measurements

Cells were seeded onto SeaHorse Bioscience XF24 plates (100850-001, Agilent Technologies) in the corresponding media alone or in the presence of BCAA- and AAA- containing dipeptides 48 h before analysis. The instrument was calibrated the day before the experiment, following manufacturer's instructions. On the day of the experiment, during sensor calibration, cells were kept in a 37°C incubator without CO_2 in 700 µL of respiration buffer (DMEM, 5 mM glucose, 2 mM glutamine, Phenol Red, non-EAAs and when indicated, BCAA- and AA-containing dipeptides). After sensor calibration, plates were immediately placed into the calibrated Seahorse XF24 flux analyzer for mitochondrial bioenergetic analysis. Injection ports on sensor cartridge were loaded with 1.25 µM oligomycin (complex V inhibitor) to distinguish the percentage of oxygen consumption devoted to ATP synthesis and the percentage of oxygen consumption required to overcome the natural proton leak across the inner mitochondrial membrane; 0.1 mM rotenone (complex I inhibitor) and 0.1 mM antimycin A (complex III inhibitor) were used to calculate the remaining respiration caused by oxidative side reactions. When indicated, 1 µM FCCP (ionophore that transports hydrogen ions through the mitochondrial membrane) was used to calculate the "spare" respiratory capacity of cells, which is defined as the quantitative difference between maximal uncontrolled OCR and the initial basal OCR. After each addition, four data points of 3 minutes were taken to determine the OCR (pmols O2/minute). OCR values were corrected by protein concentration.

7.17 Statistical analysis

In the present thesis quantification data correspond to the mean ± SEM of the independent experiments (n) indicated for each graph. Statistical significance *, $p \leq 0.05$; **, $p \leq 0.01$; ***, $p \leq 0.001$ vs. WT or control cells or #, $p \leq 0.05$; ##, $p \leq 0.01$; ###, $p \leq 0.001$ vs. KO cells was analysed using a two-tailed Student's t-test. For the paper entitled *CD98hc (SLC3A2) sustains amino acid and nucleotide availability for protein synthesis and cell cycle progression* attached in **Appendix III**, comparison of group means was performed using linear models with or without

random effects depending on the data as indicated its *Materials and Methods* section. The correct model for each dataset was chosen as follows: a mixed effect model was used when the variance explained by the replicate was larger than zero. Technical replicates were collapsed through the mean before log transforming when a linear model was chosen. Experiment was included as a fixed covariable if the model was significantly improved.

Resumen en castellano

CD98hc sostiene la disponibilidad de aminoácidos y glucosa, la homeostasis óxido-reducción y el metabolismo energético y de nucleótidos.

8. 1 Introducción

Los organismos vivos requieren energía para mantener sus funciones vitales a nivel celular. Para ello, todas las células incorporan nutrientes del medio extracelular, los cuales son posteriormente transformados a través de diversas vías metabólicas, proporcionando así la energía y materiales necesarios para el mantenimiento de las funciones y estructuras celulares (Vander Heiden et al. 2011). De entre estos nutrientes, los aminoácidos (AAs) son esenciales para la supervivencia celular, no sólo porque forman los bloques fundamentales de las proteínas, sino también por ser moléculas generadoras de energía, señalizadoras y precursoras de otros metabolitos importantes (Christensen 1990).

El paso de los AAs a través de la membrana plasmática está mediado por unas proteínas transmembrana que establecen el transporte de estos AAs desde el medio extracelular al interior de la célula, o viceversa (Cooper, 2000). Alteraciones en su funcionamiento o expresión están asociadas con una gran variedad de patologías y enfermedades (Bröer and Palacín 2011), poniendo de manifiesto la relevancia de estos transportadores para el correcto funcionamiento celular.

8.1.1 Transportadores heteroméricos de aminoácidos

Los transportadores de AAs se clasifican en diferentes familias en función de su homología de secuencia y de sus propiedades funcionales, tales como la especificidad de sustrato, el mecanismo de transporte o el acoplamiento a iones.

Los transportadores heteroméricos de AAs (HATs) son una de las once familias de proteínas implicadas en el transporte de AAs a través de la membrana plasmática

en mamíferos. Están formados por una subunidad pesada y una ligera unidas por un puente disulfuro (Fotiadis, Kanai, and Palacín 2013).

Las subunidades pesadas son glicoproteínas formadas por un extremo N-terminal intracelular, un solo segmento transmembrana y un extremo extracelular C-terminal llamado ectodominio. Sólo dos miembros constituyen las subunidades pesadas de la familia: rBAT (SLC3A1) y CD98hc (SLC3A2 o 4F2hc).

Por el contrario, las subunidades ligeras están formadas por 12 segmentos transmembrana con ambos extremos localizados en el interior de la célula (Gasol et al. 2004). Ocho cadenas ligeras han sido identificadas de la familia SLC7, dos de ellas se unen a rBAT: $b^{0,+}$AT (SLC7A9) y AGT1 (SLC7A13), mientras que CD98hc puede dimerizar con seis cadenas ligeras diferentes: LAT1, y^+LAT2, y^+LAT1, LAT2, asc1 y xCT (SLC7A5, 6, 7, 8, 10 y 11 respectivamente) (Fotiadis, Kanai, and Palacín 2013; Nagamori et al. 2016).

Las cadenas ligeras poseen la actividad catalítica del transportador con diferente especificidad de sustrato, intercambiando AAs a través de la membrana plasmática con una estequiometria 1:1. A su vez, las subunidades pesadas son las encargadas de reconocer y direccionar las subunidades ligeras a la membrana plasmática celular (Reig et al., 2002).

8.1.2 Transportadores asociados con CD98hc: asequibilidad de AAs y homeostasis óxido-reducción

Gran parte de esta tesis está dedicada al estudio de las funciones celulares que dependen de la subunidad pesada CD98hc, y para dicho estudio, se ha utilizado un modelo celular que expresa las siguientes cadenas ligeras:

y^+LAT2: el transportador desconocido

y^+LAT2-CD98hc intercambia AAs básicos (AA^+), independientemente de sodio, por AAs neutros (AA^0), de forma sodio-dependiente (D Torrents et al. 1998). Presenta una amplia distribución, incluyendo: intestino, cerebro, testículos, riñón,

corazón y glándula parótida (Bröer et al. 2000). A pesar de que su función fisiológica es aún desconocida, se cree que podría tener un papel fundamental en el mantenimiento celular del balance entre AA^0s and AA^+s.

xCT: control de estrés oxidativo

CD98hc-xCT es un intercambiador de cistina por glutamato (Sato et al. 1999). Teniendo en cuenta el bajo contenido intracelular de cistina, la dirección fisiológica de este intercambio consiste en la salida de glutamato para favorecer la entrada de cistina, la cual es rápidamente reducida a cisteína (Bannai 1986). La cisteína es considerada el precursor limitante en la síntesis del glutatión (GSH), el cual funciona como sustrato en importantes reacciones de oxidación-reducción y es considerado fundamental para combatir el estrés oxidativo. A pesar de que la cisteína no es un AA esencial (EAA, *essential* AA), el sistema de transporte x_c^- es considerado fundamental en muchas líneas celulares en cultivo (Bannai 1986).

Por otra parte, varios estudios realizados recientemente, han asociado esta subunidad ligera con un tipo de muerte celular no apoptótico e inducido por hierro denominado ferroptosis. La ferroptosis es desencadenada por la acumulación de especies reactivas de oxígeno (ROS, *reactive oxygen species*). Como consecuencia, se generan peróxidos lipídicos que desestabilizan las membranas celulares dando lugar a la muerte de la célula (W. S. Yang, Sriramaratnam, et al. 2014). Dixon y colaboradores demostraron por primera vez que la inhibición de xCT con sulfasalacina, un inhibidor específico de este transportador, daba lugar a este fenómeno debido al agotamiento intracelular de GSH (Dixon et al. 2014; Dixon et al. 2012).

Además, CD98hc-xCT es un transportador sobreexpresado en cáncer, como parte del programa celular que inducen las células cancerosas para sobrevivir en condiciones de estrés oxidativo persistente (**sección 8.1.3**).

LAT1: Asequibilidad de AAs esenciales

LAT1 es el responsable del transporte de AA^0s, grandes, ramificados (BCAA, *branched chain* AAs) y aromáticos (AAA, *aromatic* AAs) en casi todos los tipos de células (Uchino et al. 2002; Verrey et al. 1998).

Estos EAAs son reguladores de importantes vías de señalización que controlan la síntesis proteica celular, como mTORC (*mammalian Mechanistic Target of Rapamycin*) o la respuesta integrada al estrés (ISR, *integrated stress response*) mediada por eIF2 (*Eukaryotic Initiation Factor 2*) (Kimball and Jefferson 2005). CD98hc-LAT1, como transportador fundamental de estos AAs, está involucrado en la regulación de ambas vías.

La vía de señalización de mTORC1

mTORC forma parte de dos complejos: mTORC1 y mTORC2, de entre los cuales, mTORC1 juega un papel fundamental en el crecimiento y proliferación celular, regulando la síntesis y degradación de proteínas en respuesta a los niveles de nutrientes, factores de crecimiento y señales de estrés celular (Efeyan, Comb, and Sabatini 2015). mTORC1 funciona como un sensor de AAs, de manera que frente a una limitación en el contenido intracelular de éstos, mTORC1 se activa, siendo particularmente sensible a cambios en la concentración de leucina, arginina y glutamina. La activación de esta vía de señalización implica la reducción general de la síntesis proteica y la activación de un programa metabólico focalizado en la recuperación de la homeostasis celular (Blommaart, Luiken, Blommaart, van Woerkom, & Meijer, 1995; Hara et al., 1998; Nicklin et al., 2009).

Principalmente, dos proteínas diana de la activación de mTORC1 participan en la regulación de la iniciación de la traducción y elongación de proteínas: la quinasa S6K y la proteína ligada al factor eucariótico de iniciación 4E (4EBP1, *eukaryotic initiation factor 4E binding protein*) (Cargnello, Tcherkezian, and Roux 2015). S6K en su estado activo fosforila diferentes sustratos, entre los que destaca la activación de la proteína ribosomal S6 (Magnuson, Ekim, and Fingar 2011). Por otro lado, mTORC1, al fosforilar e inhibir 4EBP1, impide que éste se una al factor eucariótico

de iniciación 4E (eIF4E), promoviendo así el acoplamiento de proteínas activadoras del complejo e incrementando la iniciación de la traducción (Gingras et al. 1999).

Los resultados obtenidos en numerosos estudios evidencian el importante papel de CD98hc-LAT1 en la regulación de esta vía de señalización. De hecho, la eliminación de este transportador, tanto genética (Y. Cormerais et al. 2016; Elorza et al. 2012), como química (Y. Cormerais et al., 2016; Nicklin et al., 2009; Oda et al., 2009), tiene como consecuencia la inhibición de mTORC1 junto con una disminución de la síntesis proteica y el crecimiento celular.

La respuesta integrada al estrés mediada por eIF2

Un evento crítico para el inicio de la traducción es la unión de la subunidad ribosomal 40S libre con el complejo ternario constituido por el factor eIF2, GTP y un ARN de transferencia (ARNt) con el aminoácido iniciador metionina (Kimball and Jefferson 2005). En la formación de este complejo interviene el factor intercambiador de nucleótidos de guanina eIF2B, que activa eIF2·GDP en forma de eIF2·GTP. En situaciones de estrés, esta reacción es inhibida mediante la fosforilación del residuo Ser-51 de la subunidad α del factor eIF2 (Krishnamoorthy et al. 2002).

La fosforilación de eIF2α provoca la inhibición generalizada de la síntesis de proteínas, mientras que al mismo tiempo, se produce la activación de la traducción de ciertos ARN mensajeros (ARNm) implicados en la respuesta a estrés celular (Taniuchi et al., 2016). Es el caso del ARNm del factor de transcripción ATF4, que media un programa de expresión génica, llamada ISR, que permite que la célula se adapte a la situación de estrés que provocó la fosforilación de eIF2α y la inhibición global de la traducción (Harding et al. 2000).

En respuesta a diferentes tipos de estrés, cuatro quinasas regulan la síntesis de proteínas en células eucariotas mediante la fosforilación de eIF2α: HRI (*heme regulated inhibitor*), mayoritariamente activada en casos de deficiencia de hierro o estrés oxidativo (L. Lu, Han, & Chen, 2001; Suragani et al., 2012; Tidke, Maurya, Kulkarni, Devasagayam, & Pal, 2016); PKR (*protein kinase R*), regulada por ARN

de cadena doble (Galluzzi et al. 2008); PERK (*PKR-like endoplasmic reticulum kinase*), activada por estrés en el retículo endoplásmico (Bertolotti et al. 2000); y GCN2 (*general control non-derepressible-2*), inducida en situaciones de privación de AAs (Wek, Zhu, and Wek 1995).

En este contexto, dos estudios han demostrado que la eliminación de LAT1 induce la activación de GCN2 y posterior fosforilación de eIF2α (Y. Cormerais et al. 2016; Yann Cormerais et al. 2019).

8.1.3 La importancia de CD98hc en cáncer

Podría decirse que la flexibilidad metabólica es una de las características más relevantes de las células tumorales. La plasticidad tumoral comprende una serie de cambios en el catabolismo y anabolismo de estas células para mantener la homeostasis en un contexto de proliferación aberrante y estrictos requerimientos metabólicos, energéticos y nutricionales (Pavlova and Thompson 2016). La sobreexpresión de CD98hc forma parte de este programa de supervivencia, debido, tanto a su función de transporte, como a su interacción con integrinas, CD98hc actúa como un oncogén, estimulando el crecimiento, la proliferación independiente de anclaje, la migración y la supervivencia celular (McCracken and Edinger, 2013).

8.1.3.1 La función de CD98hc asociada a transporte

Las células cancerosas aumentan sus capacidades nutricionales y antioxidantes induciendo la expresión de los transportadores CD98hc-LAT1 y CD98hc-xCT.

CD98hc-LAT1 está sobreexpresado en numerosos tipos de cáncer y en la mayoría de líneas tumorales testadas (Hayashi & Anzai, 2017). Además, su expresión está asociada con mal pronóstico y mayor resistencia a quimioterapia (Namikawa et al. 2015; Sakata et al. 2009; Sommer et al. 2018; Yanagisawa et al. 2014).

Las células cancerosas obtienen considerables ventajas de la sobreexpresión de LAT1, llevando a cabo las siguientes funciones: i) abastecer la incrementada demanda de nutrientes, tales como EAAs, para la síntesis de proteínas y el

suministro de energía (Ganapathy, Thangaraju, and Prasad, 2009), ii) mantener la activación persistente de mTORC1 (Pavlova and Thompson 2016) y iii) activar la glutaminolisis por medio del transporte de leucina, que activa alostéricamente la enzima glutamato deshidrogenasa (GDH) (Yielding and Tomkins 1961).

Los niveles de expresión de xCT son elevados en un amplio espectro de tumores humanos (Koppula et al. 2017), y del mismo modo que LAT1, con frecuencia, esta sobreexpresión está asociada con metástasis, malignidad y resistencia a tratamientos anti-tumorales.(Cobler et al. 2018; Kinhosita et al. 2013; Toyoda et al. 2014).

La reprogramación metabólica llevada a cabo por las células tumorales tiene como consecuencia un aumento del estrés oxidativo celular, es por eso que estas células necesitan incrementar la biosíntesis de antioxidantes, incluido el GSH (Chio and Tuveson 2017). En este contexto, la inducción de xCT suministra la cistina necesaria para la producción de GSH, potenciando el restablecimiento del equilibrio de óxido-reducción y fomentando la flexibilidad metabólica de estas células.

Dado que tanto LAT1 como xCT han sido propuestos como potenciales dianas terapéuticas contra el cáncer, diferentes enfoques farmacológicos y genéticos han sido desarrollados para bloquear su función. Algunos de los inhibidores más relevantes son BCH (Kim et al. 2008; Oda et al. 2009) o JPH203 (Rosilio et al. 2015; Yothaisong et al. 2017), inhibidores específicos de LAT1, o sulfosalacina (Gout et al. 2001) y erastina (Dixon et al. 2012), en cuanto a los inhibidores de xCT. A pesar de que ha sido demostrado que estos fármacos reducen notablemente el desarrollo del tumor, sus efectos secundarios y su relativa eficiencia a bajas dosis restringe su uso en enfoques clínicos (Augustyn et al. 2016; Timmerman et al. 2013; Yang et al. 2014).

8.1.3.2 CD98hc y señalización de integrinas

Las integrinas son receptores de adhesión celular heterodiméricos, formados por dos subunidades de tipo β y α. Cada una de ellas consta de un único dominio transmembrana con una cola citoplasmática C-terminal y conectado a un extremo N-terminal extracelular (Barczyk, Carracedo, and Gullberg 2010). Las integrinas forman parte de las proteínas de la matriz extracelular y están expresadas de forma anómala en células tumorales, desempeñando un papel fundamental en la progresión y metástasis del tumor, ya que aumentan la migración, invasión, proliferación y supervivencia celular (Desgrosellier and Cheresh 2010).

Además de su función como transportador de AAs, CD98hc interactúa con las integrinas β1 y β3 amplificando su señal. En este sentido, se ha demostrado que las células que carecen de CD98hc presentan funciones anómalas de propagación y migración dependientes de integrinas, y además, están menos protegidas contra la apoptosis inducida por la privación de anclaje (anoiquis) (Feral et al. 2005).

8.1.4 CD98hc: conexiones metabólicas

Además de la función dual clásica de CD98hc, como transportador de AAs y mediador de la función de integrinas, CD98hc interactúa con otras proteínas transmembrana con funciones relevantes en el metabolismo energético celular, lo que sugiere que podría estar implicado en su regulación.

8.1.4.1 CD98hc y el transportador de glucosa GLUT1

El metabolismo glucolítico gobierna varias funciones celulares, ya que la glucosa es oxidada en diferentes vías metabólicas para generar una de las fuentes más importante de energía en células eucariotas. Estas funciones dependen en primer lugar de la captación de glucosa, que en la mayoría de las células de mamíferos está controlada principalmente por los miembros de la familia de transportadores de glucosa GLUTs (SLC2A)(Carvalho et al. 2011).

Ohno y colaboradores demostraron que CD98hc interacciona directamente con GLUT1, estabilizándolo y protegiéndolo de la degradación lisosomal, lo que da lugar a un aumento del transporte de glucosa (Ohno et al., 2011).

GLUT1 se expresa de manera aberrante en muchos tumores, ya que las células cancerosas requieren de un mayor suministro de energía para mantener su exacerbada proliferación (Cantuaria et al. 2001; Hao et al. 2009; Rudlowski, MD et al. 2003; B. Zhang, Xie, and Li 2019). La glucosa sostiene las principales vías metabólicas de provisión de energía: la glucólisis y la fosforilación oxidativa. Además, la ruta de las pentosas fosfato, la vía de la hexosaminas, la gluconeogénesis y la vía de biosíntesis de serina, también dependen de la asequibilidad de este metabolito (Hay 2016).

La ruta de las pentosas fosfato (PPP*, Pentose phosphate pathway*) deriva de la glucólisis y tiene un papel crucial en la síntesis de ribonucleótidos, además de ser una fuente importante de NADPH (Cho et al. 2018). Para mantener la homeostasis, las células proliferativas necesitan reponer los nucleótidos a la misma velocidad a la que se dividen. Es por eso que la progresión del ciclo celular está estrechamente conectada con la capacidad de la célula para adquirir nutrientes, generar energía y sintetizar nucleótidos (Lane and Fan, 2015). La PPP es una de las principales vías metabólicas que generan los sustratos necesarios parar sintetizar nucleótidos *de novo*, ya que controla la producción de ribosa-5 fosfato (5P), esencial para la generación de todos los ribonucleótidos (Cho et al. 2018).

Por tanto, CD98hc podría estar involucrado en la regulación del metabolismo glucolítico, lo que a su vez podría tener un impacto relevante en la regulación del ciclo celular.

8.1.4.2 El supercomplejo metabólico CD98hc-LAT1-MCT-CD147

CD147 (también llamado basigin, EMMPRIN, TCSF y HT7) es una glicoproteína transmembrana multifuncional expresada en una variedad de tejidos y células

humanas perteneciente a la superfamilia de inmunoglobulinas. Además, se sobreexpresa en un amplio espectro de tumores malignos humanos, potenciando la progresión tumoral mediante diferentes mecanismos moleculares (Xin et al. 2016).

Entre sus funciones principales, CD147 es la proteína auxiliar de los transportadores de lactato MCT1 y MCT4 (*monocarboxilate transporters*), asegurando su correcta expresión en la membrana plasmática y regulando su actividad como transportadores del ácido láctico producido por la glucólisis anaeróbica (Kirk et al. 2000).

La observación de que las células tumorales absorben y catabolizan la glucosa a una tasa notablemente más alta que su tejido de origen, fue reportada por primera vez por Warburg en los años 50, lo que se conoce como el *efecto Warburg* (Warburg 1956). Este descubrimiento le llevó a asumir que la respiración a través de la fosforilación oxidativa mitocondrial (OXPHOS) estaba alterada en las células cancerosas. Después de un intenso debate en los años subsiguientes, se ha demostrado que los tumores pueden mantener altas tasas metabólicas por ambas vías. Sin embargo, siendo el microambiente tumoral hipóxico, las células cancerosas dependen mayoritariamente de la glucólisis anaeróbica como fuente generadora de energía (Hay 2016).

Para poder llevar a cabo este *switch* metabólico, el ácido láctico generado como producto final de la glucólisis anaeróbica ha de ser liberado al medio extracelular a través de los MCTs, especialmente a través de MCT1, el miembro de esta familia más expresado en tumores (Pérez-Escuredo et al. 2016).

El lactato excretado por la célula estimula la angiogénesis, la motilidad y la migración de las células cancerosas. Además, la producción de lactato es vital para la autosuficiencia de estas células, ya que permite la regeneración de dinucleótido de nicotinamida y adenina (NAD^+), necesario para la continuación de la glucólisis (San-Millán and Brooks 2017).

Teniendo en cuenta todo esto, el bloqueo de la producción y transporte de lactato a través de la inactivación de los MCT o de CD147 se ha convertido en una atractiva estrategia contra el cáncer, ya que interrumpiría el *efecto Warburg* en esas células.

En este contexto, Xu y Hemler encontraron que CD98hc forma parte del supercomplejo metabólico MCT-CD147-CD98hc-LAT1, demostrando además, que la expresión de CD98hc y CD147 está correlacionada (Xu and Hemler 2005). Este hallazgo sugiere que CD98hc podría estar implicado en la regulación de la expresión y actividad de los MCTs, y que por tanto, podría jugar un papel importante en la flexibilidad metabólica tumoral (Ždralević et al. 2017).

8.1.5 Estrés replicativo y su impacto en la progresión del ciclo celular

Como se refleja en las secciones anteriores, la proliferación, y por tanto la progresión del ciclo celular, es un proceso altamente exigente, subordinado a la capacidad de la célula para adquirir nutrientes, mantener el equilibrio de óxido-reducción y también para producir la energía y sustratos necesarios para mantener la constante biosíntesis de nucleótidos (Cooper, 2000). CD98hc es capaz de regular estos tres procesos clave, y por tanto, podría tener un papel crucial en la regulación de la división celular.

Cada vez que una célula se divide, miles de millones de nucleótidos han de ser incorporados con absoluta precisión de manera coordinada y acorde con la sucesión del ciclo celular. El estrés oxidativo (Barzilai and Yamamoto 2004; Maser et al. 1997), la limitación de los factores de replicación esenciales, incluidos los nucleótidos (Poli et al. 2012), la sobreexpresión o activación constitutiva de oncogenes (Halazonetis, Gorgoulis, and Bartek 2008) o la alteración de la síntesis proteica (Rosner et al. 2009), son algunas de las situaciones que interfieren con la replicación del ADN, generando estrés replicativo.

Con el objetivo de preservar la integridad genómica, las células eucariotas son capaces de activar La respuesta a daño en el ADN (DDR, *DNA damage response*), una compleja y sofisticada vía de señalización que detecta lesiones en el ADN y pone en marcha mecanismos de reparación (Mazouzi, Velimezi, and Loizou, 2014). Estas lesiones son detectadas por *sensores* que reconocen las lesiones en sí mismas o las alteraciones de la cromatina causadas por el daño del ADN. Después, los *transductores* transfieren la señal de daño a los *efectores*, los cuales detienen o ralentizan el ciclo celular para activar la reparación a través de programas de transcripción, pudiendo incluso desencadenar la muerte celular si el daño no consigue ser reparado (Maréchal and Zou 2013).

Generalmente, las lesiones en el ADN desencadenan la generación de tramos de ADN monocatenario (ADNss, *single strand DNA*), reconocidos rápidamente por la proteína de replicación A (RPA). RPA actúa como una plataforma de señalización, reclutando una amplia variedad de proteínas, incluida la quinasa ATR (*ataxia-telangiectasia mutated*), que transfiere la señal a diferentes efectores. De entre los numerosos efectores, cabe destacar la fosforilación y posterior activación de la quinasa de punto de control 1 (CHK1), que se difunde globalmente a través del núcleo, donde inhibe la nueva replicación y activa la reparación de los daños generados (Vassin et al. 2009).

8.2 Objetivos

CD98hc es una proteína multifuncional involucrada en un gran número de funciones. Es la proteína auxiliar para seis transportadores HAT diferentes (LAT1, LAT2, xCT, y^+LAT1, y^+LAT2 y asc1), entre los cuales CD98hc-LAT1 y CD98hc-xCT están sobreexpresados en cáncer y se asocian con un fenotipo de tumor agresivo y de mal pronóstico.

Resultados previos obtenidos por Laura Rodríguez de la Ballina en nuestro grupo, determinaron que, tanto la función de transporte, como la señalización de

integrinas, ambas mediadas por CD98hc, son necesarias para la proliferación celular *in vivo*. Sin embargo, la función de integrinas es prescindible *in vitro*, de manera que las funciones CD98hc independientes de esta señalización pueden ser estudiadas en dichas condiciones.

Además, investigaciones llevadas a cabo por otros grupos, junto con los resultados obtenidos a lo largo de esta tesis, sugieren que CD98hc podría tener un papel fundamental en el metabolismo energético de la célula y en la progresión del ciclo celular, ninguno de los cuales ha sido estudiado con anterioridad.

Por todo esto, los objetivos del presente estudio son los siguientes:

I. Estudiar el papel de la función de transporte de aminoácidos asociada a CD98hc en proliferación celular y homeostasis óxido-reducción y evaluar las posibles vías de señalización involucradas en ambos procesos.

II. Investigar la implicación de CD98hc en la biosíntesis de nucleótidos y la progresión del ciclo celular.

III. Explorar cuál es el impacto de CD98hc en el metabolismo energético celular.

8.3 Resultados y discusión

Para llevar a cabo el estudio de las funciones celulares que dependen de CD98hc *in vitro*, se han utilizado fibroblastos salvajes (WT, *wild type*) y deficientes de CD98hc (KO, *knock out*) derivados de células madre de ratón como modelo celular. Los fibroblastos WT presentan los transportadores asociados a CD98hc: xCT, LAT1 y y^+LAT2, cuya actividad de transporte y expresión está ausente en las células CD98hc KO (de la Ballina et al., 2016).

8.3.1 CD98hc protege a las células frente al estrés oxidativo manteniendo su viabilidad

Las células CD98hc KO no son capaces de sobrevivir en condiciones rutinarias de cultivo y mueren por ferroptosis, tal como lo indican los altos niveles de expresión de gamma-glutamilciclotransferasa 1 (CHAC1), marcador de este tipo de muerte celular (Bassi et al. 2014), a menos que el medio sea suplementado con un agente reductor como β-ME. La suplementación con β-ME permite la reducción de la cistina extracelular en cisteína libre, que puede ser transportada posteriormente por otros transportadores no asociados CD98hc, recuperando los niveles de GSH y por tanto la homeostasis óxido-reducción de la célula (Conrad & Sato, 2012). Nuestros resultados son acordes con los obtenidos en otros estudios realizados en células deficientes de xCT (Arensman et al. 2019; Dixon et al. 2014; Sato et al. 2005) o células carentes de cisteína (Chen et al. 2017).

Aunque en condiciones normales la expresión de xCT *in vivo* no es tan crítica como en cultivo celular, especialmente debido a los diferentes niveles de oxígeno (O_2) en ambas condiciones (Jagannathan, Cuddapah, and Costa 2016), los tumores, debido a su reprogramación metabólica, dependen en gran medida de la maquinaria antioxidante de sus células. En estos casos, la eliminación de xCT puede ofrecer un punto de vulnerabilidad en cuanto a la progresión del cáncer.

Incluso cuando la ferroptosis está bloqueada por la suplementación con β-ME, las células CD98hc KO presentan un elevado estrés oxidativo. Dado que la inhibición específica de xCT con SAS en células WT no promueve la inducción de estrés oxidativo en presencia de β-ME, es posible que otra fuente, independientemente de la pérdida de xCT, esté subyacente al estrés oxidativo existente en las células CD98hc KO. Probablemente, el aumento de ROS observado en estas células esté relacionado con los cambios metabólicos que les permiten sobrevivir en ausencia de CD98hc (**sección 8.3.4**).

Además, nuestros datos sugieren que el aumento del estrés oxidativo podría ser la causa de la fosforilación de eIF2α en células deficientes de CD98hc a través de la

activación de la quinasa HRI, cuya expresión está aumentada en estas células. La activación de HRI en respuesta a altos niveles tóxicos de ROS ha sido demostrada con anterioridad en diferentes estudios (Lu, Han, and Chen 2001d; McEwen et al. 2005; Suragani et al. 2012; Tidke et al. 2016), respaldando nuestra hipótesis.

8.3.2 CD98hc sostiene la adecuada asequibilidad de AA requerida para la proliferación celular

La pérdida de la expresión y función de los transportadores asociados a CD98hc en las células KO, da lugar a un desbalance en el contenido intracelular de AAs, de manera que éstas presentan un aumento en el contenido intracelular tanto de AA^{+}s (arginina, lisina e histidina) como de AA^{0}s (alanina, serina, asparagina, glutamina y metionina). Por el contrario, los BCAAs (valina, leucina e isoleucina) y AAAs (fenilalanina y tirosina) se muestran notablemente disminudos en estas células.

La especificidad de sustrato de diferentes transportadores de AAs a menudo se solapa para garantizar que el sistema no se vea afectado si falla uno de los transportadores (Vilches et al. 2018b). Sin embargo, nuestros resultados indican que los transportadores asociados a CD98hc no son redundantes y por tanto son esenciales para mantener la homeostasis celular.

Además, los datos obtenidos en este estudio permiten conectar CD98hc tanto con estrés oxidativo como nutricional. Con el objetivo de disociar ambos tipos de estrés y poder estudiar qué funciones celulares dependían de la asequibilidad de BCAAs y AAAs mediada por CD98hc, independientemente del estrés oxidativo o de otras posibles alteraciones metabólicas presentes en las células deficientes de CD98hc, células WT fueron cultivadas en medio de cultivo con concentraciones reducidas de BCAAs y AAAs, y con concentraciones estándar de cistina y β-ME. Este nuevo modelo celular fue denominado low 6AA, por su bajo contenido en leucina, isoleucina, valina, triptófano, tirosina y fenilalanina.

Curiosamente, las células low 6AA también presentan un desbalance del contenido intracelular, muy similar al observado en las células CD98hc KO. Dicho

desequilibrio está mediado en cierta manera por la modulación de otros transportadores no asociados con CD98hc, como los transportadores catiónicos de AAs (CATs), aumentados tanto em células CD98hc KO, como en células low 6AA, y también en otros modelos generados en otros estudios, como en células KO de LAT1 (Tărlungeanu et al. 2016).

Acorde con nuestro objetivo, las células low 6AA no presentan estrés oxidativo ni tampoco un incremento en los niveles de fosforilación de eIF2α. Aunque está bien establecido que en condiciones de privación de AAs, los ARNt descargados activan la quinasa GCN2 (Dong et al. 2000; Wek, Zhu, and Wek 1995), que a su vez fosforila el eIF2α (Anthony et al. 2001; Harding et al. 2000; P. Zhang et al. 2002), nuestros resultados demuestran que la limitación de BCAAs y AAAs no induce la activación de eIF2α en nuestro modelo. En esta misma línea, no tenemos conocimiento de que se haya evaluado la carga de los ARNt o la activación de GCN2 en condiciones de restricción parcial de AAs, como es nuestro caso, en lugar de en contextos de privación total de AAs. Nuestros resultados indican que la restricción de BCAA y AAA no es suficiente para causar un aumento sustancial en los niveles de ARNt descargados, sugiriendo por tanto, que, aunque no podamos descartar su participación, GCN2 no gobierna la activación de la vía ISR mediada por P-eIF2α en las células CD98hc KO. Dicho supuesto es coherente con la hipótesis de que la activación de esta respuesta esté posiblemente mediada por estrés oxidativo y no nutricional.

La escasez de BCAAs y AAAs, de acuerdo con los resultados obtenidos en otros estudios (Cormerais et al., 2016; Elorza et al., 2012; Moberg et al., 2016; Neishabouri, Hutson, and Davoodi, 2015; Nicklin et al., 2009; Persaud et al. 2018), inhiben la vía de mTORC1 en células CD98hc KO y low 6AA. Además, la activación de la vía se recupera cuando los AAs deficitarios son suplementados en el medio celular de las células CD98hc KO en forma de dipéptidos, los cuales pueden entrar a través del transportador PEPT1, sobreexpresado en estas células.

En la misma línea, la limitación del acceso a BCAAs y AAAs causa una proliferación celular deficiente, que es recuperada mediante la adición en el medio de cultivo celular de los dipéptidos que contienen estos AAs.

Al mismo tiempo, los datos obtenidos en este estudio muestran que la eliminación de CD98hc conduce a una reducción global de la síntesis de proteínas, probablemente regida por la inhibición de mTORC1, aunque no podemos descartar la participación P-eIF2α en este proceso.

8.3.3 CD98hc es fundamental para la síntesis de nucleótidos, necesarios para la progresión del ciclo celular

La progresión del ciclo celular depende en gran medida de la capacidad de la célula para adquirir nutrientes y producir energía para impulsar la biosíntesis constante de nucleótidos (DeBerardinis et al., 2007; Moffatt and Ashihara, 2002). Cuando éstos son limitantes, la integridad del genoma puede verse afectada de diversas maneras (Bester et al. 2011; Giannattasio and Branzei 2017; Zeman and Cimprich 2014).

Nuestros resultados indican que la falta de CD98hc promueve una reducción dramática en el conjunto general de los nucleótidos, lo que da lugar a la activación de la DDR dependiente de ATR-CHK1 y consecuentemente, a la detención protectora del ciclo celular en la fase de síntesis de ADN (fase S).

Además, estos hallazgos son respaldados por los datos obtenidos en el estudio transcriptómico llevado a cabo en células WT y CD98hc KO. Por una parte, dicho análisis evidencia alteraciones en el ciclo celular de las células deficientes de CD98hc, ya que la expresión de grupos de genes relacionados con este proceso está gravemente afectada. Asimismo, la expresión de un amplio listado de genes relacionados con estrés replicativo y reparación de daño en el ADN están altamente inducida en las células CD98hc KO. Del mismo modo, los datos recogidos en el transcriptoma indican que la inducción de la DDR en las células

deficientes de CD98hc da lugar a la activación del punto de control (*checkpoint*) G2/M, disminuyendo el tránsito de las células que entran en la fase mitótica.

Con el objetivo de investigar si la restricción de BCAAs y AAAs planteaba una limitación para llevar a cabo la replicación del ADN de manera adecuada en las células CD98hc KO, se evaluaron los principales marcadores de la vía de señalización DDR y la tasa mitótica de las células low 6AA. Consistentemente, estas células presentan estrés replicativo y una reducción en el número de mitosis comparado con las células control. Sin embargo, al contrario que en las células deficientes de CD98hc, las células low 6AA presentan una disminución únicamente en el contenido de los desoxinucleótidos.

Estos resultados indican que el mecanismo que subyace al estrés replicativo en ambos modelos es diferente, sugiriendo que en las células low 6AA la reducción de los ribonucleótidos a desoxinucleótidos esté probablemente comprometida, mientras que en las células CD98hc KO se trate de un problema que afecte a la síntesis general de nucleótidos.

Mediante un análisis metabolómico realizado en ambos modelos celulares, descubrimos que la ruta PPP estaba gravemente afectada en las células deficientes de CD98hc.

La ruta PPP es una vía de las más importantes en cuanto al catabolismo de la glucosa y la fuente principal de ribosa-5P, la cual conforma la base estructural de todos los nucleótidos (Jiang, Du, and Wu 2014). En este trabajo, proponemos que la anulación del flujo de la vía PPP y, en consecuencia, la drástica reducción de ribosa-5P, probablemente sea la causa directa de la disminución de los niveles de nucleótidos en las células deficientes de CD98hc. Respaldando esta hipótesis, otros estudios han demostrado que tanto la disponibilidad de ribosa-5P (Boer and Sperling 1995; Pilz, Willis, and Boss 1984), como la perturbación de la actividad de la vía PPP (Cosentino, Grieco, and Costanzo 2011; Fornalewicz et al. 2017; Qu et al. 2017; Yu et al. 2015), desencadenan alteraciones en la biosíntesis de nucleótidos

y en la replicación del ADN. Sin embargo, el mecanismo por el cual el flujo de la ruta PPP está interrumpido en las células CD98hc KO ha de ser clarificado.

La adición de nucleósidos en el medio celular, reconstituye las funciones normales del ciclo celular en células CD98hc KO, disminuyendo el estrés replicativo, la detención del ciclo celular en la fase S y también reanudando la tasa mitótica de estas células. Estos resultados demuestran que la limitación de nucleótidos es la causa fundamental de la disrupción de la progresión del ciclo celular mediada por la falta de CD98hc.

Por otra parte, nuestros resultados indican que la disminución en los niveles de desoxinucleótidos está causada por la supresión de la expresión de la proteína RRM2 en las células low 6AA, la única enzima que cataliza el paso limitante de la conversión *de novo* de ribonucleósidos a desoxirribonucleósidos (Aird et al. 2013; Lopez-Contreras et al. 2015). La suplementación con nucleósidos en el medio de cultivo celular recupera el estrés replicativo en estas células, indicando que la limitación de BCAAs y AAAs da lugar a una caída en los niveles de desoxinucleótidos y que ésta es la causa subyacente del problema de división celular en este modelo.

8.3.4 CD98hc regula el metabolismo energético celular

Sobre la base de los datos mostrados en las secciones anteriores, llegamos a la conclusión de que la interrupción de la ruta PPP subyacía al problema de la síntesis de nucleótidos en las células deficientes de CD98hc, probablemente debido a un problema relacionado con el metabolismo energético de estas células.

La mayoría de las células de mamíferos dependen de un suministro continuo de glucosa, es por esto que la actividad de las vías metabólicas nutridas por medio de este metabolito está rigurosamente regulada. Después de la absorción, la glucosa es oxidada para extraer energía a través de la vía de la glucólisis, así mismo, también se desvía para sustentar la vía PPP, que suministra azúcares de cinco

carbonos para la síntesis de nucleótidos y la producción de NADPH (Alberts et al. 2002).

Las células CD98hc KO, de acuerdo con los resultados obtenidos por Ohno *et al.*, presentan una reducción en los niveles de expresión de GLUT1, probablemente como consecuencia de su degradación debido a la ausencia de CD98hc. Como resultado, la incorporación de glucosa, en estas células se ve muy disminuida (Ohno et al., 2011). Sin embargo, a pesar de ello, la glucosa incorporada se acumula dentro de las células, lo que evidencia un serio impedimento para usar este metabolito como suministro de energía en las células CD98hc KO. Consistentemente, los datos obtenidos en el estudio metabolómico realizado en estas células, ponen de manifiesto la drástica reducción de la glucólisis en las células que carecen de CD98hc.

En la misma línea, nuestros resultados indican que las células CD98hc KO activan la respiración mitocondrial a través de OXPHOS para satisfacer la demanda energética impuesta por su incapacidad para sintetizar ATP por la vía glucolítica, cuyos niveles están gravemente disminuidos. Este *switch* metabólico ha sido descrito en numerosos estudios en los que la glucólisis está interrumpida por diferentes motivos (Benjamin et al. 2018; Brand et al. 2016; Cormerais et al. 2016; Fantin, St-Pierre, and Leder 2006; Granja et al. 2014; de Padua et al. 2017).

Probablemente, fruto de una adaptación para llevar a cabo esta reprogramación metabólica, las células deficientes de CD98hc presentan un incremento de la masa mitocondrial. En la línea de esta discusión, en un estudio reciente realizado por Balsa y colaboradores, se ha demostrado que la privación de glucosa causa un cambio metabólico hacia OXPHOS a expensas del aumento de los niveles de proteínas mitocondriales que forman parte de complejos de la cadena de transporte de electrones (Balsa et al. 2019).

La expresión de CD147 y MCT1, en acuerdo con los datos obtenidos en el trabajo realizado por Xu y Hemler, están disminuidos en las células carentes de CD98hc (Fei et al. 2014). Sin embargo, contrariamente a lo reportado en otros estudios

(Benjamin et al. 2018; Cormerais et al. 2016; Granja et al. 2014), esto no produce una acumulación de lactato intracelular, probablemente, tal como indican nuestros datos, porque la producción de este metabolito en nuestro modelo está disminuída. La reacción de conversión de piruvato en lactato es una de las fuentes más importantes de NAD^+, necesario para sustentar la glucólisis de la célula (Benjamin et al. 2018). Si ésta fuera la causa que compromete la vía glucolítica en las células CD98hc KO, la manipulación de la relación NAD^+/NADH podría promover potencialmente la restauración de la actividad de la vía.

Además de las conexiones mencionadas anteriormente entre el metabolismo de la glucosa y la pérdida de CD98hc, ha de tenerse en cuenta que la escasez concomitante de BCAAs y AAAs también esté posiblemente involucrada en la reprogramación metabólica descrita en el modelo CD98hc KO. De hecho, nuestros datos demuestran que la escasez de BCAAs y AAAs aumenta la respiración mitocondrial por OXPHOS en las células low 6AA. Además, la adición en el medio de cultivo celular de dipéptidos que contienen los BCAAs y AAAs limitantes reduce la tasa de la respiración mitocondrial acoplada a la producción de ATP en las células CD98hc KO. Estos resultados indican que los BCAAs y AAAs son capaces de regular el metabolismo energético de la célula, sugiriendo que la adaptación celular a la disponibilidad limitada de EAAs podría ocurrir a expensas de una mayor respiración acoplada a la producción de ATP en las mitocondrias.

En resumen, en este estudio hemos evaluado las funciones celulares que dependen de CD98hc relacionadas con la homeostasis óxido-reducción, la síntesis de proteínas, la regulación del ciclo celular y el metabolismo energético. Nuestros datos respaldan CD98hc como potencial diana terapéutica, especialmente para el tratamiento del cáncer. Por un lado, la eliminación de CD98hc regularía negativamente el crecimiento del tumor al disminuir la capacidad de éste para combatir el estrés oxidativo. Por otro lado, la ablación de CD98hc limitaría la asequibilidad de AAs para la síntesis adecuada de proteínas y la proliferación celular. Además, daría lugar a una defectuosa utilización de la glucosa, lo que desencadenaría la reducción de los niveles de ATP y bloquearía la biosíntesis de

nucleótidos, deteniendo así el ciclo celular. Finalmente, aunque no ha sido objeto de estudio en este trabajo, la pérdida de función de CD98hc comprometería las vías de señalización reguladas por integrinas, necesarias para el crecimiento, migración e invasión de los tumores.

Hasta la fecha, muchos estudios se han centrado en la búsqueda de inhibidores de xCT (Balza et al. 2013) y LAT1 (Häfliger et al., 2018; Hayashi and Anzai, 2017; Im et al., 2008; Oda et al., 2009). Sin embargo, aun siendo estrategias atractivas para combatir la proliferación del tumor, los resultados obtenidos hasta el momento han sido muy limitados. CD98hc podría representar una opción novedosa, ampliando la ventana terapéutica de la terapia del cáncer al inducir un deterioro inmediato en las diversas funciones celulares descritas anteriormente.

8.4 Conclusiones

I. CD98hc contribuye a la protección de las células frente al estrés oxidativo, previniendo la muerte celular vía ferroptosis.

II. CD98hc promueve la proliferación celular, manteneniendo un contenido de aminoácidos intracelular equilibrado para regular la vía de señalización mTORC1. Además, la eliminación de CD98hc conduce a la activación de la respuesta integrada al estrés mediada por eI2Fα, probablemente debido al aumento del estrés oxidativo. La síntesis global de proteínas está reducida en células deficientes de CD98hc, probablemente por la contribución de ambas vías de señalización.

III. CD98hc sustenta a las células con la cantidad de BCAAs y AAAs requerida para mantener la expresión de RRM2 y por tanto, la síntesis de desoxinucleótidos, necesaria para la proliferación y progresión del ciclo celular.

IV. La falta de CD98hc tiene como consecuencia una reducción de la captación de glucosa y de las vías metabólicas relacionadas con este metabolito, como la

glucólisis y la ruta de las penstosas fosfato, obligando a las células a utilizar el metabolismo oxidativo mitocondrial para mantener los niveles celulares de ATP.

V. CD98hc soporta la producción de ribosa-5P, requerida para la biosíntesis de nucleótidos. La pérdida de CD98hc promueve una reducción dramática en el contenido de nucleótidos, causando estrés replicativo, enlentecimiento del ciclo celular y disminución de la mitosis.

References

Adekola, K., Rosen, S. T. & Shanmugam, M. Glucose transporters in cancer metabolism. Curr. Opin. Oncol. 24, 650–4 (2012).

Aguilera, A. & García-Muse, T. Causes of Genome Instability. Annu. Rev. Genet. 47, 1–32 (2013).

Ahn, C. S. & Metallo, C. M. Mitochondria as biosynthetic factories for cancer proliferation. Cancer Metab. 3, 1 (2015).

Aird, K. M. et al. ATM Couples Replication Stress and Metabolic Reprogramming during Cellular Senescence. Cell Rep. 11, 893–901 (2015).

Aird, K. M. et al. Suppression of nucleotide metabolism underlies the establishment and maintenance of oncogene-induced senescence. Cell Rep. 3, 1252–65 (2013).

Alberts, B. et al. Molecular biology of the cell. (Garland Science, 2002).

Albiges, L. et al. Chk1 as a new therapeutic target in triple-negative breast cancer. Breast 23, 250–258 (2014).

Anderson, N. M., Mucka, P., Kern, J. G. & Feng, H. The emerging role and targetability of the TCA cycle in cancer metabolism. Protein Cell 9, 216–237 (2018).

Andre, H. et al. Binding of vascular anticoagulant (VAC) to planar phospholipids bilayers. J. Biol. Chem 265, 4923–4928 (1990).

Anthony, T. G. et al. Reiter, A. K., Anthony, J. C., Kimball, S. R. & Jefferson, L. S. Deficiency of dietary EAA preferentially inhibits mRNA translation of ribosomal proteins in liver of meal-fed rats. Am J Physiol Endocrinol Metab 281, E430-439 (2001).

Arensman, M. D. et al. Cystine-glutamate antiporter xCT deficiency suppresses tumor growth while preserving antitumor immunity. Proc. Natl. Acad. Sci. 116, 9533-9542 (2019).

Augustyn, E. et al. LAT-1 activity of meta-substituted phenylalanine and tyrosine analogs. Bioorg. Med. Chem. Lett. 26, 2616–2621 (2016).

Avcilar-Kucukgoze, I. et al. Discharging tRNAs: a tug of war between translation and detoxification in Escherichia coli. Nucleic Acids Res. 44, 8324–8334 (2016).

Bai, J., Greene, E., Li, W., Kidd, M. T. & Dridi, S. Branched-chain amino acids modulate the expression of hepatic fatty acid metabolism-related genes in female broiler chickens. Mol. Nutr. Food Res. 59, 1171–1181 (2015).

Balasubramanian, M. N., Butterworth, E. A. & Kilberg, M. S. Asparagine synthetase: regulation by cell stress and involvement in tumor biology. Am. J. Physiol. Endocrinol. Metab. 304, E789-99 (2013).

Balsa, E. et al. ER and Nutrient Stress Promote Assembly of Respiratory Chain Supercomplexes through the PERK-eIF2α Axis. Mol. Cell 1–14 (2019).

Balza, E., Castellani, P., Delfino, L., Truini, M. & Rubartelli, A. The pharmacologic inhibition of the xc-antioxidant system improves the antitumor efficacy of COX inhibitors in the in vivo model of 3-MCA tumorigenesis. Carcinogenesis 34, 620–626 (2013).

Bannai, S. & Tateishi, N. Role of membrane transport in metabolism and function of glutathione in mammals. J. Membr. Biol. 89, 1–8 (1986).

Bannai, S. Exchange of cystine and glutamate across plasma membrane of human fibroblasts. J. Biol. Chem. 261, 2256–2263 (1986).

Barczyk, M., Carracedo, S. & Gullberg, D. Integrins. Cell Tissue Res. 339, 269–280 (2010).

Barnum, K. J. & O'Connell, M. J. Cell cycle regulation by checkpoints. Methods Mol. Biol. 1170, 29–40 (2014).

Barzilai, A. & Yamamoto, K. I. DNA damage responses to oxidative stress. DNA Repair 3, 1109–1115 (2004).

Bassi, M. et al. Ferroptosis: An Iron-Dependent Form of Nonapoptotic Cell Death. Cell 149, 1060–1072 (2012).

Bassi, M. et al. Pharmacological inhibition of cystine-glutamate exchange induces endoplasmic reticulum stress and ferroptosis. Elife 3, e02523 (2014).

Bassi, M. T. et al. Identification and characterisation of human xCT that co-expresses, with 4F2 heavy chain, the amino acid transport activity system xc-. Pflugers Arch. 442, 286–96 (2001).

Benjamin, D. et al. Dual Inhibition of the Lactate Transporters MCT1 and MCT4 Is Synthetic Lethal with Metformin due to NAD+ Depletion in Cancer Cells. Cell Rep. 25, 3047-3058.e4 (2018).

Berg, J. M. (Jeremy M., Tymoczko, J. L., Stryer, L. & Stryer, L. Biochemistry. (W.H. Freeman, 2002).

Berlanga, J. J., Herrero, S. & de Haro, C. Characterization of the hemin-sensitive eukaryotic initiation factor 2alpha kinase from mouse nonerythroid cells. J. Biol. Chem. 273, 32340–6 (1998).

Bertolotti, A., Zhang, Y., Hendershot, L. M., Harding, H. P. & Ron, D. Dynamic interaction of BiP and ER stress transducers in the unfolded-protein response. Nature 2, 1–7 (2000).

Bertran, J. et al. Expression cloning of a cDNA from rabbit kidney cortex that induces a single transport system for cystine and dibasic and neutral amino acids. Proc. Natl. Acad. Sci. U. S. A. 89, 5601–5 (1992).

Bertran, J. et al. Stimulation of system y(+)-like amino acid transport by the heavy chain of human 4F2 surface antigen in Xenopus laevis oocytes. 89, 5606–5610 (1992).

Bester, A. C. et al. Nucleotide deficiency promotes genomic instability in early stages of cancer development. Cell 145, 435–46 (2011).

Bevers, E. M., Comfurius, P., Dekkers, D. W. C. & Zwaal, R. F. A. Lipid translocation across the plasma membrane of mammalian cells. Biochim. Biophys. Acta - Mol. Cell Biol. Lipids 1439, 317–330 (1999).

Bhutia, Y. D., Babu, E., Prasad, P. D. & Ganapathy, V. The amino acid transporter SLC6A14 in cancer and its potential use in chemotherapy. Asian J. Pharm. Sci. 9, 293–303 (2014).

Bhutia, Y. D., Babu, E., Ramachandran, S. & Ganapathy, V. Amino acid transporters in cancer and their relevance to 'glutamine addiction': Novel Targets for the design of a new class of anticancer drugs. Cancer Res. 75, 1782–1788 (2015).

Bi, M. et al. Endoplasmic Reticulum and the Unfolded Protein Response: Dynamics and Metabolic Integration. International Review of Cell and Molecular Biology 301, (2013).

Birbe, E., Sahiner, U. M., Sackesen, C., Erzurum, S. & Kalayci, O. Oxidative Stress and Antioxidant Defense. World Allergy Organ 5, 0–19 (2012).

Bjursell, G. & Reichard, P. Effects of thymidine on deoxyribonucleoside triphosphate pools and deoxyribonucleic acid synthesis in Chinese hamster ovary cells. J. Biol. Chem. 248, 3904–3909 (1973).

Blommaart, E. F., Luiken, J. J., Blommaart, P. J., van Woerkom, G. M. & Meijer, A. J. Phosphorylation of ribosomal protein S6 is inhibitory for autophagy in isolated rat hepatocytes. J. Biol. Chem. 270, 2320–6 (1995).

Boado, R. J. & Pardridge, W. M. Glucose deprivation and hypoxia increase the expression of the GLUT1 glucose transporter via a specific mRNA cis-acting regulatory element. J. Neurochem. 80, 552–554 (2002).

Bodoy, S., Fotiadis, D., Stoeger, C., Kanai, Y. & Palacín, M. The small SLC43 family: Facilitator system l amino acid transporters and the orphan EEG1. Mol. Aspects Med. 34, 638–645 (2013).

Boer, P. & Sperling, O. Role of cellular ribose-5-phosphate content in the regulation of 5-phosphoribosyl-1-pyrophosphate and de novo purine synthesis in a human hepatoma cell line. Metabolism 44, 1469–1474 (1995).

Bolstad, B. M. Low Level Analysis of High-density Oligonucleotide Array Data: Background, Normalization and Summarization. PhD thesis, Univ. California, Berkeley 156 (2005).

Boroughs, L. K. & Deberardinis, R. J. Metabolic pathways promoting cancer cell survival and growth. Nat. Cell Biol. 17, 351–359 (2016).

Boulter, E. et al. Cell metabolism regulates integrin mechanosensing via an SLC3A2-dependent sphingolipid biosynthesis pathway. Nat. Commun. 9, 4862 (2018).

Brand, A. et al. LDHA-Associated Lactic Acid Production Blunts Tumor Immunosurveillance by T and NK Cells. Cell Metab. 24, 657–671 (2016).

Bröer, A., Wagner, C. A., Lang, F. & Bröer, S. The heterodimeric amino acid transporter 4F2hc/y+LAT2 mediates arginine efflux in exchange with glutamine. Biochem. J. 349 Pt 3, 787–95 (2000).

Bröer, S. & Palacín, M. The role of amino acid transporters in inherited and acquired diseases. Biochem. J. 436, 193–211 (2011).

Bröer, S. The SLC38 family of sodium-amino acid co-transporters. Pflugers Arch. Eur. J. Physiol. 466, 155–172 (2014).

Brush, M. H., Weiser, D. C. & Shenolikar, S. Growth arrest and DNA damage-inducible protein GADD34 targets protein phosphatase 1 alpha to the endoplasmic reticulum and promotes dephosphorylation of the alpha subunit of eukaryotic translation initiation factor 2. Mol. Cell. Biol. 23, 1292–303 (2003).

Bull, E. E. A. et al. Enhanced tumor cell radiosensitivity and abrogation of G2 and S phase arrest by the Hsp90 inhibitor 17-(dimethylaminoethylamino)-17-demethoxygeldanamycin. Clin. Cancer Res. 10, 8077–8084 (2004).

Burrage, L. C., Nagamani, S. C. S., Campeau, P. M. & Lee, B. H. Branched-chain amino acid metabolism: from rare Mendelian diseases to more common disorders. Hum. Mol. Genet. 23, R1-8 (2014).

Cabello, C. M. et al. Chk1 phosphorylation during mitosis. Cell Cycle 46, 220–231 (2010).

Cadenas, E., Davies, K. J. A. & Adenas, E. N. C. Mitochonrial free radical generation,oxidative stress,and aging. 29, 222–230 (2000).

Calderon-Montano, J. M. et al. Role of the Intracellular pH in the Metabolic Switch between Oxidative Phosphorylation and Aerobic Glycolysis. WebmedCentral CANCER 2, WMC001716 (2011).

Calonge, M. J. et al. Cystinuria caused by mutations in rBAT, a gene involved in the transport of cystine. Nat. Genet. 6, 420–425 (1994).

Cantuaria, G. et al. GLUT-1 expression in ovarian carcinoma: association with survival and response to chemotherapy. Cancer 92, 1144–50 (2001).

Cargnello, M., Tcherkezian, J. & Roux, P. P. The expanding role of mTOR in cancer cell growth and proliferation. Mutagenesis 30, 169–76 (2015).

Carson, P. E., Flanagan, C. L., Ickes, C. E. & Alving, A. S. Enzymatic Deficiency in Primaquine-Sensitive Erythrocytes. Am. Nat. 124, 484–485 (1956).

Carvalho, K. C. et al. GLUT1 expression in malignant tumors and its use as an immunodiagnostic marker. Clinics 66, 965–72 (2011).

Castilho, B. A. et al. Keeping the eIF2 alpha kinase Gcn2 in check. Biochim. Biophys. Acta - Mol. Cell Res. 1843, 1948–1968 (2014).

Chang, A. B., Lin, R., Studley, W. K., Tran, C. V. & Saier, Jr, M. H. Phylogeny as a guide to structure and function of membrane transport proteins. Mol. Membr. Biol. 21, 171–181 (2004).

Chantranupong, L. et al. The CASTOR proteins are arginine sensors for the mTORC1 pathway. Cell 165, 153–164 (2016).

Chen, M.-S. et al. CHAC1 degradation of glutathione enhances cystine-starvation-induced necroptosis and ferroptosis in human triple negative breast cancer cells via the GCN2-eIF2α-ATF4 pathway. Oncotarget 8, 114588 (2017).

Cheung, O. et al. Activation and Dysregulation of the Unfolded Protein Response in Nonalcoholic Fatty Liver Disease. Gastroenterology 134, 568–576 (2007).

Chio, I. I. C. & Tuveson, D. A. ROS in Cancer: The Burning Question. Trends Mol. Med. 23, 411–429 (2017).

Cho, E. S., Cha, Y. H., Kim, H. S., Kim, N. H. & Yook, J. I. The Pentose Phosphate Pathway as a Potential Target for Cancer Therapy. Biomol. Ther. 26, 29–38 (2018).

Cho, S. H., Toouli, C. D., Fujii, G. H., Crain, C. & Parry, D. Chk1 is Essential for Tumor Cell Viability Following Activation of the Replication Checkpoint. Cell Cycle 4, 131–139 (2005).

Christensen, H. N. Role of amino acid transport and countertransport in nutrition and metabolism. Physiol Rev. 70, 43-77 (1990).

Cobler, L., Zhang, H., Suri, P., Park, C. & Timmerman, L. A. xCT inhibition sensitizes tumors to ɣ-radiation via glutathione reduction. Oncotarget 9, 32280–32297 (2018).

Conrad, M. & Sato, H. The oxidative stress-inducible cystine/glutamate antiporter, system x c − : cystine supplier and beyond. Amino Acids 42, 231–246 (2012).

Cooper, G. M. Cell Membranes. (Sunderland, 2000).

Cooper, G. M. The Eukaryotic Cell Cycle. (Sunderland, 2000).

Cormerais, Y. et al. Genetic Disruption of the Multifunctional CD98/LAT1 Complex Demonstrates the Key Role of Essential Amino Acid Transport in the Control of mTORC1 and Tumor Growth. Cancer Res. 76, 4481–4492 (2016).

Cormerais, Y. et al. Inhibition of the amino-acid transporter LAT1 demonstrates anti-neoplastic activity in medulloblastoma. J. Cell. Mol. Med. 2711–2718 (2019).

Cosentino, C., Grieco, D. & Costanzo, V. ATM activates the pentose phosphate pathway promoting anti-oxidant defence and DNA repair. EMBO J. 30, 546–55 (2011).

Crabtree, H. G. The carbohydrate metabolism of certain pathological overgrowths. Biochem. J. 22, 1289–98 (1928).

Csibi, A. et al. The mTORC1/S6K1 pathway regulates glutamine metabolism through the eif4b-dependent control of c-Myc translation. Curr. Biol. 24, 2274–2280 (2014).

Cunningham, J. T., Moreno, M. V, Lodi, A. & Ruggero, D. Protein and nucleotide biosynthesis are coupled through asingle rate limiting enzyme, PRPS2, to drive cancer. Cell 157, 1088–1103 (2014).

Cuyàs, E., Corominas-Faja, B., Joven, J. & Menendez, J. A. Cell Cycle Regulation by the Nutrient-Sensing Mammalian Target of Rapamycin (mTOR) Pathway. Methods Mol. Biol. 1170, 113–144 (2014).

Dai, Y. & Grant, S. New insights into checkpoint kinase 1 in the DNA damage response signaling network. Clin. Cancer Res. 16, 376–83 (2010).

Daniel, H. & Kottra, G. The proton oligopeptide cotransporter family SLC15 in physiology and pharmacology. Pflugers Arch. Eur. J. Physiol. 447, 610–618 (2004).

David, L. et al. CHK1 as a therapeutic target to bypass chemoresistance in AML. Sci. Signal 9, (2016).

de la Ballina, L. R. Characterization of the multifunctional protein 4F2hc. PhD thesis. Univ. Barcelona (2011).

de la Ballina, L. R. et al. Amino Acid Transport Associated to Cluster of Differentiation 98 Heavy Chain (CD98hc) Is at the Cross-road of Oxidative Stress and Amino Acid Availability. J. Biol. Chem. 291, 9700–9711 (2016).

de Padua, M. C. et al. Disrupting glucose-6-phosphate isomerase fully suppresses the Warburg effect and activates OXPHOS with minimal impact on tumor growth except in hypoxia. Oncotarget 8, 87623–87637 (2017).

DeBerardinis, R. J. et al. Beyond aerobic glycolysis: transformed cells can engage in glutamine metabolism that exceeds the requirement for protein and nucleotide synthesis. Proc. Natl. Acad. Sci. U. S. A. 104, 19345–50 (2007).

Dejure, F. R. et al. The MYC mRNA 3'-UTR couples RNA polymerase II function to glutamine and ribonucleotide levels. EMBO J. 36, 1854–1868 (2017).

Desgrosellier, J. S. & Cheresh, D. A. Integrins in cancer: biological implications and therapeutic opportunities. Nat. Rev. Cancer 10, 9–22 (2010).

Dever, T. E. Gene-Specific Regulation by General Translation Factors. Cell 108, 545–556 (2002).

Deves, B. Y. R., Angelo, S. & Chavez, P. N-ethylmaleimide discriminates between two lysine transport systems in human erythrocytes. J. Physiol. 468, 753–766 (1993).

Devés, R., Chavez, P. & Boyd, C. A. R. Identifcation of a new transport system (y+ L) in human erythrocytes that recognizes lysine and leucine with high affnity. J. Physiol. 454, 491–501 (1992).

Dey, M., Cao, C., Sicheri, F. & Dever, T. E. Conserved intermolecular salt bridge required for activation of protein kinases PKR, GCN2, and PERK. J. Biol. Chem. 282, 6653–6660 (2007).

Dey, S. et al. Both transcriptional regulation and translational control of ATF4 are central to the integrated stress response. J. Biol. Chem. 285, 33165–74 (2010).

Di Giovanni, V. et al. Metabolomic Changes in Serum of Children with Different Clinical Diagnoses of Malnutrition. J. Nutr. 146, 2436–2444 (2016).

Dixon, S. J. et al. Ferroptosis: An Iron-Dependent Form of Nonapoptotic Cell Death. Cell 149, 1060–1072 (2012).

Dixon, S. J. et al. Pharmacological inhibition of cystine-glutamate exchange induces endoplasmic reticulum stress and ferroptosis. Elife (2014).

Doherty, J. R. & Cleveland, J. L. Targeting lactate metabolism for cancer therapeutics. J. Clin. Invest. 123, 3685–92 (2013).

Doherty, J. R. et al. Blocking lactate export by inhibiting the Myc target MCT1 Disables glycolysis and glutathione synthesis. Cancer Res. 74, 908–20 (2014).

Doherty, J. R., Cleveland, J. L., Doherty, J. R. & Cleveland, J. L. Targeting lactate metabolism for cancer therapeutics Find the latest version : Review series Targeting lactate metabolism for cancer therapeutics. J. Clin. Invest. 123, 3685–3692 (2013).

Dong, J., Qiu, H., Garcia-Barrio, M., Anderson, J. & Hinnebusch, A. G. Uncharged tRNA Activates GCN2 by Displacing the Protein Kinase Moiety from a Bipartite tRNA-Binding Domain open reading frames (uORFs) in the GCN4 mRNA leader underlie a specialized reinitiation mechanism that ele- vates GCN4 translation in response to sm. Mol. Cell 6, 269–279 (2000).

Donnelly, N., Gorman, A. M., Gupta, S. & Samali, A. The eIF2α kinases: their structures and functions. Cell. Mol. Life Sci. 70, 3493–3511 (2013).

Du, Y., Meng, Q., Zhang, Q. & Guo, F. Isoleucine or valine deprivation stimulates fat loss via increasing energy expenditure and regulating lipid metabolism in WAT. Amino Acids 43, 725–734 (2012).

Düvel, K. et al. Activation of a metabolic gene regulatory network downstream of mTOR complex 1. Mol. Cell 39, 171–83 (2010).

Efeyan, A., Comb, W. C. & Sabatini, D. M. Nutrient-sensing mechanisms and pathways. Nature 517, 302–10 (2015).

Elorza, A. et al. HIF2α Acts as an mTORC1 Activator through the Amino Acid Carrier SLC7A5. Mol. Cell 48, 681–691 (2012).

Errasti-Murugarren, E. et al. L amino acid transporter structure and molecular bases for the asymmetry of substrate interaction. Nat. Commun. 10, 1807 (2019).

Espino Guarch, M. et al. Mutations in L-type amino acid transporter-2 support SLC7A8 as a novel gene involved in age-related hearing loss. Elife 7, e31511 (2018).

Estévez, R. et al. The amino acid transport system y+L/4F2hc is a heteromultimeric complex. FASEB J. 12, 1319–29 (1998).

Evstafieva, A. G. et al. A sustained deficiency of mitochondrial respiratory complex III induces an apoptotic cell death through the p53-mediated inhibition of pro-survival activities of the activating transcription factor 4. Cell Death Dis. 5, e1511-10 (2014).

Fan, J. et al. Glutamine-driven oxidative phosphorylation is a major ATP source in transformed mammalian cells in both normoxia and hypoxia. Mol. Syst. Biol. 9, 712–712 (2014).

Fantin, V. R., St-Pierre, J. & Leder, P. Attenuation of LDH-A expression uncovers a link between glycolysis, mitochondrial physiology, and tumor maintenance. Cancer Cell 9, 425–434 (2006).

Fei, F. et al. CD147-CD98hc Complex Contributes to Poor Prognosis of Non-Small Cell Lung Cancer Patients Through Promoting Cell Proliferation Via the PI3K/Akt Signaling Pathway. Ann. Surg. Oncol. 21, 4359–4368 (2014).

Feliubadaló, L. et al. Non-type I cystinuria caused by mutations in SLC7A9, encoding a subunit (bo,+AT) of rBAT. Nat. Genet. 23, 52–57 (1999).

Feller, D. D. Conversion of amino acids to fatty acids. Compr. Physiol. 363–373 (2010).

Fenczik, C. A. et al. Distinct domains of CD98hc regulate integrins and amino acid transport. J. Biol. Chem. 276, 8746–52 (2001).

Fenczik, C. A., Sethi, T., Ramos, J. W., Hughes, P. E. & Ginsberg, M. H. Complementation of dominant suppression implicates CD98 in integrin activation. Nature 390, 81–85 (1997).

Feral, C. C. et al. CD98hc (SLC3A2) mediates integrin signaling. Proc. Natl. Acad. Sci. U. S. A. 102, 355–60 (2005).

Ferguson, J. F. & Wang, T. J. Branched-Chain Amino Acids and Cardiovascular Disease: Does Diet Matter? Clin. Chem. 62, 545–547 (2016).

Fingar, D. C. et al. mTOR controls cell cycle progression through its cell growth effectors S6K1 and 4E-BP1/eukaryotic translation initiation factor 4E. Mol. Cell. Biol. 24, 200–16 (2004).

Forman, H. J., Zhang, H. & Rinna, A. Glutathione: overview of its protective roles, measurement, and biosynthesis. Mol. Aspects Med. 30, 1–12 (2009).

Fornalewicz, K., Wieczorek, A., Węgrzyn, G. & Łyżeń, R. Silencing of the pentose phosphate pathway genes influences DNA replication in human fibroblasts. Gene 635, 33–38 (2017).

Fotiadis, D., Kanai, Y. & Palacín, M. The SLC3 and SLC7 families of amino acid transporters. Mol. Aspects Med. 34, 139–158 (2013).

Fuchs, B. C. & Bode, B. P. Amino acid transporters ASCT2 and LAT1 in cancer: Partners in crime? Semin. Cancer Biol. 15, 254–266 (2005).

Galluzzi, L., Brenner, C., Morselli, E., Touat, Z. & Kroemer, G. Viral control of mitochondrial apoptosis. PLoS Pathog. 4, (2008).

Ganapathy, V., Thangaraju, M. & Prasad, P. D. Nutrient transporters in cancer: Relevance to Warburg hypothesis and beyond. Pharmacol. Ther. 121, 29–40 (2009).

Gao, P. et al. c-Myc suppression of miR-23a/b enhances mitochondrial glutaminase expression and glutamine metabolism. Nature 458, 762–765 (2009).

García, M. A., Meurs, E. F. & Esteban, M. The dsRNA protein kinase PKR: Virus and cell control. Biochimie 89, 799–811 (2007).

Gasol, E., Jiménez-Vidal, M., Chillarón, J., Zorzano, A. & Palacín, M. Membrane topology of system xc- light subunit reveals a re-entrant loop with substrate-restricted accessibility. J. Biol. Chem. 279, 31228–36 (2004).

Geillinger, K. E. et al. Nrf2 regulates the expression of the peptide transporter PEPT1 in the human colon carcinoma cell line Caco-2. Biochim. Biophys. Acta. 1840, 1747–1754 (2014).

Gerlinger, M. et al. Genome-wide RNA interference analysis of renal carcinoma survival regulators identifies MCT4 as a Warburg effect metabolic target. J. Pathol. 227, 146–56 (2012).

Giannattasio, M. & Branzei, D. S-phase checkpoint regulations that preserve replication and chromosome integrity upon dNTP depletion. Cell. Mol. Life Sci. 74, 2361–2380 (2017).

Giglia-Mari, G., Zotter, A. & Vermeulen, W. DNA damage response. Cold Spring Harb. Perspect. Biol. 3, a000745 (2011).

Gingras, A. C. et al. Regulation of 4E-BP1 phosphorylation: A novel two step mechanism. Genes Dev. 13, 1422–1437 (1999).

Goberdhan, D. C. I., Wilson, C. & Harris, A. L. Amino Acid Sensing by mTORC1: Intracellular Transporters Mark the Spot. Cell Metab. 23, 580–589 (2016).

Gout, P. W., Buckley, A. R., Simms, C. R. & Bruchovsky, N. Sulfasalazine, a potent suppressor of lymphoma growth by inhibition of the x(c)- cystine transporter: a new action for an old drug. Leukemia 15, 1633–40 (2001).

Granja, S., Marchiq, I., Baltazar, F. & Pouysségur, J. Gene Disruption Using Zinc Finger Nuclease Technology. PLoS One 6, e21045 (2011).

Guarino, E., Salguero, I. & Kearsey, S. E. Cellular regulation of ribonucleotide reductase in eukaryotes. Semin. Cell Dev. Biol. 30, 97–103 (2014).

Guo, F. & Cavener, D. R. The GCN2 eIF2α Kinase Regulates Fatty-Acid Homeostasis in the Liver during Deprivation of an Essential Amino Acid. Cell Metab. 5, 103–114 (2007).

Häfliger, P. et al. The LAT1 inhibitor JPH203 reduces growth of thyroid carcinoma in a fully immunocompetent mouse model. J. Exp. Clin. Cancer Res. 37, 1–15 (2018).

Halazonetis, T. D., Gorgoulis, V. G. & Bartek, J. An Oncogene-Induced DNA Damage Model for Cancer Development. Science 319, 1352–1355 (2008).

Hanczko, R. et al. Prevention of hepatocarcinogenesis and increased susceptibility to acetaminophen-induced liver failure in transaldolase-deficient mice by N-acetylcysteine. J. Clin. Invest. 119, 1546–57 (2009).

Hansen, C. G., Ng, Y. L. D., Lam, W.-L. M., Plouffe, S. W. & Guan, K.-L. The Hippo pathway effectors YAP and TAZ promote cell growth by modulating amino acid signaling to mTORC1. Cell Res. 25, 1299–313 (2015).

Hao, L.-S. et al. [Expression of glucose transporter 1 in human breast carcinoma and its clinical significance]. Sichuan Da Xue Xue Bao. Yi Xue Ban 40, 44–7 (2009).

Hara, K. et al. Amino acid sufficiency and mTOR regulate p70 S6 kinase and eIF-4E BP1 through a common effector mechanism. J Biol Chem 273, 14484–14494 (1998).

Hardie, D. G. AMP-activated/SNF1 protein kinases: Conserved guardians of cellular energy. Nat. Rev. Mol. Cell Biol. 8, 774–785 (2007).

Harding, H. P. et al. An Integrated Stress Response Regulates Amino Acid Metabolism and Resistance to Oxidative Stress National Institute of Environmental Health Sciences. Mol. Cell 11, 619–633 (2003).

Harding, H. P. et al. Ppp1r15 gene knockout reveals an essential role for translation initiation factor 2 alpha (eIF2α) dephosphorylation in mammalian development. Proc. Natl. Acad. Sci. 106, 1832–1837 (2009).

Harding, H. P. et al. Regulated Translation Initiation Controls Stress-Induced Gene Expression in Mammalian Cells. Mol. Cell 6, 1099–1108 (2000).

Hay, N. Reprogramming glucose metabolism in cancer: Can it be exploited for cancer therapy? Nat. Rev. Cancer 16, 635–649 (2016).

Hayashi, K. & Anzai, N. Novel therapeutic approaches targeting L-type amino acid transporters for cancer treatment. World J. Gastrointest. Oncol. 9, 21–29 (2017).

Hediger, M. A., Clémençon, B., Burrier, R. E. & Bruford, E. A. The ABCs of membrane transporters in health and disease (SLC series): introduction. Mol. Aspects Med. 34, 95–107 (2013).

Hemler, M. E. & Strominger, J. L. Characterization of antigen recognized by the monoclonal antibody (4F2): different molecular forms on human T and B lymphoblastoid cell lines. J. Immunol. 129, 623–8 (1982).

Hendzel, M. J. et al. Mitosis-specific phosphorylation of histone H3 initiates primarily within pericentromeric heterochromatin during G2 and spreads in an ordered fashion coincident with mitotic chromosome condensation. Chromosoma 106, 348–360 (1997).

Hernández-Alvarez, M. I. et al. Early-onset and classical forms of type 2 diabetes show impaired expression of genes involved in muscle branched-chain amino acids metabolism. Sci. Rep. 7, 13850 (2017).

Herzig, S. & Shaw, R. J. AMPK: guardian of metabolism and mitochondrial homeostasis. Nat. Rev. Mol. Cell Biol. 19, 121–135 (2018).

Hsu, J. W. et al. Dietary Supplementation with Aromatic Amino Acids Increases Protein Synthesis in Children with Severe Acute Malnutrition1–4. J. Nutr. 144, 660–666 (2014).

Huang, P. et al. RNA interference targeting CD147 inhibits the proliferation, invasiveness, and metastatic activity of thyroid carcinoma cells by down-regulating glycolysis. Int. J. Clin. Exp. Pathol. 8, 309–18 (2015).

Hwang, B.-J., Adhikary, G., Eckert, R. L. & Lu, A.-L. Chk1 inhibition as a novel therapeutic strategy in melanoma. Oncotarget 9, 30450–30464 (2018).

Im, C. S. K. et al. BCH, an inhibitor of system L amino acid transporters, induces apoptosis in cancer cells. Biol. Pharm. Bull. 31, 1096–100 (2008).

Inoki, K., Zhu, T. & Guan, K.-L. TSC2 Mediates Cellular Energy Response to Control Cell Growth and Survival phosphorylation decreases the ability of TSC2 to inhibit the phosphorylation of ribosomal S6 kinase (S6K) and eukaryotic initiation factor 4E binding protein-1 (4EBP1). Cell 115, 577–590 (2003).

Irizarry, R. A. et al. Exploration, Normalization, and Summaries of High Density Oligonucleotide Array Probe Level Data. Biostatistics 4, 249–264 (2003).

Irizarry, R. A. et al. Summaries of Affymetrix GeneChip probe level data. Nucleic Acids Res. 31, e15 (2003).

Jagannathan, L., Cuddapah, S. & Costa, M. Oxidative Stress Under Ambient and Physiological Oxygen Tension in Tissue Culture. Curr. Pharmacol. Reports 2, 64–72 (2016).

Jensen, P. K. Antimycin-insensitive oxidation of succinate and reduced nicotinamide-adenine dinucleotide in electron-transport particles. II. Steroid effects. Biochim. Biophys. Acta 122, 167–74 (1966).

Jiang, P., Du, W. & Wu, M. Regulation of the pentose phosphate pathway in cancer. Protein Cell 5, 1–11 (2014).

Joshi, M., Kulkarni, A. & Pal, J. K. Small molecule modulators of eukaryotic initiation factor 2α kinases, the key regulators of protein synthesis. Biochimie 95, 1980–1990 (2013).

Kaleeba, J. A. R. & Berger, E. A. Kaposi's sarcoma-associated herpesvirus fusion-entry receptor: cystine transporter xCT. Science 311, 1921–4 (2006).

Kaneko, Y. et al. Cell cycle-dependent and ATM-independent expression of human Chk1 kinase. Oncogene 18, 3673–3681 (1999).

Kasuga, M. et al. Role of S6K1 in regulation of SREBP1c expression in the liver. Biochem. Biophys. Res. Commun. 412, 197–202 (2011).

Kim, C. S. et al. BCH, an inhibitor of system L amino acid transporters, induces apoptosis in cancer cells. Biol. Pharm. Bull. 31, 1096–100 (2008).

Kim, J. H. et al. Phospholipase D1 Mediates AMP-Activated Protein Kinase Signaling for Glucose Uptake. PLoS One 5, (2010).

Kimball, S. R. & Jefferson, L. S. Role of amino acids in the translational control of protein synthesis in mammals. Semin. Cell Dev. Biol. 16, 21–27 (2005).

Kinhosita, H. et al. Cystine/glutamic acid transporter is a novel marker for predicting poor survival in patients with hepatocellular carcinoma. Oncol. Rep. 29, 685–689 (2013).

Kirk, P. et al. CD147 is tightly associated with lactate transporters MCT1 and MCT4 and facilitates their cell surface expression. EMBO J. 19, 3896–904 (2000).

Köhler, P. The strategies of energy conservation in helminths. Mol. Biochem. Parasitol. 17, 1–18 (1985).

Koppula, P., Zhang, Y., Shi, J., Li, W. & Gan, B. The glutamate/cystine antiporter SLC7A11/xCT enhances cancer cell dependency on glucose by exporting glutamate. J. Biol. Chem. 292, 14240–14249 (2017).

Krämer, A. et al. Centrosome-associated Chk1 prevents premature activation of cyclin-B–Cdk1 kinase. Nat. Cell Biol. 6, 884–891 (2004).

Kramer, G., Cimadevilla, J. M. & Hardesty, B. Specificity of the protein kinase activity associated with the hemin-controlled repressor of rabbit reticulocyte. Proc Natl Acad Sci U. S. A. 73, 3078–3082 (1976).

Krishnamoorthy, T., Pavitt, G. D., Zhang, F., Dever, T. E. & Hinnebusch, A. G. Tight Binding of the Phosphorylated Subunit of Initiation Factor 2 (eIF2) to the Regulatory Subunits of Guanine Nucleotide Exchange Factor eIF2B Is Required for Inhibition of Translation Initiation. Mol. Cell. Biol. 21, 5018–5030 (2002).

Kumar, R., Krause, G. S., Yoshida, H., Mori, K. & DeGracia, D. J. Dysfunction of the unfolded protein response during global brain ischemia and reperfusion. J. Cereb. Blood Flow Metab. 23, 462–471 (2003).

Lane, A. N. & Fan, T. W.-M. Regulation of mammalian nucleotide metabolism and biosynthesis. Nucleic Acids Res. 43, 2466–85 (2015).

Le Floch, R. et al. CD147 subunit of lactate/H+ symporters MCT1 and hypoxia-inducible MCT4 is critical for energetics and growth of glycolytic tumors. Proc. Natl. Acad. Sci. U. S. A. 108, 16663–8 (2011).

Le, A. et al. Inhibition of lactate dehydrogenase A induces oxidative stress and inhibits tumor progression. Proc. Natl. Acad. Sci. 107, 2037–2042 (2010).

Leontieva, O. V., Demidenko, Z. N. & Blagosklonny, M. V. Contact inhibition and high cell density deactivate the mammalian target of rapamycin pathway, thus suppressing the senescence program. Proc. Natl. Acad. Sci. U. S. A. 111, 8832 (2014).

Lerin, C. et al. Defects in muscle branched-chain amino acid oxidation contribute to impaired lipid metabolism. Mol. Metab. 5, 926–936 (2016).

Levin, D. H., Ranu, R., Ernst, V. & London, I. M. Regulation of protein synthesis in reticulocyte lysates: Phosphorylation of methionyl-tRNAf binding factor by protein kinase activity of translational inhibitor isolated from heme- deficient lysates. Pnas 73, 3112–3116 (1976).

Lezza, A. M. S. Mitochondrial transcription factor A (TFAM): One actor for different roles. Front. Biol. (Beijing). 7, 30–39 (2012).

Li, M. Y. et al. Radiotherapy induces cell cycle arrest and cell apoptosis in nasopharyngeal carcinoma via the ATM and Smad pathways. Cancer Biol. Ther. 18, 681–693 (2017).

Li, T. et al. Defective Branched-Chain Amino Acid Catabolism Disrupts Glucose Metabolism and Sensitizes the Heart to Ischemia-Reperfusion Injury. Cell Metab. 25, 374–385 (2017).

Li, X., Gu, J. & Zhou, Q. Review of aerobic glycolysis and its key enzymes – new targets for lung cancer therapy. Thorac. Cancer 6, 17 (2015).

Lieberman, M., Marks, A. D. & Peet, A. Marks' basic medical biochemistry : a clinical approach. (Lippincott Williams & Wilkins, 2013).

Lim, S. & Kaldis, P. Cdks, cyclins and CKIs: roles beyond cell cycle regulation. Development 140, 3079–3093 (2013).

Liu, C. et al. SLC3A2 is a novel endoplasmic reticulum stress-related signaling protein that regulates the unfolded protein response and apoptosis. 1–14 (2018).

Long, Y. C. & Zierath, J. R. AMP-activated protein kinase signaling in metabolic regulation. In Vivo 116, (2006).

Lopez-Contreras, A. J. et al. Increased Rrm2 gene dosage reduces fragile site breakage and prolongs survival of ATR mutant mice. Genes Dev. 29, 690–5 (2015).

López-Contreras, A. J., Gutierrez-Martinez, P., Specks, J., Rodrigo-Perez, S. & Fernandez-Capetillo, O. An extra allele of Chk1 limits oncogene-induced replicative stress and promotes transformation. J. Exp. Med. 209, 455–61 (2012).

Lu, L., Han, A. P. & Chen, J. J. Translation initiation control by heme-regulated eukaryotic initiation factor 2alpha kinase in erythroid cells under cytoplasmic stresses. Mol. Cell. Biol. 21, 7971–80 (2001).

Lu, P. D., Harding, H. P. & Ron, D. Translation reinitiation at alternative open reading frames regulates gene expression in an integrated stress response. J. Cell Biol. 167, 27–33 (2004).

Lu, S. C. Regulation of glutathione synthesis. Mol. Aspects Med. 30, 42–59 (2009).

Ma, H. T. & Poon, R. Y. C. Synchronization of HeLa Cells. Methods Mol Biol. 761, 151-161 (2011).

Ma, Q. Role of Nrf2 in Oxidative Stress and Toxicity. Annu. Rev. Pharmacol. Toxicol. 53, 401–426 (2013).

Ma, Y. & Hendershot, L. M. Delineation of a Negative Feedback Regulatory Loop That Controls Protein Translation during Endoplasmic Reticulum Stress. J. Biol. Chem. 278, 34864–34873 (2003).

Magnuson, B., Ekim, B. & Fingar, D. C. Regulation and function of ribosomal protein S6 kinase (S6K) within mTOR signalling networks. Biochem. J. 441, 1–21 (2011).

Mak, J. P. Y., Man, W. Y., Chow, J. P. H., Ma, H. T. & Poon, R. Y. C. Pharmacological inactivation of CHK1 and WEE1 induces mitotic catastrophe in nasopharyngeal carcinoma cells. Oncotarget 6, 21074–84 (2015).

Manic, G., Obrist, F., Sistigu, A. & Vitale, I. Trial Watch: Targeting ATM–CHK2 and ATR–CHK1 pathways for anticancer therapy. Mol. Cell. Oncol. 2, 1–17 (2015).

Mannava, S. et al. Direct role of nucleotide metabolism in C-MYC-dependent proliferation of melanoma cells. Cell Cycle 7, 2392–400 (2008).

Marchiq, I., Le Floch, R., Roux, D., Simon, M.-P. & Pouyssegur, J. Genetic Disruption of Lactate/H+ Symporters (MCTs) and Their Subunit CD147/BASIGIN Sensitizes Glycolytic Tumor Cells to Phenformin. Cancer Res. 75, 171–180 (2015).

Marciano, R., Leprivier, G. & Rotblat, B. Puromycin labeling does not allow protein synthesis to be measured in energy-starved cells. Cell Death Dis. 9, 39 (2018).

Marechal, A. & Zou, L. DNA Damage Sensing by the ATM and ATR Kinases. Cold Spring Harb. Perspect. Biol. 5, a012716–a012716 (2013).

Maréchal, A. & Zou, L. DNA Damage Sensing by the ATM and ATR kinases. Cold Spring Harb. Perspect. Biol. 5, 1–18 (2013).

Maser, R. S., Monsen, K. J., Nelms, B. E. & Petrini, J. H. hMre11 and hRad50 nuclear foci are induced during the normal cellular response to DNA double-strand breaks. Mol. Cell. Biol. 17, 6087–96 (1997).

Mastroberardino, L. et al. Amino-acid transport by heterodimers of 4F2hc/CD98 and members of a permease family. Nature 395, 288–291 (1998).

Mayers, J. R. et al. Tissue of origin dictates branched-chain amino acid metabolism in mutant Kras-driven cancers. Science 353, 1161–1165 (2016).

Mazouzi, A., Velimezi, G. & Loizou, J. I. DNA replication stress: Causes, resolution and disease. Exp. Cell Res. 329, 85–93 (2014).

McCracken, A. N. & Edinger, A. L. Nutrient transporters: the Achilles' heel of anabolism. Trends Endocrinol. Metab. 24, 200–8 (2013).

McEwen, E. et al. Heme-regulated inhibitor kinase-mediated phosphorylation of eukaryotic translation initiation factor 2 inhibits translation, induces stress granule formation, and mediates survival upon arsenite exposure. J. Biol. Chem. 280, 16925–33 (2005).

Milkereit, R. et al. LAPTM4b recruits the LAT1-4F2hc Leu transporter to lysosomes and promotes mTORC1 activation. Nat. Commun. 6, 7250 (2015).

Mills, C. C., Kolb, E. A. & Sampson, V. B. Development of chemotherapy with cell-cycle inhibitors for adult and pediatric cancer therapy. Cancer Res. 78, 320–325 (2018).

Moberg, M. et al. Activation of mTORC1 by leucine is potentiated by branched-chain amino acids and even more so by essential amino acids following resistance exercise. Am. J. Physiol. - Cell Physiol. 310, C874–C884 (2016).

Moffatt, B. A. & Ashihara, H. Purine and pyrimidine nucleotide synthesis and metabolism. Arab. B. 1, e0018 (2002).

Motohashi, H. & Yamamoto, M. Nrf2-Keap1 defines a physiologically important stress response mechanism. Trends Mol. Med. 10, 549–57 (2004).

Mueckler, M. & Thorens, B. The SLC2 (GLUT) family of membrane transporters. Mol. Aspects Med. 34, 121–38 (2013).

Muñoz, J. P. & Zorzano, A. Mitochondrial medicine: Volume II, manipulating mitochondrial function. Methods Mol. Biol. 1265, E1 (2015).

Muramatsu, T. Basigin (CD147), a multifunctional transmembrane glycoprotein with various binding partners. J. Biochem. 159, 481–90 (2016).

Murphy, M. P. How mitochondria produce reactive oxygen species. Biochem. J. 417, 1 (2009).

Nagamori, S. et al. Novel cystine transporter in renal proximal tubule identified as a missing partner of cystinuria-related plasma membrane protein rBAT/SLC3A1. Proc. Natl. Acad. Sci. U. S. A. 113, 775–80 (2016).

Nam, E. A. & Cortez, D. ATR signalling: more than meeting at the fork. Biochem. J. 436, 527–36 (2011).

Nam, K., Oh, S. & Shin, I. Ablation of CD44 induces glycolysis-to-oxidative phosphorylation transition via modulation of the c-Src-Akt-LKB1-AMPK pathway. Biochem. J. 473, 3013–3030 (2016).

Namikawa, M. et al. Expression of amino acid transporters (LAT1, ASCT2 and xCT) as clinical significance in hepatocellular carcinoma. Hepatol. Res. 45, 1014–1022 (2015).

Napolitano, L. et al. Potent inhibitors of human LAT1 (SLC7A5) transporter based on dithiazole and dithiazine compounds for development of anticancer drugs. Biochem. Pharmacol. 143, 39–52 (2017).

Neishabouri, S. H., Hutson, S. M. & Davoodi, J. Chronic activation of mTOR complex 1 by branched chain amino acids and organ hypertrophy. Amino Acids 47, 1167–1182 (2015).

Neretti, N. et al. Global Regulation of Nucleotide Biosynthetic Genes by c-Myc. PLoS One 3, e2722 (2008).

Nicholson, B., Sawamura, T., Masaki, T. & MacLeod, C. L. Increased Cat3-mediated cationic amino acid transport functionally compensates in Cat1 knockout cell lines. J. Biol. Chem. 273, 14663–14666 (1998).

Nicklin, P. et al. Bidirectional transport of amino acids regulates mTOR and autophagy. Cell 136, 521–34 (2009).

Nordlund, P. & Reichard, P. Ribonucleotide Reductases. Annu. Rev. Biochem. 75, 681–706 (2006).

Novoa, I., Zeng, H., Harding, H. P. & Ron, D. Feedback inhibition of the unfolded protein response by GADD34-mediated dephosphorylation of eIF2alpha. J. Cell Biol. 153, 1011–22 (2001).

Obrig, T., Culp, W., Mckeehan, W. & Hardesty, B. The Mechanism by which Cycloheximide and Related Glutarimide Antibiotics Inhibit PeptideSynthesis on Reticulocyte Ribosomes. J. Biol. Chem. 246, 174-181 (1971).

Oda, K. et al. l-Type amino acid transporter 1 inhibitors inhibit tumor cell growth. Cancer Sci. 101, 173–179 (2009).

Ohno, H. et al. 4F2hc stabilizes GLUT1 protein and increases glucose transport activity. Am. J. Physiol. Physiol. 300, C1047–C1054 (2011).

Ohshima, Y. et al. Efficacy of system l amino acid transporter 1 inhibition as a therapeutic target in esophageal squamous cell carcinoma. Cancer Sci. 107, 1499–1505 (2016).

Ohtsuki, S., Yamaguchi, H., Kang, Y.-S., Hori, S. & Terasaki, T. Reduction of L-Type Amino Acid Transporter 1 mRNA Expression in Brain Capillaries in a Mouse Model of Parkinson's Disease. Biol. Pharm. Bull. 33, 1250–1252 (2010).

Okuno, S. et al. Role of cystine transport in intracellular glutathione level and cisplatin resistance in human ovarian cancer cell lines. Br. J. Cancer 88, 951–956 (2003).

Otani, K. et al. Cell-cycle-controlled radiation therapy was effective for treating a murine malignant melanoma cell line in vitro and in vivo. Sci. Rep. 6, 1–8 (2016).

Oyarzabal, A. et al. Mitochondrial response to the BCKDK-deficiency: Some clues to understand the positive dietary response in this form of autism. Biochim. Biophys. Acta - Mol. Basis Dis. 1862, 592–600 (2016).

Patil, M., Pabla, N. & Dong, Z. Checkpoint kinase 1 in DNA damage response and cell cycle regulation. Cell. Mol. Life Sci. 70, 4009–21 (2013).

Patra, K. C. & Hay, N. The pentose phosphate pathway and cancer. Trends Biochem. Sci. 39, 347–354 (2014).

Pavlova, N. N. & Thompson, C. B. The Emerging Hallmarks of Cancer Metabolism. Cell Metab. 23, 27–47 (2016).

Pérez-Escuredo, J. et al. Monocarboxylate transporters in the brain and in cancer. Biochim. Biophys. Acta - Mol. Cell Res. 1863, 2481–2497 (2016).

Persaud, A., Cormerais, Y., Pouyssegur, J. & Rotin, D. Dynamin inhibitors block activation of mTORC1 by amino acids independently of dynamin. J. Cell Sci. 131, jcs211755 (2018).

Pfeiffer, R. et al. Functional heterodimeric amino acid transporters lacking cysteine residues involved in disulfide bond. FEBS Lett. 439, 157–162 (1998).

Pilz, R. B., Willis, R. C. & Boss, G. R. The influence of ribose 5-phophate availability on purine synthesis of cultured human lymphoblasts and mitogen-stimulated lymphocytes. J. Biol. Chem. 259, 2927–2935 (1984).

Pinheiro, C. et al. Reprogramming energy metabolism and inducing angiogenesis: co-expression of monocarboxylate transporters with VEGF family members in cervical adenocarcinomas. BMC Cancer 15, 835 (2015).

Poli, J. et al. dNTP pools determine fork progression and origin usage under replication stress. EMBO J. 31, 883–894 (2012).

Qu, J. et al. Phosphoglycerate mutase 1 regulates dNTP pool and promotes homologous recombination repair in cancer cells. J. Cell Biol. 216, 409–424 (2017).

R Core Development Team. R: A language and environment for statistical computing. R Foundation for Statistical Computing. 2, (2008).

Reig, N. et al. The light subunit of system b(o,+) is fully functional in the absence of the heavy subunit. EMBO J. 21, 4906–14 (2002).

Reinhold, W. C., Sunshine, M., Varma, S., Doroshow, J. H. & Pommier, Y. Using CellMiner 1.6 for Systems Pharmacology and Genomic Analysis of the NCI-60. Clin. Cancer Res. 21, 3841–3852 (2015).

Roberts, L. D., Souza, A. L., Gerszten, R. E. & Clish, C. B. Targeted metabolomics. Curr. Protoc. Mol. Biol. Chapter 30, Unit 30.2.1-24 (2012).

Rosell, A. et al. Structural bases for the interaction and stabilization of the human amino acid transporter LAT2 with its ancillary protein 4F2hc. Proc. Natl. Acad. Sci. U. S. A. 111, 2966–71 (2014).

Rosilio, C. et al. L-type amino-acid transporter 1 (LAT1): a therapeutic target supporting growth and survival of T-cell lymphoblastic lymphoma/T-cell acute lymphoblastic leukemia. Leukemia 29, 1253–1266 (2015).

Rosner, M., Fuchs, C., Siegel, N., Valli, A. & Hengstschlager, M. Functional interaction of mammalian target of rapamycin complexes in regulating mammalian cell size and cell cycle. Hum. Mol. Genet. 18, 3298–3310 (2009).

Rudlowski, MD, C. et al. GLUT1 Messenger RNA and Protein Induction Relates to the Malignant Transformation of Cervical Cancer. Am. J. Clin. Pathol. 120, 691–698 (2003).

Ruiz, S. et al. Limiting replication stress during somatic cell reprogramming reduces genomic instability in induced pluripotent stem cells. Nat. Commun. 6, 8036 (2015).

Sakata, T. et al. L-type amino-acid transporter 1 as a novel biomarker for high-grade malignancy in prostate cancer. Pathol. Int. 59, 7–18 (2009).

Salaun, P., Rannou, Y. & Prigent, C. Cdk1, Plks, Auroras, and Neks: the mitotic bodyguards. Adv. Exp. Med. Biol. 617, 41–56 (2008).

Sancak, Y. et al. The Rag GTPases bind raptor and mediate amino acid signalingto mTORC1. Science (80-.). 320, 1496–1501 (2008).

San-Millán, I. & Brooks, G. A. Reexamining cancer metabolism: lactate production for carcinogenesis could be the purpose and explanation of the Warburg Effect. Carcinogenesis 38, 119–133 (2017).

Sasaki, H. et al. Electrophile response element-mediated induction of the cystine/glutamate exchange transporter gene expression. J. Biol. Chem. 277, 44765–71 (2002).

Sato, H. et al. Redox imbalance in cystine/glutamate transporter-deficient mice. J. Biol. Chem. 280, 37423–37429 (2005).

Sato, H. et al. Transcriptional control of cystine/glutamate transporter gene by amino acid deprivation. Biochem. Biophys. Res. Commun. 325, 109–116 (2004).

Sato, H., Tamba, M., Ishii, T. & Bannai, S. Cloning and expression of a plasma membrane cystine/glutamate exchange transporter composed of two distinct proteins. J. Biol. Chem. 274, 11455–8 (1999).

Scalise, M., Pochini, L., Galluccio, M., Console, L. & Indiveri, C. Glutamine Transport and Mitochondrial Metabolism in Cancer Cell Growth. Front. Oncol. 7, 306 (2017).

Schadewaldt, P. & Wendel, U. Metabolism of branched-chain amino acids in maple syrup urine disease. Eur. J. Pediatr. 156 Suppl 1, S62-6 (1997).

Schmidt, E. K., Clavarino, G., Ceppi, M. & Pierre, P. SUnSET, a nonradioactive method to monitor protein synthesis. Nat. Methods 6, 275–277 (2009).

Sehgal, P. et al. Inhibition of the sarco/endoplasmic reticulum (ER) Ca2-ATPase by thapsigargin analogs induces cell death via ER Ca2 depletion and the unfolded protein response. J. Biol. Chem. 292, 19656–19673 (2017).

Shin, G. et al. GENT: Gene Expression Database of Normal and Tumor Tissues. Cancer Inform. 10, CIN.S7226 (2011).

Shiotani, B. & Zou, L. ATR signaling at a glance. J. Cell Sci. 122, 301–4 (2009).

Sommer, A.-K. et al. A proteomic analysis of chemoresistance development via sequential treatment with doxorubicin reveals novel players in MCF 7 breast cancer cells. Int. J. Mol. Med. 42, 1987–1997 (2018).

Stambaugh, R. & Post, D. Substrate and product inhibition of rabbit muscle lactic dehydrogenase heart (H4) and muscle (M4) isozymes. J. Biol. Chem. 241, 1462–7 (1966).

Stančíková, M. & Rovenský, J. Metabolism of Aromatic Amino Acids. Adv Protein Chem. 10, 131-150 (1955).

Stincone, A. et al. The return of metabolism: biochemistry and physiology of the pentose phosphate pathway. Biol. Rev. Camb. Philos. Soc. 90, 927–63 (2015).

Subramanian, A. et al. Gene set enrichment analysis: A knowledge-based approach for interpreting genome-wide expression profiles. Proc. Natl. Acad. Sci. 102, 15545–15550 (2005).

Suragani, R. N. V. S. et al. Heme-regulated eIF2α kinase activated Atf4 signaling pathway in oxidative stress and erythropoiesis. Blood 119, 5276–84 (2012).

Takayanagi, S., Fukuda, R., Takeuchi, Y., Tsukada, S. & Yoshida, K. Gene regulatory network of unfolded protein response genes in endoplasmic reticulum stress. Cell Stress Chaperones 18, 11–23 (2013).

Taniuchi, S., Miyake, M., Tsugawa, K., Oyadomari, M. & Oyadomari, S. Integrated stress response of vertebrates is regulated by four eIF2α kinases. Sci. Rep. 6, 32886 (2016).

Tărlungeanu, D. C. et al. Impaired Amino Acid Transport at the Blood Brain Barrier Is a Cause of Autism Spectrum Disorder. Cell 167, 1481-1494.e18 (2016).

Tarver, H. & Schmidt, C. Radioactive sulfur studies? J. Biol. Chem. 146, (1942).

Tate, S. S., Yan, N. & Udenfriend, S. Expression cloning of a Na(+)-independent neutral amino acid transporter from rat kidney. Proc. Natl. Acad. Sci. U. S. A. 89, 1–5 (1992).

Thanasoula, M., Escandell, J. M., Suwaki, N. & Tarsounas, M. ATM/ATR checkpoint activation downregulates CDC25C to prevent mitotic entry with uncapped telomeres. EMBO J. 31, 3398–410 (2012).

Thoreen, C. C. & Sabatini, D. M. Rapamycin inhibits mTORC1, but not completely. Autophagy 8627, 725–726 (2009).

Thorens, B. & Mueckler, M. Glucose transporters in the 21st Century. Am. J. Physiol. Endocrinol. Metab. 298, E141-5 (2010).

Tidke, P. R., Maurya, D. K., Kulkarni, A. P., Devasagayam, T. P. A. & Pal, J. K. Radiation-induced oxidative stress regulates protein synthesis by modulating the expression of heme-regulated eIF2α kinase in human K562 cells. Indian J. Biochem. Biophys. 53, 95–103 (2016).

Timmerman, L. A. et al. Glutamine Sensitivity Analysis identifies the xCT Antiporter as a Common Triple Negative Breast Tumor Therapeutic Target. Cancer Cell 24, 450-465 (2013).

Titov, D. V et al. Complementation of mitochondrial electron transport chain by manipulation of the NAD+/NADH ratio. Science 352, 231–5 (2016).

Torrents, D. et al. Identification and characterization of a membrane protein (y+L amino acid transporter-1) that associates with 4F2hc to encode the amino acid transport activity y+L. A candidate gene for lysinuric protein intolerance. J. Biol. Chem. 273, 32437–45 (1998).

Torrents, D. et al. Identification of SLC7A7, encoding y+LAT-1, as the lysinuric protein intolerance gene. Nat. Genet. 21, 293–296 (1999).

Toyoda, M. et al. Prognostic significance of amino-acid transporter expression (LAT1, ASCT2 and xCT) in surgically resected tongue cancer. Br. J. Cancer 110, 2506–2513 (2014).

Toyoda, M. et al. Prognostic significance of amino-acid transporter expression (LAT1, ASCT2, and xCT) in surgically resected tongue cancer. Br. J. Cancer 110, 2506–2513 (2014).

Uchino, H. et al. Expression Cloning and Characterization of a Transporter for Large Neutral Amino Acids Activated by the Heavy Chain of 4F2 Antigen (CD98). J. Biol. Chem. 273, 23629–23632 (2002).

Van Engeland, M., Kuijpers, H. J. H., Ramaekers, F. C. S., Reutelingsperger, C. P. M. & Schutte, B. Plasma membrane alterations and cytoskeletal changes in apoptosis. Exp. Cell Res. 235, 421–430 (1997).

van Genderen, H. et al. In vitro measurement of cell death with the annexin A5 affinity assay. Nat. Protoc. 1, 363–367 (2006).

Van Hooser, a et al. Histone H3 phosphorylation is required for the initiation, but not maintenance, of mammalian chromosome condensation. J. Cell Sci. 111, 3497–3506 (1998).

Vander Heiden, M. G. et al. Metabolic pathway alterations that support cell proliferation. Cold Spring Harb. Symp. Quant. Biol. 76, 325–34 (2011).

Vassin, V. M., Anantha, R. W., Sokolova, E., Kanner, S. & Borowiec, J. A. Human RPA phosphorylation by ATR stimulates DNA synthesis and prevents ssDNA accumulation during DNA-replication stress. J. Cell Sci. 122, 4070–80 (2009).

Verlinden, L. et al. The E2F-Regulated Gene Chk1 Is Highly Expressed in Triple-Negative Estrogen Receptor–/Progesterone Receptor–/HER-2– Breast Carcinomas. Cancer Res. 67, 6574–6581 (2007).

Verrey, F. et al. Amino-acid transport by heterodimers of 4F2hc/CD98 and members of a permease family. Nature 395, 288–291 (1998).

Verrey, F. et al. CATs and HATs: the SLC7 family of amino acid transporters. Pflügers Arch. Eur. J. Physiol. 447, 532–542 (2004).

Vilches, C. et al. Cooperation of Antiporter LAT2/CD98hc with Uniporter TAT1 for Renal Reabsorption of Neutral Amino Acids. J. Am. Soc. Nephrol. 29, 1624–1635 (2018).

Vučetić, M., Cormerais, Y., Parks, S. K. & Pouysségur, J. The Central Role of Amino Acids in Cancer Redox Homeostasis: Vulnerability Points of the Cancer Redox Code. Front. Oncol. 7, 319 (2017).

Walters, D. K., Arendt, B. K. & Jelinek, D. F. CD147 regulates the expression of MCT1 and lactate export in multiple myeloma cells. Cell Cycle 12, 3175–83 (2013).

Wang, H. et al. Sestrin2 is a leucine sensor for the mTORC1 pathway. Science 2674, 1–9 (2015).

Wang, Q. et al. Androgen receptor and nutrient signaling pathways coordinate the demand for increased amino acid transport during prostate cancer progression. Cancer Res. 71, 7525–7536 (2011).

Wang, S. et al. The amino acid transporter SLC38A9 is a key component of a lysosomal membrane complex that signals arginine sufficiency to mTORC1. Science 347, 188–194 (2015).

Wang, X. et al. Chemotherapy-induced differential cell cycle arrest in B-cell lymphomas affects their sensitivity to Wee1 inhibition. Haematologica 103, 466–476 (2018).

Warburg, O. On the origin of cancer cells. Science 123, 309–14 (1956).

Wek, S. A., Zhu, S. & Wek, R. C. The histidyl-tRNA synthetase-related sequence in the eIF-2 alpha protein kinase GCN2 interacts with tRNA and is required for activation in response to starvation for different amino acids. Mol. Cell. Biol. 15, 4497–4506 (1995).

Wells, R. G. & Hediger, M. A. Cloning of a rat kidney cDNA that stimulates dibasic and neutral amino acid transport and has sequence similarity to glucosidases. Proc. Natl. Acad. Sci. U. S. A. 89, 5596–600 (1992).

Wells, R. G., Lee, W. S., Kanai, Y., Leiden, J. M. & Hediger, M. A. The 4F2 antigen heavy chain induces uptake of neutral and dibasic amino acids in Xenopus oocytes. J. Biol. Chem. 267, 15285–15288 (1992).

Wheaton, W. W. & Chandel, N. S. Hypoxia. 2. Hypoxia regulates cellular metabolism. Am. J. Physiol. - Cell Physiol. 300, C385 (2011).

Woehlbier, U. & Hetz, C. Modulating stress responses by the UPRosome: A matter of life and death. Trends Biochem. Sci. 36, 329–337 (2011).

Wouters, B. G. & Koritzinsky, M. Hypoxia signalling through mTOR and the unfolded protein response in cancer. Nat. Rev. Cancer 8, 851–64 (2008).

Wu, D. et al. limma powers differential expression analyses for RNA-sequencing and microarray studies. Nucleic Acids Res. 43, e47–e47 (2015).

Wu, Q., Beland, F. A., Chang, C.-W. & Fang, J.-L. Role of DNA Repair Pathways in Response to Zidovudine-induced DNA Damage in Immortalized Human Liver THLE2 Cells. Int. J. Biomed. Sci. 9, 18–25 (2013).

Würtz, P. et al. Branched-chain and aromatic amino acids are predictors of insulin resistance in young adults. Diabetes Care 36, 648–55 (2013).

Xin, X. et al. CD147/EMMPRIN overexpression and prognosis in cancer: A systematic review and meta-analysis. Sci. Rep. 6, 32804 (2016).

Xu, D. & Hemler, M. E. Metabolic activation-related CD147-CD98 complex. Mol. Cell. Proteomics 4, 1061–71 (2005).

Yan, R., Zhao, X., Lei, J. & Zhou, Q. Structure of the human LAT1–4F2hc heteromeric amino acid transporter complex. Nat. 568, 127-130 (2019).

Yanagisawa, N. et al. High expression of L-type amino acid transporter 1 as a prognostic marker in bile duct adenocarcinomas. Cancer Med. 3, 1246–55 (2014).

Yang, L., Venneti, S. & Nagrath, D. Glutaminolysis: A Hallmark of Cancer Metabolism. Annu. Rev. Biomed. Eng. 19, 163–194 (2017).

Yang, W. S. et al. Regulation of ferroptotic cancer cell death by GPX4. Cell 156, 317–331 (2014).

Yang, X. et al. LncRNA PDIA3P interacts with c-Myc to regulate cell proliferation via induction of pentose phosphate pathway in multiple myeloma. Biochem. Biophys. Res. Commun. 498, 207–213 (2018).

Yielding, K. L. & Tomkins, G. M. An effect of L-leucine and other essential amino acids on the structure and activity of glutamic dehydrogenase. Proc. Natl. Acad. Sci. U. S. A. 47, 983–9 (1961).

Yoshino, J., Baur, J. A. & Imai, S. NAD+ Intermediates: The Biology and Therapeutic Potential of NMN and NR. Cell Metab. 27, 513–528 (2018).

Yoshioka, K. et al. A novel fluorescent derivative of glucose applicable to the assessment of glucose uptake activity of Escherichia coli. Biochim. Biophys. Acta. 1289, 5–9 (1996).

Yothaisong, S. et al. Inhibition of l -type amino acid transporter 1 activity as a new therapeutic target for cholangiocarcinoma treatment. Tumor Biol. 39, 1-14 (2017).

Young, J. D., Yao, S. Y. M., Baldwin, J. M., Cass, C. E. & Baldwin, S. A. The human concentrative and equilibrative nucleoside transporter families, SLC28 and SLC29. Mol. Aspects Med. 34, 529–547 (2013).

Yu, H.-P. et al. TIGAR regulates DNA damage and repair through pentosephosphate pathway and Cdk5-ATM pathway. Sci. Rep. 5, 9853 (2015).

Zannini, L., Delia, D. & Buscemi, G. CHK2 kinase in the DNA damage response and beyond. J. Mol. Cell Biol. 6, 442–457 (2014).

Ždralević, M. et al. Disrupting the 'Warburg effect' re-routes cancer cells to OXPHOS offering a vulnerability point via 'ferroptosis'-induced cell death. Adv. Biol. Regul. 68, 55–63 (2018).

Ždralević, M. et al. Disrupting the 'Warburg effect' re-routes cancer cells to OXPHOS offering a vulnerability point via 'ferroptosis'-induced cell death. Adv. Biol. Regul. 68, 55–63 (2018).

Ždralević, M. et al. Double genetic disruption of lactate dehydrogenases A and B is required to ablate the "Warburg effect" restricting tumor growth to oxidative metabolism. J. Biol. Chem. 293, 15947–15961 (2018).

Ždralević, M., Marchiq, I., Padua, M. M. C. de, Parks, S. K. & Pouysségur, J. Metabolic Plasiticy in Cancers—Distinct Role of Glycolytic Enzymes GPI, LDHs or Membrane Transporters MCTs. Front. Oncol. 7, 313 (2017).

Zeman, M. K. & Cimprich, K. A. Causes and consequences of replication stress. Nat. Cell Biol. 16, 2–9 (2014).

Zhang, B., Xie, Z. & Li, B. The clinicopathologic impacts and prognostic significance of GLUT1 expression in patients with lung cancer: A meta-analysis. Gene 689, 76–83 (2019).

Zhang, H. S. & Wang, S. Q. Nrf2 is involved in the effect of tanshinone IIA on intracellular redox status in human aortic smooth muscle cells. Biochem. Pharmacol. 73, 1358–1366 (2007).

Zhang, P. et al. The GCN2 eIF2alpha kinase is required for adaptation to amino acid deprivation in mice. Mol. Cell. Biol. 22, 6681–8 (2002).

Zhang, S., Zeng, X., Ren, M., Mao, X. & Qiao, S. Novel metabolic and physiological functions of branched chain amino acids: A review. J. Anim. Sci. Biotechnol. 8, 4–15 (2017).

Zhang, Y. & Hunter, T. Roles of Chk1 in cell biology and cancer therapy. Int. J. cancer 134, 1013–23 (2014).

Zhang, Y.-W. et al. Genotoxic Stress Targets Human Chk1 for Degradation by the Ubiquitin-Proteasome Pathway. Mol. Cell 19, 607–618 (2005).

Zhou, B. S. & Elledge, S. J. Checkpoints in Perspective. Nature 408, 433–439 (2000).

Zoncu, R. et al. mTORC1 senses lysosomal amino acids through an inside-out mechanism that requires the vacuolar H(+)-ATPase. Science 334, 678–683 (2011).

Zou, L. & Elledge, S. J. Sensing DNA damage through ATRIP recognition of RPA-ssDNA complexes. Science 300, 1542–8 (2003).

Appendix I

I.I A human cellular model to study the roles of CD98hc

With the aim of studying the role of CD98hc in a human cellular model, a CD98hc KO was generated using CRISPR/Cas9 tecnhology in HEK 293T cells as described in **Materials and Methods, 7.1.2.**

While these cells were being characterized, we established a collaboration with the group of Functional Proteomics and Metabolic Pathways, leading by Ruth Birner-Grünberger, in The Medical University of Graz (Austria). In that group, Robert Fuchs and collaborators were focused in the study of the mechanisms underlying the pro-apoptotic action of the quinazoline-derived α1-adrenoceptor antagonists (mainly Prazosin) on cancer cells. In a proteomics approach aimed at identifying potential membrane proteins with binding affinity to quinazolines, they detected the CD98hc, LAT1 and CD147 as possible protein-candidates interacting with Prazosin. In this regard, clones 19 and 20 of CD98hc KO HEK293T cells were used by Ruth Birner-Grünberger's group as a cellular model to address that research question.

The results obtained in that study are published in an article entitled: **Prazosin induced lysosomal tubulation interferes with cytokinesis and the endocytic sorting of the tumour antigen CD98hc** (attached bellow).

Furthermore, during their investigation, they provided us with additional data that was useful to further characterize these cells while corroborating some of our results in a human cellular model. For instance, we confirmed that CD98hc is required for proper cell proliferation in HEK293T cells (**Figure 106A**). Moreover, the lack of CD98hc leads to increased cell death by apoptosis in this model, supporting our results (**Figure 106B**). In addition, Fuchs and co-workers assesed wheter the presence of CD98hc affected the endoreduplication (DNA replication bypassing mitosis, which leads to polyploidy) mediated by Prazosin. Altough cell cycle phase distributions were not analysed in detail, we used data from the endoreduplicatipon analysis to evauluate wheter the progression of the cell cycle was affected in the CD98hc KO HEK 293T cells. As shown in **Figure 106C**, CD98hc KO clones 19 and 20 present increased S- and G2-phases, likely due to alterations during the DNA synthesis, like CD98hc KO mouse fibroblasts.

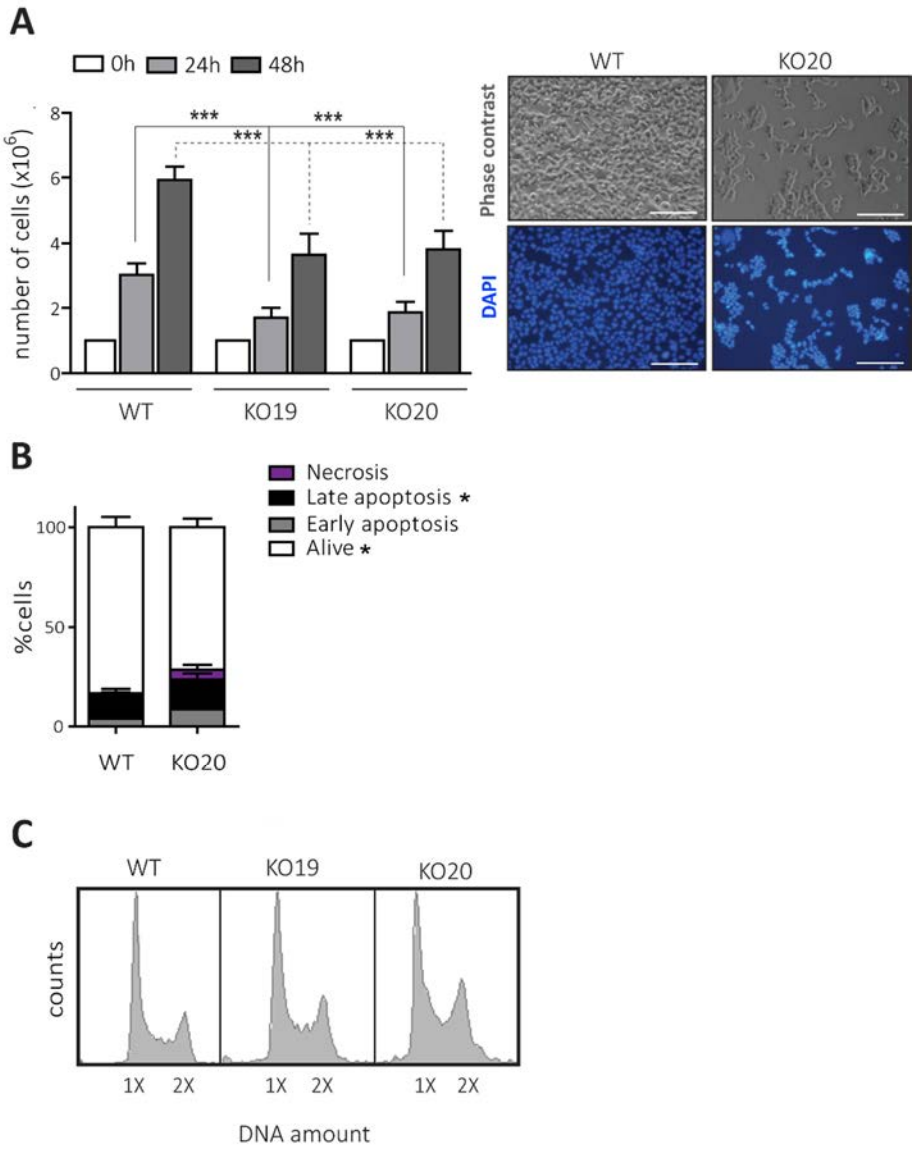

Figure 106. Characterization of CD98hc KO HEK 293T cells. A, CD98hc KO clones 19 and 20 present a proliferation delay compared to WT cells. Cells were counted at 24 and 48 h. n=3 (left panel). WT and CD98hc KO (clone 20) cells were analysed by microscopy. Scale bar is 100 microns. A representative image is shown (right panel). **B**, the loss of CD98hc induces apoptosis in HEK 293T cells. Apoptosis and necrosis were analysed by using an annexin V binding and SYTOX Green stains, respectively. n=3. **C**, CD98hc depletion leads to altered cell cyle progression. DNA content was evaluated by using propidium iodidide staining. A representative image is shown. Quantification data correspond to the mean ± SEM of the independent experiments (n) indicated in each graph. Statistical significance * $p \leq 0.05$; ***, $p \leq 0.001$ vs. WT HEK 293T cells was analysed using a Student's t-test. *These data were obtained from experiments performed by Robert Fuchs.*

In addition, the intracellular AA content was evaluated in these cells, and surprisingly, we found no differences between WT and CD98hc KO cells in this model, suggesting that cells lacking CD98hc adapted by upregulating any other tranporter non-associated to CD98hc (**Figure 107**). AA uptake assays should be performed in order to elucidate wheter the transport mediated by CD98hc-associated transporters is reduced and which other transporters have been induced if any.

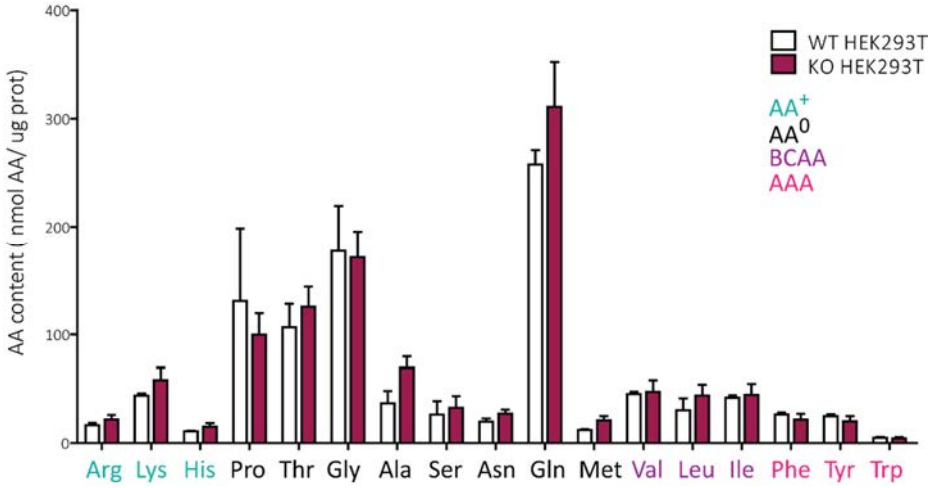

Figure 107. The intracellular AA content is not affected in CD98hc KO HEK 293T cells. Samples from WT and CD98hc KO HEK 293T cells were processed as described in *Materials and Methods* and quantitative analysis of AAs (nmol AA/µg protein) was performed. AAs are grouped by side chain properties as indicated. Quantification data correspond to the mean ± SEM of three independent experiments.

However, even presenting a balanced intracellular AA concentration, cells lacking CD98hc show defective cell proliferation, viability and cell cycle progression (**Figure 106**), pointing to the relevance of AA flux rather than AA concentration in those cellular functions.

Additional research is needed in order to further characterise this cellular model and corroborate the universality of the results reported in this thesis.

I.II Prazosin induced lysosomal tubulation interferes with cytokinesis and theendocytic sorting of the tumour antigen CD98hc

Robert Fuchs, Anika Stracke, Viktoria Holzmann, Gerfried Luschin-Ebengreuth, Nathalie Meier-Allard, Nadine Ebner, Teresa Maria Lassacher, Markus Absenger-Novak, Eleonore Fröhlich, Matthias Schittmayer, Sara Cano Crespo, Manuel Palacin, Beate Rinner,Ruth Birner-Gruenberger

BBA - Molecular Cell Research 1865 (2018) 1211–1229

Contents lists available at ScienceDirect

BBA - Molecular Cell Research

journal homepage: www.elsevier.com/locate/bbamcr

Prazosin induced lysosomal tubulation interferes with cytokinesis and the endocytic sorting of the tumour antigen CD98hc

Robert Fuchs[a,*], Anika Stracke[a], Viktoria Holzmann[a,b], Gerfried Luschin-Ebengreuth[a], Nathalie Meier-Allard[a], Nadine Ebner[a], Teresa Maria Lassacher[a], Markus Absenger-Novak[c], Eleonore Fröhlich[c], Matthias Schittmayer[d,e], Sara Cano Crespo[f], Manuel Palacin[f], Beate Rinner[g], Ruth Birner-Gruenberger[d,e]

[a] Chair of Immunology and Pathophysiology, Otto Loewi Research Center, Medical University of Graz, Heinrichstraße 31, 8010 Graz, Austria
[b] FH JOANNEUM – University of Applied Sciences, Alte Poststraße 149, 8020 Graz, Austria
[c] Centre for Medical Research, Medical University of Graz, Stiftingtalstrasse 24, 8010 Graz, Austria
[d] Research Unit Functional Proteomics and Metabolic Pathways, Institute of Pathology, Medical University of Graz, Auenbruggerplatz 25, 8036 Graz, Austria
[e] Omics Center Graz, BioTechMed-Graz, Stiftingtalstrasse 24, 8010 Graz, Austria
[f] Institute for Research in Biomedicine (IRB-Barcelona), Barcelona Institute of Science and Technology (BIST), Department of Biochemistry and Molecular Biomedicine, University of Barcelona, and CIBERER, Parc Científic de Barcelona. Baldiri I Reixac 10-12, 08028 Barcelona, Spain
[g] Biomedical Research, Medical University of Graz, Roseggerweg 48, 8036 Graz, Austria

ARTICLE INFO

Keywords:
Cancer
CD98hc/4F2/SLC3A2
Prazosin
Lysosomes
Lysomototropic agents
Apoptosis

ABSTRACT

The quinazoline based drug prazosin (PRZ) is a potent inducer of apoptosis in human cancer cells. We recently reported that PRZ enters cells via endocytosis and induces tubulation of the endolysosomal system. In a proteomics approach aimed at identifying potential membrane proteins with binding affinity to quinazolines, we detected the oncoprotein CD98hc. We confirmed shuttling of CD98hc towards lysosomes and upregulation of CD98hc expression in PRZ treated cells. Gene knockout (KO) experiments revealed that endocytosis of PRZ still occurs in the absence of CD98hc - suggesting that PRZ does not enter the cell via CD98hc but misroutes the protein towards tubular lysosomes. Lysosomal tubulation interfered with completion of cytokinesis and provoked endoreplication. CD98hc KO cells showed reduced endoreplication capacity and lower sensitivity towards PRZ induced apoptosis than wild type cells. Thus, loss of CD98hc does not affect endocytosis of PRZ and lysosomal tubulation, but the ability for endoreplication and survival of cells. Furthermore, we found that glutamine, lysomototropic agents – namely chloroquine and NH_4Cl – as well as inhibition of v-ATPase, interfere with the intracellular transport of CD98hc. In summary, our study further emphasizes lysosomes as target organelles to inhibit proliferation and to induce cell death in cancer. Most importantly, we demonstrate for the first time that the intracellular trafficking of CD98hc can be modulated by small molecules. Since CD98hc is considered as a potential drug target in several types of human malignancies, our study possesses translational significance suggesting, that old drugs are able to act on a novel target.

1. Introduction

Quinazoline based α1-adrenergic antagonists like prazosin (PRZ), doxazosin and terazosin were introduced into medicine for treatment of hypertension and benign prostate hyperplasia. Surprisingly, several studies have shown that quinazolines induce apoptosis in various types of malignant cells. Kyprianou et al. were the first to demonstrate that quinazoline based α1-adrenergic antagonists are able to induce apoptosis in prostate cancer cells [1]. Most interestingly, it turned out that the pro-apoptotic action of quinazolines is completely independent of α1-adrenergic receptors [1–7]. This fact is supported by the drug doses required to induce apoptosis in cancer cells. Only nM concentrations of quinazolines are needed to block adrenergic receptors, whereas μM concentrations are required to stop proliferation and to induce apoptosis in cancer cells. To date, cancer research on quinazolines in the human system thus has been limited to in vitro studies, because various severe side effects, primarily concerning the regulation of blood pressure, are suspected in vivo. Several animal studies using xenograft models have, however, proven that quinazolines are also able to inhibit human tumour growth in vivo [7–10]. Since the first demonstration of

* Corresponding author.
E-mail address: robert.fuchs@medunigraz.at (R. Fuchs).

https://doi.org/10.1016/j.bbamcr.2018.06.006
Received 21 February 2018; Received in revised form 28 May 2018; Accepted 12 June 2018
Available online 15 June 2018

the pro-apoptotic action of quinazolines in the prostate, numerous studies have demonstrated similar pro-apoptotic activity in breast cancer cells, leukaemia, pituitary adenoma, bladder cancer, renal cancer and most recently in glioblastoma as well [1–5, 7–12].

Our group discovered that the α1-adrenergic antagonist PRZ is able to induce apoptosis in leukaemia cells via a mechanism independent of adrenergic receptors [5,12]. We further found that PRZ is also able to induce apoptosis in cells derived from medullary thyroid carcinoma - a malignancy characterized by high resistance against chemotherapy - which further emphasizes the potent anti-tumour effects of PRZ [13]. Besides direct anti-proliferative and pro-apoptotic activity further studies have revealed that quinazolines activate anoikis - a protective effect against metastasis – and pronouncedly inhibit tumour-angiogenesis [8,9,14]. In summary, data in the literature highlight manifold anti-tumour actions of quinazolines in vitro and in vivo. Even though some details about the effects of quinazolines on apoptotic signalling pathways are known, the main drug targets triggering pro-apoptotic effects still need to be defined. We found that quinazolines enter cells via endocytosis and subsequently induce a tubular morphologic reorganisation of the LAMP1 positive endolysosomal system [15]. In order to discover proteins with affinity to quinazolines, we performed native gel electrophoresis of proteins bound to the fluorescent PRZ-derivative BODIPY® FL Prazosin (QAPB) and subsequently performed mass spectrometric analysis of fluorescent protein bands after in-gel tryptic digestion [15]. We identified up to 700 different proteins (unpublished results), initially questioning the specificity of our approach. As a starting point we focused on membrane proteins since PRZ was shown to enter cells via endocytosis and to interfere with endocytic sorting [6,15]. Among those we recurrently found CD98 heavy chain (CD98hc, SLC3A2, 4F2, 4F2hc), an oncoprotein controlling cellular amino acid homeostasis and integrin function [16]. CD98hc acts as a chaperone for various amino acid transporters like LAT1, LAT2, y + LAT1, y + LAT2 and xCT, which import essential amino acids (AA) in antiport with glutamine into the cell and thereby provide AA for protein synthesis and production of the antioxidant glutathione [16,17]. Furthermore, CD98hc regulates autophagy and promotes cell growth and protein synthesis via the PI3K-AKT-mechanistic Target of Rapamycin (mTOR) pathway [16,18]. Santiago-Gómez et al. discovered recently that CD98hc participates in tumour progression by inhibition of β-catenin proteasomal degradation via AKT/GSK-3β signalling [19]. In earlier studies Feral et al. had already shown that CD98hc is associated with β1 integrins and contributes to integrin-dependent cell spreading, cell migration and protection from apoptosis [20,21]. Poettler et al. demonstrated that CD98hc drives integrin-dependent renal cancer cell behaviour [22]. In line with the observations of Poettler et al., Kyprianou's group found that quinazolines interrupt intracellular survival signals and induce anoikis in cancer by targeting integrin mediated cell-cell and cell-extracellular matrix interactions [14,23]. These results concerning integrin signalling represent an obvious link between CD98hc and the pro-apoptotic signalling of quinazolines.

Based on our findings in proteomics analysis and the multifactorial significance of CD98hc in cancer cells, we investigated a possible role of CD98hc in quinazoline induced apoptosis. We also tested whether the lysomototropic agents chloroquine and ammonia [24–26] and the v-ATPase inhibitor bafilomycin A1, which attenuate the cytotoxicity of PRZ [15], interfere with the trafficking of CD98hc. Since CD98hc is currently seen as potential drug target in several types of human malignancies [16,21], the primary motivation and goal of our study was to uncover possible interactions of old drugs with this novel target.

2. Materials and methods

2.1. Cancer cell culture

K562 chronic myeloid leukaemia cells, obtained from ATCC (Manassas, VA, USA) and LNCaP prostate cancer cells (CLS Cell Lines Service GmbH, Eppelheim, Germany) were cultivated in RPMI-1640 medium (Sigma, St. Louis, MO, USA) supplemented with 10% foetal bovine serum (FBS, Merck/Biochrom, Berlin, Germany), 2 mM L-glutamine (Sigma) and 100 U/ml penicillin and 0.1 mg/ml streptomycin ("Penstrep", Sigma). In some experiments the standard medium was supplemented with MEM amino acid concentrate (Sigma) or additional AA mainly obtained from Carl Roth (Karlsruhe, Germany). In all cell culture experiments with PRZ the described RPMI-1640 standard medium was also used.

2.2. Drugs and reagents

Bafilomycin A1 (BafA1), bis-2-(5-phenylacetamido-1,3,4-thiadiazol-2-yl)ethyl sulphide (BPTES), chloroquine diphosphate salt (CHQ), cytochalasin-D (Cyto-D), 6-Diazo-5-oxo-L-norleucine (DON), *E. coli* derived asparaginase (L-ASP), glutathione (GSH), L-methionine sulfoximine (MSO), *n*-acetylcysteine (NAC), nocodazole (NDZ), Pit-1 and prazosin hydrochloride (PRZ) were purchased from Sigma. Rapamycin was obtained from LC Laboratories (Woburn, MA, USA) and NVP-BEZ235 (BEZ235) from the Cayman Chemical Company (Ann Arbor, MI, USA). Depending on solubility, drugs were either solved in cell culture proved dimethyl sulfoxide (DMSO, Sigma) or double distilled water (Fresenius Kabi, Graz, Austria).

2.3. Analysis of cellular proliferation and viability

Proliferation of K562 cells was assessed with a CASY® Cell Counter and Analyser System (OMNI Life Science, Bremen, Germany). For proliferation assays, K562 cells were cultivated in 24 well plates with a starting cell number of 2×10^4 cells/ml. Every condition was analysed in duplicate. For flow cytometry assays, western blotting experiments and qPCR 1×10^6 K562 cells were cultivated in 10 ml medium in 25 cm^2 cell culture flasks. Proliferation and viability of LNCaP cells were assessed using the WST-1 reagent (Roche, Mannheim, Germany) following the manufacturer's instructions. Cells were harvested by trypsination, washed once in medium without glutamine and were cultivated in 96 well tissue culture plates, starting with a cell number of 1×10^4 cells in 50 µl medium without glutamine. Cells were allowed to attach to the surface of the plate overnight, before addition of different concentrations of glutamine or NH_4Cl ± prazosin to reach a final volume of 100 µl/well. Afterwards, cells were cultivated for 24 h or 48 h. Absorption at 450 nm and as a reference at 650 nm was determined with a Sunrise™ absorbance reader (Tecan, Männedorf, Switzerland) and/or with a BMG Labtech SPECTROstar Nano microplate reader (Ortenberg, Germany). All conditions were tested in triplicates. Cell death of K562 and HEK293T cells was also tested with the WST-1 assay analysing samples of cell suspensions in sextuplicates (K562) or triplicates (HEK293T) following cultivation.

2.4. CRISPR/Cas9-mediated CD98hc knockout in HEK293T cells

The cell line HEK293T, obtained from ATCC, was maintained in DMEM medium with high glucose (Sigma) supplemented with 10% FBS, "Penstrep" and 100 µM 2-mercaptoethanol (βME, Sigma). To generate CD98hc knockout (KO) cells, the CRISPR/Cas9 system was used according to the manufacturer's instructions (Santa Cruz Biotechnology/SCBT, Dallas, TX, USA). HEK293T cells were co-transfected with the CD98hc CRISPR/Cas9 KO plasmid (sc-400501; SCBT) and the CD98hc homology-directed repair (HDR) plasmid (sc-400501-HDR; SCBT). The CD98hc CRISPR/Cas9 KO plasmid consists of a pool of three plasmids designed to disrupt gene expression by causing a double-strand break in 5′-GATTCTCTATGTCCCGAACC-3′, 5′-TCGGGACATAG AGAATCTGA-3′ and 5′-TCATCCCCGTAGCTGAAAAC-3′. The CD98hc HDR plasmid contains a puromycin resistance gene to allow selection of stably transfected cells with successful integration. Briefly, cells

(1×10^5 cells per well) were seeded onto 6-well culture plates in 2 ml of DMEM per well, 24 h prior to transfection and grown to 80% confluency. Cells were transfected with 1 μg of CD98hc CRISPR/Cas9 KO plasmid and 1 μg of CD98hc HDR plasmid (SCBT) using polyethylenimine (Polysciences Europe GMBH, Eppelheim, Germany) and NaCl and incubated at 37 °C, 5% CO_2 for 48 h. Successful co-transfection of the CRISPR/Cas9 KO plasmid and HDR plasmid was visually confirmed by detection of the green fluorescent protein (GFP) and the red fluorescent protein (RFP), respectively, by fluorescence microscopy. DMEM medium was exchanged with fresh medium containing puromycin (1 μg/ml, SCBT). Expanded pools of cells resistant to puromycin were maintained for three passages in the corresponding selective medium and were further enriched for cells expressing high levels of RFP by sorting on a Becton Dickinson (BD) FACSAria™ Fusion Cell Sorter (San Jose, CA, USA) at the Scientific and Technological Centers of the University of Barcelona/CCiTUB). The same sorter was used to deposit single cells into 96-well plates for clonal selection. Several clones were obtained, expanded and assayed for CD98hc expression. In all HEK293T cell culture experiments with prazosin, RPMI-1640 standard medium with addition of βME was used.

2.5. Real time quantitative PCR

Expression of human CD98hc (SLC3A2) at the mRNA-level was analysed versus 18S rRNA using TaqMan® chemistry (Thermo-Fisher/Applied Biosystems, Foster City, CA, USA). RNA was extracted with TRI-Reagent RT (MRC Inc., Cincinnati, OH, USA) according to the manufacturer's protocol. Extracted RNA was quantified and analysed using a NanoDrop ND-1000 spectrophotometer (Thermo-Fisher/Peqlab, Erlangen, Germany) and RNA-gel electrophoresis. Extracted RNA was reverse transcribed with the High Capacity cDNA Reverse Transcription Kit (Thermo-Fisher/Applied Biosystems). For TaqMan®-analysis inventoried assays of Thermo-Fisher/Applied Biosystems (SLC3A2: assay number: Hs00374243_m1 and Eukaryotic 18S rRNA Endogenous Control, assay number: Hs99999901_s1) were used. Quantitative RT-PCR was performed on a CFX96™ - Real-Time PCR Detection System (Bio-Rad) using the 2-ΔΔCT algorithm for quantification of relative gene expression of controls versus treated samples. Each sample was measured in triplicates.

2.6. Western blotting

Cells were harvested and washed twice with calcium/magnesium free phosphate buffered saline (CMF-PBS) at 4 °C. Cells were lysed with a lysing buffer containing 50 mM Tris base, 10 mM EDTA, 1% Triton X-100 and the cOmplete™ Protease Inhibitor Cocktail (Roche). Protein concentration was determined using the Pierce™ BCA Protein Assay Kit (Thermo Fisher Scientific, Waltham, MA, USA). For SDS-PAGE, 10% separating gels and 4% stacking gels were used. Ten μg of total protein mixed with Laemmli buffer were loaded on SDS-gels per lane. Before loading, the samples were denatured at 95 °C for 5 min. PageRuler™ Prestained Protein Ladder (Thermo Fisher) was used as molecular weight marker. For the blotting procedure a Bio-Rad Wet/Tank Blotting System and PVDF membranes (Amersham™ Hybond® P western blotting membranes, GE-Healthcare, Piscataway, NJ, USA) were used. The membrane was blocked in 5% non-fat milk in Tris Buffered Saline (T-BST) containing 0.1% Tween® 20 detergent for 1 h at room temperature (RT). After blocking, the membranes were incubated with the respective primary antibody overnight at 4 °C. The following primary antibodies were used: mouse CD98hc (E-5, SCBT), rabbit GSK-3α (D80E6, Cell Signaling Technology/CST, Danvers, MA, USA), rabbit phospho (Ser21) - GSK-3α (36E9, CST), polyclonal rabbit GAPDH (BioLegend), polyclonal rabbit AMPKα (BioLegend), rabbit phospho (Thr172) - AMPKα (40H9, CST) and polyclonal rabbit β-actin (Sigma). After washing, the membrane was incubated with the corresponding horseradish peroxidase (HRP) labelled secondary antibody (goat anti-rabbit IgG (H + L)-HRP conjugate/Bio-Rad, or F(ab')2-goat anti-mouse IgG (H + L), HRP/Sigma) for 1 h at RT. To visualise the antigen-antibody-antibody complex, we used the HRP substrate Clarity™ Western ECL (Bio-Rad) and a ChemiDoc™ Touch Imaging System (Bio-Rad). ImageJ was used for semi-quantitative analysis of band intensity.

2.7. Flow cytometry (FACS) assays

FACS analysis was performed to assess surface expression of CD98hc and CD107a (LAMP1) in K562 cells. After they were harvested and washed once with CMF-PBS buffer, cells were resuspended in CMF-PBS supplemented with 10% FBS (staining buffer) and cell numbers were assessed. For each tested condition, 2×10^5 cells in a total volume of 200 μl staining buffer were incubated with a fluorescein isothiocyanate (FITC) labelled anti-human CD98hc mouse antibody (MEM-108, BioLegend) in parallel with an allophycocyanin (APC) labelled anti-human CD107a mouse antibody (H4A3, BioLegend) in the dark for 1 h at 4 °C. In parallel, cells for each condition were stained with the same concentration of matching isotype-antibodies (FITC-mouse IgG1, κ/BioLegend and APC-mouse IgG1, κ/Thermo Fisher/eBioscience). Afterwards, cells were washed twice with CMF-PBS and resuspended in staining buffer. Until analysis samples were shielded from light and kept on ice. Flow cytometry was performed with a BD LSRFortessa™ flow cytometer running BD FACSDiva™ software. Light scattering characteristics of cells were used to discriminate dead cells as described previously [27]. Emitted mean fluorescence-area (FL-A) was used for data analysis. To assess the mode of cell death, FACS analysis of cleaved (activated) caspase-3 and Annexin V (AV)/cell-impermeant DNA binding dye - double staining was done. To stain active caspase-3 5×10^5 cells were fixed with Cytofix/Cytoperm (BD) for 20 min at 4 °C and stained with an Alexa Fluor 647-labelled antibody against active caspase-3 obtained from BD according to the manufacturer's instructions. For AV staining cells were harvested and washed once with staining buffer. Then, 1×10^5 cells were stained in AV staining buffer (BioLegend), either with AV-APC (BioLegend) and propidium iodide (PI, Thermo Fisher/eBioscience), or Pacific Blue™ AV (BioLegend) combined with the SYTOX Green Nucleic Acid Stain (Thermo Fisher) at RT and shielded from light for 20 min. For analysis of DNA-content, cells were fixed with ice cold 70% ethanol and stained with PI according to standard protocols. Cells were analysed either with a BD LSR II or a BD LSRFortessa flow cytometer.

2.8. Fluorescence labelling of adherent growing living cells

Cells were stained as recently described with the fluorescent prazosin derivative BODIPY® FL Prazosin (QAPB) and the red fluorescent lysomototropic dye Lysotracker® Red (LT), both obtained from Thermo Fisher/Molecular Probes (Eugene, OR, USA) [15]. QAPB was added directly to the culture at a final concentration of 100 nM (LNCaP) or 200 nM (HEK293T) to survey drug-trafficking in living cells. LT-staining was performed after cell cultivation. To identify apoptotic cells directly in cell cultures at the endpoint of the experiment, the CellEvent™ Caspase-3/7 Green ReadyProbes® Reagent or the Hoechst 33342 nuclear dye (both obtained from Thermo Fisher/Molecular Probes) were used according to the manufacturer's instructions. LAMP1-GFP, LAMP1-RFP or Rab5-RFP fusion proteins were expressed transiently in LNCaP cells using the CellLight® BacMam 2.0 technology (Molecular Probes/Thermo Fisher). The fluorescence of stained cells was analysed with an Eclipse TE300 (Nikon, Tokyo, Japan) inverted microscope, the LSM 510 META scanning laser confocal microscope (Zeiss, Jena, Germany) and/or a ZOE™ Fluorescent Cell Imager (Bio-Rad). Live cell imaging studies observing lysosomal tubulation in LAMP1-RFP expressing LNCaP cells were performed using a Zeiss Cell Observer.

2.9. Immunofluorescence staining

Indirect immunofluorescence (IF) staining followed standard protocols as described in previous studies [15]. The following primary antibodies were used: mouse CD98hc (either MEM-108/BioLegend, or UM7F8/BD Pharmingen), mouse LAMP1 (H4A3, BioLegend), rabbit LAMP1 (D2D11, CST), mouse CD44 (BJ18, BioLegend), mouse CD59 [p282 (H19)] (BioLegend), mouse CD147 (HIM6, BioLegend) and mouse alpha tubulin (DM A1, Thermo Fisher). For fluorescent visualisation of primary antibody binding, matching secondary antibodies labelled with either Cy3 or Alexa Fluor® 555 or DyLight® 488 obtained from Jackson ImmunoResearch (West Grove, PA, USA) or BioLegend were used. 4′, 6-Diamidin-2-phenylindol (DAPI, 1 μg/ml, Sigma) was routinely used to counterstain nuclei but is not shown in every image compilation. In some experiments actin fibres were visualised with phalloidin staining using phalloidin-tetramethylrhodamine B isothiocyanate (Sigma). A Leica DM 4000 fluorescence microscope (Wetzlar, Germany) was used to monitor and document IF-stained cells.

2.10. Statistics

Data are presented as mean values + or ± standard deviation calculated with Microsoft Excel. Significance was calculated using Sigma Plot 13 (Systat Software Inc., San Jose, CA, USA). Normal distribution of data was tested with the Shapiro–Wilk test. Multiple testing or testing of several treatment groups versus a single control group was done with one-way ANOVA with Holm-Sidak post hoc testing, assuming normal distribution of data. For multiple testing or testing several treatment groups versus a single control group in data sets lacking normal distribution, one-way ANOVA on the ranks and Student-Newman-Keuls (NKS) post hoc test or Dunnett's method were used as appropriate. The overall significance level was set at $p \leq 0.05$. To test for possible treatment interactions, the free software tool Combenefit 2.021 (Cancer Research UK/University of Cambridge, Cambridge, UK) was employed, following the Bliss independence model and one sample *t*-test for testing significance of possible drug interactions.

3. Results

3.1. Prazosin reroutes CD98hc towards tubular lysosomes

Because we had detected CD98hc in a BODIPY® FL Prazosin (QAPB) positive protein fraction [15] (unpublished results), we initially analysed the pattern of CD98hc in prazosin (PRZ) treated LNCaP prostate cancer cells with indirect immunofluorescence (IF). We found CD98hc mainly located at the cell membrane in untreated cells, whereas in PRZ treated cells, CD98hc appeared in tubular structures (Fig. 1). Since one of the main cytotoxic mechanisms of PRZ is lysosomal tubulation [15], we investigated a possible association of CD98hc with LAMP1 positive tubules. In fact, double IF assays showed perfect analogy of CD98hc with morphologically altered lysosomes in PRZ treated cells (Fig. 1). We obtained similar effects in the leukaemia cell line K562, which was used as a second model in our study [5,12,15] (Suppl. Fig. 1). Because CD98hc is a known cargo of clathrin independent endocytosis (CIE) which employs tubular carriers for the endocytic recycling of proteins back to the cell membrane [28], we wanted to investigate whether the trafficking of other CIE cargo proteins such as CD44, CD59, and CD147 (basigin) was affected by PRZ as well [28,29]. CD147 was of particular interest, since CD98hc is associated with basigin [30]. As reported by Verkaik et al. [31], we also saw no expression of CD44 in LNCaP cells (Suppl. Fig. 2). We found CD59 expressed in LNCaP cells, but the fluorescence pattern of CD59 was not affected by PRZ treatment (Suppl. Fig. 2). Basigin showed a pronounced association with the cell membrane in untreated and PRZ treated cells, but in contrast to CD98hc, no striking tubular pattern appeared in PRZ treated cells (Suppl. Fig. 2). This data suggests that PRZ does not affect clathrin independent endocytosis in general but specifically targets CD98hc to newly formed lysosomal tubular structures.

3.2. Membrane derived CD98hc is shuttled towards tubular lysosomes

To investigate whether membrane derived CD98hc is shuttled towards lysosomes in PRZ treated cells, we directly added the CD98hc (MEM-108) antibody routinely used in our IF experiments to cultures of LNCaP cells and treated them with PRZ for 24 h without prior removal of the antibody solution. Following fixation and incubation with the secondary antibody we observed an almost identical pattern of CD98hc as in cells stained according to the standard IF protocol (Fig. 2). In cells treated with PRZ, but not in control cells, we observed lysosomal accumulation of CD98hc and the formation of the tubular LAMP1/CD98hc pattern. In contrast, addition of an anti CD44 antibody, used as isotype control for the CD98hc antibody, to the culture gave no specific signal. Because the antibody solution contained a low concentration of NaN_3, we also tested the effects of NaN_3 on the pattern of CD98hc in PRZ treated cells. Interestingly, the supplementation of the medium with azide equivalent to the antibody solution showed no effect on untreated cells but resulted in polar accumulation of CD98hc and attenuation of the formation of the tubular CD98hc fluorescence pattern in PRZ treated cells, suggesting that the tubulation process depends on ATP (not shown). In summary, the main outcome of these experiments is that the CD98hc protein that accumulates in the lysosomes of PRZ treated cells at least partially originates from the cell membrane.

3.3. Prazosin induces de novo synthesis of CD98hc

IF-assays have shown that the localization of CD98hc changes from a surface to a lysosomal pattern in response to PRZ treatment. To test whether PRZ also induces expression changes of CD98hc in K562 cells, we used qPCR to quantify CD98hc mRNA levels, flow cytometry to assess cell membrane bound CD98hc protein and western blotting (WB) to screen for changes in total CD98hc-expression. qPCR and WB assays showed a dose dependent increase of CD98hc-transcription and translation (Fig. 3). But even though the accumulation of CD98hc in the lysosomes of PRZ treated cells suggested a possible lack of CD98hc at the cell membrane, CD98hc surface expression in PRZ treated cells remained almost constant (Fig. 3). There was only a slight (~20%) reduction of CD98hc expression in cells treated with 20 μM PRZ. WB experiments in the LNCaP cell line as well showed a dose dependent upregulation of CD98hc in response to PRZ treatment (Fig. 3), whereas the level of membrane bound CD98hc remained almost constant as assessed by flow cytometry (data not shown).

3.4. CRISPR/Cas9-knockout of the SLC3A2 gene in HEK293T cells does not inhibit endocytosis of quinazolines and lysosomal tubulation but interferes with pro-apoptotic signalling in response to prazosin

In order to establish a functional connection between CD98hc, PRZ induced lysosomal tubulation and apoptosis, a CRISPR/Cas9-mediated gene knockout (KO) of SLC3A2 - the gene coding for CD98hc - was realized in the HEK293T (HEK) cell line. The HEK cell line is an established model for research on CD98hc [30]. Successful KO of CD98hc was confirmed with WB (Fig. 4A), IF (Fig. 4C) and PCR/qPCR (not shown). Using this model, we observed that the adhesive behaviour of CD98hc KO cells was impaired compared to wild type (WT) cells. KO cells showed adhesive growth, but were very prone towards detachment in response to vibration or agitation. There was also upregulation of CD98hc expression (Fig. 4A,B) and lysosomal tubulation (Fig. 4D) in response to PRZ treatment in HEK cells, confirming that the HEK cell line is an appropriate model for our purposes. Experiments with CD98hc KO cells clearly showed that the uptake of QAPB and lysosomal tubulation were not disabled in the absence of CD98hc (Fig. 4D); however, we observed fundamental differences in the response of HEK

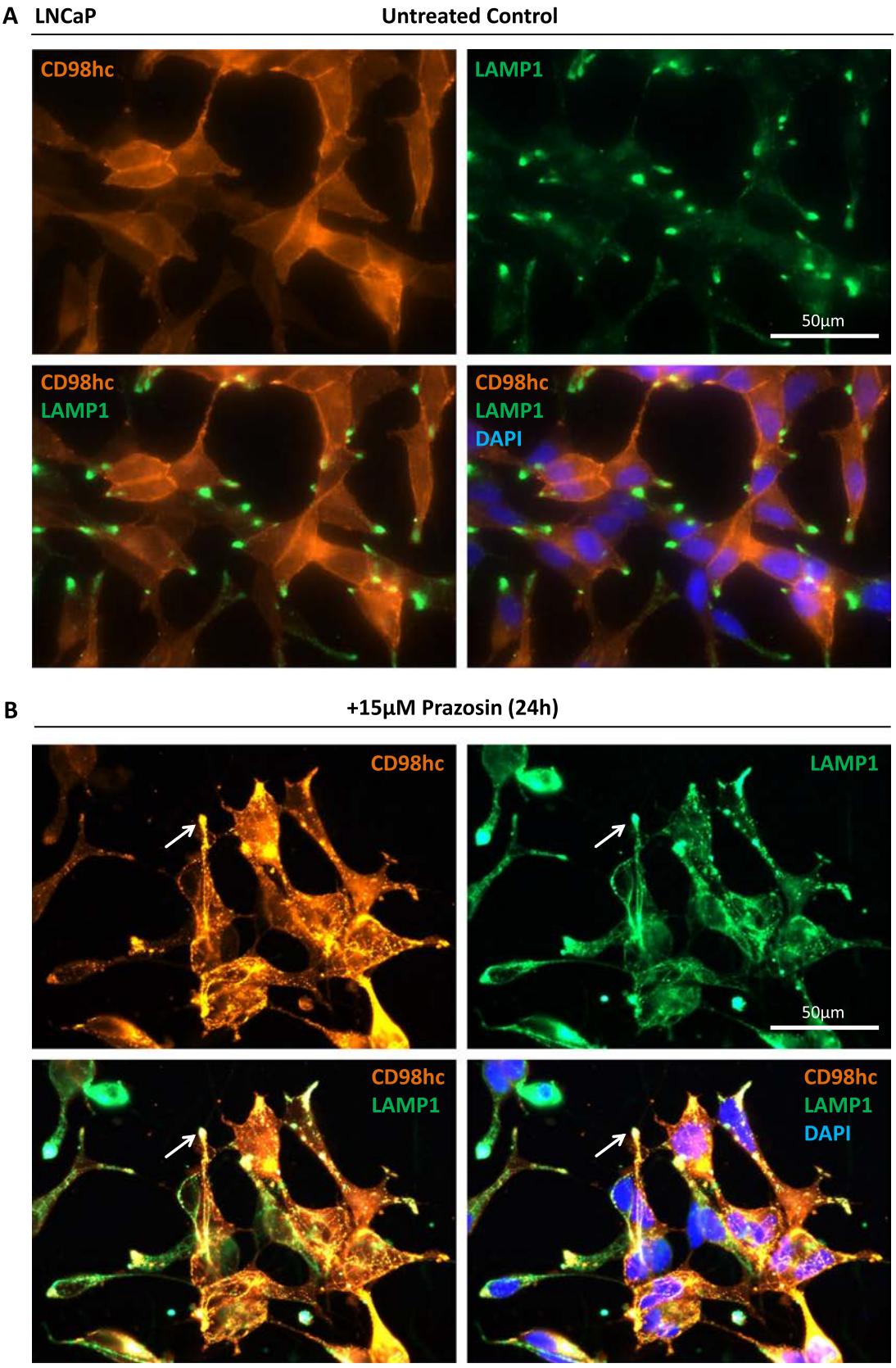

Fig. 1. Prazosin (PRZ) induced endosomal/lysosomal tubular structures in the prostate carcinoma cell line LNCaP are positive for CD98hc. LNCaP cells were treated without (A) or with 15 µM PRZ (B) for a total time of 24 h. Then, patterns of LAMP1 positive late endosomes/lysosomes and CD98hc were assessed in parallel by indirect immunofluorescence. Nuclei of cells were counterstained with DAPI. In untreated cells, CD98hc is mainly located at the cell membrane, whereas in PRZ treated cells CD98hc accumulates in LAMP1 positive tubular lysosomes (arrows).

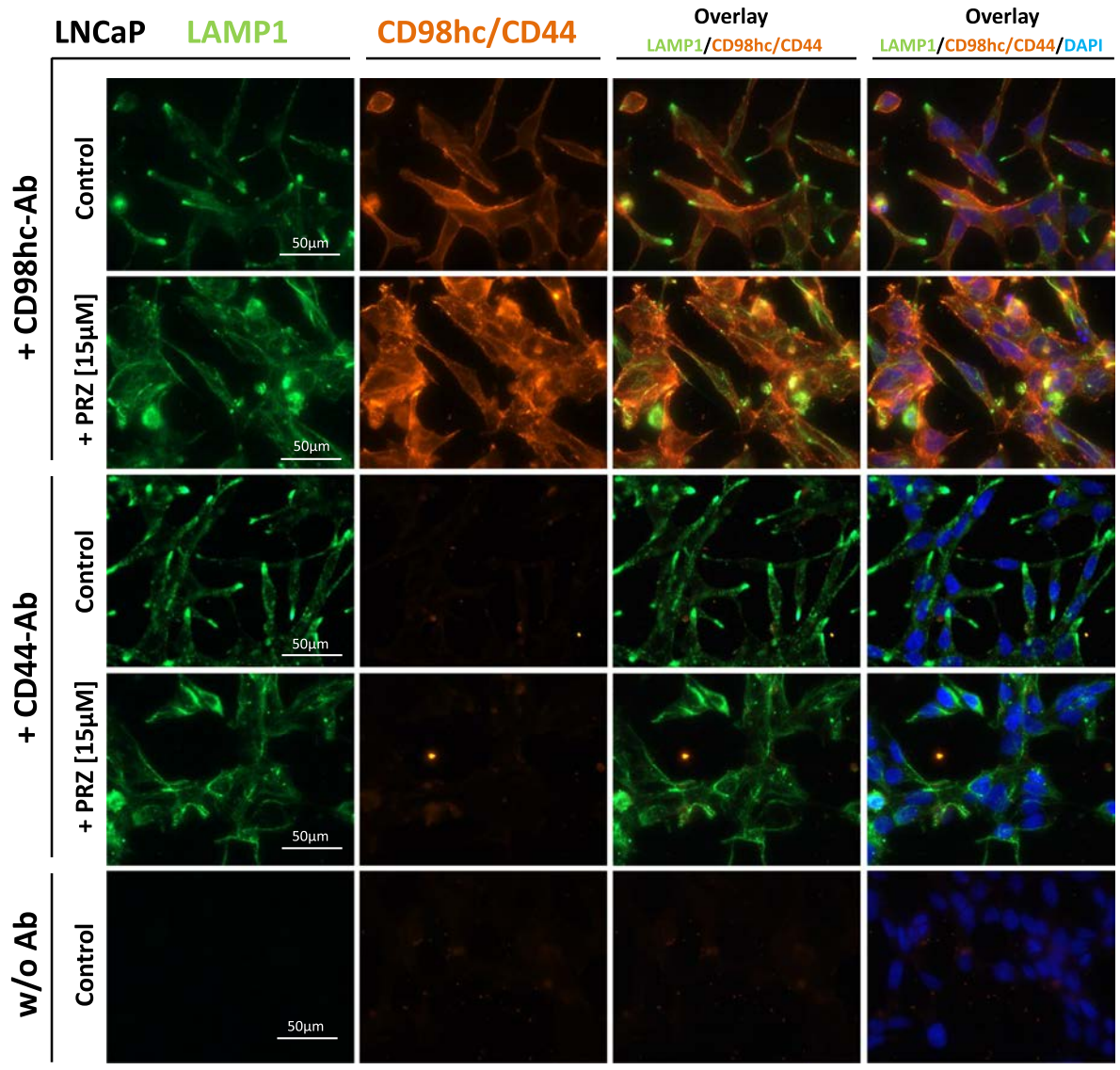

Fig. 2. CD98hc associated with the lysosomes originates from the cell membrane. LNCaP cells were incubated 15 min at 37 °C without (w/o) or with addition of an anti CD98hc (MEM-108) antibody (Ab) or an anti CD44 Ab as isotype control before treatment with 15 µM prazosin (PRZ) for 24 h. Afterwards, LAMP1/CD98hc immunofluorescence (IF) analysis was performed (w/o primary CD98hc antibody staining). Nuclei of cells were counterstained with DAPI. w/o Ab: Control cells cultivated w/o addition of PRZ/Ab and stained with both secondary Ab only. Treatment of cells with PRZ in the presence of the CD98hc Ab resulted in the typical tubular CD98hc pattern, suggesting that the CD98hc protein associated with the lysosomes in PRZ treated cells derives from the cell membrane.

cells towards PRZ treatment when CD98hc was deleted. First, we saw that PRZ treatment already induced rounding of CD98hc KO clones at concentrations of 15 µM, whereas WT cells mostly maintained their typical morphology. As a consequence, PRZ treated KO clones preferentially formed floating cell aggregates and tubular lysosomes showed pronounced perinuclear localization in these cells (Fig. 4D). Second, staining of living cells with the Hoechst nuclear dye showed the accumulation of complex nuclei in WT cells treated with 15 µM PRZ due to inhibition of cytokinesis [6,15], but this was only sparse in cultures of CD98hc KO cells (Suppl. Fig. 3). Most interestingly, within 48 h there was pronounced nuclear fragmentation in response to 30 µM PRZ in WT cells whereas nuclear fragmentation was much lower in CD98hc KO cells (Suppl. Fig. 3). To confirm these preliminary observations, we tested proliferation, viability, DNA content and apoptosis in KO clones. Cell counts showed that proliferation of CD98hc KO cells was decreased compared to WT cells (Fig. 5). In HEK cells treated either with 15 µM or 30 µM PRZ there was no increase in cell counts over a total period of 72 h, irrespective of CD98hc expression. But even though total cell numbers of PRZ treated WT cells remained constant over time, the cell volume and the DNA content of these cells were still increasing, indicating endoreplication (Fig. 5C and Suppl. Fig. 3). Within 24 h both WT cells and CD98hc KO clones treated with 15 µM PRZ showed an accumulation of cells with 4 N and > 4 N DNA content (Fig. 5C). In cells treated with 30 µM PRZ, the 4 N cell fraction was dominant. In the course of time, cells treated with 15 µM PRZ showed a continuous increase in DNA content and the parallel appearance of a pronounced Sub-G1 peak, indicating nuclear fragmentation and hence apoptosis. It was evident that the progress of the cell cycle and subsequently the accomplishment of the multinucleated phenotype and the induction of apoptosis were clearly attenuated in CD98hc KO cells. WT cells treated with 30 µM PRZ showed ongoing DNA synthesis while cytokinesis was inhibited; there was a time dependent increase of the Sub-G1 peak, which conforms to our microscopic observations of massive karyorrhexis under these conditions (Suppl. Fig. 3). Most interestingly, CD98hc KO cells treated with 30 µM PRZ were almost completely arrested in a 4 N-state at 24 h and persisted in that state for up to 72 h (Fig. 5C). WST-1-viability assays (Fig. 5B) showed only minor differences between WT cells and CD98hc KO clones concerning measured

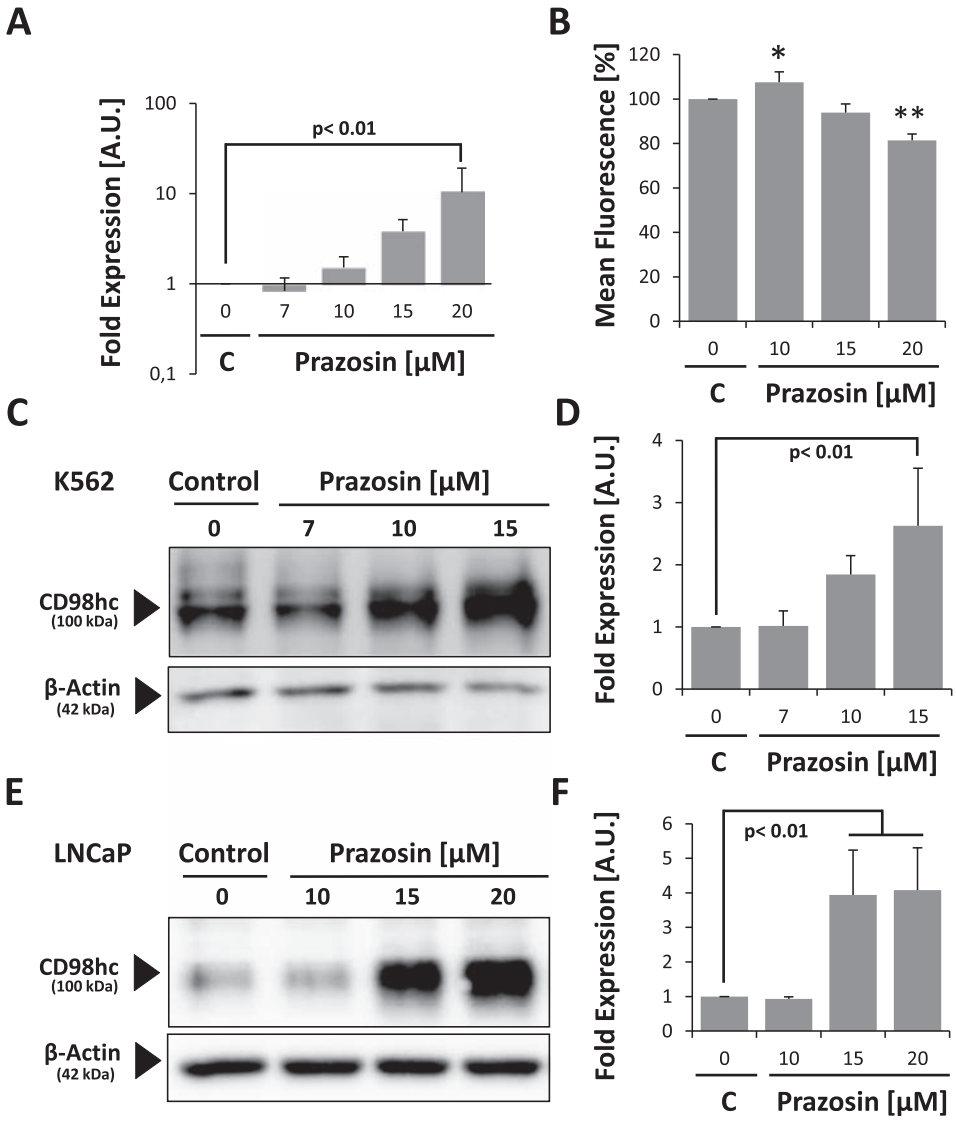

Fig. 3. Prazosin (PRZ) induces de novo synthesis of CD98hc. A–D: K562 cells were treated for 24 h with PRZ. Afterwards, CD98hc-expression was analysed by qPCR to assess CD98hc-mRNA-expression (in relation to 18sRNA) (A), flow cytometry to assess CD98hc expression at the cell membrane (B) and western blotting (WB) to analyse total CD98hc expression (C, D). A: PRZ induces transcription of CD98hc. n = 4. P-value according to Dunnett's test. A.U. = arbitrary units, C = control. B: Cell surface expression of CD98hc is only slightly reduced due to treatment with PRZ. n = 4, except PRZ [20 µM]: n = 3. *: $p < 0.01$, **: $p < 0.001$ versus control (C) according to ANOVA and Holm-Sidak post hoc analysis: C-D: Total expression of CD98hc in response to 24 h treatment with PRZ as assessed by WB. n = 4. P-value according to ANOVA and Holm-Sidak post hoc analysis. β-Actin was used as loading control. E–F: Total expression of CD98hc in LNCaP cells in response to a 24 h treatment with PRZ as assessed by WB. P-value according to ANOVA and Holm-Sidak post hoc analysis. n = 3.

optical density (OD) 450 values. At 24 h after addition of 15 µM PRZ to cultures OD values of CD98hc KO clones 1 and 2 were significantly ($p \leq 0.05$) lower compared to WT cells. These differences disappeared with drug dose and time. Cell death analysis using annexin V and the SYTOX Green Dead Cell Stain of cells (Fig. 5D) treated with 15 µM PRZ showed only slight differences in viability between WT and CD98hc KO clones. However, with 30 µM PRZ treatment, KO clones showed a significantly ($p < 0.001$) higher level of viability (i.e. a higher percentage of annexin V/SYTOX negative cells) than WT cells. The mean percentage (n = 3) of viable WT cells following 48 h treatment with 30 µM PRZ was 14 ± 5% compared to 40 ± 2% (Clone 1), respectively 41 ± 2% (Clone 2). Thus, loss of CD98hc does not affect endocytosis of PRZ and lysosomal tubulation, but does affect the progress of endoreplication and the survival of cells.

3.5. Ammonia - a by-product of glutaminolysis - preserves growth and viability of cancer cells in the presence of prazosin

Since it is known that besides AA, several xenobiotics also enter the cell via LAT1 (=CD98 light chain/CD98lc) which is coupled to CD98hc by a disulphide bridge [16,17,32], we tested whether an excess of distinct AA might interfere with the effects of 10 µM PRZ on K562 cells. In fact, among tested AA an antagonistic effect against the anti-proliferative effect of PRZ was observed for glutamine (Gln) (Fig. 6B) but not for alanine, arginine, asparagine, glycine, histidine, leucine, phenylalanine, serine, threonine, or supplementation of the growth medium with complex MEM amino acid concentrate (not shown). However, increasing Gln levels in the medium did not fully restore the growth of cells reduced in response to 10 µM PRZ. We confirmed that high Gln-concentrations in the medium ameliorated the anti-proliferative effect of low doses of PRZ over a total period of 72 h (Fig. 6C). Proliferation of untreated K562 cells was not significantly influenced by either the omission of Gln supplementation or the presence of Gln in a concentration range (0.5-10 mM) employed in common growth media formulations.

Furthermore, there was at least a modest protective effect for cysteine, which is most possibly associated with its antioxidant properties [33]. Addition of glutathione or also its antioxidant precursor *N*-acetylcysteine to the medium resulted in a similar effect as seen for cysteine (not shown). Glucose deprivation or increasing levels (2.75–33 mM) of glucose did not significantly influence the growth of K562 cells treated with 10 µM PRZ (data not shown).

In the light of CD98hc, the protective role of Gln against the cytotoxicity of PRZ was not surprising, because CD98hc is a crucial component for the maintenance of cellular Gln homeostasis, especially in malignant cells (Fig. 6A) [16,34–37]. Since our results suggested PRZ induced "glutamine addiction" of K562 cells, we tested whether targeting cellular Gln metabolism at several points - as illustrated in Fig. 6

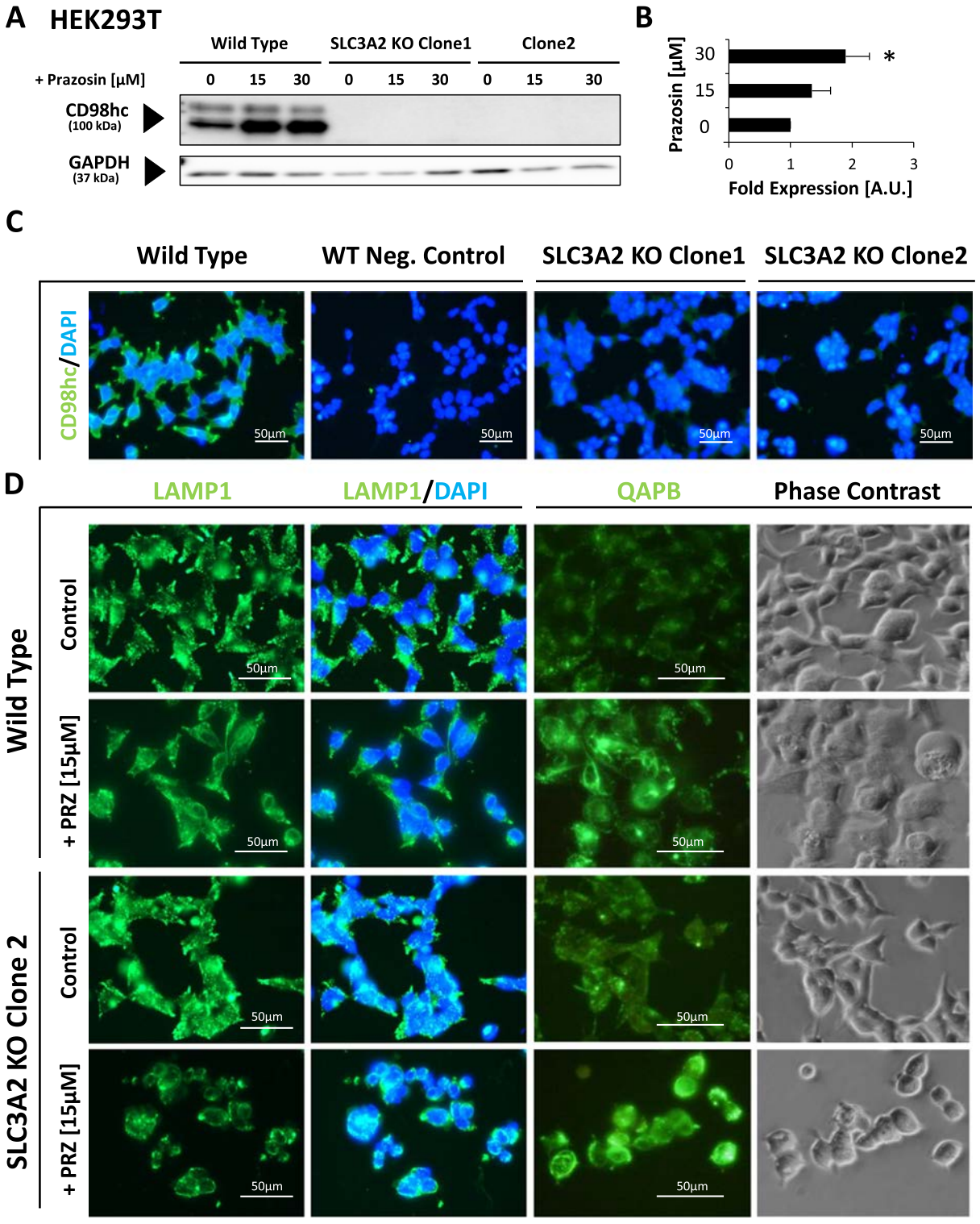

Fig. 4. Prazosin (PRZ) induced lysosomal tubulation occurs independent of CD98hc. To test whether CD98hc is required for PRZ induced lysosomal tubulation, the SLC3A2 gene-coding for CD98hc - was knocked out (KO) in HEK293T (HEK) cells. A–B: Western blotting (WB) analysis of PRZ treated HEK cells. Wild type (WT) and two KO clones were treated with PRZ for 24 h. A: A representative HEK-CD98hc plot out of four experiments is shown. As expected, no CD98hc signals were obtained in KO clones. WT cells typically presented two CD98hc bands, but only the respective lower band showed an increase of intensity in response to PRZ. GAPDH was used as loading control. B: Densitometry analysis of CD98hc lower bands. *: $p < 0.01$ compared to untreated control according to ANOVA and Holm-Sidak post-hoc testing. n = 4. C: Demonstration of KO of SLC3A2 in HEK293T cells by indirect immunofluorescence (IF) against CD98hc. Nuclei of cells were counterstained with DAPI. Two independent SLC3A2 KO clones (Clone1 and Clone2) were used in our study. WT Neg.Control = Negative Control (secondary antibody only). D: Cells were either treated for 6 h with 15 µM PRZ and lysosomes were visualised by IF staining against LAMP1 or for 24 h and stained with the fluorescent PRZ derivative QAPB. PRZ induced LAMP1 + tubular structures in both WT and KO cells. Both PRZ treated KO clones mainly lost their spindle shaped morphology and exhibited perinuclear LAMP1 + tubules. Similar results were obtained when cells were stained with QAPB.

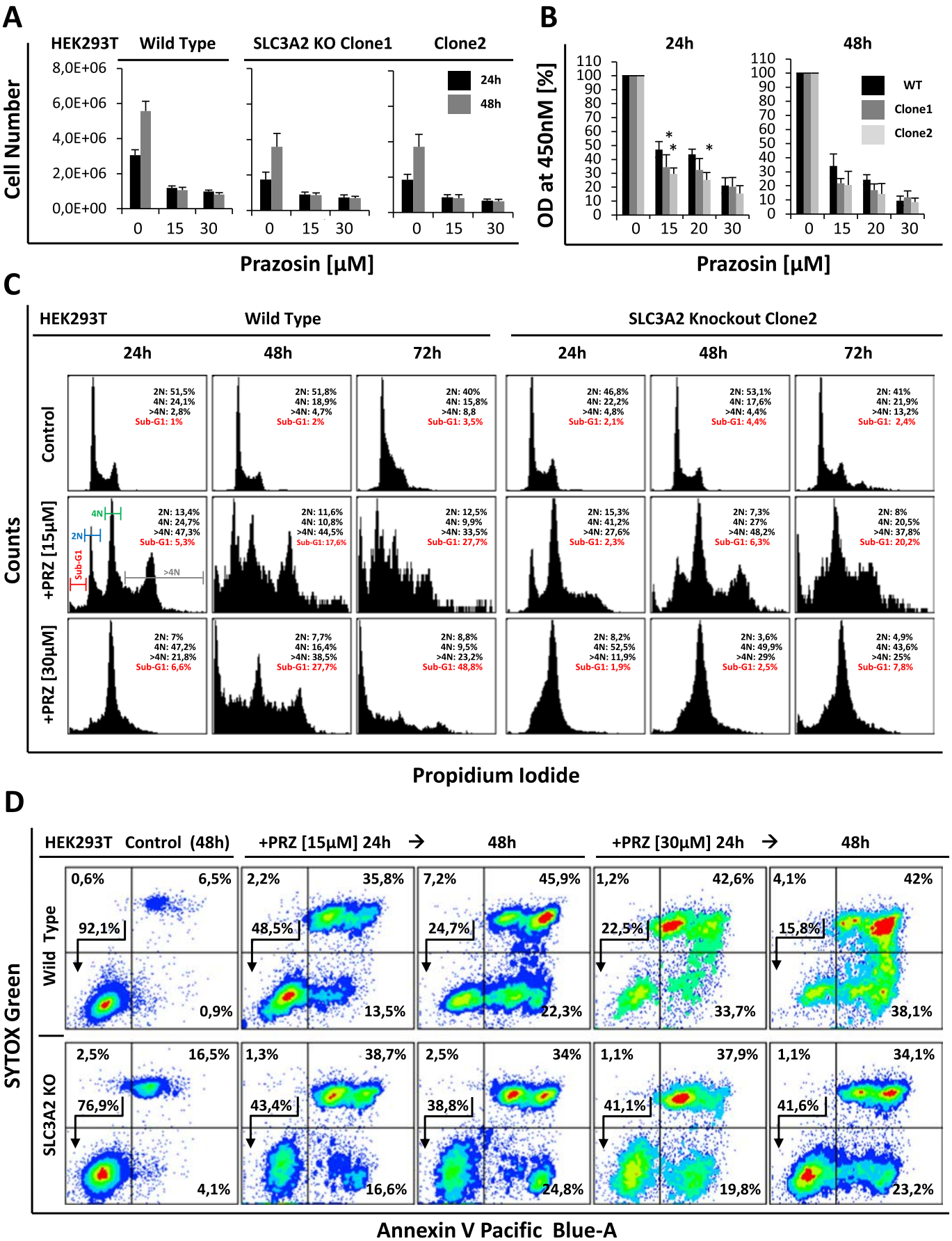

(caption on next page)

Fig. 5. The role of CD98hc in the cytotoxicity of prazosin (PRZ) on HEK293T (HEK) cells. SLC3A2 (CD98hc) was knocked out (KO) in HEK cells using CRISPR/Cas9 technology. Proliferation (A), viability (B), DNA content (C) and apoptosis/necrosis (D) of two KO clones, herein referred as Clone1 and Clone2 were analysed following 24 h or 48 h treatment with PRZ and compared to wild type (WT) cells. A: Cell counting showed an overall lower proliferative capacity of CD98hc KO clones compared to WT cells and no increase in cell counts in cultures treated with PRZ irrespective of CD98hc expression. n = 4. B: WST-1 viability assays showed a significant (*: $p \leq 0.05$) lower optical density (OD) at 450 nM of CD98hc KO clones compared to WT cells at 24 h according to ANOVA and Holm-Sidak post hoc testing. n = 3. C: DNA content profiles of HEK cells exposed to PRZ. HEK cells were treated with PRZ up to 72 h and stained afterwards with propidium iodide (PI) to assess DNA content or apoptosis. Treatment of HEK cells with PRZ resulted in the genesis of cells with 4 N or > 4 N DNA content and apoptosis, indicated by the appearance of a Sub-G1-peak. SLC3A2 KO cells treated with 30 μM PRZ were arrested in a binucleated (4 N) state and persisted in that state for up to 72 h. In contrast, WT cells did not cease DNA-synthesis in the presence of PRZ but also reached an > 4 N state and underwent apoptosis. The percentages in the upper right corner of the histograms depict the relative portions of cells with distinct DNA-content; respectively apoptotic cells (Sub-G1). The assignment of DNA content peaks is exemplified in the Wild Type-24 h-PRZ [15 μM] histogram. The presented results are representative for both SLC3A2 KO clones tested in a total of three independent experiments with similar outcome. D: Cell death analysis of PRZ treated HEK cells. HEK cells (WT versus CD98hc KO clones) were treated with PRZ and stained with Annexin V and the cell membrane impermeable DNA dye SYTOX Green. The presented plots (WT versus Clone1) are representative for three independent experiments with similar outcomes for Clone1 and Clone2.

- might enhance the cytotoxicity of PRZ. We therefore tested whether the enzyme asparaginase (L-ASP) and the glutaminase (GLS) inhibitors BPTES and DON were able to interfere with the protective effect of Gln against the cytotoxicity of PRZ on K562 cells. As a competitive Gln-analogue, DON also inhibits other Gln-metabolizing enzymes such as glutamine fructose-6-phosphate amidotransferase (GFAT) that use Gln as a nitrogen donor for the synthesis of several biomolecules [36] (Fig. 6A).

L-ASP, which deaminates the AA asparagine and to a lesser extent Gln [38] (Fig. 6A), was used to eliminate Gln in the medium. As reported by Song et al. L-ASP inhibited the growth of K562 cells dose dependently [39] and surprisingly attenuated the antiproliferative effects of PRZ (Fig. 6 and Suppl. Fig. 4A). In contrast, glutaminase inhibitors also inhibited cell growth dose dependently, but solely exhibited an additive but no synergistic inhibitory effect with PRZ and did not cancel the protective effect of high Gln doses (data not shown).

To further investigate the protective effect of L-ASP, we tested its products ammonia, glutamate and aspartate on PRZ treated cells. We observed a pronounced protective role of NH_4Cl (without affecting the pH of the medium) on PRZ treated cells but no effects with either glutamate or aspartate (Fig. 6 and Suppl. Fig. 4A). Just 1 mM NH_4Cl completely neutralized the effect of 10 μM PRZ. In order to test whether ammonia is utilized as a substrate to generate Gln via glutamate-ammonia-ligase (GLUL) [37], we used the GLUL-inhibitor methionine sulfoximine (MSO) either alone or in a cocktail with PRZ. However, even though used in concentrations up to 4 mM, MSO neither inhibited the growth of K562 cells alone, nor did it show a synergistic growth inhibitory effect with PRZ irrespective of the Gln concentration in the medium (not shown).

We also tested the effects of Gln and ammonia on cell viability to confirm results seen with cell counting. As expected, we observed a significant ($p < 0.001$) decrease in cell viability following treatment with pro-apoptotic 15 μM PRZ [12] in standard medium (without Gln) using WST-1 viability assays (Suppl. Fig. 4). In the presence of ammonia the harmful effects of PRZ were almost completely neutralized. Supplementation of the medium with 10 mM Gln also significantly ($p < 0.001$) attenuated the cytotoxicity of PRZ but did not completely restore the viability of cells. Caspase-3 activation occurred in at least a low percentage of cells treated with 15 μM PRZ without addition of Gln or ammonia, but not when supplemented with 10 mM Gln or ammonia (Suppl. Fig. 4). Annexin V/propidium iodide (AV/PI) assays confirmed ongoing apoptosis in Gln deprived PRZ treated cells (Suppl. Fig. 4). Addition of ammonia to the medium fully protected the cells against the induction of apoptosis, whereas supplementation of the medium with 10 mM Gln appeared only to slow down the progression of apoptosis.

To reproduce our results obtained in the K562 cell line in LNCaP cells, we treated the latter for a total period of 72 h with increasing concentrations of PRZ without or with 2 mM or 10 mM Gln. As reported by Dong and Yung [40] we observed that Gln deprivation inhibits the proliferation of LNCaP cells, but surprisingly, high doses of Gln also interfered with cell growth (Suppl. Fig. 5). Thus - in contrast to K562 cells - the growth behaviour of LNCaP cells is clearly influenced by Gln supply. With PRZ concentrations > 15 μM high doses of Gln exerted a protective effect on LNCaP cells. Microscopic analysis of cells treated with 30 μM PRZ under Gln free conditions additionally stained with the caspase-3/7 green reagent showed rounding, massive detachment and caspase activation, indicated by green fluorescent staining of the nuclei (Suppl. Fig. 5). Supplementation of the medium with high doses of Gln at least partially preserved the adhesive character of the cells and suppressed the induction of apoptosis although 10 mM Gln could not completely neutralize the cytotoxicity of PRZ. NH_4Cl also significantly ($p < 0.05$) interfered with the cytotoxic effect of PRZ (Suppl. Fig. 5). Microscopic analysis of cells showed dose dependent rounding, detachment and activation of effector caspases, attenuated by supplementation of the medium with NH_4Cl.

3.6. Ammonia maintains membrane expression and total expression of CD98hc in PRZ treated cells

To assess CD98hc cell membrane and total protein expression of PRZ treated cells in dependence of Gln and ammonia, we analysed cells by flow cytometry (FACS) and WB. To test whether tubular LAMP1 positive structures are in contact with the cell membrane, we used FACS to assess (in parallel to CD98hc) the expression of LAMP1 (CD107a), which is a marker for lysosomal exocytosis [41]. FACS analysis of PRZ [15 μM] treated cells showed a constant 20% reduction of membrane bound CD98hc under Gln free conditions, which could be reversed by supplementation of the medium with either Gln or NH_4Cl (Fig. 7). We detected weak expression of CD107a at the cell membrane of untreated cells that was approximately doubled by 5 mM NH_4Cl (Fig. 7). With 15 μM PRZ a fivefold increase of CD107a at the cell membrane was evident that was almost completely abolished by NH_4Cl but not by Gln.

These results imply that lysosomal tubules are indeed in contact with the cell membrane, providing a route via late endosomes/lysosomes back to the cell membrane (via lysosomal exocytosis).

Analysis of total CD98hc protein expression showed that NH_4Cl but not Gln significantly interfered with PRZ induced stimulation of CD98hc expression (Fig. 7). The supplementation of Gln free medium with NH_4Cl maintained CD98hc expression in the presence of PRZ at the same level as in untreated cells, further confirming an intriguing relationship between ammonia and PRZ.

For preliminary information on whether PRZ might alter the activation state of cellular energy sensors AMPKα and GSK3α, which are proteins downstream from CD98hc [30,42], we assessed the phosphorylation state of these proteins in K562 cells following 24 h treatment with PRZ (Fig. 7). These analyses were done in parallel with CD98hc WB as described above. GSK3α showed a significantly ($p < 0.05$) higher phosphorylation level at Ser21 in PRZ treated cells in the absence of Gln or ammonia, indicating inactivation of GSK3α via active PI3K-AKT-signalling upstream of GSK3α [43]. In the presence of ammonia PRZ induced phosphorylation of GSK3α was abolished. We also observed significant alterations in the activation state of AMPKα.

Interestingly, within 24 h ammonia and PRZ reduced the level of phosphorylation of AMPKα at Thr172 compared to untreated control (without NH_4Cl/Gln/PRZ) indicating inactivation of AMPKα and therefore a sufficient level of cellular energy. Thus, even though we only analysed a single time point, our results suggest that PRZ influences the metabolic state of the cell, but surprisingly causes no lack of energy.

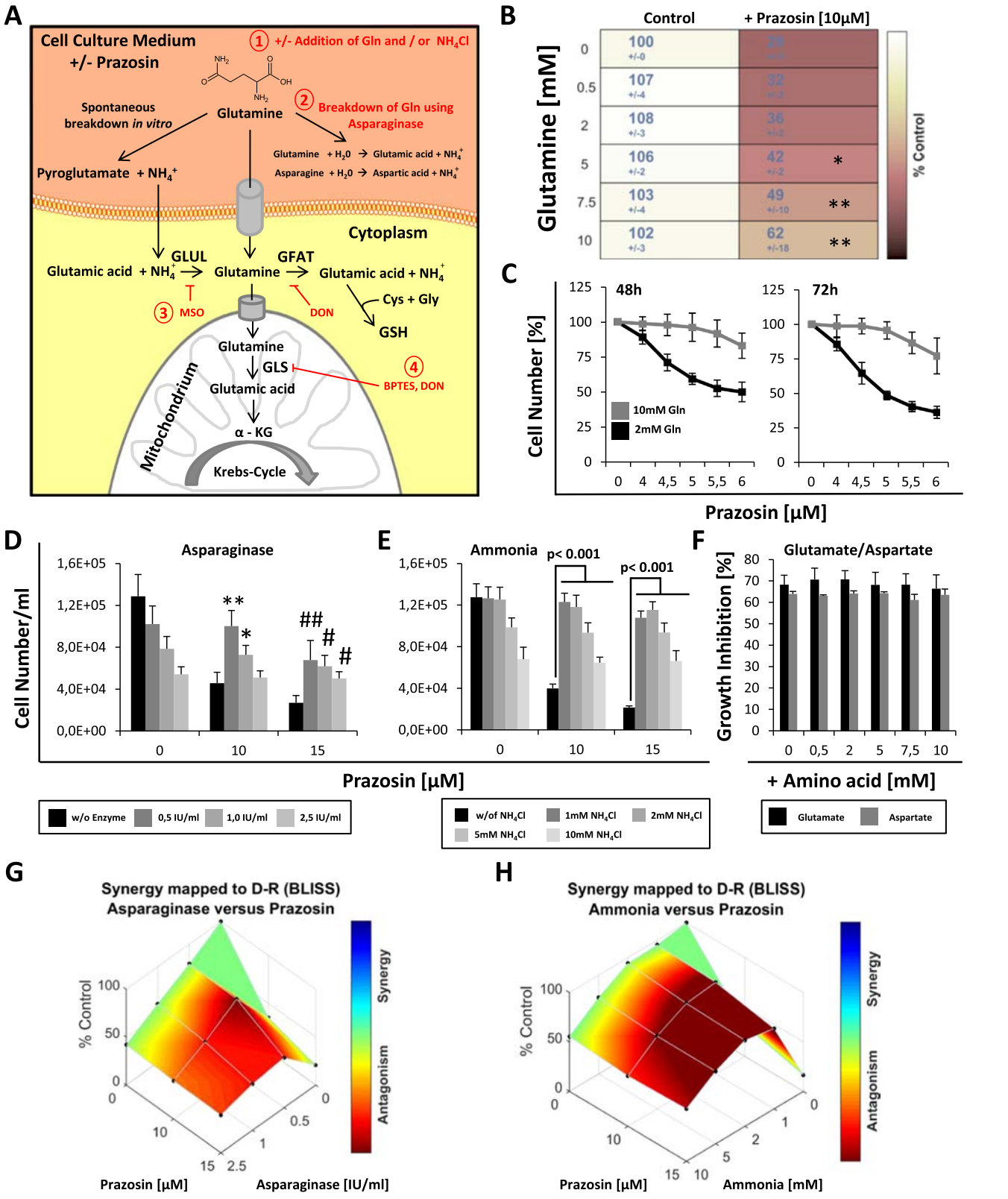

(caption on next page)

Fig. 6. Glutamine (Gln) and its metabolite ammonia preserve proliferation of K562 cells treated with prazosin (PRZ). A: Gln-metabolism of cancer cells according to Hensley et al. and Krall et al. [36,37] and description of how Gln-metabolism was manipulated in our study to test the influence of Gln-supply on the cytotoxicity of PRZ. First (1) we cultivated cells ± addition of Gln or NH_4Cl or (2) enzymatically depleted Gln using asparaginase. Spontaneous break down of Gln in vitro is a known phenomenon in cell culture. Gln is imported into the cell via various Gln-transporters. As a non-essential amino acid Gln can also be synthesized by glutamate-ammonia ligase (GLUL), inhibited by (3) methionine sulfoximine (MSO). In the cell Gln is used for the synthesis of glutathione (GSH, together with cysteine/Cys and glycine/Gly) and as nitrogen donor for various enzymatic reactions such as glutamine fructose-6-phosphate amidotransferase (GFAT) inhibited by the Gln analogue 6-Diazo-5-oxo-L-norleucin (DON). Gln is imported into mitochondria and undergoes anaplerotic reactions to generate α-ketoglutarate (α-KG) that enters the Krebs cycle [36]. The Gln degrading enzyme glutaminase (GLS) is inhibited by DON or the GLS inhibitor bis-2-(5-phenylacetamido-1,3,4-thiadiazol-2-yl)ethyl sulphide (BPTES). B–F: Proliferation of PRZ treated cells depending on Gln supply. Cell counts were assessed at given time points using an automated cell counter. B: K562 cells were treated for 48 h without (control) or with 10 μM PRZ and increasing concentrations of Gln. Control w/o Gln/PRZ = 100%, n = 7, *: $p < 0.01$, **: $p < 0.001$ versus cultivation with PRZ w/o (0) Gln according to Dunnett's test. C: K562 cells were cultivated with supply of 2 mM or 10 mM Gln for 48 h, or 72 h respectively. D: Supplementation of the medium with asparaginase restores proliferation of PRZ treated K562 cells. n = 3. *: $p < 0.05$, **: $p < 0.001$ versus PRZ [10 μM], #: $p < 0.05$, ##: $p < 0.01$ versus PRZ [15 μM] according to ANOVA and Holm-Sidak post hoc analysis. E: Supplementation of the medium with NH_4Cl restores proliferation of PRZ treated K562 cells. n = 3. P-values according to ANOVA and Holm-Sidak post hoc analysis. F: Replenishment of the growth medium with additional glutamate (Glu) or aspartate (Asp) does not influence the anti-proliferative effect of PRZ. n = 3. G–H: Combenefit synergy-mapping of combined treatments PRZ versus asparaginase (G), or PRZ versus ammonia (H).

3.7. Ammonia, glutamine, chloroquine and the v-ATPase-inhibitor bafilomycin A1 interfere with lysosomal tubulation and the trafficking of CD98hc

To assess the pattern of CD98hc and lysosomes in LNCaP cells in dependence on ammonia or Gln, we performed CD98hc/LAMP1 IF analysis, and QAPB/LT vital staining's. In the presence of ammonia, the localization and morphology of LAMP1 positive endosomes/lysosomes was only slightly affected and the pattern of CD98hc remained mostly unchanged (Fig. 8). Interestingly, the supplementation of the medium with ammonia (2 mM or 5 mM) completely abolished PRZ induced tubulation of lysosomes and lysosomal accumulation of CD98hc in the absence (not shown) or presence of Gln (Fig. 8). Analysis of lysosomes in living cells using LT and QAPB confirmed the results obtained in fixed cells (Suppl. Fig. 6). In the low concentrations used NH_4Cl did not prevent the accumulation of LT in obviously still acidic lysosomes. Over the total incubation time of 24 h, NH_4Cl did not prevent cellular uptake of QAPB but provoked a more diffuse fluorescence pattern and completely abolished the formation of QAPB positive tubules. Gln was also able to interfere with lysosomal tubulation and PRZ induced trafficking of CD98hc but the potency of Gln was much less pronounced than ammonia (Suppl. Fig. 7). We so conclude that ammonia causally interferes with PRZ induced lysosomal tubulation and resultant misrouting of CD98hc.

Since we demonstrated in our previous study that the FDA approved lysomototropic drug chloroquine (CHQ) and the v-ATPase-inhibitor bafilomycin A1 (BafA1) are able to restore the growth of cells in the presence of PRZ [15], we also tested whether these drugs are able to influence the trafficking of CD98hc either alone or in mutual reaction with PRZ. As already shown previously for CHQ [15], BafA1 also induced a dose dependent accumulation of enlarged LAMP1 positive endosomes/lysosomes in the cytoplasm (Suppl. Fig. 8) and completely eliminated PRZ induced lysosomal tubulation in LNCaP cells. We further showed that in response to either CHQ or BafA1 treatment CD98hc also accumulates in cytoplasmic vesicles in LNCaP (Suppl. Fig. 8) as well as K562 cells (not shown). In K562 cells low concentrations of both drugs (CHQ: 10-20 μM, BafA1: 1-5 nM) induced the formation of enlarged LAMP1 positive vesicles that showed co-localization with CD98hc and efficiently interfered with PRZ induced lysosomal tubulation. Furthermore, in CHQ and Baf1A treated cells there was a dose dependent increase of CD107a expression at the cell membrane, indicating lysosomal exocytosis. Interestingly, CHQ treatment alone resulted in a dose dependent decrease of CD98hc membrane expression (with 20 μM CHQ: 70 ± 5% CD98hc expression compared to untreated control, n = 7, $p < 0.001$), whereas BafA1 only marginally altered CD98hc membrane expression.

Experiments using HEK293T SLC3A2 KO cells showed that both CHQ and ammonia preserved the adhesive behaviour of KO cells in the presence of PRZ and also completely inhibited lysosomal tubulation, suggesting that the protective effects of these lysomototropic agents are not causally dependent on CD98hc expression (not shown).

3.8. Prazosin induced lysosomal tubulation is reversible, depending on an interplay of actin and microtubules but is non-sensitive towards inhibition of the canonical PI3K-AKT-mTor pathway

Since lysosomal tubulation is one of the main features of the cytotoxicity of PRZ, we aimed to further characterize this process. Besides LAMP1 positive tubules a further typical sign of PRZ-treated cells is vacuolization. We tested, whether these vacuoles represent early (sorting) endosomes or, lysosomes. We observed the appearance of Rab5 positive vacuoles parallel to Rab5 tubules, but no LAMP1 positive tubules within 10 min of treatment of LNCaP cells with 20 μM PRZ (Fig. 9A). In cells treated for 24 h with PRZ, Rab5 positive tubules were replaced by LAMP1 positive tubules. Live cell imaging studies revealed that LAMP1 + vacuoles swell and fuse with each other (Suppl. Video Files Supplemental Video FileA). Most interestingly, time-lapse microscopy also showed that LAMP1 + vacuoles arose in the cytoplasm and accumulated in the perinuclear region of PRZ treated cells. LAMP1 + tubules were obviously “growing” towards vacuoles originating from lysosomes located at the cell poles (Suppl. Video Files Supplemental Video FilesB/C). Although vacuoles also became LAMP1 positive, they did not accumulate Lysotracker® (Fig. 9B) suggesting that vacuoles are non-acidic and not physically connected with LAMP1 + tubules. Confocal microscopy showed that following 24 h PRZ treatment a minority of (small) vacuoles were positive for both Rab5 and LAMP1, whereas huge vacuoles were only positive for LAMP1 (Fig. 9C). Live cell imaging also confirmed that LAMP1 positive tubules interfered with cytokinesis, as indicated by LAMP1 + intercellular bridges between dividing cells (Suppl. Video Files Supplemental Video FilesA–C).

In experiments investigating whether PRZ induced tubulation is still reversible [6] when late endosomes/lysosomes are affected, we observed that the formation of QAPB/LAMP1 positive tubules was indeed reversible. Interestingly, tubules disappeared, but QAPB/LAMP1 positive vacuoles remained and were still visible 24 h after removal of PRZ (Fig. 9D). In summary, these experiments clearly show that PRZ induced vacuoles derive from swollen, obviously functionally impaired, early endosomes; this triggers the subsequent tubulation of lysosomes.

Zhang et al. also tested the role of the cytoskeleton in PRZ induced endosomal tubulation, but their results were inconclusive [6]. In our hands, using either cytochalasin-D (Cyto-D) or nocodazole (NDZ) to disrupt the actin cytoskeleton or microtubules, respectively, both the morphology of the cells and PRZ induced lysosomal tubulation were affected. Depolymerisation of F-actin with Cyto-D, which affects most endocytic pathways [44], interfered with the cellular transport of QAPB, indicated by QAPB-positive vesicles spread all over the cytoplasm with and without additional PRZ treatment, and also abolished the formation of the QAPB positive tubular pattern within 3 h (not

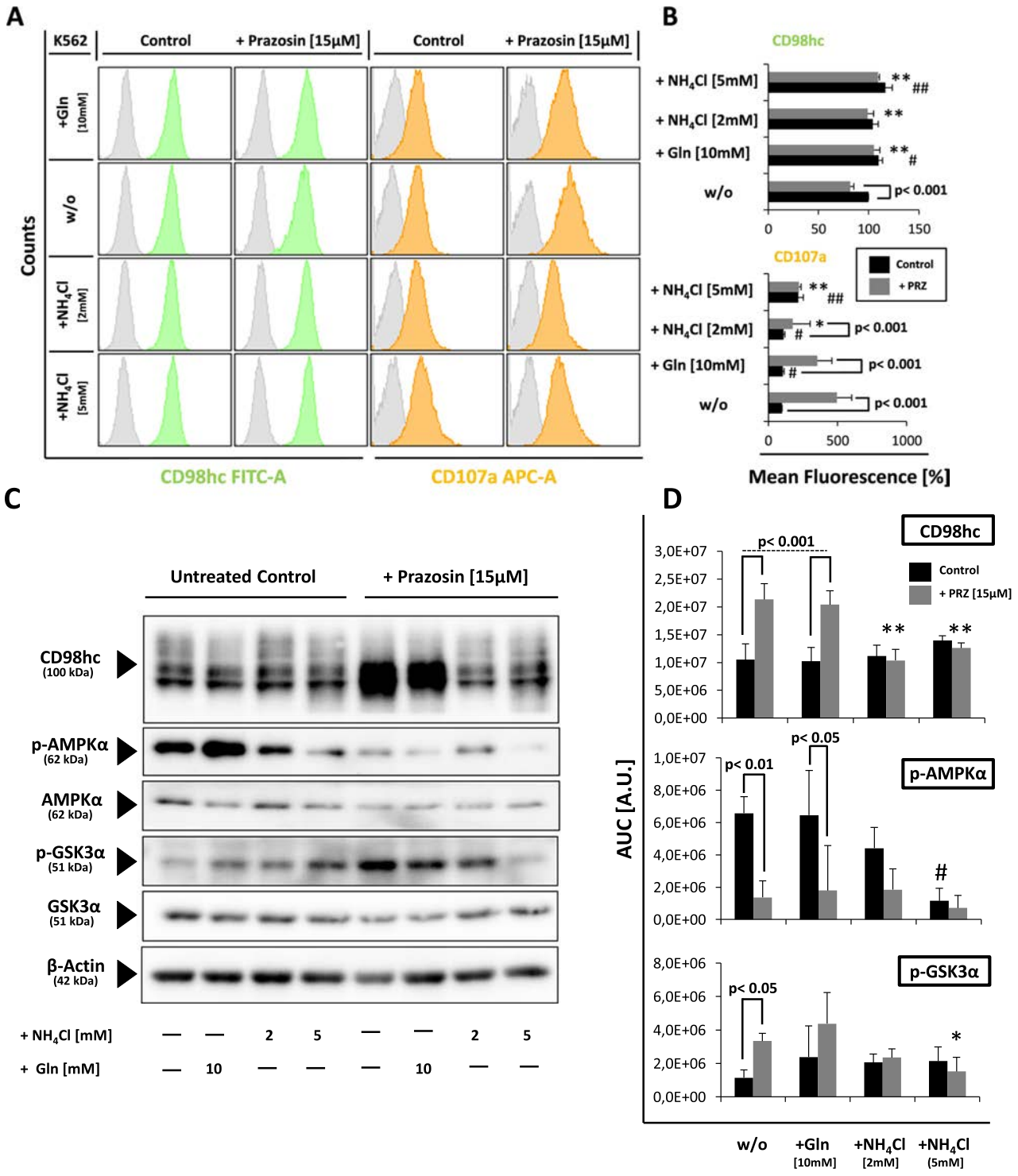

Fig. 7. PRZ modulates expression of CD98hc depending on the presence of Gln, or ammonia. A–B: CD107a (LAMP1) and CD98hc were analysed in parallel by flow cytometry following cultivation of cells with or without (w/o) 15 µM PRZ and varying supplementation of the medium with Gln or NH_4Cl. A: CD98hc/CD107a histograms of one representative experiment series. The grey peaks represent the emitted fluorescence of cells stained with an appropriate isotype-antibody. B: Statistical analysis of CD98hc/CD107a expression. *: $p < 0.01$, **: $p < 0.001$ versus PRZ-w/o, #: $p < 0.05$, ##: $p < 0.001$ versus Control-w/o according to ANOVA and Holm-Sidak post hoc analysis (CD98hc), respectively ANOVA on ranks and NKS post hoc analysis (CD107a). n = 5. C–D: Expression of CD98hc was assessed by western blotting in parallel to phosphorylation analysis of energy sensors AMPKα (p-AMPKα, Thr172) and GSKα (p-GSK3α, Ser21) following 24 h treatment of K562 cells with 15 µM PRZ either with or without (w/o) addition of Gln or NH_4Cl to the medium. C: Representative blots of one out of four independent experiment series. D: Densitometry results using ImageJ presented as area under the curve (AUC) values. n = 4 except AMPK-analysis: n = 3. *: $p < 0.05$, **: $p < 0.001$ versus PRZ-w/o, #: $p < 0.01$ versus Control-w/o, according to ANOVA or ANOVA on ranks and Holm-Sidak, or NKS post hoc analysis. A.U. = arbitrary units.

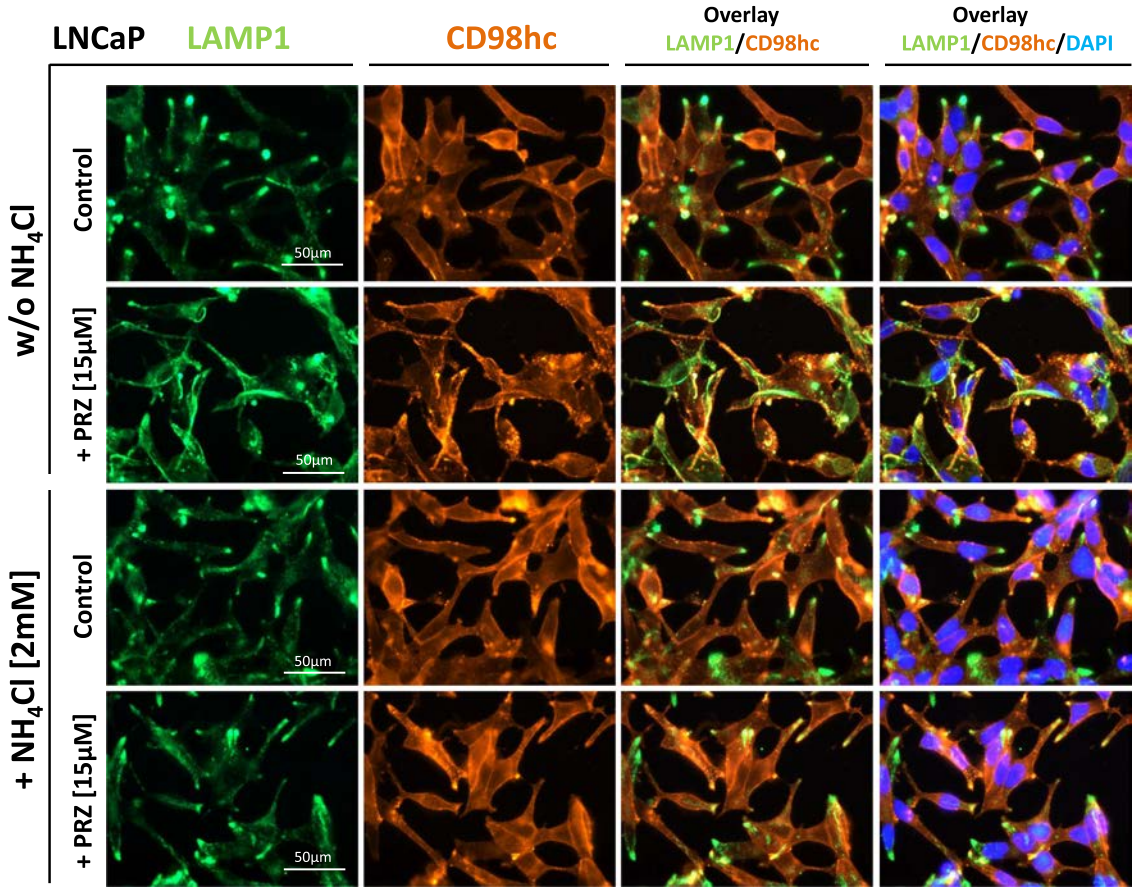

Fig. 8. Ammonia completely abrogates prazosin (PRZ) induced lysosomal tubulation. LNCaP cells were cultivated with/without (w/o) 15 µM PRZ with/w/o supplementation of the medium with 2 mM NH_4Cl for 24 h. Afterwards, cells were fixed and stained parallel with antibodies against CD98hc/LAMP1 and appropriate secondary antibodies. Nuclei were counterstained with DAPI. Within 24 h PRZ induces shuttling of CD98hc towards LAMP1 positive tubular endosomes/lysosomes. Lysosomal tubulation is completely neutralized by supplementation of the medium with NH_4Cl.

shown). Surprisingly, within 24 h we observed not solely polar protrusions as usual with PRZ, but the appearance of fine LAMP1 positive tubules all around the cell (Fig. 9E). Disruption of microtubules resulted in loss of the spindle shaped appearance of LNCaP cells. Before NDZ treated cells finally showed rounding and detached within 24 h, they spread on the surface of the flask and formed cell clusters (Fig. 9E). In NDZ treated cells, lysosomes were localized perinuclear in vesicular form in control cells, or in tubular form in the presence of PRZ (Fig. 9E). This observation is in good accordance with findings that lysosomal positioning and tubulation depend on microtubules [45–47].

A recent study by Saric et al. showed that lipopolysaccharide induced lysosomal tubulation in antigen presenting cells is abrogated by PI3K and mTor-inhibitors [46]. We tested the ability of the novel dual PI3K/mTOR inhibitor BEZ235 and the phosphatidylinositol-3,4,5-triphosphate (PIP3) antagonist Pit-1 [48] to interfere with PRZ induced lysosomal tubulation in LNCaP cells. In the presence of Pit-1 (but not BEZ235) LNCaP cells lost their spindle like morphology and formed cell clusters without visible contours of single cells. Similar effects were observed in cells treated with NDZ, but cells treated with Pit-1 showed no detachment within 24 h.

Interestingly, using these drugs either alone or in combination with QAPB/PRZ, we observed opposing results. Pre-treatment of cells with BEZ235 resulted in enhanced accumulation of QAPB and Lysotracker® (LT) in lysosomes, whereas Pit-1 inhibited the uptake of QAPB and lysosomal trapping of LT (Suppl. Fig. 9). Furthermore, lysosomal tubulation was not inhibited by BEZ235 up to concentrations of 500 nM, whereas in cells treated with 150 µM Pit-1 no lysosomal tubulation was evident with QAPB or LT. Additional IF staining showed that the morphology of LAMP1 positive endosomes/lysosomes was not altered by treatment of cells with either BEZ235 or Pit-1, suggesting a pH-dependent effect of those drugs on LT accumulation (Suppl. Fig. 9). LAMP1-IF staining further confirmed that lysosomal tubulation was completely stopped by Pit-1, but not by BEZ235. Parallel CD98hc staining showed a less pronounced tubular CD98hc fluorescence pattern and enhanced polar accumulation in PRZ/BEZ235 treated cells. In cells co-treated with Pit-1 and PRZ, the CD98hc staining remained at the cell membrane with no evident tubular structures, suggesting that endocytosis of PRZ/QAPB and subsequent lysosomal tubulation and trapping of CD98hc depend on PIP3. Experiments using the selective mTor inhibitor rapamycin (up to 1 µM) showed similar results as with BEZ235, ruling out the canonical PI3K-AKT-mTor pathway as the force driving PRZ induced lysosomal tubulation.

4. Discussion

4.1. Prazosin induced lysosomal tubulation interferes with cytokinesis

Prazosin (PRZ), the first clinically approved substance of the drug class of quinazoline-based α1-adrenoceptor antagonists, had a greater pro-apoptotic effect on malignant cells than other agents of this drug class, which is why we also focused on it [49,50]. PRZ recently attracted great attention for it anticancer potential, since Kahn et al. showed that PRZ can kill glioblastoma, a highly aggressive brain tumour with a poor prognosis [7]. Already in 2012 Zhang et al. were the first to associate PRZ with alterations in the endolysosomal system [6]. The authors showed that PRZ disturbs endocytic sorting due to an off-

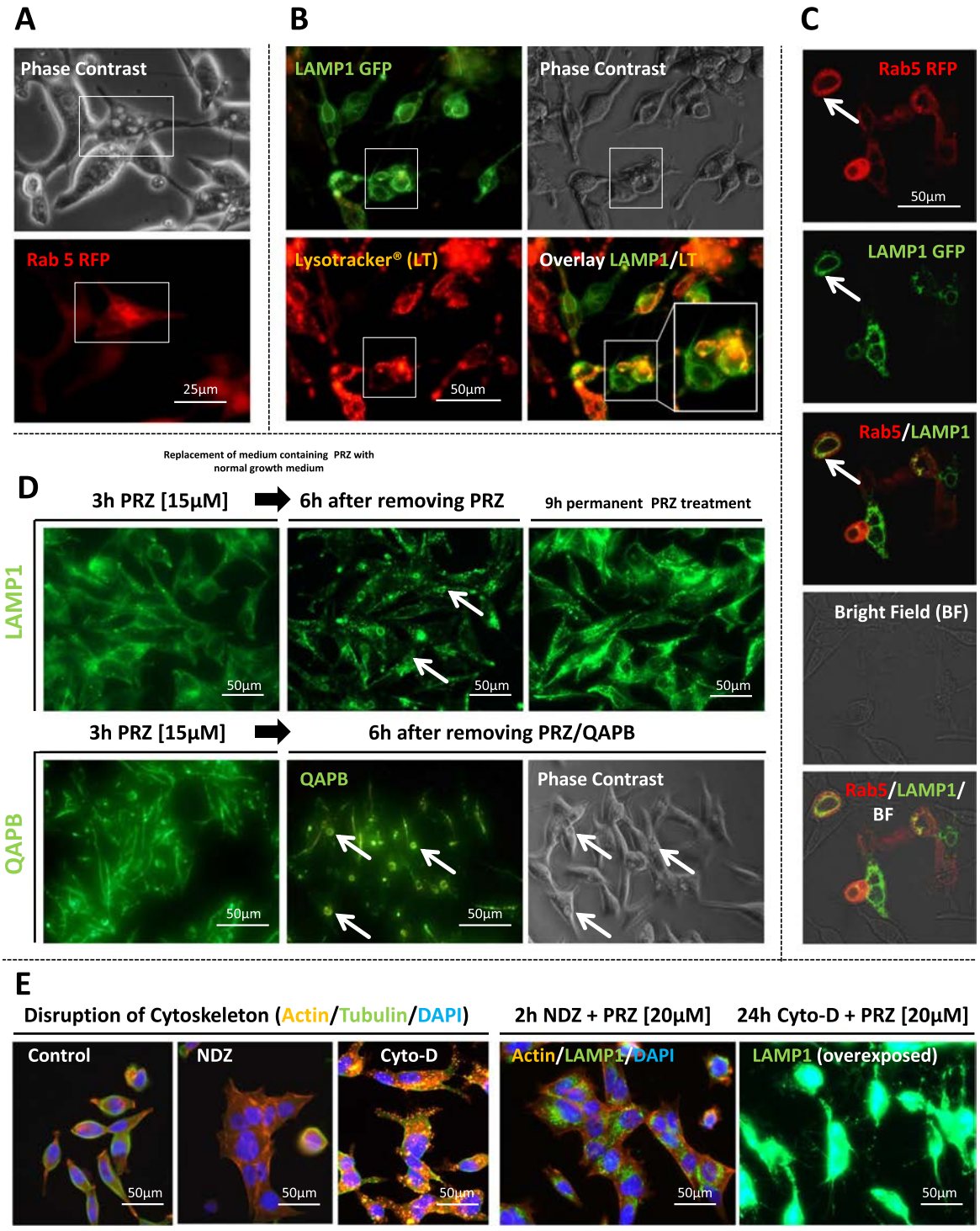

Fig. 9. Dynamics of prazosin (PRZ) induced lysosomal tubulation. A: PRZ induced vacuoles derive from Rab5 positive early endosomes. Rab5-RFP expressing LNCaP cells were treated with 20 µM PRZ for 10 min. Vacuoles (rectangles) are positive for Rab5. B: LAMP1-GFP expressing LNCaP cells were treated with 20 µM PRZ for 24 h and stained with Lysotracker® Red (LT). LAMP1 positive tubules, but not vacuoles (area shown in higher magnification in the rectangle) accumulate LT C: LNCaP cells expressing Rab5-RFP and LAMP1-GFP were exposed to 10 µM PRZ for 24 h and analysed by confocal microscopy. LAMP1 positive vacuoles appeared, but only a minority of them were Rab5 and LAMP1 double positive (arrow). D: Lysosomal tubulation is reversible. LNCaP cells were treated for 3 h (with/without addition of QAPB) with PRZ and incubated for further 6 h after removal of PRZ. Lysosomes were visualised by immunofluorescence staining; QAPB staining was observed with an inverted fluorescence microscope. Within 6 h post withdrawal of PRZ, LAMP1/QAPB positive tubules disappeared, but vacuoles remained. E: The role of microtubules (MT) and actin in PRZ induced lysosomal tubulation. In order to interfere with the functionality of MT or the actin cytoskeleton, LNCaP cells were either treated ± PRZ with 5 µM nocodazole (NDZ) for 2 h or 2 µg/ml cytochalasin-D (Cyto-D) for 24 h. Cells treated with NDZ showed a diffuse tubulin pattern. Cyto-D treatment clearly disrupted actin fibres as visualised by phalloidin staining. NDZ or combined PRZ/NDZ treatment resulted in perinuclear accumulation of vesicular or tubular (with PRZ) lysosomes. Long-term treatment of cells with Cyto-D/PRZ resulted in the formation of fine LAMP1 + protrusions all around the cell. The Cyto-D + PRZ picture was intentionally overexposed to visualise those structures.

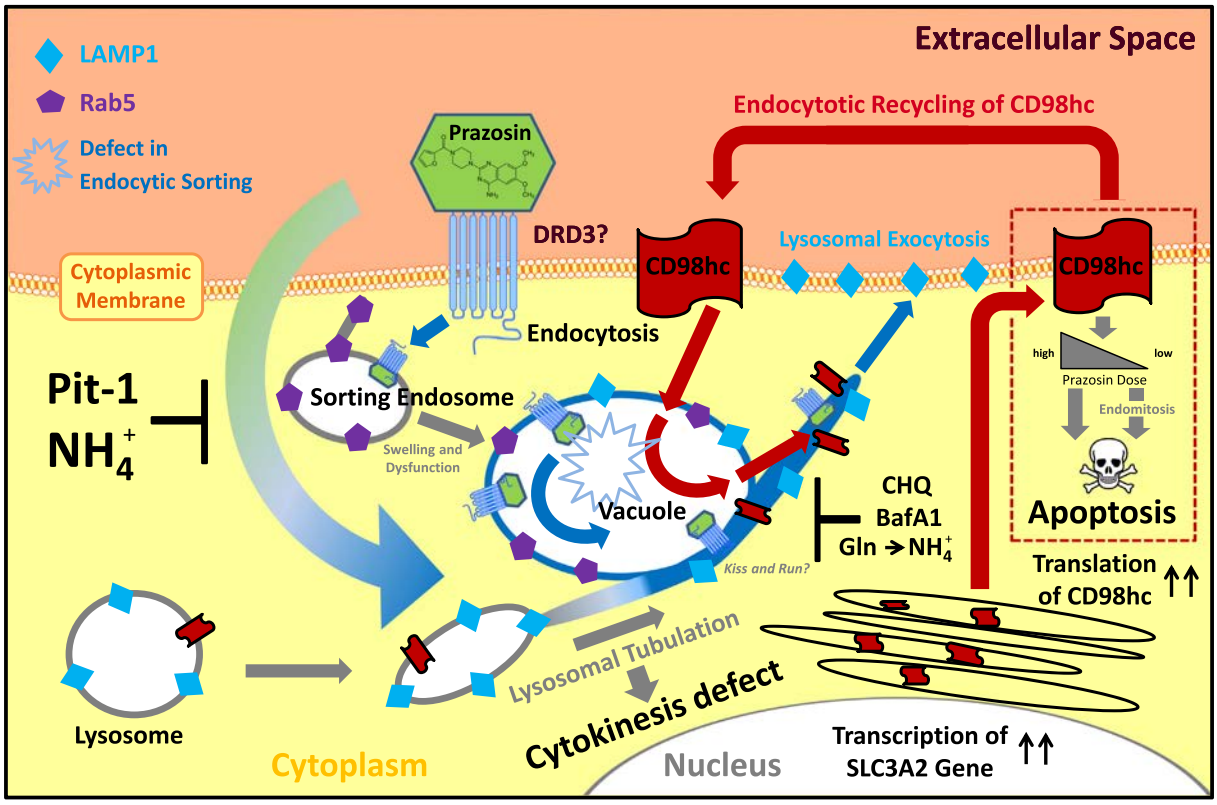

Fig. 10. Model of prazosin (PRZ) induced lysosomal tubulation and its interference with the trafficking of CD98hc. The model was created based on results obtained in our lab in the light of data obtained by Zhang et al. showing that PRZ interferes with endocytic sorting due to an interaction with dopamine receptor DRD3. [6]PRZ enters the cell via endocytosis through interaction with DRD3 or other still unknown receptors ending up in Rab5 positive early (=sorting) endosomes. This process results in obviously functionally impaired endosomes that swell and form huge LAMP1 positive vacuoles. According to our observations tubular lysosomes grow towards vacuoles but do not fuse with them suggesting a "kiss and run" exchange mechanism between vacuoles and lysosomes. Finally, tubular lysosomes, which interfere with the successful completion of cytokinesis, get in touch with the cell membrane, a process referred to as lysosomal exocytosis, indicated by increased expression of the lysosomal membrane protein LAMP1 at the cell membrane. Lysosomal tubulation interferes with the endocytic sorting of the oncoprotein CD98hc, which is misrouted towards lysosomal tubules. Transcription and translation of CD98hc are induced in response to PRZ treatment to maintain surface expression of CD98hc. Depending on PRZ dose CD98hc expression favours endoreplication and apoptosis. Lysomototropic agents – i.e. ammonia as by-product of glutaminolysis, chloroquine (CHQ) and the v-ATPase inhibitor bafilomycin A1 (BafA1) interfere with PRZ induced lysosomal tubulation and the intracellular trafficking of CD98hc. Ammonia was defined as a potent antagonist of PRZ able to completely neutralize the cytotoxicity of PRZ and obviously independent of its documented alkalizing functions on the endolysosomal system. Pit-1 inhibits endocytosis of QAPB/PRZ, PRZ induced lysosomal tubulation and subsequent lysosomal trapping of CD98hc, indicating PIP3 dependent endocytosis of quinazolines.

target interaction with dopamine receptor DRD3, causing tubulation of endosomes and subsequent inhibition of cytokinesis [6]. We further found out more about the effects of PRZ on the endolysosomal system demonstrating that during long-term treatment of cells with PRZ the lysosomes also form a tubular pattern, which is reversible by lysomotropic agents and blockade of v-ATPase [15]. Live cell imaging showed that tubular LAMP1 positive structures did indeed interfere with the process of cytokinesis. This observation goes along with the finding of Rajamanoharan et al. that lysosomal activity in close proximity to the intercellular bridge plays an essential role in cytokinesis [51]. In 2001, Bergeland et al. have already shown that during cytokinesis lysosomes accumulate in the vicinity of the microtubule organization center [52]. Concerning the kinetics of PRZ induced lysosomal tubulation (modelled in Fig. 10) we observed that vacuoles deriving from early endosomes (EE) trigger the formation of LAMP1 positive tubules. This hypothesis is supported by the appearance of swollen EE, which are the "distribution centres" of intracellular vesicle trafficking [53], convincing hints that PRZ interferes with endocytic sorting [6] and the observation that huge QAPB positive vacuoles remain in the cytoplasm of cells following removal of PRZ. The pronounced swelling of EE is most probably due to osmotic imbalances in the vesicle lumen [54]. During long-term treatment of cells with PRZ Rab5 positive tubules disappeared, but LAMP1 positive tubules arose instead. In the light of the observation that vacuoles acquire LAMP1, maturation of EE towards late endosomes is thinkable, which is known to be accompanied by loss of EE tubular domains [55]. Tubular lysosomes obviously grow towards vacuoles but do not fuse with them. Because of the dynamics of vacuoles regarding their volume and their interaction with LAMP1 positive tubules we hypothesize that vacuoles attract lysosomes and subsequently exchange quinazoline bound proteins with tubular lysosomes via a "kiss and run" mechanism [56]. Tubular lysosomes subsequently grow towards and fuse with the cell membrane, as indicated by increased expression of the lysosomal membrane protein LAMP1 at the cell surface - technically representing a kind of lysosomal exocytosis [41]. However, we have no proof to date as to whether CD98hc is also shuttled back to the membrane via this pathway. Several research groups suggested a similar mode of action for antigen presenting cells (APC) of the immune system [46,47,57]. Antigen loaded class II MHC molecules were shown to be shuttled via LAMP1 positive tubular structures towards the cell membrane using microtubules as trafficking route. Moreover, the canonical PI3K-AKT-mTor pathway was found to be essential for lysosomal tubulation in APC [46]. We did not, however, observe that BEZ235, which targets multiple members of the mTor pathway simultaneously [58], interferes with the effects of PRZ on lysosomes. This means that physiological lysosomal tubulation in APC may be somehow functionally different compared to drug (PRZ)

induced lysosomal tubulation. Even though, the sensitivity of PRZ induced lysosomal tubulation towards the PIP3 antagonist Pit-1 suggests that PIP3 has an essential role in this process. A common feature of lysosomal tubulation in APC and PRZ treated cells is its dependence on microtubules. When microtubules were disrupted in PRZ treated cells, perinuclear tubular lysosomes accumulated, suggesting that PRZ induced lysosomal tubulation not in general but that the anterograde trafficking of tubular lysosomes depends on microtubules. Furthermore, the formation of QAPB positive tubules was also sensitive towards disruption of actin fibres. PRZ induced lysosomal tubulation therefore is conducted via interaction of vesicles of the endolysosomal system with actin filaments and microtubules.

4.2. CD98hc paves the way towards Mitotic Catastrophe of PRZ treated cells

Besides the characterization of the kinetics of PRZ induced lysosomal tubulation, we aimed primarily to identify further protein targets of PRZ responsible for the pro-apoptotic effects of quinazolines. We recently described that QAPB showed a relatively stable interaction with a protein complex that provided a possible window of opportunity for the identification of proteins involved in the cytotoxicity of PRZ [15]. We identified CD98hc, a protein whose trafficking and expression is modulated by PRZ and that is also a crucial factor for growth and survival of PRZ treated cells. We demonstrated that in the presence of PRZ, CD98hc is shuttled from the cell membrane towards tubular lysosomes. This is quite interesting because it is known that CIE cargo proteins normally traffic directly into Arf6-associated tubules after internalization and avoid lysosomal degradation [59]. LAT1 is also a known CIE cargo [16,60]. Unfortunately, due to unspecific binding of the LAT1 antibody we used, we cannot yet discriminate whether PRZ shuttles solely CD98hc-monomers and/or CD98hc-LAT1 heterodimers towards lysosomes, although we have also consistently identified LAT1 in the QAPB positive protein fraction (results not shown). Enhanced shuttling of CD98hc towards lysosomes is a phenomenon that was already described in 2002 to occur in cells under withdrawal of growth factors [61]. But even though we also confirmed that CD98hc in lysosomes of PRZ treated cells originates from the cell membrane, total CD98hc expression levels were highly elevated whereas expression at the cytoplasmic membrane was only slightly reduced or remained almost constant under these conditions. Accordingly, our hypothesis was that PRZ either acts as a ligand of CD98hc, stimulating endocytosis (and recycling) of its receptor, or interferes with endocytic sorting of CD98hc in an unspecific manner. Using HEK293T CD98hc knock out (KO) clones we observed that KO cells were still able to accumulate QAPB and also showed tubular lysosomes. It was then clear that CD98hc is not required for endocytosis of quinazolines per se and is also not causally responsible for PRZ induced lysosomal tubulation. We therefore conclude that CD98hc is rerouted towards tubular lysosomes when PRZ blocks endocytic sorting (Fig. 10).

Nevertheless, we found that CD98hc is a protein that significantly influences the fate of PRZ treated cells regarding growth and survival. When treated with high doses of PRZ, HEK293T WT cells, but CD98hc KO cells only to a limited extent, were able to synthesize DNA, favouring the genesis of a multinucleated phenotype. Interestingly, CD98hc was already associated manifold with the formation, due to induction of cell fusion, and occurrence of multinucleated giant cells in various cell types, including monocytes, trophoblasts and glioblastoma cells [62–64]. Since HEK293T CD98hc KO clones showed an overall reduced proliferative potential compared to WT cells, we hypothesize that lack of CD98hc delays the induction of apoptosis in cells in which cytokinesis is inhibited. It is well known that cytokinesis failure and the subsequent appearance of a binucleated (and multinucleated) phenotype cause genetic instability and apoptosis via so-called Mitotic Catastrophe [65]. This hypothesis is supported by the findings of Lin et al. that PRZ induces DNA damage stress in PC-3 prostate cancer cells [49]. Furthermore, Spencer et al. have demonstrated recently that PRZ sensitizes prostate cancer cells to docetaxel [66]. The latter is a chemotherapeutic agent which targets microtubules and induces cell death in cancer cells through induction of Mitotic Catastrophe [67]. Since highly proliferative cells and especially cancer cells are characterized by high CD98hc expression [16], CD98hc might pave the way towards Mitotic Catastrophe in cells treated with PRZ.

In the context of CD98hc and PRZ, cellular proliferation and survival, further studies should pay special attention to the role of integrins. Similar to CD98hc [60], it was shown in cancer cells expressing p53 mutants that recycling of β1-integrin (via EE) is accelerated, whereas degradation in lysosomes is bypassed [68]. As mentioned in the introduction, on the one hand quinazolines target integrins [14] and on the other hand CD98hc is associated with integrins and promotes integrin-signalling [16,20,21]. In line with these results it was recently shown that CD98hc plays a central role in acute myelogenous leukaemia (AML) via integrin binding [69]. In 2009 we had already shown that PRZ induces pronounced apoptosis in the AML cell line HEL [12]. But an open question still remains, as to whether solely inhibition of cytokinesis [12], which is a common feature of PRZ treated cells, and/or misrouting of CD98hc and subsequent adverse effects on integrin-signalling cause PRZ induced apoptosis in HEL cells. Most interestingly, it was shown by Sachlos et al. in 2012 that AML cells express DRD3 (and other dopamine receptors), which serves as an atypical receptor for PRZ [6,70]. This finding establishes a possible connection between DRD3, PRZ and CD98hc. Generally, the pro-proliferative and anti-apoptotic roles of CD98hc seem to be strongly cell and tissue dependent. For instance, CD98hc in AML cells seems to be crucial for integrin signalling, whereas the loss of CD98hc in the colon cell line LS174T sensitizes the cells towards inhibition of LAT1, suggesting an essential role of CD98hc as chaperone for LAT1 in this cells line [71].

Besides the role of CD98hc, our data clearly shows that PRZ also induces apoptosis independent of CD98hc suggesting alternative pro-apoptotic mechanisms.

4.3. Prazosin, ammonia and CD98hc: an intriguing love triangle

We found that ammonia, a by-product of glutaminolysis and amino acid metabolism in general, is able to completely neutralize the cytotoxicity of PRZ (Fig. 10). Routinely, commercial growth media are provided without Gln, since Gln is known to break down to ammonia and pyroglutamate during storage (Fig. 6) [72,73]. In a recent study, Zhang et al. demonstrated that during incubation of DMEM-medium (without cells) under standard cell culture conditions, approximately 1 mM ammonia is generated within 24 h [73]. In preliminary experiments (not shown) we compared the cytotoxicity of PRZ in dependence on the growth medium since the standardized recipes of DMEM and RPMI significantly differ regarding their supply of AA. Interestingly, growth of cells was inhibited in RPMI medium as described here, but surprisingly, the growth inhibitory effect of PRZ was weak or absent in DMEM medium. Catalysing the breakdown of Gln with L-ASP or supplementation of the (RPMI-) medium with NH_4Cl protected the cells against the cytotoxicity of PRZ, proving that the protective effect of Gln occurs via generation of ammonia. Supplementation of the medium with NH_4Cl also completely inhibited lysosomal tubulation and subsequent misrouting and upregulation of CD98hc. We therefore assume that when there is no misrouting of CD98hc, there is also no need to upregulate CD98hc. A limitation of our study is that so far, we can only speculate about the underlying protective mechanisms of NH_4Cl. There is validated information that ammonia, similarly to CHQ and BafA1, alkalizes the pH in vesicles of the endolysosomal system. However, in order to alkalize lysosomes, much higher concentrations are routinely used than in our study [25]. At the moment, we can offer a highly speculative but interesting hypothesis that PRZ and ammonia compete for the same binding site at the dopamine receptor DRD3. Interestingly, Zhang et al., who have already shown that PRZ enters the cell via

DRD3, also recently demonstrated that DRD3 acts as a cellular ammonia sensor but as yet no studies on the interaction of ammonia and PRZ at DRD3 have been published [73]. Our study is the first to partially close this gap, demonstrating an antagonistic effect of ammonia on the cytotoxicity of PRZ. It is well known that ammonia is a metabolite that is highly enriched in tumours, whereby enhanced glutaminolysis of tumour cells is seen as major source of ammonia [25,26]. Therefore, the antagonistic effects of ammonia might be important to overcome for the possible future use of quinazolines in chemotherapy.

Regarding the trafficking of CD98hc we also observed that treatment with CHQ and BafA1 results in accumulation of CD98hc in the cytoplasm. It is well known that luminal acidification of the endocytic pathway is required for vesicle trafficking and associated cellular functions [74]. Nonetheless, our study shows for the first time that the trafficking of CD98hc, which has an important role in cellular amino acid homeostasis, is sensitive towards manipulation of endocytic pH. Our study so revealed a new link between cellular pH control and bioenergetic mechanisms [75].

4.4. Conclusions

In synopsis, our study sheds new light on the process of PRZ induced lysosomal tubulation and shows for the first time that the endocytic recycling of the oncoprotein CD98hc can be modulated in vitro using FDA approved drugs. Our study further spotlights lysosomes as a hopeful new target for the treatment of cancer [76], thanks to the novel mechanism by which tubular lysosomes inhibit cytokinesis. Since CD98hc is seen as potential drug target in several types of human malignancies [16,21,70,71], our study can be expected to have high translational significance. Nevertheless, intensive research is still needed to translate our research into clinical practice and to fully understand the interactions between the intriguing love triangle of prazosin, ammonia and CD98hc.

Supplementary data to this article can be found online at https://doi.org/10.1016/j.bbamcr.2018.06.006.

Transparency document

The Transparency document associated with this article can be found, in online version.

Declarations

Acknowledgements

We wish to thank Eugenia Lamont for proofreading the manuscript and Katharina Meditz and Marie-Therese Frisch for competent technical support. Furthermore, we want to thank Andrea Groselj-Strele for her help concerning analysis of drug interaction studies.

Funding

This work was supported by a grant from the Austrian Science Fund (FWF), P24006 (to RF); the Franz Lanyar Foundation (to RF) and by private donations obtained with a fund-raising campaign kindly initiated by MEFOgraz (to RF). The identity of donors remained completely anonymous for all authors involved, excluding any conflict of interest in this regard. Furthermore, our study was supported by the Spanish Ministry of Science and Innovation, SAF2015-64869-R-FEDER (to MP) and the Government of Catalonia, Grant SGR2009-1355 (to MP). SCC is a recipient of a Severo Ochoa Fellowship.

Authors' contributions

RF designed the study, performed experiments, analysed and interpreted data and wrote the manuscript. AS, MS, RBG, and BR contributed to conception, interpretation of data, design of the study and development of methodology. AS, VH, GLE, NMA, NE, TML, MS, and BR performed experiments and contributed to data analysis and interpretation. SCC and MP generated and provided CD98hc knockout cells and discussed obtained data. MAN contributed to the acquisition of data. AS, TML, EF, SCC, MP, BR and RBG contributed to reviewing of the manuscript. EF contributed to study supervision and provided essential materials. All authors read and approved the final version of the manuscript.

Competing interests

The authors declare that they have no competing interests.

References

[1] C.M. Benning, N. Kyprianou, Quinazoline-derived alpha1-adrenoceptor antagonists induce prostate cancer cell apoptosis via an alpha1-adrenoceptor-independent action, Cancer Res. 62 (2002) 597–602.
[2] J.R. Gonzalez-Juanatey, M.J. Iglesias, C. Alcaide, R. Pineiro, F. Lago, Doxazosin induces apoptosis in cardiomyocytes cultured in vitro by a mechanism that is independent of alpha1-adrenergic blockade, Circulation 107 (2003) 127–131.
[3] M.A. Fernando, A.P. Heaney, Alpha1-adrenergic receptor antagonists: novel therapy for pituitary adenomas, Mol. Endocrinol. 19 (2005) 3085–3096.
[4] H. Hui, M.A. Fernando, A.P. Heaney, The alpha1-adrenergic receptor antagonist doxazosin inhibits EGFR and NF-kappaB signalling to induce breast cancer cell apoptosis, Eur. J. Cancer 44 (2008) 160–166.
[5] R. Fuchs, E. Schraml, G. Leitinger, I. Stelzer, N. Allard, H.S. Haas, et al., alpha1-Adrenergic drugs modulate differentiation and cell death of human erythroleukemia cells through non adrenergic mechanism, Exp. Cell Res. 317 (2011) 2239–2251.
[6] X. Zhang, W. Wang, A.V. Bedigian, M.L. Coughlin, T.J. Mitchison, U.S. Eggert, Dopamine receptor D3 regulates endocytic sorting by a prazosin-sensitive interaction with the coatomer COPI, Proc. Natl. Acad. Sci. U. S. A. 109 (2012) 12485–12490.
[7] S.A. Kahn, S.L. Costa, S. Gholamin, R.T. Nitta, L.G. Dubois, M. Feve, et al., The antihypertensive drug prazosin inhibits glioblastoma growth via the PKC-dependent inhibition of the AKT pathway, Embo Mol. Med. 8 (2016) 511–526.
[8] M.S. Park, B.R. Kim, S.M. Dong, S.H. Lee, D.Y. Kim, S.B. Rho, The antihypertension drug doxazosin inhibits tumor growth and angiogenesis by decreasing VEGFR-2/Akt/mTOR signaling and VEGF and HIF-1alpha expression, Oncotarget 5 (2014) 4935–4944.
[9] C.F. Chiang, E.L. Son, G.J. Wu, Oral treatment of the TRAMP mice with doxazosin suppresses prostate tumor growth and metastasis, Prostate 64 (2005) 408–418.
[10] N. Kyprianou, C.M. Benning, Suppression of human prostate cancer cell growth by alpha1-adrenoceptor antagonists doxazosin and terazosin via induction of apoptosis, Cancer Res. 60 (2000) 4550–4555.
[11] E.J. Siddiqui, M. Shabbir, C.S. Thompson, F.H. Mumtaz, D.P. Mikhailidis, Growth inhibitory effect of doxazosin on prostate and bladder cancer cells. Is the serotonin receptor pathway involved? Anticancer Res. 25 (2005) 4281–4286.
[12] R. Fuchs, I. Stelzer, H.S. Haas, G. Leitinger, K. Schauenstein, A. Sadjak, The alpha1-adrenergic receptor antagonists, benoxathian and prazosin, induce apoptosis and a switch towards megakaryocytic differentiation in human erythroleukemia cells, Ann. Hematol. 88 (2009) 989–997.
[13] R. Fuchs, G. Schwach, A. Stracke, N. Meier-Allard, M. Absenger, E. Ingolic, et al., The anti-hypertensive drug prazosin induces apoptosis in the medullary thyroid carcinoma cell line TT, Anticancer Res. 35 (2015) 31–38.
[14] S. Sakamoto, S. Schwarze, N. Kyprianou, Anoikis disruption of focal adhesion-Akt signaling impairs renal cell carcinoma, Eur. Urol. 59 (2011) 734–744.
[15] R. Fuchs, A. Stracke, N. Ebner, C.W. Zeller, A.M. Raninger, M. Schittmayer, et al., The cytotoxicity of the alpha1-adrenoceptor antagonist prazosin is linked to an endocytotic mechanism equivalent to transport-P, Toxicology 338 (2015) 17–29.
[16] J.M. Cantor, M.H. Ginsberg, CD98 at the crossroads of adaptive immunity and cancer, J. Cell Sci. 125 (2012) 1373–1382.
[17] L.R. de la Ballina, S. Cano-Crespo, E. Gonzalez-Munoz, S. Bial, S. Estrach, L. Cailleteau, et al., Amino acid transport associated to cluster of differentiation 98 heavy chain (CD98hc) is at the cross-road of oxidative stress and amino acid availability, J. Biol. Chem. 291 (2016) 9700–9711.
[18] R. Milkereit, A. Persaud, L. Vanoaica, A. Guetg, F. Verrey, D. Rotin, LAPTM4b recruits the LAT1-4F2hc Leu transporter to lysosomes and promotes mTORC1 activation, Nat. Commun. 6 (2015) 7250.
[19] A. Santiago-Gomez, J.I. Barrasa, N. Olmo, E. Lecona, H. Burghardt, M. Palacin, et al., 4F2hc-silencing impairs tumorigenicity of HeLa cells via modulation of galectin-3 and beta-catenin signaling, and MMP-2 expression, Bba-Mol. Cell Res. 1833 (2013) 2045–2056.
[20] C.C. Feral, N. Nishiya, C.A. Fenczik, H. Stuhlmann, M. Slepak, M.H. Ginsberg, CD98hc (SLC3A2) mediates integrin signaling, Proc. Natl. Acad. Sci. U. S. A. 102 (2005) 355–360.
[21] G.W. Prager, C.C. Feral, C. Kim, J. Han, M.H. Ginsberg, CD98hc (SLC3A2) interaction with the integrin beta subunit cytoplasmic domain mediates adhesive signaling, J. Biol. Chem. 282 (2007) 24477–24484.

[22] M. Poettler, M. Unseld, K. Braemswig, A. Haitel, C.C. Zielinski, G.W. Prager, CD98hc (SLC3A2) drives integrin-dependent renal cancer cell behavior, Mol. Cancer 12 (2013) 169.
[23] J.B. Garrison, N. Kyprianou, Doxazosin induces apoptosis of benign and malignant prostate cells via a death receptor-mediated pathway, Cancer Res. 66 (2006) 464–472.
[24] G. Manic, F. Obrist, G. Kroemer, I. Vitale, L. Galluzzi, Chloroquine and hydroxychloroquine for cancer therapy, Mol. Cell Oncol. 1 (2014) e29911.
[25] C.H. Eng, K. Yu, J. Lucas, E. White, R.T. Abraham, Ammonia derived from glutaminolysis is a diffusible regulator of autophagy, Sci. Signal. 3 (2010) ra31.
[26] A. Merhi, P. Delree, A.M. Marini, The metabolic waste ammonium regulates mTORC2 and mTORC1 signaling, Sci. Rep. 7 (2017) 44602.
[27] R. Fuchs, E. Schraml, G. Leitinger, I. Letofsky-Papst, I. Stelzer, H.S. Haas, et al., alpha1-adrenergic drugs exhibit affinity to a thapsigargin-sensitive binding site and interfere with the intracellular Ca2+ homeostasis in human erythroleukemia cells, Exp. Cell Res. 317 (2011) 2969–2980.
[28] C.A. Eyster, J.D. Higginson, R. Huebner, N. Porat-Shliom, R. Weigert, W.W. Wu, et al., Discovery of new cargo proteins that enter cells through Clathrin-independent endocytosis, Traffic 10 (2009) 590–599.
[29] M. Capestrano, S. Mariggio, G. Perinetti, A.V. Egorova, S. Iacobacci, M. Santoro, et al., Cytosolic phospholipase A(2)epsilon drives recycling through the clathrin-independent endocytic route, J. Cell Sci. 127 (2014) 977–993.
[30] D.S. Xu, M.E. Hemler, Metabolic activation-related CD147-CD98 complex, Mol. Cell. Proteomics 4 (2005) 1061–1071.
[31] N.S. Verkaik, J. Trapman, J.C. Romijn, T.H. Van der Kwast, G.J. Van Steenbrugge, Down-regulation of CD44 expression in human prostatic carcinoma cell lines is correlated with DNA hypermethylation, Int. J. Cancer 80 (1999) 439–443.
[32] E.G. Geier, A. Schlessinger, H. Fan, J.E. Gable, J.J. Irwin, A. Sali, et al., Structure-based ligand discovery for the large-neutral amino acid transporter 1, LAT-1, Proc. Natl. Acad. Sci. U. S. A. 110 (2013) 5480–5485.
[33] C. Kerksick, D. Willoughby, The antioxidant role of glutathione and N-acetyl-cysteine supplements and exercise-induced oxidative stress, J. Int. Soc. Sport Nutr. 2 (2005).
[34] P. Nicklin, P. Bergman, B.L. Zhang, E. Triantafellow, H. Wang, B. Nyfeler, et al., Bidirectional transport of amino acids regulates mTOR and autophagy, Cell 136 (2009) 521–534.
[35] L. Pochini, M. Scalise, M. Galluccio, C. Indiveri, Membrane transporters for the special amino acid glutamine: structure/function relationships and relevance to human health, Front. Chem. 2 (2014).
[36] C.T. Hensley, A.T. Wasti, R.J. Deberardinis, Glutamine and cancer: cell biology, physiology, and clinical opportunities, J. Clin. Invest. 123 (2013) 3678–3684.
[37] A.S. Krall, H.R. Christofk, Rethinking glutamine addiction, Nat. Cell Biol. 17 (2015) 1515–1517.
[38] R. Pieters, S.P. Hunger, J. Boos, C. Rizzari, L. Silverman, A. Baruchel, et al., L-asparaginase treatment in acute lymphoblastic leukemia, Am. Cancer Soc. 117 (2011) 238–249.
[39] P. Song, L. Ye, J.J. Fan, Y.B. Li, X. Zeng, Z.Y. Wang, et al., Asparaginase induces apoptosis and cytoprotective autophagy in chronic myeloid leukemia cells, Oncotarget 6 (2015) 3861–3873.
[40] Y.S. Dong, H.C. Yung, Glutamine deprivation induces growth inhibition in human prostate carcinoma LnCap cells, J. Cancer Prev. 16 (2011) 41–50.
[41] M.A. Samie, H. Xu, Lysosomal exocytosis and lipid storage disorders, J. Lipid Res. 55 (2014) 995–1009.
[42] F. Fei, X.F. Li, L. Xu, D.Y. Li, Z.P. Zhang, X. Guo, et al., CD147-CD98hc complex contributes to poor prognosis of non-small cell lung cancer patients through promoting cell proliferation via the PI3K/Akt signaling pathway, Ann. Surg. Oncol. 21 (2014) 4359–4368.
[43] P.P. Ruvolo, Y.H. Qiu, K.R. Coombes, N. Zhang, E.S. Neeley, V.R. Ruvolo, et al., Phosphorylation of GSK3 alpha/beta correlates with activation of AKT and is prognostic for poor overall survival in acute myeloid leukemia patients, Bba Clin. 4 (2015) 59–68.
[44] D. Dutta, J.G. Donaldson, Search for inhibitors of endocytosis: intended specificity and unintended consequences, Cell Logist. 2 (2012) 203–208.
[45] J. Pu, C.M. Guardia, T. Keren-Kaplan, J.S. Bonifacino, Mechanisms and functions of lysosome positioning, J. Cell Sci. 129 (2016) 4329–4339.
[46] A. Saric, V.E. Hipolito, J.G. Kay, J. Canton, C.N. Antonescu, R.J. Botelho, mTOR controls lysosome tubulation and antigen presentation in macrophages and dendritic cells, Mol. Biol. Cell 27 (2016) 321–333.
[47] X. Li, N. Rydzewski, A. Hider, X. Zhang, J. Yang, W. Wang, et al., A molecular mechanism to regulate lysosome motility for lysosome positioning and tubulation, Nat. Cell Biol. 18 (2016) 404–417.
[48] B. Miao, I. Skidan, J. Yang, A. Lugovskoy, M. Reibarkh, K. Long, et al., Small molecule inhibition of phosphatidylinositol-3,4,5-triphosphate (PIP3) binding to pleckstrin homology domains, Proc. Natl. Acad. Sci. U. S. A. 107 (2010) 20126–20131.
[49] S.C. Lin, S.C. Chueh, C.J. Hsiao, T.K. Li, T.H. Chen, C.H. Liao, et al., Prazosin displays anticancer activity against human prostate cancers: targeting DNA and cell cycle, Neoplasia 9 (2007) 830–839.
[50] A. Forbes, S. Anoopkumar-Dukie, R. Chess-Williams, C. McDermott, Relative cytotoxic potencies and cell death mechanisms of α1-adrenoceptor antagonists in prostate cancer cell lines, Prostate 76 (2016) 757–766.
[51] D. Rajamanoharan, H.V. Mccue, R.D. Burgoyne, L.P. Haynes, Modulation of phosphatidylinositol 4-phosphate levels by CaBP7 controls cytokinesis in mammalian cells, Mol. Biol. Cell 26 (2015) 1428–1439.
[52] T. Bergeland, J. Widerberg, O. Bakke, T.W. Nordeng, Mitotic partitioning of endosomes and lysosomes, Curr. Biol. 11 (2001) 644–651.
[53] M. Jovic, M. Sharma, J. Rahajeng, S. Caplan, The early endosome: a busy sorting station for proteins at the crossroads, Histol. Histopathol. 25 (2010) 99–112.
[54] N.D. Sonawane, F.C. Szoka, A.S. Verkman, Chloride accumulation and swelling in endosomes enhances DNA transfer by polyamine-DNA polyplexes, J. Biol. Chem. 278 (2003) 44826–44831.
[55] J. Huotari, A. Helenius, Endosome maturation, EMBO J. 30 (2011) 3481–3500.
[56] S. Duclos, R. Corsini, M. Desjardins, Remodeling of endosomes during lysosome biogenesis involves 'kiss and run' fusion events regulated by rab5, J. Cell Sci. 116 (2003) 907–918.
[57] J.M. Vyas, A.G. Van der Veen, H.L. Ploegh, The known unknowns of antigen processing and presentation, Nat. Rev. Immunol. 8 (2008) 607–618.
[58] Z.Y. Yu, G.F. Xie, G.T. Zhou, Y. Cheng, G.T. Zhang, G.M. Yao, et al., NVP-BEZ235, a novel dual PI3K-mTOR inhibitor displays anti-glioma activity and reduces chemoresistance to temozolomide in human glioma cells, Cancer Lett. 367 (2015) 58–68.
[59] D. Dutta, J.G. Donaldson, Sorting of Clathrin-independent cargo proteins depends on Rab35 delivered by Clathrin-mediated endocytosis, Traffic 16 (2015) 994–1009.
[60] L. Maldonado-Baez, C. Williamson, J.G. Donaldson, Clathrin-independent endocytosis: a cargo-centric view, Exp. Cell Res. 319 (2013) 2759–2769.
[61] A.L. Edinger, C.B. Thompson, Akt maintains cell size and survival by increasing mTOR-dependent nutrient uptake, Mol. Biol. Cell 13 (2002) 2276–2288.
[62] M. Tajima, S. Higuchi, Y. Higuchi, N. Miyamoto, A. Uchida, M. Ito, et al., Suppression of FRP-1/CD98-mediated multinucleated giant cell and osteoclast formation by an anti-FRP-1/CD98 mAb, HBJ 127, that inhibits c-src expression, Cell. Immunol. 193 (1999) 162–169.
[63] P. Dalton, H.C. Christian, C.W.G. Redman, I.L. Sargent, C.A.R. Boyd, Membrane trafficking of CD98 and its ligand galectin 3 in BeWo cells - implication for placental cell fusion, FEBS J. 274 (2007) 2715–2727.
[64] H. Takeuchi, T. Kubota, R. Kitai, T. Nakagawa, N. Hashimoto, CD98 immunoreactivity in multinucleated giant cells of glioblastomas: an immunohistochemical double labeling study, Neuropathology 28 (2008) 127–131.
[65] I. Vitale, L. Galluzzi, M. Castedo, G. Kroemer, Mitotic catastrophe: a mechanism for avoiding genomic instability, Nat. Rev. Mol. Cell Biol. 12 (2011) 384–391.
[66] B.H. Spencer, C.M. McDermott, R. Chess-Williams, D. Christie, S. Anoopkumar-Dukie, Prazosin but not tamsulosin sensitises PC-3 and LNCaP prostate cancer cells to docetaxel, Pharmacology 17 (2018) 10–18.
[67] D.L. Morse, H. Gray, C.M. Payne, R.J. Gillies, Docetaxel induces cell death through mitotic catastrophe in human breast cancer cells, Mol. Cancer Ther. 4 (2005) 1495–1504.
[68] I. Mellman, Y. Yarden, Endocytosis and cancer, Csh Perspect. Biol. 5 (2013).
[69] J. Bajaj, T. Konuma, N.K. Lytle, H.Y. Kwon, J.N. Ablack, J.M. Cantor, et al., CD98-mediated adhesive signaling enables the establishment and propagation of acute myelogenous leukemia, Cancer Cell 30 (2016) 792–805.
[70] E. Sachlos, R.M. Risueno, S. Laronde, Z. Shapovalova, J.H. Lee, J. Russell, et al., Identification of drugs including a dopamine receptor antagonist that selectively target cancer stem cells, Cell 149 (2012) 1284–1297.
[71] Y. Cormerais, S. Giuliano, R. Lefloch, B. Front, J. Durivault, E. Tambutte, et al., Genetic disruption of the multifunctional CD98/LAT1 complex demonstrates the key role of essential amino acid transport in the control of mTORC1 and tumor growth, Cancer Res. 76 (2016) 4481–4492.
[72] S. Heeneman, N.E.P. Deutz, W.A. Buurman, The concentrations of glutamine and ammonia in commercially available cell-culture media, J. Immunol. Methods 166 (1993) 85–91.
[73] Z.Y. Li, X.M. Ji, W.C. Wang, J.J. Liu, X.F. Liang, H. Wu, et al., Ammonia induces autophagy through dopamine receptor D3 and MTOR, PLoS One 11 (2016).
[74] C.L. Brett, D.N. Tukaye, S. Mukherjee, R.J. Rao, The yeast endosomal Na+(K+)/H + exchanger Nhx1 regulates cellular pH to control vesicle trafficking, Mol. Biol. Cell 16 (2005) 1396–1405.
[75] S.K. Parks, J. Chiche, J. Pouyssegur, Disrupting proton dynamics and energy metabolism for cancer therapy, Nat. Rev. Cancer 13 (2013) 611–623.
[76] S.F. Piao, R.K. Amaravadi, Targeting the lysosome in cancer, Ann. N. Y. Acad. Sci. 1371 (2016) 45–54.

Appendix II

Amino Acid Transport Associated to Cluster of Differentiation 98 Heavy Chain (CD98hc) is at the Cross-road of Oxidative Stress and Amino Acid Availability

Laura R. de la Ballina, Sara Cano-Crespo, Elena González-Muñoz, Susanna Bial, Soline Estrach, Laurence Cailleteau, Floriane Tissot, Hannelore Daniel, Antonio Zorzano, Mark H. Ginsberg, Manuel Palacín and Chloé C. Féral

THE JOURNAL OF BIOLOGICAL CHEMISTRY VOL. 291, NO. 18, pp. 9700–9711, April 29, 2016

Amino Acid Transport Associated to Cluster of Differentiation 98 Heavy Chain (CD98hc) Is at the Cross-road of Oxidative Stress and Amino Acid Availability*

Received for publication, November 16, 2015, and in revised form, February 25, 2016 Published, JBC Papers in Press, March 5, 2016, DOI 10.1074/jbc.M115.704254

Laura R. de la Ballina[‡§1], Sara Cano-Crespo[‡¶2,3], Elena González-Muñoz[‡‖2], Susanna Bial[‡¶], Soline Estrach[§], Laurence Cailleteau[§], Floriane Tissot[§4], Hannelore Daniel[**], Antonio Zorzano[‡ ‡‡], Mark H. Ginsberg[§§], Manuel Palacín[‡¶5,6], and Chloé C. Féral[§5,7]

From the [‡]Institute for Research in Biomedicine (IRB Barcelona), Barcelona Institute of Science and Technology, Baldiri Reixac 10, 08028 Barcelona, Spain and Department of Biochemistry and Molecular Biology, University of Barcelona, 08028 Barcelona, Spain, [§]INSERM, U1081, Institute for Research on Cancer and Aging, Nice (IRCAN), University of Nice Sophia-Antipolis, CNRS UMR 7284, 06107 Nice, France, [¶]Spanish Biomedical Research Network in Rare Diseases (CIBERER U-731), 08028 Barcelona, Spain, [‖]The Andalusian Cellular Reprogramming Laboratory (LARCEL), Fundación Progreso y Salud, 41092 Seville, Spain, [**]ZIEL Research Center of Nutrition and Food Sciences, Molecular Nutrition and Biochemistry Unit, Technische Universität München, Gregor-Mendel-Strasse 2, 85350 Freising, Germany, [‡‡]Spanish Biomedical Research Network in Diabetes and Associated Metabolic Diseases (CIBERDEM), 08028 Barcelona, Spain, and [§§]Department of Medicine, University of California, San Diego, La Jolla, California 92093

CD98hc functions as an amino acid (AA) transporter (together with another subunit) and integrin signaling enhancer. It is overexpressed in highly proliferative cells in both physiological and pathological conditions. CD98hc deletion induces strong impairment of cell proliferation *in vivo* and *in vitro*. Here, we investigate CD98hc-associated AA transport in cell survival and proliferation. By using chimeric versions of CD98hc, the two functions of the protein can be uncoupled. Although recovering the CD98hc AA transport capacity restores the *in vivo* and *in vitro* proliferation of CD98hc-null cells, reconstitution of the integrin signaling function of CD98hc is unable to restore *in vitro* proliferation of those cells. CD98hc-associated transporters (*i.e.* xCT, LAT1, and y^+LAT2 in wild-type cells) are crucial to control reactive oxygen species and intracellular AA levels, thus sustaining cell survival and proliferation. Moreover, in CD98hc-null cells the deficiency of CD98hc/xCT cannot be compensated, leading to cell death by ferroptosis. Supplementation of culture media with β-mercaptoethanol rescues CD98hc-deficient cell survival. Under such conditions null cells show oxidative stress and intracellular AA imbalance and, consequently, limited proliferation. CD98hc-null cells also present reduced intracellular levels of branched-chain and aromatic amino acids (BCAAs and ARO AAs, respectively) and induced expression of peptide transporter 1 (PEPT1). Interestingly, external supply of dipeptides containing BCAAs and ARO AAs rescues cell proliferation and compensates for impaired uptake of CD98hc/LAT1 and CD98hc/y^+LAT2. Our data establish CD98hc as a master protective gene at the cross-road of redox control and AA availability, making it a relevant therapeutic target in cancer.

Proliferative cells have an increased demand for nutrients such as glucose, AAs,[8] fatty acids, and vitamins. Heteromeric amino acid transporters are among several families of solute carriers (SLC Tables website) that mediate the influx or efflux of solutes (AAs among others) through the plasma membrane of mammalian cells. Heteromeric amino acid transporters are composed of a heavy (SLC3 family) and a light (L-type amino acid transporters (LATs) from SLC7 family) subunit, linked by a disulfide bridge (1). The heavy chain carries the complex to the plasma membrane (2), whereas the light chain constitutes

* This work was supported by grants from the Fondation ARC pour la Recherche sur le Cancer (ARC R14029AA) from the Ligue Contre le Cancer (R14035A) through the "Investments for the Future" LABEX SIGNALIFE, program reference ANR-11-LABX-0028-01 and by grants from the Spanish Ministerio de Economia y Competitividad (SAF2012-40080-C02–01 and SAF2015-64869-R) and the Generalitat de Catalunya (SGR2009-1355). IRB Barcelona is the recipient of a Severo Ochoa Award of Excellence from the Spanish Ministerio de Economia y Competitividad. The authors declare no competing financial interests.

[1] To whom correspondence may be addressed: Institute for Research in Biomedicine (IRB Barcelona), Baldiri Reixac 10, E-08028 Barcelona, Spain. Tel.: 34-93-403-47-01; E-mail: larual_rb@yahoo.es.

[2] Both authors share second authorship.

[3] Recipient of a Severo Ochoa doctoral fellowship.

[4] Recipient of a doctoral fellowship from INSERM Region Provence-Alpes Cote d'Azur/Cancéropôle PACA.

[5] Both authors share last authorship.

[6] To whom correspondence may be addressed: Institute for Research in Biomedicine (IRB Barcelona), Parc Científic de Barcelona, Baldiri Reixac 10, E-08028 Barcelona, Spain. Tel.: 34-93-403-71-99; E-mail: manuel.palacin@irbbarcelona.org.

[7] To whom correspondence may be addressed: INSERM, U1081, IRCAN, Université Nice-Sophia Antipolis, 28 avenue de Valombrose, F-06107 Nice, France. Tel.: 33-4-93-37-76-93; E-mail: chloe.feral@inserm.fr.

[8] The abbreviations used are: AA, amino acid; CD98hc, cluster of differentiation 98 heavy chain; β-ME, β-mercaptoethanol; BCAA, branched-chain amino acid; ARO AA, aromatic amino acid; PEPT1, peptide transporter 1; SLC, solute carrier; LAT, L-type amino acid transporter; ES cell, embryonic stem cell; AA^+, cationic amino acid; AA^0, neutral amino acid; SAS, sulfasalazine; NAC, *N*-acetylcysteine; Vit E, vitamin E; H_2DCFDA, 2′,7′-dichlorodihydrofluorescein diacetate; CHAC1, cation transport regulator homolog 1; RPLP0, ribosomal phosphoprotein, large, P0; Nrf2, nuclear factor erythroid 2-related factor; SNAT, sodium-coupled amino acid transporter; S6, ribosomal protein S6; eIF2α, eukaryotic initiation factor 2; ATF4, activating transcription factor 4; ER, endoplasmic reticulum; BCH, 2-aminobicyclo [2,2,1] heptane-2-carboxylic acid; CAT, cationic amino acid transporter; mTOR, mechanistic target of rapamycin; mTORC1, mTOR complex 1; ED, ectodomain.

the catalytic part of the transporter (3, 4). CD98hc (aka SLC3A2, 4F2, FRP1), the only ubiquitously expressed heavy subunit of heteromeric amino acid transporters, can bind to any of six light subunits (LAT1, LAT2, xCT, y^+LAT1, y^+LAT2, and asc1), which confer substrate specificity to the heterodimer, referred to as CD98 (1). All together these transporters cover a broad substrate spectrum, including all essential amino acids. Most heteromeric amino acid transporters are obligatory antiporters, meaning they mediate the simultaneous translocation of two AAs across the membrane in opposite directions (in a 1:1 stoichiometry). As a consequence of this mechanism of transport CD98 heterodimers are unable to generate net AA import. However, their up-regulation can increase the uptake of specific AAs (in exchange with others), rendering the proper AA pool to support cell growth.

Besides its function as transporter, CD98hc behaves as a co-receptor of β integrins and amplifies their downstream signaling (5, 6). A large body of evidence implicates CD98hc in cell proliferation during physiological and pathological conditions (7–9). Furthermore, the lack of CD98hc in mouse embryonic stem (ES) cells (in which exon 1, encoding the transmembrane domain of CD98hc, is replaced by a neomycin cassette) blocks cell proliferation *in vivo* (6). The CD98hc function as integrin signaling enhancer is sufficient to partially rescue the *in vivo* proliferation defect of CD98hc-null ES cells (6).

In this study we analyzed the role of CD98hc-associated AA transport in cell proliferation and teratoma formation. Interestingly, CD98hc presents specific binding capacity domains; whereas the intracellular domain is necessary and sufficient for interactions with β1 integrins (thus regulating their signaling capacities), the ectodomain (ED) is required for AA catalytic subunit association (10). We show that impaired proliferation of previously generated CD98hc-null ES cells and ES-derived fibroblasts (6) is restored by expression of chimeras that bind the AA transport catalytic subunits. Furthermore, such chimeras are able to specifically promote all AA transport activities observed in wild-type (WT) cells (namely CD98hc/xCT, system x_c^-; CD98hc/LAT1, system L and CD98hc/y^+LAT2, system y^+L). Next, we established the biological consequences of deleting CD98hc-mediated AA transport activities and found that ES-derived fibroblasts cannot compensate this deletion. Thus, invalidation of xCT activity results in iron-dependent oxidative (non-apoptotic) cell death called ferroptosis (11, 12). Culture medium supplementation with β-ME prevents ferroptosis and restores cell survival. In such conditions CD98hc-deficient cells present: (i) accumulation of reactive oxygen species, ii) modulation of CD98hc-independent AA transporters and up-regulation of peptide transporter PEPT1, (iii) intracellular AA imbalance with dramatic increase in cationic AAs (AA^+) and neutral AAs (AA^0) but reduced levels of BCAAs and ARO AAs, and (iv) concomitant limited cell proliferation. An external supply of BCAAs and ARO AAs in the form of dipeptides rescues cell proliferation. Thus, only medium supplementations (with β-ME and BCAA- and ARO AA-containing dipeptides) can compensate for disrupted uptake of essential amino acids by CD98hc-dependent transport systems x_c^-, L, and y^+L. Taken together, our results highlight the critical role of CD98hc-associated AA transport for cell survival and proliferation. We show that CD98hc functions as an integrative and protective hub between oxidative stress and low AA availability.

Experimental Procedures

Cell Culture—Wild-type and CD98hc-null mouse ES cells as well as corresponding ES-derived fibroblasts were cultured in complete DMEM high glucose (Gibco) medium supplemented with 10% v/v FBS (HyClone), 20 mM Hepes, pH 7.3, 100 μM non-essential amino acids (Gibco), 2 mM L-glutamine (Gibco), and if not stated otherwise, 100 μM β-ME (Sigma) at 37 °C and 5% v/v CO_2 in an humidified incubator.

Induction of Teratomas—A suspension of ES cells (1.5×10^6 cells per site) was injected subcutaneously into athymic BALB/c WEHI nude mice. After 33 days, teratomas were recovered and measured. To ensure similar expression levels in reconstitution experiments, each cell line was supplemented with CD98hc-null ES cells so that a similar number of expressing cells was injected with each clone.

Cell Proliferation Assay—On day 0, wild-type and CD98hc-null ES-derived fibroblasts were seeded in duplicate at 1×10^4 cells per 35-mm diameter dish. After 24 h of growth in complete supplemented DMEM medium (detailed above), cells were washed twice with PBS and put to grow in DMEM media with the corresponding additional supplementations (1 mM sulfasalazine (SAS), 1 mM *N*-acetylcysteine (NAC), 1 μg/ml vitamin E (Vit E), or BCAA- and ARO AA-containing dipeptides (see below) as indicated).

Flow Cytometry with 2′,7′-Dichlorodihydrofluorescein Diacetate (H_2DCFDA)-stained Cells—Briefly, cells were plated and cultured in normal conditions. Forty-eight hours after plating cells were washed with Hanks' balanced salt solution (HBSS) once and incubated with 1 μM H_2DCFDA (Molecular Probes) for 30 min at 37 °C. Then cells were harvested and washed in Hanks' balanced salt solution, and levels of intracellular fluorescence (non-fluorescent H_2DCFDA is converted to highly fluorescent 2′,7′-dichlorofluorescein (DCF) upon cleavage of the acetate groups by intracellular esterases and oxidation) were analyzed using a FACS Calibur.

Quantitative PCR/RNA Preparation—RNAs were extracted from cultured ES-derived fibroblasts using TRIzol reagent (Gibco). Reverse transcription was performed using Superscript II reverse transcriptase (Invitrogen). Sets of specific primers (cation transport regulator homolog 1 (CHAC1), sense (5′-CTTGAAGACCGTGAGGGCTG-3′), antisense (5′-GTGGGGTGGCCACATAGG); PEPT1, sense (5′-GCCGGACCAGATGCAGACGG-3′), antisense (5′-GCGGGTACACCACAGCGTCC-3′)) were used for amplification using 7900 HT Real Time PCR System (Applied Biosystems). Samples were normalized to ribosomal phosphoprotein, large, P0 (RPLP0) (sense, 5′-CACTGGTCTAGGACCCGAGAAG-3′; antisense, 5′-GGTGCCTCTGGAGATTTTCG-3′), using the ΔCt method. Statistical significance was determined by means of Student's *t* test.

AA Uptake Measurement—Transport activities were tested on whole cells as previously described (3) by measuring the transport of corresponding radiolabeled AA (10 μM). Transport activities were confirmed using 1 mM specific inhibitors (and pretreating cells with 1 mM *N*-ethylmaleimide for 3 min when needed) as indicated in the figure legends. (See Figs. 3 and 4.)

Western Blot—Whole cell lysates were prepared in radioimmunoprecipitation assay (RIPA) buffer (150 mM NaCl, 10 mM Tris, pH 7.2, 0.1% w/v SDS, 1% w/v Triton X-100, 1% w/v deoxycholate, 5 mM EDTA, 1 mM $NaVO_4$, 5 mM NaF, 1 mM PMSF, and protease inhibitor mixture (Roche Applied Science)) and centrifuged at 10,000 × *g* for 15 min at 4 °C. Protein lysates were quantified using the bicinchoninic acid (BCA) method (Thermo Scientific Pierce). Proteins were loaded (10 μg of total protein per lane) and resolved in 10% w/v or 12.5% w/v acrylamide gels by SDS-PAGE and transferred to Immobilon membranes (Millipore). They were then immunoblotted (see below) and detected by the ECL method.

Primary Antibodies—The following primary antibodies were used and validated for protein immunoblotting. (i) Anti-Nrf2 is a rabbit polyclonal antibody against synthetic peptide within human nuclear factor erythroid 2-related factor (Nrf2) C terminus; Abcam #ab62352 lot #GR149891–2; 1:2500; used to recognize mouse Nrf2. This antibody revealed a single band (with same mobility as the one validated in a previous report (13)) that responded to Nrf2 up-regulation in CD98hc-null cells treated with 25 μM *tert*-butylhydroquinone for 2 h. (ii) Anti-SNAT1 is a rabbit polyclonal antibody raised against human sodium-coupled amino acid transporter 1 (SNAT1); Santa Cruz #sc-67080 lot #G0208; 1:500. It reacts against mouse SNAT1, with several bands appearing in the film. Specificity of the ~50-kDa band was validated by its distinct disappearance after SNAT1 silencing in ES-derived wild-type fibroblasts and in mouse embryonic fibroblasts after lentivirus-mediated transduction of SNAT1 shRNA (Sigma, #TRCN0000069230) compared with control transduction with scrambled RNA (Sigma, #SHC00). (iii) Anti-p-S6 is a rabbit polyclonal antibody against a synthetic phosphopeptide corresponding to residues surrounding Ser-235 and Ser-236 of human ribosomal protein S6 (S6); Cell Signaling #2211S lot #22 Ref.02/2014; 1:2000. It reacts with S6 only when phosphorylated at serine 235 and 236 as shown in the datasheet. This antibody detected a single band, which decreased after treatment of murine fibroblasts with 2 μM rapamycin for 3 h, proving its specificity. (iv) Anti-S6 is a mouse monoclonal antibody against human S6; Santa Cruz #sc-74459 lot #G0708; 1:8000. This antibody reacts specifically against murine S6 as shown by the presence of a single band in the gels, corresponding to the size of the band revealed by anti-p-S6 but not responding to treatment with rapamycin. (v) Anti-p-eIF2α is a rabbit polyclonal antibody against a synthetic phosphopeptide corresponding to residues surrounding Ser-51 of the α subunit of human eukaryotic initiation factor 2 (eIF2); Cell Signaling #9721 lot #9 Ref.04/2012; 1:1000. Specificity against murine eIF2α was validated by up-regulation of phosphorylated-eIF2α after murine fibroblasts treatment with 10 nM thapsigargin for 3 h. (vi) Anti-eIF2α is a rabbit polyclonal antibody produced by immunizing animals with a synthetic peptide derived from the C-terminal sequence of eIF2α; Cell Signaling #9722 lot #13 Ref.04/2013; 1:1000. It was used to recognize murine total eIF2α. Specificity was validated by the presence of a unique band in the gels with the same size as p-eIF2α but not responding to thapsigargin treatment. (vii) Anti-ATF4 is a rabbit monoclonal antibody against human activating transcription factor 4 (ATF4); Cell Signaling D4B8 #11815 lot # 2; 1:1000. It was validated by up-regulation of the protein after thapsigargin treatment. (viii) Anti-PEPT1 is a custom made rabbit polyclonal antibody against human PEPT1. It was kindly provided and validated by Dr. H. Daniel (14, 15); 1:5000. (ix) Anti-tubulin (Sigma #T5168 lot #103M4773V; 1:1000) was used as a loading control, and correlation between total protein loaded and tubulin signal was checked.

Intracellular AA Quantification—Pelleted cells were weighed, and norleucine was added as an internal standard. Samples were deproteinized with 10% v/v trifluoroacetic acid and lysed by repeated freeze-thaw cycles. After centrifugation at maximum speed, supernatants were ultrafiltered through a 10-kDa spin column (Millipore) and dried using a vacuum chamber. Pellets were resuspended in loading buffer (Biochrom Ltd.), filtered, and injected for HPLC analysis. Quantitative analysis of AAs was performed using a Biochrom 30 amino acid analyzer (Biochrom Ltd.). AA peaks were identified on the basis of the retention times of the corresponding standards. Quantification was normalized by total protein.

Dipeptide Synthesis and Supplementation—BCAA- or ARO AA- and L-Ala dipeptides were synthesized following standard procedures by the ICTS "NANBIOSIS," more specifically by the Synthesis of Peptides Unit (U3) of the CIBER in Bioengineering, Biomaterials and Nanomedicine (CIBER-BBN) at the Barcelona Science Park. Briefly, dipeptides were synthesized in solution by coupling of the corresponding protected N- and C-terminal AAs using 2-(1H-benzotriazol-1-yl)-1,1,3-tetramethylmethyluronium hexafluoro phosphate (HBTU) in dimethylformamide as the coupling reagent. Once the reaction was finalized, protected dipeptides were precipitated with cold water, centrifuged, and washed again with cold water. Protecting groups were eliminated by the addition of trifluoroacetic acid, and after 1 h final dipeptides were precipitated by the addition on cold diethyl ether. Dipeptides were redissolved in H_2O and lyophilized. Purity was estimated by HPLC and HPLC-MS. Each dipeptide was supplemented at a concentration of 0.25× of the corresponding BCAA (isoleucine, leucine, and valine) or ARO AA (phenylalanine, tyrosine, and tryptophan) concentration in complete DMEM medium.

Results

CD98hc-associated AA Transport Function Is Sufficient to Support Cell Proliferation in Vivo—We previously found that (i) CD98hc-deficient ES cells fail to proliferate and form teratomas *in vivo* (6) and (ii) that the intracellular domain of CD98hc, required for enhanced β1 integrin signaling, rescues teratoma growth, although teratomas are as not as large as when CD98hc-null ES cells are reconstituted with wild-type CD98hc (6). Here we asked whether the partial teratoma growth observed could be ascribed to the lack of CD98hc-mediated AA transport function. Rescue experiments using CD98hc-CD69 chimeras (C69T98E98 and C98T69E98) (depicted in Fig. 1*A*) only able to bind CD98hc AA transport subunits but not integrins (10) showed restoration of *in vivo* cell proliferation. Importantly, reconstitution of CD98hc-null ES cells with wild-type CD98hc induced the strongest growth (Fig. 1, *B* and *C*). As expected, when CD98hc-null cells were reconstituted with CD69, no teratomas were formed (Fig. 1, *B*, *lower right panel*,

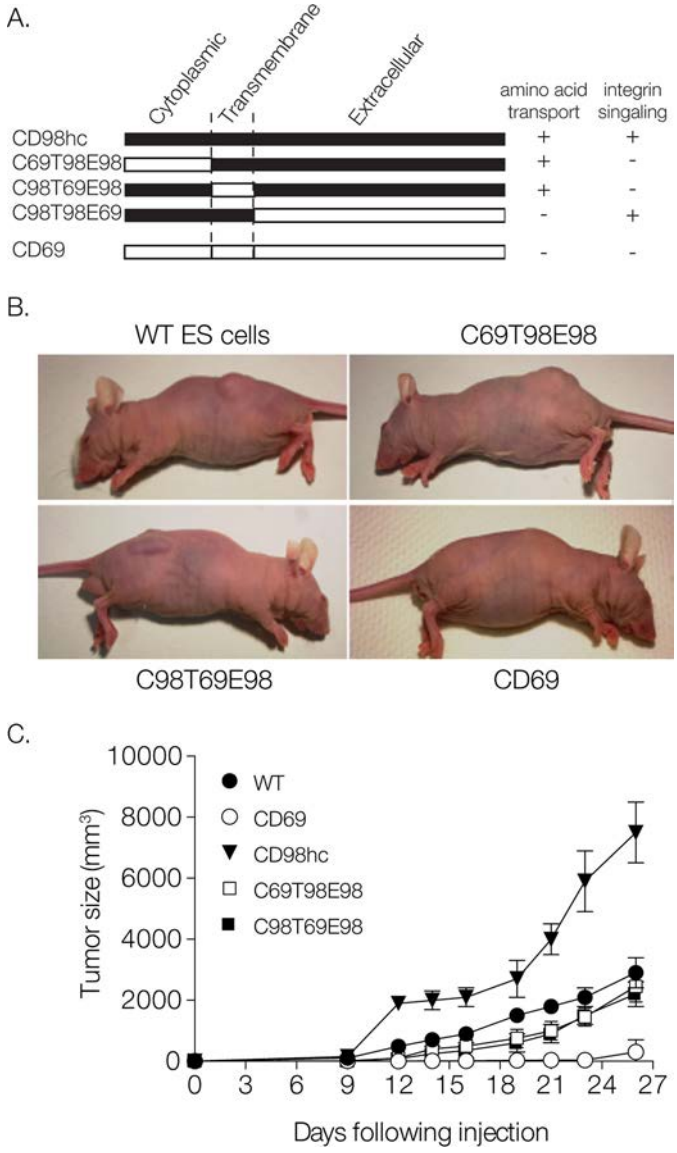

FIGURE 1. **CD98hc AA transport capacity restores cell proliferation *in vivo*.** *A*, depiction of chimeras of CD98hc and CD69 (type II transmembrane protein with functions unrelated to CD98hc) and their interactions with integrins or amino acid transporters. CD98hc protein is depicted in *black*, and CD69 is shown in *white*. Each chimera is defined by its cytoplasmic (*C*), transmembrane (*T*), and extracellular (*E*) domain derived from either CD98hc (*98*) or CD69 (*69*). *B*, mice were injected with corresponding ES cells and analyzed after 26 days. *C*, depicted is the quantification of tumor volumes (mean values ± S.E.) determined at various time points as previously described (6) for wild-type ES cells (●) and CD98hc-null ES cells reconstituted with CD69 (CD69, ○), full-length CD98hc (CD98hc, ▼), or with chimeras recovering only AA transport, namely C69T98E98 (□) or C98T69E98 (■). A similar expression level of full-length CD98hc and AA transport chimeras was confirmed by FACS (10).

and *C*). Thus, we show that (i) the portion of CD98hc that binds AA transporters promotes cell proliferation *in vivo* and (ii) maximal cell growth rates are only achieved when both CD98hc activities (AA transport and enhanced integrin signaling) are functional. These results suggest that both functions act in synergy to induce teratoma formation.

CD98hc Protects Cells against Oxidative Stress Leading to Cell Survival—Next, we analyzed the consequences of the lack of CD98hc-mediated AA transport activities. System x_c^- (CD98hc/xCT) is required for cystine uptake in exchange with glutamate. Hence, it plays a vital role in both redox control and cellular growth by supplying intracellular cysteine, a rate-limiting AA in the synthesis of GSH and necessary for protein synthesis (16). CD98hc-deficient ES-derived fibroblasts generated previously (6) did not survive under standard culture conditions (Fig. 2*A*, *left panel*) unless medium was supplemented with β-ME (Fig. 2*A*, *central panel*). xCT deficiency leads to ferroptosis. Up-regulation of endoplasmic reticulum (ER) stress response gene CHAC1 serves as a ferroptosis marker and can be reverted by adding β-ME to culture media (12), as shown in CD98hc-deficient cells (Fig. 2*B*) and in wild-type cells in which xCT transporter has been inhibited with sulfasalazine (*SAS*) (Fig. 2*B*). β-ME supplementation allowed reduction of extracellular cystine into free cysteine, which was subsequently imported by CD98hc-independent transporters (Fig. 2*A*, *right panel*), thus guaranteeing cell survival. We tested the effect of *N*-acetylcysteine (*NAC*) as an alternative source of cysteine and Vit E as an anti-oxidant (Fig. 2*C*) on cell survival. Vit E had no positive effect. In contrast, NAC protected CD98hc-null cells from death induced by the withdrawal of β-ME, thus rescuing cell proliferation (Fig. 2*C*). However, even when supplemented with β-ME, CD98hc-null fibroblasts showed a 1.4-fold increase of redox-sensitive probe H_2DCFDA labeling compared with wild-type fibroblasts (Fig. 2*D*). Because of the limitations in the reliability of such probe to accurately measure reactive oxygen species (17), we also analyzed in cells cultured in β-ME-supplemented medium the expression of the master regulator of intracellular antioxidant response Nrf2 (18). It presented indeed an increased expression (~9-fold) in CD98hc-null fibroblasts compared with the wild-type cells (Fig. 2*E*). In contrast, inhibition of xCT by SAS did not increase Nrf2 expression (Fig. 2*E*). Thus, CD98hc is required for *in vitro* cell survival because of its role in cystine uptake via x_c^- system, protecting cells from ferroptosis. Moreover, CD98hc ablation induces oxidative stress that is independent of xCT activity and non-reverted by β-ME.

CD98hc-mediated AA Transport (via xCT, LAT1, and y^+LAT2) Is Sufficient for Proper in Vitro Cell Proliferation—Both wild-type ES-induced teratomas (*in vivo*) and ES-derived fibroblasts (*in vitro*) express identical CD98hc-associated transporters as revealed by their mRNA expression (not shown): xCT (more expressed in cultured cells than *in vivo*, probably due to higher oxygen tension in culture than *in vivo* conditions (19)), LAT1, y^+LAT2, and to a lesser extent Asc1. Thus, the ES-derived fibroblasts provide a suitable *in vitro* model to establish the role of CD98hc-dependent AA transport in cell proliferation. Wild-type ES-derived fibroblasts presented transport activities corresponding to system x_c^-, system L, and system y^+L (Fig. 3*A*, *upper* and *middle panels*). CD98hc drives the trafficking of associated light chains to the plasma membrane (20). Thus, CD98hc-null cells should lack all CD98hc-associated transport subunits in the plasma membrane. Consistently, the system x_c^-, L, and y^+L transport activities were absent in CD98hc-deficient cells (Fig. 3*A*, *middle panel*). We show that the chimeras previously described to induce leucine transport (C69T98E98 and C98T69E98) (10) (Fig. 3*A*, *lower panel*) indeed recovered all CD98hc-mediated transport activities present in wild-type ES-derived fibroblasts (Fig. 3*A*, *middle panel*). In sharp contrast, the integrin-signaling

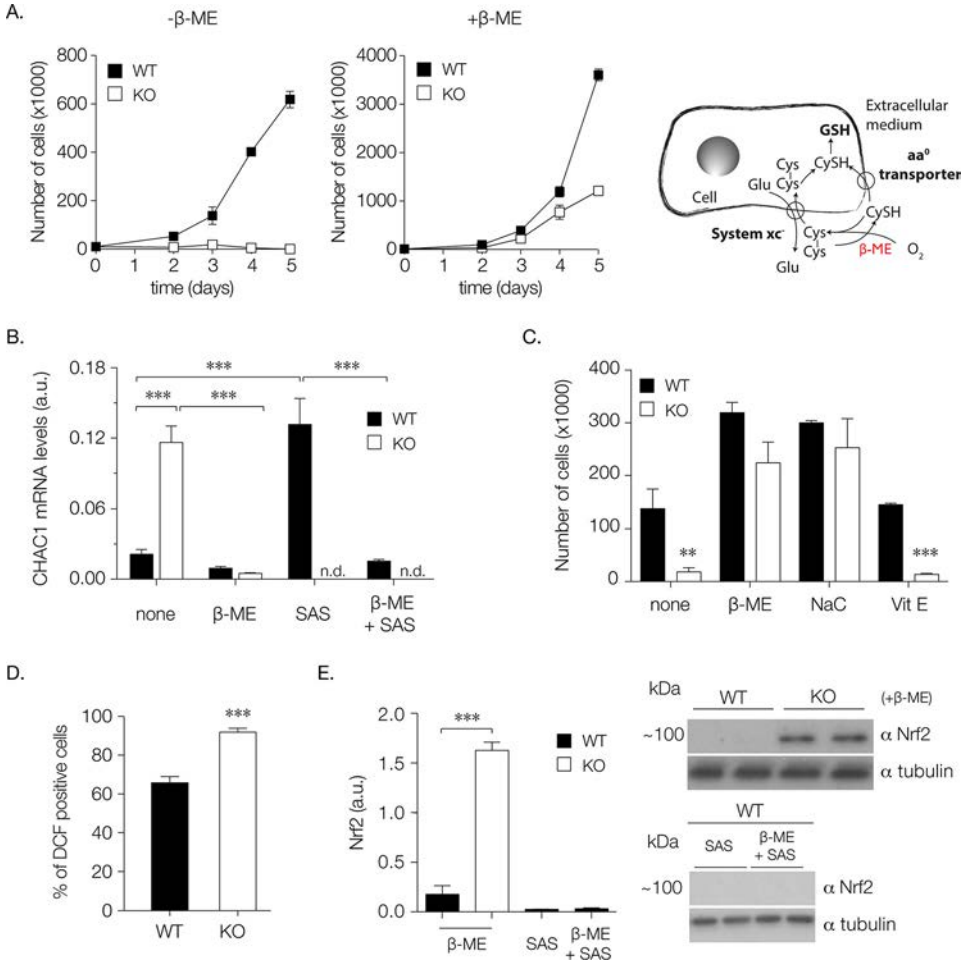

FIGURE 2. ***β*-Mercaptoethanol inhibits ferroptosis induced by depletion of CD98hc/xCT transporter and restores CD98hc-null cell survival.** *A*, WT and CD98hc-null (*KO*) fibroblast proliferation was compared in the absence (−) (*left panel*) and presence (+) (*middle panel*) of β-ME for 5 days. Cell counts at several time points are shown as the mean ± S.E. Similar results were obtained at least 3 times. Cystine (Cys-Cys) is transported by system x_c^- inside the cell where it is reduced to cysteine (CysSH, essential for the formation of reduced GSH). By supplementing the culture medium with β-ME, free CysSH is available extracellularly and can be imported inside the cell by CD98hc-independent neutral AA transporters (*right panel*). *B*, CHAC1 mRNA expression levels in WT (*solid bar*) and CD98hc-deficient fibroblasts (*KO*, *open bar*) grown with no additives (*none*) and in the presence of 100 μM β-ME, 1 mM SAS, or the combination of both (*β-ME + SAS*). RPLP0 was used as a housekeeping gene (not depicted). *n.d.*, not determined. Data are presented as the mean ± S.E. of eight independent experiments. *a.u.*, arbitrary units. *C*, WT (*solid bar*) and CD98hc-deficient (*KO*, *open bar*) fibroblasts were grown with no additives (*none*) or with 100 μM β-ME, 1 mM NAC, or 1 μg/ml Vit E for 48 h. Cell counts are expressed as the mean ± S.E. of duplicates. A representative experiment is shown; similar results were obtained at least 3 times. *D*, percentage of cells positive for the free radical sensor H_2DCFDA measured by flow cytometry. Data shows the mean ± S.E. of 12 measurements. E, Nrf2 protein expression in WT (*solid bar*) and CD98hc-null fibroblasts (*KO*, *open bar*) grown in the presence of 100 μM β-ME, 1 mM SAS, or the combination of both (*β-ME + SAS*). A representative Western blot of two independent experiments is shown. Data are normalized by tubulin expression. Quantification corresponds to the mean ± S.E. of six measurements. **, $p < 0.01$; ***, $p < 0.001$; Student's *t* test.

chimera (CD98T98E69) (Fig. 3*A*, *lower panel*) cannot mediate AA transport (Fig. 3*A*, *middle panel*). Next, to specifically study the effect of CD98hc-mediated AA transport on intrinsic cell proliferation capacity, we compared the *in vitro* cell proliferation rate of CD98hc-null fibroblasts when rescued with chimeras (described above) capable of restoring AA transport or integrin binding (10). First, we show that CD98hc-deficient cells present a major delay in proliferation *in vitro* compared with wild-type cells. This delay was rescued by reconstitution with full-length CD98hc (Fig. 3*B*, *upper panel*). Second, we observed a restoration of *in vitro* cell proliferation comparable with wild-type or full-length CD98hc-expressing cells only when null cells were reconstituted with AA transport chimeras (C69T98E98 and C98T69E98) (Fig. 3*B*, *lower panel*). Conversely, when only the capacity of integrin signaling (C98T98E69) was reconstituted in CD98hc-null cells, *in vitro* cell proliferation was still impaired (Fig. 3*B*, *lower panel*). Thus, CD98hc AA transport capacity is sufficient to drive proliferation *in vitro*, whereas the function as integrin signaling enhancer is dispensable. These results highlight the essential requirement of CD98hc-dependent AA transport for cell proliferation regardless of the surrounding environment.

CD98hc Supports the Balance of Intracellular AA Content—Deficiency of CD98hc and associated transporters had an impact on the intracellular AA content of CD98hc-null fibroblasts (Fig. 4*A*). The cell content of both AA^+ (Arg, Lys, and His) and AA^0 (Ala, Ser, Asn, Gln, and Met) was increased (2.9–4.3-fold and 1.2–2.7-fold, respectively) in CD98hc-deficient compared with wild-type fibroblasts. In contrast, BCAAs (Val, Leu, and Ile) and ARO AAs (Phe and Tyr) showed an intracellular content decrease of 0.5–0.6-fold in CD98hc-null when compared with wild-type cells (Fig. 4*A*). Analysis of the trans-

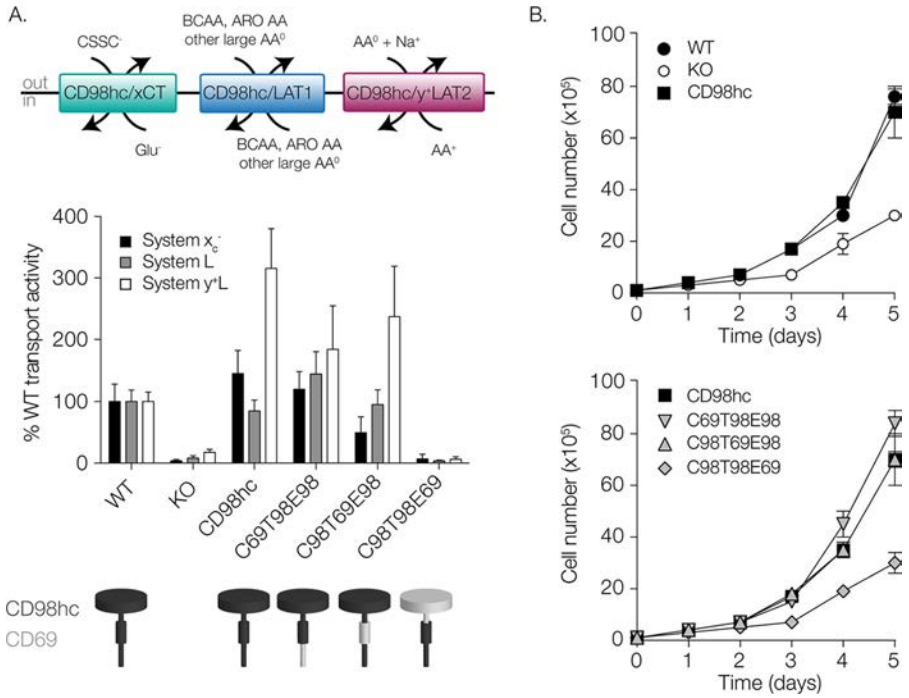

FIGURE 3. **CD98hc AA transport function is required for efficient cell proliferation *in vitro*.** *A*, depicted are the activities of transporters xCT (exchange of the anionic forms of cystine and glutamate), LAT1 (exchange of BCAAs, ARO AAs, and other large neutral AAs), and y^+LAT2 (exchange of cationic AAs and neutral AAs plus Na^+) across the plasma membrane (*upper panel*). AA transport activities of corresponding systems x_c^- (*black*), L (*gray*), and y^+L (*white*) in wild-type fibroblasts (*WT*), CD98hc-deficient (*KO*) fibroblasts, and CD98hc-null fibroblasts recovered with full-length CD98hc or chimeras recovering AA transport (C69T98E98 and C98T69E98) or integrin signaling (C98T98E69). Uptake activity is shown as a percentage of the levels of transport at 2 min (linear conditions) of wild-type cells for each CD98hc-associated transport system. Activities of the transport systems were determined as the uptake of the corresponding radiolabeled amino acid minus its uptake in the presence of specific inhibitor. Thus, system x_c^- represents the Na^+-independent uptake of L-Glu (10 μM) inhibitable by (*S*)-4-carboxyphenylglycine (1 mM); system L corresponds to the Na^+-independent L-Ile (10 μM) uptake that can be inhibited by 2-aminobicyclo [2,2,1] heptane-2-carboxylic acid (*BCH*) (1 mM), and system y^+L corresponds to the L-Arg (10 μM) uptake non-inhibitable by *N*-ethylmaleimide (1 mM) and inhibitable by L-Leu (1 mM) only when Na^+ is present. Transport data correspond to the mean ± S.E. of at least eight independent measurements (*middle panel*). Protein domains are depicted (CD98hc in *black*, CD69 in *gray*) (*lower panel*). *B*, Wild-type (WT, *black circle*) or CD98hc-deficient (*KO*, *white circle*) fibroblasts recovered with full-length CD98hc (*CD98hc*, *black square*) (*upper panel*) or CD98hc-null fibroblasts recovered with chimeras restoring AA transport (C69T98E98, *inverted grey triangle*, C98T69E98, *grey triangle*) or integrin signaling (C98T98E69, *grey diamond*) functions (*lower panel*, CD98hc is repeated as a reference) were seeded on day 0 and grown in the presence of β-ME for 5 days. Cells were counted every day. Results are expressed as the mean ± S.E. of duplicates. The experiment was repeated at least three times.

port of AAs with altered intracellular content revealed that, in the absence of CD98hc, the expression and activity of CD98hc-independent transporters was modulated. L-Arg uptake was much higher (~240%) in CD98hc-deficient than in wild-type ES-derived fibroblasts (Fig. 4*B*). We identified this transport activity as exclusively system y^+ (as *N*-ethylmaleimide specifically inactivates system y^+ without affecting system y^+L; Ref. 21), which presented an ~8-fold increase when compared with wild-type cells (Fig. 4*B*). Next, we tested whether the expression levels of cationic amino acid transporters (CATs) (system y^+) could account for such dramatically increased transport activity. In this regard we detected a 145-fold specific increase in CAT3 (but not CAT1 and CAT2) mRNA levels in CD98hc-null compared with wild-type fibroblasts (data not shown). Using the CAT3-specific inhibitor D-arginine (22), we measured an ~12-fold increase in CAT3 activity in CD98hc-null compared with wild-type cells (Fig. 4*C*). CAT3 is a CD98hc-independent transporter that mediates the Na^+-independent transport of cationic amino acids (1). Thus, the up-regulation of CAT3 in fibroblasts lacking CD98hc is in accordance with increased AA^+ intracellular content in such cells (Fig. 4*A*) as arginine, lysine, and histidine are substrates of murine CAT3 (22, 23). Regarding the transport of AA^0, by analyzing L-Ala uptake, we identified the presence of system A, a co-transporter of Na^+ and neutral AAs, mainly excluding BCAAs and ARO AAs (24) (Fig. 4*D*, *gray column*), system N, a Na^+-dependent transporter of neutral AAs (24) (Fig. 4*D*, *white column*), and others (part of L-Ala uptake was not ascribed to any specific transporter but could represent systems ASC, B^0 or $B^{0,+}$) (Fig. 4*D*, *black column*) in wild-type ES-derived fibroblasts. Depletion of CD98hc resulted in the disappearance of CD98hc-independent system A transport activity (Fig. 4*D*, *gray column*) along with the expression of SNAT1 transporter (Fig. 4*E*) (no differences in mRNA expression of SNAT2, the other system A isoform, were observed) (not shown). In contrast, system N was not changed in CD98hc-ablated cells (Fig. 4*C*, *white column*). System N couples AA import with H^+ efflux (1 AA: 1 Na^+ [symport]:1 H^+ [antiport]), making it less concentrative than system A (24). Despite the depletion of system A, the intracellular content of AA^0 (Ala, Ser, Asn, Gln, and Met) was increased in CD98hc-null cells (Fig. 4*A*). Thus, AA^0 accumulation would be generated by unidentified causes (*e.g.* reduced consumption rate) not related to AA^0 uptake. Ablation of CD98hc abrogated LAT1 transport activity (system L) (Fig. 3*A*, *middle panel*). LAT1 exchanges large AA^0, including BCAAs, ARO AAs, and histidine, methionine, and glutamine across the plasma membrane

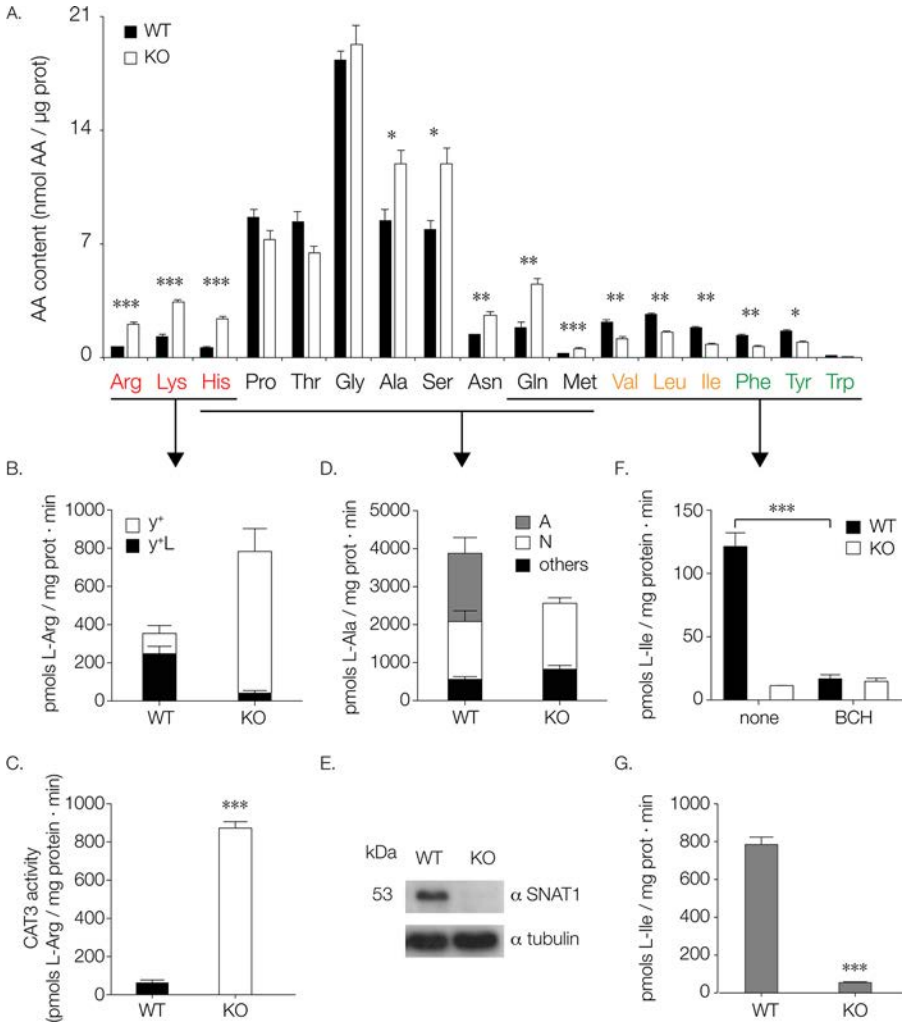

FIGURE 4. **CD98hc depletion leads to imbalanced intracellular AA content and to adaptations of CD98hc-independent transporters.** *A*, samples from WT (*solid bar*) and CD98hc-null (*KO*, *open bar*) fibroblasts were processed as described under "Experimental Procedures," and quantitative analysis of AAs was performed. Results are expressed as the mean ± S.E. of three independent measurements. AA^+ are presented in *red*, BCAAs are depicted in *yellow*, ARO AAs are in *green*, and the rest of AA^0 are in *black*. AAs are grouped and *underlined* to indicate that they are substrates of the corresponding transport system (below). *B*, Na^+-dependent L-Arg (10 μM) uptake at 2 min inhibitable by *N*-ethylmaleimide (1 mM) alone (system y^+, *white column*) or in combination with L-Leu (1 mM) (system y^+L, *black column*). Transport data correspond to the mean ± S.E. of at least 12 independent measurements. *C*, CAT3 transport activity measured as Na^+-independent uptake of L-Arg (10 μM) by WT (*solid bar*) and CD98hc-null (*KO*, *open bar*) fibroblasts inhibitable by D-Arg (5 mM) in the presence of L-Leu (1 mM). Transport data correspond to the mean ± S.E. of three independent experiments. *D*, Na^+-dependent L-Ala (100 μM) uptake at 2 min inhibitable by *N*-(methylamino)isobutyric acid (10 mM) alone (*system A*, *gray column*) or in combination with L-Asn (10 mM) (*system N*, *white column*). Residual transport is depicted as others (*black column*). Transport data correspond to the mean ± S.E. of at least eight independent measurements. *E*, protein expression of SNAT1 in WT and CD98hc-null (*KO*) fibroblasts. A representative Western blot is shown. Data are normalized by tubulin expression. Three independent experiments showed similar results. *F*, Na^+-independent L-Ile (10 μM) uptake at 2 min in the absence (none) and presence of BCH (1 mM) in WT (*solid bar*) and CD98hc-deficient (*KO*, *open bar*) fibroblasts. Transport data correspond to the mean ± S.E. of at least eight independent measurements. *G*, L-Ile (10 μM) uptake levels at 2 min in the presence of Na^+ in WT (*solid bar*) and CD98hc-null fibroblasts (*KO*, *open bar*). Transport data correspond to the mean ± S.E. of at least 12 independent measurements. *, $p < 0.05$; **, $p < 0.01$; ***, $p < 0.001$; Student's *t* test.

(25). System L has four isoforms, two associated with CD98hc (LAT1 and LAT2) and two independent of CD98hc (LAT3 and LAT4) (1, 26). All these transporters are Na^+-independent and can be inhibited by BCH, the leucine analog 2-aminobicyclo [2,2,1] heptane-2-carboxylic acid. Interestingly, in CD98hc-null cells, there was no Na^+-independent transport of L-Ile inhibitable by BCH (Fig. 4*F*). Thus, no CD98hc-independent isoform of system L compensated for LAT1 ablation. Moreover, CD98hc-deficient cells presented only ~10% of wild-type L-Ile uptake in Na^+-containing transport medium (Fig. 4*G*), thus arguing in favor of the absence of an efficient compensation for LAT1 by a Na^+-dependent transporter. Reduced intracellular BCAA and ARO AA content in CD98hc-null cells (Fig. 4*A*) is consistent with this lack of compensation for LAT1 transport and might underlie the proliferation defect of such cells.

Neither the Mechanistic Target of Rapamycin (mTOR) nor the Integrated Stress Response Is Responsible for CD98hc-null Cell Proliferation Deficiency—The mTOR and its downstream effector mTOR complex 1 (mTORC1) play a central role in cell growth and proliferation by responding to amino acid (*i.e.* leucine, arginine, glutamine) availability (27–30). mTORC1 phosphorylates and activates ribosomal protein S6 (S6) kinase that, in turn, mediates the phosphorylation of S6, an integral component of the 40S subunit of the ribosome (29, 31). In protein synthesis no AA can compensate for the absence of another;

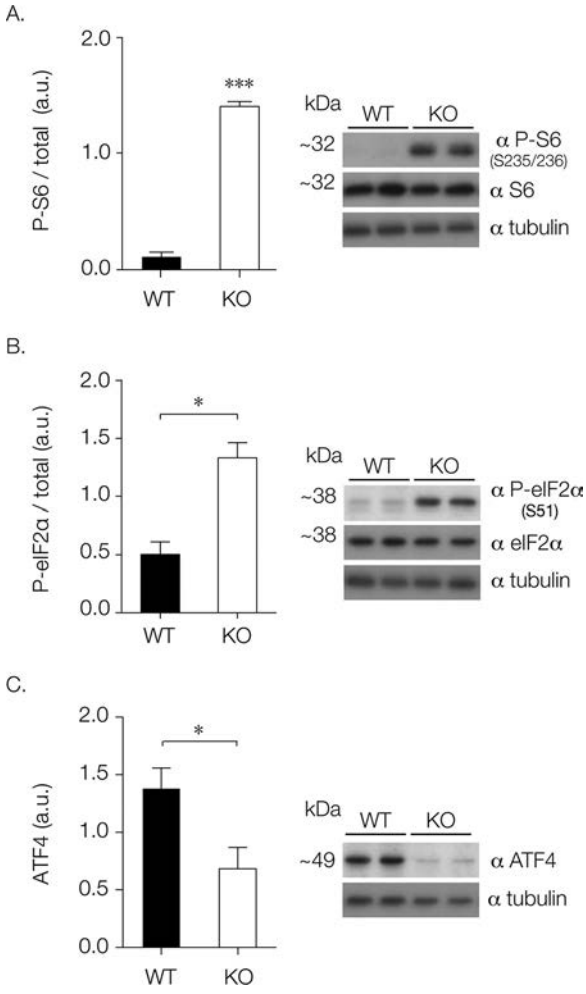

FIGURE 5. **Stress responses triggered in CD98hc-depleted fibroblasts.** *A*, mTORC1 is activated in CD98hc-deficient fibroblasts. Phosphorylation of S6 is compared between WT (*solid bar*) and CD98hc-null (*KO*, *open bar*) fibroblasts. *a.u.*, arbitrary units. *B*, eIF2α phosphorylation is compared between WT (*solid bar*) and CD98hc-null (*KO*, *open bar*) fibroblasts. *C*, ATF4 protein expression in WT (*solid bar*) and CD98hc-null (*KO*, *open bar*) cells. *A–C*, representative Western blots of two independent experiments are shown. Data are normalized by tubulin expression. Quantification corresponds to the mean ± S.E. of at least three independent experiments run in duplicates. *, $p < 0.05$; ***, $p < 0.001$; Student's *t* test.

thus, we thought that the intracellular BCAA and ARO AA shortage of CD98hc-deficient cells could induce protein synthesis repression via mTOR inactivation. Contrary to our hypothesis, we found an increased phosphorylation state of S6 in CD98hc-null compared with wild-type cells (Fig. 5*A*). In fact, increased activity of mTORC1 in fibroblasts deficient for CD98hc could be attributed to the high content of AA^+ and glutamine in such cells (Fig. 4*A*), as arginine and glutamine are also regulators of mTORC1 (32–34). Alternatively to mTORC1, eukaryotic cells respond to stress (such as oxidative stress or AA deprivation) by phosphorylating the α subunit of the eIF2, which represses global translation coincident with preferential translation of ATF4, a master regulator controlling the transcription of pro-survival target genes (35). This pathway is collectively referred to as integrated stress response. We analyzed the phosphorylation state of eIF2α in CD98hc-null cells, which was markedly increased (~3-fold) in comparison with wild-type cells (Fig. 5*B*), thereby suggesting the activation of the eIF2α-mediated stress response pathway. However, despite the strong phosphorylation of eIF2α, ATF4 mRNA (data not shown) and protein levels (Fig. 5*C*) were substantially repressed in CD98hc-deficient fibroblasts. Dysfunctional integrated stress response (suppressed ATF4 expression in the presence of phosphorylated eIF2α) has been reported in cells affected by chronic stresses (36–40). This could be the case for CD98hc-null ES-derived fibroblasts, which present chronic oxidative stress and imbalanced intracellular AA content. Moreover, CD98hc-deficient cell proliferation was restored without affecting the phosphorylation state of eIF2α (see below), offering serious doubts about the role of phosphorylated eIF2α in blocking general protein synthesis of ES-derived fibroblasts lacking CD98hc. In all, despite our attempts to decipher the molecular mechanisms behind, we cannot yet explain the cause for proliferation impairment in CD98hc-null cells.

CD98hc-deficient Cell Proliferation Is Restored after BCAA and ARO AA Supplementation—As shown above, in the absence of LAT1 activity and presenting only an ~10% of L-Ile uptake (Fig. 3*A*, *middle panel*, and Fig. 4*G*), CD98hc-deficient cells maintained a considerable (yet reduced) intracellular content of the LAT1 substrates valine, leucine, isoleucine, phenylalanine, and tyrosine (Fig. 4*A*). This observation suggests a diminished cell metabolism or alternative sources of these AAs. In this regard, we observed an overexpression of mRNA (Fig. 6*A*) and protein (Fig. 6*B*) levels of peptide transporter PEPT1 (whereas PEPT2 mRNA expression was not affected) (data not shown) in CD98hc-deficient fibroblasts when compared with wild-type fibroblasts. PEPT1 is a proton-dependent transporter responsible for cellular uptake of di- and tripeptides (41). We took advantage of this overexpression to supplement culture media of CD98hc-KO cells with alanyl dipeptides containing BCAAs and ARO AAs. Intriguingly, the proliferation capacity of CD98hc-deficient fibroblasts was restored to levels of wild-type cells after being grown in dipeptide-supplemented media for 5 days (Fig. 6*C*), whereas control-supplementation (L-Ala) showed no effect (Fig. 6*C*, *right panel*). Next, we performed a time-course analysis and found that up-regulation of PEPT1 expression matched the rescue of cell proliferation, with the highest mRNA and protein expression being reached at days 5–6 after cell seeding (data not shown). Therefore, cell proliferation was restored when fibroblasts expressed the transporter that allows extra uptake of dipeptides containing BCAAs and ARO AAs. Strikingly, the intracellular AA content of dipeptide-supplemented fibroblasts showed no recovery of either BCAA or ARO AA content (Fig. 6*D*); neither phosphorylation of eIF2α nor ATF4 repression was alleviated in the presence of BCAA- and ARO AA-containing dipeptides (data not shown). CD98hc-null ES-derived fibroblasts grown in peptide-supplemented media proliferated normally in the presence of phosphorylated eIF2α, supporting a dysfunctional role of the phosphorylation of the initiation factor on protein synthesis in these cells. Our results reveal the strong dependence of ES-derived fibroblasts on adequate BCAA and ARO AA availability for cell proliferation and the strict requirement of CD98hc/LAT1 and CD98hc/y^+LAT2 for mediating the transport of such essential AAs.

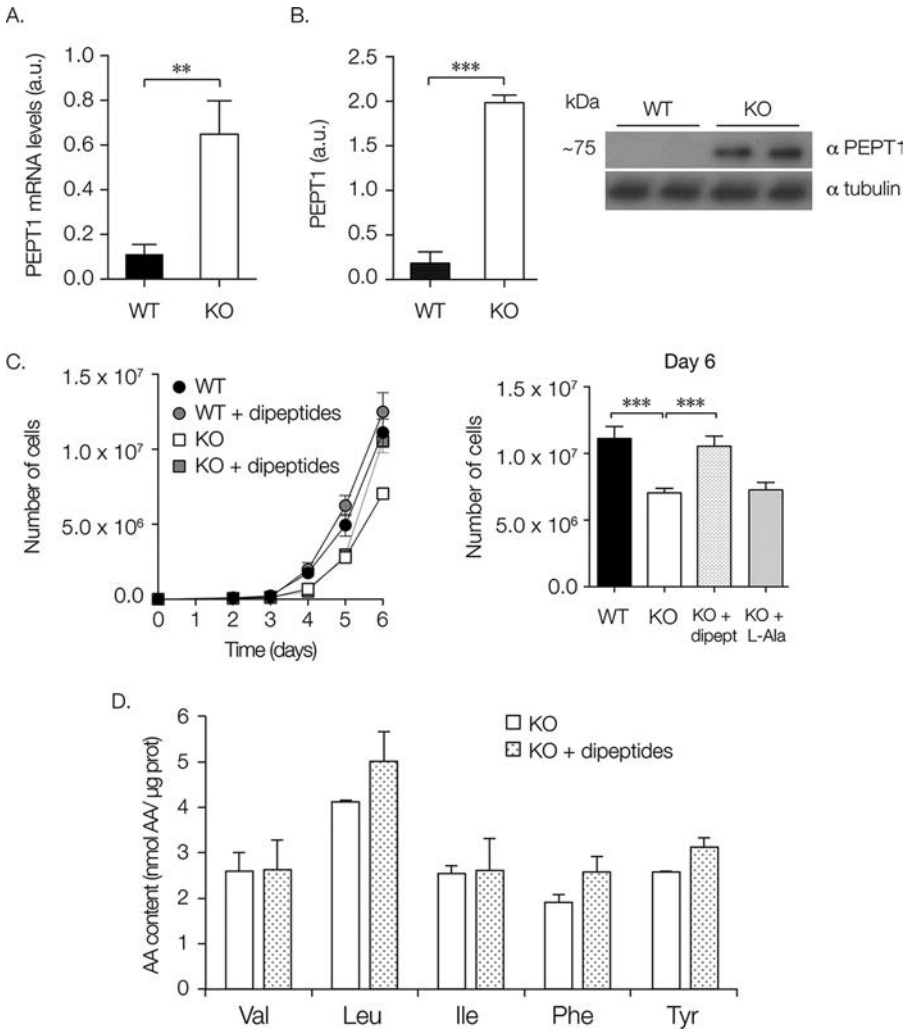

FIGURE 6. **Supplementation with BCAA- and ARO AA-containing dipeptides restores proliferation of CD98hc-null fibroblasts.** *A*, PEPT1 mRNA expression levels in WT and CD98hc-deficient (*KO*) fibroblasts. RPLP0 was used as a housekeeping gene (not depicted). Data are presented as the mean ± S.E. of three independent experiments. *a.u.*, arbitrary units. *B*, PEPT1 protein expression in WT and CD98hc-null (*KO*) fibroblasts. Representative Western blot of two independent experiments is shown. Data are normalized by tubulin expression. Quantification corresponds to the mean ± S.E. of eight measurements (*right panel*). *C*, proliferation of WT and CD98hc-null (*KO*) fibroblasts grown with no additives or in the presence of BCAA- and ARO AA- containing dipeptides (*WT + dipeptides* and *KO + dipeptides*) was measured over 6 days. Cell counts at several time points are shown as the mean ± S.E. of three independent experiments (*left panel*). Cell count at day 6 including KO + Ala as control (*right panel*). *D*, samples from CD98hc-null (*KO*, *open bar*) and CD98hc-null + dipeptides (*KO + dipeptides*, *dotted open bar*) fibroblasts were processed as described under "Experimental Procedures," and quantitative analysis of BCAAs and ARO AAs was performed. Results are expressed as the mean ± S.E. of three independent measurements. **, $p < 0.01$; ***, $p < 0.001$; Student's *t* test.

Discussion

Proliferating cells must meet specific energetic and biosynthetic demands (42). Their adaptation involves the expression of nutrient transporters, in particular for AAs that cells are unable to store. In this study we unveil the role of CD98hc-mediated AA transport in teratoma formation and proliferation *in vivo*. We show that CD98hc AA transport function is required for adequate provision of AAs to cells, protecting them against oxidative stress and allowing normal cell proliferation, both *in vitro* and *in vivo*.

We show that expression of the CD98hc portion able to bind integrins (C98T98E69) in CD98hc-null cells is not sufficient to restore *in vitro* cell proliferation, in contrast with *in vivo* teratoma formation (6), suggesting a specific integrin mediated regulation depending on the properties of the surrounding environment (43). In parallel, expression of any of the chimeras deficient for integrin interaction but containing the CD98hc-ED (C69T98E98, C98T69E98) (6, 10) rescues *in vivo* and *in vitro* cell proliferation of CD98hc-deficient cells.

Our data suggest that the ED of CD98hc (absent in the chimera exclusively recovering β1 integrin signaling) is crucial for the proper functioning of associated transporters, as CD98hc-null cells expressing ED-containing chimeras catalyze all AA transport activities present in wild-type cells (systems x_c^-, L, and y^+L). This observation is in agreement with a recent structural model of CD98hc heterodimers, which shows that CD98hc-ED interacts with the corresponding associated transporter, thus stabilizing it (4).

Distinct AA transporters often share the same substrates, thereby ensuring that the system remains unaffected if one transporter fails. Here we report a general change in intracellular AA content after invalidation of a transporter component, showing that redundancy is not observed with CD98hc-associated transporters. Consequently, CD98hc/

xCT and CD98hc/LAT1 (up-regulated in highly proliferative cells; Ref. 44) and CD98hc/y^+LAT2 are essential for cell survival and proliferation.

In vitro in high oxygen tension, cells rely on membrane expression of CD98hc-associated cystine transporter xCT (20), which protects them from cell death by ferroptosis (11). We show that CD98hc-null ES-derived fibroblasts do not survive under routine culture conditions but grow normally in the presence of β-ME or NAC. Our results are in good agreement with the work by Sato *et al.* (45) on fibroblasts isolated from xCT deficient embryos. However, whereas Vit E restores cell survival in xCT-null fibroblasts (45), it has no effect on CD98hc-deficient fibroblasts. This aggravated phenotype might be due to the lack of other transporters (LAT1 and y^+LAT2) along with xCT in CD98hc-null cells. Moreover, even when ferroptosis is blocked by β-ME supplementation (consistently with Ref. 12), CD98hc-null fibroblasts still present, with no obvious explanation, accumulation of 2′,7′-dichlorofluorescein signal and increased Nrf2 expression. Although it is known as a master regulator of oxidative stress, Nrf2 also participates in intermediary metabolism and mitochondrial physiology (46). Because pharmacological inhibition of xCT does not promote Nrf2 activation, one might question whether the observed increased Nrf2 in CD98hc-nulls is directly related to oxidative stress. Further investigation will be needed to clarify this process.

LAT1 is the other CD98 catalytic subunit overexpressed in highly proliferative cells (44). Although inhibition of LAT1 affects cell proliferation (47, 48), its genetic or chemical ablation results in mTOR inhibition and impaired cell growth (27, 28, 48–50). Our data indicate that >90% of L-isoleucine uptake is lost when CD98hc is absent. Moreover, CD98hc/LAT1 loss leads to cellular depletion of several essential AAs (BCAAs leucine, isoleucine, and valine and ARO AAs phenylalanine and tyrosine), which surprisingly does not impair mTORC1 activity. We hypothesize that the high intracellular content of other AAs such as arginine and glutamine is sufficient to sustain mTORC1 activity (as observed in Refs. 32–34) in CD98hc-null cells. Nonetheless, even with active mTORC1 CD98hc-null cells present a major defect in cell proliferation. In the absence of CD98hc, oxidative stress and/or scarcity of BCAAs and ARO AAs may underlie eIF2α phosphorylation; however, p-eIF2α does not appear to play a relevant role in the restriction of general translation of CD98hc-null ES-derived fibroblasts.

Isolated cells (both normal and malignant) depend on 13 AAs for *in vitro* survival. Over and above the eight AAs required for nitrogen balance (isoleucine, leucine, lysine, methionine, phenylalanine, threonine, tryptophan, and valine), cell cultures require arginine, cysteine/cystine, glutamine, histidine, and tyrosine (51). Despite the absence of LAT1 activity, CD98hc-deficient cells maintain a considerable intracellular concentration of the BCAA and ARO AA substrates of LAT1. We could explain these somewhat unexpected results by the strong up-regulation of di- and tri-peptide transporter PEPT1 (41) expression in CD98hc-deficient cells. Providing dipeptides as an alternative source of BCAAs and ARO AAs is sufficient to recover proper cell proliferation. However, it neither alleviates stress sensed by eIF2α nor restores the intracellular BCAA and ARO AA content, pointing to the relevance of AA flux rather than AA concentration. PEPT1 has been described to participate in tumor cell growth (52); our data now point to its relevant role in cell proliferation.

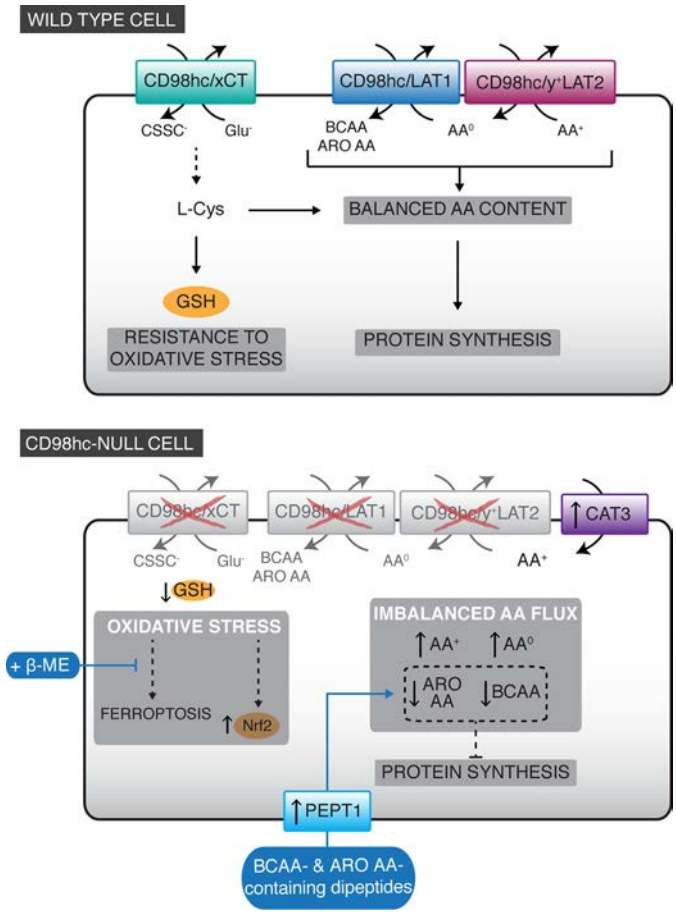

FIGURE 7. **CD98hc serves as a hub of the stress response network.** In wild-type fibroblasts (*upper panel*) CD98hc-associated transporters (LAT1, xCT, and y^+LAT2) ensure that cells have a balanced AA content, which allows them to counterbalance oxidative stress (via CD98hc/xCT) and to fuel protein synthesis and concomitant cell proliferation. When CD98hc is not present (*lower panel*), all associated transporters fail to reach the plasma membrane, and therefore, there is no effective AA transport activity of LAT1, xCT, and y^+LAT2 transporters. β-ME supplementation is then required to inhibit cell death by ferroptosis. In supplemented culture media, CD98hc-null cells present reactive oxygen species accumulation (triggering Nrf2) and imbalanced AA flux (increased concentration of AA^+ caused by up-regulation of CAT3 CD98hc-independent AA transporter, accumulation of AA^0, and shortage of BCAAs and ARO AAs), which lead to a defect in cell proliferation. External supply of BCAAs and ARO AAs in the form of dipeptides (which can enter the cell via PEPT1 di- and tripeptide transporter and compensate for the lack of CD98hc/LAT1 and CD98hc/y^+LAT2 transport activities) restores cell proliferation.

By controlling expression at the plasma membrane and coupling transport activities of xCT, LAT1, and y^+LAT2, CD98hc confers protection against oxidative and nutritional stresses (ensuring a balanced AA content and a proper supply of essential amino acids) and, thus, provides cells with a proliferative advantage (Fig. 7). Each function of CD98hc, AA transport activity (presented herein), or integrin signaling (6), rescues *in vivo* cell proliferation. Moreover, our results strongly suggest that both functions can act in synergy, providing cells with hyperproliferative capacity *in vivo* (as can be observed in teratomas formed when full-length CD98hc is expressed in CD98hc-null ES cells). These findings have relevant implica-

tions in pathophysiological scenarios. For instance, CD98hc and the associated catalytic subunits LAT1 and xCT, as well as integrins, are overexpressed in most tumors (8, 44, 53), thus promoting cell growth. By expressing such transporters coupled with extracellular matrix receptors, cells can control AA adequacy, reactive oxygen species impact, and anchoring/migration, leading to sustain cell proliferation, critical for tumor cells (54). To date, many studies have focused on the search for either transporter (xCT, LAT1) inhibitors or integrin antagonists as anti-cancer strategies (47, 48, 55, 56). Even though these molecules are appealing targets, encouraging, yet limited results, have been obtained so far. Targeting CD98hc could represent a novel option, widening the therapeutic window of cancer therapy by inducing an immediate blockage of AA transport activities mediated by xCT and LAT1 (with extremely limited compensation capacities) as well as a strong impairment in integrin signaling. CD98hc-targeting drugs could be delivered locally to tumors where this protein is strongly overexpressed. Generating drugs against CD98hc that could inhibit such a pivotal signal integrator would be of potential great use specifically for anti-cancer therapeutic purposes.

Author Contributions—L. R. B., S. C.-C., E. G.-M., M. P., and C. C. F. designed the research. L. R. B., S. C.-C., S. B., S. E., L. C., F. T., and C. C. F. performed the research. L. R. B., M. P., and C. C. F. analyzed and interpreted the data. E. G.-M., H. D., and M. H. G. contributed new reagents and analytic tools. L. R. B., A. Z., M. P., and C. C. F. participated in the conception and design of the article. A. Z. did a critical revision of the article. L. R. B., A. Z., M. H. G., M. P., and C. C. F. gave final approval of the version to be published. L. R. B., M. P., and C. C. F. wrote the article.

Acknowledgments—We greatly acknowledge the IRCAN core facilities (supported by le Conseil Général 06, FEDER, le Ministère de l'Enseignement Supérieur, la Région Provence Alpes-Côte d'Azur and INSERM) and the Synthesis of Peptides Unit (U3) of the CIBER in Bioengineering, Biomaterials and Nanomedicine (CIBER-BBN) at the Barcelona Science Park. We thank Dr. Juan Pablo Muñoz and Dr. Sónia R. Veiga for technical advice, constructive comments, and enlightening discussions.

References

1. Fotiadis, D., Kanai, Y., and Palacín, M. (2013) The SLC3 and SLC7 families of amino acid transporters. *Mol. Aspects. Med.* **34,** 139–158
2. Pfeiffer, R., Spindler, B., Loffing, J., Skelly, P. J., Shoemaker, C. B., and Verrey, F. (1998) Functional heterodimeric amino acid transporters lacking cysteine residues involved in disulfide bond. *FEBS Lett.* **439,** 157–162
3. Reig, N., Chillarón, J., Bartoccioni, P., Fernández, E., Bendahan, A., Zorzano, A., Kanner, B., Palacín, M., and Bertran, J. (2002) The light subunit of system b(o,+) is fully functional in the absence of the heavy subunit. *EMBO J.* **21,** 4906–4914
4. Rosell, A., Meury, M., Álvarez-Marimon, E., Costa, M., Pérez-Cano, L., Zorzano, A., Fernández-Recio, J., Palacín, M., and Fotiadis, D. (2014) Structural bases for the interaction and stabilization of the human amino acid transporter LAT2 with its ancillary protein 4f2hc. *Proc. Natl. Acad. Sci. U.S.A.* **111,** 2966–2971
5. Fenczik, C. A., Sethi, T., Ramos, J. W., Hughes, P. E., and Ginsberg, M. H. (1997) Complementation of dominant suppression implicates CD98 in integrin activation. *Nature* **390,** 81–85
6. Feral, C. C., Nishiya, N., Fenczik, C. A., Stuhlmann, H., Slepak, M., and Ginsberg, M. H. (2005) CD98hc (SLC3A2) mediates integrin signaling. *Proc. Natl. Acad. Sci. U.S.A.* **102,** 355–360
7. Nguyen, H. T., Dalmasso, G., Torkvist, L., Halfvarson, J., Yan, Y., Laroui, H., Shmerling, D., Tallone, T., D'Amato, M., Sitaraman, S. V., and Merlin, D. (2011) CD98 expression modulates intestinal homeostasis, inflammation, and colitis-associated cancer in mice. *J. Clin. Invest.* **121,** 1733–1747
8. Cantor, J. M., and Ginsberg, M. H. (2012) CD98 at the crossroads of adaptive immunity and cancer. *J. Cell Sci.* **125,** 1373–1382
9. Estrach, S., Lee, S. A., Boulter, E., Pisano, S., Errante, A., Tissot, F. S., Cailleteau, L., Pons, C., Ginsberg, M. H., and Féral, C. C. (2014) CD98hc (SLC3A2) loss protects against ras-driven tumorigenesis by modulating integrin-mediated mechanotransduction. *Cancer Res.* **74,** 6878–6889
10. Fenczik, C. A., Zent, R., Dellos, M., Calderwood, D. A., Satriano, J., Kelly, C., and Ginsberg, M. H. (2001) Distinct domains of cd98hc regulate integrins and amino acid transport. *J. Biol. Chem.* **276,** 8746–8752
11. Dixon, S. J., Lemberg, K. M., Lamprecht, M. R., Skouta, R., Zaitsev, E. M., Gleason, C. E., Patel, D. N., Bauer, A. J., Cantley, A. M., Yang, W. S., Morrison, B., 3rd, and Stockwell, B. R. (2012) Ferroptosis: an iron-dependent form of nonapoptotic cell death. *Cell* **149,** 1060–1072
12. Dixon, S. J., Patel, D. N., Welsch, M., Skouta, R., Lee, E. D., Hayano, M., Thomas, A. G., Gleason, C. E., Tatonetti, N. P., Slusher, B. S., and Stockwell, B. R. (2014) Pharmacological inhibition of cystine-glutamate exchange induces endoplasmic reticulum stress and ferroptosis. *Elife* **3,** e02523
13. Lau, A., Tian, W., Whitman, S. A., and Zhang, D. D. (2013) The predicted molecular weight of nrf2: it is what it is not. *Antioxid. Redox. Signal.* **18,** 91–93
14. Wuensch, T., Schulz, S., Ullrich, S., Lill, N., Stelzl, T., Rubio-Aliaga, I., Loh, G., Chamaillard, M., Haller, D., and Daniel, H. (2013) The peptide transporter PEPT1 is expressed in distal colon in rodents and humans and contributes to water absorption. *Am. J. Physiol. Gastrointest. Liver. Physiol.* **305,** G66–G73
15. Wuensch, T., Ullrich, S., Schulz, S., Chamaillard, M., Schaltenberg, N., Rath, E., Goebel, U., Sartor, R. B., Prager, M., Büning, C., Bugert, P., Witt, H., Haller, D., and Daniel, H. (2014) Colonic expression of the peptide transporter PEPT1 is down-regulated during intestinal inflammation and is not required for nod2-dependent immune activation. *Inflamm. Bowel. Dis.* **20,** 671–684
16. Conrad, M., and Sato, H. (2012) The oxidative stress-inducible cystine/glutamate antiporter, system x (c) (−): cystine supplier and beyond. *Amino Acids* **42,** 231–246
17. Kalyanaraman, B., Darley-Usmar, V., Davies, K. J., Dennery, P. A., Forman, H. J., Grisham, M. B., Mann, G. E., Moore, K., Roberts, L. J., 2nd, and Ischiropoulos, H. (2012) Measuring reactive oxygen and nitrogen species with fluorescent probes: Challenges and limitations. *Free. Radic. Biol. Med.* **52,** 1–6
18. Gorrini, C., Harris, I. S., and Mak, T. W. (2013) Modulation of oxidative stress as an anticancer strategy. *Nat. Rev. Drug. Discov.* **12,** 931–947
19. Sato, H., Tamba, M., Kuriyama-Matsumura, K., Okuno, S., and Bannai, S. (2000) Molecular cloning and expression of human xct, the light chain of amino acid transport system xc-. *Antioxid. Redox. Signal.* **2,** 665–671
20. Palacín, M., and Kanai, Y. (2004) The ancillary proteins of hats: SLC3 family of amino acid transporters. *Pflugers. Arch.* **447,** 490–494
21. Devés, R., Angelo, S., and Chávez, P. (1993) *N*-ethylmaleimide discriminates between two lysine transport systems in human erythrocytes. *J. Physiol.* **468,** 753–766
22. Nicholson, B., Sawamura, T., Masaki, T., and MacLeod, C. L. (1998) Increased cat3-mediated cationic amino acid transport functionally compensates in cat1 knockout cell lines. *J. Biol. Chem.* **273,** 14663–14666
23. Ito, K., and Groudine, M. (1997) A new member of the cationic amino acid transporter family is preferentially expressed in adult mouse brain. *J. Biol. Chem.* **272,** 26780–26786
24. Bröer, S. (2014) The SLC38 family of sodium-amino acid co-transporters. *Pflugers. Arch* **466,** 155–172
25. Kanai, Y., Segawa, H., Miyamoto, K. i., Uchino, H., Takeda, E., and Endou, H. (1998) Expression cloning and characterization of a transporter for large neutral amino acids activated by the heavy chain of 4F2 antigen (CD98). *J. Biol. Chem.* **273,** 23629–23632
26. Bodoy, S., Fotiadis, D., Stoeger, C., Kanai, Y., and Palacín, M. (2013) The

small SLC43 family: facilitator system l amino acid transporters and the orphan EEG1. *Mol. Aspects. Med.* **34,** 638–645
27. Nicklin, P., Bergman, P., Zhang, B., Triantafellow, E., Wang, H., Nyfeler, B., Yang, H., Hild, M., Kung, C., Wilson, C., Myer, V. E., MacKeigan, J. P., Porter, J. A., Wang, Y. K., Cantley, L. C., Finan, P. M., and Murphy, L. O. (2009) Bidirectional transport of amino acids regulates mtor and autophagy. *Cell* **136,** 521–534
28. Elorza, A., Soro-Arnáiz, I., Meléndez-Rodríguez, F., Rodríguez-Vaello, V., Marsboom, G., de Cárcer, G., Acosta-Iborra, B., Albacete-Albacete, L., Ordóñez, A., Serrano-Oviedo, L., Giménez-Bachs, J. M., Vara-Vega, A., Salinas, A., Sánchez-Prieto, R., Martín del Río, R., et al. (2012) HIF2α acts as an mtorc1 activator through the amino acid carrier SLC7A5. *Mol. Cell* **48,** 681–691
29. Cargnello, M., Tcherkezian, J., and Roux, P. P. (2015) The expanding role of mtor in cancer cell growth and proliferation. *Mutagenesis* **30,** 169–176
30. Efeyan, A., Comb, W. C., and Sabatini, D. M. (2015) Nutrient-sensing mechanisms and pathways. *Nature* **517,** 302–310
31. Albert, V., and Hall, M. N. (2015) MTOR signaling in cellular and organismal energetics. *Curr. Opin. Cell Biol.* **33,** 55–66
32. Rebsamen, M., Pochini, L., Stasyk, T., de Araújo, M. E., Galluccio, M., Kandasamy, R. K., Snijder, B., Fauster, A., Rudashevskaya, E. L., Bruckner, M., Scorzoni, S., Filipek, P. A., Huber, K. V., Bigenzahn, J. W., Heinz, L. X., et al. (2015) SLC38A9 is a component of the lysosomal amino acid sensing machinery that controls mtorc1. *Nature* **519,** 477–481
33. Wang, S., Tsun, Z. Y., Wolfson, R. L., Shen, K., Wyant, G. A., Plovanich, M. E., Yuan, E. D., Jones, T. D., Chantranupong, L., Comb, W., Wang, T., Bar-Peled, L., Zoncu, R., Straub, C., Kim, C., et al. (2015) Metabolism: lysosomal amino acid transporter SLC38A9 signals arginine sufficiency to mtorc1. *Science* **347,** 188–194
34. Jewell, J. L., Kim, Y. C., Russell, R. C., Yu, F. X., Park, H. W., Plouffe, S. W., Tagliabracci, V. S., and Guan, K. L. (2015) Metabolism: differential regulation of mtorc1 by leucine and glutamine. *Science* **347,** 194–198
35. Harding, H. P., Zhang, Y., Zeng, H., Novoa, I., Lu, P. D., Calfon, M., Sadri, N., Yun, C., Popko, B., Paules, R., Stojdl, D. F., Bell, J. C., Hettmann, T., Leiden, J. M., and Ron, D. (2003) An integrated stress response regulates amino acid metabolism and resistance to oxidative stress. *Mol. Cell* **11,** 619–633
36. Evstafieva, A. G., Garaeva, A. A., Khutornenko, A. A., Klepikova, A. V., Logacheva, M. D., Penin, A. A., Novakovsky, G. E., Kovaleva, I. E., and Chumakov, P. M. (2014) A sustained deficiency of mitochondrial respiratory complex III induces an apoptotic cell death through the p53-mediated inhibition of pro-survival activities of the activating transcription factor 4. *Cell. Death. Dis.* **5,** e1511
37. Dey, S., Baird, T. D., Zhou, D., Palam, L. R., Spandau, D. F., and Wek, R. C. (2010) Both transcriptional regulation and translational control of ATF4 are central to the integrated stress response. *J. Biol. Chem.* **285,** 33165–33174
38. Kumar, R., Krause, G. S., Yoshida, H., Mori, K., and DeGracia, D. J. (2003) Dysfunction of the unfolded protein response during global brain ischemia and reperfusion. *J. Cereb. Blood. Flow. Metab.* **23,** 462–471
39. Puri, P., Mirshahi, F., Cheung, O., Natarajan, R., Maher, J. W., Kellum, J. M., and Sanyal, A. J. (2008) Activation and dysregulation of the unfolded protein response in nonalcoholic fatty liver disease. *Gastroenterology* **134,** 568–576
40. Woehlbier, U., and Hetz, C. (2011) Modulating stress responses by the uprosome: a matter of life and death. *Trends Biochem. Sci.* **36,** 329–337
41. Daniel, H., and Kottra, G. (2004) The proton oligopeptide cotransporter family SLC15 in physiology and pharmacology. *Pflugers. Arch* **447,** 610–618
42. Cantor, J. R., and Sabatini, D. M. (2012) Cancer cell metabolism: one hallmark, many faces. *Cancer. Discov.* **2,** 881–898
43. Schwartz, M. A. (2010) Integrins and extracellular matrix in mechanotransduction. *Cold. Spring. Harb. Perspect. Biol.* **2,** a005066
44. McCracken, A. N., and Edinger, A. L. (2013) Nutrient transporters: the Achilles' heel of anabolism. *Trends. Endocrinol. Metab.* **24,** 200–208
45. Sato, H., Shiiya, A., Kimata, M., Maebara, K., Tamba, M., Sakakura, Y., Makino, N., Sugiyama, F., Yagami, K., Moriguchi, T., Takahashi, S., and Bannai, S. (2005) Redox imbalance in cystine/glutamate transporter-deficient mice. *J. Biol. Chem.* **280,** 37423–37429
46. Dinkova-Kostova, A. T., Baird, L., Holmström, K. M., Meyer, C. J., and Abramov, A. Y. (2015) The spatiotemporal regulation of the keap1-nrf2 pathway and its importance in cellular bioenergetics. *Biochem. Soc. Trans.* **43,** 602–610
47. Kim, C. S., Cho, S. H., Chun, H. S., Lee, S. Y., Endou, H., Kanai, Y., and Kim, do, K. (2008) BCH, an inhibitor of system L amino acid transporters, induces apoptosis in cancer cells. *Biol. Pharm. Bull.* **31,** 1096–1100
48. Oda, K., Hosoda, N., Endo, H., Saito, K., Tsujihara, K., Yamamura, M., Sakata, T., Anzai, N., Wempe, M. F., Kanai, Y., and Endou, H. (2010) L-Type amino acid transporter 1 inhibitors inhibit tumor cell growth. *Cancer Sci.* **101,** 173–179
49. Poncet, N., Mitchell, F. E., Ibrahim, A. F., McGuire, V. A., English, G., Arthur, J. S., Shi, Y. B., and Taylor, P. M. (2014) The catalytic subunit of the system l1 amino acid transporter (slc7a5) facilitates nutrient signalling in mouse skeletal muscle. *PLoS One* **9,** e89547
50. Milkereit, R., Persaud, A., Vanoaica, L., Guetg, A., Verrey, F., and Rotin, D. (2015) LAPTM4b recruits the lat1–4f2hc leu transporter to lysosomes and promotes mtorc1 activation. *Nat. Commun.* **6,** 7250
51. Eagle, H. (1959) Amino acid metabolism in mammalian cell cultures. *Science* **130,** 432–437
52. Mitsuoka, K., Kato, Y., Miyoshi, S., Murakami, Y., Hiraiwa, M., Kubo, Y., Nishimura, S., and Tsuji, A. (2010) Inhibition of oligopeptide transporter suppress growth of human pancreatic cancer cells. *Eur. J. Pharm. Sci.* **40,** 202–208
53. Desgrosellier, J. S., and Cheresh, D. A. (2010) Integrins in cancer: biological implications and therapeutic opportunities. *Nat. Rev. Cancer* **10,** 9–22
54. Hanahan, D., and Weinberg, R. A. (2011) Hallmarks of cancer: the next generation. *Cell* **144,** 646–674
55. Balza, E., Castellani, P., Delfino, L., Truini, M., and Rubartelli, A. (2013) The pharmacologic inhibition of the xc- antioxidant system improves the antitumor efficacy of COX inhibitors in the *in vivo* model of 3-MCA tumorigenesis. *Carcinogenesis* **34,** 620–626
56. Millard, M., Odde, S., and Neamati, N. (2011) Integrin targeted therapeutics. *Theranostics* **1,** 154–188

Appendix III

CD98hc (SLC3A2) sustains amino acid and nucleotide availability for cell cycle progression

Sara Cano-Crespo, Josep Chillarón, Alexandra Junza, Gonzalo Fernández-Miranda, Judit García, Christine Polte, Laura R. de la Ballina, Zoya Ignatova, Óscar Yanes, Antonio Zorzano, Camille Stephan-Otto Attolini and Manuel Palacin.

Under revison

CD98hc (SLC3A2) sustains amino acid and nucleotide availability for cell cycle progression

Sara Cano-Crespo[1*], Josep Chillarón[2], Alexandra Junza[3,4], Gonzalo Fernández-Miranda[1], Judit García[4,5], Christine Polte[6], Laura R. de la Ballina[7,8], Zoya Ignatova[6], Óscar Yanes[3,4], Antonio Zorzano[1,9,10], Camille Stephan-Otto Attolini[1] and Manuel Palacin[1,4,10*].

[*]Corresponding authors

Sara Cano-Crespo, sara.cano@irbbarcelona.org
Josep Chillarón, jchillaron@ub.edu
Alexandra Junza, alexandra.junza@urv.cat
Gonzalo Fernández-Miranda, gonzalo.fernandez@irbbarcelona.org
Judit García, JUGARCIA@clinic.cat
Christine Polte, Christine.Polte@chemie.uni-hamburg.de
Laura R. de la Ballina, l.r.de.l.ballina@medisin.uio.no
Zoya Ignatova, zoya.ignatova@chemie.uni-hamburg.de
Óscar Yanes, oscar.yanes@urv.cat
Antonio Zorzano, antonio.zorzano@irbbarcelona.org
Camille Stephan-Otto Attolini, camille.stephan@irbbarcelona.org
Manuel Palacín, manuel.palacin@irbbarcelona.org

[1] Institute for Research in Biomedicine (IRB Barcelona), The Barcelona Institute of Science and Technology, Barcelona 08028, Spain.

[2] Department of Cell Biology, Physiology and Immunology, Faculty of Biology, Universitat de Barcelona, Barcelona 08028, Spain.

[3] Metabolomics Platform, IISPV, Department of Electronic Engineering (DEEEA), Universitat Rovira i Virgili, Tarragona 43003, Spain.

[4] Centro de Investigación Biomédica en Red de Enfermedades Raras (CIBERER), Madrid 28029, Spain.

[5] Secció Errors Congènits del Metabolisme-IBC, Servei de Bioquímica i Genètica Molecular, Hospital Clínic, Barcelona, Spain.

[6] Institute of Biochemistry and Molecular Biology University of Hamburg, Hamburg 20246, Germany.

[7] Department of Molecular Medicine, Institute of Basic Medical Sciences, Faculty of Medicine, University of Oslo, Oslo 0372, Norway.

[8] Centre for Cancer Cell Reprogramming, Institute for Clinical Medicine, Faculty of Medicine, University of Oslo, Oslo 0372, Norway.

[9] Centro de Investigación Biomédica en Red de Diabetes y Enfermedades Metabólicas Asociadas (CIBERDEM), Madrid 28029, Spain.

[10] Department of Biochemistry and Molecular Biomedicine, Faculty of Biology, University of Barcelona, Barcelona 08028, Spain.

Abstract

CD98 heavy chain (CD98hc) forms heteromeric amino acid (AA) transporters by interacting with different light chains. Cancer cells overexpress CD98hc-transporters in order to meet their increased nutritional and antioxidant demands, since they provide branched-chain AA (BCAA) and aromatic AA (AAA) availability while protecting cells from oxidative stress.

Here we show that BCAA and AAA shortage phenocopy part of the phenotype driven by CD98hc ablation (mTORC1 signalling downregulation without inducing oxidative stress and eIF2α phosphorylation). Furthermore, our data indicate that CD98hc regulates nucleotide metabolism through the pentose phosphate pathway (PPP) flux. Thus, loss of CD98hc triggered a dramatic reduction in the nucleotide pool, which caused replicative stress (RS) in these cells, as evidenced by the enhanced DNA Damage Response (DDR), S-phase delay and diminished rate of mitosis, all recovered by nucleoside supplementation. In addition, proper BCAA and AAA availability sustains the expression of Ribonucleotide reductase (RNR) required for the synthesis of deoxynucleotides. In this regard, BCAA and AAA shortage resulted in decreased content of deoxynucleotides that triggers RS, also recovered by nucleoside supplementation.

On the basis of our findings, we conclude that CD98hc plays a central role in cellular nutrition, redox homeostasis and nucleotide availability, all key for cell proliferation.

Introduction

Amino acid (AA) transporters are pivotal for human physiology [1]. Heteromeric Amino Acid Transporters (HATs) are disulphide-bound heterodimers composed by a heavy subunit from the SLC3 family (CD98hc (SLC3A2) or rBAT (SLC3A1)) and a light subunit from the SLC7 family [2]. CD98hc-associated transporters have two well established roles [3]. CD98hc confers the complex the capacity to potentiate integrin-dependent signals via direct binding with cytoplasmic tails of β-integrin subunits [3–5], while the light chain, which can be LAT1, LAT2, xCT, y^+LAT1, y^+LAT2 or asc1, mediates AA transport, conferring substrate specificity to the heterodimer [6].

A growing body of evidence shows that the AA transport function of CD98hc plays a crucial role in the growth, proliferation, survival and metastasis of cancer cells [7,8]. Rapidly proliferating cells extensively reprogram metabolic pathways to meet their increased demand of AAs, which are used not only as building blocks for protein synthesis but also as nitrogen and carbon sources for the synthesis of nucleotides, amino sugars, and glutathione (GSH) [9,10]. In this regard, cancer cells are able to upregulate their nutritional and antioxidant capacity by overexpressing the AA transporters CD98hc-LAT1 ((L)-type amino acid transporter 1) and CD98hc-xCT (cystine/glutamate transporter) [11,12].

We previously studied the effects of the ablation of CD98hc from fibroblasts derived from embryonic stem (ES) cells that expressed LAT1-, xCT- and y^+LAT2-CD98hc associated transporters [4,13]. CD98hc knock out (KO) fibroblasts failed to survive in standard culture conditions due to cell death by ferroptosis [13–15]. This phenomenon is attributed to the loss of CD98hc-xCT, a transporter that sustains cellular redox homeostasis by taking up cyst(e)ine, which is necessary for GSH biosynthesis [16–18]. Although the addition of β-mercaptoethanol (β-ME) to the culture media rescued cell death, CD98hc KO cells still presented increased oxidative stress [13]. Moreover, these cells showed a shortage in the intracellular branched-chain AA (BCAA) and aromatic AA (AAA) content, which led to defective cell proliferation [13,19,20]. These results allowed us to establish that the AA transport function of CD98hc lies at the cross-road of oxidative and nutritional stress. However, the relative contribution of each stressor to the phenotype of CD98hc KO cells remained unknown.

Nutritional status regulates cell cycle progression in part by controlling protein synthesis via the mammalian target of rapamycin complex 1 (mTORC1) [21–23]. Moreover, nucleotide biosynthesis pathways have strict energetic and nutritional requirements. Indeed, *de novo* synthesis of purine and pyrimidine nucleotides relies on metabolic pathways that provide carbon and nitrogen precursors, including the AAs aspartate, glutamine, serine and glycine, as well as glucose and CO_2. The major feeder pathways are glycolysis, the pentose phosphate pathway (PPP), the serine-glycine pathway, the tricarboxylic acid (TCA) cycle, and glutamine amidotransferase reactions [24]. Interestingly, BCAAs have been shown to constitute a potential alternative source of nitrogen for the synthesis of nucleotides [25]. Moreover, BCAAs can control glucose metabolism by regulating pyruvate dehydrogenase (PDH) activity [26], and like AAAs, can be shunted via anaplerosis to replenish the TCA cycle [27,28]. However, little attention has been devoted to the involvement of BCAA and

AAA availability in nucleotide metabolism. Furthermore, CD98hc may also regulate glucose metabolism via direct interaction and stabilisation of Glucose transporter 1 (GLUT1) [29]. Given these observations, we hypothesised that CD98hc participate in cellular nucleotide metabolism and therefore in cell cycle regulation, since nucleotide availability is tightly related to the adequacy of the progression of cell division [30,31].

The data provided herein indicate that CD98hc regulates the cellular nucleotide content likely through the flux of the PPP. In addition, BCAA and AAA availability has an impact in the reduction of ribonucleotides to the corresponding deoxynucleotides, thereby having the capacity to balance the cellular nucleotide content. Our results highlight a novel role of CD98hc and BCAA/AAA availability in cell cycle regulation, since both are required for the maintenance of an adequate nucleotide pool for DNA synthesis, thereby protecting cells from DNA replication stress (RS).

Results

BCAA and AAA shortage phenocopy part of the phenotype driven by CD98hc ablation: mTORC1 signalling downregulation without oxidative stress and eIF2α phosphorylation

Fibroblasts derived from ES cells lacking CD98hc-related transporters showed a shortage of BCAAs and AAAs and increased reactive oxygen species (ROS) [13]. In order to dissociate oxidative from nutritional stress, we generated a cellular model with only one of the stressors. To this end, we cultured wild-type (WT) cells in media with reduced concentrations of BCAAs and AAAs, considered within the lower physiological levels in plasma (Figure S1a), under standard cell culture concentrations of cyst(e)ine and β-ME. Cell culture medium was optimised to phenocopy the proliferation defect (Figure 1a) reported in the CD98hc KO model [13]. These cells (hereafter referred to as low 6AA cells) showed a dramatic decrease in the content of BCAAs and AAAs compared with those cultured in complete media (control cells) (Figure 1b). Strikingly, the intracellular levels of cationic (AA^+) and neutral (AA^0) AAs were increased in low 6AA cells (Figure 1b). This imbalance in the intracellular AA content (Figure S1b) resembled that observed in CD98hc KO cells [13]. The alteration in the expression of other transporters in low 6AA cells may account for the increase in the AA^+ concentration [13], as indicated by higher mRNA expression levels of the AA^+ transporters CAT1 and CAT3 (y^+ transport system) and

y^+LAT1 (y^+L transport system) in these cells (Figure S1c). This finding is consistent with increased L-arginine uptake by both the y^+ and y^+L transport systems in low 6AA cells (Figure S1D). In the light of these results, extracellular BCAA and AAA restriction is sufficient to trigger the intracellular imbalance of AAs observed in cells lacking CD98hc. Oxidative stress was not increased in low 6AA cells, since no differences were found compared to control cells in the redox-sensitive H_2DCFDA labelling (Figure 1c). In addition, the protein levels of Nuclear factor (erythroid-derived 2)-like 2 (Nrf2), considered a master regulator of intracellular antioxidant response [32], were not increased in low 6AA and control cells (Figure 1d). This observation indicates that in contrast to CD98hc KO cells (Figures S1e and S1f), low 6AA cells did not present oxidative stress. Together, these findings indicate that low 6AA cells are a suitable cellular model in which to study the effects of cellular BCAA and AAA deficiency, independently of oxidative stress and other possible metabolic alterations that might be associated with CD98hc ablation.

The nutrient-sensing pathway mTORC1 responds to AA deprivation by downregulating global protein synthesis while reprograming cells for their particular needs [33]. mTORC1 activation stimulates the subsequent phosphorylation of components of the translational machinery, including the ribosomal protein S6, one of the most widely studied downstream effector targets of this pathway [34]. Consistent with the AA shortage, CD98hc KO cells showed lower levels of phosphorylated S6 (P-S6) in comparison to WT cells (Figure 1e), in agreement with the alterations reported in cells lacking CD98hc-LAT1 [8,19,35].The addition of BCAA- and AAA-containing dipeptides to the culture media partially restored S6 phosphorylation (Figure 1e). In addition, low 6AA cells also presented repressed mTORC1 activation, as revealed by decreased P-S6 protein levels (Figure 1f). These results indicate that the shortage of BCAAs and AAAs in CD98hc KO cells is responsible of the downregulation of mTORC1 pathway, which may repress protein synthesis in these cells.

AA deprivation, among other stress stimuli, leads to the activation of the eIF2-mediated ISR [36,37]. eIF2α phosphorylation reduces the overall rate of translation, allowing cells to overcome the stress or promoting their elimination if the damage cannot be repaired [38]. In line with previous results [13], CD98hc KO cells presented a marked increase in the phosphorylated levels of eIF2α (P-eIF2α) compared to WT cells (Figure 1g). Interestingly, the levels of P-eIF2α did not change after addition of BCAA- and AAA-containing dipeptides (Figure 1g), thereby suggesting that nutritional status is not the trigger of the eIF2α-mediated ISR pathway activation in CD98hc KO cells. The phosphorylation of the

α subunit of eIF2 caused by AA deprivation is mediated by the kinase general control non-derepressible-2 (GCN2) [39], which is activated through the binding of uncharged transfer RNAs (tRNAs) [40]. Importantly, tRNA charging levels, measured by the tRNA-tailored microarrays, were only marginally affected in CD98hc KO cells (Figure S1g), which suggests that GCN2 is not upstream of eIF2α phosphorylation in these cells. Moreover, phosphorylated levels of eIF2α remained unaffected in low 6AA cells when compared to control cells (Figure 1h), which reinforce the notion that eIF2-mediated ISR activation is unlikely to be related to the shortage of BCAAs and AAAs that resulted from CD98hc ablation. Most likely, mTORC1 downregulation and increased P-eIF2α is upstream of the decreased general protein synthesis found in CD98hc KO cells (Figure 1i).

Transcriptome analysis reveals putative cell cycle alterations in CD98hc KO cells

Besides protein synthesis, other cellular processes are known to be regulated by the nutritional status of the cell. In order to study additional alterations that could take place in cells surviving loss of CD98hc and by consequence their associated transport activities and AA unavailability, a comparative transcriptome analysis was performed in CD98hc KO and WT cells. Strikingly, we found that 20% of the genes were differentially expressed in both groups (biological fold change > 2 and adjusted p-value < 0.05; GEO accession code: GSE126781). Supporting this, Gene Set Enrichment Analysis (GSEA) using KEGG database identified several gene categories altered between WT and CD98hc KO cells. Remarkably, we found a notable enrichment in gene sets closely related to the cell cycle, including mismatch repair, DNA replication and nucleotide excision repair (Figures 2a and S2; GEO accession code: GSE126781). Furthermore, gene sets associated with RNA and AA metabolism in CD98hc KO cells were also enriched, which may be caused by BCAA and AAA deficiency and defective protein synthesis (Figures 2a and S2; GEO accession code: GSE126781).

Cells lacking CD98hc fail to progress adequately through the S-phase of the cell cycle

On the basis of these data, we analysed cell cycle phase distributions by measuring DNA content using flow cytometry in CD98hc KO and WT cells (Figure 2b). Compared to WT, CD98hc KO cells showed increased S- (65 ± 0.7% vs. 53.3 ± 2.2%) and G2/M-phases (16 ± 0.5% vs. 14 ± 0.6%) at the expense of a reduction in G1-phase (18.8 ± 0.9% vs. 32.7 ± 2.5%)

(Figure 2b). The increase in S-phase population cannot be attributed to an enhanced proliferative rate, since cells lacking CD98hc presented a major delay in proliferation in comparison to WT cells [13]. Alternatively, the lack of CD98hc may slow down the progression of cells that are in the S-phase. To test whether CD98hc KO cells presented delayed DNA replication, cells were synchronised in S-phase with a double block of thymidine [41]. The treatment achieved the retention of around 75% of cells in the DNA-synthesis phase (Figure 2c). S-phase progression was then monitored. Remarkably, 4 h after release, 70.7 ± 3.4% of CD98hc KO cells remained in S-phase as compared to 47.7± 1.8% in the case of WT cells (Figure 2c). This observation confirms that cells lacking CD98hc fail to progress adequately through DNA synthesis phase.

BCAA and AAA limitation reproduces the replicative stress (RS) observed in CD98hc KO cells

During S-phase, cells must faithfully duplicate their genomes. As a consequence of DNA damage, cells suffer RS, which is characterised by the activation of the DNA damage response (DDR) pathway and often accompanied by cell cycle arrest [42,43]. We took advantage of the transcriptome analysis performed in WT and CD98hc KO cells to further interrogate whether the observed cell cycle arrest was accompanied by DNA damage and RS in CD98hc KO cells. For this purpose, we created the DDR gene set, which comprised 97 genes related to the regulation of DNA replication and repair and involved in DNA damage signalling pathways. The selection was carried out following the bibliography and available gene lists from commercial arrays (RT² Profiler™ PCR Array Human DNA Repair (PAHS-042Z), QUIAGEN;) [44,45]. This gene set was significantly enriched in CD98hc KO cells (P-val<0.001, NES = 1.83, FDR<0.001) (Figures 3a and S3a).

RS usually results in the development of stretches of single-stranded DNA (ssDNA) rapidly coated by replication protein A (RPA), which functions as a signalling platform to recruit a wide variety of RS-response proteins involved in the DDR [46]. The phosphorylation of RPA and checkpoint kinase 1 (CHK1), the final transducer of this signalling pathway, is widely accepted as the most specific indicator of DDR activation [47–49]. CD98hc KO cells presented enhanced DDR activation as demonstrated by the increased in phosphorylated and total levels of CHK1 and RPA (Figure 3b), in line with the transcriptomic analysis (Figure 3a). The overexpression of these two DDR markers is probably the outcome of adaptation, which ensures that CD98hc KO cells survive in a

context of chronic RS. This phenomenon is also observed in tumour cells subjected to chronic RS imposed by the tumour microenvironment [50–55]. Apoptosis is often associated with inappropriate DNA damage resolution [56]. Furthermore, CD98hc KO cells presented increased apoptotic cell death (Figure S3b), which was already indicated by the results of the transcriptome analysis (Figure 3a).

To address whether BCAA and AAA limitation poses a challenge for the integrity of DNA replication in CD98hc KO cells, we evaluated the same DDR indicators in low 6AA cells. CHK1 and RPA phosphorylation was strongly upregulated in low 6AA cells compared to the control cells (Figure 3c). In this case, the total levels of both proteins were decreased in low 6AA cells (Figure 3c). The observed coupling between activating phosphorylation and subsequent downregulation of total levels of CHK1 has been described as a mechanism through which detrimental accumulation of this protein upon acute induction of genotoxic stresses is prevented [57]. Taken together, these results indicate that loss of CD98hc and shortage of BCAAs and AAAs compromise the cell cycle, triggering RS.

CD98hc and BCAA/AAA availability are required for correct completion of the cell division cycle

A key role of CHK1 within the DNA surveillance program is to stop cells from undergoing mitosis, thereby preventing the propagation of error-containing copies of the genome to daughter cells [58]. In this regard, we found an increase in the expression of genes involved in the transition from G2-phase to mitosis in CD98hc KO cells, according to the Hallmark database (Figure S3c). This observation suggests that the entry into mitosis is compromised by the activation of the CHK1-mediated G2/M checkpoint. Mitosis was analysed by immunofluorescence using the marker phospho-histone H3 (P-H3). Specific phosphorylation at serine 10 (Ser10) of histone H3 starts during late G2-phase and peaks during mitosis, when it undergoes different localization patterns during the mitotic phases, depending on chromatin condensation [59,60]. Thus, only patterns corresponding to cells undergoing mitosis were selected for quantification. CD98hc KO cells showed an impaired mitotic rate compared to WT cells (2.64% ± 0.3 vs. 3.8% ± 0.4%) (Figure 3d). This outcome was consistent with the increase in the percentage of CD98hc KO cells in the G2/M fraction (Figure 2b), which may reflect a delay in the G2-phase caused by mitotic blockage [61]. Mitotic activity was also strongly diminished in low 6AA cells (0.80 ± 0.1% vs. 3.67 ±

0.3 %) (Figure 3e), thereby indicating that BCAA and AAA availability is essential for cell division.

CD98hc KO cells present a defective PPP and a general reduction in nucleotide pool levels

To gain further insight into the link between the lack of CD98hc and the reported DNA damage, we performed a targeted metabolomics assay to quantify the nucleotide content of these cells. Notably, CD98hc KO cells showed a remarkable general decrease in nucleotide levels when compared to WT cells (Figure 4a). This finding suggests that the alteration underlying this massive reduction compromised the biosynthesis of both purine and pyrimidine nucleotides before the formation of their precursors (Figure 4a). Ribose 5-phosphate (R5P), which is both a product and an intermediate of the PPP, plays a critical role in *de novo* nucleic acid synthesis. In this regard, R5P functions as the scaffold for purine biosynthesis, but it also conforms the five-carbon sugar molecule of both purine and pyrimidine ribonucleotides [62]. In order to analyse the activity of the PPP, we used fully labelled glucose (U-^{13}C6-Glucose) in combination with gas chromatography-coupled to mass spectrometry (GC-MS). The PPP flux was abrogated in CD98hc KO cells in comparison to WT cells, as indicated by the absence of ^{13}C-R5P (M+5) (Figure 4b). In addition, total levels of R5P were measured, and accordingly, they were prominently decreased in the KO cells (Figure 4c). Taken together, these results suggest that CD98hc KO cells present an impaired nucleotide synthesis as a result of reduced R5P production, which is attributable to a decrease in PPP flux.

We next examined whether low 6AA cells also present same alterations in nucleotide metabolism. Interestingly, in this case we only found a reduction in the deoxynucleotide content (Figure 4d). This result suggests that low 6AA cells present an impaired conversion of nucleotides to deoxynucleotides. The Ribonucleotide Reductase (RNR) is the only enzyme able to catalyse this rate-limiting step [63]. Its activity is determined by the levels of its Ribonucleotide reductase regulatory subunit M2 (RRM2) [64]. Protein levels of RRM2 were found to be strongly diminished in low 6AA compared to control cells (Figure 4e). As expected, PPP activity was not affected in the former cells as indicated by levels of ^{13}C-R5P (M+5) (Figure 4f). These results strongly suggest that the decrease in deoxynucleotide levels is caused by suppression of RRM2 expression in low 6AA cells.

Shortage of nucleotides causes RS in CD98hc KO cells

We next sought to assess whether the decrease in nucleotides was responsible for the RS in CD98hc KO cells. To test this hypothesis, we examined whether supplementation of nucleosides in the culture media could rescue S-phase delay in these cells. Hence, cell culture media was supplemented with the five (A, U, C, G and T) nucleosides, and cell cycle distribution was evaluated after 48 h. The percentage of cells that remained in the S fraction after nucleoside addition decreased from 66.6 ± 3.8 % to 57.8 ± 5.4 % in CD98hc KO cells (Figure 5a), whereas the addition of nucleosides did not change cell cycle distribution in WT cells. This observation indicates that the shortage of nucleosides poses a replication barrier that delays the S-phase transition in Cd98hc KO cells. To further corroborate our hypothesis, we next studied the effects of exogenous nucleosides on the activation of the DDR signalling pathway in CD98hc KO cells. The phosphorylation of CHK1 and RPA was strongly reduced in CD98hc KO cells supplemented with exogenous nucleosides, compared to non-treated cells; while the total levels of the two proteins remained unchanged after supplementation (Figure 5b). Finally, we examined the effects of nucleoside addition on progression through the cell division cycle. To this end, we used P-H3-labelling by immunofluorescence in order to select and quantify cells undergoing mitosis. The mitotic rate was significantly recovered in nucleoside supplemented-CD98hc KO cells (Figure 5c). The RS triggered by BCAA and AAA shortage was also recovered after addition of exogenous nucleosides, since the DDR was reversed in low 6AA cells (Figure S4). On the basis of our observations, we conclude that a shortage of nucleotides jeopardises faithful DNA replication in CD98hc KO cells, resulting in RS and cell cycle arrest.

Discussion

All cells take up nutrients from the surrounding environment into metabolic pathways in order to fuel the wide variety of functions that they exert [65]. However, proliferating cells, including cancer cells, have an increased nutritional demand compared to normal cells since they must double their biomass in each cell cycle. In this regard, AA transporters play a key role in meeting this metabolic challenge [66–68]. Our results highlight that CD98hc functions as a regulatory hub, orchestrating not only cellular nutrient and redox homeostasis but also nucleotide metabolism. In this regard, we used low 6AA cells as a

novel model through which to study the impact of BCAA and AAA shortage on protein synthesis and cell cycle regulation, independently of oxidative stress and other metabolic alterations present in CD98hc KO cells.

Proteins account for ~ 50-60% of the total cellular biomass [69], thus, protein synthesis positively correlates with cell proliferation [70]. Our results show that ablation of CD98hc leads to a reduced protein synthesis rate, in line with the decrease in proliferation already described in CD98hc KO cells [13]. In this regard, we identified alterations in both mTORC1 and eIF2 nutrient-sensing pathways, both of which regulate protein synthesis (Figure 6). Our results indicate that mTORC1 downregulation is driven by BCAA and AAA shortage, in agreement with previously reported results (Figure 6) [8,19,71–74]. In support of this notion, the addition of BCAA- and AAA-containing dipeptides partially rescues cell proliferation [13] and mTORC1 activity in CD98hc KO cells. Furthermore, low 6AA cells present similar mTORC1 pathway inhibition to that observed on CD98hc KO cells.

In contrast, we show that BCAA and AAA limitation does not induce the phosphorylation of eIF2α in our model. This finding is supported by the observation that the supplementation with dipeptides as an alternative source of BCAAs and AAAs did not ameliorate the activation of eIF2α in CD98hc KO cells. It is well established that, in conditions of AA starvation, uncharged tRNAs activate GCN2 [75,76], which in turn phosphorylates eIF2α [77–79]. However, to the best of our knowledge, neither tRNA charging nor direct activation of GCN2 has been evaluated after partial AA restriction rather than full deprivation. Our results show that BCAA and AAA restriction is not enough to cause a substantial increase in the level of deacylated tRNAs. Thus, our data suggest that GCN2 does not govern the activated eIF2-mediated ISR pathway in the CD98hc KO model, although its participation in the response cannot be ruled out. In this regard, a reduction of BCAAs and AAAs in WT cells (low 6AA cells) did not trigger any detectable change in the activity of eIF2α, despite the impaired proliferation rate present in these cells. An alternative explanation for the observed activation of the ISR could be that increased levels of oxidative stress in CD98hc KO cells mediate eIF2α phosphorylation (Figure 6) through activation of the kinase heme-regulated inhibitor (HRI), which is activated in response to oxidative stress [80–83].

In addition to protein synthesis, other cellular processes, such as the cell cycle, are regulated by the nutritional status of the cell [84–86]. The progression of the cell cycle is

tightly dependent on the ability of the cell to acquire nutrients and produce energy to drive the constant *de novo* biosynthesis of nucleotides [87,88], which, when limiting, may affect genome integrity in diverse ways [89–91]. Our results indicate that CD98hc is essential for the biosynthesis of nucleotides (Figure 6). Consistent with this, lack of CD98hc promotes a dramatic reduction in the nucleotide pool, which leads to ATR-CHK1-dependent DDR activation and subsequent protective arrest in S-phase. The induction of the DDR in CD98hc KO cells subjected to chronic RS is likely to be governed by the overexpression of the components of the pathway, probably as a result of a chronic adaptation. In support of this notion, other studies have proposed that this behaviour is an adaptation to the chronic RS in cancer [50–55]. Moreover, we report that a shortage of BCAAs and AAAs entails DNA damage and subsequent RS in low 6AA cells. In this case, these cells present markedly increased phosphorylated levels of CHK1 and RPA, probably due to acute nutritional stress. Data provided by the transcriptome analysis suggest that the reduced mitotic rate in CD98hc KO cells is due to the activation of the G2/M checkpoint, which also involves the activation of CHK1 [92,93].

The addition of nucleosides rescued the replication-induced DNA damage in CD98hc KO cells, as reflected in the marked decrease of the phosphorylation of RPA and CHK1. Consistently, nucleoside-supplemented CD98hc KO cells resumed cycle progression, thus reversing the observed S-phase arrest. Finally, the provision of nucleosides also rescued the slowed entry into mitosis. Collectively, these findings unveil that CD98hc is critical for the prevention of derangements in nucleotide levels.

The PPP is a major pathway for glucose catabolism and the main source of R5P, which forms the sugar backbone of all nucleotides [94]. In this study, we propose that the abrogation of the PPP flux and, consequently, the drastic reduction of R5P, explains the decreased levels of nucleotides in CD98hc KO cells (Figure 6). In support of this notion, other studies have demonstrated that both R5P availability [95,96] and impaired PPP activity [97–100] trigger alterations in nucleotide biosynthesis and DNA replication. However, the mechanism by which the PPP is downregulated in CD98hc KO cells remains to be determined. A potential explanation may lie in the reported reduction of glucose uptake in cells lacking CD98hc due to decreased protein levels of GLUT1 [29], corroborated in our model (data not shown). In support of this hypothesis, other studies have linked glucose restriction with cell cycle arrest and nucleotide depletion [101–103]. On the basis of our data, we conclude that the mechanism by which the lack of CD98hc promotes a decrease in nucleotide levels is

unlikely to be determined exclusively by the shortage of BCAAs and AAAs in CD98hc KO cells, since low 6AA cells did not present altered PPP activity and showed a reduction only in the deoxynucleotide pool. The intracellular concentration of deoxynucleotides is tightly regulated by the expression of RRM2, the only enzyme that catalyses the rate-limiting step for the *de novo* conversion of ribonucleosides to deoxyribonucleosides [104,105]. Consistently, low 6AA cells presented a severe downregulation of RRM2 protein levels, which probably underlies the RS reported in this model (Figure 6). However, the link between BCAA and AAA restriction and RRM2 downregulation in low 6AA cells remains to be elucidated. In this regard, the ability of the oncogenic protein c-myc to control DNA replication is well established [106–108]. It has been reported that c-myc enhances the biosynthesis of nucleotides by promoting deoxynucleotide synthesis through the upregulation of RRM2 [109,110]. Thus, it is feasible that low 6AA cells showed reduced c-myc expression. In support of this notion, Csibi and co-workers demonstrated that the mTORC1 pathway, which is downregulated in low 6AA cells, positively regulates c-myc translation [111].

In summary, in this study we have evaluated the extensive cellular functions related to protein synthesis and cell cycle regulation that rely on CD98hc (Figure 6). Our data further support CD98hc as a putative target in pathophysiological scenarios, especially in the context of cancer treatment. On the one hand, targeting CD98hc downregulates tumour growth by decreasing the redox counterbalance capacity mediated by CD98hc-xCT [112,113], by limiting the required balance in the AA content for proper protein synthesis and cell proliferation, mostly harmonised by CD98hc-LAT1 [114–118], and by compromising integrin-regulated signalling pathways [4,5,13]. On the other hand, here we demonstrate that BCAAs and AAAs are required for deoxynucleotide synthesis. In addition, CD98hc regulates the PPP flux; thereby its ablation causes a broader alteration in the nucleotide synthesis. Consequently, the ablation of CD98hc triggers RS and cell cycle arrest. Such a therapeutic strategy would be beneficial for cancer treatment, as it would impair tumour cell proliferation. Moreover, the arrest in S-phase may enhance the sensitivity of cancer cells to chemotherapeutic [119,120] and radiotherapeutics [121–123] agents. Thus, combinatorial therapy involving the ablation of CD98hc emerges as a promising strategy for the treatment of cancer.

Methods

Cell culture

WT and CD98hc KO fibroblasts derived from mouse embryonic stem cells were generated by Chloé C. Féral (Université de Nice - Sophia Antipolis, Nice, France) [4]. WT and KO cells were cultured in DMEM high glucose (21969035, ThermoFisher) medium supplemented with 10% v/v FBS (SH30066.03, HyClone), 20 mM Hepes, pH 7.3, 100 μM non-essential amino acids (11140035, ThermoFisher), 2 mM l-glutamine (25030-024, ThermoFisher), 100 μM β-mercaptoethanol (31350010, ThermoFisher) and 100 U/mL Penicillin-Streptomycin (15140122, ThermoFisher). WT cells named as control and low 6AA cells were cultured for 3 days in DMEM medium (D9800-13, Stratech) supplemented with 10% v/v FBS (SH30066.03, HyClone), 20 mM Hepes, pH 7.3, 100 μM non-essential amino acids (11140035, ThermoFisher), 2 mM l-glutamine (25030-024, ThermoFisher), 100 μM β-mercaptoethanol (31350010, ThermoFisher), 100 U/mL Penicillin-Streptomycin (15140122, ThermoFisher), 25 mM glucose, 1 mM sodium pyruvate, 44 mM sodium bicarbonate and the same concentration of amino acids as complete DMEM media, with the exception of BCAAs and AAAs in low 6AA media (16 μM L-Isoleucine, 16 μM L-Leucine, 8 μM L- Phenylalanine, 1.5 μM L-Tryptophan, 7.8 μM L-Tyrosine and 16 μM L-Valine). Total AA concentrations are indicated in Figure S2A. Cells were maintained at 37°C and 5% v/v CO_2 in a humidified incubator and were periodically tested with a PCR detection kit to ensure that they were mycoplasma-free (MP0035, Sigma-Aldrich).

Dipeptide and nucleoside supplementation

BCAA- and AAA-containing dipeptides were synthesised by the Synthesis of Peptides Unit (U3) of the CIBER in Bioengineering, Biomaterials and Nanomedicine (CIBER-BBN) at the Barcelona Science Park, as reported in [13]. Where indicated, dipeptides were supplemented in complete DMEM medium. BCAA: isoleucine (200 μM), leucine (200 μM), and valine (25 μM), or AAA: phenylalanine (25 μM), tyrosine (200 μM), and tryptophan (100 μM).

Where indicated, nucleosides (ES-008-D, EmbryoMax) were supplemented for 48 h (150 μM cytidine, 150 μM guanosine, 150 μM uridine, 150 μM adenosine and 50 μM thymidine).

Protein synthesis measurement

Cells were washed twice with Phosphate-Buffered-Saline (PBS) and incubated for 1 min at 37°C with labelling media (Met/Cys-free DMEM with the usual supplements, dialysed FBS and 120 UCi/mL of ^{35}S-Methionine/Cysteine (Perkin Elmer)). Next, cycloheximide (C4859, Sigma-Aldrich) was added for 1 min at 37°C at a final concentration of 100 μg/mL. Cells were then washed three times with cold PBS (plus 5 mM Met and Cys). They were then harvested in 0.5 mL of cold PBS and pelleted by centrifugation for 3 min at 3000 *g* at 4°C. Cells were lysed for 30 min at 4°C with NET buffer (50 mM Tris HCl pH 7.4, 150 mM NaCl, 5 mM EDTA, 0.5 % IGEPAL, with protease inhibitors) and, after centrifugation for 10 min at 10000 *g*, the supernatant was precipitated with cold 10 % Trichloroacetic acid in order to measure the amount of intracellular radioactivity incorporated into protein. The percentage of intracellular radioactivity incorporated was calculated.

Immunoblotting

Cells were lysed in radioimmunoprecipitation assay (RIPA) buffer (150 mM NaCl, 10 mM Tris, pH 7.2, 0.1% w/v SDS, 1% w/v Triton X-100, 1% w/v deoxycholate, 5 mM EDTA, phosphatase inhibitor cocktail (524628-1SET, Merck Chemicals & Life Science S.A.) and protease inhibitor mixture (11836153001, Sigma-Aldrich). After centrifugation at 10,000 *g* for 15 min at 4°C, protein concentrations were determined using the Pierce BCA protein assay (23225, Cultek). Protein extracts (20 μg, unless specified otherwise) were separated by electrophoresis on 10% or 15% SDS polyacrylamide gel and transferred onto Immobilon membranes (IPVH00010, Millipore). Membranes were blocked in 5% non-fat milk or 3% BSA according to datasheet specifications and incubated with the following anti-mouse antibodies: anti-P-S6 (#2211S, Cell Signaling, 1:2000); anti-S6 (sc-74459, Santa Cruz, 1:8000); anti-P-eIF2α (#9721, Cell Signaling, 1:1000); anti-eIF2α (#9722, Cell Signaling, 1:1000); anti-HRI (sc-21949, Santa Cruz, 1:500); anti-P-p70 S6K (#1679234S, Cell Signaling, 1:1000); anti-p70 S6K (#9202S, Cell Signaling, 1:1000); anti-P-CHK1 (#2348, Cell Signaling, 1:2000); anti-CHK1 (#2360, Cell Signaling, 1:2000); anti-P-RPA32(A300-245A-T, Bionova Cientifica, 1:2000); anti-RPA32 (1672208T, S.G. Servicios Hospitalarios, 1:2000); anti-Nrf2 (ab62352, Abcam, 1:1000); anti-RRM2 (GTX103193, GeneTex, 1:1000); anti-tubulin (#T5168, Sigma-Aldrich, 1:1000); anti-Vinculin (ab18058, Abcam, 1:5000); and anti-β-Actin (A1978,Sigma-Aldrich, 1:5000). Immunoreactive bands were detected with horseradish peroxidase anti-mouse (715-035-150, Jackson Immuno Research Europe,

1:10.000), anti-rabbit (711-035-152, Jackson Immuno Research Europe, 1:10.000), or anti-rat (SC-2956, Santa Cruz, 1:15.000) antibodies using the ECL system (RPN2106, Sigma-Aldrich). Analysis and quantification of immunoblotting were performed using ImageJ software.

Cell proliferation assay

Control and low 6AA cells were seeded in duplicate in corresponding media at 1×10^4 cells per 35-mm diameter dish. Cells were collected and counted at indicated time points using the Neubauer chamber method.

Annexin V/PI apoptosis staining

The annexin V–FITC (A23204, Invitrogen) and propidium iodide (IP) (P4864, Sigma-Aldrich) double staining technique was used to evaluate apoptosis. Cells were seeded in 6-well plates at a density of of 1×10^5 cell/mL. A positive control was performed by treating cells with 1 µM of staurosporine (S5921, Sigma-Aldrich) for 3 h. Cells were then harvested, washed in PBS and centrifuged. They were resuspended in 100 µl of Annexin V binding buffer. Samples were incubated with 5 µL of annexin V conjugate and 1 µL of IP for 15 min at room temperature (RT). Then, 300 µL of binding buffer was added to each sample, which was then subjected to flow cytometry (Gallios Flow Cytometer, Beckman Coulter). FSC-Area (forward scatter) and SSC-Area (side scatter) gating was applied to discriminate single cell population from debris. FITC and PI fluorescence were detected at 515 nm and 620 nm respectively. Ten-thousand events were recorded for each sample. Fluorescence was displayed on a scatter plot with PI and FITC quadrant gates. Data acquisition was performed using FlowJO software.

Cell cycle analysis

Cells were seeded in 6-well plates at a density of 1×10^5 cell/mL with no additives or in the presence of nucleosides. When indicated, cells were synchronised by double thymidine block [41,124]. In that case, cells were incubated with 2 mM of thymidine (T1895, Sigma-Aldrich) for 16 h. Next, they were incubated for 8 h in complete medium without thymidine, and another block (2 mM thymidine) was performed for 16 h. After the double block, cells were released in complete medium for the indicated times. For cell cycle analysis, the unattached cells were collected from the growth media and pooled before

washing the culture with PBS. Next, PBS was pooled and cells were trypsinised. Cells were then fixed in 70% ethanol and stored at -20°C for at least 2 h. Before the analysis, cells were centrifuged and resuspended in PI/ Triton X-100 (9036-19-5, Merck) staining solution with RNase A (740505, Cultek) (0.1% (v/v) Triton X-100, 2 mg RNase, 500 µM PI) for 30 min at RT. Samples were then subjected to flow cytometry (Coulter EPICS (R) XL Flow Cytometry System). Forward and side scatter area gating were used to identify singlets. Interval gates were placed on the detected peaks corresponding to the phases of the cell cycle. Percentage of cells in G1-, S-, and G2/M-phases was determined using MCycle software. Cell cycle profiles were generated using FlowJO software.

Quantification of intracellular ROS levels by dichlorofluorescein assay

The levels of intracellular free radicals were assayed by measuring intracellular oxidation of H_2DCFDA. Cells were seeded onto 6-well plates in corresponding media in normal conditions. Cultures were incubated with 1 µM non-fluorescent H_2DCFDA (C6827, Thermo Fisher). After a 30-min incubation, H_2DCFDA is converted to highly fluorescent 2′, 7′-dichlorofluorescein (DCF) upon cleavage of the acetate groups by intracellular esterases and oxidation. Cells were then harvested and washed in PBS, and intracellular fluorescence was measured using the Gallios Flow Cytometer system (Beckman Coulter).

Gene expression analysis

Total RNA from the cell culture was extracted using an RNA extraction kit (12183018A, PURELINK RNA MINI KIT, Invitrogen) following the manufacturer's instructions. RNA was reverse-transcribed with the reverse transcriptase SuperScript RTII (18064014, Invitrogen). Quantitative real-time PCR was performed using the ABI Prism 7900 HT real-time PCR machine (Applied Biosystems) and the SYBR Green PCR Master Mix (4368702, Thermofisher). The following sets of specific primers were used: cationic amino acid transporter-1 (CAT1) (sense, 5′-GGACACGGAGCGGAAAATACACC-3′; antisense 5′-GCTCCCTGCTGTACTGGTTCATGGTC-3′); cationic amino acid transporter-3 (CAT3) (sense, 5′-GGCTCCCTCTGTGCACTTTCTA-3′; antisense 5′-TAGCAAGGACACGGAACAGGA-3′); and y+L amino acid transporter-1 (y^+LAT1) (sense, 5′-CTAAAGGGCAATGCGAGCAAGCTG-3′; antisense, 5′-GGTGGTACCCAGTTCAGCGTAACAAAG). Samples were normalised to ribosomal

phosphoprotein, large, P0 (RPLP0) (sense, 5′-CACTGGTCTAGGACCCGAGAAG-3′; antisense, 5′-GGTGCCTCTGGAGATTTTCG-3′).

RNA expression profiling

Total RNA from the cell culture was extracted using an RNA extraction kit (12183018A, PURELINK RNA MINI KIT, Invitrogen) following the manufacturer's instructions. RNA integrity was assessed using RNA Nano Assay (Agilent Bioanalyzer 2100) and RNA quantification were executed using Nanodrop ND 1000 Spectrophotometer. cDNA library preparation and amplification were performed from 25 ng total RNA using WTA2 (Sigma-Aldrich) with 17 cycles of amplification. 8 µg of cDNA was subsequently fragmented by DNAseI and biotinylated by terminal transferase obtained from GeneChip Mapping 250k Nsp Assay Kit (Affymetrix). The hybridisation mixture was prepared following the Gene Atlas protocol (Affymetrix). Each sample target was hybridised to a Mouse Genome 430 PM array. After hybridisation for 16 h at 45°C, washing and staining was performed in the GeneAtlas Fluidics Station (Affymetrix). The arrays were scanned in a GeneAtlas Imaging Station (Affymetrix). All processing was performed following the manufacturer's recommendations. CEL files were generated from DAT files using Affymetrix Command Console software. To generate the log2 expression estimates, overall array intensity was normalised between arrays and the probe intensity of all probes in a probe set was summarised to a single value using the RMA (Robust Multichip Average) algorithm [125]. Microarray processing was performed at Functional Genomics Facility at IRB Barcelona.

Bioinformatic analyses

Affymetrix arrays were normalized using RNA. Background correction and summarization [126] as implemented in the "affyPLM" package [127] from the R statistical framework [128]. Annotations for the HT-430 array version na34 were downloaded from Affymetrix (Affymetrix Analysis Center. Netaffx https://www.affymetrix.com/analysis/index.affx). A linear model was fitted in order to identify differentially expressed genes between conditions of interest with batch scan as covariate. The "lmFit" function from the "limma" package [129] was used for fitting the model. Gene set enrichment analysis (GSEA), as implemented in [130], was performed on all the genes in the array ranked by the t-statistic obtained from the model. For each gene,

the t-statistic of the most variable probe was used as a representative. We also ran GSEA on custom gene sets.

Immunofluorescence analysis of mitosis

Cells were fixed in 4% paraformaldehyde (PFA) (sc-281692, Santa Cruz) in PBS for 20 min and washed with 50 mM NH_4Cl. They were then permeabilised and blocked in 0.1% triton X-100 (9036-19-5, Merck), 2% FBS (F7524, Sigma-Aldrich) in PBS for 10 min. The coverslips were incubated with anti-phospho-Histone (P-H3) antibody (06-570, Merck) diluted 1:100 in 2% FBS PBS for 30 min. They were then washed with PBS, incubated in secondary antibody diluted 1:400 in 2% FBS PBS for 30 min and washed again with 0.5% triton X-100 PBS. They were then washed with PBS, stained with Hoechst 33342 (H3570, Invitrogen) diluted 1:20.000 in PBS and then washed again with PBS. Coverslips were mounted on microscope slides with Flouromount (17984-25, Fisher Scientic). WideField images were obtained using Olympus IX 81 microscope with objective lenses of 20x/ 0.45 LUCPlanFL N and 40x/ 0.75 UPlan FL N and ScanR Acquisition Software v2.3. Nuclei segmentation was performed using a tailor-made ImageJ macro. Mitosis was measured manually. Image processing and quantification were performed using ImageJ software.

AA uptake measurement

Transport activities were studied on whole cells as previously described [131] by measuring the transport of 10 µM L-[2,3-^{3}H]-Arginine (American Radiolabeled Chemicals). To distinguish between y^+ and y^+L transport systems, L-arginine uptake assays were performed in Na^+ media in the absence or presence of 1 mM L-leucine.

Metabolite extraction

Cells were cultured for 16 h in the presence of fully labelled glucose (^{13}C6-glucose, Sigma-Aldrich). Media were also collected. Cell pellets were scrapped, collected and frozen. Briefly, the pellets were resuspended in 300 µl of cold acetonitrile:methanol:water (5:4:1, v:v:v) containing ^{13}C-glycerol (5 µl/ml) as internal standard. 10 µl of ^{13}C3-glycerol (150 µl/ml) was also added to 200 µl of medium. Metabolites from cells were extracted with three rounds of liquid N2 immersion and sonication, followed by 1 h in ice before centrifugation at 14,500 rpm (10 min at 4 ºC). Samples of media were lyophilised and resuspended in 500 µl of cold acetonitrile:methanol:water (5:4:1, v:v:v). After vortexing,

they were placed in ice for 1 h and centrifuged at 14,500 rpm (10 min at 4 °C). Metabolite extractions of cells and media were split in aliquots of 200 and 400 µL for GC-MS, respectively, and 50 µL for LC-MS analysis.

GC-MS analysis

Samples were dried under a stream of N2 gas and lyophilised before chemical derivatisation with 40 µl methoxyamine in pyridine (30 µg/ml) for 45 min at 60°C. Samples were also silylated using 25 µl N-methyl-N-trimethylsilyltrifluoroacetamide with 1% trimethylchlorosilane (Thermo Fisher Scientific) for 30 min at 60°C to increase the volatility of metabolites. A 7890A GC system coupled to a 7000 QqQ mass spectrometer (Agilent Technologies) was used for isotopologue determination. Derivatised samples were injected (1 µl) into the gas chromatograph system with a split inlet (5:1) equipped with a J&W Scientific HP-5ms stationary phase column (30 m × 0.25 mm i.d., 0.1 µm film, Agilent Technologies). Helium at a flow of 1.5 ml/min was used as carrier gas. The temperature gradient was from 70 to 190°C at a heating rate of 11°C/min and from 190 to 325°C at 21°C/min. Metabolites were ionized using positive chemical ionization (CI) with isobutene as reagent gas. Mass spectral data on the 7000 QqQ were acquired in scan mode monitoring Ribose-5P (RT (min): 13.92; m/z: 620.

LC-MS analysis

To determine nucleotides, cell extracts were analysed using an UHPLC system coupled to a 6490 QqQ mass spectrometer (Agilent Technologies). Cell extracts were injected (5 µl) and metabolites were separated using an InfinityLab Poroshell 120 HILIC-Z column (2.7 µm, 2.1×100 mm, Agilent). The mobile phases used for the metabolite separation were A: 50 mM ammonium acetate with 5 µM medrionic acid; and B: acetonitrile. The chromatographic gradient was isocratic for 0.5 min at 80% B, from 0.5 to 7.5 min decreased to 70% B and from 7.5 to 8.5 min decreased to 50%, and maintained for 30 sec. From 9.0 min to 9.2 min the percentage of B rose quickly to 80 % and finally the column was equilibrated at 80 % B until min 11. Flow rate was 0.7 mL/min. The QqQ mass spectrometer worked in MRM mode using the transitions in Table 1 to determine nucleotides. The electrospray ionization source (ESI) worked in positive and negative mode.

Table 1.

Metabolite	RT (min)	1st Transition (CE (V))	2nd Transition (CE (V))	Polarity
AMP	3.13	348 →136 (16)	348 → 199(56)	Positive
ADP	4.64	428 → 136 (32)	428 → 348 (16)	Positive
dAMP	2.79	332 → 136 (8)	332 → 81 (12)	Positive
dADP	4.34	412 → 136 (20)	412 → 81 (36)	Positive
CMP	4.40	324 → 112 (8)	324 → 95 (48)	Positive
CDP	5.89	404 → 112 (12)	404 → 95 (56)	Positive
dCMP	3.92	308 → 112 (12)	308 → 95 (56)	Positive
dCDP	5.51	388 → 112 (12)	388 → 81 (20)	Positive
GMP	4.46	364 → 152 (8)	364 → 135 (52)	Positive
GDP	5.88	444 → 152 (32)	444 → 135 (60)	Positive
dGMP	4.01	348 → 152 (8)	348 → 135 (56)	Positive
UMP	3.19	325 → 97 (8)	325 → 41 (48)	Positive
UDP	4.67	403 → 159 (24)	403 → 79 (52)	Negative
dTDP	3.89	401 → 79 (60)	401 → 159 (24)	Negative
IMP	3.76	349 → 137 (16)	349 → 110 (60)	Positive

tRNA aminoacylation array

To determine the fraction of aminoacyl-tRNAs from the total tRNAs, we used tRNA-tailored microarrays and the protocol described earlier [132]. Total RNA was isolated using acidic phenol (pH 4.5) to preserve the aminoacyl moiety. The arrays were normalised to spike-standards, and quantification and normalisation was performed using in-house Phyton and R scripts.

Intracellular AA quantification

Intracellular amino acid content was analysed using the Mass Trak Amino Acid Derivatization kit (186003836, Waters) and following the manufacturer's instructions. Cells were collected and homogenised in water. 100 µL of 50 µM norvaline was added to 100 µL of each sample as an internal standard. Samples were vortex for 10 sec and centrifuged at 16,000 g for 5 min. Next, 20 µL of supernatant from each sample was mixed with 60 µL of NaOH 0.5M/Borate buffer in a chromatography injection vial. After vortexing for 10 sec, 20 µL of 6-aminoquinolyl-N-hydroxysuccinimidyl carbamate (AQC)

solution was added to the vials for AA derivatisation. Samples were then vortexed for 20 sec and incubated for 1 min at room temperature followed by 10 min at 55°C. Sample preparations were injected into an Ultra High Performance Liquid Chromatograph (Shimadzu) (injection volume: 1 µL). Chromatography was performed using MassTrak AAA columns (2.1 x 150 mm, 1.7 µm) (Waters). Solutions A and B were used as mobile phases (A: MassTrak AAA Eluent A Concentrate, diluted 1:10; B: MassTrak AAA Eluent B) and MassTrak standard gradient was used as provided in the kit. Detection was performed at 260 nm. AAs were quantified with Labsolutions software (Shimadzu).

Statistical analysis

Comparison of group means was performed using linear models with or without random effects depending on the data. Linear models were fitted with the R [128] function "lm" and mixed effects models with the "lmer" function of the lme4 R package [133]. Whenever necessary, experiment was included as a fixed effect covariable. For the mixed effect models technical replicate was taken as a random effect. All data was log transformed except for panel 3C. The correct model for each dataset was chosen as follows: a mixed effect model was used when the variance explained by the replicate was larger than zero. Technical replicates were collapsed through the mean before log transforming when a linear model was chosen. Experiment was included as a fixed covariable if the model was significantly improved (F-test p-value lower than 0.25). Figures 1D, 1E, 1H, S1 (left and right graphs), 3C (lower right panel) and 4E were analysed with a linear model, while all other panels were analysed with mixed effects models. In figures S1C (left and middle graphs), 3B (upper graphs) and 4E, experiment was included as a fixed effect. In figures, 1E, 1H, S1 (left and right graphs) and 3C (lower right panel), replicates were collapsed to one observation through the mean. If not aforementioned a Statistical significance was analysed using a two-tailed Student's t-test.

List of abbreviations

The abbreviations used are: CD98hc, cluster of differentiation 98 heavy chain; AA, amino acid; SLC, solute carrier; LAT1, L-type amino acid transporter 1; LAT2, L-type amino acid transporter 2; y+LAT1 y+L amino acid transporter 1; y+LAT2 y+L amino acid transporter 2; asc1, alanine-serine-cysteine-1; mTORC1, mTOR complex 1; BCAA, branched-chain

amino acid; AAA, aromatic amino acid; ROS, reactive oxygen species; eIF2, Eukaryotic Initiation Factor 2; ISR, Integrated Stress Response; PPP, pentose phosphate pathway; R5P, Ribose 5-phosphate; DDR, DNA damage response; HAT, heteromeric amino acid transporter; GSH, glutathione; FES, fibroblasts derived from embryonic stem cells; β-ME, β mercaptoethanol; EAA, essential amino acid; PEPT1, peptide transporter 1; PPP, pentose phosphate pathway; TCA, tricarboxylic acid cycle; PDH, pyruvate dehydrogenase; GLUT1, glucose transporter 1; CD147, cluster of differentiation 147; MCT1, monocarboxylate transporter 1; RS, replication stress; S6, ribosomal protein S6; PERK, PKR-like ER kinase; PKR, protein kinase double-stranded RNA-dependent; GCN2, general control non-derepressible-2; HRI, heme-regulated inhibitor; BiP, immunoglobulin heavy chain-binding protein; XBP1, X-box binding protein 1; CHOP, C/EBP [CCAAT/enhancer-binding protein]-homologous protein; AA+, cationic amino acid; AA0, neutral amino acid; H2DCFDA, 2',7'-dichlorodihydrofluorescein diacetate; DCF, fluorescent 2′, 7′-dichlorofluorescein; Nrf2, nuclear factor erythroid 2-related factor; t BHQ, tert-butylhydroquinone; DDR, DNA damage response pathway; RPLP0, ribosomal phosphoprotein, large, P0; CAT, cationic amino acid transporter; RIPA, radio-immunoprecipitation assay; BCA, bicinchoninic acid assay; ES, Enrichment Score, NES, Normalised enrichment score; FDR, False discovery rate; RPA, replication protein A; CHK1, checkpoint kinase 1; GC-MS, gas chromatography-coupled to mass spectrometry; RNR, Ribonucleotide Reductase; RRM2, Ribonucleotide Reductase Regulatory Subunit M2; H3, histone 3; GSEA, gene set enrichment analysis; IP, propidium iodide; LG-MS, liquid chromatography–mass spectrometry; AMP, adenosine monophosphate; ADP, adenosine diphosphate; dADP, deoxy-adenosine diphosphate; dAMP, deoxy-adenosine monophosphate; CMP, cytidine monophosphate; CDP, cytidine diphosphate; dCMP, deoxy-cytidine monophosphate; dCDP, deoxy- cytidine diphosphate; GMP, guanosine monophosphate; GDP, guanosine diphosphate; dGMP, deoxy- guanosine monophosphate; UMP, uridine monophosphate; UDP, uridine diphosphate; dTDP, deoxythymidine diphosphate and IMP, inosine monophosphate.

Acknowledgments

We thank all the members of Manuel Palacín's and Antonio Zorzano's laboratory for support and technical advice. Special thanks go to Dr. Jordi Duran, Dr. Aida Rodriguez-Nuevo and Dr. Juan Pablo Muñoz for their constructive comments and discussions. We

also wish to thank the Functional Genomics, Biostatistics/bioinformatics, and Advanced Digital Microscopy Facilities of IRB Barcelona for their invaluable assistance, as well as the Flow Cytometry Facility of the Parc Científic de Barcelona (PCB).

Availability of data and material

The raw RNA expression array data that support the findings of this study have been deposited in GEO with the accession code GSE126781.

The rest of the data generated or analysed during this study are included in this published article and its supplementary information files.

Competing interests

The authors declare that they have no competing interests.

Funding

This work has been supported by the Spanish Ministry of Science and Innovation SAF2015-64869-R-FEDER, Fundació la Marató TV3 (20132330), and Generalitat de Catalunya Grants SGR2009-1355 and SGR2017-961. We gratefully acknowledge institutional funding from the Spanish Ministry of Economy, Industry and Competitiveness (MINECO) through the Centres of Excellence Severo Ochoa award, and from the CERCA Programme of the Catalan Government. Sara Cano-Crespo was a recipient of a Severo Ochoa doctoral fellowship.

Authors' contributions

SCC designed research, performed the research, analysed results and wrote the paper. JC performed protein synthesis and AA uptake measurements and wrote the paper. AJ and OY performed metabolite extraction, GC-MS analysis and LC-MS analysis. GFM and LRB designed research. JG performed intracellular AA quantification. CP and ZI performed the tRNA array. AZ did a critical revision of the article. CSOA performed the statistical and

bioinfomatic analysis. MP designed research, analysed results and wrote the paper. All authors read and approved the final manuscript.

Bibliography

1. Bröer, S. & Palacín, M. The role of amino acid transporters in inherited and acquired diseases. *Biochem. J.* **436,** 193–211 (2011).
2. Fotiadis, D., Kanai, Y. & Palacín, M. The SLC3 and SLC7 families of amino acid transporters. *Mol. Aspects Med.* **34,** 139–158 (2013).
3. Fenczik, C. A. *et al.* Distinct Domains of CD98hc Regulate Integrins and Amino Acid Transport. *J. Biol. Chem.* **276,** 8746–8752 (2001).
4. Feral, C. C. *et al.* CD98hc (SLC3A2) mediates integrin signaling. *Proc. Natl. Acad. Sci. U. S. A.* **102,** 355–60 (2005).
5. Fenczik, C. A., Sethi, T., Ramos, J. W., Hughes, P. E. & Ginsberg, M. H. Complementation of dominant suppression implicates CD98 in integrin activation. *Nature* **390,** 81–85 (1997).
6. Palacín, M. & Kanai, Y. The ancillary proteins of HATs: SLC3 family of amino acid transporters. *Pflugers Arch.* **447,** 490–494 (2004).
7. Haining, Z. *et al.* Relation of LAT1/4F2hc expression with pathological grade, proliferation and angiogenesis in human gliomas. *BMC Clin. Pathol.* **12,** 4 (2012).
8. Cormerais, Y. *et al.* Genetic Disruption of the Multifunctional CD98/LAT1 Complex Demonstrates the Key Role of Essential Amino Acid Transport in the Control of mTORC1 and Tumor Growth. *Cancer Res.* **76,** 4481–4492 (2016).
9. Ganapathy, V., Thangaraju, M. & Prasad, P. D. Nutrient transporters in cancer: Relevance to Warburg hypothesis and beyond. *Pharmacol. Ther.* **121,** 29–40 (2009).
10. Vučetić, M., Cormerais, Y., Parks, S. K. & Pouysségur, J. The Central Role of Amino Acids in Cancer Redox Homeostasis: Vulnerability Points of the Cancer Redox Code. *Front. Oncol.* **7,** 319 (2017).
11. McCracken, A. N. & Edinger, A. L. Nutrient transporters: the Achilles' heel of anabolism. *Trends Endocrinol. Metab.* **24,** 200–8 (2013).
12. Cantor, J. M. & Ginsberg, M. H. CD98 at the crossroads of adaptive immunity and cancer. *J. Cell Sci.* **125,** 1373–82 (2012).
13. de la Ballina, L. R. *et al.* Amino Acid Transport Associated to Cluster of Differentiation 98 Heavy Chain (CD98hc) Is at the Cross-road of Oxidative Stress and Amino Acid Availability. *J. Biol. Chem.* **291,** 9700–11 (2016).
14. Dixon, S. J. *et al.* Ferroptosis: An Iron-Dependent Form of Nonapoptotic Cell Death. *Cell* **149,** 1060–1072 (2012).
15. Dixon, S. J. *et al.* Pharmacological inhibition of cystine-glutamate exchange induces endoplasmic reticulum stress and ferroptosis. *Elife* **3**, e02523 (2014).
16. Okuno, S. *et al.* Role of cystine transport in intracellular glutathione level and cisplatin resistance in human ovarian cancer cell lines. *Br. J. Cancer* **88,** 951–956 (2003).
17. Sato, H. *et al.* Redox imbalance in cystine/glutamate transporter-deficient mice. *J. Biol. Chem.* **280,** 37423–37429 (2005).
18. Forman, H. J., Zhang, H. & Rinna, A. Glutathione: overview of its protective roles, measurement, and biosynthesis. *Mol. Aspects Med.* **30,** 1–12 (2009).
19. Elorza, A. *et al.* HIF2α Acts as an mTORC1 Activator through the Amino Acid Carrier SLC7A5. *Mol. Cell* **48,** 681–691 (2012).
20. Milkereit, R. *et al.* LAPTM4b recruits the LAT1-4F2hc Leu transporter to lysosomes and promotes mTORC1 activation. *Nat. Commun.* **6,** 7250 (2015).
21. Cuyàs, E., Corominas-Faja, B., Joven, J. & Menendez, J. A. Cell cycle regulation by the nutrient-sensing mammalian target of rapamycin (mTOR) pathway. *Methods Mol Biol.* **1170**, 113–144 (2014).
22. Rosner, M., Fuchs, C., Siegel, N., Valli, A. & Hengstschlager, M. Functional interaction of mammalian target of rapamycin complexes in regulating mammalian cell size and cell cycle. *Hum. Mol. Genet.* **18,** 3298–3310 (2009).
23. Fingar, D. C. *et al.* mTOR controls cell cycle progression through its cell growth effectors S6K1 and 4E-BP1/eukaryotic translation initiation factor 4E. *Mol. Cell. Biol.* **24,** 200–16 (2004).
24. Lane, A. N. & Fan, T. W.-M. Regulation of mammalian nucleotide metabolism and biosynthesis. *Nucleic Acids Res.* **43,** 2466–85 (2015).

25. Mayers, J. R. *et al.* Tissue of origin dictates branched-chain amino acid metabolism in mutant Kras-driven cancers. *Science.* **353,** 1161–1165 (2016).
26. Li, T. *et al.* Defective Branched-Chain Amino Acid Catabolism Disrupts Glucose Metabolism and Sensitizes the Heart to Ischemia-Reperfusion Injury. *Cell Metab.* **25,** 374–385 (2017).
27. Stančíková, M. & Rovenský, J. Metabolism of Aromatic Amino Acids. *Alkaptonuria and Ochronosis.* 9–12 (2015).
28. Lerin, C. *et al.* Defects in muscle branched-chain amino acid oxidation contribute to impaired lipid metabolism. *Mol. Metab.* **5,** 926–936 (2016).
29. Ohno, H. *et al.* 4F2hc stabilizes GLUT1 protein and increases glucose transport activity. *Am. J. Physiol. Physiol.* **300,** C1047–C1054 (2011).
30. Garzón, J. *et al.* Shortage of dNTPs underlies altered replication dynamics and DNA breakage in the absence of the APC/C cofactor Cdh1. *Oncogene* **36,** 5808–5818 (2017).
31. Poli, J. *et al.* dNTP pools determine fork progression and origin usage under replication stress. *EMBO J.* **31,** 883–94 (2012).
32. Ma, Q. Role of Nrf2 in Oxidative Stress and Toxicity. *Annu. Rev. Pharmacol. Toxicol.* **53,** 401–426 (2013).
33. Efeyan, A., Comb, W. C. & Sabatini, D. M. Nutrient-sensing mechanisms and pathways. *Nature* **517,** 302–10 (2015).
34. Cargnello, M., Tcherkezian, J. & Roux, P. P. The expanding role of mTOR in cancer cell growth and proliferation. *Mutagenesis* **30,** 169–76 (2015).
35. Nicklin, P. *et al.* Bidirectional transport of amino acids regulates mTOR and autophagy. *Cell* **136,** 521–34 (2009).
36. Castilho, B. A. *et al.* Keeping the eIF2 alpha kinase Gcn2 in check. *Biochim. Biophys. Acta - Mol. Cell Res.* **1843,** 1948–1968 (2014).
37. Taniuchi, S., Miyake, M., Tsugawa, K., Oyadomari, M. & Oyadomari, S. Integrated stress response of vertebrates is regulated by four eIF2α kinases. *Sci. Rep.* **6,** 32886 (2016).
38. Dever, T. E. Gene-Specific Regulation by General Translation Factors. *Cell* **108,** 545–556 (2002).
39. Donnelly, N., Gorman, A. M., Gupta, S. & Samali, A. The eIF2α kinases: their structures and functions. *Cell. Mol. Life Sci.* **70,** 3493–3511 (2013).
40. Joshi, M., Kulkarni, A. & Pal, J. K. Small molecule modulators of eukaryotic initiation factor 2α kinases, the key regulators of protein synthesis. *Biochimie* **95,** 1980–1990 (2013).
41. Bjursell, G. & Reichard, P. Effects of thymidine on deoxyribonucleoside triphosphate pools and deoxyribonucleic acid synthesis in Chinese hamster ovary cells. *J. Biol. Chem.* **248,** 3904–3909 (1973).
42. Giglia-Mari, G., Zotter, A. & Vermeulen, W. DNA damage response. *Cold Spring Harb. Perspect. Biol.* **3,** a000745 (2011).
43. Zhou, B. S. & Elledge, S. J. Checkpoints in Perspective. *Nature* **408,** 433–439 (2000).
44. Wu, Q., Beland, F. A., Chang, C.-W. & Fang, J.-L. Role of DNA Repair Pathways in Response to Zidovudine-induced DNA Damage in Immortalized Human Liver THLE2 Cells. *Int. J. Biomed. Sci.* **9,** 18–25 (2013).
45. Shiotani, B. & Zou, L. ATR signaling at a glance. *J. Cell Sci.* **122,** 301–4 (2009).
46. Zou, L. & Elledge, S. J. Sensing DNA damage through ATRIP recognition of RPA-ssDNA complexes. *Science* **300,** 1542–8 (2003).
47. Nam, E. A. & Cortez, D. ATR signalling: more than meeting at the fork. *Biochem. J.* **436,** 527–36 (2011).
48. Marechal, A. & Zou, L. DNA Damage Sensing by the ATM and ATR Kinases. *Cold Spring Harb. Perspect. Biol.* **5,** a012716–a012716 (2013).
49. Dai, Y. & Grant, S. New insights into checkpoint kinase 1 in the DNA damage response signaling network. *Clin. Cancer Res.* **16,** 376–83 (2010).
50. Hwang, B.-J., Adhikary, G., Eckert, R. L. & Lu, A.-L. Chk1 inhibition as a novel therapeutic strategy in melanoma. *Oncotarget* **9,** 30450–30464 (2018).
51. Mak, J. P. Y., Man, W. Y., Chow, J. P. H., Ma, H. T. & Poon, R. Y. C. Pharmacological inactivation of CHK1 and WEE1 induces mitotic catastrophe in nasopharyngeal carcinoma cells. *Oncotarget* **6,** 21074–84 (2015).
52. David, L. *et al.* CHK1 as a therapeutic target to bypass chemoresistance in AML. *Sci. Signal.* **9,** (2016).
53. Albiges, L. *et al.* Chk1 as a new therapeutic target in triple-negative breast cancer. *Breast* **23,** 250–258 (2014).
54. Cho, S. H., Toouli, C. D., Fujii, G. H., Crain, C. & Parry, D. Chk1 is Essential for Tumor Cell Viability Following Activation of the Replication Checkpoint. *Cell Cycle* **4,** 131–139 (2005).
55. Verlinden, L. *et al.* The E2F-Regulated Gene *Chk1* Is Highly Expressed in Triple-Negative Estrogen Receptor–/Progesterone Receptor–/HER-2– Breast Carcinomas. *Cancer Res.* **67,** 6574–6581 (2007).

56. Mazouzi, A., Velimezi, G. & Loizou, J. I. DNA replication stress: Causes, resolution and disease. *Exp. Cell Res.* **329,** 85–93 (2014).
57. Zhang, Y.-W. *et al.* Genotoxic Stress Targets Human Chk1 for Degradation by the Ubiquitin-Proteasome Pathway. *Mol. Cell* **19,** 607–618 (2005).
58. Zhang, Y. & Hunter, T. Roles of Chk1 in cell biology and cancer therapy. *Int. J. cancer* **134,** 1013–23 (2014).
59. Van Hooser, a *et al.* Histone H3 phosphorylation is required for the initiation, but not maintenance, of mammalian chromosome condensation. *J. Cell Sci.* **111,** 3497–3506 (1998).
60. Hendzel, M. J. *et al.* Mitosis-specific phosphorylation of histone H3 initiates primarily within pericentromeric heterochromatin during G2 and spreads in an ordered fashion coincident with mitotic chromosome condensation. *Chromosoma* **106,** 348–360 (1997).
61. Patil, M., Pabla, N. & Dong, Z. Checkpoint kinase 1 in DNA damage response and cell cycle regulation. *Cell. Mol. Life Sci.* **70,** 4009–4021 (2013).
62. Stincone, A. *et al.* The return of metabolism: biochemistry and physiology of the pentose phosphate pathway. *Biol. Rev. Camb. Philos. Soc.* **90,** 927–63 (2015).
63. Guarino, E., Salguero, I. & Kearsey, S. E. Cellular regulation of ribonucleotide reductase in eukaryotes. *Semin. Cell Dev. Biol.* **30,** 97–103 (2014).
64. Nordlund, P. & Reichard, P. Ribonucleotide Reductases. *Annu. Rev. Biochem.* **75,** 681–706 (2006).
65. Vander Heiden, M. G. *et al.* Metabolic pathway alterations that support cell proliferation. *Cold Spring Harb. Symp. Quant. Biol.* **76,** 325–34 (2011).
66. Bhutia, Y. D., Babu, E., Ramachandran, S. & Ganapathy, V. Amino acid transporters in cancer and their relevance to 'glutamine addiction': Novel Targets for the design of a new class of anticancer drugs. *Cancer Res.* **75,** 1782–1788 (2015).
67. Fuchs, B. C. & Bode, B. P. Amino acid transporters ASCT2 and LAT1 in cancer: Partners in crime? *Semin. Cancer Biol.* **15,** 254–266 (2005).
68. Bhutia, Y. D., Babu, E., Prasad, P. D. & Ganapathy, V. The amino acid transporter SLC6A14 in cancer and its potential use in chemotherapy. *Asian J. Pharm. Sci.* **9,** 293–303 (2014).
69. Alberts, B. *et al. Molecular biology of the cell.* (Garland Science, 2002).
70. Dolfi, S. C. *et al.* The metabolic demands of cancer cells are coupled to their size and protein synthesis rates. *Cancer Metab.* **1,** 20 (2013).
71. Nicklin, P. *et al.* Bidirectional transport of amino acids regulates mTOR and autophagy. *Cell* **136,** 521–34 (2009).
72. Neishabouri, S. H., Hutson, S. M. & Davoodi, J. Chronic activation of mTOR complex 1 by branched chain amino acids and organ hypertrophy. *Amino Acids* **47,** 1167–1182 (2015).
73. Moberg, M. *et al.* Activation of mTORC1 by leucine is potentiated by branched-chain amino acids and even more so by essential amino acids following resistance exercise. *Am. J. Physiol. - Cell Physiol.* **310,** C874–C884 (2016).
74. Persaud, A., Cormerais, Y., Pouyssegur, J. & Rotin, D. Dynamin inhibitors block activation of mTORC1 by amino acids independently of dynamin. *J. Cell Sci.* **131,** jcs211755 (2018).
75. Wek, S. A., Zhu, S. & Wek, R. C. The histidyl-tRNA synthetase-related sequence in the eIF-2 alpha protein kinase GCN2 interacts with tRNA and is required for activation in response to starvation for different amino acids. *Mol. Cell. Biol.* **15,** 4497–4506 (1995).
76. Dong, J., Qiu, H., Garcia-Barrio, M., Anderson, J. & Hinnebusch, A. G. Uncharged tRNA Activates GCN2 by Displacing the Protein Kinase Moiety from a Bipartite tRNA-Binding Domain open reading frames (uORFs) in the GCN4 mRNA leader underlie a specialized reinitiation mechanism that ele- vates GCN4 translation in response to sm. *Mol. Cell* **6,** 269–279 (2000).
77. Zhang, P. *et al.* The GCN2 eIF2alpha kinase is required for adaptation to amino acid deprivation in mice. *Mol. Cell. Biol.* **22,** 6681–8 (2002).
78. Harding, H. P. *et al.* Regulated Translation Initiation Controls Stress-Induced Gene Expression in Mammalian Cells. *Mol. Cell* **6,** 1099–1108 (2000).
79. Anthony, T. G., Reiter, A. K., Anthony, J. C., Kimball, S. R. & Jefferson, L. S. Deficiency of dietary EAA preferentially inhibits mRNA translation of ribosomal proteins in liver of meal-fed rats. *Am J Physiol Endocrinol Metab* **281,** E430-439 (2001).
80. Suragani, R. N. V. S. *et al.* Heme-regulated eIF2α kinase activated Atf4 signaling pathway in oxidative stress and erythropoiesis. *Blood* **119,** 5276–84 (2012).
81. Lu, L., Han, A. P. & Chen, J. J. Translation initiation control by heme-regulated eukaryotic initiation factor 2alpha kinase in erythroid cells under cytoplasmic stresses. *Mol. Cell. Biol.* **21,** 7971–80 (2001).
82. Tidke, P. R., Maurya, D. K., Kulkarni, A. P., Devasagayam, T. P. A. & Pal, J. K. Radiation-induced oxidative stress regulates protein synthesis by modulating the expression of heme-regulated eIF2α kinase in human K562 cells. *Indian J. Biochem. Biophys.* **53,** 95–103 (2016).

83. McEwen, E. *et al.* Heme-regulated inhibitor kinase-mediated phosphorylation of eukaryotic translation initiation factor 2 inhibits translation, induces stress granule formation, and mediates survival upon arsenite exposure. *J. Biol. Chem.* **280,** 16925–33 (2005).
84. Brunner, M. Regulation of DNA synthesis by amino acid limitation. *Cancer Res.* **33,** 29–32 (1973).
85. Wang, X. & Proud, C. G. Nutrient control of TORC1, a cell-cycle regulator. *Trends Cell Biol.* **19,** 260–267 (2009).
86. Visagie, M. H. *et al.* Influence of partial and complete glutamine-and glucose deprivation of breast- and cervical tumorigenic cell lines. *Cell Biosci.* **5,** 37 (2015).
87. DeBerardinis, R. J. *et al.* Beyond aerobic glycolysis: transformed cells can engage in glutamine metabolism that exceeds the requirement for protein and nucleotide synthesis. *Proc. Natl. Acad. Sci. U. S. A.* **104,** 19345–50 (2007).
88. Moffatt, B. A. & Ashihara, H. Purine and pyrimidine nucleotide synthesis and metabolism. *Arab. B.* **1,** e0018 (2002).
89. Zeman, M. K. & Cimprich, K. A. Causes and consequences of replication stress. *Nat. Cell Biol.* **16,** 2–9 (2014).
90. Bester, A. C. *et al.* Nucleotide deficiency promotes genomic instability in early stages of cancer development. *Cell* **145,** 435–46 (2011).
91. Giannattasio, M. & Branzei, D. S-phase checkpoint regulations that preserve replication and chromosome integrity upon dNTP depletion. *Cell. Mol. Life Sci.* **74,** 2361–2380 (2017).
92. Krämer, A. *et al.* Centrosome-associated Chk1 prevents premature activation of cyclin-B–Cdk1 kinase. *Nat. Cell Biol.* **6,** 884–891 (2004).
93. Thanasoula, M., Escandell, J. M., Suwaki, N. & Tarsounas, M. ATM/ATR checkpoint activation downregulates CDC25C to prevent mitotic entry with uncapped telomeres. *EMBO J.* **31,** 3398–410 (2012).
94. Jiang, P., Du, W. & Wu, M. Regulation of the pentose phosphate pathway in cancer. *Protein Cell* **5,** 1–11 (2014).
95. Boer, P. & Sperling, O. Role of cellular ribose-5-phosphate content in the regulation of 5-phosphoribosyl-1-pyrophosphate and de novo purine synthesis in a human hepatoma cell line. *Metabolism* **44,** 1469–1474 (1995).
96. Pilz, R. B., Willis, R. C. & Boss, G. R. The influence of ribose 5-phophate availability on purine synthesis of cultured human lymphoblasts and mitogen-stimulated lymphocytes. *J. Biol. Chem.* **259,** 2927–2935 (1984).
97. Fornalewicz, K., Wieczorek, A., Węgrzyn, G. & Łyżeń, R. Silencing of the pentose phosphate pathway genes influences DNA replication in human fibroblasts. *Gene* **635,** 33–38 (2017).
98. Cosentino, C., Grieco, D. & Costanzo, V. ATM activates the pentose phosphate pathway promoting anti-oxidant defence and DNA repair. *EMBO J.* **30,** 546–55 (2011).
99. Qu, J. *et al.* Phosphoglycerate mutase 1 regulates dNTP pool and promotes homologous recombination repair in cancer cells. *J. Cell Biol.* **216,** 409–424 (2017).
100. Yu, H.-P. *et al.* TIGAR regulates DNA damage and repair through pentosephosphate pathway and Cdk5-ATM pathway. *Sci. Rep.* **5,** 9853 (2015).
101. Masuda, F. *et al.* Glucose restriction induces transient G2 cell cycle arrest extending cellular chronological lifespan. *Sci. Rep.* **6,** 19629 (2016).
102. Detimary, P., Van den Berghe, G. & Henquin, J. C. Concentration dependence and time course of the effects of glucose on adenine and guanine nucleotides in mouse pancreatic islets. *J. Biol. Chem.* **271,** 20559–65 (1996).
103. Nakano, H. *et al.* Glucose inhibits cardiac muscle maturation through nucleotide biosynthesis. *Elife* **6,** (2017).
104. Aird, K. M. *et al.* Suppression of nucleotide metabolism underlies the establishment and maintenance of oncogene-induced senescence. *Cell Rep.* **3,** 1252–65 (2013).
105. Lopez-Contreras, A. J. *et al.* Increased Rrm2 gene dosage reduces fragile site breakage and prolongs survival of ATR mutant mice. *Genes Dev.* **29,** 690–5 (2015).
106. Dejure, F. R. *et al.* The MYC mRNA 3'-UTR couples RNA polymerase II function to glutamine and ribonucleotide levels. *EMBO J.* **36,** 1854–1868 (2017).
107. Gao, P. *et al.* c-Myc suppression of miR-23a/b enhances mitochondrial glutaminase expression and glutamine metabolism. *Nature* **458,** 762–765 (2009).
108. Aird, K. M. *et al.* ATM Couples Replication Stress and Metabolic Reprogramming during Cellular Senescence. *Cell Rep.* **11,** 893–901 (2015).
109. Mannava, S. *et al.* Direct role of nucleotide metabolism in C-MYC-dependent proliferation of melanoma cells. *Cell Cycle* **7,** 2392–400 (2008).
110. Neretti, N. *et al.* Global Regulation of Nucleotide Biosynthetic Genes by c-Myc. *PLoS One* **3,** e2722 (2008).

111. Csibi, A. *et al.* The mTORC1/S6K1 pathway regulates glutamine metabolism through the eif4b-dependent control of c-Myc translation. *Curr. Biol.* **24,** 2274–2280 (2014).
112. Zhang, H., Park, C., Cobler, L., Suri, P. & Timmerman, L. A. xCT inhibition sensitizes tumors to γ-radiation via glutathione reduction. *Oncotarget* **9,** 32280–32297 (2018).
113. Balza, E., Castellani, P., Delfino, L., Truini, M. & Rubartelli, A. The pharmacologic inhibition of the xc-antioxidant system improves the antitumor efficacy of COX inhibitors in the in vivo model of 3-MCA tumorigenesis. *Carcinogenesis* **34,** 620–626 (2013).
114. Häfliger, P. *et al.* The LAT1 inhibitor JPH203 reduces growth of thyroid carcinoma in a fully immunocompetent mouse model. *J. Exp. Clin. Cancer Res.* **37,** 1–15 (2018).
115. Hayashi, K. & Anzai, N. Novel therapeutic approaches targeting L-type amino acid transporters for cancer treatment. *World J. Gastrointest. Oncol.* **9,** 21 (2017).
116. Marshall, A. D. *et al.* LAT1 is a putative therapeutic target in endometrioid endometrial carcinoma. *Int. J. Cancer* **139,** 2529–2539 (2016).
117. Im, C. S. K. *et al.* BCH, an inhibitor of system L amino acid transporters, induces apoptosis in cancer cells. *Biol. Pharm. Bull.* **31,** 1096–100 (2008).
118. Oda, K. *et al.* l-Type amino acid transporter 1 inhibitors inhibit tumor cell growth. *Cancer Sci.* **101,** 173–179 (2009).
119. Wang, X. *et al.* Chemotherapy-induced differential cell cycle arrest in B-cell lymphomas affects their sensitivity to Wee1 inhibition. *Haematologica* **103,** 466–476 (2018).
120. Mills, C. C., Kolb, E. A. & Sampson, V. B. Development of chemotherapy with cell-cycle inhibitors for adult and pediatric cancer therapy. *Cancer Res.* **78,** 320–325 (2018).
121. Bull, E. E. A. *et al.* Enhanced tumor cell radiosensitivity and abrogation of G2and S phase arrest by the Hsp90 inhibitor 17-(dimethylaminoethylamino)-17- demethoxygeldanamycin. *Clin. Cancer Res.* **10,** 8077–8084 (2004).
122. Li, M. Y. *et al.* Radiotherapy induces cell cycle arrest and cell apoptosis in nasopharyngeal carcinoma via the ATM and Smad pathways. *Cancer Biol. Ther.* **18,** 681–693 (2017).
123. Otani, K. *et al.* Cell-cycle-controlled radiation therapy was effective for treating a murine malignant melanoma cell line in vitro and in vivo. *Sci. Rep.* **6,** 1–8 (2016).
124. Ma, H. T. & Poon, R. Y. C. Synchronization of HeLa Cells. *Methods Mol Biol.* **761,** 151–161 (2011).
125. Irizarry, R. A. *et al.* Summaries of Affymetrix GeneChip probe level data. *Nucleic Acids Res.* **31,** e15 (2003).
126. Irizarry, R. A. *et al.* Exploration , Normalization , and Summaries of High Density Oligonucleotide Array Probe Level Data. *Biostatistics* **4,** 249–264 (2003).
127. Bolstad, B. M. Low Level Analysis of High-density Oligonucleotide Array Data: Background, Normalization and Summarization. *PhD thesis, Univ. California, Berkeley* 156 (2005).
128. R Core Development Team. *R: A language and environment for statistical computing. R Foundation for Statistical Computing*. **2,** (2008).
129. Wu, D. *et al.* limma powers differential expression analyses for RNA-sequencing and microarray studies. *Nucleic Acids Res.* **43,** e47–e47 (2015).
130. Subramanian, A. *et al.* Gene set enrichment analysis: A knowledge-based approach for interpreting genome-wide expression profiles. *Proc. Natl. Acad. Sci.* **102,** 15545–15550 (2005).
131. Reig, N. *et al.* The light subunit of system b(o,+) is fully functional in the absence of the heavy subunit. *EMBO J.* **21,** 4906–14 (2002).
132. Avcilar-Kucukgoze, I. *et al.* Discharging tRNAs: a tug of war between translation and detoxification in *Escherichia coli*. *Nucleic Acids Res.* **44,** 8324–8334 (2016).
133. Bates, D., Mächler, M., Bolker, B. & Walker, S. Fitting Linear Mixed-Effects Models using lme4. *J. Stat. Softw.* **67,** (2014).

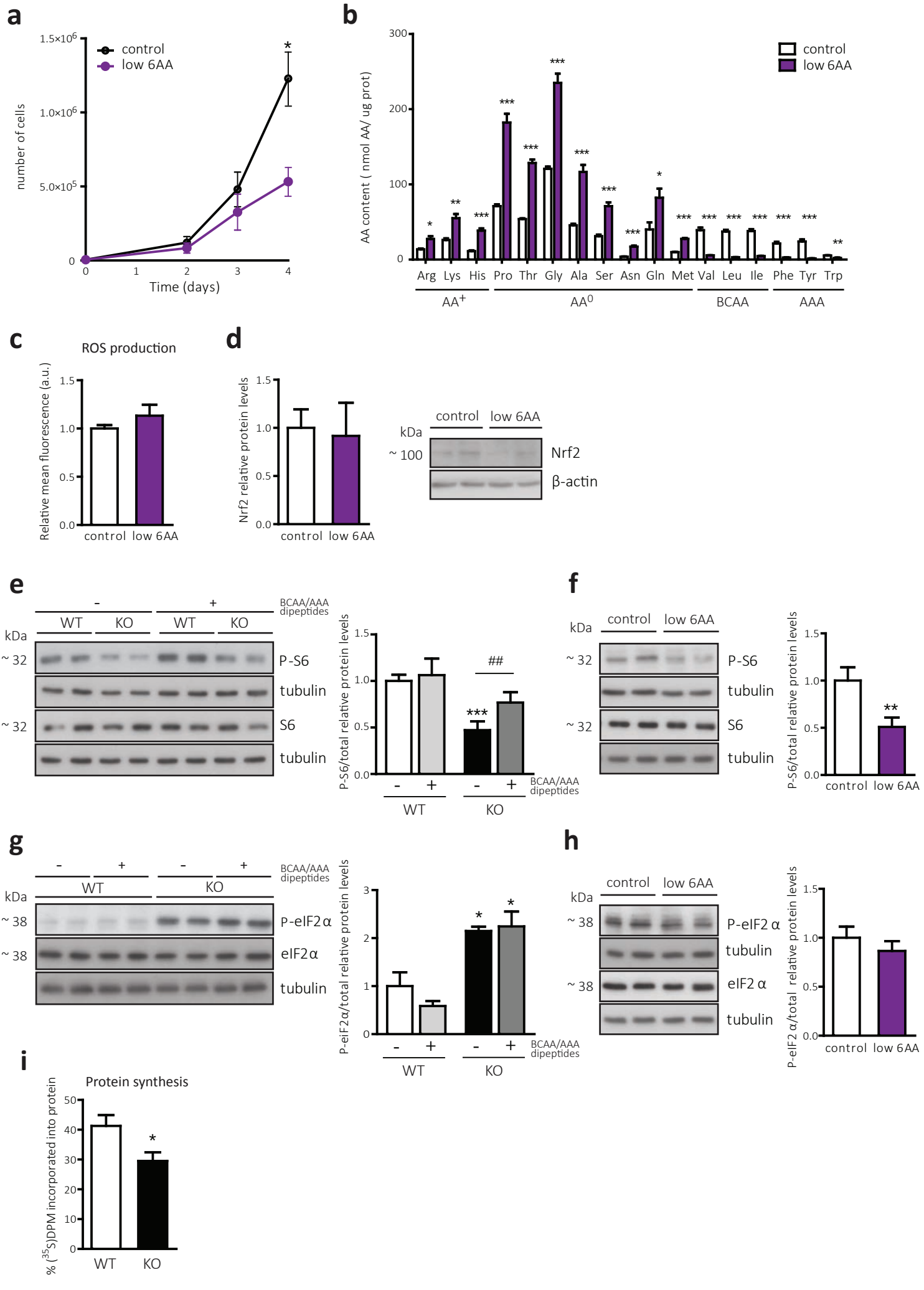
a
number of cells
1.5×10^6
1.0×10^6
5.0×10^5
0
control
low 6AA
*
0 1 2 3 4
Time (days)
b
AA content (nmol AA/ ug prot)
300
200
100
0
control
low 6AA
Arg Lys His Pro Thr Gly Ala Ser Asn Gln Met Val Leu Ile Phe Tyr Trp
AA+
AA0
BCAA
AAA
c
ROS production
Relative mean fluorescence (a.u.)
1.5
1.0
0.5
0.0
control low 6AA
d
Nrf2 relative protein levels
control low 6AA
kDa
~ 100
control low 6AA
Nrf2
β-actin
e
BCAA/AAA dipeptides
WT KO WT KO
kDa
~ 32
P-S6
tubulin
~ 32
S6
tubulin
P-S6/total relative protein levels
##
***
WT
KO
f
control low 6AA
kDa
~ 32
P-S6
tubulin
~ 32
S6
tubulin
P-S6/total relative protein levels
**
control low 6AA
g
BCAA/AAA dipeptides
WT KO
kDa
~ 38
P-eIF2α
~ 38
eIF2α
tubulin
P-eIF2α/total relative protein levels
WT
KO
h
control low 6AA
kDa
~ 38
P-eIF2 α
tubulin
~ 38
eIF2 α
tubulin
P-eIF2 α/total relative protein levels
control low 6AA
i
Protein synthesis
% ([35S]DPM incorporated into protein
50
40
30
20
10
0
*
WT KO

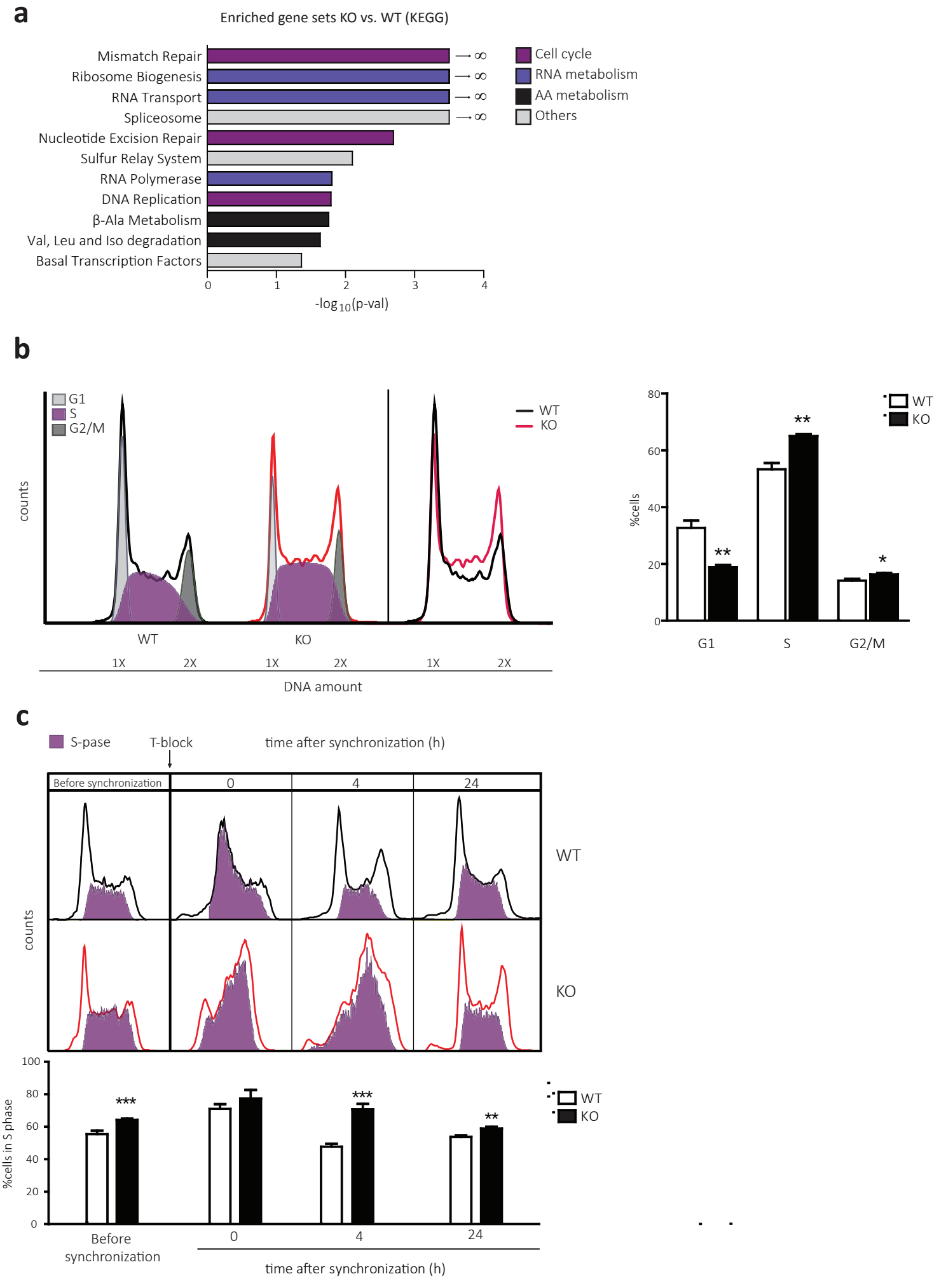
a
Enriched gene sets KO vs. WT (KEGG)
Mismatch Repair
Ribosome Biogenesis
RNA Transport
Spliceosome
Nucleotide Excision Repair
Sulfur Relay System
RNA Polymerase
DNA Replication
β-Ala Metabolism
Val, Leu and Iso degradation
Basal Transcription Factors
Cell cycle
RNA metabolism
AA metabolism
Others
-log10(p-val)
b
G1
S
G2/M
WT
KO
counts
1X
2X
DNA amount
%cells
G1
S
G2/M
c
S-pase
T-block
time after synchronization (h)
Before synchronization
0
4
24
counts
%cells in S phase
Before synchronization
time after synchronization (h)

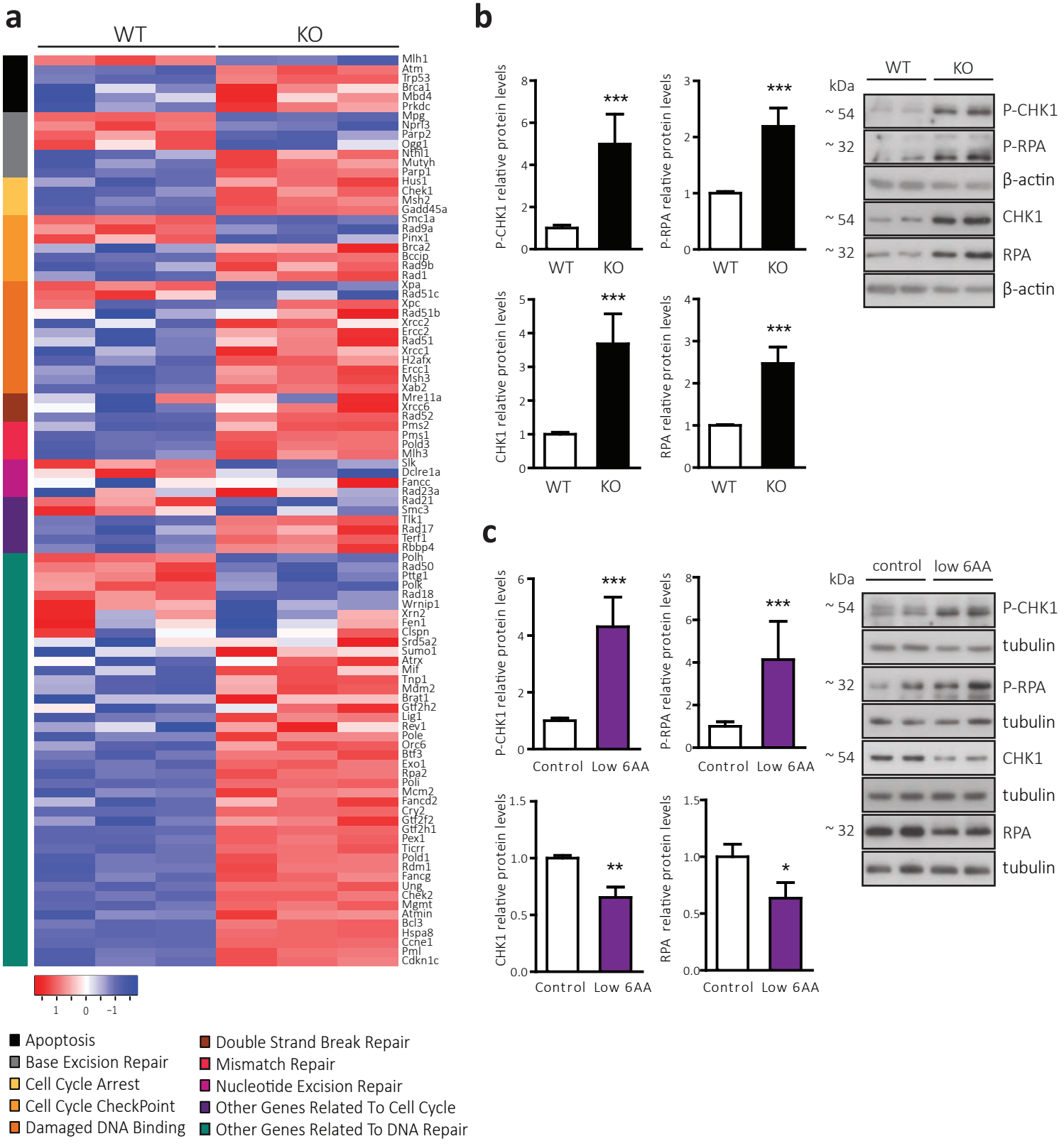
a
WT
KO
Mlh1
Atm
Trp53
Brca1
Mbd4
Prkdc
Mpg
Nprl3
Parp2
Ogg1
Nthl1
Mutyh
Parp1
Hus1
Chek1
Msh2
Gadd45a
Smc1a
Rad9a
Pinx1
Brca2
Bccip
Rad9b
Rad1
Xpa
Rad51c
Xpc
Rad51b
Xrcc2
Ercc2
Rad51
Xrcc1
H2afx
Ercc1
Msh3
Xab2
Mre11a
Xrcc6
Rad52
Pms2
Pms1
Pold3
Mlh3
Slk
Dclre1a
Fancc
Rad23a
Rad21
Smc3
Tlk1
Rad17
Terf1
Rbbp4
Polh
Rad50
Ptpt1
Polk
Rad18
Wrnip1
Xrn2
Fen1
Clspn
Srd5a2
Sumo1
Atrx
Mif
Tnp1
Mdm2
Brat1
Gtf2h2
Lig1
Rev1
Pole
Orc6
Btf3
Exo1
Rpa2
Poli
Mcm2
Fancd2
Cry2
Gtf2f2
Gtf2h1
Pex1
Ticrr
Pold1
Rdm1
Fancg
Ung
Chek2
Mgmt
Atmin
Bcl3
Hspa8
Ccne1
Pml
Cdkn1c
1
0
-1
Apoptosis
Base Excision Repair
Cell Cycle Arrest
Cell Cycle CheckPoint
Damaged DNA Binding
Double Strand Break Repair
Mismatch Repair
Nucleotide Excision Repair
Other Genes Related To Cell Cycle
Other Genes Related To DNA Repair
b
P-CHK1 relative protein levels
P-RPA relative protein levels
CHK1 relative protein levels
RPA relative protein levels
***
WT
KO
kDa
~ 54
~ 32
P-CHK1
P-RPA
β-actin
CHK1
RPA
β-actin
c
control
low 6AA
Control
Low 6AA
**
*
tubulin
d
P-H3
DAPI/P-H3
WT
KO
% mitosis
e
control
low 6AA

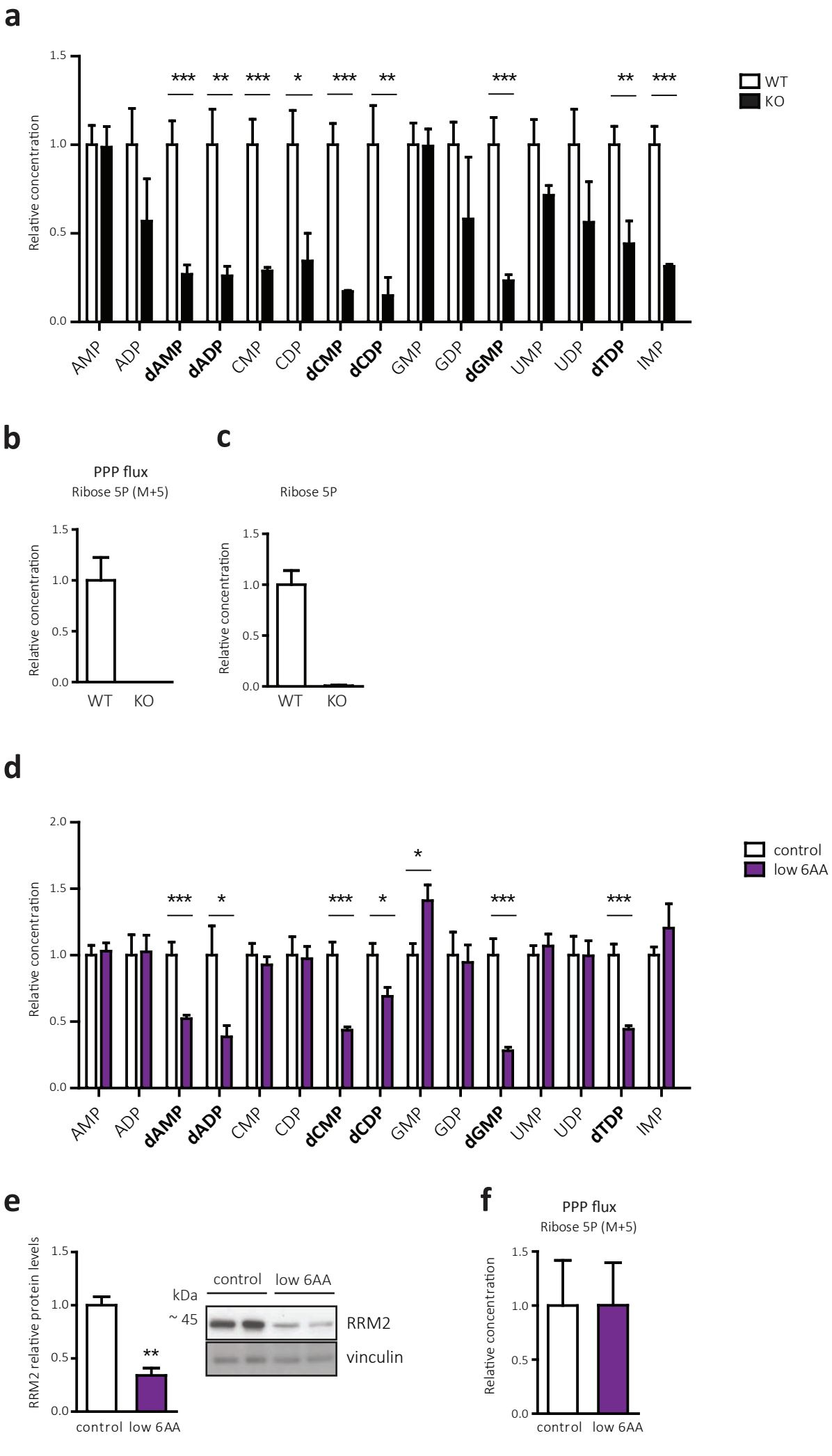
a
Relative concentration
1.5
1.0
0.5
0.0
***
**
***
*
***
**
***
**
***
WT
KO
AMP
ADP
dAMP
dADP
CMP
CDP
dCMP
dCDP
GMP
GDP
dGMP
UMP
UDP
dTDP
IMP
b
PPP flux
Ribose 5P (M+5)
Relative concentration
WT
KO
c
Ribose 5P
Relative concentration
WT
KO
d
Relative concentration
2.0
1.5
1.0
0.5
0.0
***
*
***
*
*
***
***
control
low 6AA
AMP
ADP
dAMP
dADP
CMP
CDP
dCMP
dCDP
GMP
GDP
dGMP
UMP
UDP
dTDP
IMP
e
RRM2 relative protein levels
1.5
1.0
0.5
0.0
**
control
low 6AA
kDa
~ 45
control
low 6AA
RRM2
vinculin
f
PPP flux
Ribose 5P (M+5)
Relative concentration
1.5
1.0
0.5
0.0
control
low 6AA

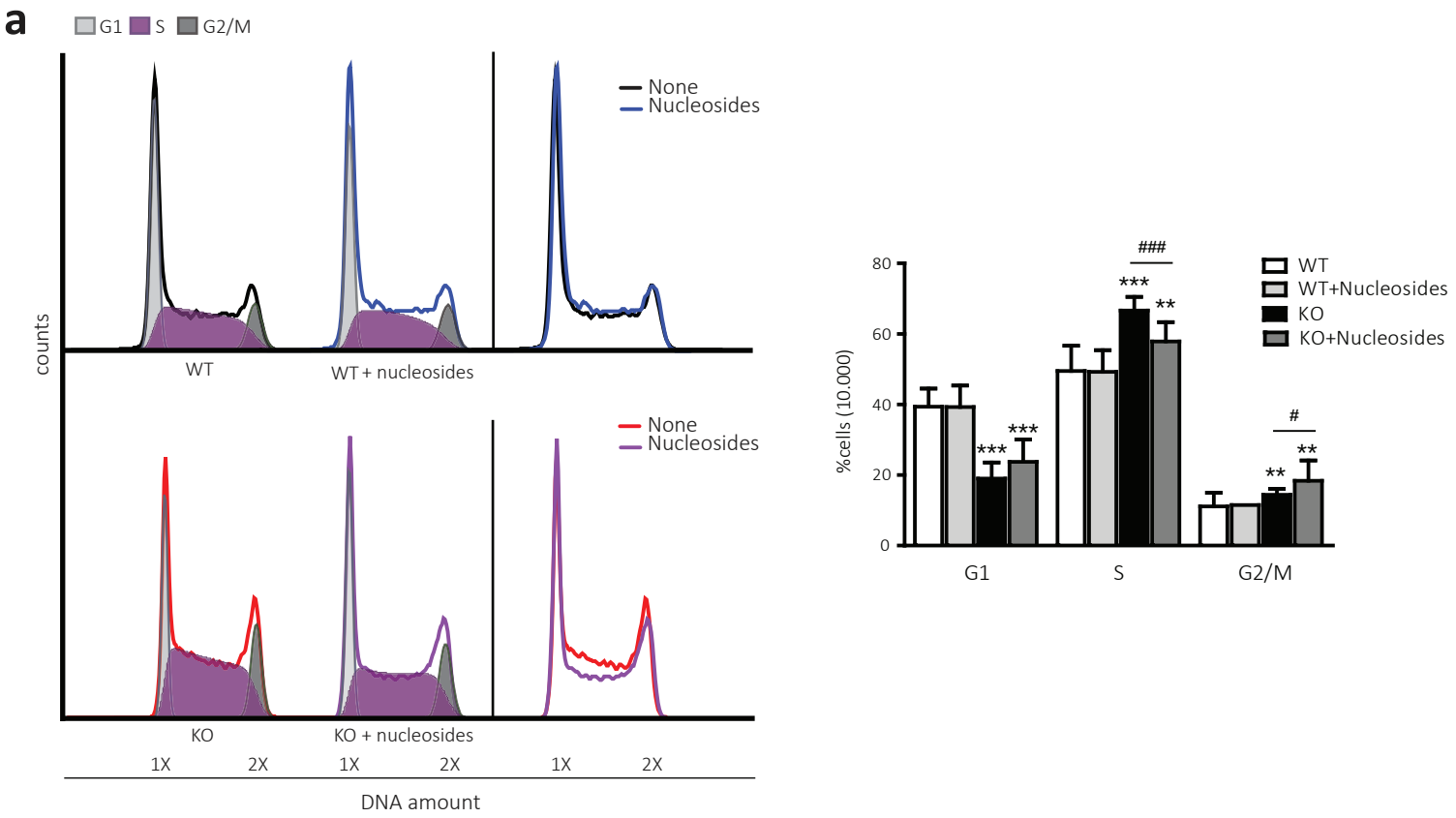
a
G1
S
G2/M
None
Nucleosides
counts
WT
WT + nucleosides
KO
KO + nucleosides
1X
2X
DNA amount
%cells (10.000)
WT
WT+Nucleosides
KO
KO+Nucleosides
G1
S
G2/M

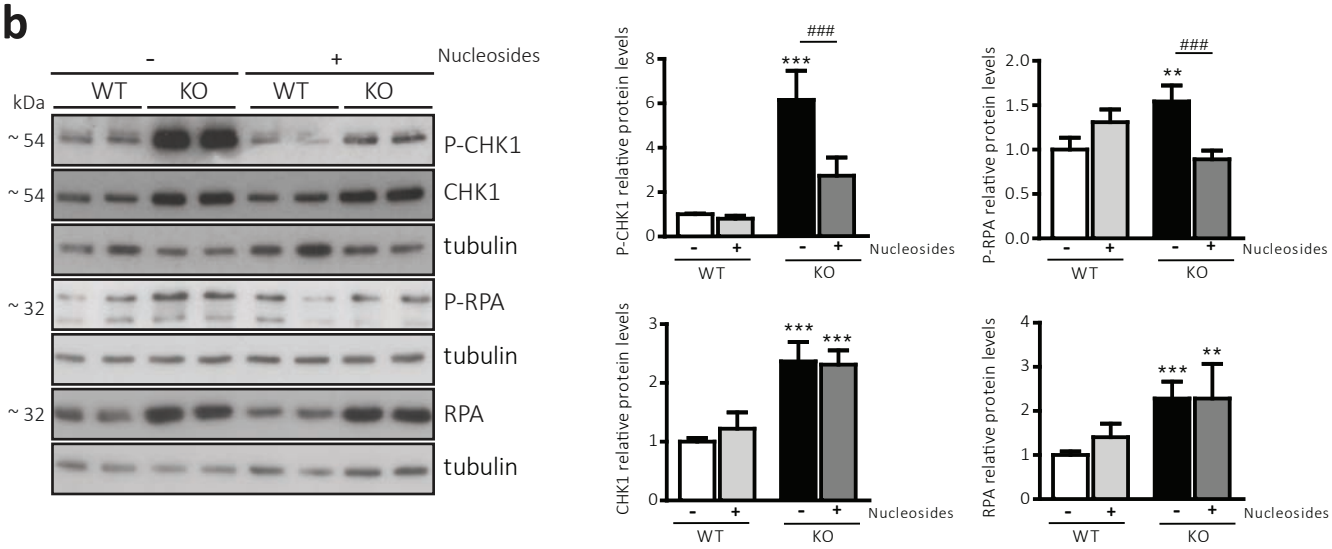
b
Nucleosides
kDa
WT
KO
~ 54
P-CHK1
CHK1
tubulin
~ 32
P-RPA
RPA
P-CHK1 relative protein levels
P-RPA relative protein levels
CHK1 relative protein levels
RPA relative protein levels

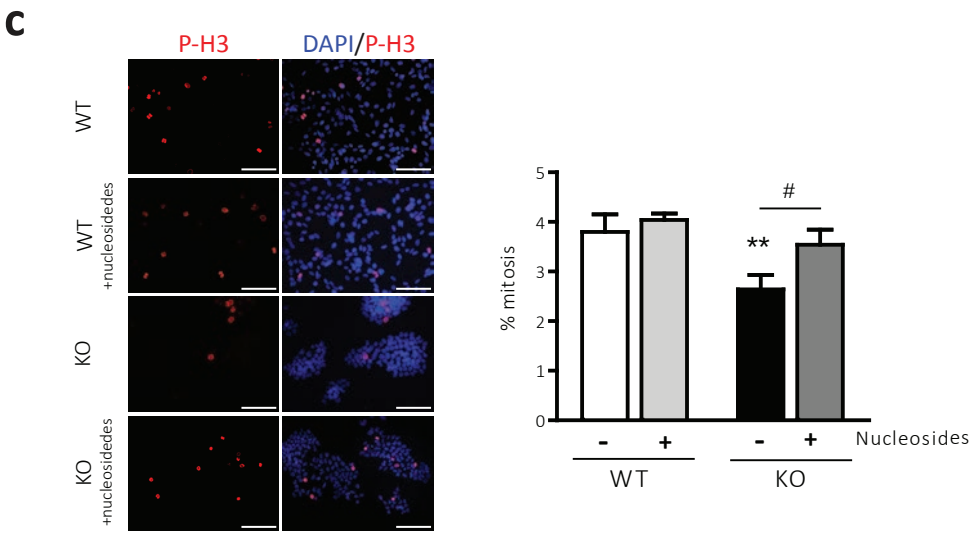
c
P-H3
DAPI/P-H3
WT
WT +nucleosidedes
KO
KO +nucleosidedes
% mitosis
Nucleosides

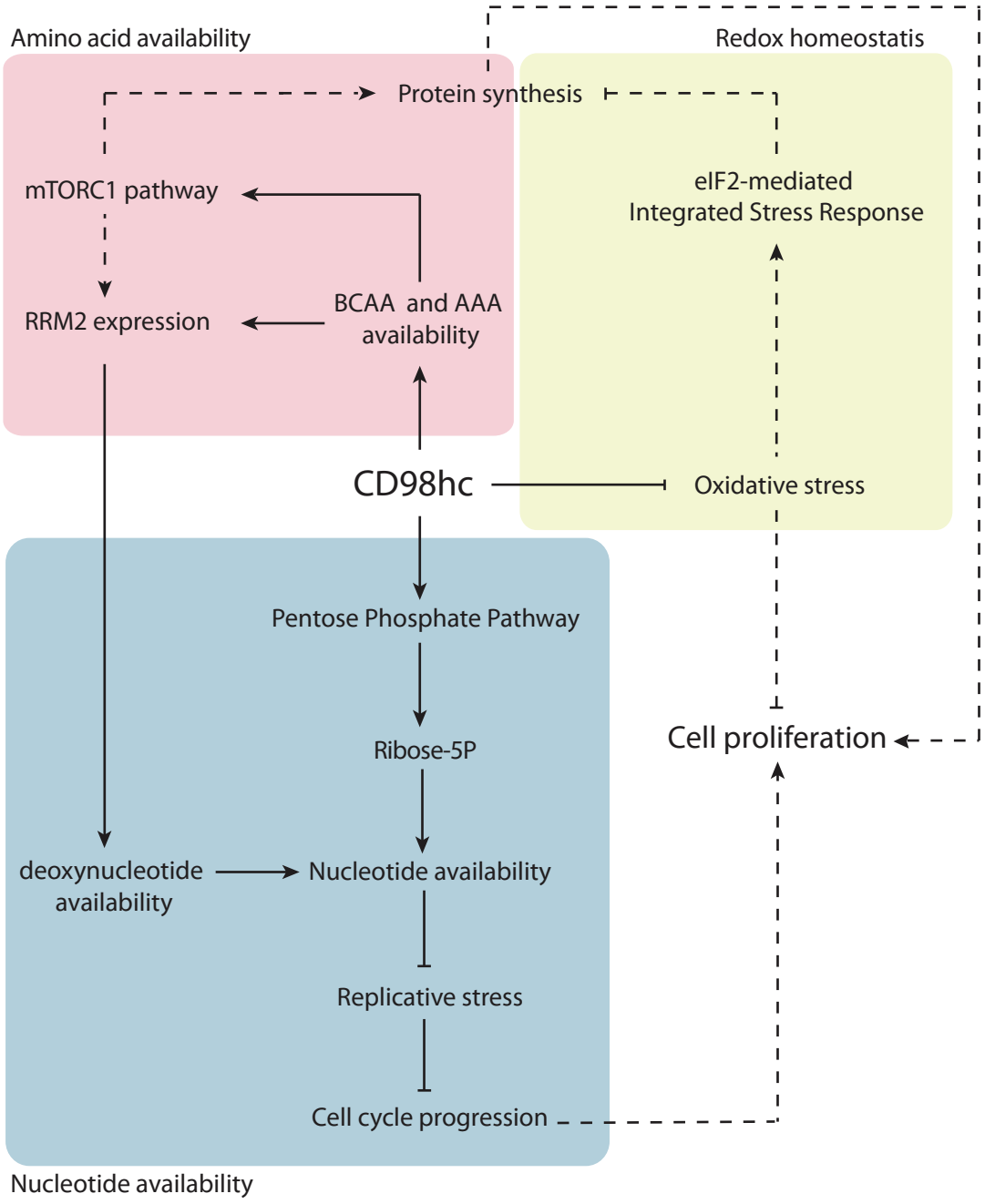
Amino acid availability
Redox homeostatis
Protein synthesis
mTORC1 pathway
eIF2-mediated
Integrated Stress Response
RRM2 expression
BCAA and AAA
availability
CD98hc
Oxidative stress
Pentose Phosphate Pathway
Ribose-5P
Cell proliferation
deoxynucleotide
availability
Nucleotide availability
Replicative stress
Cell cycle progression
Nucleotide availability

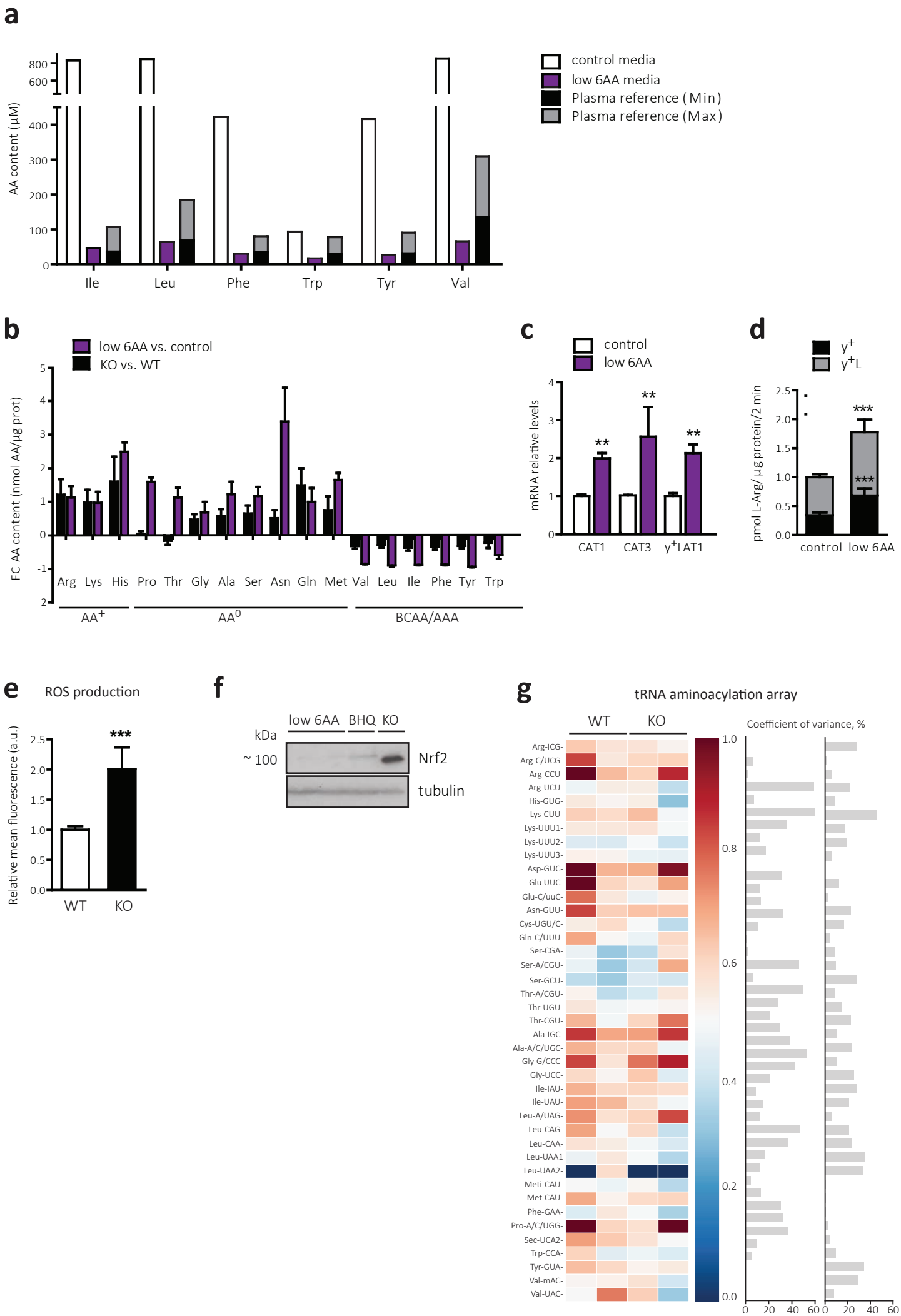
a
AA content (µM)
800
600
400
300
200
100
0
Ile
Leu
Phe
Trp
Tyr
Val
control media
low 6AA media
Plasma reference (Min)
Plasma reference (Max)
b
low 6AA vs. control
KO vs. WT
FC AA content (nmol AA/µg prot)
5
4
3
2
1
0
-1
-2
Arg Lys His Pro Thr Gly Ala Ser Asn Gln Met Val Leu Ile Phe Tyr Trp
AA+
AA0
BCAA/AAA
c
control
low 6AA
mRNA relative levels
4
3
2
1
0
**
**
**
CAT1
CAT3
y+LAT1
d
y+
y+L
pmol L-Arg/ µg protein/2 min
2.5
2.0
1.5
1.0
0.5
0.0
***
***
control
low 6AA
e
ROS production
Relative mean fluorescence (a.u.)
2.5
2.0
1.5
1.0
0.5
0.0
***
WT
KO
f
low 6AA
BHQ
KO
kDa
~ 100
Nrf2
tubulin
g
tRNA aminoacylation array
WT
KO
Coefficient of variance, %
Arg-ICG-
Arg-C/UCG-
Arg-CCU-
Arg-UCU-
His-GUG-
Lys-CUU-
Lys-UUU1-
Lys-UUU2-
Lys-UUU3-
Asp-GUC-
Glu UUC-
Glu-C/uuC-
Asn-GUU-
Cys-UGU/C-
Gln-C/UUU-
Ser-CGA-
Ser-A/CGU-
Ser-GCU-
Thr-A/CGU-
Thr-UGU-
Thr-CGU-
Ala-IGC-
Ala-A/C/UGC-
Gly-G/CCC-
Gly-UCC-
Ile-IAU-
Ile-UAU-
Leu-A/UAG-
Leu-CAG-
Leu-CAA-
Leu-UAA1
Leu-UAA2-
Meti-CAU-
Met-CAU-
Phe-GAA-
Pro-A/C/UGG-
Sec-UCA2-
Trp-CCA-
Tyr-GUA-
Val-mAC-
Val-UAC-
1.0
0.8
0.6
0.4
0.2
0.0
0 20 40 60
0 20 40 60

KO vs. WT

Cell cycle related gene sets

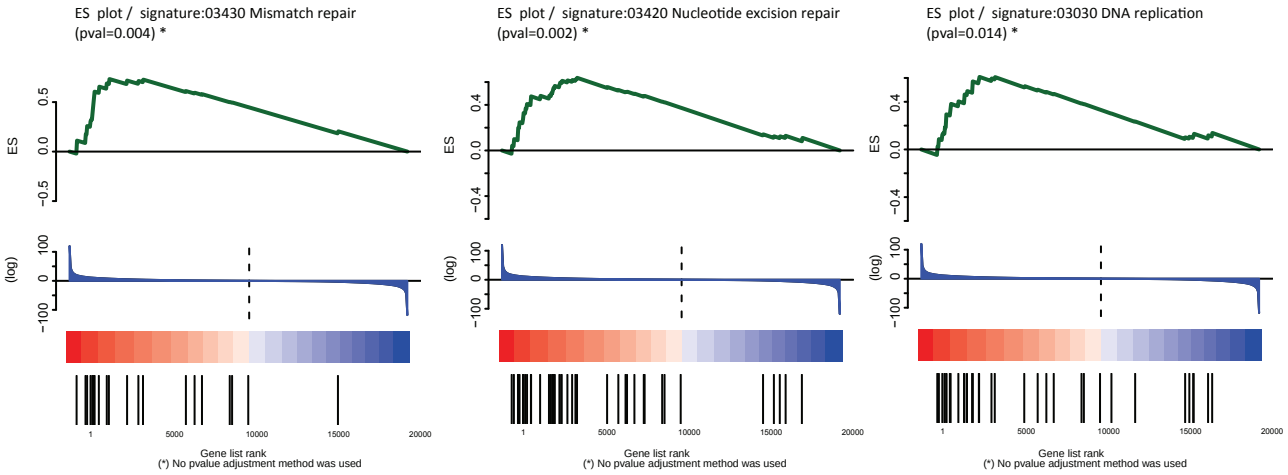

Amino acid metabolism related gene sets

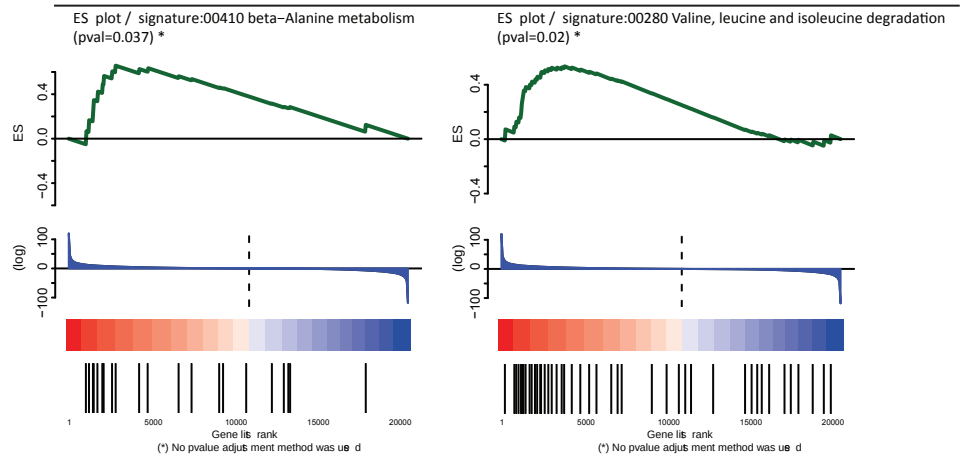

RNA metabolism related gene sets

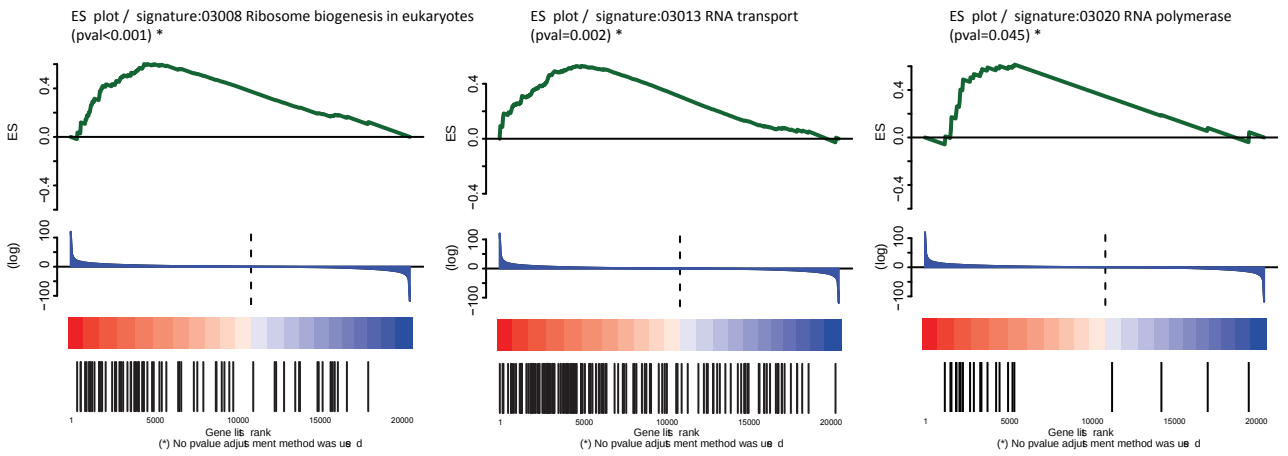

Gene set	NES	p-val	FDR
03008 RIBOSOME BIOGENESIS IN EUKARYOTES	1.81	0.000	0.034
03430 MISMATCH REPAIR	1.77	0.004	0.035
03013 RNA TRANSPORT	1.76	0.002	0.025
03420 NUCLEOTIDE EXCISION REPAIR	1.71	0.002	0.039
03030 DNA REPLICATION	1.65	0.014	0.069
00410 BETA-ALANINE METABOLISM	1.61	0.037	0.078
00280 VALINE, LEUCINE AND ISOLEUCINE DEGRADATION	1.53	0.020	0.138
03020 RNA POLYMERASE	1.52	0.045	0.130

a

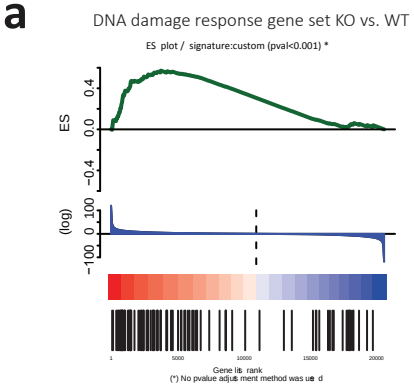
DNA damage response gene set KO vs. WT
ES plot / signature:custom (pval<0.001) *
ES
(log)
Gene list rank
(*) No pvalue adjustment method was used

b

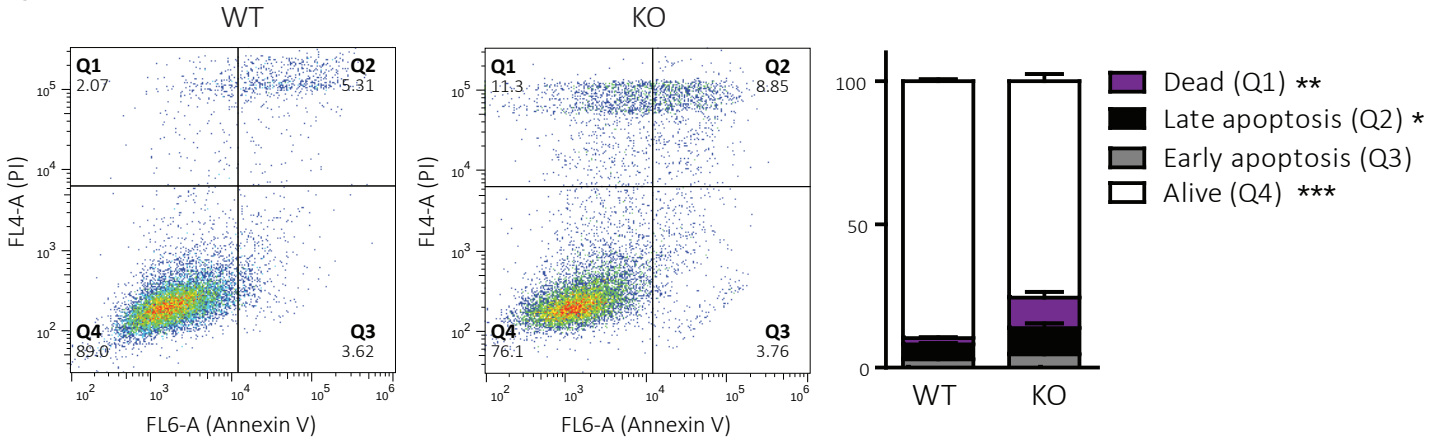
WT
KO
Q1
2.07
Q2
5.31
Q4
89.0
Q3
3.62
Q1
11.3
Q2
8.85
Q4
76.1
Q3
3.76
FL4-A (PI)
FL6-A (Annexin V)
100
50
0
WT
KO
Dead (Q1) **
Late apoptosis (Q2) *
Early apoptosis (Q3)
Alive (Q4) ***

c

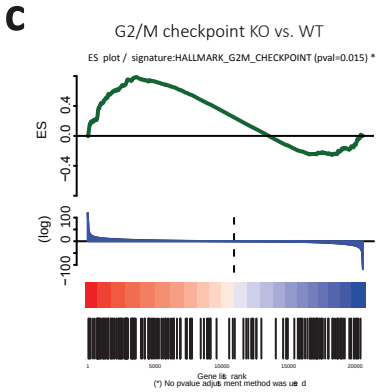
G2/M checkpoint KO vs. WT
ES plot / signature:HALLMARK_G2M_CHECKPOINT (pval=0.015) *
ES
(log)
Gene list rank
(*) No pvalue adjustment method was used

Figure S4

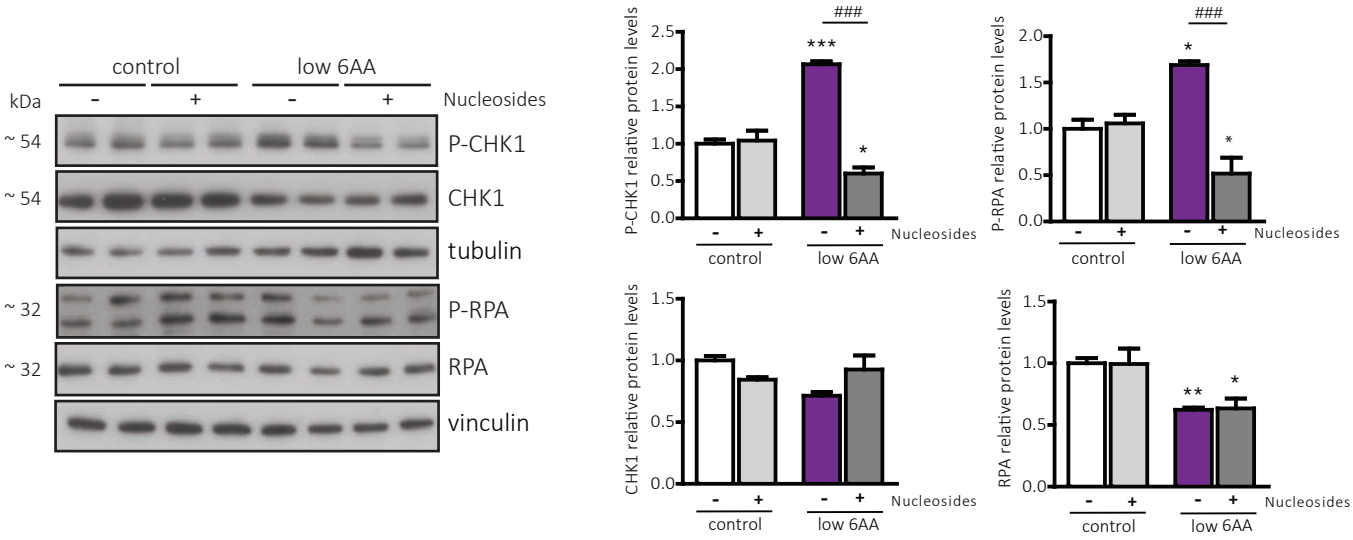
control
low 6AA
kDa
- + - +
Nucleosides
~ 54
P-CHK1
~ 54
CHK1
tubulin
~ 32
P-RPA
~ 32
RPA
vinculin
P-CHK1 relative protein levels
###
***
*
- + - +
Nucleosides
control
low 6AA
P-RPA relative protein levels
###
*
*
- + - +
Nucleosides
control
low 6AA
CHK1 relative protein levels
- + - +
Nucleosides
control
low 6AA
RPA relative protein levels
**
*
- + - +
Nucleosides
control
low 6AA

Legends

Figure 1. CD98hc ablation leads to BCAA and AAA shortage-dependent mTORC1 inactivation and –independent eIF2-mediated ISR with reduced general protein synthesis.

a, Proliferation of control and low 6AA cells was measured over 4 days. n=3.

b, Intracellular AA content (nmol AA/µg protein) in control and low 6AA cells. AAs are grouped by side chain properties as indicated. n=5.

c, ROS levels quantified by flow cytometry using the free radical sensor H_2DCFDA (DCF). Bars represent the mean DCF fluorescence in control and low 6AA cells. a.u., arbitrary units. n>6.

d, Comparison of Nrf2 protein expression between control and low 6AA cells. 50 µg of protein extract was loaded. Data are normalised by β-actin expression. n=4.

e, Comparison of S6 phosphorylation between WT and CD98hc KO cells with no additives or in the presence of BCAA- and AAA- containing dipeptides. Data are normalised by tubulin expression. n=4.

f, Comparison of S6 phosphorylation between control and low 6AA cells. Data are normalised by tubulin expression. n=4.

g, Comparison of eIF2α phosphorylation between WT and CD98hc KO cells with no additives or in the presence of BCAA- and AAA- containing dipeptides. Data are normalised by tubulin expression. n=3.

h, Comparison of eIF2α phosphorylation between control and low 6AA cells. Data are normalised by tubulin expression. n=3.

i, Comparison of ^{35}S-methionine incorporation into protein between WT and CD98hc KO cells. DPM, disintegrations per minute. n=4.

Quantification data correspond to the mean ± SEM of the independent experiments (n) indicated for each graph normalised to control or WT cells. Statistical significance *, $p \leq 0.05$; **, $p \leq 0.01$; ***, $p \leq 0.001$ vs. control or WT cells, #, $p \leq 0.05$; ##, $p \leq 0.01$; ###, $p \leq 0.001$ vs. KO cells was analysed using a Student's t-test (panels A, B, C and I) or a linear model (panels D, E, F, G and H).

Figure 2. CD98hc depletion leads to delayed S-phase.

a, Gene Set Enrichment Analysis (GSEA) of transcriptional data from WT and CD98hc KO cells was performed. Bars represent significantly positively enriched gene sets (nominal p-value < 5%, FDR < 25%) in CD98hc KO cells compared to WT cells according to the KEGG data base. Bars are coloured following the functional characterisation indicated in the legend. X-axis: $-\log_{10}$ (p-val).

b, Cell cycle distribution measured by flow cytometry using propidium iodide (PI) staining. 10,000 cells/condition were analysed. A representative cell cycle profile of WT and CD98hc KO cells is shown, along with the overlap of their profiles (left panel). The graphical representation of cell cycle distribution (right panel) shows the percentage of cells in G1, S and G2/M phases in WT and CD98hc KO cells. n=4.

c, WT and CD98hc KO cells were synchronised in S-phase with a double thymidine block as indicated in *Methods*. The DNA content was analysed by flow cytometry using propidium iodide staining. 10,000 cells/condition were analysed. The percentage of cells in each cell cycle stage was measured at the indicated times after the release of the thymidine block. A representative cell cycle profile with highlighted S-phase is shown for each time point (upper panel). The percentage of WT and CD98hc KO cells in S-phase out of total was quantified at the indicated time points for (lower panel). n=4.

Quantification data correspond to the mean ± SEM of the independent experiments (n) indicated for each graph. Statistical significance *, $p \leq 0.05$; **, $p \leq 0.01$; ***, $p \leq 0.001$ vs. WT cells was analysed using a Student's t-test.

Figure 3. CD98hc deletion and BCAA and AAA shortage lead to replicative stress and impaired mitotic rate

a, Heat map of RNA expression level in WT and CD98hc KO cells of 97 genes involved in DNA damage signalling pathways. The genes featured were selected as indicated in *Methods* and grouped in the specified categories. Rows: genes; columns: samples. Range of colours (red/high to blue/low) shows the range of expression values after scaling within each sample.

b, Comparison of phosphorylated and total protein levels of CHK1 and RPA between WT and CD98hc KO cells. Data are normalised by β-actin expression. n=5.

c, Comparison of phosphorylated and total protein levels of CHK1 and RPA between control and low 6AA cells. Data are normalised by tubulin expression. n=3.

d, Comparison of mitotic rate between WT and CD98hc KO by immunofluorescence. The phosphorylation of Histone H3 (P-H3, red) was used as a marker for cells undergoing mitosis. DNA was stained with DAPI (blue) (left panel). Scale bar is 50 microns. More than 30,000 nuclei/condition were analysed. The percentage of mitotic cells is shown (right panel). n=7.

e, Comparison of mitotic rate between control and low 6AA cells by immunofluorescence. The phosphorylation of Histone H3 (P-H3, red) was used as a marker for cells undergoing mitosis. DNA was stained with DAPI (blue) (left panel). Scale bar is 50 microns. More than 30,000 nuclei/condition were analysed. The percentage of mitotic cells is shown (right panel). n=7.

Quantification data correspond to the mean ± SEM of the independent experiments (n) indicated for each graph normalised to WT or control cells. Statistical significance *, $p \leq 0.05$; **, $p \leq 0.01$; ***, $p \leq 0.001$ vs. WT or control was analysed using a linear model (panels B and C) or a Student's t-test (panels D and E).

Figure 4. CD98hc and BCAA and AAA availability are required for correct maintenance of the intracellular nucleotide pool

a, Content of nucleotides in WT and CD98hc KO cells measured by a targeted metabolomics assay. Data are normalized to cell number. n=5.

b, PPP activity was analysed by stable isotope tracer-based metabolomics in WT and CD98 KO cells. Cells were cultured with 5 mM fully labelled glucose (U-^{13}C6-Glucose) for 16 h. Ribose-5P with five ^{13}C carbon atoms (M+5) was compared between WT and CD98hc KO cells. Data are normalized to cell number. n=5.

c, Comparison of total content of ribose 5-P between WT and CD98hc KO cells. Data are normalized to cell number. n=5.

d, Content of nucleotides in control and low 6AA cells measured by a targeted metabolomics assay. Data are normalized to cell number. n=5.

e, Comparison of RRM2 protein expression between control and low 6AA cells. Data are normalised by vinculin expression. n=4.

f, PPP activity was analysed by stable isotope tracer-based metabolomics in control and low 6AA cells. Cells were cultured with 5 mM fully labelled glucose (U-^{13}C6-Glucose) for 16 h. Ribose-5P with five ^{13}C carbon atoms (M+5) was compared between control and low 6AA cells. n=5.

Quantification data correspond to the mean ± SEM of the independent experiments (n) indicated for each graph normalised to WT or control cells. Statistical significance *, $p \leq 0.05$; **, $p \leq 0.01$; ***, $p \leq 0.001$ vs. WT or control cells was analysed using a Student's t-test (panels A, B, C, D and G) or a linear model (panels E and F).

Figure 5. Nucleosides reverse cell cycle alterations in CD98hc KO cells

a, Cell cycle distribution was measured by flow cytometry using propidium iodide (PI) staining. A representative cell cycle profile of WT and CD98hc KO cells with no additives or in the presence of nucleosides (48 h) is shown, along with the overlap of their profiles (left panel). The graphical representation of cell cycle distribution shows the percentage of cells in G1, S and G2/M phases (right panel). n=4.

b, Comparison of phosphorylated and total protein levels of CHK1 (n=6) and RPA (n=4) between WT and CD98hc KO cells with no additives or in the presence of nucleosides (48 h). Data are normalised by tubulin expression.

c, Comparison of mitotic rate between WT and CD98hc KO cells with no additives or in the presence of nucleosides (48 h) by immunofluorescence. The phosphorylation of Histone H3 (P-H3, red) was used as a marker for cells undergoing mitosis. DNA was stained with DAPI (blue) (left panel). Scale bar is 50 microns. Quantification of the percentage of mitotic cells is shown. More than 30,000 nuclei/condition from six independent experiments were analysed (right panel).

Quantification data correspond to the mean ± SEM of the independent experiments (n) indicated for each graph normalised to WT. Statistical significance *, $p \leq 0.05$; **, $p \leq 0.01$; ***, $p \leq 0.001$ vs. WT or #, $p \leq 0.05$; ##, $p \leq 0.01$; ###, $p \leq 0.001$ vs. KO cells was analysed using a Student's t-test (panels A and C) or a linear model (Panel B).

Figure 6. CD98hc sustains cellular nutrition, redox homeostasis and nucleotide availability, all key for cell proliferation.

Solid lines represent established connexions proposed in this work. Dashed lines represent connexions suggested by the data provided herein and literature.

Figure S1. Characterisation of cell adaptations to AA shortage

a, Final BCAA and AAA concentrations (μM) in control and low 6AA media are indicated and compared with minimum and maximum physiological reference values in human plasma.

b, Comparative quantitative analysis of the intracellular AA content (nmol AA/μg protein) in CD98hc KO (n=7) and low 6AA cells (n=5). The fold change (FC, (KO or low/WT or control)-1) of the AA concentration is shown. AAs are grouped by side chain properties as indicated.

c, Comparison of CAT1, CAT3 and y^+LAT1 mRNA expression levels between control and low 6AA cells. n=3.

d, L-arg (10 μM) uptake at 2 min (linear conditions of uptake) in control and low 6AA cells is indicated. L-Arg uptake inhibitable by 1 mM L-Leu + Na^+ was identified as system y^+L, the remaining transport was attributed to system y^+. n=4.

e, ROS levels quantified by flow cytometry using the free radical sensor H_2DCFDA (DCF). Bars represent the mean DCF fluorescence in WT and CD98hc KO cells. a.u., arbitrary units. n>6.

f, Comparison of Nrf2 protein expression between low 6AA and CD98hc KO cells. 50 μg of protein extracts were loaded. Tert-butylhydroquinone (BHQ) treatment (50 μM, 1 h) was used as a control. n>4.

g, tRNA microarrays of aminoacyl-tRNAs in CD98hc KO and WT cells. Representative array of two independent biological replicates replicates which are highly similar as assessed by covariance analysis (right plots) for each isoacceptor. tRNAs are depicted by their anticodon and cognate amino acid.

Quantification data correspond to the mean ± SEM of the independent experiments (n) indicated for each graph normalised to control or WT cells. Statistical significance *, $p \leq 0.05$; **, $p \leq 0.01$; ***, $p \leq 0.001$ vs. control or WT cells was analysed using a linear model (panel C) or a Student's t-test (panels D and E).

Figure S2. GSEA reveals positive enrichment in gene sets related to cell cycle, AA metabolism and RNA metabolism in CD98hc KO cells

Enrichment plots for the indicated gene sets obtained from gene set enrichment analysis (GSEA) using KEGG data base of transcriptional data from WT and CD98hc KO cells (upper panel). Y-axis: value of the enrichment score; X-axis: genes ranked by t-statistic. Bottom: plot of the ranked list of all genes. P-value (p-val), Normalized Enrichment Score (NES) and False Discovery Rate (FDR) are indicated for the included enrichment plots (lower panel).

Figure S3. CD98hc KO cells activate the DNA Damage Response and induce apoptosis

a, Enrichment plot for the gene set DNA Damage Response from gene set enrichment analysis (GSEA) of transcriptional data from WT and CD98hc KO cells. Y-axis: value of the enrichment score; X-axis: genes ranked by t-statistic. Bottom: plot of the ranked list of all genes. P-value=0.00, Normalized Enrichment Score (NES) =1.83 and False Discovery Rate (FDR) =0.00.

b, Apoptosis in WT and CD98hc KO cells was measured by Annexin V and propidium iodide (PI) staining followed by flow cytometry analysis. Representative diagrams are shown (left panel). Y-axis: PI fluorescence; X-axis: Annexin V fluorescence. The analysis allows us to distinguish between living cells (lower left quadrant, Q4), early apoptotic cells (lower right quadrant, Q3), late apoptotic cells (upper right quadrant, Q2), and dead cells (upper left quadrant, Q1). The percentage

of cells in each state was calculated and represented in a histogram (right panel). Quantification data correspond to the mean ± SEM of 7 independent experiments. Statistical significance *, $p \leq 0.05$; **, $p \leq 0.01$; ***, $p \leq 0.001$ vs. WT was analysed using a Student's t-test.

c, Enrichment plot for the gene set G2/M checkpoint from gene set enrichment analysis (GSEA) using Hallmarks data base of transcriptional data from WT and CD98hc KO cells. Y-axis: value of the enrichment score; X-axis: genes ranked by t-statistic. Bottom: plot of the ranked list of all genes. P-value=0.015, Normalised Enrichment Score (NES) =1.37 and False Discovery Rate (FDR) =0.13.

Figure S4. Nucleosides reverse the replicative stress caused by BCAA and AAA deprivation in low 6AA cells.

Comparison of phosphorylated and total protein levels of CHK1 and RPA between control and low 6AA cells with no additives ($n \geq 6$) or in the presence of nucleosides (48 h) ($n=4$). Data are normalised by tubulin or vinculin expression. Quantification data correspond to the mean ± SEM of the independent experiments (n) indicated for each graph normalised to control cells. Statistical significance *, $p \leq 0.05$; **, $p \leq 0.01$; ***, $p \leq 0.001$ vs. control or #, $p \leq 0.05$; ##, $p \leq 0.01$; ###, $p \leq 0.001$ vs. low 6AA cells was analysed using a linear model.